DE MONTFORT UNIVERSITY LEICESTER

FACULTY OF HEALTH AND LIFE SCIENCES

REMEDIATION OF TEXTILE AND MINING INFLUENCED EFFLUENTS USING NOVEL HETEROGENEOUS PAN CATALYST AND MODIFIED PAN MESH

A thesis submitted in the partial fulfilment for the degree of Doctor of Philosophy (Ph.D.) in Environmental Technology

By

Pushpa Datta Upreti

Supervisor: Prof. Dr. Katherine D. Huddersman

March 2018

DEDICATION

I would like to dedicate this thesis in memory of my beloved late parents:

Mr. Ganesh Datta Upreti

&

Mrs. Maheshwori Upreti

Who sacrificed own happiness for my success and could not be there when it is happening!!!

ACKNOWLEDGEMENT

First, I would like to express my deepest and sincere gratitude to my supervisor Prof. Dr. Katherine D. Huddersman for her continual invaluable guidance and support without which this project would not come to this stage. I am deeply indebted to her for the opportunities, from the laboratory to the pilot trials, provided to me. Her support was more than one could hope for from a supervisor, an exceptional supervisor. Her efforts enlightened me with life-long research skills.

I would like to thank my second supervisor Prof. Dr. Martin Grootveld.

I would like to express my sincere thanks to Dr. George Tangyie Chi for his invaluable feedback and guidance. I would like to thank Dr. Walkiria Schlindwein for feedback and discussions during annual reviews.

I would like to thank technicians, especially Unmesh Deshai, Nazmin Juma and Rachel Armitage, of the Faculty of Health and Life Sciences for their support. I would like to remember my colleagues Aghogho Ekpruke, Emmanuel Ushie, Dr. Caroline Akinremi, Elmajid Yusuf and Dr. Leo Ihonre Asuelimen in the research group for their friendship and stress-free friendly environment making this programme memorable.

I am deeply indebted to my family, Dhruba Datta Upreti – brother; Apsara Upreti – sister-in-law; Barsha Belbase – wife; Avani Upreti – niece; Samriddha Upreti – son and Avan Upreti – nephew for their love and always being there to support and encourage me. I would like to appreciate all the relatives, friends and social committee co-workers for their encouragement and positive vibes.

I would like to thank Innovate UK for the opportunity of innovation voucher and Jersey Dyer, Leicester for the part of SME in the scheme. I would like to express my sincere gratitude to The Coal Authority (CA) for managing the sponsorship of the metal removal project from the Department for Environment, Food & Rural Affairs (DEFRA). My special thanks goes to Isla Ismail, the then project manager from CA. I would like to appreciate all the related staff from The CA, The Environment Agency, Severn Trent Services and Integrated Water Services for their help.

PUBLICATION

A part of chapter six of this research has led to the publication of the following conference proceeding.

Upreti, Pushpa; Tangyie, George Chi; Huddersman, Katherine; Smail, Isla (2016): Field trial of an ion exchange based metal removal technology in the treatment of mine waters. – In: Drebenstedt, C. & Paul, M.: IMWA 2016 – Mining Meets Water – Conflicts and Solutions. – p. 828 – 835; Freiberg / Germany (TU Bergakademie Freiberg).

ABSTRACT

The effectiveness of a modified PAN catalyst and hydrogen peroxide system in the treatment of textile effluent and a modified ion exchange PAN mesh in the remediation of non-coal mine drainage was investigated. The results show a tremendous potential in the treatment of such wastewaters.

The treatment process for textile effluent was optimized in batch mode of operation. The influence of pH and catalyst was more pronounced compared to that of H_2O_2. At optimum conditions, 99.5 % decolourization and 91.9 % loss of aromaticity and 70 % mineralization were achieved in 100 minutes. The sorption of dye onto the catalyst is favourable and can be best described by a Langmuir adsorption isotherm model. The model predicts a maximum adsorption capacity for the PAN catalyst as 0.68 mg of RO16 per gram of catalyst. A direct relationship between pH, temperature and iron leaching was established. The leached iron has no significant contribution, by means of homogeneous catalysis, in the removal of dye. The system was successful in treating a real dye-bath effluent that was much more concentrated than usual textile effluents.

The continuous flow treatment in a prototype of a rotating discs contactor revealed that 99.2 %, 73 %, 64.4 % and 50 % removal efficiencies for decolourization, loss of aromaticity, COD and mineralization at optimum conditions. The breakthrough of the system occurred after 50 days. The system was successfully regenerated in-situ three times and the lifetime of the catalyst extended to 103 days in total, decolourizing 25.3 g of RO16 dye from 546.7 L solution. The deactivation of catalyst occurred mainly due to the loss of iron and partially due to loss of functional groups that ligate iron. Similar to the batch experiments, the leached iron, in continuous flow experiment, has insignificant contribution in removing dye through homogeneous catalysis.

The ion exchange capacity of the modified PAN fibre was determined though acid-base titration. The sorption of zinc onto ion exchange mesh is favourable and can be best described by Langmuir adsorption isotherm model. The pH of the medium was found to be the most influential parameter with maximum sorption observed at pH ≥ 5.5 at contact time ≥ 4 hours in batch mode of operation.

A pilot scale field trial was performed to remediate mine effluent with elevated concentration of zinc, cadmium and lead demonstrates a tremendous potential applicability. According to analyses by UKAS accredited laboratory, the 170 days long trial successfully removed 5.59 kg, 8.53 g and 18.18 g of zinc-total, cadmium-total and lead-total from 131.46 m^3 of mine effluent. The system also removed suspended solids, iron, copper, arsenic, nickel, aluminium, boron, manganese and nitrate (NO_3-N). The performance of the system was not affected by the in-situ regeneration and seasonal variation in temperature. The best performance of the system was observed when the contact time ≥ 1.33 hours. The metal removal mechanism was ion exchange initiated (co)precipitation / sorption of metals onto the surface of ion exchange mesh. This technology can be applied in the remediation of all type of mine waters though pre-treatment to adjust pH and alkalinity may be needed.

TABLE OF CONTENT

LIST OF FIGURES

LIST OF TABLES

LIST OF APPENDICES

LIST OF ABBREVIATIONS

AAS - Atomic Absorption Spectrophotometer

AATCC – American Association of Textile Chemists and Colourists

ALD – Anoxic Limestone Drain

AMD – Acid Mine Drainage

AOP – Advanced Oxidation Process

BOD – Biological Oxygen Demand

C.I. – Colour Index

CEPA – Canadian Environmental Protection Act

CNN – Cable News Network

COD – Chemical Oxygen Demand

DNA – Deoxyribonucleic Acid

EC – European commission

EEC – European Economic Community

EGS – Environmental Scientific Group

EQS – Environment Quality Standard

ETAD - Ecological and Toxicological Association of the Dyestuffs Manufacturing Industry

EU – European Union

GARD – Global Acid Rock Drainage

IARC – International Agency for Research on Cancer

ICP-MS – Inductively Coupled Plasma – Mass Spectroscopy

INAP – The International Network for Acid Prevention

ITRC – Interstate Technology Regulatory Council

IWS – Integrated Water Services

LD_{50} – Lethal Dose that kills 50 % of the test organisms

LOD – Limit of Detection

MIW – Mining Influenced Water

NPCS – Niir Project Consultancy Services

ODAS – Oxidation, Dosing with Alkali and Sedimentation

OFAT – One-factor-at-a-time

OLD – Oxic Limestone Drain

OPEX – Operating Expense

PAN – Polyacrylonitrile

PPE – Personal Protective Equipment

PRB – Permeable Reactive Barrier

RAPS – Reducing and Alkalinity Producing System

RBC – Rotating Biological Contactor

REACH – Registration, Evaluation, Authorization and Restriction of Chemicals

RO16 – Reactive Orange 16

RT – Resident / Retention Time

SAPS – Successive Alkalinity Producing System

SDC – Society of Dyers and Colourists

SPs – Specific Pollutants

STS – Severn Trent Water Services

STY – Space Time Yield

TC – Total Carbon

TIC – Total Inorganic Carbon

TOC – Total Organic Carbon

TOF – Turnover Frequency

TON – Turnover Number

UK – United Kingdom

UKAS – United Kingdom Accreditation Service

UKTAG – United Kingdom Technical Advisory Group

USA – United States of America

USEPA – United States Environmental Protection Agency

WFD – Water Framework Directive

WHO – World Health Organization

CHAPTER ONE

1. INTRODUCTION

1.1. INTRODUCTION TO THE THESIS

The natural environment has been systematically exploited, modified and destructed since human beings learnt to use fire, domesticate animals and grow plants for food. Natural resources are being exploited drastically all over the world to fulfil the basic needs, for example, safe drinking water and clothing of booming population.

Water is a basic form of life on earth. The significance of water resources can be reflected through a hypothesis, "*the next world war will be fought over water*", introduced to public forums (Gleick *et al.*, 2006; Goldenberg, 2014; Engelke, 2016). Water is polluted by human activities such as agriculture, domestic and industrial. Discharge of organic and inorganic toxic compounds into water system increased significantly after 1850, as a result of the industrial revolution (Timmy and Satake, 1989). Industries produce waste materials and by-products during the manufacturing and processing. Textile and mining industries are amongst the top polluting industries. The problems and potential solutions related to these industries are introduced separately in the following sections.

1.2. PROBLEM STATEMENT – TEXTILE INDUSTRY EFFLUENTS

Textile industry has one of the largest water footprints (Annie, 2018) and discharges large volumes of effluents containing harmful organic compounds such as dyes and surfactants (Carmen and Daniela, 2012). Based on the discharged volume and composition of effluent, textile industry is rated as the most polluting amongst all industrial sectors (Vandevivere, Bianchi and Verstraete, 1998). It is estimated that about 12 m^3 (2,641 gallons) of water is consumed to produce one pair of jeans (Annie, 2018) and an average sized textile mill with the production capacity of 8,000 kg clothes per day discharges one million litres (1000 m^3) of effluent to water systems (Choudhury, 2006). The effluent contains wide range of organic compounds, for example dyes and their breakdown products, additives, auxiliary chemicals and surfactants. The notorious effect of textile effluents can often be seen in water systems around the manufacturing areas of Nepal, India, China and other developing countries (Muthu, 2017; Annie, 2018). These organic compounds are not easily acquiescent to chemical and biological treatment (Vandevivere, Bianchi and Verstraete, 1998; Dantas *et al.*, 2006).

It is estimated that more than 100,000 different dyes are commercially available (Robinson *et al.*, 2001; Singh, 2006; Valh and Marechal, 2009; Soon and Hameed, 2011). The annual production of these dyes is up to 7×10^5 million tonnes (Butler *et al.*, 2016). About 67 % (Pereira and Alves, 2016) to 80 % (Gürses, 2016) of the total dyes

produced worldwide is consumed by textile industry. A large fraction, 25 % (Carmen and Daniela, 2012) to around 30 % (Vandevivere, Bianchi and Verstraete, 1998), of applied dyes is lost during dyeing process. In case of reactive azo dyes, a loss of 50 % (Abdullah, Wong and Yaziz, 2010; Tizaoui and Grima, 2011; Chequer *et al.*, 2013) to 70 % (Øllgaard *et al.*, 1998) has been reported. Consequently, the effluent from textile industry contains up to 20 % (Carmen and Daniela, 2012) or 600 - 800 mg/L (Vandevivere, Bianchi and Verstraete, 1998) of applied dyes of which 80 % (Øllgaard *et al.*, 1998) are azo dyes. Dyes are also used in religious occasions, for example, the Hindu festival of colours, commonly known as Holi. As shown in Figure 1-1, Holi is one of the religious sources for environmental exposure of dyes.

Figure 1-1: Environmental exposure of dyes during 'Fagu Purnima', also known as 'Holi', in Nepal. Source: (NepaliSansar, 2018).

The discharge of textile effluent into the natural water system is undesirable, not only because of their turbid appearance, but also due to putative toxicity and carcinogenicity. In fact, many dyes are made of known carcinogens, for example benzidine, naphthalene and other aromatic compounds (Banat *et al.*, 1996; Anjaneyulu, Chary and Raj, 2005; Carmen and Daniela, 2012). Formation of the parent toxic amines due to the reduction of azo and nitro compounds in sediments and intestinal environment has already been established (Chung, Fulk and Egan, 1978; Weber and Wolfe, 1987).

Most of the dyes are non-biodegradable and they can have carcinogenic action or cause allergies, dermatitis, skin irritation or tissular changes. Several azo dyes cause damage

of DNA that can lead to genesis of malignant tumours (Carmen and Daniela, 2012). Adsorption of azo dyes and their breakdown products (toxic amines) through gastrointestinal tract, skin and lungs has caused a high potential health risk (Börnic and Schmidt, 2006).

Azo dyes are the most common in use and they represent ≥ 70 % of all textile dyestuffs (Supaka *et al.*, 2004; Anjaneyulu, Chary and Raj, 2005; Saratale *et al.*, 2011; Brillas and Martínez-Huitle, 2015; Wawrzkiewicz and Hubicki, 2015). These dyes are intentionally designed to resist degradation and hence these are resistant to biodegradation under aerobic conditions (Banat *et al.*, 1996; Vandevivere, Bianchi and Verstraete, 1998; Carmen and Daniela, 2012). Ecotoxicological studies conducted in England show that over 18 % of 200 dyes tested significantly inhibited respiration rate of biomass from sewage (Cooper, 1995). Ecological and Toxicological Association of the Dyestuffs Manufacturing Industry (ETAD) conducted a survey of some 4,000 dyes and found that the lethal dose (LD_{50}) of over 90 % dyes had values greater than 2 g/kg (Robinson *et al.*, 2001). Thus, treatment of textile effluent before discharging into the public water system is necessary

1.2.1. SOLUTION FOR THE TREATMENT OF TEXTILE EFFLUENTS

Large-scale production and extensive application of dyes cause a serious concern to the environmental and public health. Therefore, strict environmental legislation has been introduced in order to prevent them entering into the environment. Developed countries are becoming stricter in their regulations whereas developing countries also have introduced environmental laws. For example, in UK, environmental policy allows zero synthetic chemicals to be released into the marine environment. European community (EC) regulations are also becoming stricter. Enforcement of these laws compels textile industries to treat their effluents before releasing into the environment (Robinson *et al.*, 2001).

A wide range of methods and their combinations has been employed in the treatment of textile effluent. These methods can be classified into three main categories: physical, biological and chemical. These methods involve adsorption on inorganic or organic matrices, filtration, decolourization by photo-catalysis, and / or oxidation processes, microbiological or enzymatic decomposition and so on (Hao, Kim and Chiang, 2000; Forgacs, Cserháti and Oros, 2004). Irrespective of differences in treatment technologies, the overall aim of them is to complete mineralization of the pollutants. Biological

treatment methods, for example, activated sludge, are widely accepted and relatively cost effective. However, complete mineralization of finishing agents (e.g. surfactants, dyes and softeners) using conventional biological treatment methods is often not possible (Weschenfelder *et al.*, 2007). Phase separation methods concentrate pollutants and experience disposal problems as a result (Andreozzi *et al.*, 1999). Therefore, destructive methods, for example, advanced oxidation processes (AOPs), are the alternative.

AOPs are the processes in which oxidation of organic pollutants primarily occurs through the generation of extremely reactive non-selective entities known as the hydroxyl radicals ($^{\bullet}OH$). These processes often include the use of ozone, ultraviolet light and hydrogen peroxide (H_2O_2) in combination or in the presence of catalyst especially in the case of hydrogen peroxide. Heterogeneous Fenton process is one of the most promising amongst AOPs. Fenton-based processes are increasingly applied in the treatment of wastewater or landfill leachate due to cost-effective and easy operation features (Glaze and Kang, 1989; Andreozzi *et al.*, 1999; Arslan and Balcioğlu, 1999; Parson, 2004; Muñoz *et al.*, 2006). Thus, this thesis also employed a heterogeneous catalyst, modified PAN-Fe^{3+}, which was developed at De Montfort University (DMU) and relies on Fenton's mechanism.

1.3. PROBLEM STATEMENT – MINING INFLUENCED EFFLUENTS

Mining related pollution, especially the mining influenced water (MIW), represents a severe environmental problem in countries which have a mining history such as the UK (National Rivers Authority, 1994; Johnston *et al.*, 2008; Whysner *et al.*, 2012). Mining related pollution is difficult to deal with as post mining impacts last for a very long time, for centuries even after the cessation of active mining. The abandoned mines are the biggest sources of water pollution in the UK (National Rivers Authority, 1994; Younger, Banwart and Hedin, 2002; Johnston *et al.*, 2008). Mining related contamination of soils and sediments affected rivers, lakes, estuaries and floodplains. Eight of twelve river basin districts in the UK have been influenced by abandoned mines (Hudson-Edwards *et al.*, 2008; Johnston and Rolley, 2008).

Mining influenced water from metal mining is circum-neutral (around pH 7) and that from coal mining is acidic-ferruginous, both waters contain very high concentrations of metals commonly known as 'heavy metals' such as zinc, lead and cadmium (Younger, Banwart and Hedin, 2002; Miller, Wildeman and Figueroa, 2013). Some authors reported that the term 'heavy metals' is misleading and useless (MacKay, MacKay and Henderson, 2002,

p. 44; Smith and Nordberg, 2014, p. 15). Thus, here forward, they will be referred as metals only. These metals are toxic to aquatic environment, livestock and human beings. Consequently, human suffering from anaemia, pulmonary distress, skin irritation, kidney damage, skeletal deformity, fertility problem, neuro-psychological development etc. due to metals such as zinc, cadmium and lead have been reported (Herber, Verschoor and Wibowo, 1988; WHO, 1996; Mohan and Singh, 2002; Fu and Wang, 2011). Water crisis in Flint, Michigan, USA caused due to elevated concentration of lead (see Figure 1-2) is a recent infamous case of metal pollution. Thus, to prevent removal of these metals from water before discharging into the public water system is necessary.

Figure 1-2: A picture captioned 'Flint Water Crisis " Ground Zero"' reflecting the Flint Water Crisis. Source: (American Chemical Society, 2017).

1.3.1. REMEDIATION OF MINING INFLUENCED EFFLUENTS

Mining influenced effluents can be either acidic, circum-neutral or saline. A range of methods exists for the remediation of such waters. These methods are broadly classified into passive and active treatment methods (Brown, Barley and Wood, 2002; Younger, Banwart and Hedin, 2002; Miller et al., 2011; Pearce, 2014; USEPA, 2014). Further information on these methods can be found in chapter three.

Passive treatment methods require large land space. Thus, application of passive treatment methods in the UK is problematic as most of the mining sites are located in the areas with steep sided valleys with minimal land space (Warrender, 2009; Pearce, 2014).

Active treatment methods can be controlled with the workforce on site thus better suited to working mines, mine with large discharge rate and little land space (Brown, Barley and Wood, 2002; Younger, Banwart and Hedin, 2002). Amongst the various active treatment

methods, sorption (ion exchange and adsorption) based processes are potential alternatives (Gode and Pehlivan, 2006). Ion exchange process is gaining more interest due to high efficiency, selectivity, better recovery of metal value, less sludge production and low operational costs (Alyüz and Veli, 2009; Fu and Wang, 2011).

Synthetic ion exchangers are commonly preferred in water treatment as they are inexpensive and effective in removing metals (Alchin and Wansbrough, 2002; Chen *et al.*, 2006; Gode and Pehlivan, 2006; Alyüz and Veli, 2009; Fu and Wang, 2011). Thus, this thesis also employed a potential ion exchanger, a modified fibrous PAN mesh, developed at DMU, in the remediation of circum-neutral mine effluent.

1.4. AIMS AND OBJECTIVES

The general aim of this research, treatment of wastewaters, is subdivided:

a) To study the effectiveness of a novel heterogeneous modified polyacrilonitrile (PAN)-(Fe^{3+}) catalyst and hydrogen peroxide system for the treatment of textile effluent and;
b) To study the effectiveness of a modified fibrous ion exchange PAN mesh for the remediation of mining influenced effluents.

1.4.1. OBJECTIVES – TREATMENT OF TEXTILE EFFLUENTS

The aim of this project mentioned in section 1.4 a) was achieved through the following objectives;

- To investigate the influence of process parameters on removal of dyes
- To investigate the influence of process parameters on sorption capacity of modified PAN catalyst
- To investigate the extent of catalyst loss with respect to the process parameters
- To investigate the extent of decolourization, loss of aromaticity and mineralization in batch and continuous flow mode of operations
- To investigate the lifetime of the modified PAN catalyst in a continuous flow treatment
- To investigate the mechanism of catalyst deactivation
- To investigate the effectiveness of regeneration of deactivated catalyst

1.4.2. OBJECTIVES - REMEDIATION OF MINING INFLUENCED EFFLUENTS

The aim of this project mentioned in section 1.4 b) was achieved through the following objectives;

- To determine the ion exchange capacity of functionalized fibrous PAN mesh

- To determine the metal removal capacity of the ion exchange PAN mesh in batch mode of operation
- To determine the metal removal capacity of the ion exchange PAN mesh at pilot scale continuous flow experiment with real mining influenced effluent
- To determine the effectiveness of regeneration of the deactivated ion exchange PAN mesh

1.5. THESIS STRUCTURE

Chapter 1 – Introduction: This chapter introduces to global water pollution, problems arising from the effluents discharged by textile and mining industries and highlights potential solutions to such problems. This chapter also introduces to aim and objectives of this project.

Chapter 2 - Literature review on treatment of textile effluents: This chapter introduces to dyes (history, consumption and related problems) and technologies available for the treatment of textile effluents.

Chapter 3 - Literature review on remediation of mining influenced effluents: This chapter introduces to history of mining and its environmental impacts, mine water chemistry and potential technologies available to remediate mining influenced effluents.

Chapter 4 - Optimization of reaction process: This chapter explains the importance of process optimization and presents the results and discussions of sorption and equilibrium study, influences of process parameters, extent of catalyst loss, heterogeneous versus homogeneous catalyses, and treatment of real dye-bath effluent.

Chapter 5 - Continuous flow treatment and lifetime of the modified PAN catalyst: This chapter introduces to the upscaling of treatment process and continuous flow treatment systems. Results for extent of decolourization, loss of aromaticity, mineralization, mechanism of catalyst deactivation and regeneration of deactivated PAN catalyst etc. obtained from the continuous flow treatment of dye performed with a bench scale prototype rotating discs contactor are discussed in this chapter.

Chapter 6 – Remediation of mine water drainage: This chapter presents the results of ion exchange and metal uptake capacities of modified PAN mesh, equilibrium study, a pilot scale field trial for the remediation of non-coal mine drainage and effectiveness of regeneration of exposed ion exchange PAN mesh.

Chapter 7 - Conclusions and recommendations: This chapter provides a general summary of the main finding of this project and a list of future works that will help better understanding of the technologies used in this project.

CHAPTER TWO

2. LITERATURE REVIEW: TREATMENT OF TEXTILE EFFLUENTS

2.1. DYES: DEFINITION AND HISTORY

The history of dyes has been prevalent to ancient time. Archaeologists found linens in Egypt that can be traced back to 5,000 B.C. Before introduction of synthetic dyes, natural sources such as Brazilwood, cochineal insects (female) Mexican or Peruvian cactus and vegetable leaves were used to extract dyes (Baumann and Lacasse, 2004; Butler *et al.*, 2016).

The first synthetic dye, Mauveine also known as aniline purple or Perkin's mauve, was accidently discovered by William Perkin in 1856. Then, synthesis of dyes expanded rapidly and 10,000 new synthetic dyes had been developed and manufactured by the end of 19th century (Hunger, 2003; Butler *et al.*, 2016; Gürses *et al.*, 2016; Pereira and Alves, 2016). Today, dyes become an inevitable part of human life. Dyes are used in textile industry (Sokolowska-gajda, Freeman and Reife, 1996; Shore, 2002; Zollinger, 2003; Baumann and Lacasse, 2004; Pereira and Alves, 2016), leather industry (Tunay *et al.*, 1999) religious and cultural festivals (Narayanan, 2015), food technology, agricultural research (Cook and Linden, 1997), light-harvesting arrays (Wagner and Lindsey, 2009), hair colouring, ground water tracing (Field *et al.*, 1995) etc.

A dye can be defined as a substance that strongly absorbs light in the visible range (400 nm to 700 nm) of the electromagnetic spectrum and has an affinity for the substrate to which it is applied. Affinity can be best explained as the alignment of a specific dye on a fabric (Baumann and Lacasse, 2004; Butler *et al.*, 2016; Pereira and Alves, 2016). According to the Ecological and Toxicological Association of Dyes and Organic Pigment Manufacturers (ETAD), "*Dyes are intensely coloured or fluorescent organic substances only, which impart colour to a substrate by selective absorption of light. They are soluble and / or go through an application process which, at least temporarily, destroys any crystal structure by absorption, solution and mechanical retention, or by ionic or covalent chemical bonds"* (SDC & AATCC, 2017).

Dyes belong to a subcategory known as colorants, substances that absorb light within the visible range of electromagnetic spectrum, are divided into dyes and pigments. The property that differentiate dyes and pigments is solubility. Dyes are soluble in water and / or organic solvents whereas pigments are insoluble in both media (Allen, 1971; WHO-IARC, 2010). In general, dyes are soluble in the application medium thus disperse at molecular level whereas pigments are insoluble to the application medium and disperse as particles (Gürses *et al.*, 2016). Dyes are applied onto the substrates whereas pigments are combined with the substrates (Butler *et al.*, 2016).

Mostly, natural dyes are used for foodstuffs whereas synthetic dyes are primarily used for colouration of textiles, although substantial amounts are used for colouring of diverse materials such as paper, leather, plastics, petroleum products and other consumables. Dyes make the world colourful and enjoyable but also pose serious problems to the environment (NPCS Board of Consultants and Engineers, 2009; Valh and Marechal, 2009).

2.1.1. CHEMICAL STRUCTURE OF DYE AND COMPONENT RESPONSIBLE FOR DYE COLOUR

Otto Witt (1876) made a first general theory explaining the depth of colour to molecular structure and found that all the dyes contained three essential components known as chromogen, chromophore and auxochrome (Shore, 2002; Gürses *et al.*, 2016).

The group of atoms that is responsible for the appearance of colour of the compound through absorption of light is the chromophore group, i.e., a delocalized electron system with conjugated bonds, double or single. The chromophores generally contain heteroatoms and the common examples of chromophores include azo (–N=N-); carbonyl (=C=O); ethylene (=C=C=); methine (-CH=); carbon-nitrogen (-C=N, =C=NH, -CH=N); nitroso (-NO or N-OH); nitro ($-NO_2$ or NO-OH); carbon-sulphur (C=S, ≡C-S-S-C≡) and quinoid / chinoid groups (Pahari and Chauhan, 2006; Carmen and Daniela, 2012; Gürses *et al.*, 2016; Pereira and Alves, 2016).

Auxochromes are the electron withdrawing or donating substituents on the opposite side of the molecule that intensify the colour of dye molecule. In other words, the auxochrome groups are the ionisable groups. The common examples of auxochromes include amino ($–NH_3$), carboxyl (-COOH), hydroxyl (-OH), amine ($-NH_2$) and sulfonate ($-SO_3H$) (Valh and Marechal, 2009; Carmen and Daniela, 2012; Pereira and Alves, 2016). The attachment of auxochromes in the basic chromophore may modify the intensity of absorption band of the dye due to bathochromic and hypsochromic shifts. Bathochromic or red shift causes the absorption maxima shift towards longer wavelength of lower frequency whereas hypsochromic or blue shift causes absorption maxima shift towards lower wavelength (Pahari and Chauhan, 2006).

The chromophoric groups are responsible for the absorption of electromagnetic radiation in the visible range and the auxochromic groups are responsible for dyes affinity for dyed materials (Wawrzkiewicz and Hubicki, 2015). The chromogen is chemical compound that

is coloured either due to presence of chromophore and auxochrome or could be made coloured by the attachment of suitable substituent (Gürses *et al.*, 2016).

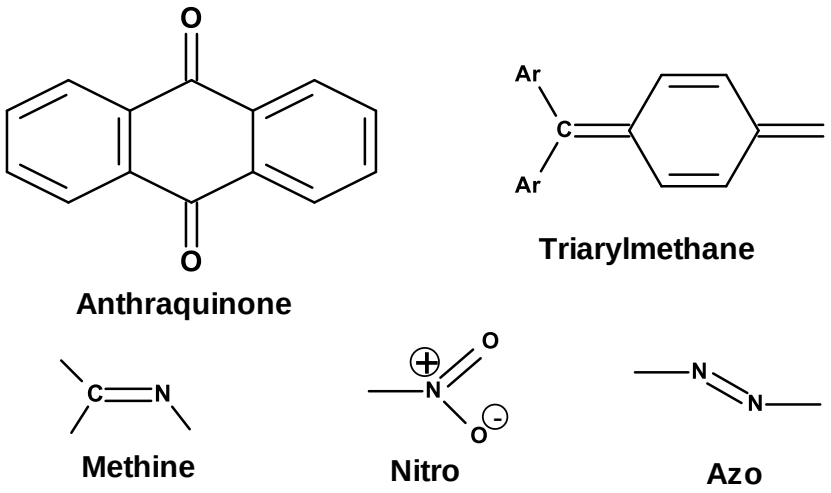

Figure 2-1: Examples of chromophoric groups present in dyes. Source: (WHO-IARC, 2010; Gürses et al., 2016).

The essential characteristics for a dye molecule to possess colour are:

- absorption within the visible range of electromagnetic spectrum,
- contain at least one chromophore,
- have a conjugated system, i.e. structure with alternating single or double bonds, and
- exhibit resonance (stabilizing force) of electrons in organic compounds.

The colour is lost if any one of these features lack from the molecular structure of dye. Although, auxochromes are not responsible for colour their presence can shift the colour and solubility of the dye (WHO-IARC, 2010; Gürses *et al.*, 2016).

2.1.2. CLASSIFICATION OF DYES

The classification of dyes has become mandatory due to growing number and varieties. The first systematic classification of dyes based on chemical structure with subgrouping according to hue started in 1880s (Waring and Geoffrey, 1990; Shore, 2002).There are several methods for dye classification. Dyes can be classified according to their chemical structure (chromogen), usage or application to textile fibres, origin, and physical properties. Amongst these, the former two are commonly used by dye chemists and technologists (Allen, 1971; Waring and Geoffrey, 1990; Shore, 2002; Hunger, 2003; Valh and Marechal, 2009; Khalid, Arshad and Crowley, 2010; Butler *et al.*, 2016; Gürses *et*

al., 2016; Pereira and Alves, 2016). These are discussed separately in the following sections.

The Colour Index (C.I.) method considers the chemical structure and application type, colour or hue and shade. In the C.I. classification, a five-digit C.I. number is assigned once the manufacturer discloses the chemical structure of a dye. The first and second words represent the classification system and hue or shade of the dye respectively (Hunger, 2003; Gürses *et al.*, 2016; Pereira and Alves, 2016). For example, C.I. Acid Yellow 36 (CI13065) is an acidic type and yellow coloured.

Chemical classification of dye is further divided into several groups: based on the presence of different structural units (azo, anthraquinone, indigo etc.), method and domain of usage (acid, direct, basic, reactive, reductive, disperse etc.), chromogen (absorptive, fluorescent, dyes with energy transfer etc.), nature of donor – acceptor couple (1-aminoanthraquinone, p-nitroaniline etc.), and nature of polyenes (polyolefins, cyanines etc.) (Waring and Geoffrey, 1990; Shore, 2002; Hunger, 2003; Valh and Marechal, 2009; Pereira and Alves, 2016).

Due to the complications of the colour nomenclature based on chemistry, the classification based on application or usage is considered more useful. Based on application dyes are divided into several groups: acid, azoic, basic, direct, disperse, fluorescent, food, ingrain, leather, mordant, natural, oxidation, reactive, vat, solvent and sulphur (Waring and Geoffrey, 1990; Shore, 2002; Hunger, 2003; Baumann and Lacasse, 2004; Valh and Marechal, 2009; Gürses *et al.*, 2016; Pereira and Alves, 2016). The major types are azo, acid, direct, disperse, sulphur and fibre reactive (USEPA, 1985).

The dyes can be classified into water-soluble cationic and anionic dyes and water insoluble dyes – non-ionic dyes. The cationic dyes are basic dyes whereas anionic dyes are acidic, direct and reactive dyes. The non-ionic dyes are disperse, mordant (substance that fixes a dyestuff in or on a material) and solvent dyes which are known to have low water solubility (Allen, 1971; Øllgaard *et al.*, 1998). This project used a reactive azo dye as a model compound.

2.1.2.1. AZO DYES

Azo dyes are the most widely used and studied synthetic dyes and represent over 50 % (Waring and Geoffrey, 1990; Tizaoui and Grima, 2011), ≥ 60 % (Allen, 1971; Hunger, 2003; Gürses *et al.*, 2016), ≥ 70 % (Supaka *et al.*, 2004; Anjaneyulu, Chary and Raj,

2005; Saratale *et al.*, 2011; Brillas and Martínez-Huitle, 2015; Wawrzkiewicz and Hubicki, 2015) of all commercial dyes. They are characterized by the presence of one or more azo (-N=N-) bonds (Allen, 1971; Bilgi and Demir, 2005; Valh and Marechal, 2009; Tizaoui and Grima, 2011; Gürses *et al.*, 2016) and further divided into four subgroups depending on the number of azo bonds (monoazo, diazo, triazo and polyazo) (Allen, 1971; Shore, 2002; Baumann and Lacasse, 2004; Pereira and Alves, 2016). The azo bond is attached to two moieties of which at least one but, usually, both are aromatic (Waring and Geoffrey, 1990; Gürses *et al.*, 2016). Azo dyes can be tautomerized. The possible tautomers are azo / hydrazine for hydroxyazo dyes, azo / imino for aminoazo dyes, and azonium / ammonium for protonated azo dyes (Waring and Geoffrey, 1990). Azo dyes have benzene and naphthalene groups in the form of chloro [-Cl], nitro [-NO_2], amino [-NH_2], methyl [-CH_3], hydroxyl [-OH], and carboxyl [-COOH] (Saratale *et al.*, 2011; Butler *et al.*, 2016). Azo dyes are mostly used for orange, yellow and red colours (Valh and Marechal, 2009). Based on the charge of attached group, azo dyes can be classified as cationic, anionic and non-ionic. Ionic azo dyes dissociate completely or partially in an aqueous solution and the solubility ranges from 100 mg/L to 80 g/L. However, the solubility of non-ionic azo dyes limited in the range of 0.2 mg/L to 34.3 mg/L only. Azo dyes do not occur naturally (Øllgaard *et al.*, 1998; Madan, 2013).

The synthetic azo dyes are formulations of several components and the specific dye content varies in the range of 10 – 98 %. The majority of commercial azo dyes, by application, belongs to acid, basic, direct, disperse, mordant, solvent and reactive dyes. The examples of azo dyes include Acid Red, Reactive Orange 16 (RO16) (Remazol Brilliant Orange 3R, C.I.177757) (Øllgaard *et al.*, 1998).

2.1.2.1.1. REACTIVE DYES

Reactive dyes are water-soluble and contain special functional groups capable of forming covalent bonds with the substrates possessing hydroxyl and amino groups. They have excellent fastness (the ability to maintain colour without fading or washing away) to washing as the bond is strongly held. Thus, the dye becomes part of the substrate and energy requires to break the bond is similar to that degrade the substrate itself. They are the best choice for dyeing cellulose and cotton fibres. The principal group of reactive dyes include azo dyes. Reactive Orange 16 and Reactive Black 5 are examples of reactive dye (Øllgaard *et al.*, 1998; Hunger, 2003; Baumann and Lacasse, 2004; NPCS Board of Consultants and Engineers, 2009). Typical fixation of reactive dyes falls within the range of 60 % to 90 % (Butler *et al.*, 2016).

2.1.3. WORLDWIDE CONSUMPTION OF DYES

Literature shows no exact data for the quantity of available types of dyes and their production. The estimated number of available types of dyes ranges from 10,000 (Balan and Monteiro, 2001; Abdullah, Wong and Yaziz, 2010; Chequer *et al.*, 2013; Karthik and Rathinamoorthy, 2015), 30,000 (Hu and Pei, 2002) 40,000 (Pereira and Alves, 2016) to over 100,000 (Robinson *et al.*, 2001; Singh, 2006; Valh and Marechal, 2009; Soon and Hameed, 2011). Similarly, the estimated annual global production of dyes also varies from 4.5×10^5 tonnes (Pereira and Alves, 2016), 7×10^5 tonnes (Robinson *et al.*, 2001; Singh, 2006; Valh and Marechal, 2009; Abdullah, Wong and Yaziz, 2010; Chen *et al.*, 2010; Soon and Hameed, 2011), 7.5×10^5 to 8×10^5 tonnes (Catanho, Malpass and Motheo, 2006; Chequer *et al.*, 2013; Karthik and Rathinamoorthy, 2015), 1×10^6 tonnes (Hu and Pei, 2002; Hunger, 2003) to 7×10^5 million tonnes (Butler *et al.*, 2016).

Despite of differences on the quantity of the available dyes and their production scale, all literature agrees that the major consumer of produced dyes is the textile industry. Dyeing of textiles consumes over half (Freedonia, 2015), two-third (Pereira and Alves, 2016), 80 % (Gürses *et al.*, 2016) of the total dyes produced worldwide.

A study conducted by Freedonia (Freedonia, 2015) revealed that the global demand for dyes is expected to increase by 6 % per year in 2019. The major dyes used in textile industry are azo, anthraquinone, indigoid, sulfur, reactive, disperse etc. (Forgacs, Cserháti and Oros, 2004; Khalid, Arshad and Crowley, 2010). By chemical composition, azo dyes constitute the largest class and account for up to 50 % (Zollinger, 2003; Abdullah, Wong and Yaziz, 2010; Pereira and Alves, 2016), 60 % to 70 % (Øllgaard *et al.*, 1998; Khalid, Arshad and Crowley, 2010; Chequer *et al.*, 2013), 60 % to 80 % (Risk and Policy Analysis Ltd., 1997) of dyes used in textile industry. There are more than 3,000 azo colorants out of which at least 120 compounds are restricted in some countries (Øllgaard *et al.*, 1998). Application-wise reactive and disperse dyes account for over 50 % of total global dye demand. Production of dyes strongly linked with textile industry as demand of textile steadily increasing following the worldwide population growth and improving gross domestic product (GDP) in many countries (Hunger, 2003). The demand growth will be in developing countries, especially in Asia / Pacific region, China as a dominant, will be the main consumer of these dyes (Freedonia, 2015).

2.1.4. CHARACTERIZATION OF TEXTILE EFFLUENT

Textile effluents not only contain dyes but also other chemical substances used during various production stages. These can be grouped into functional (effect) chemical substances, auxiliary chemical substances and chemical substances not intentionally added. The functional chemicals include dyestuffs and pigments, crease resistant agents, oil, anti-shrinking agents, stabilizers, biocides etc. The auxiliary chemical substances include organic solvents, salts, surfactants, acids and bases, softeners etc. and unintended chemicals include impurities and degradation products such as formaldehyde, polyaromatic hydrocarbons (PAHs), arylamines and toxic metals (Swedish Chemicals Agency, 2014; Karthik and Rathinamoorthy, 2015). The effluents from textile plant are classified as the most polluting of all industrial sectors (Chequer et al., 2013). These effluents are characterized by the presence of high colour, chemical oxygen demand (COD), suspended solids, low biodegradability, temperature, impurities, surfactants, auxiliaries and metals such as chromium, mercury, lead, cadmium, zinc, copper etc. and largely fluctuating pH (Horning, 1978; Shore, 2002; Bisschops and Spanjers, 2003; Hunger, 2003; Tizaoui and Grima, 2011; Ghaly *et al.*, 2014).

Literature review shows that COD, pH, colour, suspended solids and biological oxygen demand (BOD_5) are the major parameters used for textile effluent characterization. A range of characteristic parameters related to textile effluent are discussed elsewhere (Bisschops and Spanjers, 2003). Appendix 9-1 shows a list of characteristic parameters and their load in raw textile effluent.

2.1.5. ENVIRONMENTAL EXPOSURE AND FATE OF DYES

Typical pollutants associated with the dyes are shown in

Table 2-1. The environmental media for emission of dyes are air, soil and water. The release of dyes to the air during processing and use phase is negligible. Emission of dyes during incineration of waste also assumed to be negligible as organic molecules decomposed by high temperature during incineration. Release to the soil is generally negligible, except from disposal of de-inking sludge and its application to agricultural soil. Dyes may release to soil and groundwater if the agricultural soil is fertilized with sludge and landfill deposit containing dyes. Therefore, the water is the main environmental medium for discharged dyes. The major route of discharge of dyes during production and use phase is through wastewater effluent from the processing industries, mainly the textile (Øllgaard *et al.*, 1998).

Table 2-1: Typical pollutants generated by synthetic dyes.

Dye Classes	Typical pollutants associated with the dyes
Acid	Colour, organic acids, and unfixed dyes
Direct	Colour, salts, unfixed dyes, fixing agents, surfactants, levelling and retarding agents, diluents
Disperse	Colour, organic acids, carriers, levelling agents, phosphates, lubricants, and dispersants
Reactive	Colour, alkali, oxidizing and reducing agents, and unfixed dye
Sulfur	Colour, alkali, oxidizing and reducing agents, and unfixed dye
Vat	Colour, alkali, oxidizing and reducing agents

Source: reproduced from (Adinew, 2012; Karthik and Rathinamoorthy, 2015).

Textile industries generate large amounts of effluent containing organic and inorganic compounds. The amount of effluent varies depending on the type of fabric used. It is estimated that 80 L to 150 L of water is needed to produce 1 kg of fabric (Tizaoui and Grima, 2011; Ghaly *et al.*, 2014), 12 m^3 (2,641 gallons) for a pair of jeans (Annie, 2018) and about 1,000 m^3 to 3,000 m^3 of water is discharged after processing 10 – 12 tonnes of textiles per day (Pagga and Brown, 1986; Al-Kdasi *et al.*, 2005; Ghaly *et al.*, 2014).

Majority of literature reported that 10 % - 20 % of the globally produced dye is discharged in effluents during textile production and processing (Catanho, Malpass and Motheo, 2006; Singh, 2006; Muhammad *et al.*, 2008; Rauf and Ashraf, 2009; Şengil and Özacar, 2009; Valh and Marechal, 2009; Abdullah, Wong and Yaziz, 2010; Soon and Hameed, 2011; Karthik and Rathinamoorthy, 2015). In case of reactive azo dyes, a loss of 50 % (Singh, 2006; Muhammad *et al.*, 2008; Abdullah, Wong and Yaziz, 2010; Khalid, Arshad and Crowley, 2010; Tizaoui and Grima, 2011; Chequer *et al.*, 2013) to 70 % (Øllgaard *et al.*, 1998) has been reported. Globally, textile industries discharge an estimated amount of 200,000 tonnes (Chequer *et al.*, 2013) to 600,000 tonnes (Hu and Pei, 2002) of dyes into the environment every year and majority (Øllgaard *et al.*, 1998) up to 80 % of which are azo dyes. Annual release of hazardous acid and direct dyes to the EU environment from washing of cotton and polyamide textiles was estimated to be in the range of 4,000 kg to 44,000 kg. This figure can increase above 220 tonnes if all acid and direct dyes used in polyamide and cotton are included and might exceed five times (>1,100 tonnes) if less optimal processes are used during the textile production. It is estimated that over

80 % of the wastewater in the EU is currently put through secondary treatment, suggesting that a part of acid and direct dyes are discharged more or less directly to the environment after laundering (Swedish Chemicals Agency, 2014).

It is also estimated that 57.1 % of the landfills in the EU are occupied with textiles waste and up to 90 % of the initially used dyes could eventually end up to the environment when complete degradation of the textiles occurred (European Commission, 2013; European Comission, 2014; Swedish Chemicals Agency, 2014).

Azo dyes are of primary concern due to their widespread use, potential to form toxic aromatic products and low removal during primary and secondary wastewater treatment (Abdullah, Wong and Yaziz, 2010).

Figure 2-2: Dyes, environmental exposure and biological effect.

A) Dyes in an open market (Rozas, 2017).
B) Textile effluent containing unreacted dyes (Annie, 2009).
C) Soil contaminated by effluent released from a dye factory in Henan province, China, September, 2014 (Vietnamnet, 2016).
D) Burial of ducks died after consuming contaminated effluent from a local tannery in Vellore, India, July 2016 (Chronicle, 2016).

Dyes impart colour on aquatic systems which not only affects the aesthetic value of aquatic system but also interferes with the penetration of sunlight thereby retards photosynthesis and solubility of gases and inhibits the growth of aquatic fauna and flora (Şengil and Özacar, 2009). Dyes also attribute to the higher biological oxygen demand

(BOD) of the aquatic system and reduce the reoxygenation process and eventually inhibit the growth of photoautotrophic organisms (Ghaly *et al.*, 2014). The residual colour usually arises from the dyes which have poor biodegradability and high chemical stability. The complex composition (aromatic amide groups with alkyl, sulfonic acid, nitro, hydroxyl, halogen substituent and inorganic sodium salts) of synthetic dyes makes them resistant to mild degradation (Soon and Hameed, 2011). It is reported that only 47 % of dyestuffs are biodegradable (Pagga and Brown, 1986; Al-Kdasi *et al.*, 2005). A study of sewage treatment plants shows that biodegradation of dyes merely occurred when 40 % – 80 % of decolourization occurred via adsorption onto the biomass. Biodegradation is hindered when the dyes are strongly adsorbed to the sediment (Brown and Anliker, 1988; Weber, 1991; Zissi and Lyberatos, 1996; Øllgaard *et al.*, 1998; Shore, 2002).

The electron-withdrawing character of the azo substituent generates electron deficiency and makes azo dyes less susceptible to oxidative catabolism (Knackmuss, 1996). Azo dyes are expected to have high to moderate mobility in soil, sediment and particulate matter. However, due to their inherent affinity to substrate, they tend to adsorb onto these media. Moreover, dyes are designed to have high degree of chemical and photolytic stability. Thus, they are persistent in the aerobic environment (Pagga and Brown, 1986; Øllgaard *et al.*, 1998) and eventually end up in anaerobic sediments, shallow aquifers and ground water (Razo-Flores *et al.*, 1997).

Azo dyes can undergo biodegradation in both aerobic and anaerobic environments with the reductive cleavage of the azo-bond as an initial step in both cases. No further degradation occurs in anaerobic conditions whereas in aerobic conditions initial step of azo-bond cleavage proceeds by hydroxylation and ring opening of the aromatic intermediates (Zissi and Lyberatos, 1996). The degradation of azo dyes due to reductive cleavage leads to the formation of aromatic amines that generally do not degrade and accumulate in anaerobic environment thereby end up in sediments dominated by anaerobic conditions. However, the aromatic amines with the presence of carboxyl and / or hydroxyl groups can degrade in aerobic environment (Razo-Flores *et al.*, 1997; Sponza and Işik, 2007).

2.1.6. TOXICITY AND EFFECTS OF DYES ON BIOLOGICAL SYSTEM

Only few dyes are defined according to European Union (EU) criteria for classification of dangerous substances based on REACH (Registration, Evaluation, Authorization and Restriction of Chemicals) regulation. The LD_{50}, lethal dose that kills the half of the

population, values of majority of the azo dyes are in the range of 250 - 2,000 mg/kg body weight and only a few dyes have LD_{50} below 250 mg/kg body weight (Clarke and Anliker, 1980). Some dyes have very high LD_{50} values, for example, LD_{50} of Reactive Black 5 is 14 g/kg body weight (Hunger, 1991).

The extent of toxicity of the textile effluents varies among industries. An estimated amount of 2 – 20 % of the acid and direct dyes are hazardous to human health and / or the environment (Swedish Chemicals Agency, 2014). The physico-chemical parameters of cleavage products and impurities of azo dyes generally vary within four groups: aniline, toluidine, benzidine and naphthalene which are potentially carcinogenic, mutagenic and / or toxic to reproduction (Hunger, 1991; Øllgaard *et al.*, 1998). Approximately 500 azo dyes listed in the Colour Index are synthesized based on carcinogenic amines regulated under REACH. In total, 22 aromatic amines that can be released from azo dyes are listed under REACH restriction. A majority of azo dyes can undergo via reductive cleavage and form regulated and non-regulated aryl amines (Swedish Chemicals Agency, 2014). These amines are highly toxic (carcinogenic and / or genotoxic) as they can convert haemoglobin in the blood to the methaemoglobin by preventing oxygen uptake and result in cyanosis of lips and nose, weakness and dizziness (Øllgaard *et al.*, 1998; Sponza and Işik, 2007; Swedish Chemicals Agency, 2014).

If an azo dye is stable in the hydroxyazo tautomeric form then the dye itself can be an active carcinogen. However, dyes existing in ketohydrazone form can be reduced to metabolites such as aromatic amines that are likely carcinogen (Shore, 2002). Azo dyes related carcinogenic activities such as bladder cancer, splenic sarcomas, hepatocellular carcinomas and lung tumours are discussed in the literature (Øllgaard *et al.*, 1998; Marin-morales, Ventura-camargo and Marin-morales, 2013).

The sensitizing effect of azo dyes (red azoic dye) was observed in 1930 as 20 % of the cotton dyeing workers in an industry had eczema. Certain dyes are known to accelerate skin reddening effect of sunlight exposure. The disperse dyes used in textiles are the common sensitizing dyes. It is found that contact dermatitis is linked to the wearing of clothes, especially nylon dyed with disperse dyes. Disperse dyes such as Disperse Orange 1/3/76; Disperse Red 1/17 and Disperse Yellow 3/4 showed sensitizing properties during clinical patch tests and found associated with contact dermatitis (Øllgaard *et al.*, 1998; Shore, 2002; Marin-morales, Ventura-camargo and Marin-morales, 2013; Swedish Chemicals Agency, 2014). After having a report of severe sensitizing effect from reactive dyes, UK Health and Safety Executive conducted a study

in 440 workers from 51 dye houses and found that 15 % of them showed occupational related respiratory and nasal symptoms and 21 had allergy attributed from the contact with one or more reactive dyes (Shore, 2002).

Absorption of azo dyes through skin is doubtful. However, the aromatic component amines of azo dyes may be absorbed through lungs, skin and the intestine. Ingested azo dyes in human body may be cleaved via reduction and form aromatic amines which were originally used to synthesize the dyes. Bacteria in human intestine and skin and liver enzymes are also capable of azo cleavage. A distribution study of Direct Red 2 and Direct Blue 15 conducted in rats showed higher levels of 14C in liver, kidney and lung than other tissues after 72 hours of single oral consumption (Øllgaard *et al.*, 1998; Marin-morales, Ventura-camargo and Marin-morales, 2013). Highly purified azo dyes have less potential to cause mutagenicity. However, aromatic amines that contain higher amounts of impurities may have mutagenic effect. Mutagenic activities of azo dyes such as C.I. Solvent Yellow 14, C.I. Disperse Orange 1, C.I. Disperse Blue 291 are discussed. Azo dye, namely Congo Red related dysfunction in the reproductive organs of rodents is also documented (Øllgaard *et al.*, 1998; Chequer *et al.*, 2013; Marin-morales, Ventura-camargo and Marin-morales, 2013).

The azo dyes are the potential risk to human health. The direct dyes are associated with the increased risk of cancer and developmental effects and the acid dyes are associated with allergic reaction. Acid and direct dyes can be linked to a potential large-scale human exposure, particularly to children sucking or chewing on textiles or ingesting indoor dust. They can also enter to human via food chain as they easily leached to environment due to relatively weaker bonding to textiles and accumulate in aquatic food chain (Øllgaard *et al.*, 1998; Swedish Chemicals Agency, 2014).

Aquatic toxicity of five dyes (three textile and two food) before and after the treatment (Photo-Fenton) was assessed using freshwater organisms and three different observations were reported: 1) formation of more toxic daughter products; 2) generation of more toxic intermediate products at the beginning and further oxidized to non-toxic products; and 3) generation of non-toxic products (Luna *et al.*, 2014). The first two observations emphasize the fact that incomplete mineralization, which could be true in case of complete decolourization, of dyes can be more harmful to the environment. In other words, optimization of treatment process should not be considered based on decolourization rate only.

A case from Vellore, India reported by Deccan Chronicle, an e-paper, in July, 2016 highlights the death of over 3,400 ducks after consuming contaminated effluent, blueish in colour, believed to be discharged from a local tannery (see Figure 2-2 D). A review highlighting uses and problems of different dyes can be find elsewhere (Nidheesh, Gandhimathi and Ramesh, 2013, pp. 2103–5).

2.1.7. ENVIRONMENTAL LEGISLATION FOR WATER QUALITY

Environmental legislation has been adopted by several countries in order to control the use of hazardous chemicals. However, there is no consensus amongst the countries concerning the discharge limits. Countries like United States of America (USA), Canada, Australia and the EU have own environmental legislation whereas some countries, e.g. Thailand, have adopted the American system and others, e.g. Turkey and Morocco, the EU model. Some countries, e.g. India, Pakistan and Malaysia, recommend the non-mandatory limits (Chequer *et al.*, 2013; Marin-morales, Ventura-camargo and Marin-morales, 2013).

In the USA, the Pollution Prevention Act of 1990 enforces the manufacturers and related companies to report their activities based on the usage of hazardous chemicals (Christie, 2007). The Toxic Substances Control Act was developed for the control of benzidine-based substances in 1996. In 2010, United States Environment Protection Agency (USEPA) addressed 48 dyes derived from benzidine and its derivatives.

In Canada, The Canadian Environmental Protection Act (CEPA), 1999 governs the use of hazardous chemicals. India legislated the Environment Protection Act, 1986 and prohibited the handling of 112 azo- and benzidine-based dyes (Environment Canada and Health Canada, 2012). In Turkey, Istanbul Water and Sewerage Administration controls and inspects the wastewater discharges (Tüfekci, Sivri and Toroz, 2007).

In the EU, the discharge of chemicals to the water bodies is governed by Water Framework Directive (WFD) known as 2000/60/EC introduced in October 2000. Article 16 of the WFD governs the strategy for water pollution and the strategy begins with the listing of priority substances. Article 1(c) states that the future reviews of the substances in the priority list under the Article 16 (4) of WFD will contribute to the cessation of emissions, discharges and losses of all hazardous substances by 2020 by progressively adding substances to the list. WFD covers discharges to rivers, lakes, groundwater, estuaries and coastal waters. The Europe's Black and Grey listed dangerous substances are integrated in the WFD (Christie, 2007). The Black List substances e.g. cadmium and

mercury are hazardous because of their toxicity, persistence and bio-accumulative and carcinogenic properties. The Grey List substances are those which have an adverse impact on the aquatic environment but the severity of the impact varies with respect to location and receiving waters (Wolf and Stanley, 2003). WFD dictates that Member States to identify Specific Pollutants and set standard for them. Specific Pollutants are toxic substances which are covered by Annex VIII, points 1 to 9 of WFD. The use of azo dyes that have carcinogenic breakdown products is restricted by EU Directive 76/769/EEC.

In the UK, UKTAG identifies the Specific Pollutants and recommends standards for them. UKTAG recommends standards based on the hazardous properties such as toxicity, persistence and potential to accumulate in organisms and potential environmental exposure to the substance including extent and pattern of use (WFD-UKTAG, 2015).

Under the UK law, the use of non-biodegradable and inorganic dyes and auxiliary chemicals, metal or reactive dyes should be justified. Dyes with solid pigments should only be used if where they can be abated by clarification. The textile effluent should have absorbance less than 0.1 in the range 400 nm to 800 nm (Environment Agency, 2009).

Discharge limits of hazardous substances in different countries varies accordingly with the differences in the legislation. Appendix 9-1 shows the discharge limits for water quality parameters in various countries.

2.1.8. REACTIVE ORANGE 16 – THE MODEL DYE

RO16 is an anionic sulfonated reactive azo dye with two sulfonate groups (Gomes *et al.*, 2011) and bears azo group as chromophore and a sulphatoethylsulfone as the reactive group (Purnama, 2005; Ma *et al.*, 2014). RO16 has been extensively used in industry in printing process and textile industry dyeing cotton, silk (Purnama, 2005; Gomes *et al.*, 2011; Ma *et al.*, 2014) and cellulose fibres (Tizaoui and Grima, 2011). The fixation efficiency of RO16 is 55 - 60 % (Esteves and Sousa, 2015). Figure 2-3 and Table 2-2 present the chemical structure in azo and hydrazone forms and the general characteristics of RO16 respectively.

RO16 is recalcitrant to biodegradation (Chen, 2009; Tizaoui and Grima, 2011) and conventional treatment methods (Gomes *et al.*, 2011; Ma *et al.*, 2014). A study on treatment of simulated textile wastewater conducted by Spagni et al., 2010 evidenced that the biological treatment of RO16 resulted in the formation of sulfonated aromatic

amines which are recalcitrant to biodegradation. Moreover, citing to (Taylor, Brown and Vito, 1993), (Tizaoui and Grima, 2011) mentioned that biodegradation of RO16 resulted in the formation of potential carcinogenic recalcitrant aromatic amines. Thus, presence of RO16 in textile effluent pose an environmental concern and its selection as a model dye is verifiable.

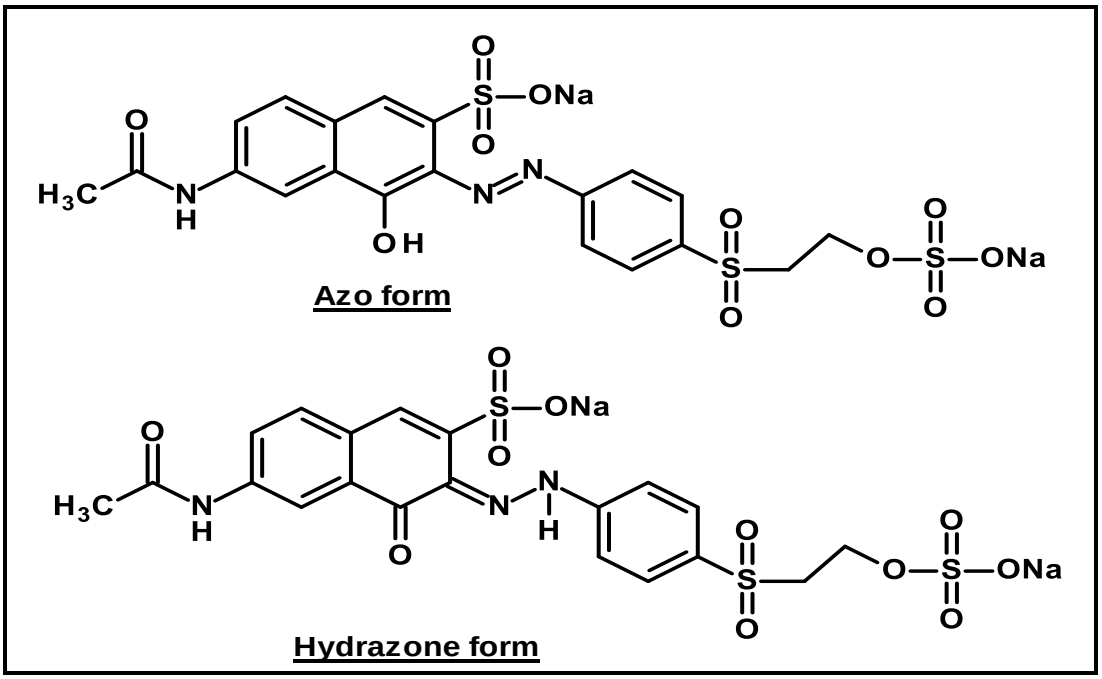

Figure 2-3: Chemical structure showing azo and hydrazon tautomeric forms of Reactive Orange 16.

Azo dyes with hydroxyl groups generally exhibit azo-hydrazone tautomerism. Thus, RO16, an azo dye, also exhibits tautomerism. According to (Sukhdev, Manjunatha and Puttaswamy, 2017), hydrazone form of dye is favoured in aqueous phase. Accordingly, this form is believed to be involved in the chemical reactions during this research.

Table 2-2: Characteristics of Reactive Orange 16.

Characteristics	**Description**
Synonym	Remazol Brilliant Orange 3R
Molecular formula	$C_{20}H_{12}N_3O_{11}S_{12}Na_2$
Molecular weight	617.54 g/mol
IUPAC name (Azo form)	Disodium6-acetamido-4-hydroxy-3[[3-[[2-(sulphonatooxy)ethyl]sulphonyl]phenyl]azo]naphthalene-2-sulphonate
H-Bond donor	2

Characteristics	Description
H-Bond acceptor	13
Maximum absorption wavelength, λ_{max} (nm)	494
Extinction coefficient (L mol^{-1} cm^{-1})	≥ 11,000 in 491 nm to 497 nm and 294 nm to 300 nm ≥ 6,000 in 385 nm to 391 nm ≥ 13,000 in 251 nm to 257 nm
CAS / EC-No.	12225-83-1 / 235-431-5
Colour Index number	17757
Classification according to EU-GHS/CLP	Irritating to eyes, respiratory system and skin. May cause sensitization by inhalation and skin contact.

Source: (Won, Choi and Yun, 2006; Sigma-Aldrich, 2017b; NCBI, 2018).

2.2. TREATMENT TECHNOLOGIES FOR DYE REMOVAL

In view of the environmental contamination and possible health effect of dyes, a range of technologies has been developed for the removal of dyes from the environmental matrices such as water. These technologies have been broadly categorized into biological, physical and chemical (Robinson *et al.*, 2001; Forgacs, Cserháti and Oros, 2004; Saratale *et al.*, 2011; Marin-morales, Ventura-camargo and Marin-morales, 2013; Tijani *et al.*, 2014; Yagub *et al.*, 2014; Arslan *et al.*, 2016). A brief review of these technologies is given in the following sections.

2.2.1. BIOLOGICAL TREATMENT METHODS

Biological treatment methods involves the use of microorganisms such as bacteria, fungi, yeast, actinomycetes, algae and plants for the biodegradation of pollutants in the effluent. Figure 2-4 presents a range of biological treatment methods available for the treatment of wastewater. In biological treatment of textile effluent, microorganisms acclimatize themselves to the textile dyes and develop new resistant strains which can transform toxic dyes to less harmful forms. The degradation mechanism is based on the action of the enzymes produced by microorganisms. The treatment efficiency of biological system solely depends on the adaptability of selected microbes and the enzymatic activity (Saratale *et al.*, 2011; Holkar *et al.*, 2016). A review of microorganisms used for the decolourization of several synthetic dyes can be found elsewhere (Forgacs, Cserháti and Oros, 2004, p. 956).

On the basis of oxygen requirement, biological methods can be classified into anaerobic, aerobic and anoxic or facultative or a combination of these (Arslan *et al.*, 2016; Holkar *et al.*, 2016). Although aerobic treatment is widely used, it is often less effective in facilitating degradation of dyes compared to anaerobic treatment. The decolourization of (azo) dyes proceeds via reductive cleavage facilitated by anaerobic conditions (Khalid, Arshad and Crowley, 2010). Anaerobic processes are more satisfactory and produce less sludge compared to aerobic processes. The toxic intermediate products formed during anaerobic process have to be treated by aerobic process, i.e. two separate processes are required. Microbial degradation is dependent on several physicochemical parameters including oxygen, temperature, pH, concentration and structure of dye, sources of carbon and nitrogen, amount of electron donor as well as redox mediator (Forgacs, Cserháti and Oros, 2004; Holkar *et al.*, 2016).

Several strains of bacteria have been used to decolourize and degrade azo dyes. Bacterial decolourization of azo dyes occurs via reductive cleavage of azo bonds resulting in the formation of colourless hazardous aromatic amines. These aromatic amines are further degraded aerobically or anaerobically to form less hazardous products. A list of bacteria capable to decolourize azo dyes can be found elsewhere (Khalid, Arshad and Crowley, 2010, pp. 12 & 19; Saratale *et al.*, 2011, p. 142; Gupta *et al.*, 2015, p. 78; Holkar *et al.*, 2016, p. 359).

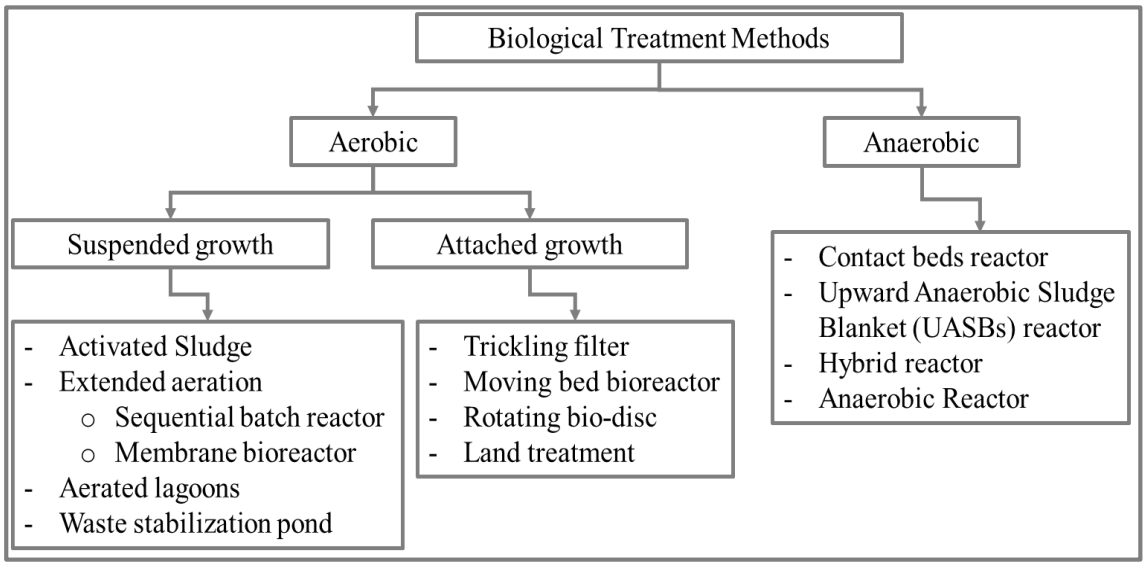

Figure 2-4: Biological methods for the treatment of wastewater. Source: (Arslan et al., 2016, p. 13).

Alike bacteria, a wide variety of fungi have been used to decolourize and degrade a wide range of dyes. Amongst these varieties, the use of white-rot fungi has been widely reported. The intra and extracellular enzymes containing lignin peroxidase, manganese

peroxidase and laccase are capable to degrade dyes present in the textile effluent. Use of fungi for the decolourization of dyes has been reviewed and the extensive list of fungi can be found elsewhere (Srinivasan and Viraraghavan, 2010, p. 1917; Gupta *et al.*, 2015, p. 80; Holkar *et al.*, 2016, p. 357).

Algae have been also used for the degradation of dyes. The removal of dyes using algae occurs via three mechanisms: consumption of dyes for their own growth, conversion of dyes into colourless intermediates or carbon dioxide and water, adsorption of chromophores on algae (Holkar *et al.*, 2016). A range of algae capable to decolourize dyes can be found elsewhere (Srinivasan and Viraraghavan, 2010, p. 1926; Holkar *et al.*, 2016, p. 358).

Biological degradation of a pollutant refers to its elimination by means of metabolic activity of living organisms, generally microorganisms, particularly the bacteria and fungi that live in natural water and soil. In this regards, conventional biological treatment methods may not be successful in the treatment of effluents containing toxic and recalcitrant organic pollutants (EC, 2003b EUR 20418 EN/2; Oller, Malato and Sánchez-pérez, 2011).

2.2.2. CONVENTIONAL PHYSICOCHEMICAL METHODS

Physical treatment technologies are governed by means of physical forces and thereby tend to transfer the pollutant to a different phase. Phase separating methods do not destroy the pollutants rather concentrate in different phase and generate sludge that can be a cause of secondary pollution (Gomes *et al.*, 2011; Saratale *et al.*, 2011; Marin-morales, Ventura-camargo and Marin-morales, 2013). Physicochemical methods include different precipitation methods (coagulation, flocculation and sedimentation), adsorption, filtration (micro, ultra and nano), reverse osmosis, ion exchange, irradiation, cavitation, and oxidation (Slokar and Marechal, 1998; Robinson *et al.*, 2001; Şengil and Özacar, 2009; Gupta *et al.*, 2015; Arslan *et al.*, 2016; Holkar *et al.*, 2016).

2.2.2.1. COAGULATION AND FLOCCULATION (C & F)

C & F processes aim to destabilize and form aggregation of small colloidal particles using coagulants such as aluminum sulfate ($Al_2(SO_4)_3$), aluminum chloride (Al_2Cl_3) and ferric sulfate ($Fe_2(SO_4)_3$. The bigger aggregates thus formed can be removed by sedimentation (Arslan *et al.*, 2016). C & F processes are effective mainly for sulfur and disperse dyes (Saratale *et al.*, 2011; Holkar *et al.*, 2016). The applicability of C & F processes is limited

due to their low colour removal efficiency, production of large amount of sludge, neurotoxicity and chromaticity colour or aggressive action caused by high residual concentration of aluminum and ferric-based salts respectively (Saratale *et al.*, 2011; Arslan *et al.*, 2016; Li *et al.*, 2016). Electrocoagulation has been developed to overcome the limitations of conventional C & F (Şengil and Özacar, 2009). The use of hybrid polymers as improvised coagulants flocculants is increasing. Some latest examples are lignin-based (Li *et al.*, 2016), chitosan-based (Dharani and Balasubramanian, 2015), polyaluminum chloride based (Yeap *et al.*, 2014) and kaolin-TiO_2-polyacrylamide (Wei *et al.*, 2017).

2.2.2.2. ADSORPTION

Adsorption is a process by which ions or molecules in one phase (solution) have an affinity to amass and concentrate on the surface of another phase (sorbent) (Karthik and Rathinamoorthy, 2015). It is probably the most effective technique amongst physical processes. Although adsorption results in higher efficiency for the removal of a wide range of dyes, its success depends on the selection of suitable adsorbent based on affinity, capacity and the possibility of regeneration (Saratale *et al.*, 2011; Holkar *et al.*, 2016). Colour removal based on mechanisms involving adsorption and ion exchange are influenced by pH, surface area of sorbent, substrate concentration, substrate-sorbent interaction, particle size, temperature and residence time (Slokar and Marechal, 1998; Robinson *et al.*, 2001; Yagub *et al.*, 2014). The effects of pH, temperature, initial concentration of dye and amount of adsorbent on adsorption of different dyes have been reviewed elsewhere (Yagub *et al.*, 2014). The adsorption of cationic dyes favoured at pH > pH_{PZC} and that of anionic dyes favoured at pH < pH_{PZC}. The pH_{PZC} is the pH at which surface charge is zero, known as point of zero charge (PZC) (Yagub *et al.*, 2014).

Adsorption of dyes also depends on dye properties such as number and position of substituents (auxochromes) in the dye molecule, type and molecular structure. Dyes interact differently with the active groups on the surface of adsorbents. Presence of hydroxyl, nitro and azo groups in the dye molecule increases adsorption whereas sulfonic acid groups decrease adsorption (Srinivasan and Viraraghavan, 2010). Apart from the most extensively used adsorbent, the activated carbon, a range of low-cost adsorbents including biological, natural (in)organic materials, agricultural and industrial waste products have been used. Adsorption capacities of these adsorbents for varieties of dyes are reviewed elsewhere (Salleh *et al.*, 2011; Yagub *et al.*, 2014; Gupta *et al.*,

2015; Holkar *et al.*, 2016). More information about adsorption process and adsorbents is provided in section 3.3.2.7, p.73.

2.2.2.3. ION EXCHANGE

Ion exchange, though not very common, is also applied in the treatment of dyes. Ion exchange process and ion exchangers, with regard to metal removal are discussed in section 3.3.2.8, p. 75. Electrochemical ion exchange process, an advanced form of ion exchange, with an electrical driving force enhances the ion exchange to adsorb ionic species from a solution (Sharma, Saxena and Gaur, 2014).

The cationic dyes are basic dyes which are quarternary salts bearing positive charge (cation) most often on the atom N (ammonium salts), rarely on C (carbonium), O (oxonium) and S (sulfone). These cations can be exchanged with the cations on the ion exchangers. The anionic dyes belongs to acidic, direct and reactive groups whose anions are generally Cl^-, SO_4^{2-}, HSO_4^-, or COO^- (Wawrzkiewicz, 2013). The chromophores and auxochromes of dyes used by textile industry are defined as typical anionic groups. These groups can be exchanged with anions from anionic exchangers (Arslan *et al.*, 2016). Ion exchange process has been used in the removal of both anionic (Greluk and Hubicki, 2013; Wawrzkiewicz and Hubicki, 2015) and cationic (Wawrzkiewicz, 2013) dyes.

2.2.2.4. FILTRATION

Filtration methods have been used in textile industry to clarify, concentrate and separate hydrolysed dyestuffs and dyeing auxiliaries from the effluent. These methods are resistant to temperature, an adverse chemical environment and microbial attack. However, the concentrated residue left after separation arises many problems such as disposal, fouling and clogging of membranes (Robinson *et al.*, 2001; Saratale *et al.*, 2011; Karthik and Rathinamoorthy, 2015; Holkar *et al.*, 2016). Filtration methods include ultrafiltration, nanofiltration, microfiltration and reverse osmosis. More information can be found in section 3.3.2.5 p.72.

2.2.2.5. OXIDATION METHODS

Oxidation methods are based on conventional oxidants such as oxygen or air, chlorine, potassium permanganate, sodium hypochlorite, ozone and H_2O_2 (direct oxidation of substrate) etc. (Parson, 2004; Pera-titus *et al.*, 2004; Oliveira *et al.*, 2010; Sharma *et al.*, 2012). Colour removal, taste and odour control, and disinfection are the main application

areas for these oxidation methods. Conventional oxidants, such as chlorine, are selective to pollutants (Sharma *et al.*, 2012). The decolourization of azo dyes (Reactive, Acid, Direct, Cationic and Fluorescent) using chlorine (Oliveira *et al.*, 2010), permanganate (Xu *et al.*, 2005) and hypochlorite (Pizzolato *et al.*, 2002) has been investigated. The mechanism of decolourization is the cleavage of the chromophore groups that are responsible for dye colour. The authors reported that mineralization was incomplete and hazardous by-products such as organochlorides, chlorophenol etc. were formed. On the other hand, oxidation by H_2O_2 and ozone on their own is not effective for certain refractory pollutants because of low reaction rates (Neyens and Baeyens, 2003). Accordingly, alternatives to conventional oxidation methods, for example advanced oxidation processes, are advised. This is also supported by (Slokar and Marechal, 1998; Oliveira *et al.*, 2010).

2.2.3. ADVANCED OXIDATION PROCESSES (AOPS)

Advanced oxidation process was first mentioned by William H Glaze in 1989 (Glaze and Kang, 1989; Boczkaj and Fernandes, 2017). Comninellis *et al.*, 2008 broadly defined AOPs as *"aqueous phase oxidation methods based on the intermediacy of highly reactive species such as (primarily but not exclusively) hydroxyl radicals in the mechanisms leading to the destruction of the target pollutant"*. AOPs are the alternative to conventional physicochemical and biological treatment methods (Pizzolato *et al.*, 2002; Babuponnusami and Muthukumar, 2014; Pereira and Alves, 2016; Fida *et al.*, 2017), hence thought to fulfil the gap between the treatability attained by the conventional processes and the stringent environmental regulations (Dewil *et al.*, 2017).

AOPs aim at the mineralization of refractory contaminants to carbon dioxide, water and inorganics or, at least, at their transformation into harmless products. AOPs, despite of using different oxidants, are characterized by the production of non-selective, unstable and extraordinarily reactive species, the hydroxyl radical ($^{\bullet}OH$), with oxidation potential of 2.80 V (Andreozzi *et al.*, 1999; Parson, 2004; Asghar, Raman and Daud, 2015; Pereira and Alves, 2016; Hassaan and Nemr, 2017). The radical species generated from the redox reaction are highly reactive and unstable due to their unpaired electrons. The $^{\bullet}OH$, with an average lifetime of only about 10 microseconds (Hoigné, 1997), then attack organic molecules, see Equation 2-1, with rate constants in the range of $10^6 – 10^9$ $Lmol^{-1}s^{-1}$. The $^{\bullet}OH$ is more reactive to double bonds (C=C) in the structure of compounds than saturated molecules. Moreover, the reactivity of $^{\bullet}OH$ towards oxidative species

decreases with lower molecular weight and higher oxidation level (Andreozzi *et al.*, 1999; Shahidi, Roy and Azzouz, 2015; Boczkaj and Fernandes, 2017).

Table 2-3: Standard reduction potential of oxidants alone and relative to chlorine.

Oxidants	Oxidation potential (V)	Oxidation potential relative to chlorine (V)
Fluorine (F_2)	3.03	2.23
Hydroxyl radical ($^{\bullet}OH$)	2.80	2.05
Atomic oxygen (O)	2.42	1.78
Ozone (O_3)	2.07	1.52
Hydrogen peroxide (H_2O_2)	1.77	1.30
Potassium permanganate ($KMnO_4$)	1.67	1.23
Hypobromous acid (HBrO)	1.59	1.17
Chlorine dioxide (ClO_2)	1.50	1.10
Hypochlorous acid (HClO)	1.49	1.10
Chlorine (Cl_2)	1.36	1.00
Bromine (Br_2)	1.09	0.80

Source: (Parson, 2004; Pera-titus *et al.*, 2004; Babuponnusami and Muthukumar, 2014; Hassaan and Nemr, 2017).

The oxidation potential of common oxidants alone and relative to chlorine is given in Table 2-3. AOPs are considered as the most environmentally friendly and clean methods as they can be processed at or near ambient temperature and pressure without generating secondary waste stream (Babuponnusami and Muthukumar, 2014; Tijani *et al.*, 2014; Gupta *et al.*, 2015; Dewil *et al.*, 2017). However, AOPs are generally suitable for effluents with COD contents of ≤ 5 g/L (Andreozzi *et al.*, 1999; Rodríguez, 2003).

$$HO^{\bullet} + Organic\ species \rightarrow CO_2 + H_2O + inorganic\ ions \qquad \textbf{Equation 2-1}$$

AOPs have two inherent components: generation of an oxidizing agent, e.g. $^{\bullet}OH$, and the oxidation reaction. The versatility of AOPs is enhanced by the fact that $^{\bullet}OH$ can be generated in various ways (Andreozzi *et al.*, 1999; Ranade and Bhandari, 2014; Gupta *et al.*, 2015; Hassaan and Nemr, 2017). These ways can be broadly categorized into two: with and without energy requirement. Figure 2-5 presents further classification of

AOPs. The application and effectiveness of these AOPs are reviewed somewhere else (Sharma, Saxena and Gaur, 2014, pp. 3–5).

The efficacy of AOPs for a given wastewater is a function of the treatment aim itself and the composition and concentration load of the waste stream. The higher the pollution load and the desired extent of removal, the tougher the treatment conditions to be applied are. In such, different AOPs can be coupled in order to enhance the treatment performance (Comninellis *et al.*, 2008). This can be done by:

- Simultaneous application of two or more AOPs (hybridization of AOPs), e.g. MW / UV / Fenton oxidation.
- Sequential application of two or more AOPs, e.g. Fenton oxidation followed by electrochemical treatment.
- Pre-treatment of waste stream prior to AOPs, e.g. separation followed by Fenton oxidation.
- Pre-treatment by AOPs to enhance biodegradability, e.g. Fenton oxidation followed by biological treatment.
- Combination of conventional physicochemical, AOP and biological treatment methods.

Literature shows that one of the most extensively studied AOPs is Fenton oxidation process (Andreozzi *et al.*, 1999; J. Herney Ramirez *et al.*, 2007; Ramirez *et al.*, 2009; Soon and Hameed, 2011; Babuponnusami and Muthukumar, 2014; Bokare and Choi, 2014; Asghar, Raman and Daud, 2015; Wang *et al.*, 2016) which was also the technique applied in this study thus discussed in detail below.

2.2.3.1. FENTON OXIDATION

The Fenton reaction was discovered, while investigating the oxidation of tartaric acid by hydrogen peroxide in the presence of iron, and reported by H.J.H. Fenton in 1894 (Fenton, 1894). Haber and Weiss, 1934, proposed hydroxyl radical (•OH) as an active oxidant generated by the Fenton reaction (Pignatello, Oliveros and Mackay, 2006).

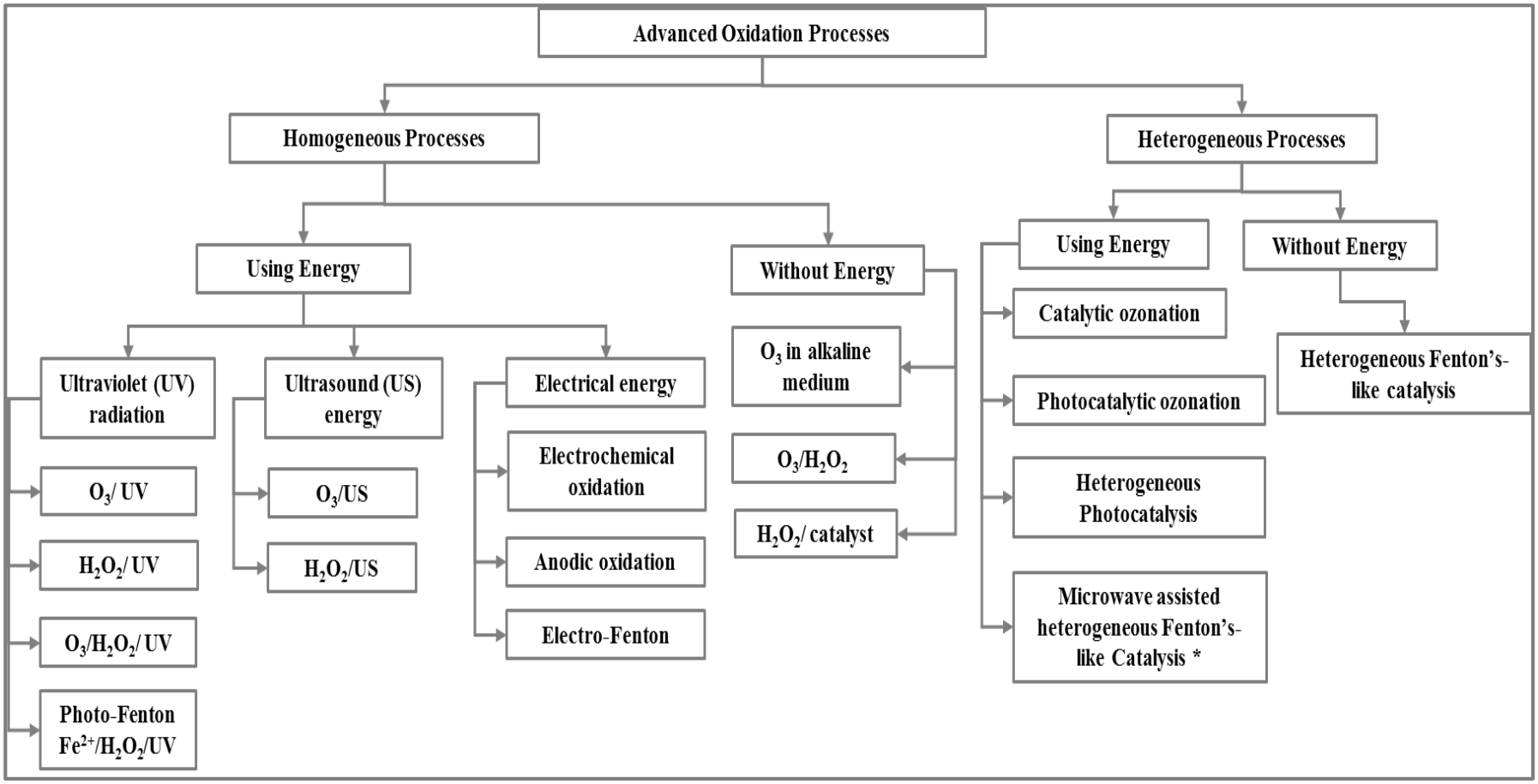

Figure 2-5: Advanced oxidation technologies for wastewater treatment.

Source: Modified from (Sharma, Ruparelia and Patel, 2011, p. 2; Tijani *et al.*, 2014, p. 4), * introduced in author's research group at DMU.

There are some intense and controversial discussions about the chain mechanism and the species responsible for oxidation involved in Fenton system. The debate is whether the oxidation is based on free radical mechanism or ferryl ion mechanism involving high-valent oxo-iron (Fe^{IV}) species. However, there is a consensus among the majority of the literature that catalytic decomposition of H_2O_2 generates hydroxyl radical.

The simplicity of Fenton oxidation attracted much attention and hence is widely studied. The studies of Fenton oxidation applied to effluents from olive mill (Rivas *et al.*, 2003; Bianco, Michelis and Vegliò, 2011), textile and dye (Arslan-Alaton, 2007; Kušić, Božić and Koprivanac, 2007), chemical laboratory (Benatti, Tavares and Guedes, 2006), pulp mill (Catalkaya and Kargi, 2007), pharmaceuticals (Tekin *et al.*, 2006), petroleum refinery (Coelho, Castro and Sant' Anna Jr., 2006) and effluents containing pesticide (Badawy, Ghaly and Gad-allah, 2006), cosmetics (Bautista *et al.*, 2007), phenolic (Lopez *et al.*, 2005; Martins, Rossi and Quinta-Ferreira, 2010), photographic processing effluents (Yang, Ishtchenko and Huddersman, 2006) etc.

2.2.3.1.1. CONVENTIONAL FENTON OXIDATION

Fenton process involves a mixture of H_2O_2 and aqueous ferrous iron (Fe^{2+}), generally known as Fenton's reagent, under acidic condition. The Fenton reaction occurs when H_2O_2 is activated by Fe^{2+} ions to generate hydroxyl radicals thereby oxidizing Fe^{2+} to ferric (Fe^{3+}) ions. The active sites in Fenton based reactions are derived from the hydrated iron cations in aqueous solution. The reactions involved in Fenton oxidation are given below (Andreozzi *et al.*, 1999; Chiron *et al.*, 2000; Chamarro, Marco and Esplugas, 2001; Neamtu *et al.*, 2003; Neyens and Baeyens, 2003; Parson, 2004; Martins, Rossi and Quinta-Ferreira, 2010; Soon and Hameed, 2011; Nidheesh, Gandhimathi and Ramesh, 2013; Babuponnusami and Muthukumar, 2014; Bokare and Choi, 2014; Asghar, Raman and Daud, 2015).

$Fe^{2+} + H_2O_2 \rightarrow Fe^{3+} + OH^- + HO^{\bullet}$	(Chain initiation) $k = 40 - 100\ L\ mol^{-1}S^{-1}$	***Equation 2-2***
$HO^{\bullet} + Fe^{2+} \rightarrow OH^- + Fe^{3+}$	(Chain termination) $k = 2.5 - 5\ \times 10^8\ L\ mol^{-1}S^{-1}$	***Equation 2-3***
$Fe^{3+} + H_2O_2\ \rightarrow Fe^{2+} + HO_2^{\bullet} + H^+$	$k = 9.1 \times 10^{-7} - 0.01\ L\ mol^{-1}S^{-1}$	***Equation 2-4***
$Fe^{2+} + HO_2^{\bullet} \rightarrow Fe^{3+} + HO_2^-$	$k = 0.72 - 1.5\ \times 10^6\ L\ mol^{-1}S^{-1}$	***Equation 2-5***
$Fe^{3+} + HO_2^{\bullet} \rightarrow Fe^{2+} + O_2 + H^+$	$k = 0.33 - 2.1 \times 10^6\ L\ mol^{-1}S^{-1}$	***Equation 2-6***

$HO^{\bullet} + H_2O_2 \rightarrow H_2O + HO_2^{\bullet}$	$k = 1.7 - 4.5 \times 10^7\ L\ mol^{-1}S^{-1}$	***Equation 2-7***
$2H_2O_2 \rightarrow O_2 + 2H_2O$	$k = 0.001S^{-1}$	***Equation 2-8***
	Disproportionation reaction	
$HO^{\bullet} + HO^{\bullet} \rightarrow H_2O_2$	$k = 5 - 8 \times 10^9\ L\ mol^{-1}S^{-1}$	***Equation 2-9***
	Chain termination	
$HO_2^{\bullet} + HO_2^{\bullet} \rightarrow H_2O_2 + O_2$	$k = 0.8 - 2.2 \times 10^6\ L\ mol^{-1}S^{-1}$	***Equation 2-10***
	Chain termination	

The Equation 2-2 to Equation 2-10 represent traditionally accepted Fenton mechanism. The range of kinetic constants given above are taken from literature (Neyens and Baeyens, 2003; J. Herney Ramirez *et al.*, 2007; Babuponnusami and Muthukumar, 2014; Bokare and Choi, 2014). Equation 2-2, the core of Fenton reaction, involves the oxidation of ferrous ions (Fe^{2+}) to ferric ions (Fe^{3+}) resulting in the generation of hydroxyl radicals ($^{\bullet}OH$) while decomposing H_2O_2. The $^{\bullet}OH$ then initiates the radical chain oxidations. The excess H_2O_2 in the system can react with the generated ferric ions (Fe^{3+}) and regenerate ferrous ions (Fe^{2+}) according to Equation 2-4. Hydroperoxyl radical ($HO_2^{\bullet}$) can react with Fe^{2+} and Fe^{3+} and consume ferrous ions as in Equation 2-5 and regenerate Fe^{2+} according to Equation 2-6 respectively. The cyclic mechanism continues as long as H_2O_2 is accessible in the system. These reactions are advantageous as regenerated Fe^{2+} reacts further and produce more $^{\bullet}OH$ (Neyens and Baeyens, 2003; Nidheesh, Gandhimathi and Ramesh, 2013; Bokare and Choi, 2014).

Hydroxyl radical, due to non-selective nature, can be self-scavenged according to Equation 2-3, Equation 2-7, and Equation 2-9 thereby limits the rate. Similarly, Equation 2-5 to Equation 2-8 represent the rate limiting reactions due to consumption of H_2O_2 and ferric ions (Neyens and Baeyens, 2003; Nidheesh, Gandhimathi and Ramesh, 2013; Bokare and Choi, 2014). However, hydroperoxyl radicals, less reactive than $^{\bullet}OH$, generated in Equation 2-4 and Equation 2-7 may attack some organic substrates (Babuponnusami and Muthukumar, 2014).

In the presence of organic substrate (RH), such as dye, hydroxyl radical reacts by abstracting proton (H^+) from RH and generate organic radical ($R^{\bullet}$), as in Equation 2-11. In the presence of iron salts, the organic radical thus generated undergo a series of reactions, Equation 2-12 and Equation 2-13, to regenerate and terminate Fe^{2+}. Complete mineralization of RH to CO_2 and H_2O is possible if reactants (H_2O_2 and Fe^{2+}/Fe^{3+}) are sufficiently present (Neyens and Baeyens, 2003; Pignatello, Oliveros and Mackay, 2006;

Bokare and Choi, 2014). However, species such as chlorinated alkanes, n-paraffins and short chain carboxylic acids (oxalic, acetic, maleic, malonic) are known as recalcitrant to Fenton oxidation (Chamarro, Marco and Esplugas, 2001).

In the presence of air in the system, organic radicals may react with molecular O_2 according to Equation 2-15 to produce hydroperoxyl radical ($HO_2^{\bullet}$) and its conjugate base superoxide radical ($O_2^{\bullet-}$), organic peroxyl radicals ($ROO^{\bullet}$), or organic oxyl radicals ($RO^{\bullet}$) (Pignatello, Oliveros and Mackay, 2006). Oxidation of organic free radical by Fe^{3+}, as in Equation 2-12, competes with the chain termination reaction (Equation 2-3) and the propagation reaction (Equation 2-11). Such competition for $^{\bullet}OH$ between ferrous and ferric ions and substrate leads to non-productive decomposition of H_2O_2. This eventually limits the yield of oxidized organic compounds. Thus, in order to maximize the efficacy of degradation process, it is important to establish stoichiometric relationship between Fe^{2+}, substrate (RH) and Fe^{3+} (Neyens and Baeyens, 2003).

$$RH + OH^{\bullet} \rightarrow H_2O + R^{\bullet} \rightarrow Further\ oxidation \quad \textbf{Equation 2-11}$$

$$R^{\bullet} + Fe^{3+} \rightarrow R^{+} + Fe^{2+} \quad \textbf{Equation 2-12}$$

$$R^{\bullet} + Fe^{2+} \rightarrow R^{-} + Fe^{3+} \quad \textbf{Equation 2-13}$$

$$R^{\bullet} + H_2O_2 \rightarrow ROH + HO^{\bullet} \quad \textbf{Equation 2-14}$$

$$R^{\bullet} + O_2 \rightarrow ROO^{\bullet} \rightarrow\rightarrow RO^{\bullet} \quad \textbf{Equation 2-15}$$

Both ferrous and ferric ions can act as coagulants. Thus, Fenton process is considered to have dual functions: oxidation and coagulation. The ferrous ions generated from redox reaction reacts with hydroxyl ions and form hydroxo complexes. Similarly, the ferric ions generated during the Fenton mechanism can react with hydroxide ions to form ferric hydroxide precipitates. The coagulation function depends on the ratio of H_2O_2 and iron salts employed. Chemical coagulation occurs if the amounts of Fe^{2+} exceeds the amount of H_2O_2 in the system (Neyens and Baeyens, 2003; Benatti, Tavares and Guedes, 2006; Nidheesh, Gandhimathi and Ramesh, 2013).

The advantages of conventional Fenton process include high performance, simplicity of operation involving non-toxic reagents, operating at ambient pressure and temperature, requires no external energy sources, ease of integration with existing treatment processes and shortest reaction time amongst all conventional AOPs. The disadvantages include performance based on narrow pH range, high operating cost, difficulties in recycling of the catalyst, generation of large amount of iron-rich sludge, requires iron at concentration much higher than discharge limit (2 mg/L) set by EU

directives for direct discharge of wastewater into the environment (Bokare and Choi, 2014; Wang *et al.*, 2016).

2.2.3.1.2. MODIFIED FENTON OXIDATION

In order to overcome the disadvantages of conventional Fenton process, researchers have been focussing to modify conventional Fenton process. Modified Fenton systems are collectively known as Fenton-like systems representing any deviation from the classical Fenton process (Yap, Gan and Ng, 2011; Bokare and Choi, 2014). Fenton-like processes can be established simply by replacing ferrous ion in Fenton reagent by ferric ion, combination of other transition metal ions or metal ion-organic ligand complexes (Wang *et al.*, 2016). Some examples of modified Fenton processes include iron on activated carbon (AC-Fe)/H_2O_2 (Sun *et al.*, 2014), iron (III)/H_2O_2 (Chi, Nagy and Huddersman, 2011; Chi *et al.*, 2013), UV-A/Fe^{3+}/H_2O_2 and UV-A/Cu^{2+}/H_2O_2 (Ghiselli *et al.*, 2004), iron(III) on rice husk ash/H_2O_2, saponite/H_2O_2 (J. Herney Ramirez *et al.*, 2007), schorl (Xu *et al.*, 2014), nano zero-valent iron (Babuponnusami and Muthukumar, 2012), electro-Fenton-like (Şengil and Özacar, 2009; Bensalah *et al.*, 2013), microwave assisted Fenton (Carta and Desogus, 2013) and cavitation-Fenton-like (Elshafei *et al.*, 2014). Iron-free heterogeneous and homogeneous Fenton processes have been also developed by replacing iron with aluminum (Al), cerium (Ce), cobalt (Co), manganese (Mn), cupper (Cu), ruthenium (Ru) and polyoxometalates (POMs) (Bokare and Choi, 2014).

In Fenton-like systems involving Fe^{3+}/H_2O_2, production of hydroxyl radical occurs in a two-stage process. The reaction proceeds by the formation of a Fe (III)-H_2O_2 complex. Spectral analysis performed by (De-Laat and Gallard, 1999) evidenced the formation of two Fe(III)-hydroperoxy complexes: $Fe^{III}(OOH)^{2+}$ as in Equation 2-16 and $Fe^{III}(OH)(OOH)^{2+}$ as in Equation 2-18. These complexes further decompose in a uni-molecular mechanism to produce Fe^{2+} ions and hydroperoxide / superoxide radicals ($OOH^{\bullet}$/$O_2^{\bullet}$) according to Equation 2-17 and Equation 2-19, Thus, the Fe^{2+} ions catalyze the H_2O_2 decomposition to generate hydroxyl and hydroperoxyl radicals according to Equation 2-2 and the Fenton cycle continues (De-Laat and Gallard, 1999; Pignatello, Oliveros and Mackay, 2006; Jiang *et al.*, 2010; Hasan, Aziz and Daud, 2012). The reaction rate constants are taken from the literature (Jiang *et al.*, 2010).

$$Fe^{3+} + H_2O_2 \rightleftharpoons [Fe^{III}(OOH)]^{2+} + H^+ \qquad k = 3.1 \times 10^{-3} \qquad \textbf{Equation 2-16}$$

$$Fe^{III}(OOH)^{2+} \rightarrow HO_2^{\bullet} + Fe^{2+} \qquad k = 2.7 \times 10^{-3}\ S^{-1} \qquad \textbf{Equation 2-17}$$

$$FeOH^{2+} + H_2O_2 \rightleftharpoons Fe^{III}(OH)(HOO)^{2+} + H^+ \qquad k = 2 \times 10^{-4} \qquad \textbf{Equation 2-18}$$

$$Fe^{III}(OH)(HOO)^{+} \rightarrow Fe^{2+} + HO_2^{\bullet} + OH^- \qquad k = 2.7 \times 10^{-3}\ S^{-1} \qquad \textbf{Equation 2-19}$$

The difference between the rate constants for ferrous and ferric ions in above equations evidence that reactions with ferric ions, the Fenton-like oxidation, is much slower than that of conventional Fenton oxidation. Fenton-like processes include both homogeneous and heterogeneous systems, which are discussed below.

2.2.3.1.3. HOMOGENEOUS VERSUS HETEROGENEOUS FENTON OXIDATION CATALYSIS

Jöns Jacob Berzelius first used the term catalysis in 1836 (Robertson, 1975). A process in which the rate of reaction is enhanced by the presence of a substance, the catalyst, is known as catalysis. "*A catalyst transforms reactants into products, through an uninterrupted and repeated cycle of elementary steps, until the last step in the cycle regenerates the catalyst in its original form"* (Panel on New Directions in Catalytic Science and Technology, 1992, p. 12; Augugliaro *et al.*, 2010, p. 16; Suib, 2013). The atoms of a catalyst that participate in the transformation of reactants to products are known as active sites. Catalysis can be divided into two major categories: heterogeneous and homogeneous. Figure 2-6 shows diversity of Fenton-like processes by means of heterogeneous catalysts.

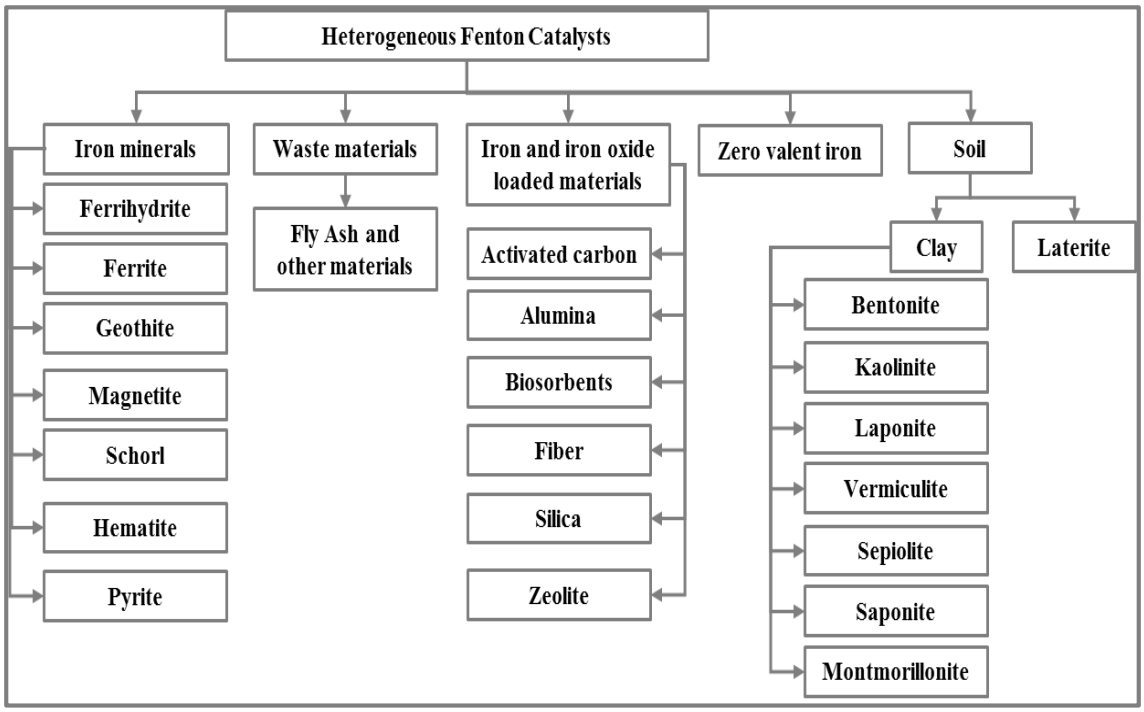

Figure 2-6: Diversity of Fenton-like processes in terms of heterogeneous catalysts. Source: Reproduced from (Nidheesh, 2015, p. 40554).

Fenton process can be performed in both homogeneous and heterogeneous systems. The fundamental difference between two processes is the position where the catalytic reaction occurs. In the homogeneous Fenton process, catalysis can occur in the liquid phase where as in the heterogeneous process the catalysis always occurs on the surface of the catalyst. This explains why heterogeneous Fenton processes are slower compared to homogeneous Fenton processes (Wang *et al.*, 2016). The general differences between two processes are presented in Table 2-4.

Table 2-4: Differences between homogeneous and heterogeneous Fenton processes.

Phenomena	**Homogeneous Fenton process**	**Heterogeneous Fenton process**
Phase	- Same phase as the reagents	- Involves solid-liquid phase
Mechanism	- Chemical reaction is involved solely in the degradation process	- Dual processes of physical absorption and desorption in addition to chemical reaction take place
Catalytic activities	- Fast	- Slow and reaction rate can be enhanced by the application of ultraviolet irradiation source - Nano size solid catalyst can accelerate the reaction rate
Active sites	- Fe^{2+}, Fe^{3+}, Fe-OOH^{2+}, iron complexes ion	- Dispersed on surface in the form of iron oxides, iron complexes ion, iron ions
pH	- Tight acidic pH range for the reaction and need pH adjustment before and after	- Broad pH range
Sludge treatment	- High amount of treated effluent is precipitated as	- Minimal ferric hydroxide is formed due to leaching of

Phenomena	Homogeneous Fenton process	Heterogeneous Fenton process
	ferric hydroxide sludge when the reaction solution was neutralized in the post-treatment - High catalyst loss after reaction takes place.	the active components into the bulk solution
Catalyst loss	Additional recovery and separation steps are required for the catalyst after treatment in order to comply with environmental regulation	- Iron loss is limited because the active phase is anchored on the surface of porous materials
Catalyst recovery	- Possible but time consuming and cost ineffective	- Easy to recover and recycling is guaranteed
Deactivation	- Irreversible reaction with products - Refractory towards certain chemical pollutants slow down the reaction	- The leaching of active sites from the support occurred at low pH and subsequently catalytic activity is lost - Degradation is slowed down due to catalyst poisoning

Source: reproduced from (Soon and Hameed, 2011, p. 4).

2.2.3.1.4. FACTORS AFFECTING FENTON BASED PROCESSES

The efficacy and kinetics of Fenton / Fenton-like processes are influenced by several factors. The most influencing five factors are pH, concentration of H_2O_2, amount of iron and its speciation, temperature, concentration of substrate (≈ initial COD). Presence of inorganic anions, dissolved oxygen, source of light (sunlight, UV, LED etc.), ligand structures, and mixing or homogeneity of the system also influence Fenton process (De-Laat and Gallard, 1999; Neyens and Baeyens, 2003; Rivas *et al.*, 2003; Pignatello,

Oliveros and Mackay, 2006; Emami *et al.*, 2010; Nidheesh, Gandhimathi and Ramesh, 2013; Babuponnusami and Muthukumar, 2014).

Presence of anions such as sulfate, phosphate, fluoride, chloride, bromide and organosulfonate may inhibit degradation process by scavenging •OH, precipitating iron or coordinating to dissolved Fe(III) to form less reactive complexes (Pignatello, Oliveros and Mackay, 2006).

Investigation on the influence of the structure of organic pollutants on mineralization by •OH revealed that alicyclic compounds were susceptible to •OH than the aromatic compounds, (Ruppert *et al.*, 1993; Neyens and Baeyens, 2003). The compounds having carbon double bonds are more reactive towards •OH than saturated molecules (Boczkaj and Fernandes, 2017). The structure of dyes also determines the extent of removal efficiency. Decolourization of acid, reactive, disperse, direct and basic dyes bearing azoic, anthraquinone, phthalocyanine, methine and oxazine structures was studied by (Kuo, 1992). The study revealed that the decolourization is affected by different types of dye structures (Kuo, 1992). The degradation of dyes such as Alizarian Violet 3B with Quinone structure was more effective compared with the dyes without Quinone structure, such as Malachite Green (Ma *et al.*, 2005). Hydroquinones with m*eta*-dihydroxy groups are far less oxidizable (Pignatello, Oliveros and Mackay, 2006).

The molecular structure of dyes affects the decolourization efficiency in microbial decomposition. Dyes with low molecular weights and simple structures exhibit higher removal efficiency compared to the dyes with high molecular weight and highly substituted. Monoazo dyes decolourize faster than diazo or triazo dyes (Pearce, Lloyd and Guthrie, 2003). Azo compounds that have a hydroxyl (-OH) or an amino ($-NH_2$) groups are more likely to be decomposed than those compounds with a methyl ($-CH_3$), methoxy, sulpho or nitro ($-NO_2$) groups (Shaul *et al.*, 1991; Nigam *et al.*, 1996; Pearce, Lloyd and Guthrie, 2003). Dyes in azo tautomeric form are relatively more stable than in hydrazone tautomeric form (Shore, 2002).

The influence of five main parameters on Fenton and Fenton-like processes are discussed below.

2.2.3.1.5. INFLUENCE OF PH

The pH of the medium is probably the most influential parameter in Fenton based processes. Since the variation in pH of the reaction medium leads to the variation in the degree of ionization of the substrate molecules and the surface properties (charge) of

the adsorbent, the modified PAN catalyst in the context of this project (Yagub *et al.*, 2014). Most of the literature agree that the optimum pH for Fenton and Fenton-like systems is around pH 3 (Pignatello, Oliveros and Mackay, 2006), falling within a narrow pH range of 2 to 4 (Andreozzi *et al.*, 1999; Rivas *et al.*, 2003; Bokare and Choi, 2014). However, basic pH can also be the optimum in the removal of some organic compounds such as dibutyl sulfide, 4-chloro-2-nitrophenol and linear alkyl benzene (Boczkaj and Fernandes, 2017). The reactivity of iron in Fenton-based processes strictly dependent on the pH-dependent speciation of iron species (Fe^{2+}, Fe^{3+} and Fe (III) hydroxides). Figure 2-7 presents pH-dependent speciation of iron species in aqueous solution and the dotted green line marks optimum pH range (Bokare and Choi, 2014).

Production of $^{\bullet}OH$ is influenced by pH mainly due to the speciation of iron and H_2O_2. Production of $^{\bullet}OH$ decreases at higher pH due to the auto decomposition of H_2O_2 according to Equation 2-8 and formation of relatively inactive oxohydroxides and ferric hydroxide (Pignatello, Oliveros and Mackay, 2006; Babuponnusami and Muthukumar, 2014). The oxidation potential of $^{\bullet}OH$ decreases rapidly with increasing pH (Neyens and Baeyens, 2003; Nidheesh, Gandhimathi and Ramesh, 2013). At alkaline medium H_2O_2 reacts with hydroxyl ions (OH^-) as shown in Equation 2-22 to form perhydroxyl ions (Boczkaj and Fernandes, 2017).

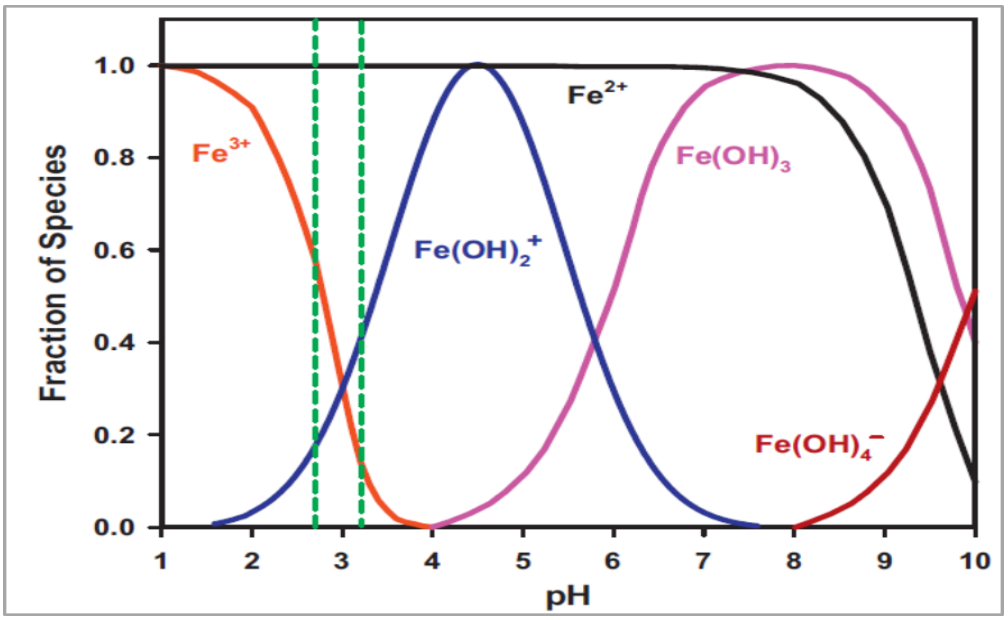

Figure 2-7: pH-dependent speciation of iron species in aqueous solution. Source:(Bokare and Choi, 2014, p. 124).

At low pH, iron exists predominantly as the hexaquo ion $[Fe(H_2O)_6]^{2+}$ which is relatively less reactive to H_2O_2 than other iron species. On the other hand, reactivity of H_2O_2

reduces due to the formation of oxonium ion $(H_3O_2)^+$ through the solvation of H_2O_2, according to Equation 2-20 at high concentration of H^+, i.e. pH < 2.0. Excess protons (H^+) also consume hydroxyl radicals according to Equation 2-21 (Nidheesh, Gandhimathi and Ramesh, 2013; Babuponnusami and Muthukumar, 2014; Fida *et al.*, 2017). Iron leaching increases with decreasing pH as the solubility of metals is favoured at low pH (He *et al.*, 2016).

The first step of the reaction in heterogeneous catalysis is the adsorption of reactants onto the catalyst (Jacques, 2017). Thus, variation in pH varies the degree of ionization of the adsorptive molecule (the substrate) and the surface of adsorbent (the catalyst). The pH at point of zero charge, pH_{zpc}, can be used to describe the adsorption mechanism of dyes. Accordingly, adsorption of cationic dye is favoured at pH > pH_{zpc} whereas adsorption of anionic dye is favoured at pH < pH_{zpc} where the surface becomes positively charged (Yagub *et al.*, 2014).

$$H_2O_2 + H^+ \rightarrow H_3O_2^+ \qquad \textbf{Equation 2-20}$$

$$HO^\bullet + H^+ + e^- \rightarrow H_2O \qquad \textbf{Equation 2-21}$$

$$H_2O_2 + OH^- \rightleftharpoons HO_2^- + H_2O \qquad \textbf{Equation 2-22}$$

2.2.3.1.6. INFLUENCE OF HYDROGEN PEROXIDE CONCENTRATION

Concentration of hydrogen peroxide plays an important role in Fenton based processes. The H_2O_2 concentration is important to achieve better degradation efficiency (Chamarro, Marco and Esplugas, 2001). H_2O_2 alone does not generate $^\bullet$OH (Boczkaj and Fernandes, 2017). Generally, oxidation of substrates increases with increasing H_2O_2 dose until an optimum concentration, if enough active sites are present in the system. This is due to the increasing production of $^\bullet$OH (Babuponnusami and Muthukumar, 2014). However, beyond optimum concentration, H_2O_2 acts as a scavenger of $^\bullet$OH. The excess H_2O_2 reacts with $^\bullet$OH in the system according to Equation 2-7 to generate less reactive perhydroxyl radicals ($HO_2^\bullet$) (Nidheesh, Gandhimathi and Ramesh, 2013). Thus, performance of system reduces when performed with higher initial concentration of H_2O_2. Also, this inefficient decomposition lead to the wastage of H_2O_2 thereby increases the operation cost (OPEX) (Rivas *et al.*, 2003).

In Fenton-like processes, hydrogen peroxide is known to form iron complexes according to Equation 2-16 and Equation 2-18. Extreme high concentration (~ 9 M) of H_2O_2 may lead to the formation of other complexes such as $Fe(H_2O_2)^{3+}$ and $Fe(H_2O_2)(HO_2)^{2+}$ (Lewis, Richards and Salter, 1963; Gallard, De Laat and Legube, 1999; Pignatello,

Oliveros and Mackay, 2006). In order to proceed as in Equation 2-4, at least one coordination position on Fe(III) must be open or occupied by a labile ligand such as H_2O (Graf *et al.*, 1984; Pignatello, Oliveros and Mackay, 2006).

2.2.3.1.7. INFLUENCE OF AMOUNT OF CATALYST

The amount of catalyst plays an important role in reaction kinetics (Chamarro, Marco and Esplugas, 2001). The rate of degradation generally increases with increasing amount of catalyst. This is mainly due to the addition of more active sites which lead to catalytic decomposition of oxidant and produce more hydroxyl radicals ($^{\bullet}OH$). In heterogeneous system, increasing amount of catalyst not only increases the active sites but also enhances the adsorption process. However, beyond the optimum amount, the catalyst can scavenge $^{\bullet}OH$ according to Equation 2-3. In Fe^{3+}/H_2O_2 system, excess concentration of Fe^{3+} can react with H_2O_2 to produce less reactive hydroperxyl radicals according to Equation 2-16 and Equation 2-17 (Nidheesh, Gandhimathi and Ramesh, 2013; Fida *et al.*, 2017). This will decrease the rate of oxidation. The activity of catalyst also relies on the characteristics of the iron salts such as crystallinity and surface area. Production of $^{\bullet}OH$ depends on the surface reaction between iron and the adsorbed H_2O_2 on the solid's surface (Dantas *et al.*, 2006).

2.2.3.1.8. INFLUENCE OF TEMPERATURE

Temperature plays an important role in the treatment of wastewater. Alike H_2O_2 and catalyst, generally, rate of reaction increases with increase in temperature. This can be explained in terms of Arrhenius law which invokes the exponential dependency of the kinetic constant on reaction temperature (J. Herney Ramirez *et al.*, 2007). The increase in reaction rate with increase in temperature results from the increase in $^{\bullet}OH$ production (Emami *et al.*, 2010). However, Fenton based processes can have negative effect of low and high temperatures. Low temperature slows down the reaction according to Arrhenius law. At very high temperature, thermal decomposition of H_2O_2 occurs as in Equation 2-8 and leads towards inefficient consumption of H_2O_2. This results in production of less $^{\bullet}OH$ thus hinders the degradation process. The solubility of oxygen decreases with increasing temperature which can have negative effect on COD removal (Nidheesh, Gandhimathi and Ramesh, 2013; Babuponnusami and Muthukumar, 2014).

2.2.3.1.9. INFLUENCE OF SUBSTRATE CONCENTRATION

Most of the literature agree that degradation rate decreases with the increasing initial concentration of substrate (≈ initial COD). The generation of $^{\bullet}OH$ on the surface of

catalyst may be hindered due to the limited access of H_2O_2 to the catalyst surface. This is possible as the number of substrate molecules, compared to the number H_2O_2 molecules, increase with the increase in concentration of substrate. The excess substrate molecules / ions can occupy the active sites on the catalyst surface (Idel-aouad *et al.*, 2011; Nidheesh, Gandhimathi and Ramesh, 2013). Further to this, the intermediate products may compete with the substrate for the active sites and $^{\bullet}OH$ (Panda, Sahoo and Mohapatra, 2011).

In contrast to the above explanation, improved degradation rate with increasing initial substrate concentration was also reported. Kasiri, Aleboyeh and Aleboyeh, 2008 and Hassan and Hameed, 2011 observed higher removal efficiencies with increasing initial concentration of dyes. Authors argued the phenomenon based on collision theory of chemical reactions. They explained that for a chemical reaction to occur or to break or form chemical bonds, the reacting molecules must collide in correct orientation so that they possess a minimum energy equivalent or more than activation energy. The authors further argued that increasing the concentration of substrate (number of dye molecules) enhances the frequency of effective collisions between substrate and $^{\bullet}OH$ which eventually leading to the higher removal efficiency (Hassan and Hameed, 2011).

2.2.3.2. MODIFIED FIBROUS POLYACRYLONITRILE (PAN) CATALYST

It is already mentioned that Fenton-like processes have been developed to overcome the disadvantages of conventional Fenton process. Heterogeneous catalyst have been developed to overcome the disadvantages of homogeneous catalysis. Accordingly, a number of heterogeneous catalysts have been applied in the treatment wastewater (J. Herney Ramirez *et al.*, 2007; Kasiri, Aleboyeh and Aleboyeh, 2008; Melero *et al.*, 2009; Soon and Hameed, 2011; Hassan and Hameed, 2011; Duarte *et al.*, 2013; Satishkumar *et al.*, 2013; Yao *et al.*, 2013; Cihanoğlu, Gündüz and Dükkanci, 2015; Rahim Pouran *et al.*, 2015; Khataee *et al.*, 2015; Lv *et al.*, 2015; Nidheesh, 2015; Queirós *et al.*, 2015).

PAN fibre was modified at De Montfort University to produce a fibrous catalyst (Ishtchenko, Huddersman and Vitkovskaya, 2003). The PAN fibre representing a copolymer of acrylonitrile (92.3 %), itaconic acid (1.5 %) and methylmethacrylate (6.2 %) was produced as a self-supporting mesh with excellent hydrodynamic properties by incorporation of polypropylene. Modification of PAN component of mesh was achieved in three consecutive stages (Ishtchenko, Huddersman and Vitkovskaya, 2003):

Stage one: Treatment of mesh by boiling in solution containing hydrazine, hydroxylamine and sodium hydroxide (NaOH).

Stage two: Treatment of modified mesh from stage one by NaOH solution.

Stage three: Impregnation of transition metal such as iron onto the modified mesh from stage two to produce a novel heterogeneous fibrous PAN catalyst to undergo Fenton-like process.

Figure 2-8: Modified heterogeneous fibrous PAN catalyst used in the treatment of dyes.

The modified fibrous mesh was impregnated with transition metals (Iron, cobalt, copper and nickel) and successfully converted to an active Fenton-like catalyst (Ishtchenko, Huddersman and Vitkovskaya, 2003). The mechanical and physicochemical properties of the catalyst were investigated and subsequently applied to the treatment of various wastewaters. These include photographic waste (Yang, Ishtchenko and Huddersman, 2006), microbiological contaminated waters (Boateng *et al.*, 2011; Price *et al.*, 2012), maleic acid (Chi and Huddersman, 2011), phenols (Alsamkari, 2011), municipal wastewater (Chi *et al.*, 2013), humic acid and polycyclic aromatic hydrocarbons (PAHs) (Asuelimen, 2015) and BTEX contaminated produced waters (Ekpurke, 2018).

During the developmental phase, this modified PAN catalyst was tested against the real textile effluent obtained from one of the local textile factory in Leicester, UK (Ishtchenko, Huddersman and Vitkovskaya, 2003). However, the detail investigation of the process parameters, both in batch and continuous flow modes, process optimization, lifetime of the catalyst, mechanism of catalyst deactivation and regeneration schemes etc. were not studied. Thus, this study was focussed to explore the effectiveness of modified PAN catalyst in the treatment of textile effluent in light to the afore mentioned parameters.

CHAPTER THREE

3. LITERATURE REVIEW – REMEDIATION OF MINING INFLUENCED EFFLUENTS

3.1. MINING AND THE ENVIRONMENT

Mining is the activity of extracting minerals and geological materials such as coal and metals from the earth by digging. Mining expanded worldwide in the 20th century. In Britain, the history of mining for coal, metal ores and other minerals pre-date the Bronze Age and mining output reached to the climax after the industrial revolution as the demand for metals and coal was at its height (Younger, Banwart and Hedin, 2002; Johnston *et al.*, 2008).

Although mining supplied enormous amount of mineral wealth to human, the potential and the actual destruction of the natural environment resulting from the mines, both working and abandoned, is severe. During the peak time of mining industry, over 25,000 km^2 of land surfaces in the UK was affected by coal mining alone. Thus, mining related pollution, especially the water, represents a severe environmental problem in countries which have a mining history such as the UK (National Rivers Authority, 1994; Johnston *et al.*, 2008). The negative impacts of mining on the water environment arise from the six distinct phases of the mining life-cycle (Younger, Banwart and Hedin, 2002):

i) *The mining process itself* – affects the water environment mainly through the disruption of existing hydrogeological pathways.
ii) *Mineral processing operations* – water after washing of ores become polluted and failures of tailings dams release pollution to the water system.
iii) *The dewatering* – leads to the pollution of surface and ground waters and depression of water table which can result in decreased flows into water bodies, lowering of water table, land subsidence due to compaction or collapse of voids.
iv) *Seepage of contaminated leachate from waste rock piles and tailings dams* – release of acidic leachates from re-vegetated waste rock piles and unlined bases of old tailings dams. Highly polluted surface runoff can arise from the unreclaimed spoil.
v) *Flooding of workings after extraction has ceased* – the flooding of abandoned mine workings occurs due to the water table rebound or groundwater rebound. Water quality deteriorates during the process of rebound due to the sudden dissolution of acid-generating salts, the secondary minerals formed during the weathering / oxidation of pyrite (FeS_2) above the water table.
vi) *Discharge of untreated waters after flooding is complete* – can lead to pollution of surface water and over-lying aquifers, localised flooding and clogging of sewers.

Figure 3-1 presents a highly idealized diagram reflecting mining activities and the related pathways (excludes direct discharges) for the transport of metals to the aquatic environment.

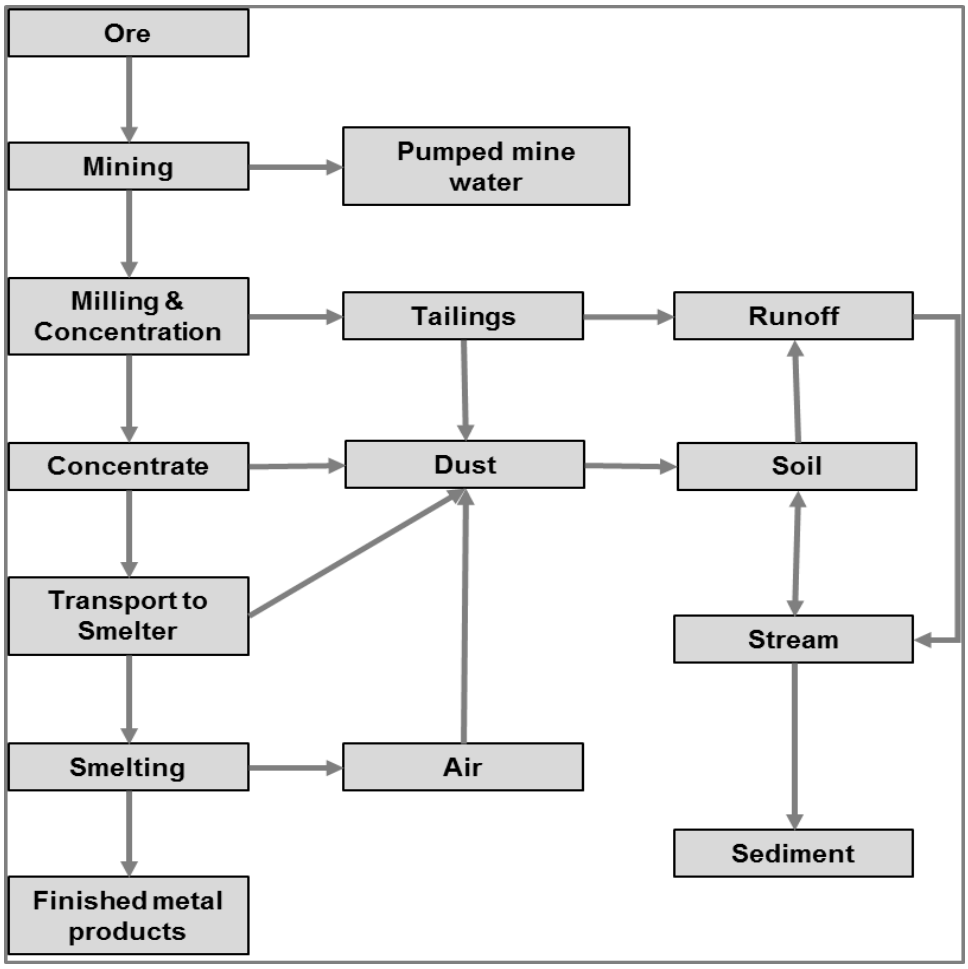

Figure 3-1: Schematic diagram showing mining activities and transport of contaminants to the aquatic environment. (Source: reproduced from (Kelly, 1988, p. 10).

Water pollution arises from the large-scale disturbance of land associated with thousands of abandoned coal, metal and other mines. The waters in working mines are controlled by pumping whereas in closed mines, groundwater level finally reaches to the surface and discharges via adits, springs, seepage to the aquifer or riverbed. Diffuse pollution arising from mining related land disturbance has been reported to contribute 45 % to 95 % of the total polluting load (Mullinger, 2004; Mayes *et al.*, 2006; Johnston, Parker and Pritchard, 2007; Johnston *et al.*, 2008). The abandoned mines are the biggest sources of water pollution in the UK as the last major mine closed in the 1990s and there are no working mines (National Rivers Authority, 1994; Younger, Banwart and Hedin, 2002; Johnston *et al.*, 2008).

Mining related pollution is difficult to address as it lasts for a very long time even after the cessation of active mine. A typical example is the discharge of acidic, ferruginous waters into the River Esk in Dalkeith, Scotland by the old coal workings excavated in the thirteenth century (Younger and Adams, 1999; Johnston *et al.*, 2008). Earlier reports claimed that pollution arising from the abandoned mines was the cause of 7 % to 9 % of rivers and 14 % of groundwater (by area) in England and Wales and 2 % to 6 % respectively in Scotland be at risk of not achieving the good chemical and ecological status set by Water Framework Directive (WFD) (Johnston, Parker and Pritchard, 2007; Johnston and Rolley, 2008). It has been reported that 71 % of the surface water resources that did not meet the cadmium quality standard are in metal mining areas (Johnston and Rolley, 2008). USEPA reported that an approximate 20,000 km of streams and rivers in the eastern US are polluted by Acid Mine Drainages (AMDs) (Ziemkiewicz et al., 2003; USEPA 2014).

Mining is also associated to the contamination of soils and sediments. A long-term negative impact of metal mining is due to the contamination of river, lake, estuary and floodplain by fine-grained (< 2 mm) suspended sediment with metals such as cadmium, lead, zinc, copper and arsenic metalloid. Metal contamination in some floodplains is so severe that they are no longer suitable for grazing livestock (Hudson-Edwards *et al.*, 2008; Johnston *et al.*, 2008). The abandoned mines were identified as a significant problem in eight of the twelve river basin districts in the UK. Metal mining affected an estimated area of 12,000 km^2 river catchments (Johnston and Rolley, 2008) in northern England. Over 90 % of surface and subsurface floodplain soils exceed background concentrations and guideline limits and similar consequences are expected in metal mining catchments in south-west England (Cornwall) and mid-Wales. British rivers have not been remediated to improve sediment contaminated with metals released from metal mines (Hudson-Edwards *et al.*, 2008; Johnston *et al.*, 2008). Figure 3-2 shows the catchments in the UK sensitive to sediment-borne metal contamination from metal mining.

Mining can result in negative ecological and economic impacts. The mine discharges with low pH / ochre / elevated metal concentrations can decimate freshwater ecology and aquatic biodiversity. Similarly, polluted water can be unaesthetic and become unfit for fishing, irrigation, livestock watering and water sports and can reduce the economic and social values (National Rivers Authority, 1994; Hudson-Edwards *et al.*, 2008; Johnston *et al.*, 2008).

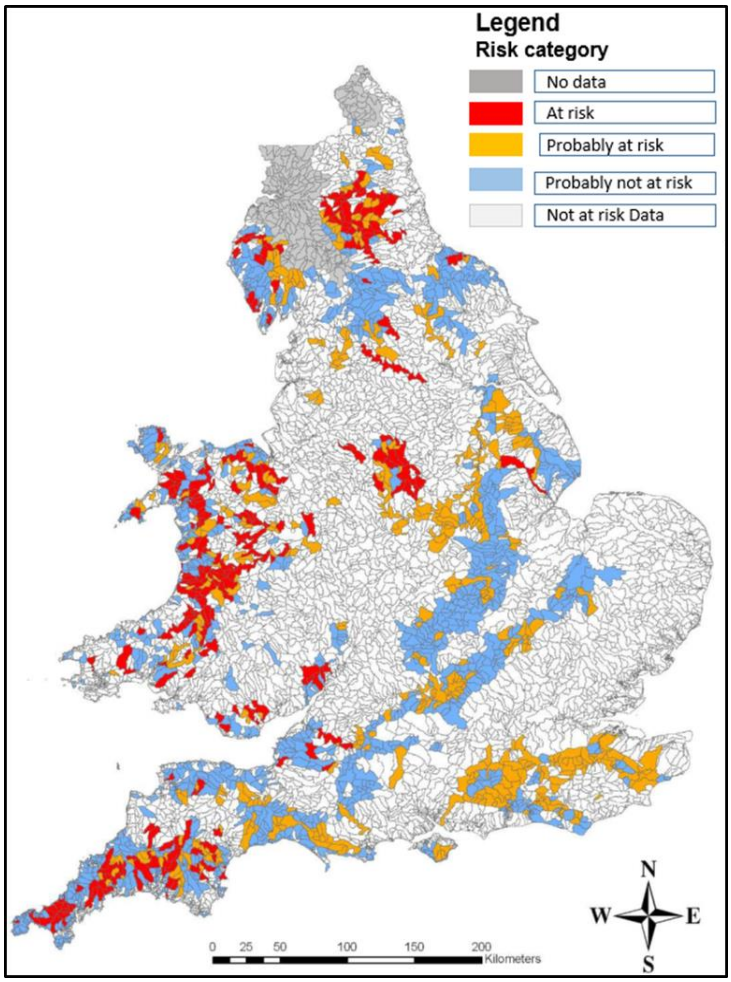

Figure 3-2: Catchments in the UK sensitive to sediment-borne metal contamination arising from mining. Source: (Hudson-Edwards et al., 2008, p. 26).

3.1.1. THE CHEMISTRY OF MINE WATERS

The nature and effect of mine water can also vary between shallow and deeper level workings and adits within the same mining area. The mine water chemistry varies significantly depending on a number of factors such as geochemistry of the area, geochemical situation at the point source of weathering, the nature of the mine waste, host rocks and gangue minerals. Accordingly, mine drainage waters can be alkaline, moderately or highly saline, acidic and ferruginous or alkaline and ferruginous (National Rivers Authority, 1994; Younger, Banwart and Hedin, 2002; Johnston *et al.*, 2008). The chemistry of mine water is the consequence of the competing process of acid formation and neutralization (Warrender, 2009). In general, mining sites rich in sulfide containing minerals such as sphalerite (ZnS), galena (PbS), arsenopyrite (FeAsS), pyrite/marcasite (FeS_2), millerite (NiS), greenockite (CdS), covellite (CuS), chalcopyrite ($CuFeS_2$) and poor in carbonate containing minerals such as calcite ($CaCO_3$), dolomite ($CaMg(CO_3)_2$, magnesite ($MgCO_3$), siderite ($FeCO_3$) produce acidic drainage whilst carbonate-rich

mines produce circum-neutral or alkaline drainage (Younger, Banwart and Hedin, 2002; Ziemkiewicz, Skousen and Simmons, 2003; Warrender, 2009).

The stable minerals and coal ores become chemically unstable after excavation and exposure to the atmosphere. The chemical weathering of sulfide minerals undergo through a series of geochemical and microbial-mediated reactions that release contaminants into the hydrological cycle thus bioavailable as potentially toxic solutes. Metal ions are released from the weathering of sulfide containing minerals mentioned above (Younger, Banwart and Hedin, 2002). The rebound water may appear clear due to low dissolved oxygen and soluble iron. However, a yellowish-orange precipitate, commonly known as ochre, will form once the rebound water comes in contact with oxygen (National Rivers Authority, 1994; Johnston *et al.*, 2008). Figure 3-3 summarizes the sources and pathways of mine water pollution.

3.1.1.1. MINE WATER FROM THE COAL MINE

Drainage water from coal mines are generally acidic and ferruginous and known as acid mine drainages (AMDs). The formation of AMDs is well studied. AMDs formed as a result of weathering and oxidation of a principal mineral in coal and the mudstones, the pyrite or marcasite (Iron sulfide, FeS_2), in the presence of dissolved oxygen. Weathering and oxidation of pyrite undergo several complex interacting microbial, chemical and physical processes involving oxidation-reduction reactions (Nordstrom, 1982; Langmuir, 1997; Younger, Banwart and Hedin, 2002; Wingenfelder *et al.*, 2005; Manhan, 2011).

The overall process of AMDs formation can be summarized by Equation 3-1. In the presence of dissolved oxygen, pyrite and water produce insoluble hydroxide of iron, the ochre (see Figure 3-4), and sulfuric acid. However, in natural environment, in addition or instead of ochre, many other iron minerals may form (Nordstrom, 1982; Warrender, 2009; Manhan, 2011).

$$FeS_2(s) + \frac{15}{4}O_2(aq) + \frac{7}{2}H_2O(l) \rightarrow Fe(OH)_3(s) + 2H_2SO_4(aq) \qquad \textit{Equation 3-1}$$

Weathering of pyrite can produce sulfate and release soluble ferrous iron (Fe^{2+}) and acidity as indicated by the formation of protons in Equation 3-2 (Langmuir, 1997; Brown, Barley and Wood, 2002; Younger, Banwart and Hedin, 2002; Manhan, 2011). In the presence of excess dissolved oxygen or oxygenation from atmosphere, the dissolved ferrous iron (Fe^{2+}) produced in Equation 3-2 further oxidized to ferric iron (Fe^{3+}) as shown in Equation 3-3 thereby consumes acidity.

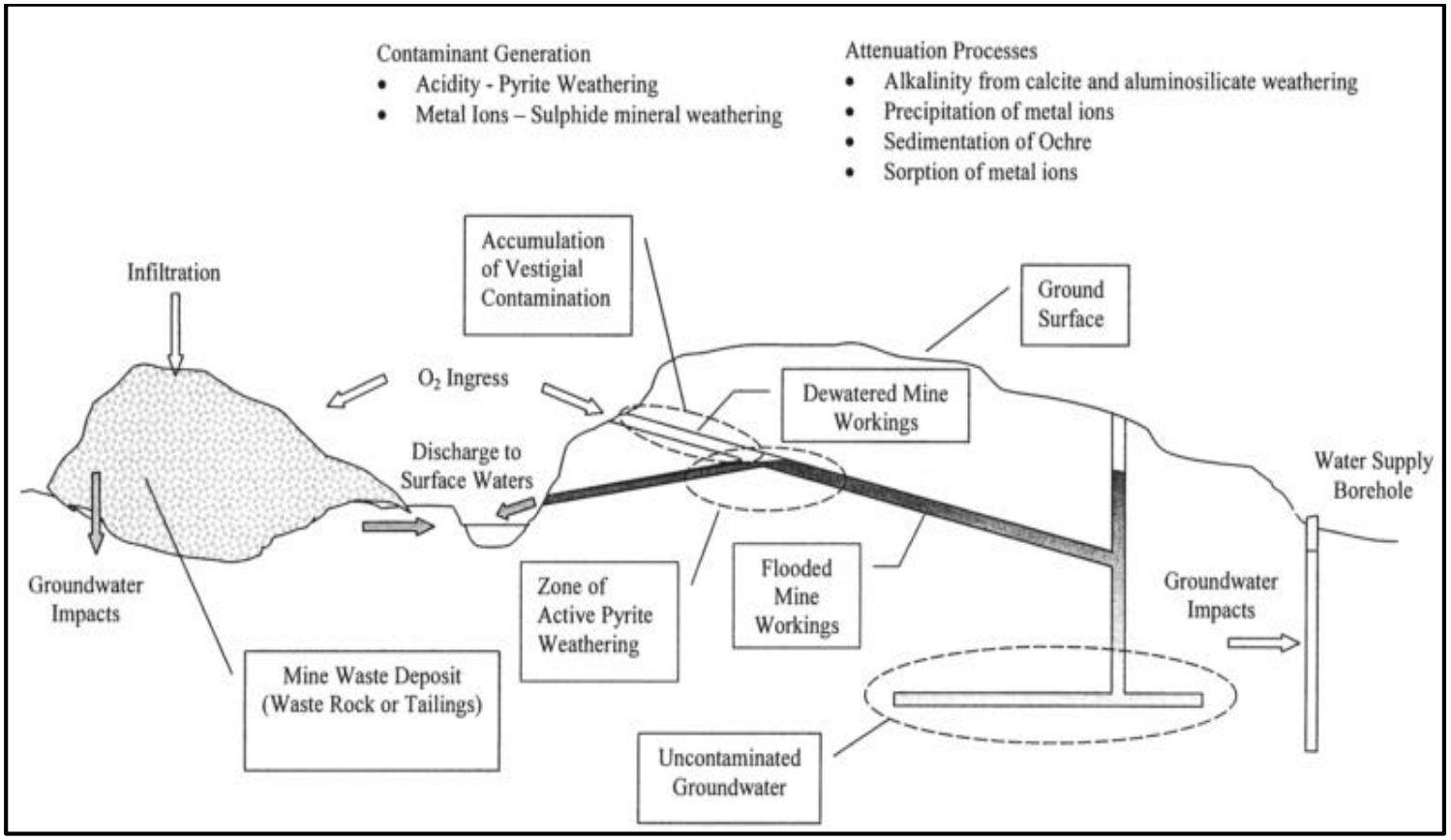

Figure 3-3: Sources and pathways of mine water pollution. Source: (Younger, Banwart and Hedin, 2002; Johnston et al., 2008).

$$2FeS_2(s) + 7O_2(aq) + 2H_2O \rightarrow 2Fe^{2+} + 4SO_4^{2-} + 4H^+$$ ***Equation 3-2***

$$2Fe^{2+} + \frac{1}{2}O_2 + 2H^+ \rightarrow 2Fe^{3+} + H_2O$$ ***Equation 3-3***

The ferric iron thus generated in Equation 3-3 can lead to the production of acidity in much greater extent through Equation 3-4 and Equation 3-5. Ferric iron either further reacts to precipitate as iron oxyhydroxide forming ochre as represented by Equation 3-4 or acts as the oxidant in the weathering of pyrite to release ferrous iron and acidity as represented in Equation 3-5 (Nordstrom, 1982; Langmuir, 1997; Younger, Banwart and Hedin, 2002; Manhan, 2011).

$$2Fe^{3+} + 6H_2O \rightleftharpoons 2Fe(OH)_3(s) + 6H^+$$ ***Equation 3-4***

$$14Fe^{3+} + FeS_2(s) + 8H_2O \rightarrow 2SO_4^{2-} + 15Fe^{2+} + 16H^+$$ ***Equation 3-5***

The ferrous iron produced during Fe^{3+} / pyrite oxidation (Equation 3-5) can be re-oxidized according to Equation *3-3* and the reaction cycle continues until oxygen is no longer available. If oxygen becomes limited then Equation 3-5 can proceed to completion, yielding ferrous iron in the solution (Langmuir, 1997).

It is clear from Equation 3-2 and Equation 3-5 that the acidity solely depends upon the oxidizing agent. With one mole of FeS_2 (pyrite), two moles of H^+ are produced in Equation 3-2 with oxygen as an oxidant whereas 16 moles of H^+ are produced with Fe^{3+} as an oxidant. The Fe^{3+} / pyrite oxidation depends on the availability of Fe^{3+}, which eventually depends on the rate of Fe^{2+} oxidation via Equation 3-3 which is generally slow in acidic conditions and dominates at pH < 3 (Langmuir, 1997; Younger, Banwart and Hedin, 2002).

Figure 3-4: Deposition of ochre downstream of an abandoned coal mine, Aberbaiden Colliery, South Wales. (Source: D Johnston-Environment Agency).

$$Fe^{2+} + \frac{1}{4}O_2 + \frac{5}{2}H_2O \rightarrow Fe(OH)_3 + 2H^+$$ ***Equation 3-6***

At low pH (< 3), increasing rate of pyrite weathering results due to catalysis of reaction (Equation 3-3) by acidophilic bacteria such as *Thiobacillus* (*T. thiooxidans* and *T. ferroxidans*). If the pH of the solution rises above three or near neutral due to partial neutralization and natural attenuation, the oxidation of Fe^{2+} occurs much faster via Equation 3-6. The neutralization and natural attenuation occur when the drainage water is diluted by the receiving waters. The weathering of carbonate and silicate minerals also helps to consume acidity and buffer the solution (Nordstrom, 1982; Langmuir, 1997; Younger, Banwart and Hedin, 2002; Warrender, 2009; Manhan, 2011).

Table 3-1 presents the pH and the concentrations of metals in the receiving water bodies impacted by the drainage from the coal mines. The pH of the receiving water ranges from 2.3 to 7.8. The solubility of many base metals such as Zn, Cd and Pb is enhanced by the low pH resulted from the oxidation of pyrite. Therefore, AMDs released from coal mines are generally characterised by the elevated concentrations of metals, especially the iron. The higher concentration of other metals is due to the co-precipitation with iron oxyhydroxide (Garrel and Thompson, 1960; Smith, 1999; Mestre, 2009; Warrender, 2009).

Table 3-1: pH and concentration (mg/L) of metals in the receiving water bodies impacted by coalmine drainage.

River	pH	Fe	Mn	Cu	Cd	Ni	Zn	Pb	SO_4^{2-}
Matsuo mine drainage (Japan)	2.3	237	-	-	-	-	-	-	-
Drift min discharge (Wales, UK)	7.8	15.79	3.12	-	-	-	1.30	-	612
Avon mine drainage (Ireland)	2.67	996	-	0.916	-	-	229	-	10203
Kimblesworth mine drainage (UK)	6.95	1.87	0.63	-	-	-	-	-	307.7
Bulhouse mine drainage (UK)	5.61	62	11.5	0.019	0.046	0.021	0.156	0.003	231.5
River Akagawa (Japan)	3.7	10	0.87	3.6	96	22	62	14	-

River	pH	Fe	Mn	Cu	Cd	Ni	Zn	Pb	SO_4^{2-}
Taff Bargoed (Wales, UK)	7.8	1.8	0.2	-	-	-	0.07	-	110
Avoca River (Ireland)	5.8	1400	-	610	-	-	640	-	28
Rio Tinto (Spain)	2.7	489	25	0.274	0.493	0.06	55	0.508	2583
Slippery Rock Creek (USA)	6.3	0.4	4.1	-	-	-	0.07	-	255
Racoon Creek (USA)	3.2	-	3.4	-	-	-	-	-	411
Indian Creek USA	6.0	1.5	-	-	-	-	-	-	65.8
River Don UK	6.3	11.72	3.05	0.001	0.045	0.0005	0.007	0.005	65.4

Source: reproduced from (Mestre, 2009, p. 56).

3.1.1.2. MINE WATER FROM THE METAL MINES

Drainage water from metal mines are characterized by circum-neutral pH if either pyrite is absent within the mining ore or host rock or gangue (the commercially valueless material in which ore is found) contain carbonate minerals. Weathering of mineral ores other than pyrite does not produce acidity and presence of carbonate minerals helps neutralize and buffer the pH of water. Although acidity will not necessarily produce during weathering of sulfide minerals such as sphalerite (ZnS), galena (PbS), greenockite (CdS) and chalcopyrite ($CuFeS_2$), metal ions and SO_4^{2-} are still released into the solution (Brown, Barley and Wood, 2002; Younger, Banwart and Hedin, 2002). The oxidation reactions of these minerals are given below, Equation 3-7 to Equation 3-10.

Sphalerite $ZnS(s) + O_2(aq) \rightarrow Zn^{2+} + SO_4^{2-}$ ***Equation 3-7***

Galena $PbS(s) + O_2(aq) \rightarrow Pb^{2+} + SO_4^{2-}$ ***Equation 3-8***

Greenockite $CdS\ (s) + 2O_2(aq) \rightarrow Cd^{2+} + SO_4^{2-}$ ***Equation 3-9***

Chalcopyrite $CuFeS_2(s) + 4O_2(aq) \rightarrow Cu^{2+} + Fe^{2+} + 2SO_4^{2-}$ ***Equation 3-10***

The above reactions show that weathering of sulfide minerals result in the formation of metal-laden drainage without releasing acidity (H^+). Such drainages result in circum-neutral pH and contain high sulfate, low iron and elevated concentrations of base metals / metalloids such as Zn, Cd, Pb and As (Younger and Adams, 1999). Table 3-2 presents the pH and concentration of metals and sulfate in the receiving water bodies impacted

by metal mine drainages. The low pH at Cwm Rheidol mine drainage is due to the presence of pyrite (Warrender, 2009).

Table 3-2: pH and concentration of metals (µg/L) and sulfate (SO_4^{2-}, mg/L) in the receiving water bodies impacted by metal mine drainage.

River	pH	Fe	Mn	Cu	Cd	Ni	Cr	Zn	Pb	SO_4^{2-}
Cwm Rheidol Wales, UK	2.9	-	-	49	74	555	-	55000	26	643.5
River Gaula Norway	6.77	-	-	11	-	-	-	83	-	-
Tarapaya River Bolivia	-	-	-	13	5.0	-	-	601	56.0	-
Pilcomayo river Bolivia	-	-	-	14	0.76	-	-	238	28.5	-
Mosquito Creek USA	8.3	-	-	BD	BD	-	-	168	-	-
Jack Creek USA	-	33	-	41	9.0	-	-	942	0.5	-
Saxbäcken river Sweden	-	390	-	5.9	1.23	-	-	1480	0.4	-
Estanda stream Spain	8.23	130	27970	2570	530	-	3160	320	20200	-
Afon Rheidol Wales, UK	6.1	-	-	-	1.5	3.15	-	269.5	6.3	7.1
Afon Ystwyth Wales, UK	4.1	-	-	-	1.0	3.0	-	307	68	-
Eagle river USA	8.1	600	615	BD	BD	-	-	107	-	-

Source: reproduced from (Mestre, 2009, p. 61), BD = below detection.

Most of the circum-neutral mine drainages in the UK are situated in the areas with hydrothermal base metal sulfide deposits which are low in pyrite content. Thus, the potential contaminants in those drainages include Zn, Cd, Pb, As, Cr and Ni (Younger, Banwart and Hedin, 2002; Hartley, 2009; Warrender, 2009). Some of these metals are proven toxic to the plants, animals and human being (Kelly, 1988). This project focusses

on the primary contaminants, Zn, Cd and Pb in the circum-neutral drainage and hence a brief overview of these metals is given below.

3.1.1.2.1. ZINC (ZN)

Zinc pollution arises through the weathering of ore mineral sphalerite (ZnS) as shown in Equation 3-7. Zinc is an essential trace element in plants and animals. However, at higher concentration, it can be toxic to aquatic environment and human being. Human suffering from diarrhoea, nausea, anaemia, stomach cramps, skin irritation, vomiting, gastroenteritis and pulmonary distress have been reported due to Zn toxicity (WHO, 1996; Mayes et al., 2009; Fu and Wang, 2011). Zn can accumulate in bone and vital organs, bind to the gill epithelium or suffocate fish by enhancing excessive production of mucus (Nuttall and Younger, 2000).

Solubility of zinc in a wider pH range makes it a primary contaminant in many circum-neutral mine waters. A Eh-pH diagram elucidates the field of stability of mineral or chemical species with respect to the activities of hydrogen ions (pH) and electrons (oxidation potential) (Eh) (Geological Survey of Japan, 2005; The Editors of Encyclopaedia Britannica, 2015). The Eh-pH diagram for Zn in Figure 3-5 (left) suggests that Zn may be present as free ion (Zn^{2+}) at pH ≤ 7.5 or in complexes of oxide, sulfide and carbonate at pH > 7.5. Thus, removal of Zn from mine discharge is difficult (Hem, 1972; Kelly, 1988; Nuttall and Younger, 2000).

The updated list of hazardous substances published by (WFD-UKTAG, 2017) determined Zn as non-hazardous pollutant in groundwater. In UK, the discharge limit for Zn increases with increasing hardness (mg/L of $CaCO_3$) and maximum permitted limit is 125 µg/L for water with hardness above 250 mg/L of $CaCO_3$ (Mullinger, 2004). Hardness of water is the measure for a total amount of dissolved minerals, especially calcium and magnesium, in the water. General guidelines for classification of waters based on calcium carbonate are: 0 to 60 mg/L as soft; 61 to 120 mg/L as moderately hard; 121 to 180 mg/L as hard; and more than 180 mg/L as very hard (United States Geological Survey, 2016).

3.1.1.2.2. CADMIUM (CD)

Cadmium pollution arises through the weathering of ore mineral greenockite (CdS) as shown in Equation 3-9. Greenockite (cadmium) tends to occur naturally with other sulfide ores of zinc and lead. The Eh-pH diagram for Cd in Figure 3-5 (right) is similar to that of

Zn (Figure 3-5 left) also suggests their geochemical similarities (Hem, 1972; Brookins, 1998).

Cadmium is a very toxic to all organisms and cumulative poison in mammals. Cd is linked to kidney damage (Herber et al., 1988; Igwe, 2007), nausea, chronic pulmonary problems, muscular cramps, renal degradation, skeletal deformity (Mohan and Singh, 2002) and affect fertility in human (Kumar et al., 2000), hepatic damage and hypertension (Igwe, 2007). Cadmium is very persistent in human and has a biological half-life of 10 – 35 years. It is reported that 50 – 85 % of Cd is stored in kidney and liver, 30 – 60 % in kidney alone. "Itai-itai" disease caused by elevated concentration of Cd in drinking water in Japan is a well-known case related to cadmium toxicity (WHO, 2011).

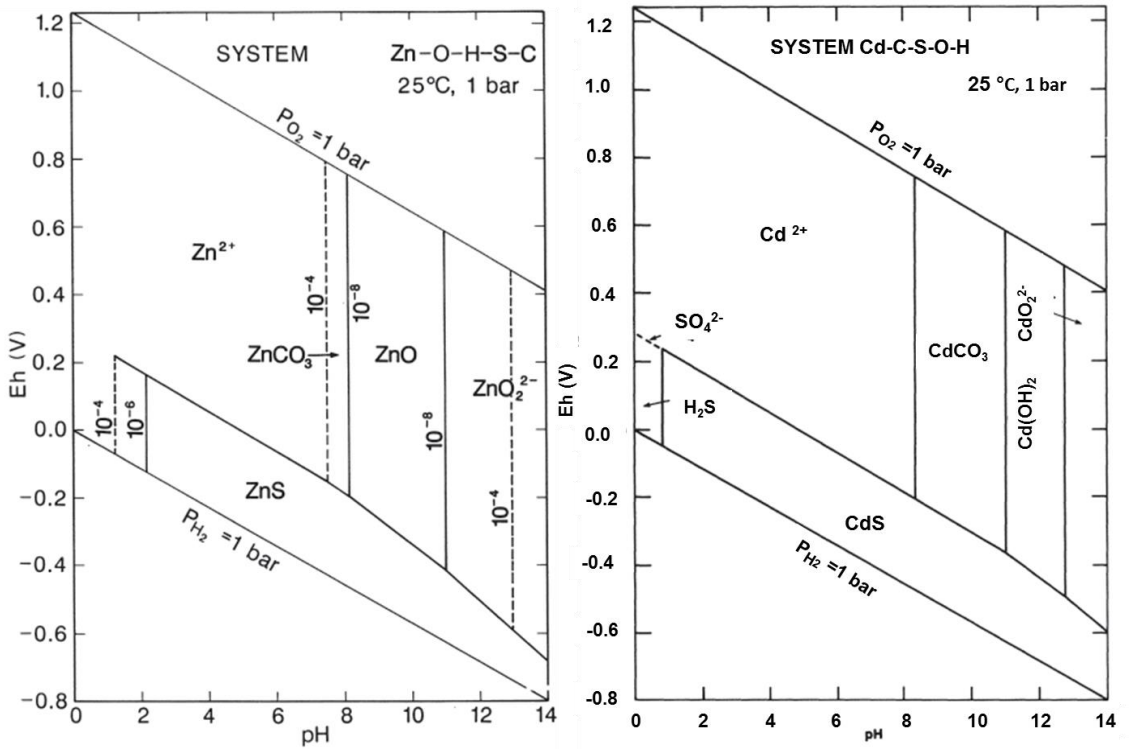

Figure 3-5: Eh-pH diagram for Zn (Zn-O-H-S-C) (left) and Cd (Cd-C-S-O-H) (right) at 25 °C and 1 atm. Source: (Hem, 1972; Brookins, 1998, pp. 54–57).

The updated list of hazardous substances published by (WFD-UKTAG, 2017) determined Cd as non-hazardous pollutant in groundwater. The EU-WFD sets concentration of Cd in surface waters at 1 µg/L.

3.1.1.2.3. LEAD (PB)

Lead is an abundant metal mostly occurs as ore mineral galena (PbS) on Earth's crust. Thus, lead pollution arises through the weathering of PbS as shown in Equation 3-8.

Although Pb occurs in various oxidation states, the most stable oxidation state under normal, oxidizing conditions is Pb (II). Presence of lead in most of the natural waters is minimal due to its low solubility and high sorption tendency onto sediments. Like Zn and Cd, below pH 7.1, Pb generally occurs in ionic form (Pb^{2+}) and above pH 7.1, it occurs as hydroxide and carbonate complexes (Hem, 1972; Kelly, 1988, p. 23; Huang, 2016).

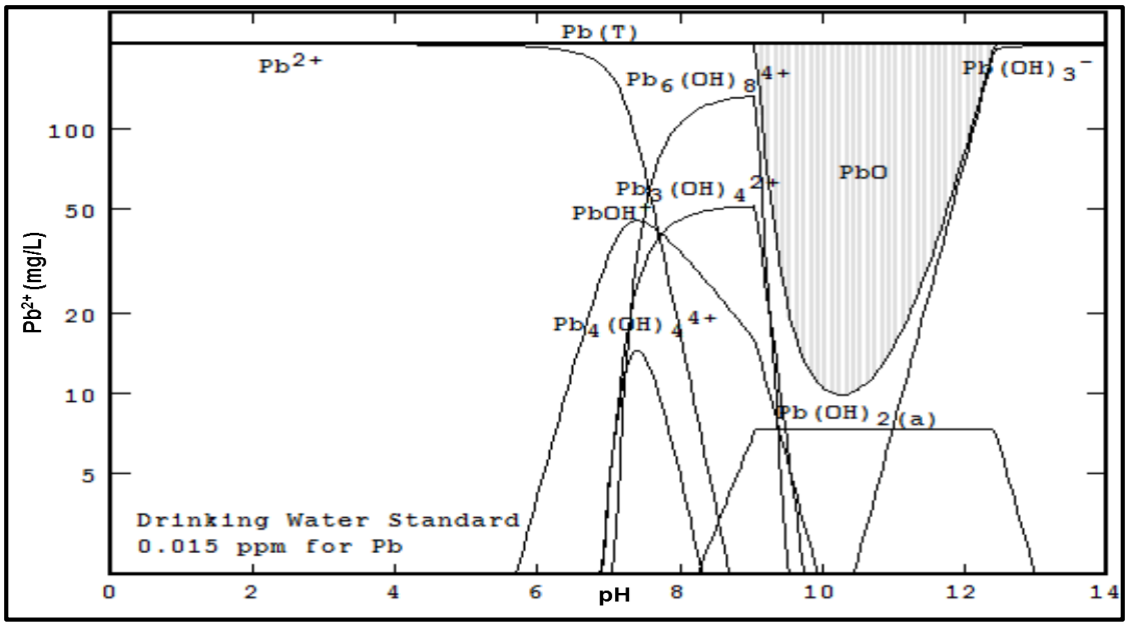

Figure 3-6: Occurrence of lead species with respect to pH of the water. Source: (Huang, 2016).

Lead is toxic to aquatic organisms, livestock and human. It has been reported that elevated concentration of lead affected neuro-psychological development in human and suffocation in fish. Lead can also damage brain functions, liver, reproductive system and kidney. The symptoms related to lead toxicity include anaemia, insomnia, headache, dizziness, weakness of muscles, hallucination and renal damages (Fu and Wang, 2011). Thus, use of lead to paint inside structures has been banned (Brookins, 1998). The water crisis in Flint, Michigan, USA, which affected over several thousand households, 100,000 residents, due to very high levels of lead in drinking water is a recent example of lead poisoning (Rifai, 2016; CNN, 2017; The Guardian, 2017). The updated list of hazardous substances published by (WFD-UKTAG, 2017) determined Pb as hazardous substance in groundwater.

3.2. ENVIRONMENTAL LEGISLATION FOR WATER QUALITY

A brief outline of environmental legislations in the EU and many other countries is given in section 2.1.7, p.23. Regarding mining influenced effluent in the UK, until recently there was no national mechanism or strategic approach for the remediation of mine water

discharged from non-coal mines (Johnston, Parker and Pritchard, 2007). The Coal Authority (CA) is now responsible for the remediation of water pollution arising from abandoned mines. However, for existing mines, the owners / operators have to comply with all current legislation (Johnston *et al.*, 2008; Coal Authority, 2016). Global and country (USA, EU, Canada, New Zealand, Australia, South Africa, Brazil and Indonesia) regulatory guidance for the mine waters is discussed elsewhere in (INAP, 2014, pp. 130–135). Discharge limits of hazardous substances in different countries is given in Appendix 9-2.

3.3. MINE WATER TREATMENT TECHNOLOGIES

The nature of mine water discharges from coal and metal mines are discussed in the sections 3.1.1.1, p.53 and 3.1.1.2, p.57 respectively. The polluted mine water discharge from a particular mine can be either acidic, circum-neutral or alkaline. Methods for the treatment of such polluted mine waters aim to neutralize acidity (raise pH), remove metals and sulfate are broadly categorized into two: the active treatment and the passive treatment (Brown, Barley and Wood, 2002; Younger, Banwart and Hedin, 2002; Miller et al., 2011; Pearce, 2014; USEPA, 2014). In practice, the selection of a treatment technology depends on the economic-environmental cost benefit analysis. A qualitative comparison of different categories of active and passive treatments is highlighted by INAP-GARD guidelines (INAP-GARD, 2014, p. 322). Some of the latest in-depth reviews of these technologies along with their application can be found in the literature (European Commission, 2003a; ITRC, 2010; Trumm, 2010; Pearce, 2014; INAP, 2014; USEPA, 2014). These technologies are briefly discussed below.

3.3.1. PASSIVE TREATMENT METHODS

Passive treatment of mine water refers to the processes that can be operated without frequent human intervention and employ naturally available construction materials such as soils and clays and treatment media such as wood chips and compost. A commonly accepted definition of passive treatment is:

"Passive treatment is the deliberate improvement of water quality using only naturally-available energy sources (e.g. gravity, microbial metabolic energy, photo-synthesis), in systems which require only infrequent (albeit regular) maintenance in order to operate effectively over the entire system design life" (Younger, Banwart and Hedin, 2002).

Passive treatment techniques aim to enhance the natural amelioration processes by raising the pH, reducing the contaminant mobility and solubility and facilitate the

precipitation, co-precipitation / sorption of metal ions. The main alkaline reagent in passive system is bicarbonate (HCO_3^-). Thus, passive treatment removes most of metal ions as their carbonate minerals (Younger, Banwart and Hedin, 2002; Warrender, 2009; USEPA, 2014). Although passive treatment is a cost-effective solution, its applicability is limited by the availability of large amount of land that determines the retention time of the mine water in the system. Thus, application of passive technologies in the UK is problematic as many mine sites are located in areas with steep sided valleys or minimal land space (Warrender, 2009; Pearce, 2014).

The mechanisms of remediation of acidic mine drainage have been well studied and there exists a range of passive treatment methods. Latest reviews of existing passive treatment methods and the related case studies reflecting costs, maintenance, effectiveness etc. can be found in (Pearce, 2014, pp. 27–33; INAP-GRAD, 2014; USEPA, 2014, pp. 73–88). A brief overview of the major passive treatment methods is given in the following sections.

3.3.1.1. ANOXIC LIMESTONE DRAINS (ALDS)

ALDs consist of cells or trenches with encapsulated limestone covered, usually 1 to 3 m, with clay or compacted soil so that inputs of atmospheric oxygen are minimized and the accumulation of CO_2 within the ALDs is maximized. The anoxic condition prevents ALDs from clogging by ochres and aluminum hydroxides. ALDs are designed to raise pH of the solution when AMD percolates through. The pH of the AMD rises due to the release of bicarbonate alkalinity via calcite ($CaCO_3$) dissolution. The divalent metals such as Fe^{2+} and Zn^{2+} remain in their reduced states due to anoxic conditions. Therefore, ALDs must be followed by a unit such as aeration cascade or aerobic wetland for metal oxidation, hydrolysis and precipitation to occur (Younger, Banwart and Hedin, 2002; USEPA, 2014).

For the successful operation of ALDs, characterization of AMDs must be done. Flow rate, dissolved oxygen, acidity and alkalinity, ferric and ferrous iron and aluminum concentration are the parameters to be considered. The speciation of iron (Fe^{2+} and Fe^{3+}) is necessary for AMDs with pH less than five. If Fe^{3+} is present, pre-treatment to reduce Fe^{3+} to Fe^{2+} is needed. This is to consume acidity as in Equation 3-3. The contact time (residence time) necessary for the maximum concentration of alkalinity is around 15 hours. ALDs are suitable only for AMDs containing less than 1 mg/L of dissolved oxygen and less than 2 mg/L each of Fe^{3+} and Al^{3+}. A vent for the release of excess CO_2 in the

ALDs helps functioning of the system (Younger, Banwart and Hedin, 2002; INAP-GARD, 2014; USEPA, 2014).

Figure 3-7: Cross-section of an Anoxic Limestone Drain (ALD). Source: (USEPA, 2014, p. 11).

3.3.1.2. OXIC LIMESTONE DRAINS (OLDS)

OLDs are physically identical to ALDs but they differ in terms of openness to atmospheric oxygen. OLDs are open to the atmospheric oxygen thus AMDs which are not suitable (AMDs containing more than 1 mg/L of dissolved oxygen and more than 2 mg/L each of Fe^{3+} and Al^{3+}) for ALDs can be treated using OLDs. The Fe^{2+}, Fe^{3+} and Al^{3+} oxidize to their hydroxides and precipitate in settling pond. The clogging of OLDs is prevented by maintaining rapid flow velocities (> 0.1 m/min) within the system and retain ferric and / or aluminum hydroxides in suspension. OLDs can generate up to 120 mg/L of alkalinity (as $CaCO_3$ equivalent) in only two to three hours residence time. OLDs are suitable for the treatment of AMDs in mountainous terrain, slopes > 20 %, where other options would be infeasible (Younger, Banwart and Hedin, 2002; INAP-GARD, 2014).

3.3.1.3. REDUCING AND ALKALINITY PRODUCING SYSTEM (RAPS)

RAPS, originally known as SAPS (Successive Alkalinity Producing Systems), are designed to counter major drawbacks of ALDs and treat AMDs without limit to the concentrations of O_2, Fe^{3+} and Al^{3+}. RAPS method is an improvised version of an ALD thus composed of an ALD overlain by a compost bed (Figure 3-8). The compost layer supply nutrients for the iron and sulfate-reducing bacteria and lies beneath 1 - 3 m of water. AMD flows into the pond on top of RAPS which then flows down through the permeable compost layer (0.15 to 0.6 m thick) which strips dissolved oxygen and reduces ferric iron (Fe^{3+}) to ferrous iron (Fe^{2+}) before passing through limestone bed (0.6

m to 1.2 m thick) which produces alkalinity. The RAPS unit is generally followed by a sedimentation pond or aerobic wetland to facilitate precipitation of metal complexes. RAPS are more efficient than simple compost wetlands and require less land. However, they require substantial driving head that makes them unsuitable in topography with less than 5 m relief (Younger, Banwart and Hedin, 2002; INAP-GARD, 2014; USEPA, 2014).

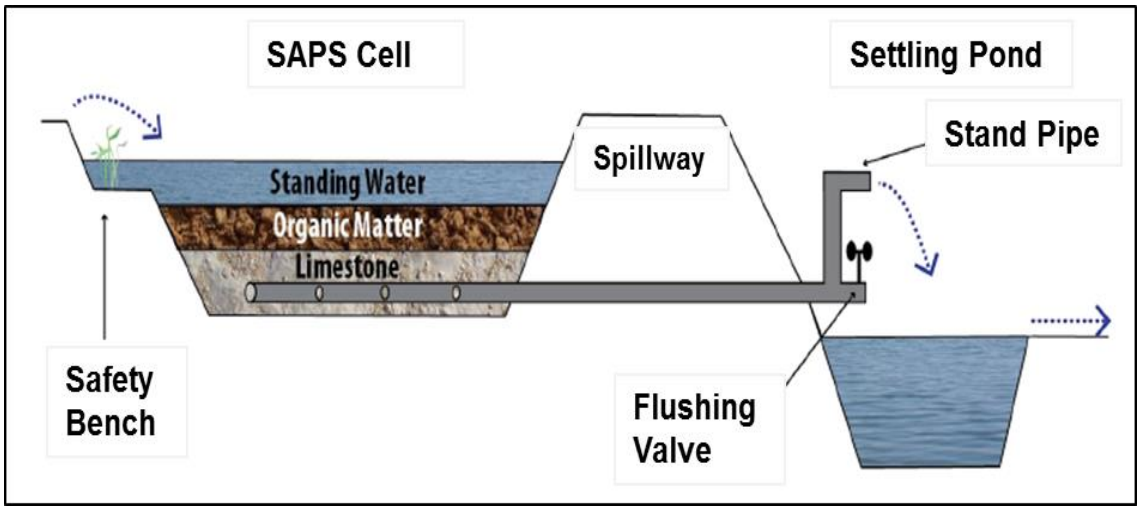

Figure 3-8: Layout of a Reducing and Alkalinity Producing System (RAPS = SAPS). Source: (USEPA, 2014, p. 16).

3.3.1.4. CONSTRUCTED WETLANDS

Constructed wetlands are biologically active systems such as bogs, swamps or marshes designed for the treatment of polluted waters. Wetlands are constructed on the land surface using crushed rocks and plants that grow in wetlands. Wetlands can be used to treat sulfate and various metals such as manganese and copper from acidic, neutral and alkaline mine drainage. Constructed wetlands can be differentiated into aerobic wetlands and compost wetlands and the flow direction can be vertical or horizontal (ITRC, 2010; USEPA, 2014).

Aerobic wetlands are constructed to enhance the oxidation and hydrolysis of dissolved metals and generally consist of wetland plants in a shallow substrate. Aerobic wetlands also known as 'Reed Beds' are proven effective in the treatment of alkaline and ferruginous mine waters. The iron is removed by means of settlement of Fe-hydroxides, filtration of suspended materials, uptake by plants, and precipitation as Fe-oxide / hydroxide. Aerobic wetlands are suitable for the treatment of AMDs due to the release of acidity (H^+) as a result of oxidation of Fe^{3+} and Al^{3+}, further mobilizing the metals (Younger, Banwart and Hedin, 2002; Ziemkiewicz, Skousen and Simmons, 2003).

Conventional aerobic wetlands are unsuited to the removal of zinc from mine waters (Pearce, 2014).

Compost wetlands, occasionally known as anaerobic wetlands, are constructed to consume acidity and precipitate metals by chemical and microbial sulfate reduction in a thick anoxic compost layer of organic material. The compost layer can be composed of animal manure, bark, sawdust, paper-making waste, peat, wood chips, crushed limestone, grass cuttings, hay etc. Compost wetlands are considered effective for the treatment of acidic mine water. The metals can be removed as sulfide, hydroxide and carbonate precipitate (Younger, Banwart and Hedin, 2002; USEPA, 2014).

The advised retention time of approximately 14 days demands an unrealistic amount of land for the construction of wetland to treat mine drainage with large flow rate. Application of conventional wetlands is neither efficient nor cost effective for the removal of zinc, cadmium and lead (Pearce, 2014). Despite extensive published literature, application of constructed wetlands limited to the treatment of storm water and municipal wastewaters (ITRC, 2010).

3.3.1.5. PERMEABLE REACTIVE BARRIERS (PRBS)

PRBs are in-situ techniques consisting of very simple engineered walls made of permeable reactive materials that are placed in the form of a 'barrier' across the flow path of polluted mine waters (see Figure 3-9). Improvement in down-stream water quality results from the adsorption and biochemical reactions that take place while polluted water flows through the barriers. PRBs rely on gradient of groundwater table. A range of reactive materials such as zero valent iron (ZVI), activated carbon, activated alumina, apatite, municipal compost, manure, peat, clay minerals, limestone and zeolites etc. have been used in PBR systems (Powell *et al.*, 1998; Younger, Banwart and Hedin, 2002). Selection of the best reacting material for the design of PRBs depends upon the target pollutant and the mine water chemistry.

There are two types of PRBs: (i) Continuous barriers, in which the barrier is installed across the groundwater contaminant plume, and (ii) Funnel-and-gate barriers, in which funnel walls divert contaminated water into a gate made of permeable reactive medium (Younger, Banwart and Hedin, 2002; Warrender, 2009). An in-depth review of potential reactive materials for PRBs can be found in (Warrender, 2009, p. 23 to 36).

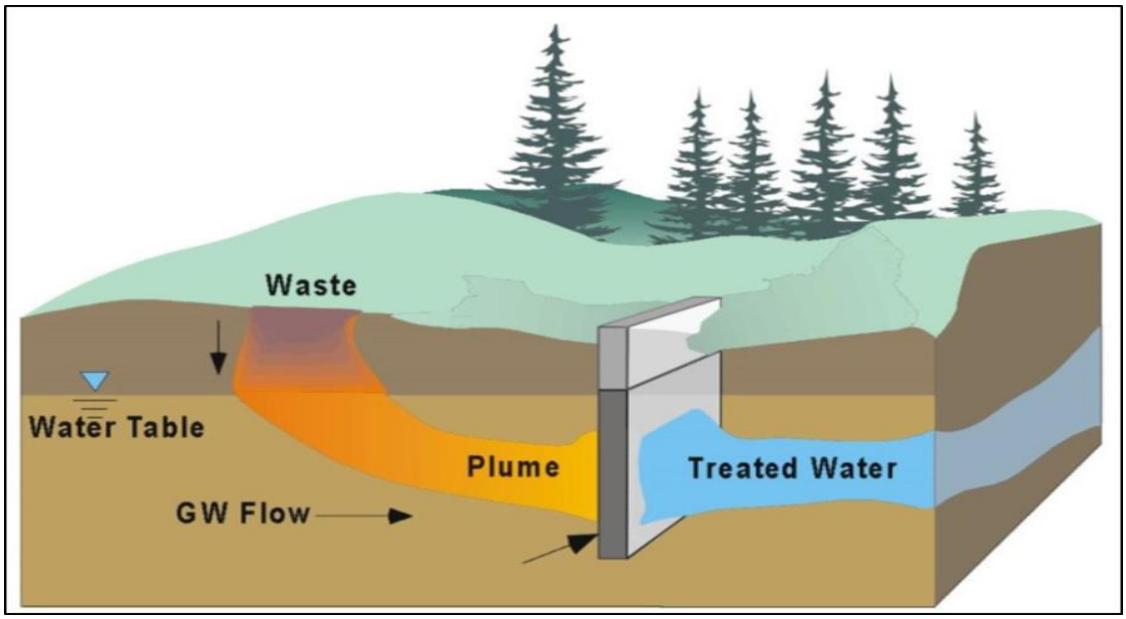

Figure 3-9: A schematic diagram of Permeable Reactive Barrier (PRBs). Source: (Powell et al., 1998, p. 1).

In summary, despite of being cheaper options, in the past decade, there has been little change or advancement of passive treatment technologies such as wetlands, aeration cascades, limestone drains and settling ponds. Removal of zinc and cadmium found to be difficult using purely passive treatment methods (Pearce, 2014).

3.3.2. ACTIVE TREATMENT METHODS

Active treatment of mine water is the application of conventional wastewater engineering and is defined as "*the improvement of water quality by methods which require ongoing inputs of artificial energy and / or (bio)chemical reagents*" (Younger, Banwart and Hedin, 2002). Thus, active treatment refers to the technologies requiring ongoing human resources for maintenance and monitoring based on external sources of energy, infrastructure and engineered systems (INAP, 2014; USEPA, 2014). Treatment processes in active technologies can be controlled as required and this can be done with the workforce or automated system on site. Therefore, active treatment technologies are better suited to working mines, mines with large flow (discharge) rate and less land-space (Brown, Barley and Wood, 2002; Younger, Banwart and Hedin, 2002).

The conventional ODAS (Oxidation, Dosing with Alkali and Sedimentation) is the most commonly-used approach amongst the variety of active treatment technologies. The others include ion exchange, (bio)sorption, sulfidization, reverse osmosis, membrane filtration and bio-sedimentation (Younger, Banwart and Hedin, 2002; Trumm, 2010;

INAP, 2014). The technologies based on ODAS approach consist of three phases (Younger, Banwart and Hedin, 2002):

a) *Oxidation (O)*: aims to transform soluble metal ions such as Fe^{2+} into less soluble oxidized forms such as Fe^{3+};

b) *Dosing of Alkali* (DA): aims to raise the pH of the acidic mine water and buffer the pH reduction arising due to release of protons during hydrolysis of insoluble metal ions such as Fe^{3+} to hydroxide solids. The main alkaline reagent in active system is hydroxyl (OH^-). Thus, active treatment removes most metal ions as their hydroxides.

c) *Sedimentation* (S): aims to remove metal hydroxide solids from solution by means of sediment. Sedimentation can be enhanced via addition of coagulants.

The nature of the mine water determines the order of above three stages (O, DA and S). Therefore, the suitable order for AMD would be DA, O and S, for highly carbonated waters would be O, DA, O and S and for waters with inert solids would be S, DA, O and S (Younger, Banwart and Hedin, 2002; Trumm, 2010). The ODAS steps are discussed below.

3.3.2.1. OXIDATION

Oxidation stage in mine water treatment is designed to supply oxygen that is required to oxidize all the soluble metal ions present in the water. Oxidation step can also help stripping off excess CO_2 from circum-neutral and strongly alkaline mine waters thereby causes the pH to rise which promotes the rate of oxidation of pollutants (Younger, Banwart and Hedin, 2002; INAP, 2014). There exist a range of oxidation techniques, the most common are given below.

3.3.2.1.1. AERATION

Aeration is the most popular oxidation technique used in mine water treatment and it can be performed before or during treatment. Aeration can be achieved via several methods. The most popular include cascade, trickle filter also known as aerated biological filters and percolating filters, in-line venturi devices (a system for speeding the flow of the fluid by constricting through a cone shape) and mechanical means, for example jetting the water at high pressure into mechanically stirred tanks. It is documented that oxidation of about 50 mg/L of Fe^{2+} via cascade aeration and 900 mg/L Fe^{2+} via in-line system venturi devices have been achieved (Brown, Barley and Wood, 2002; Younger, Banwart and

Hedin, 2002). The detailed explanation of these techniques can be found in the literature (Younger, Banwart and Hedin, 2002; INAP, 2014).

3.3.2.1.2. BIOCHEMICAL OXIDATION BY RBC

Rotating Biological Contactors (RBCs) are based on the growth of bacterial colonies on the surfaces of slow-rotating disks. RBCs are better suited for acidic mine waters as enhanced bacterial oxidation of metal ions occurs at low pH. RBCs would be suitable for small discharges rich in Fe^{3+}, aluminium or dissolved oxygen for treatment using anoxic limestone drain. Evidence shows that a RBC can remove over 90 % of initial iron content (44 mg/L up to 200 mg/L) from acidic mine water (Younger, Banwart and Hedin, 2002).

3.3.2.1.3. CHEMICAL OXIDATION

Chemical oxidation is an alternative to aeration and oxidation by RBCs. Oxidants such as H_2O_2, sodium hypochlorite (NaOCl) and potassium permanganate ($KMnO_4$) can be dosed directly into mine water stream. The dosing rate for H_2O_2 (35%) is advised as 350 µg/L per gram of Fe (II) iron in the mine water. Use of conventional oxidants such as chlorine and ozone is rare due to high cost (Younger, Banwart and Hedin, 2002).

3.3.2.2. DOSING WITH ALKALI

The purpose of alkali dosing in mine water is to raise the pH (neutralization) of AMD and promote precipitation of metals. The reactions governing precipitation of metal ions to their hydroxides and sulfides are given by Equation 3-11 and Equation 3-12 respectively. The hydroxides and sulfides of metals are amphoteric, capable of accepting or donating proton resulting in either increase or decrease pH of solution. If the pH of the solution reach beyond the point of minimum solubility then precipitated metals can be potentially remobilize back into solution. The guideline residual solubility of selected metal hydroxides and sulphides are given in Figure 3-10 and Figure 3-11 respectively (Pearce, 2014; INAP, 2014).

$$M^+(aq) + OH^-(aq) \rightarrow MOH\ (s) \qquad \textit{Equation 3-11}$$

$$2M^+(aq) + S^{2-} \rightarrow M_2S\ (s) \qquad \textit{Equation 3-12}$$

For cost effective treatment, pre-aeration before alkali dosing is advised for mine waters with high dissolved CO_2. The dose of alkali depends up on the targeted metal removal as minimum pH values for the complete precipitation of dissolved metals to their hydroxides vary significantly as shown in Table 3-3.

The common alkali used in neutralization process are lime (CaO), limestone ($CaCO_3$), caustic soda (NaOH) and sodium bicarbonate (Na_2CO_3). In general, calcium based alkali are inexpensive and react slower than sodium based alkali. Carbonate alkali raise the water pH up to 8.5 whereas hydroxide alkali can raise the pH above 10. The list of other alkali used in neutralization of mine water can be found in (Brown, Barley and Wood, 2002, p. 40).

Table 3-3: pH values for complete precipitation of dissolved metals to their hydroxides.

Metal ion	pH
Fe^{2+}	5.3[d], ~8.0[a], 8.5[b] and 9.5[c]
Fe^{3+}	2.0[d], ~ 3.5[a], 3.5[b] and 4.3[c]
Zn^{2+}	6.7[d], 8.2[b], 8.4[c] and ~8.5[a]
Pb^{2+}	6.0[d], 6.3[c] and ~6.5[a]
Cd^{2+}	6.7[d], 9.8[c] and ~ 10.0[a]
Mn^{2+}	8.5[d], 10.2[b], 10.6[c] and ~ 10.6[a]
Ni^{2+}	6.7[d], ~9.3[a] and 9.3[c]
Al^{3+}	4.1[d], ~4.5[a] and 5.2[c]
Cr^{3+}	5.3[d]
Cu^{2+}	5.3[d]
Co^{2+}	6.9[d]
Hg^{2+}	7.3[d]

Source: (INAP, 2014)[a], (Younger, Banwart and Hedin, 2002)[b], (Brown, Barley and Wood, 2002)[c] and (Igwe, 2007)[d].

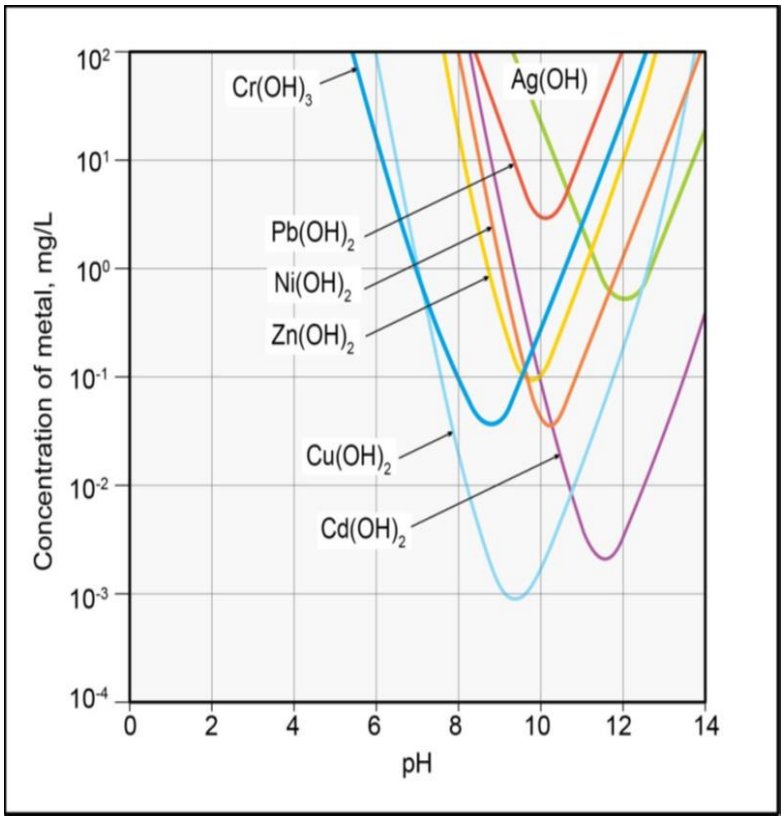

Figure 3-10: Solubility of selected metal hydroxide as a function of pH. Source: (Pearce, 2014, p. 38).

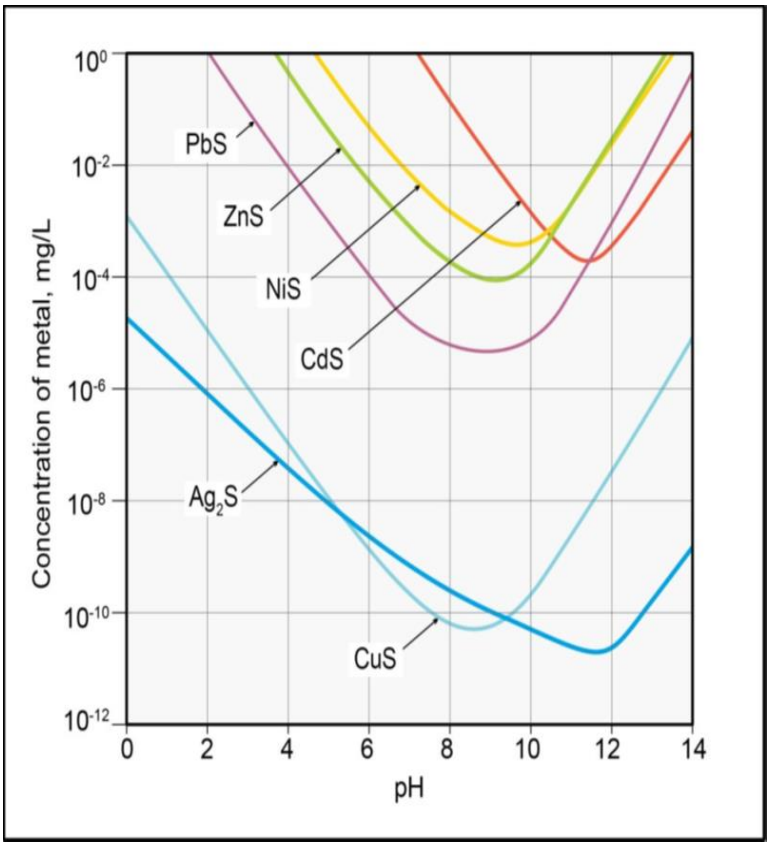

Figure 3-11: Solubility of selected metal sulfides as function of pH. Source: (Pearce, 2014, p. 41).

3.3.2.3. SEDIMENTATION

The suspended hydroxides of metals formed after alkali dosing can be removed by sedimentation. Sedimentation can be achieved via gravity settlement in ponds or clarifiers / thickeners. Sedimentation ponds are cheaper to operate but require large space. In contrast to ponds, clarifiers are more expensive to operate but require less space. Sedimentation can be enhanced via coagulation and flocculation by using chemicals such as starch and aluminium sulfate. Detail lists of chemicals for coagulation and flocculation are given in (Brown, Barley and Wood, 2002, p. 45).

3.3.2.4. SULFIDIZATION AND BIODESALINATION

Sulfidization is the conversion of sulfate (SO_4^{2-}) to sulfide species ($HS^{-\bullet}$, H_2S) under reducing conditions. The sulfide species thus converted can react rapidly with the divalent dissolved metal ions and precipitate as sulfide solids. Trivalent metal ions such as Fe^{3+} and Al^{3+} do not form sulfide precipitate at the temperature and pressure of earth surface. However, rise in pH is possible during sulfate reduction process. Therefore, precipitation of trivalent metal ions to their hydroxides may occur if the required pH values given in Table 3-3 are attained. Sulfidization is a biological treatment process which is immeasurably slow in the absence of sulfate-reducing bacteria. For sulfidization, bacteria are given a carbon source and a substrate for adhesion in the form of organic matter such as compost (Younger, Banwart and Hedin, 2002). The passive treatment system using compost wetlands are also based on sulfidization process.

Biodesalination is a treatment method which incorporates mixing of metal rich mine effluent with sulfur species rich effluent containing sulfate-reducing bacteria so that sulfidization continues and metals from mine effluent can be used to help sulfide precipitate from sulfur rich effluent. A pioneering example of biodesalination was demonstrated in South Africa by mixing mine water with tannery effluent (Younger, Banwart and Hedin, 2002).

3.3.2.5. MEMBRANE PROCESSES

Membrane processes are based on the filtration of contaminants from brackish and saline waters such as mine discharge. The polluted water is forced to pass through membrane at high pressure and the contaminants bigger than diameter of the pore size of membrane are trapped and as a consequence highly concentrated brine and sludge are left upstream. Application of membrane processes to mine discharge is challenging because of high cost, scaling and fouling potential. Membrane processes are known by

various names depending on the pore size diameter (ϕ) (Younger, Banwart and Hedin, 2002; INAP, 2014):

Microfiltration, used for bacterial removal from water, 0.1 μm ≥ ϕ < 0.45 μm.

Ultrafiltration, used for removal of colloids present in water, 0.01 μm ≥ ϕ < 0.1 μm.

Nanofiltration, used for colour removal from water, 0.001 μm ≥ ϕ < 0.01 μm.

Reverse osmosis (RO): used to remove solutes from water, ϕ < 0.001 μm. It is not common in mine water treatment due to high cost. However, it can be the option if the mine water contain economically valuable resources. For example, two full-scale RO plants have been constructed to recover salt from highly-saline mine waters of Upper Silesia, Poland (Younger, Banwart and Hedin, 2002).

3.3.2.6. EXTRACTION

Although there are some laboratory demonstration for the treatment of mine water discharges using extraction techniques, its application at larger scale is rare. Extraction can be achieved by solvent, electrochemical and biochemical methods.

Solvent extraction technique involves agitation of an immiscible organic solvent with the mine water until the targeted metal partitioned into the solvent. The solvent is then separated from the mine water and metal can be recovered. This method is used in the processing of uranium and gold (Younger, Banwart and Hedin, 2002).

Electrochemical extraction technique involves suspension of electrodes in the mine water. Electrodes are supplied with appropriate electrical current so that targeted metals can be attracted towards and precipitate onto them (Younger, Banwart and Hedin, 2002).

Biochemical extraction technique involves use of bio-surface to absorb metals. This can be done in both active and passive treatment mode. Biochemical extraction can be done via several techniques such as bio-sorption of metals by microbes, bio-concentration (phytoremediation) of metals by algal uptake and removal of metals using genetically engineered plants (hyperconcentrators) that can uptake metals at very high concentration (Younger, Banwart and Hedin, 2002).

3.3.2.7. SORPTION

Sorption is transfer of ions from liquid phase to the sorbents, the solid phase. Thus, it describes every type of removal (adsorption or absorption) of a solute to an external

surface of solids, liquids and internal surface of porous solids or liquids. The term sorption is commonly used when a specific removal mechanism is not known. Adsorption refers to the accumulation of adsorbate onto the surface of the adsorbent whereas absorption refers to the diffusion of the sorbate into the adsorbent. According to the bonding involved, sorption can be classified as Physical, Chemical and Electrostatic sorption (ion exchange) (Smith, 1999; Inglezakis and Poulopoulos, 2006; Hartley, 2009).

Physical sorption, known as physisorption, occurs without exchange of electrons. It is independent of the electronic properties of the molecules due to intermolecular attractions between favourable sites. Physisorption may occur in multiple layers as relatively weak van der Waals forces hold the adsorbate to the surface.

Chemical sorption, known as chemisorption, results in formation of chemical bond through the exchange of electrons between solute molecules and surface sites. It is characterized by interaction energies between the adsorbate and surface thus only a single layer can be adsorbed.

Electrostatic sorption occurs due to the Coulomb attractive forces between ions and charged functional groups and commonly known as ion exchange.

Sorption process is generally accomplished in three steps: transport of contaminant from solution to the sorbent surface; adsorption on to the surface of sorbent; and transport within the sorbent (Barakat, 2011). Sorption (adsorption and ion exchange) based processes are considered as potential alternatives for the treatment of aqueous solutions (Gode and Pehlivan, 2006). The modified polyacrilonitrile (PAN) mesh used in this project exhibits properties of a sorbent (adsorbent and ion exchanger). Thus, the related processes are discussed separately.

3.3.2.7.1. ADSORPTION

Sorption based processes are seen as an alternative remediation technique for wastewater treatment. Adsorption is a well-established, effective and economic technology for the remediation of mine waters (Mohan and Singh, 2002; Fu and Wang, 2011). "*Adsorption simply is the ability to adhere or attach to a substance"* (Igwe, 2007).

Metal partition between solid phase (adsorbent) and solution phase can be affected by several factors. Metals tend to present in the solution phase at low pH, reducing conditions, low particulate loads, and (or) high dissolved concentrations of a strong complexing agent. Thus, sorption of metal ions relies heavily on experimental conditions

such as solution pH, metal concentration, ligand concentration, competing ions, and particle size (Bailey *et al.*, 1999; Smith, 1999).

The design and operation of an adsorption process is flexible. Adsorbents can be regenerated in reversible adsorption process (Fu and Wang, 2011). A range of adsorbents exists from mineral, biological origin, zeolites, industrial by-products, agricultural wastes, biomass, and polymeric materials (Barakat, 2011). Despite of extensive use as an adsorbent, activated carbon remains an expensive material (Barakat, 2011; Fu and Wang, 2011; Hegazi, 2013). Thus, recent studies are focussing on the development of easily available low-cost adsorbents from biological origin. Agricultural and plant waste products such as sugarcane bagasse, papaya wood, maize leaf, rubber leaf powder, coriander, peanut hull pellets, fern tree, grape stalk wastes, neem bark, oil palm shell, rice husk, coconut shell husk, sawdust, coffee husk, potato peels, eggshell, chitosan etc., industrial by-products such as lignin, diatomite, clino-pyrrhotite, lignite, aragonite, natural zeolites, clay, kaolinite, peat etc. and algal biomass and microbial biomass have been used (Bailey *et al.*, 1999; Ngah and Hanafiah, 2008; Barakat, 2011; Fu and Wang, 2011; Hegazi, 2013).

The application of adsorbents based on plant products can result in low adsorption capacity with added total organic carbon (TOC), chemical oxygen demand (COD) and biological oxygen demand (BOD) in treated effluent. The increase in TOC, COD and BOD is due to the release of soluble organic compounds from plants. Some of the above plant products such as rice husk, sawdust, peanut husks and shells, sugarcane bagasse etc. have been chemically modified to enhance chelating efficiency and sorption capacity and minimize the contribution to TOC, COD and BOD (Ngah and Hanafiah, 2008).

3.3.2.8. ION EXCHANGE

Ion exchange mechanism is accredited to two agricultural scientists H.S. Thompson and J.T. Way who, in 1848, passed a solution of manure through a bed of ordinary loamy soil and found that ammonia was removed from the solution. Afterward, many studies were performed to test soil and clays, natural and synthetic aluminum silicates and synthetic zeolites as ion exchange materials. The first synthetic organic resins were synthesized in 1935 (Chen *et al.*, 2006; Inglezakis and Poulopoulos, 2006). Historical milestones of ion exchange process is given in (SenGupta, 2017, pp. 3–5).

Ion exchange is a specialty sorption process where undesired contaminant ions from the liquid phase interchange (exchange) with more desirable ions of a similar charge

adsorbed to solid phase. Ion exchange material can be of natural substances or synthesized. Ion exchange is influenced by capacity, sorption affinity for targeted ionic species, and desorption and regeneration efficiency for desired application (Chen *et al.*, 2006; Inglezakis and Poulopoulos, 2006; ITRC, 2010; USEPA, 2014). According to Zagorodni, 2007, *ion exchange "is the equivalent exchange of ions between two or more ionised species located in different phases, at least one of which is an ion exchanger. The process takes place without the formation of chemical bonds".*

Although ion exchange process is analogous to adsorption process in many aspects, there are distinct differences. Electrically neutral species are sorbed in adsorption whereas ions are the sorbed species in ion exchange. Ion exchange is a stoichiometric (quantitative relationships between substances that undergo a physicochemical change) process and for every ion removed from the solution, another ion of same sign is released into the solution. The ions that take part in the exchange are called counter ions. The ions in the liquid phase that have same charge as that of ion exchanger are called the co ions (Chen *et al.*, 2006; Inglezakis and Poulopoulos, 2006; Zagorodni, 2007).

Ion exchange forms the basis of several chemical processes involving substitution, separation, and removal of ions. In substitution, commercially low or no valued ions on ion exchange material are replaced with valuable ions of same charge. Separation occurs according to the affinities between ions and the ion exchange material (Chen *et al.*, 2006). The affinity of ion exchange resin is "*a product of a combination between the type of functional groups, type of matrix, cross-linking degree, ion exchange capacity, swelling, and even the composition of the surrounding media"* (Zagorodni, 2007).

Ion exchange process is gaining interest due to its high efficiency, selectivity, better recovery of metal value, less sludge production, and low operational costs (Alyüz and Veli, 2009; Fu and Wang, 2011). Today, ion exchange is applied to multidiscipline. A list of applications of ion exchange technology is given elsewhere (Zagorodni, 2007, p. 4). According to European Commission, ion exchange is one of the best available techniques (BAT) for the treatment of wastewaters polluted by metals and inorganic salts (Inglezakis and Poulopoulos, 2006). In water treatment, ion exchange can be applied for the removal of hardness, alkalinity, radioactive waste, ammonia and metals (Alchin and Wansbrough, 2002; USEPA, 2014). It is found that ion exchange works best for waters in the pH range of four to eight, low amount of iron, aluminum and suspended solids. The presence of iron and aluminum can form precipitates and armour the ion exchanger, especially the resin (ITRC, 2010).

3.3.2.8.1. ION EXCHANGERS (RESINS AND FIBRES)

Ion exchangers are cross-linked insoluble polymers that are capable of exchanging ions attached on their fixed sites, without physical alteration, to the ions in a solution that is passed through them. The charge of the ions exchanged determines the type of exchangers, cation or anion exchangers. Amphoteric ion exchangers are capable of exchanging both cation and anion. Ion exchangers can be natural products such as soil and zeolites or synthetic. Synthetic exchangers are commonly preferred in water treatment as they are inexpensive and effective in removing metals (Alchin and Wansbrough, 2002; Chen *et al.*, 2006; Gode and Pehlivan, 2006; Alyüz and Veli, 2009; Fu and Wang, 2011).

3.3.2.8.2. PROPERTIES OF ION EXCHANGE RESINS

The differences in origin, composition and structures of ion exchangers result in different sorption properties that distinguish them as ion exchangers. The properties that characterize the performance of ion exchangers can be classified into physical and chemical and are summarized in Table 3-4. More information about these properties can be found in the literature (Harland, 1994, pp. 49–88; Chen *et al.*, 2006, pp. 263–270; Zagorodni, 2007, pp. 9–54)

Table 3-4: Main properties of ion exchangers.

Chemical properties	Physical properties
Matrix (polymer structure)	Physical structure and morphology
Cross-linking degree	Particle size
Type of functional groups	Pore size and morphology
Ion exchange capacity	Surface area
Ionic form	Partial volume in swollen state
Selectivity	
Swelling	

Source: (Harland, 1994; Chen *et al.*, 2006; Zagorodni, 2007).

3.3.2.8.3. ION EXCHANGE FIBRES

The physicochemical limitations of ion exchange resins such as filter ripening and pore clogging, slow exhaustion and regeneration kinetics due to mass transfer limitation, size

constraints, vulnerability to damage etc. have been overcome by developing many functional polymers as highly effective fibrous adsorbents, the ion exchange fibres. The fibrous structure provides numerous advantages: short diffusion passes providing up to hundred times faster sorption rates; mechanically durable; allow designing of packet reactors with minimal pressure drops; allow unusual possibilities for new technological designs; simplification of the overall synthesis; environmentally friendly (Zagorodni, 2007; Jassal et al., 2014; Xu *et al.*, 2017).

A range of modified fibres such as polyester, polyacrylonitrile (PAN), polypropylene etc. containing varied functional moieties such as hydrated ferric oxide, carboxyl, amide, amidoxime etc. have been developed. These fibres contain large specific surface area and quick mass transfer velocity (Ishtchenko et al., 2003; Wei *et al.*, 2005; Vatutsina *et al.*, 2007; Jassal *et al.*, 2014; Xing et al., 2015; Deng et al., 2016; Xu *et al.*, 2017). PAN fibre is one of the widely used material which is discussed in the following section.

3.3.2.8.3.1. MODIFIED POLYACRYLONITRILE (PAN) FIBRE

The starting material of PAN is acrylonitrile (CH_2=CHCN). According to the contents of acrylonitrile units, PAN fibres are classified into two: acrylic fibre proper (≥ 85 % acrylonitrile units) and modified acrylic fibres, also known as modacrylic fibres (35 – 85 % acrylonitrile units) (Sebesta et al., 1995). PAN is considered as the most promising fibre-forming polymer. PAN fibre has large surface area, high thermal, mechanical and chemical stability, abrasion resistance, desirable chemical resistance, resistant to corrosion and mildew, low flammability and low cost (Zhang et al., 2009; Jassal *et al.*, 2014; Xing *et al.*, 2015; Deng *et al.*, 2016; Xu *et al.*, 2017).

PAN only dissolves in aprotic polar organic solvents such as acetonitrile and Acetone, concentrated sulphuric acid and nitric acid and concentrated aqueous solutions of some inorganic salts. PAN forms hydrogen bonds, transition metal ion complexes, donor-acceptor complexes and undergoes a number of chemical transformations. It yields primary polyamine by hydrogenation, poly(hydroxamic acid) and poly(amidoxime) with hydroxylamine, and polyacrylic acid by alkaline hydrolysis (Sebesta *et al.*, 1995).

Additionally, PAN fibre contains an abundance of (cyano) nitrile groups that can be easily modified into several functional moieties such as carboxyl, amide, amidoxime (Zhang et al., 2009; Jassal *et al.*, 2014; Xing *et al.*, 2015; Xu *et al.*, 2017). The raw PAN fibre that has no ability to bind metal ions can be modified with low-molecular weight ligands and activate the metal binding ability (Deng *et al.*, 2016).

Acidic, neutral and alkaline hydrolysis of nitrile groups in PAN hydrolyze to amides, cyclic imides, carboxylates and poly (acrylic acid) (Sebesta *et al.*, 1995). Fibrous ion exchangers developed from PAN contain both cation and anion exchange groups, substantially larger amount of anionic groups than cationic (carboxylic acid) groups. The pH of the medium determines the type of ions exchange. At high pH they function as cation exchangers (Vatutsina *et al.*, 2007; Chaudhary and Farrell, 2014).

A range of functionalized PAN fibres have been developed for the removal of metal ions such as mercury (Deng et al., 2015; Xu *et al.*, 2017), copper (Jassal *et al.*, 2014; Deng *et al.*, 2015), cadmium and lead (Zhang et al., 2009; Deng *et al.*, 2016), silver (Xing *et al.*, 2015), zinc (Zhang et al., 1994). PAN fibre was modified at De Montfort University, see step two in section 2.2.3.2, p. 46 to produce an ion exchange fibrous mesh shown in Figure 3-12 (Ishtchenko, Huddersman and Vitkovskaya, 2003).

During modification of PAN, carboxylic acid groups form through hydrolysis of nitrile groups (Vatutsina *et al.*, 2007; Orlova, 2010). Carboxylate groups can be formed by the hydrolysis of amide end groups. Polyconjugated cyclic structures can also be formed due to incomplete hydrolysis of nitrile group with NaOH. Polyconjugated cyclic structures, carboxyl and amide end groups formed on the modified PAN mesh are able to ligate the metal cations to the fibre (Ishtchenko, Huddersman and Vitkovskaya, 2003).

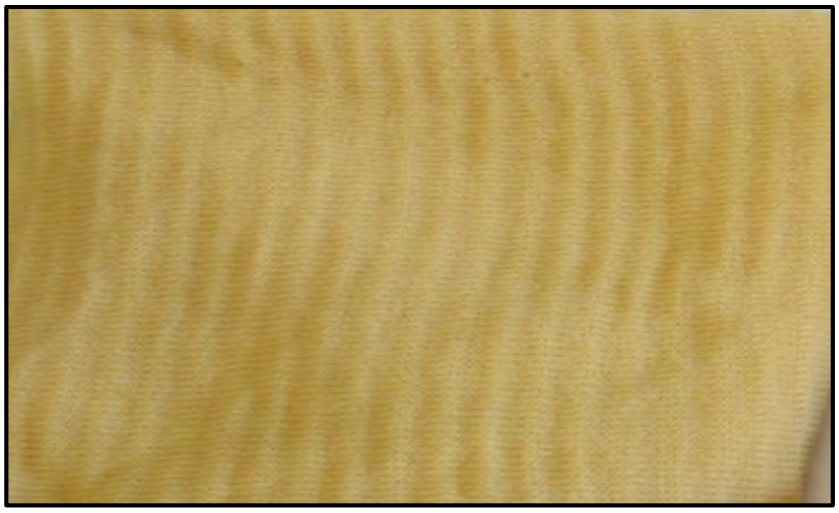

Figure 3-12: Modified PAN ion exchange mesh used in the remediation of mining influenced effluent.

Hydrolysis at high pH of hydrazine or polyamine may convert nitrile groups to carboxamide and carboxylate functional groups which can be introduced to fibre by further treatment with NaOH (Chaudhary and Farrell, 2014). Formation of hydrazide group by cross-linking of hydrazine with PAN fibre has been reported (Liu et al., 1999).

Formation of anion exchange groups such as amine and amino (NH, NH_2) on modified PAN fibre, during hydrazine modification, has also been reported (Chaudhary and Farrell, 2014).

In summary, modified PAN mesh shown in Figure 3-12 contains both cation and anion exchange groups and hence behaves as an ion exchanger. The pH determines the cation and anion exchange properties of the modified PAN mesh. The ion exchange capacity of modified PAN mesh reported by (Orlova, 2010) shows existence of ~ 80 % cation exchange groups on the modified PAN mesh. It was the same mesh used in this project for the remediation of circum-neutral mine water. Since, modified PAN mesh was produced after NaOH (alkali) treatment, the carboxylic groups are mostly in the form of carboxylate (-COONa) form and only few in (-COOH) form. In such, the ion exchange mechanism takes place as in Equation 3-13. The modified PAN mesh also has complexometric oxime groups arising from treatment with hydroxylamine.

$$2RCOONa + M^{2+} \rightarrow (RCOO)_2M + 2Na^{+}$$ ***Equation 3-13***

Where M and R represent metal ions in the solution and PAN fibre respectively.

CHAPTER FOUR

4. OPTIMIZATION OF DYE TREATMENT PROCESS

4.1. INTRODUCTION

The environmental and biological health problems associated with the dyes and textile effluents discussed in chapter two highlighted the need for a proper treatment before discharging into the natural water system. Chapter two also provides a brief discussion of the technologies available for the treatment of refractory organic pollutants such as synthetic azo dyes. Advanced oxidation processes (AOPs), such as Fenton-like oxidation, are considered the best alternative for the treatment of such recalcitrant substances (Slokar and Marechal, 1998; Pizzolato *et al.*, 2002; Oliveira *et al.*, 2010; Dewil *et al.*, 2017).

In light of advantages of simple separation of catalyst, no post-treatment sludge handling, facile recovery and recycling of solid phase catalyst, the heterogeneous Fenton processes are more attractive and demanding (Sheldon and Downing, 1999; Arends and Sheldon, 2001; Menini *et al.*, 2004; Guimarães *et al.*, 2008). Fenton-like process relying on the heterogeneous modified PAN catalyst / hydrogen peroxide (Fe^{3+} / H_2O_2) system was introduced by (Ishtchenko, Huddersman and Vitkovskaya, 2003) to overcome the problems entailing with homogeneous processes. This system was successfully applied for the remediation of environmental matrices mentioned in section 2.2.3.2, p.46. The same system was applied in this study to optimize the reaction process for the treatment of dyes.

Reactive Orange 16 (RO16), an azo dye, was chosen as a model dye and used without further purification in batch experiments. Suitable analytical methods were used to analyze compounds of interest. Optimization of the process was done by varying the process parameters: amount of catalyst, amount of hydrogen peroxide, pH, temperature, and initial concentration of the dye.

4.2. AIM AND OBJECTIVES

This study (chapter) aimed at optimization of the batch treatment process for the catalytic decomposition of azo dye using Fenton-like heterogeneous process involving modified PAN catalyst and hydrogen peroxide.

To achieve the aim of this study, the set objectives were:

- To investigate the dye removal efficiencies with respect to the influence of process parameters:
  - Modified PAN catalyst,

- Hydrogen peroxide concentration,
- pH of the reaction medium,
- Temperature of the reaction medium, and
- Initial concentration of dye

➢ To investigate the extent of sorption
- Equilibrium adsorption isotherms
- Influence of pH on adsorption

➢ To investigate the extent of degradation and mineralization

➢ To investigate the extent of decolourization and loss of aromaticity

➢ To investigate the extent of catalyst loss with respect to process parameters

➢ To investigate the removal efficiency contributed by homogeneous Fenton-like system.

4.3. MATERIALS AND METHODS

The reagents, materials and methodologies used in this study are given separately in the following sections.

4.3.1. REAGENTS

All the reagents used in this thesis are listed in Table 4-1. These reagents were used without further purification. The required solutions and dilutions were made using double distilled water.

Table 4-1: Reagents used in this thesis.

S.N.	Reagents	Molecular formula / Molecular weight (g/mol)	Purity	Supplier
1	Hydrogen Peroxide	H_2O_2 / 34.01	30 % wt/v	Fisher Scientific
2	Sodium Hydroxide	NaOH / 40.0	40 % wt/v	,,
3	Iron (III) Sulfate pentahydrate	$Fe_2(SO_4)_3.5H_2O$ / 489.96	General purpose grade	,,
4	Buffer Solution pH 4	-	-	,,
5	Buffer Solution pH 7	-	-	,,
6	Iron Standard for A.A.S.	-	1,000 mg/L in nitric acid	,,

S.N.	Reagents	Molecular formula / Molecular weight (g/mol)	Purity	Supplier
7	Iron (II) Sulfate heptahydrate	$FeSO_4.7H_2O$ / 278.02	≥ 98 %	FSA
8	Hydrochloric Acid	HCl / 36.45	ca. 37 % wt/v	Acros Organics
9	COD vials (LCI 400)	-	(0-1,000 mg/L O_2)	Hach Lange
10	Phosphoric Acid	H_3PO_4 / 98.0	≥ 85 %	Sigma Aldrich
11	Sodium Sulfate Decahydrate	$Na_2SO_4.10H_2O$ / 322.19	≥ 98 %	,,
12	Reactive Orange 16	$C_{20}H_{17}N_3Na_2O_{11}S_3$ / 617.54	50 %	,,
13	Sulfuric Acid	H_2SO_4 / 98.079	≥ 95 %	,,
14	Potassium Hydrogen Phthalate (KHP)	$C_8H_5KO_4$ / 204.22	≥ 99.95 %	,,
15	Sodium Carbonate	Na_2CO_3 / 105.98	≥ 99.9 %	BDH
16	Acetone	-	-	
17	Sodium Hydroxide	NaOH /40.0	40 % wt/v	Fisher Scientific
18	Zinc, Cadmium and Lead standards for AAS	-	1,000 mg/L in nitric acid	,,
19	Methyl Orange	-	-	,,
20	Zinc sulfate heptahydrate	$ZnSO_4.7H_2O$ / 287.56	99 %	Acros Organics

4.3.2. MATERIALS AND INSTRUMENTS

Apart from the conventional glassware (beaker, volumetric flask, Erlenmeyer flask, graduated and bulb pipettes) used in the laboratory; the other materials and instruments used in this thesis are listed in Table 4-2.

Table 4-2: Materials and instruments used in this thesis.

S.N.	Materials	Manufacturer / Model
1	G100 Gilson Pipette	HTL / 49011535
2	Magnetic stirrer and flea	-
3	Modified PAN Catalyst	DMU
4	Analytical Balance	KERN & Sohn GmbH /ALJ-220-4
5	Quartz cuvette	-
6	Peroxide Check strips	Water Works / (0 to 100 mg/L)
7	THERMALOX range Catalyst Rods	Analytical Sciences
8	THERMALOX range Quartz Wool	,,
9	THERMALOX Analyzer	Analytical Sciences Ltd.
10	pH meter	JENWAY / 305
11	Spectrophotometer (UV-VIS)	Thermo Scientific / Evolution 220
12	FTIR-ATR	Bruker / Alpha
13	Spectrophotometer (VIS)	Hach Lange / DR 3800
14	Atomic Absorption Spectrophotometer (AAS)	Perkin Elmer Instruments, LLC / 939/595
15	Heating Block	Hach Lange / LT 200
16	Data Logger	MadgeTech / pHTemp2000
17	Peristaltic Pump	ISMATEC / MV-GE
18	Motor	GGM Co. Ltd. / K9IG40NH-T5
19	Syringe (used for THERMALOX)	SGE Analytical Science
20	Conductivity meter	Mettler Toledo / S230-Kit SevenCompact
21	Borosilicate tube	-
22	Silicon tubing	Cole Parmer
23	Rotator drive and drum	Stuart

4.3.3. ANALYTICAL PARAMETERS AND METHODOLOGY

The methodology for the analytical parameters measured in this study are given in the following sections.

4.3.3.1. pH

The pH meter was calibrated, on daily basis, using reference standard buffer solutions at pH 4 and pH 7. The electrode was washed with double distilled water before measuring sample. The electrode was immersed into the solution and left until a stable reading was achieved. The pH of the solution on the bench was measured using JENWAY 305 pH meter.

4.3.3.2. Decolourization of Reactive Orange 16 (RO16)

Decolourization of Reactive Orange 16 was measured by analysing absorbance of samples taken with respect to the time. Absorbance was recorded using UV-Vis spectrophotometer in scan mode of operation. The UV-Vis spectrophotometer was set to record absorbance spectrum at 2 nm bandwidth with integration time of 0.05 second, data interval of 0.50 nm, scan speed of 600 nm/min and high smoothness. Double distilled water was used to auto zero the base line. The samples were withdrawn with respect to time were scanned in the wavelength range of 550 nm to 190 nm. RO16 exhibits four characteristic bands (the peaks) at maximum wavelengths (λmax) of 254 nm, 297 nm, 387 nm and 493.5 nm respectively. The absorbance (Y) recorded at these wavelengths were converted to concentrations (X) of RO16 using calibration functions, Equation 4-1 to Equation 4-4 respectively, obtained from the calibration curves as shown in Figure 4-1.

λ_{max} = 254 nm, $Y = 0.0531X + 0.0164$ ***Equation 4-1***

λ_{max} = 297 nm, $Y = 0.0497X + 0.0098$ ***Equation 4-2***

λ_{max} = 387 nm, $Y = 0.0311X + 0.005$ ***Equation 4-3***

λ_{max} = 493.5 nm, $Y = 0.0516X + 0.0095$ ***Equation 4-4***

The removal efficiency (R) of RO16 was calculated by the Equation 4-5.

$$R(\%) = \frac{(A_0 - A_t)}{A_0} * 100$$ ***Equation 4-5***

Where, A_0 is the initial absorbance and A_t is the absorbance at time t.

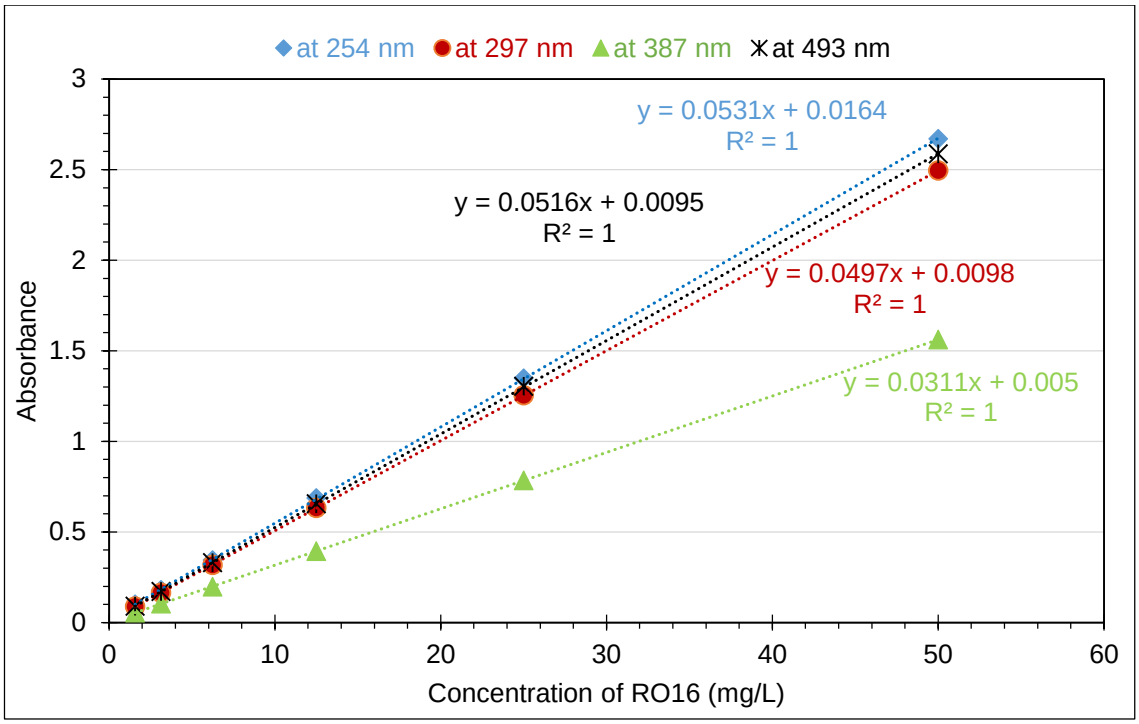

Figure 4-1: Calibration of UV/Vis spectrophotometer for the analysis of Reactive Orange 16.

4.3.3.3. MINERALIZATION

The extent of mineralization (A process in which organic substances are converted into inorganic compounds such as water and carbon dioxide) of Reactive Orange 16 was determined by analyzing the total organic carbon (TOC) content at regular time intervals. TOC was analyzed using THERMALOX TOC analyzer; model number 2001, version 2.5, equipped with two ovens that allow to measure total carbon (TC) and total inorganic carbon (TIC) content of the samples respectively.

Potassium hydrogen phthalate (KHP) (2.1255 g) was dissolved in one litre double distilled water to get a stock solution of concentration equivalent to 1,000 mg/L C of TC. Similarly, 8.8243 g of Sodium carbonate (Na_2CO_3) was dissolved in one litre double distilled water to obtain a stock solution of concentration equivalent to 1,000 mg/L C of TIC. Calibration standards for TC and TIC were prepared by serial dilution of respective stock solutions. Calibrations for TC and TIC were performed using 30 µL of respective calibration standards.

All the carbon species in the sample were converted to carbon dioxide (CO_2) through thermal catalytic oxidation in the heated quartz reactor containing platinum catalyst rods at 678 °C in TC oven. The inorganic species of carbon in the sample react with phosphoric acid (H_3PO_4) heated at 120 °C in TIC oven and form CO_2. The CO_2 free

carrier gas, oxygen, with flow rate of 200 mL/min then sweeps the resulting CO_2 in the samples to nondispersive infrared (NDIR) detector. The corresponding peak area (Y) obtained from the detection of CO_2 was then converted to concentration (X) of TIC and TC using the calibration Equation 4-6 and Equation 4-7 respectively determined from the calibration curves as shown in Figure 4-2. Then, TOC value of the sample was determined by subtracting TIC value from TC value using Equation 4-8.

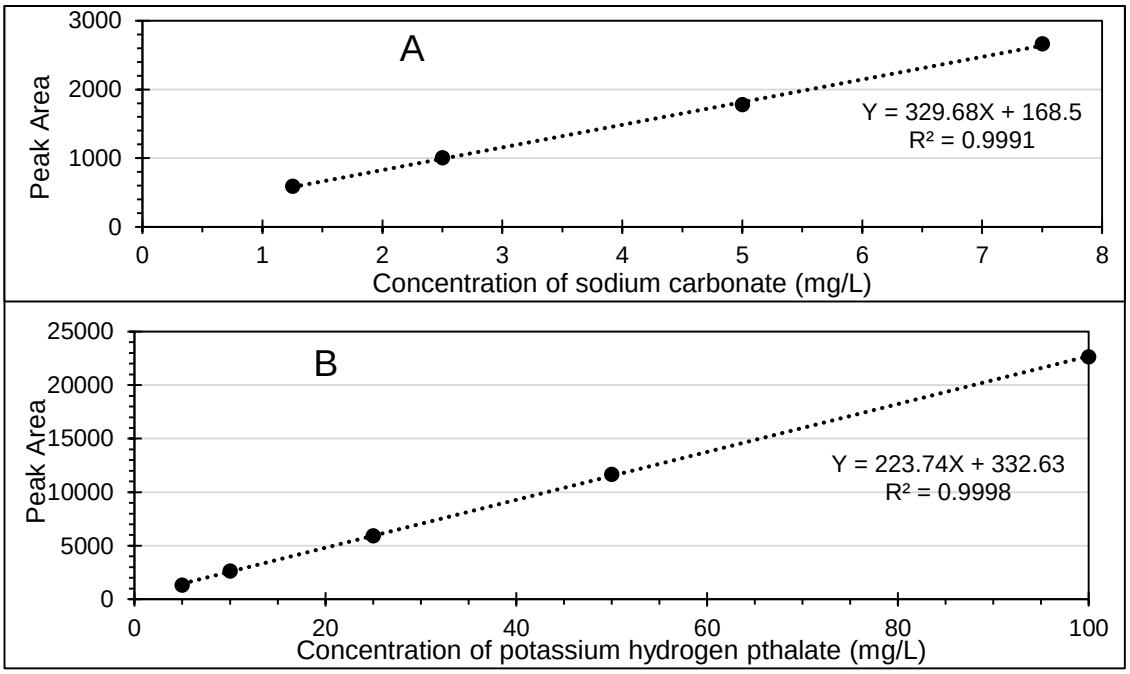

Figure 4-2: Calibration for A) Total Inorganic Carbon (TIC) and B) Total Carbon using THERMALOX analyzer.

$$Y = 329.68X + 168.5 \quad \textit{Equation 4-6}$$

$$Y = 223.74X + 332.63 \quad \textit{Equation 4-7}$$

$$TOC(mg/L) = TC\ (mg/L) - TIC\ (mg/L) \quad \textit{Equation 4-8}$$

4.3.3.4. CHEMICAL OXYGEN DEMAND (COD)

Chemical oxygen demand (COD) was measured using ISO 15705 standard cuvette vials (LCI 400), compatible with DR 3800 spectrophotometer, measuring range of 0 – 1,000 mg/L of O_2, supplied by Hach. 2 mL sample was introduced into the pre-shaken vial and shaken thoroughly. Then, the mixture was digested in a pre-heated (148 °C) heating block for two hours. The sample was allowed to cool down to room temperature and direct value for COD was obtained using DR 3800 spectrophotometer. Contribution from H_2O_2, if present, was deducted by converting residual H_2O_2 concentration according to Equation 4-9 derived from the calibration curve shown in Figure 4-3.

$$Y = 2.0308X + 7.5686$$ ***Equation 4-9***

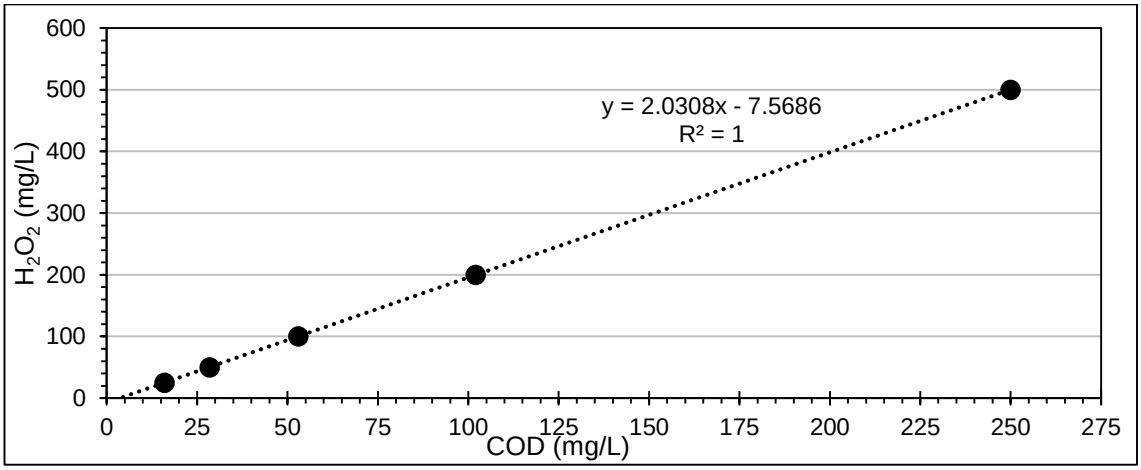

Figure 4-3: Calibration for the contribution to COD by residual hydrogen peroxide.

4.3.3.5. SORPTION OF RO16 ONTO THE MODIFIED PAN CATALYST

The adsorption of RO16 onto the modified PAN catalyst was determined by performing experiments (two replicates) using Radley's Carousel as shown in Figure 4-5. Equal mass of modified PAN catalyst (2 g) normalized at pH 3 was inserted into each of the 50 mL RO16 solutions of initial concentrations (12.5 mg/L, 25 mg/L, 50 mg/L and 60 mg/L). Before inserting the catalyst into the solution, pH and temperature were adjusted to pH 3 and 30 °C respectively. The solution was mixed continuously with a magnetic stirrer rotating at a speed of 400 rotations per minute (rpm). The aliquots were taken and analyzed using UV-Vis spectrophotometer (details given in section 4.3.3.2, p. 86). The absorbances were converted to corresponding residual concentrations using calibration function. The adsorption capacity at equilibrium, q_e (mg/g), was calculated using Equation 4-10.

$$q_e = \frac{(C_0 - C_e)V}{m}$$ ***Equation 4-10***

Where C_0 and C_e are the dye concentrations (mg/L) before exposure (t = 0 min) and at equilibrium time respectively; V is the volume of dye solution used (L); and m is the mass of the modified PAN catalyst used (g).

Adsorption of RO16 as a function of pH was also studied. The experiments were performed with 6 g modified PAN catalyst normalized at desired pH in the range of pH 2 to pH 7. The normalized catalyst was inserted into 100 mL of RO16 solution, initial concentration of 50 mg/L at 30 °C. The rest of the experimental setting was similar to the one described above. The adsorption efficiency (%) was calculated as shown in Equation 4-5.

4.3.3.6. LOSS OF CATALYST (≈ IRON LEACHING)

The concentration of leached iron in the solution was measured using atomic absorption spectrophotometer (AAS) equipped with hollow cathode lamp (Co, Cr, Cu, Fe, Mn, Ni) and fuelled with acetylene and air as oxidant. The emission wavelength was measured at 248.33 nm. Before analysis, samples (30 mL) were acidified using 100 µL of conc. HCl.

Iron standard for AAS (1,000 mg/L in HNO_3) was used to prepare calibration standards ranged from 0.625 mg/L to 10 mg/L. AAS signal was auto-zeroed with double distilled water and calibration was performed. Then, leached iron in the samples was analyzed by aspirating samples to AAS to obtain signal corresponding to iron concentration. Each sample was analyzed in triplicate and three signals were averaged to obtain the mean signal for the corresponding sample. The signal (Y) then converted to concentration of iron (X) using calibration Equation 4-11 derived from the calibration curve shown in Figure 4-4.

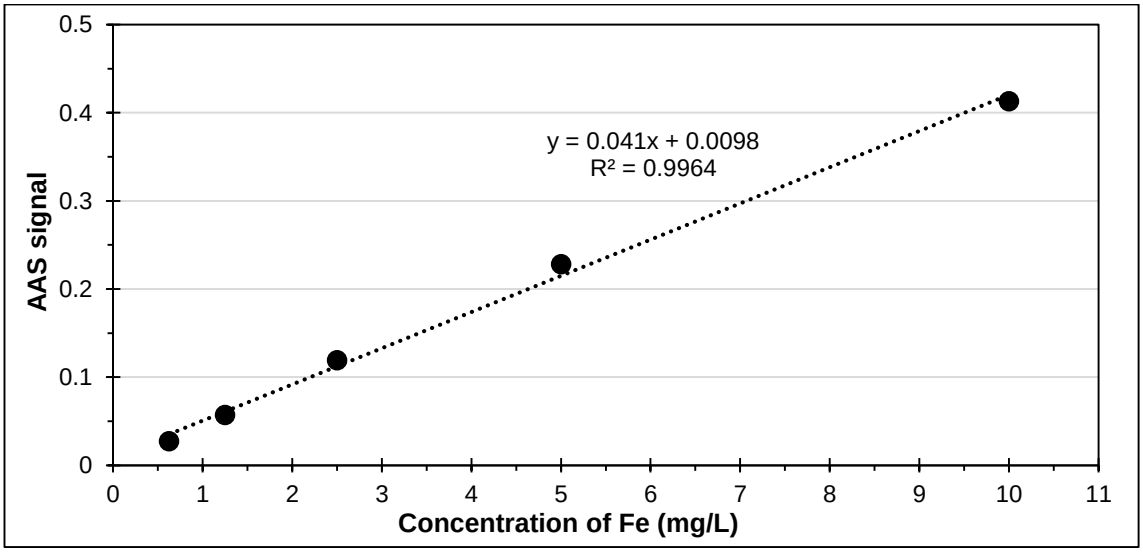

Figure 4-4: Calibration of atomic absorption spectrophotometer (AAS) for the analysis of iron.

$$Y = 0.041X + 0.0098$$ ***Equation 4-11***

4.3.3.7. HOMOGENEOUS CATALYSIS

Investigation on homogeneous catalysis was performed using the leached iron in the solution exposed with an optimum amount of catalyst (6 g) and H_2O_2. 100 mL of H_2O_2 solution (C_0 = 125 mg/L) at pH 3 and 30 °C was prepared and an optimum amount of catalyst (6 g) was submerged into the solution and left for four hours. The solution was filtered through 0.45 µm syringe filter to remove modified PAN catalyst fibrils. The

solution was kept in an airtight, well-stirred volumetric flask for few days to allow decomposition of the residual H_2O_2. Then, the solution was warmed to attain a temperature of 30 °C and used to prepare solution containing RO16 (C_0 = 50 mg/L) and H_2O_2 (C_0 = 125 mg/L). The samples were withdrawn with respect to time to determine the removal efficiency.

4.3.3.8. EFFECT OF DISSOLVED OXYGEN ON DECOLOURIZATION OF RO16

The effect of dissolved oxygen on decolourization of RO16 was investigated by performing experiment in the presence and absence of dissolved oxygen in the system. The dissolved oxygen was removed by sparging the solution with helium gas. The modified PAN catalyst was submerged into 48.75 mL of double distilled water, pH adjusted to 3, and sparged with helium gas for one hour. Then, 1.25 mL of RO16 solution (C = 2 g/L) and required quantity of H_2O_2 were quickly transferred into the system to obtain 50 mg/L of RO16. The system was sparged continuously throughout the experiment.

4.3.3.9. SAMPLING AND TREATMENT OF DYE-BATH EFFLUENT

The dye bath water sample was collected from a local dyer, Jersey Dyer, in Leicester on 20th March 2015. It was not possible to sample the real effluent generated by the Dyer as their collection tank was not accessible and the dye-baths were operating at different times using different dyes. Therefore, the effluent samples were taken from the first wash of each individual dye-bath and mixed together to simulate a real effluent. The sample was transported to De Montfort University and stored in the fridge.

The sample container was shaken before taking samples for experiments. Then, the samples were warmed up to desired temperature and pH was adjusted using hydrochloric acid (0.1M) and sodium hydroxide (0.1M). Heating plate with stirring facility was used to heat and stir the samples. A magnetic flea was used for the effective mixing of samples. Duplicate experiments were performed using 100 mL of wastewater in Dreschel bottles. Glass stoppers were used to prevent the loss of sample volume due to evaporation. The experiment was performed without further dilution. However, the samples for UV/Vis analyses were diluted five folds and the absorbances of samples were recorded using Thermo Scientific Evolution 220 spectrophotometer. The obtained absorbances were then multiplied by dilution factor to get the actual absorbances. Then average of two experiments was taken to represent the residual concentration of contaminants.

4.4. EXPERIMENTATION

Degradation of RO16 was investigated in batch experiments. The batch experiments were performed in a thermostated Radleys 6 Reaction Station Carousel, shown in Figure 4-5, that consists of six 250 mL capacity reaction vessels. The experimental set up involved the following steps.

4.4.1. PREPARATION OF THE CATALYST

The catalyst was first washed with tap water to get rid of loose iron and then normalized to desired pH. The details of washing and pH normalization are given below.

4.4.1.1. WASHING OF CATALYST

The catalyst was thoroughly washed with tap water until the washed water appeared colourless. The washing of catalyst is to get rid of loose iron so that homogeneous catalysis can be prevented, if not minimized. The presence or absence of loose iron on the catalyst after washing was checked by pressing the washed catalyst in between white tissues. Then, the tissues were air dried in room temperature and brown stains / spots as a result of loose iron acted as an indicator.

Figure 4-5: Thermostated Radleys 6 Reaction Station Carousel used for experimentation in batch mode.

4.4.1.2. pH NORMALIZATION OF MODIFIED PAN CATALYST

To normalise the catalyst to a desired pH, the catalyst was placed into a beaker filled with double distilled water and pH was adjusted using 0.1M HCl and 0.1M NaOH. The water was stirred with a magnetic flea to homogenize the added acid or alkali. The addition of HCl and / or NaOH was continued until the pH of the solution stabilized (at

least for 30 minutes) to the desired pH. Then, the catalyst was pressed in between white tissues and dried at room temperature.

4.4.2. EXPERIMENTAL PROCEDURES

Double distilled water was spiked with the pollutant (RO16) to obtain the required initial concentration of the substrate. Then, pH of the solution was adjusted using 0.1M HCl and NaOH. 100 mL of the pH-adjusted solution was transferred into the reactor vessel and allowed to attain desired temperature. The zero minute reading was recorded at this point. Then, required amount of H_2O_2 was added to obtain the desired initial concentration of H_2O_2. The pH-normalized catalyst was cut into smaller pieces, tapped with fingers to get rid of loose fibrils and weighed. Finally, the reaction was commenced by inserting a desired amount of pH-normalized catalyst into the solution. Aliquots were taken from the reactor vessel at selected time intervals and analyzed. The samples were returned to the reactor vessel after UV/Vis analysis. All the experiments were performed in duplicate under a constant temperature of 30 °C. An average of two replicates was taken and plotted as a function of time. Table 4-3 presents the list of experiments with varying experimental conditions used in the study of degradation of RO16.

Apart from the experiments listed in Table 4-3, an experiment was performed to determine the stability and half-life of RO16. For this, RO16 solution (C_0 = 50 mg/L) at pH 3 was placed in a volumetric flask, closed with a stopper and stirred with a magnetic flea. The flask was shaken upside down and samples were taken as a function of time.

Table 4-3: List of experiments used in the study of RO16 degradation.

Experiments	Study objective	Process parameters				
		Amount of PAN catalyst (g)	**Amount of H_2O_2 (mg/L)**	**pH**	**Initial conc. of RO16 (mg/L)**	**Temperature (°C)**
1	Effect of Catalyst	**0**	500	3	50	30
2		**2**	500	3	50	30
3		**4**	500	3	50	30
4		**6**	500	3	50	30
5		**8**	500	3	50	30
6		6	0	3	50	30

Experiments	Study objective	Process parameters				
		Amount of PAN catalyst (g)	**Amount of H_2O_2 (mg/L)**	**pH**	**Initial conc. of RO16 (mg/L)**	**Temperature (°C)**
7	Effect of H_2O_2	6	**62.5**	3	50	30
8		6	**125**	3	50	30
9		6	**250**	3	50	30
10 (= 4)		6	**500**	3	50	30
11		6	**1000**	3	50	30
12	Effect of pH	6	125	**2**	50	30
13 (= 8)		6	125	**3**	50	30
14		6	125	**4**	50	30
15		6	125	**5**	50	30
16		6	125	**7**	50	30
17	Effect of RO16 Conc.	6	125	3	**12.5**	30
18		6	125	3	**25**	30
19 (= 8)		6	125	3	**50**	30
20		6	125	3	**100**	30
21	Effect of Temp.	6	125	3	50	**20**
22		6	125	3	50	**25**
23 (= 8)		6	125	3	50	**30**
24		6	125	3	50	**35**

4.5. RESULTS AND DISCUSSIONS

4.5.1. UV-VIS SPECTRA OF RO16

The degradation of RO16 was investigated using a UV-Vis spectrophotometer. Therefore, it is important to understand the characteristic UV-Vis absorption spectrum of RO16. Figure 4-6 presents an overlay of the UV-Vis spectra for different concentrations of RO16. RO16 presents four distinct characteristic bands (peaks) at the maximum wavelengths of 254 nm, 297 nm, 387 nm and 493.5 nm respectively. These characteristic bands of RO16 agree with most of the literature (Purnama, 2005; Gomes *et al.*, 2009, 2011; Abdullah, Wong and Yaziz, 2010; Migliorini *et al.*, 2011; Tizaoui and Grima, 2011; Mitrović *et al.*, 2012). However, Bilgi and Demir, 2005 analyzed RO16 solution at pH 10

and observed only three characteristic bands at 235 nm, 315 nm and 480 nm respectively.

The band at 254 nm is due to the presence of aromatic (benzene) rings (Catanho, Malpass and Motheo, 2006; Gomes *et al.*, 2009, 2011; Mitrović *et al.*, 2012). The band at 297 nm is attributed to the structure of naphthalene rings (Mitrović *et al.*, 2012) and gamma acetylated acid, a precursor for the synthesis of RO16, see Figure 4-7 (Gomes *et al.*, 2009, 2011; Mijin *et al.*, 2016). The absorbance at these wavelengths originate due to π → π* transitions in the benzene and naphthalene rings. Thus, reduction in the absorbance at these wavelengths is indicative of degradation of the aromatic rings (Catanho, Malpass and Motheo, 2006; Gomes *et al.*, 2009; Mitrović *et al.*, 2012).

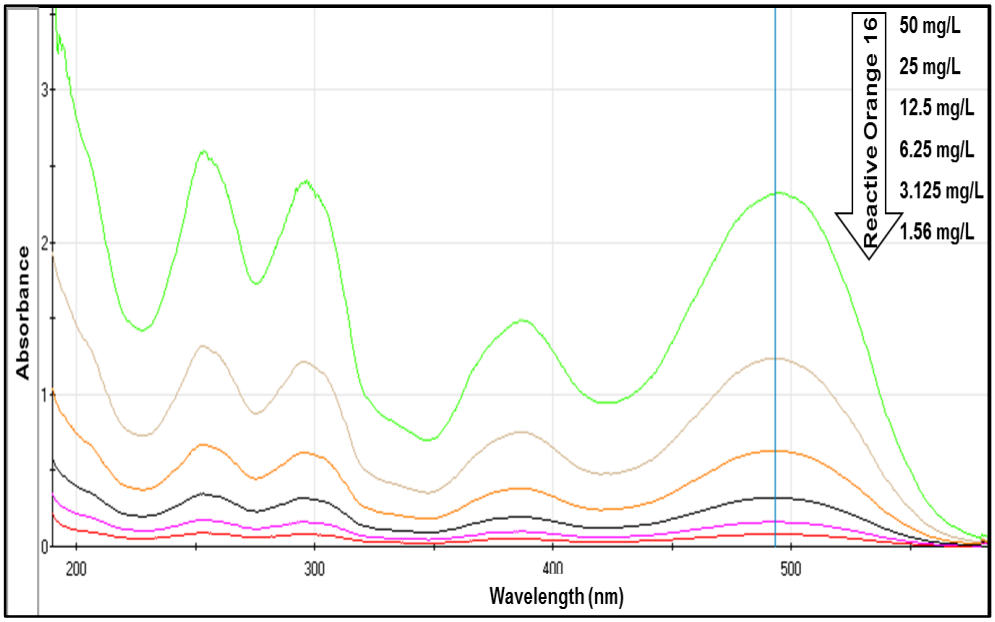

Figure 4-6: UV-Vis spectra of Reactive Orange 16.

The band at 387 nm relates to the azo group (Gomes *et al.*, 2009, 2011; Mitrović *et al.*, 2012) or the aromatic ring bonded to the azo group (Migliorini *et al.*, 2011). The last band at 493.5 nm relates to the chromophore group (Gomes *et al.*, 2009, 2011; Migliorini *et al.*, 2011) and linked to the hydrazone form of the azo dye (Mitrović *et al.*, 2012). The absorbance of band in the visible region is due to n → π* transitions of the chromophoric azo group. Thus, reduction in the absorbance in this region signifies the degradation of main chromophore of the dye and thus reflects the extent of decolourization (Migliorini *et al.*, 2011; Mitrović *et al.*, 2012).

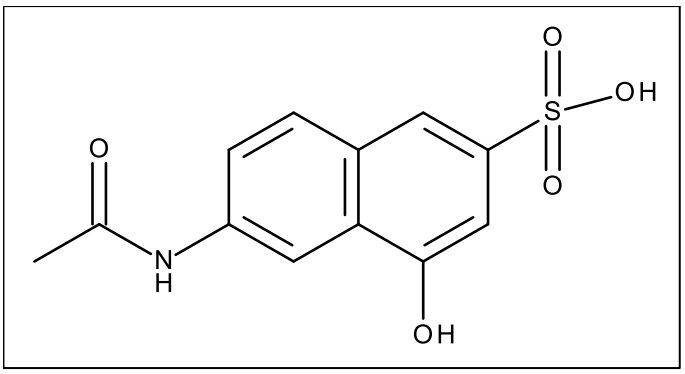

Figure 4-7: Structure of N-acetyl gamma acid. Source: (Chemical Book, 2017).

4.5.2. STABILITY OF RO16

Commercial dyes are synthesized to resist biodegradation. This is why they are persistent in the environment for longer time. They are stable to sun light and oxidation. For example, the half-life of the hydrolyzed Reactive Blue 19 at neutral pH and 25 °C is reported to be about 46 years (Chequer *et al.*, 2013). Therefore, the stability of RO16 (C_0 = 50 mg/L) in the laboratory at pH 3 was investigated as described in section 4.4.2. Figure 4-8 presents the results for the stability of RO16 in the presence and absence of oxidant (H_2O_2) at pH 3 and room temperature ranging from 20 °C to 30 °C. The stability of RO16 solution in the presence of oxidant was investigated with an initial concentration of H_2O_2 500 mg/L.

RO16 seems to be persistent in the absence of H_2O_2 under light and atmospheric oxygen. In 20 days, 99.5 % of RO16 was decolourized (Vis @ 493 nm) in the presence of H_2O_2 whereas in the absence of H_2O_2 the decolourization of RO16 was only 5.04 %. Similar trends with relatively less reduction were observed for characteristic bands at 254 nm, 297 nm and 387 nm. The slight but sudden drop in the removal RO16 in the absence of H_2O_2 on day 52 (marked with a vertical dotted line) was due to the contamination of cuvette with residual H_2O_2 in RO16 sample containing H_2O_2. The decolourization of RO16 after nine months (277 days) was 19.5 % which includes the added removal due to H_2O_2 contamination. A logarithmic model, a line of best fit ($Y = -0.012\ln(x) + 0.9968$), was developed from the data observed before contamination to predict the decolourization trend (represented by a dark blue dashed line) without the influence of H_2O_2 contamination. The extended trend line shows that the decolourization would have been about 7.1 % if contamination had not occurred.

The results discussed above agree with the literature. Abdullah et al., 2010 and Mitrović et al., 2012 observed negligible loss of RO16 due to the irradiation by UV light, direct

UV-photolysis. Similarly, authors also observed a negligible loss of RO16 with H_2O_2 only (Abdullah, Wong and Yaziz, 2010; Mitrović *et al.*, 2012).

The decolourization of RO16 in the absence of H_2O_2 does not obey the zero and first order kinetic plots. Hence, the estimated half-life of RO16 is calculated based on unitary method. The decolourization efficiency of 19.5 % in 277 days suggests an estimated half-life of RO16 of two years. Similarly, based on the predicted trend line, the half-life of RO16 is estimated as 5.4 years. The half-life of RO16 could not be compared with literature as no published literature contained such information. However, in either cases, the half-life of RO16 is much shorter than that of Reactive Blue 19 (46 years) documented by (Chequer *et al.*, 2013).

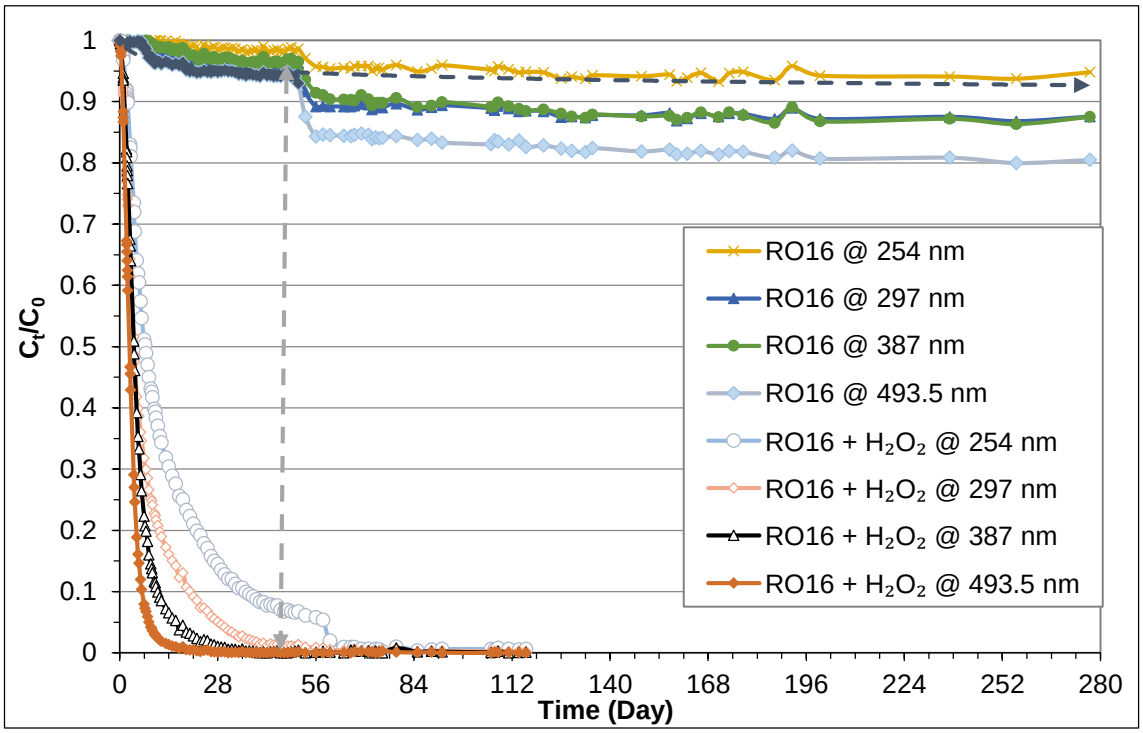

Figure 4-8: Stability of Reactive Orange 16.

[Experimental conditions: RO16 solution (C_0 = 50 mg/L) at pH 3 and room temperature].

4.5.3. SORPTION OF REACTIVE ORANGE 16 ONTO THE CATALYST

The first step in the heterogeneous catalytic reaction is the adsorption of reactants (dye and H_2O_2) onto the catalyst and favouring their activation (Jacques, 2017). Thus, adsorption of RO16 onto the modified PAN catalyst was determined according to the procedure laid out in section 4.3.3.5 and the results are presented in Figure 4-9 and Figure 4-10 respectively. A proportional decrease in absorbances, as seen in Figure 4-19-B, at four absorption bands of RO16 was expected during adsorption process.

Thus, the results below are discussed based on the analyses corresponding to absorption band at 493.5 nm only.

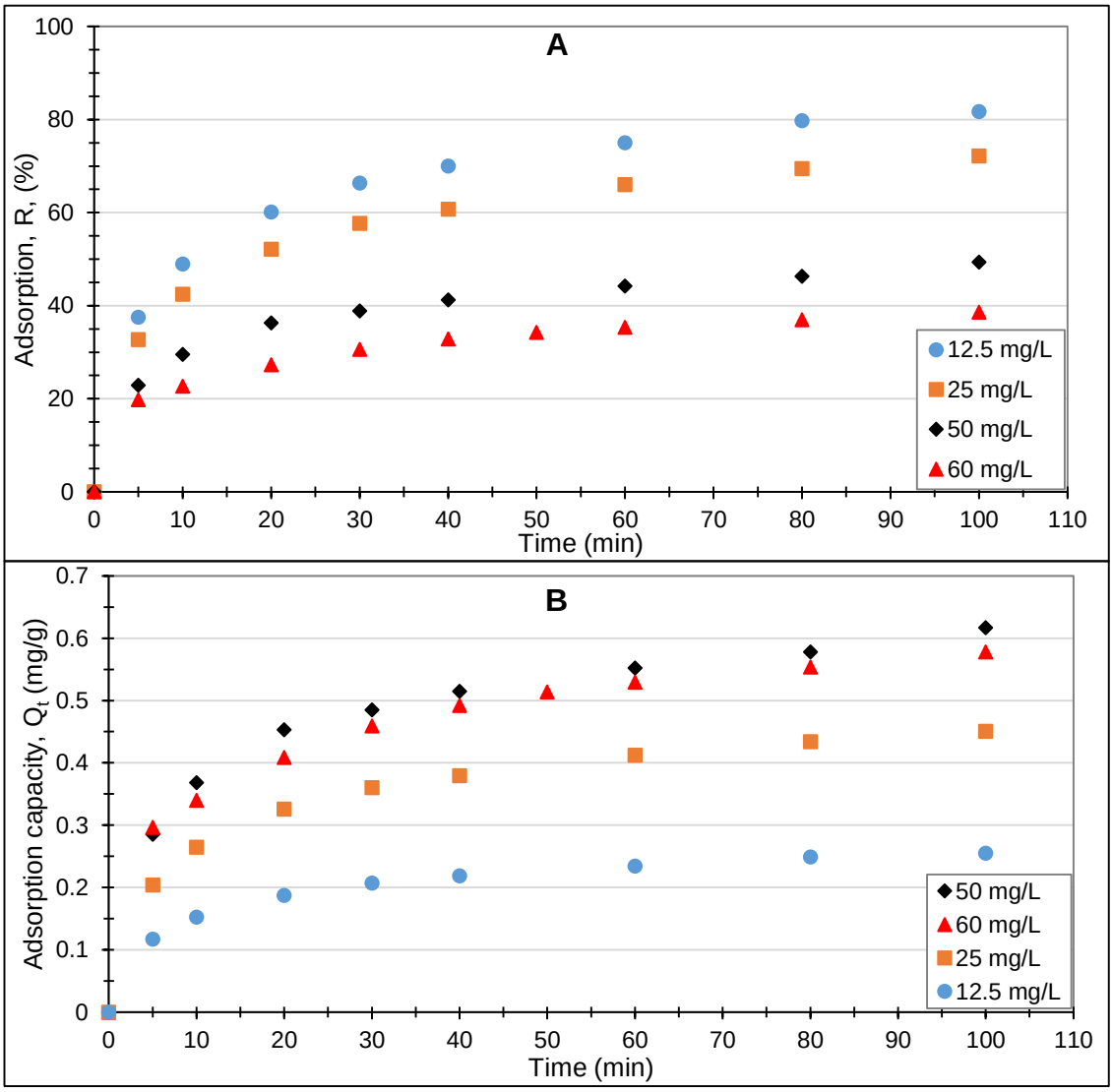

Figure 4-9: Adsorption of RO16, R (%), and adsorption capacity of the modified PAN catalyst, Q_t (mg/g) as a function of RO16 concentration and contact time.

[Experimental conditions: 2 g catalyst in 50 mL of RO16 solution at pH 3 and 30 °C].

Figure 4-9-A and Figure 4-9-B show adsorption of RO16, R (%), and adsorption capacity at time t, Q_t (mg/g), of catalyst with respect to time. The adsorption process is rapid at the beginning as more than 80 % of RO16 adsorbed in the first 40 minutes. Adsorption of RO16 gradually slows down as time proceeds nearing saturation at 100 minutes. The removal efficiency, R (%), of RO16 increases as the initial concentration (C_0) of RO16 decreases whereas the adsorption capacity, Q_t (mg/g) increases with respect to the increase in initial concentration of RO16. Figure 4-10-A shows a negative linear

correlation between initial concentration of dye and the extent of adsorption, R (%), of the catalyst. After 100 minutes, the extent of adsorption corresponding to 12.5 mg/L, 25 mg/L, 50 mg/L and 60 mg/L of RO16 become 81.7 %, 72.2 %, 49.3 % and 38.6 % respectively.

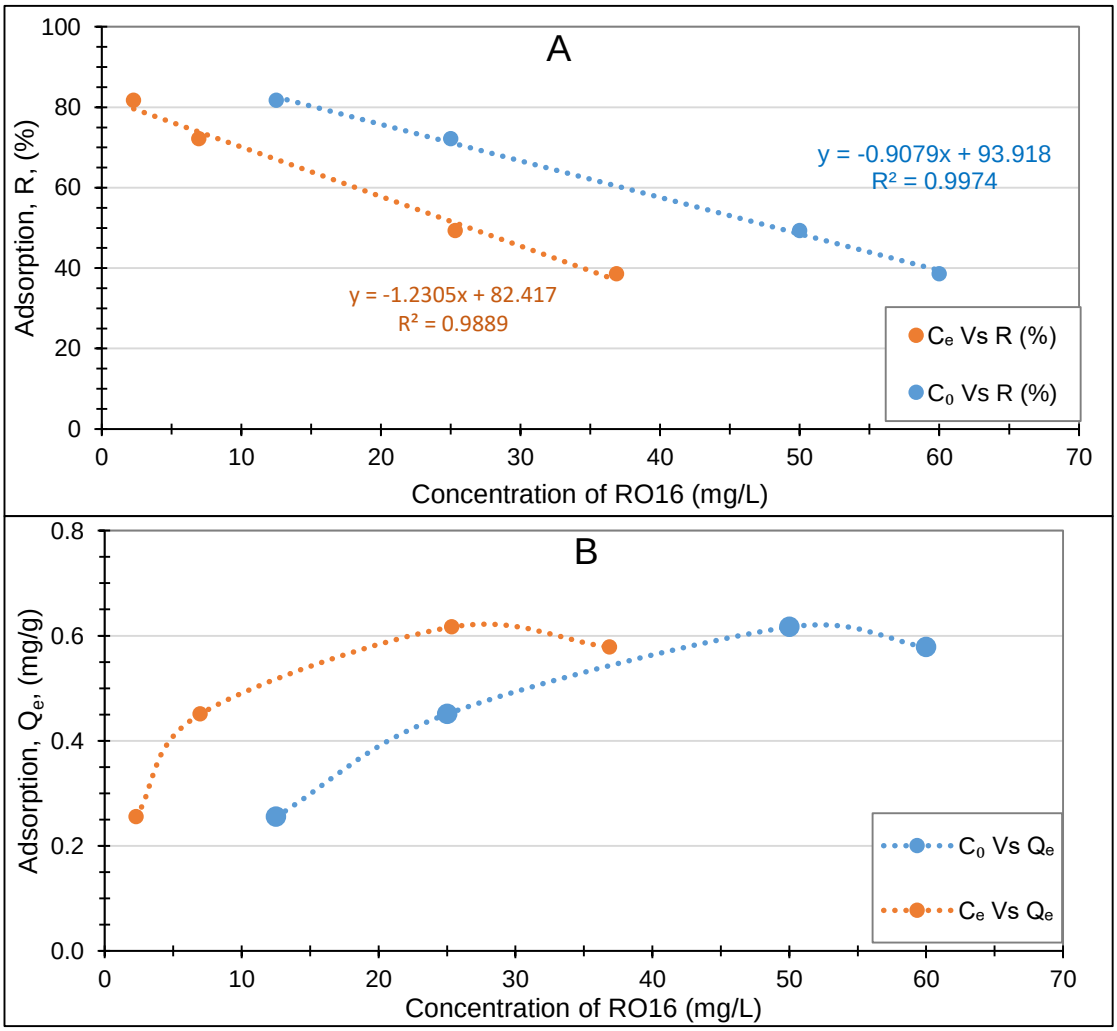

Figure 4-10: Adsorption of dye as a function of initial concentration of RO16. C_e and Q_e represent the concentration (mg/L) and adsorbed mass of RO16 at equilibrium time.

Figure 4-10-B shows the mass of RO16 adsorbed per gram of modified PAN catalyst. The adsorbed mass of RO16 increased with increasing initial concentration of dye. The adsorption of RO16 appeared to be saturated when initial concentration of RO16 reached 50 mg/L. Accordingly, the adsorption capacity (Q_e) of modified PAN catalyst at the saturation point become 0.62 mg/g catalyst. However, the true capacity may differ from the one presented above as the exposure time was not enough to reach to equilibrium. The exposure time (100 minutes) was matched with the time taken for the complete catalytic decolourization of RO16 (see Figure 4-15). Adsorption curves in

Figure 4-9 show continual increase in adsorption of RO16, suggesting that adsorption of RO16 had not reached to an equilibrium state. This was reflected as a dip in Figure 4-10-B. Thus, to obtain a true adsorption capacity, a relatively longer exposure time would be needed.

4.5.3.1. EQUILIBRIUM ADSORPTION ISOTHERMS

The relationship between the amount of sorbed dye and its equilibrium concentration can be used to describe the sorption isotherm models and the best-fit can be established based on the linear regression correlation coefficient (R^2) (Suteu, Zaharia and Malutan, 2011; Yagub *et al.*, 2014). The equilibrium sorption isotherms are one of the most important data to understand how RO16 interacts with the modified PAN catalyst and give an idea of the adsorption capacity per unit mass of catalyst, surface properties and affinities to the catalyst (Liu *et al.*, 2012; Wawrzkiewicz, 2013; Wawrzkiewicz and Hubicki, 2015). The surface phase may be considered as a monolayer or multilayer (Salleh *et al.*, 2011; Yagub *et al.*, 2014). There are several adsorption isotherm models such as Langmuir, Freundlich, Henry, Dubinin-Radushkevich (D-R), Tempkin, Dubinin-Kaganer-Radushkevich (DKR) etc. (Kubilay *et al.*, 2007; Alyüz and Veli, 2009). Amongst these, Langmuir and Freundlich models are the most common models used in the linearized form to describe the adsorption progress (Deng *et al.*, 2015).

4.5.3.1.1. THE LANGMUIR ISOTHERM MODEL

The Langmuir isotherm theory is based on the ideal monolayer coverage of adsorbate over a homogeneous adsorbent surface (Allen, Mckay and Porter, 2004; Salleh *et al.*, 2011). Thus, it assumes uniform (homogeneous) reversible adsorption on the surface and describes monolayer adsorption on a surface having a finite number of identical sites (Chen *et al.*, 2006; Liu *et al.*, 2012). The Langmuir expression is given by the Equation 4-12 (Wang, Hung and Shammas, 2007; Valh and Marechal, 2009; Salleh *et al.*, 2011; Yagub *et al.*, 2014; Deng *et al.*, 2015).

$$Q_e = \frac{Q_m K_L C_e}{1 + K_L C_e} \qquad \textit{Equation 4-12}$$

Where, Q_e = amount of RO16 adsorbed at the time of equilibrium (mg/g); Q_m = Maximum monolayer adsorption capacity of the modified PAN catalyst (mg/g); C_e = Concentration of RO16 (mg/L) at the time of equilibrium; and K_L = Langmuir adsorption isotherm constant related to the free energy adsorption (L/mg).

Rearranging the Equation 4-12, Langmuir equation can be linearized to two different forms: a) Langmuir-1 isotherm model as in Equation 4-13 (Liu *et al.*, 2012; Pandiselvi and Thambidurai, 2013; Wawrzkiewicz, 2013; Yagub *et al.*, 2014; Wawrzkiewicz and Hubicki, 2015).

$$\frac{C_e}{Q_e} = \frac{C_e}{Q_m} + \frac{1}{K_L Q_m} \qquad \textbf{Equation 4-13}$$

This is in the form of $Y = mX + c$. Thus Q_m and K_L can be calculated from the $Slope = \frac{1}{Q_m}$ and $Intercept = \frac{1}{K_L Q_m}$ of the linear plot of C_e/Q_e versus C_e. Thus, $Q_m = \frac{1}{Slope}$ and $K_L = \frac{Slope}{Intercept}$.

b) Langmuir-2 isotherm model as in Equation 4-14 (Langmuir, 1997, p. 361; Chen *et al.*, 2006; Suteu, Zaharia and Malutan, 2011; Yagub *et al.*, 2014).

$$\frac{1}{Q_e} = \frac{1}{K_L Q_m}\frac{1}{C_e} + \frac{1}{Q_m} \qquad \textbf{Equation 4-14}$$

This is also in the form of $Y = mX + c$. Thus, Q_m and K_L can be calculated from the $Slope = \frac{1}{K_L Q_m}$ and $Intercept = \frac{1}{Q_m}$ of the linear plot of $1/Q_e$ versus $1/C_e$. Thus, $Q_m = \frac{1}{Intercept}$ and $K_L = \frac{Intercept}{Slope}$.

The Langmuir isotherm models and related parameters are presented in Table 4-4 and Figure 4-11respectively. Both models show correlation coefficient close to unity ($R^2 > 0.99$), model-2 having slight better over model-1. However, the maximum adsorption capacity of the catalyst (Q_m) calculated from model-1 is closer to the practical adsorption capacity (Q_e). Although most of the literature uses the Langmuir isotherm model-1, Langmuir, 1997, p.361 argued that model-1 is linearized incorrectly thus produces an induced correction in concentration (C). This could be an explanation for having closer values of Q_m and Q_e via model-1.

The influence of the Langmuir isotherm shape on whether adsorption is favourable or unfavourable can be classified by separation factor (R_L). The separation factor which is considered as more reliable indicator of the adsorption capacity can be calculated by the relation given in Equation 4-15 (Pandiselvi and Thambidurai, 2013; Yagub *et al.*, 2014; Xiong *et al.*, 2015).

$$R_L = \frac{1}{1 + K_L C_0}$$ ***Equation 4-15***

Where, C_0 is the initial concentration (mg/L) of RO16 and K_L is the Langmuir adsorption constant (L/mg). The R_L values depicts whether monolayer adsorption is irreversible ($R_L = 0$), favourable ($0 < R_L < 1$), linear ($R_L = 1$). $R_L > 1$ is interpreted as unfavourable in the literature (Arslan and Balcioğlu, 1999; Gode and Pehlivan, 2006; Kubilay *et al.*, 2007; Ming, 2011; Yagub *et al.*, 2014; Asuelimen, 2015; Xiong *et al.*, 2015). Equation 4-15 can yield a maximum value of R_L as one when the $K_L C_0$ becomes zero. Thus, interpreting $R_L > 1$ is meaningless.

Table 4-4: Langmuir adsorption isotherm parameters for RO16.

Langmuir isotherm	**Slope**	**Intercept**	**R^2**	**Q_m (mg/g)**	**K_L (L/mg)**
Model-1	1.5555	4.5221	0.9934	0.64	0.34
Model-2	5.5484	1.4729	0.9943	0.68	0.27

The calculated values for separation factor (R_L) corresponding to initial concentrations of RO16 are presented in Table 4-5. The R_L values fall between zero and unity ($0 < R_L < 1$), thus adsorption of RO16 onto the modified PAN catalyst is favourable.

Table 4-5: Separation factors (R_L), calculated from model-2, with respect to the initial concentrations of RO16.

Initial concentration of RO16 (C_0) (mg/L)	12.5	25	50	60
Separation Factor (R_L)	0.2316	0.1309	0.0701	0.0591

The R_L decreases towards zero with respect to increase in dye concentration, possibly suggests that adsorption at high concentration could be irreversible. Similarly, R_L increases towards unity with respect to decrease in concentration, possibly suggests that adsorption at low concentration could be linear. This happens as the equilibrium concentration (C_e) becomes lower, $K_L C_e$ become much less than unity thus the denominator in Equation 4-12 become close to unity. Hence, Langmuir expression reduce to the linear form $Q_e = K_L Q_m C_e$ which is the equation of straight (linear) line passing through the origin ($Y = mx$).

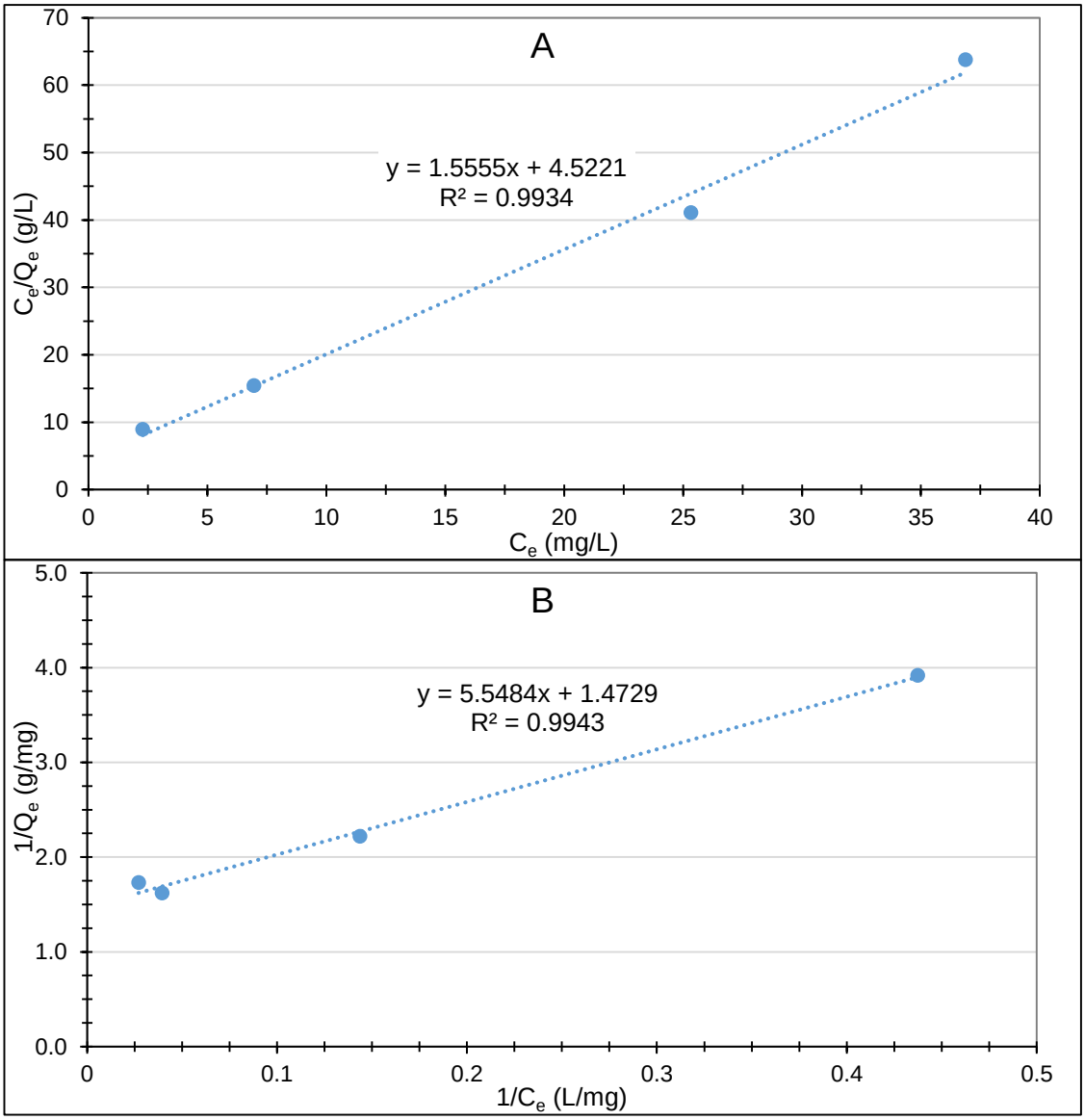

Figure 4-11: Langmuir adsorption isotherm A) model-1 and B) model-2.

4.5.3.1.2. FREUNDLICH ADSORPTION ISOTHERM MODEL

The Freundlich adsorption isotherm model is an exponential equation and assumes a heterogeneous adsorption surface that has unevenly (exponential) distributed sites with different energies of adsorption. The Freundlich model assumes multilayer adsorption. The Freundlich expression is given by the Equation 4-16 (Fytianos, Voudrias and Kokkalis, 2000; Allen, Mckay and Porter, 2004; Suteu, Zaharia and Malutan, 2011; Yagub *et al.*, 2014; Deng *et al.*, 2015).

$$Q_e = K_F C_e^{\frac{1}{n}}$$ ***Equation 4-16***

Where, Q_e (mg/g) is the amount of RO16 adsorbed by the modified PAN catalyst at the time of equilibrium, C_e (mg/L) is the equilibrium concentration of RO16, K_F (mg/g) is the adsorption capacity of modified PAN catalyst, and 1/*n* is an empirical parameter measuring intensity of adsorption. n = 1 indicates the partition between two phases is independent of the concentration where $K_F \equiv K_L$ (linear isotherm), 1/n < 1 (n >1) indicates a normal Langmuir isotherm and 1/n > 1 (n <1) is indicative to cooperative sorption (Fytianos, Voudrias and Kokkalis, 2000; Voudrias, Fytianos and Bozani, 2002; Dada *et al.*, 2012). The Freundlich equation can be linearized by taking logarithm of above equation as shown in Equation 4-17.

$$log\ Q_e = logK_F + \frac{1}{n} logC_e$$ ***Equation 4-17***

This is in the form of $Y = mX + c$. Thus, K_F and *n* can be calculated from the $Slope = \frac{1}{n}$ and $Intercept = logK_F$ of the linear plot of $logQ_e$ versus $logC_e$. Thus, $K_F = antilog\ (Intercept)$ and $n = \frac{1}{Slope}$.

Table 4-6: Parameters related to Freundlich adsorption isotherm model.

Freundlich isotherm model	**Slope**	**Intercept**	**R^2**	***n***	**K_F (mg/g)**
	0.301	-0.6606	0.9063	3.3223	0.22

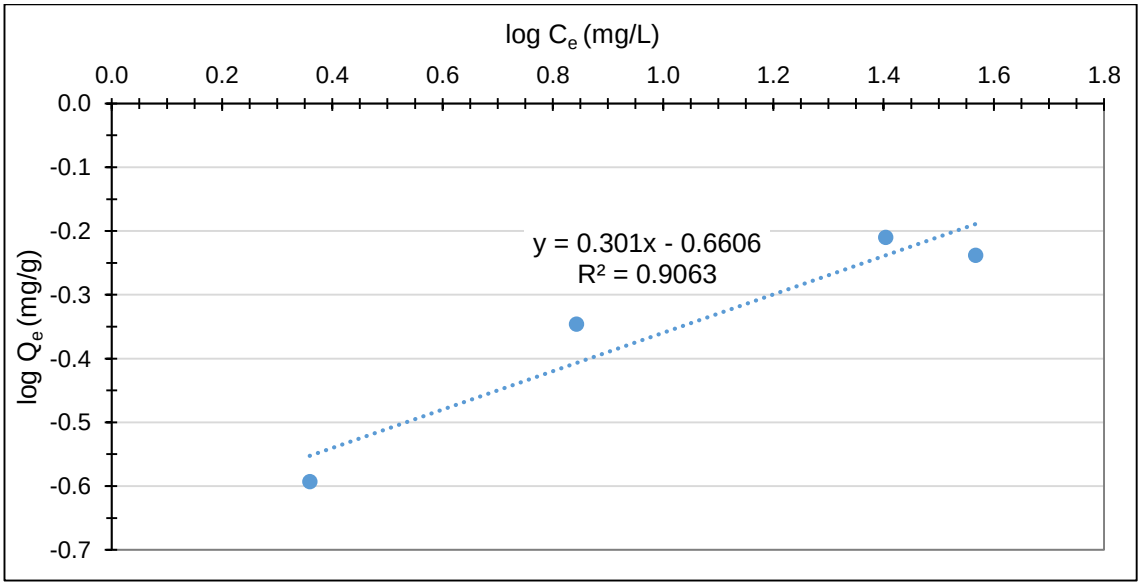

Figure 4-12: Freundlich isotherm for the adsorption of RO16 onto the modified PAN catalyst.

Freundlich adsorption isotherm model and related parameters are presented in Table 4-6 and Figure 4-12 respectively. Since 1/n < 1, i.e. n >1, the adsorption can be explained as a normal Langmuir isotherm. Dada et.al, 2012 mentioned that adsorption is favourable if *n* lies between one and ten. However, some literature (Langmuir, 1997; Allen, Mckay and Porter, 2004) expressed Freundlich model as $Q_e = K_F C_e^n$ and quoted the values of *n* from 0.6 to 3.3, but usually between 0.9 and 1.4. In such case, the conditions for *n* given above may not be true. The authors did not classify the nature of adsorption based on value of *n*.

4.5.3.1.3. SELECTION OF THE BEST-FIT ADSORPTION MODEL

Despite of using different forms of Langmuir and Freundlich models, all literature cited above used R^2 values (goodness of fit criterion) to give an indication as to which model can be chosen to give the best-fit. Table 4-4 and Table 4-6 show higher value of R^2 for Langmuir models (R^2 > 0.99). Langmuir model-2 has a slightly better R^2 than model-1. In addition, the line of the best-fit also represents more experimental data points. Thus, Langmuir model-2 is considered as the best-fit model to describe the adsorption of RO16 onto the modified PAN catalyst. The best-fit of Langmuir isotherm model indicates the presence of monolayer sorption of RO16 onto the homogeneous surface of the modified PAN catalyst (Deng *et al.*, 2015, 2016). Accordingly, the maximum monolayer adsorption capacity (Q_m) of modified PAN catalyst at pH 3 and 30 °C is calculated as 0.68 mg/g, close to the experimentally derived value (0.62 mg/g).

The R^2 (> 0.9) value for Freundlich model may still be considered good but Figure 4-12 shows that the line of the best-fit obtained does not represent any of the experimental data points. Furthermore, the computed adsorption capacity (K_F = 0.2185) of modified PAN catalyst is ~ 3 times less than the practical value. Thus, Freundlich model is not suitable to describe the adsorption of RO16 onto the modified PAN catalyst.

The maximum adsorption capacities corresponding to the given equilibrium concentrations were calculated using model parameters (K_L, Q_m, K_F and *n*) of Langmuir and Freundlich isotherm models. Figure 4-13 presents the experimental and modelled isotherms and confirms the fitting of Langmuir isotherm model and hence the presence of monolayer adsorption of RO16 onto the homogeneous surface of modified PAN catalyst. The maximum monolayer adsorption capacity (Q_m) of modified PAN catalyst is much less than the adsorbents reported such as waste materials from raw agricultural by-product (Yagub *et al.*, 2014, p. 179), agricultural solid waste (Salleh *et al.*, 2011, p.

9), anion exchangers (Wawrzkiewicz and Hubicki, 2015, pp. 51–53) and cation exchangers and a range of natural and synthetic adsorbents (Wawrzkiewicz, 2013, p. 419).

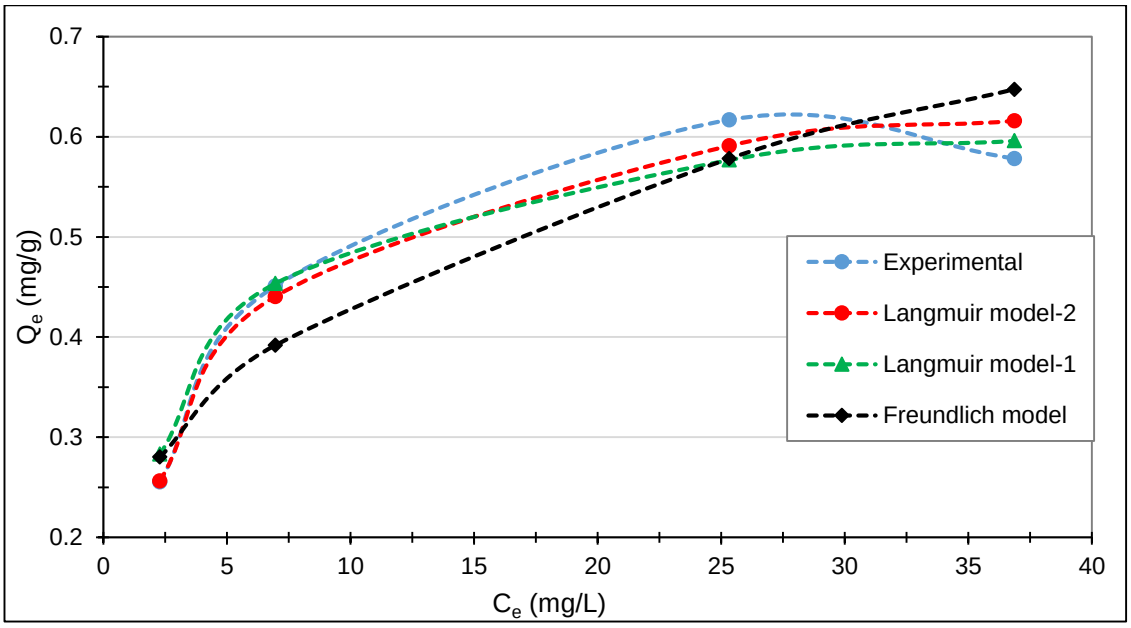

Figure 4-13: Cross verification of Langmuir and Freundlich adsorption isotherm models.

4.5.3.1.4. INFLUENCE OF PH ON SORPTION OF RO16

The pH of the adsorbate exerts profound influence on the adsorption of substrate molecule by influencing the ionization / dissociation of the dye molecules and the surface properties of the modified PAN catalyst (Pandiselvi and Thambidurai, 2013; Deng *et al.*, 2015). Thus, influence of pH on adsorption of RO16 onto the modified PAN catalyst was studied in the range of pH 2 to pH 7. Figure 4-14 shows no significant difference in adsorption rates at pH 2 and pH 3. However, adsorption rates decreased when pH increased beyond three. After 100 minutes, the adsorption efficiencies corresponding to pH 2, pH 3, pH 4, pH 5 and pH 7 become 87.2 %, 84.5 %, 24.4 %, 13.3 % and - 4.0 % respectively. The variation in adsorption efficiencies with respect to pH can be explained in terms of changes in surface properties of modified PAN catalyst.

The solid surfaces at solid-solution interfaces acquire an electrical charge when in contact with an aqueous phase. The charge on the solid surfaces produces a microenvironment of electrical potential imbalance and affects the distribution of neighbouring ions. Thus, the charged solid surface attracts ions of opposite charge and repels ions of like charge. The pH of the solution determines the charge of solid surface. Generally, solution with neutral or alkaline pH results in a net negative charged surface

whereas more acidic condition yields a net positive charged surface. Accordingly, charged surface attracts cationic species from solution at neutral or alkaline pH and anionic species at acidic pH (Smith, 1999).

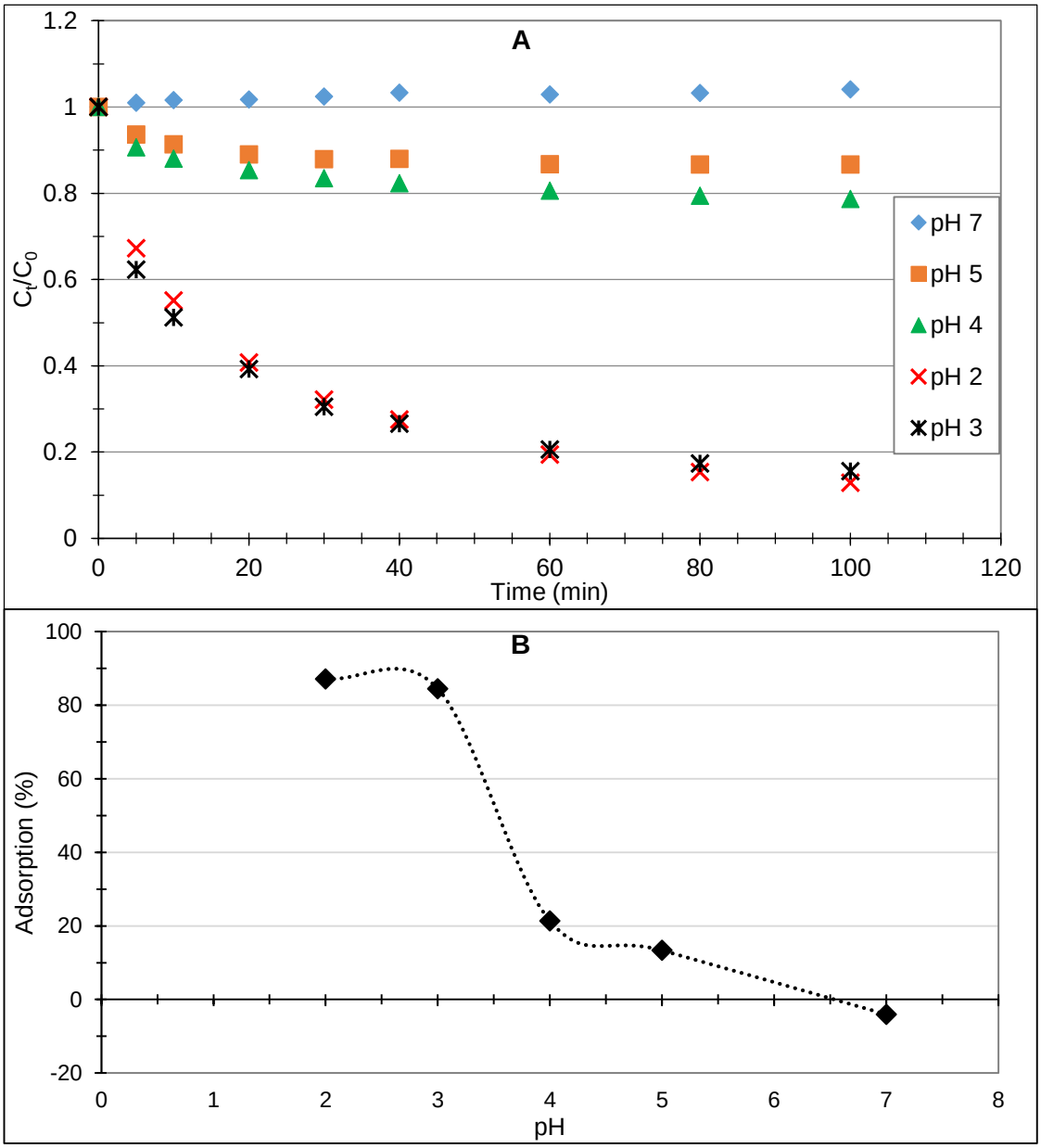

Figure 4-14: Adsorption of RO16 as a function of pH, a) with respect to time b) as a percentage of RO16 removal at time = 100 minutes.

[Experimental conditions for A: 6 g catalyst, pH 3 in 100 mL of RO16 (C_0 = 50 mg/L) at 30 °C].

At acidic pH of 2.5 to 3.5, the surface of modified PAN catalyst becomes positively charged (protonation of catalyst) as pH_{pzc}, the pH at point of zero surface charge, become higher than the pH of the solution (pH_{pzc} > pH) (Xiong *et al.*, 2015). The protonation of functional groups such as carboxyl and amine groups also occurs at low pH. At low pH,

the carboxyl and amine (-NH_2) groups exist in -COOH and -NH_3^+ forms. Thus, the electrostatic attraction between positively charged groups in the catalyst and negatively charged sulfonic group in RO16 leads to strong adsorption, the first step that facilitates heterogeneous catalysis. At pH ≥ 4, due to the presence of excess OH^- ions leads to deprotonation of functional groups on the catalyst. At alkaline pH, the carboxyl and amine functional groups exist in the form of carboxylate (-COO^-) and -NH_3OH. Thus, negatively charged surface of modified PAN catalyst become electrostatically repulsive to the negatively charged RO16 molecules thus reduces the adsorption of RO16 and hence the removal of RO16 (Purnama, 2005; Pandiselvi and Thambidurai, 2013; Yagub *et al.*, 2014). The negative removal of dye at pH 7 is due to the contribution from the catalyst which is discussed in section 4.5.4.3.

4.5.4. OPTIMIZATION OF REACTIVE ORANGE 16 DEGRADATION PROCESS

The degradation process of RO16 was optimized by evaluating the effect of the most influential five parameters (amount of catalyst, initial concentration of H_2O_2, pH, initial concentration of RO16 and temperature) discussed in the section 2.2.3.1.4, p.41. The process was optimized based on one-factor-at-a-time (OFAT) approach. OFAT approach incorporates experimentation investigating several process parameters by varying one factor at a time and keeping other factors fixed. This factor is varied until its best outcome is found (Frey and Jugulum, 2003; Frey *et al.*, 2003; Wahid and Nadir, 2013). To begin with, the best working pH of 3 was adopted from the literature. The initial amount of H_2O_2 was kept above the theoretical COD for the complete mineralization of RO16. The working concentration of RO16 was considered as the highest concentration in the linear range of calibration curve of RO16. The temperature was kept at 30 °C. The influence of each process parameter is discussed below.

4.5.4.1. INFLUENCE OF AMOUNT OF MODIFIED PAN CATALYST

The amount of catalyst in Fenton-like reaction is one of the major parameters that influences the catalytic decomposition of hydrogen peroxide to generate $^{\bullet}OH$. The influence of amount of catalyst on Fenton-like reaction is discussed in section 2.2.3.1.7, p. 45. Degradation of RO16 is dependent on the amount of catalyst and hence it is important to investigate its influence on degradation process and establish an optimum amount of catalyst for the degradation of RO16.

The influence of catalyst on degradation of RO16 was investigated by varying the amount of modified PAN catalyst in the range of 0 g to 8 g. The iron content of the modified PAN

catalyst was determined to be 9.24 mg/g of modified PAN catalyst which is equivalent to 0.165 mmol/g of modified PAN catalyst. The results of the influence of amount of modified PAN catalyst on degradation of RO16, monitored at four characteristic bands (254 nm, 297 nm, 387 nm and 493.5 nm), are shown in Figure 4-15.

The absorbance in the visible and UV region decreases faster with increasing amount of catalyst. This signifies the rates of decolourization and loss of aromaticity increase with increasing amount of catalyst. This is expected as additional amount of catalyst introduces the additional number of active sites (Fe^{3+}) to the reacting system. The additional active sites enhance the adsorption of dye. At the same time, additional active sites (Fe^{3+}) increase the availability of ferrous ions (Fe^{2+}) enhancing the catalytic decomposition of H_2O_2 thereby accelerates the generation of $^{\bullet}OH$ radicals which initiate the chain reaction according to Equation 2-2, enhancing the degradation rate of the dye (Chamarro, Marco and Esplugas, 2001; Wu *et al.*, 2009). This can be summarized as the increase in decolourization rate with increase in amount of catalyst is due to the increase in the surface area for the catalytic decomposition of H_2O_2.

It is meaningful to compare the results obtained at 40 minutes of the catalysis as decolourization of RO16 in the presence of higher amount of catalyst nearly completed in 40 minutes of catalysis. In the absence of catalyst (i.e. in the presence of H_2O_2 only), at 30 °C, decolourization of RO16 after 40 minutes and 100 minutes were 2.25 % and 7.3 % respectively. At room temperature (see Figure 4-8), decolourization of RO16 was much slower. This signifies that catalyst is needed for the degradation of the dye. The negative efficiency (increase in C_t/C_0) for the 254 nm band is due to the additional absorbance of H_2O_2 at this absorption band.

At 40 minutes, the decolourization efficiency (at 493.5 nm) improved from 79.5 % to 95.55 %, 98 %, and 99 % when amount of catalyst increased from 2 g to 4 g, 6 g and 8 g respectively. Similar effect of catalyst was observed for the loss of aromaticity, monitored at 254 nm. Accordingly, loss of aromaticity improved from 48.4 % to 65 %, 76.1 % and 79.6 % when the amount of catalyst increased from 2 g to 4 g, 6 g, and 8 g respectively. Similar trends were noted with respect to the absorption bands corresponding at 297 nm and 387 nm. Similar effect of catalyst on degradation of RO16 was observed by other researchers (Purnama, 2005; Chen, 2009; Abdullah, Wong and Yaziz, 2010; Su *et al.*, 2011; Sukhdev, Manjunatha and Puttaswamy, 2017).

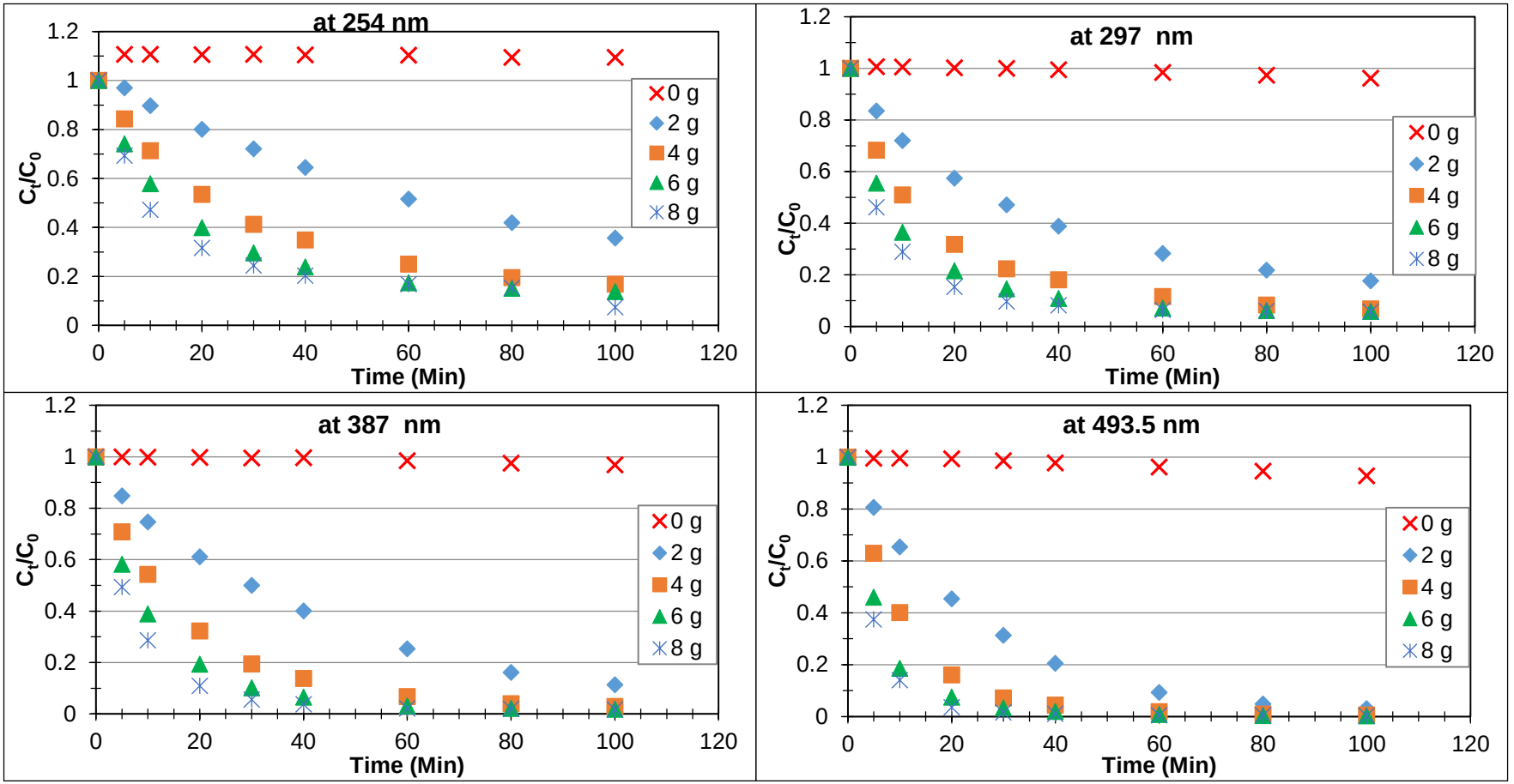

Figure 4-15: Influence of amount of catalyst on degradation of RO16.

[Experimental conditions: 500 mg/L H_2O_2, pH 3 in 100 mL of RO16 solution (C_0 = 50 mg/L) at 30 °C.]

Although degradation of RO16 with 8 g of modified PAN catalyst seems slightly better over 6 g, there is no significant difference between the two amounts of catalyst. Thus, an optimum amount of catalyst is considered as 6 g.

The degradation of RO16 at 493.5 nm absorption band occurs relatively faster than at 387 nm, 297 and 254 nm. The degradation of RO16 corresponding to these bands were found in the order of 493.5 nm > 387 nm > 297 nm > 254 nm. This suggests that the reaction proceeds with the cleavage of azo bond (-N=N-), the chromophoric part of the dye, followed by the removal of aromaticity (the naphthalene and benzene rings) respectively. This observation agrees with the published literature (Purnama, 2005).

After 100 minutes of catalysis, as shown in Figure 4-16, the pH of the reacting solution dropped by ~ 0.5 units from an initial pH of 3.0. However, as expected, there was no change in pH of the solution that had only H_2O_2. The drop of pH is indicative to the formation of acidic products such as organic acids. The biggest drop in pH was observed in the presence of 4 g and 6 g catalyst, suggesting the optimum mass of catalyst lies in between 4 g to 6 g.

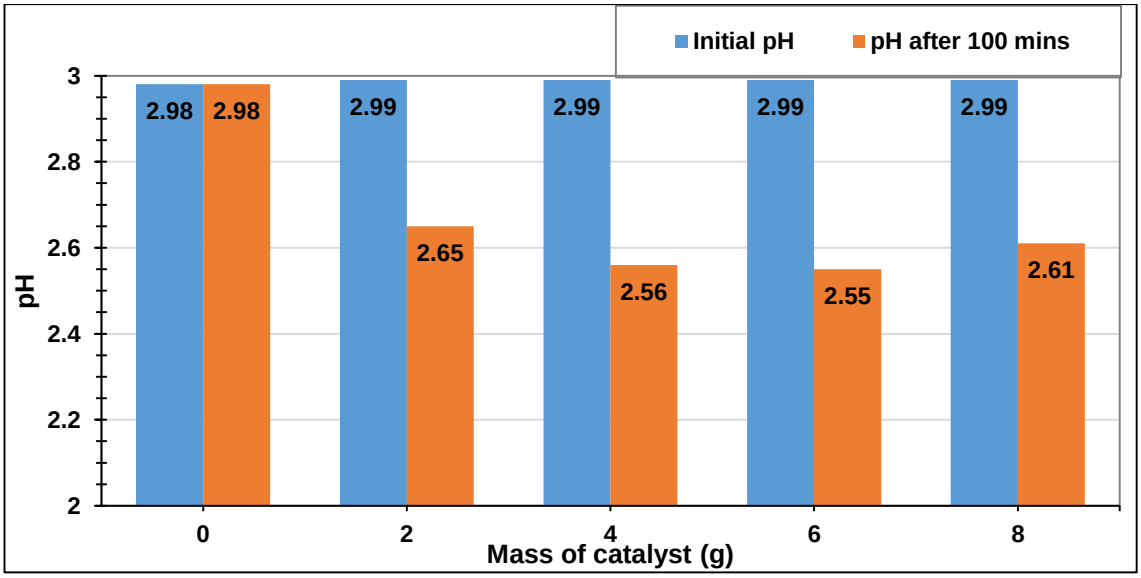

Figure 4-16: pH variation during the reaction process with respect to varying amount of catalyst.

[Experimental conditions are same as in Figure 4-15].

4.5.4.2. INFLUENCE OF HYDROGEN PEROXIDE ON DEGRADATION OF RO16

Initial concentration of H_2O_2 plays an important role in Fenton-like process. The influence of H_2O_2 on Fenton-like process, in terms of chemistry, is discussed in section 2.2.3.1.6 p. 44. In addition to the chemical aspect, in a full-scale treatment plant, H_2O_2 is one of

the major sources of operating expenditure (OPEX). Thus, it is inevitable to optimize the initial concentration of H_2O_2 in order to achieve a cost-effective treatment process. Therefore, the influence of initial concentration of H_2O_2 on degradation of RO16 was evaluated by varying the H_2O_2 concentration whilst keeping the optimum amount of modified PAN catalyst at pH 3. The influence of H_2O_2 was investigated in the concentration range of 0 mg/L to 1,000 mg/L and the results are presented in Figure 4-17.

The decolourization efficiencies (at 493.5 nm) of RO16 after 40 minutes of catalysis corresponding to 62.5 mg/L, 125 mg/L, 250 mg/L, 500 mg/L and 1,000 mg/L of H_2O_2 are 98.2 %, 98.7 %, 98.67 %, 98 % and 97.8 % respectively. Similarly, the loss of aromaticity (at 254 nm) of RO16 after 40 minutes of catalysis corresponding to 62.5 mg/L, 125 mg/L, 250 mg/L, 500 mg/L and 1,000 mg/L of H_2O_2 are 83.6 %, 86.3 %, 82.1 %, 76.1 % and 65.1 % respectively. The degradation trends corresponding to the absorption bands at 297 nm and 387 nm are similar to those at 254 nm and 493.5 nm. The results reveal that the influence of H_2O_2 on removal of RO16 is not significant as that of catalyst and pH.

The removal efficiency of RO16 improved slightly when dosage of H_2O_2 increased from 62.5 mg/L to 125 mg/L. However, there was no improvement with H_2O_2 dosages beyond 125 mg/L. In fact, the removal efficiency decreased slightly with increasing dosages of H_2O_2. This phenomenon is widely discussed in literature as hydroxyl radical scavenging effect of H_2O_2. Removal efficiency of organic contaminants is generally expected to increase with increasing dose of H_2O_2 until an optimum concentration is reached. Beyond optimum concentration, the excess H_2O_2 in the system competes with the substrate by reacting with $^{\bullet}OH$ according to Equation 2-7 to generate less reactive perhydroxy radicals ($^{\bullet}OOH$) which eventually retards the degradation efficiency. (Abdullah, Wong and Yaziz, 2010; Martins, Rossi and Quinta-Ferreira, 2010; Su *et al.*, 2011; Babuponnusami and Muthukumar, 2012; Mitrović *et al.*, 2012; Nidheesh, Gandhimathi and Ramesh, 2013).

The higher consumption of H_2O_2 with respect to higher dosage of H_2O_2 was observed during the continuous flow treatment of RO16 (see 5.5.1.2, p.158). The consumption of H_2O_2 increased from 48.3 mg/L to 113.3 mg/L and 200.4 mg/L when the initial concentrations of H_2O_2 increased from 50 mg/L to 125 mg/L and 250 mg/L respectively.

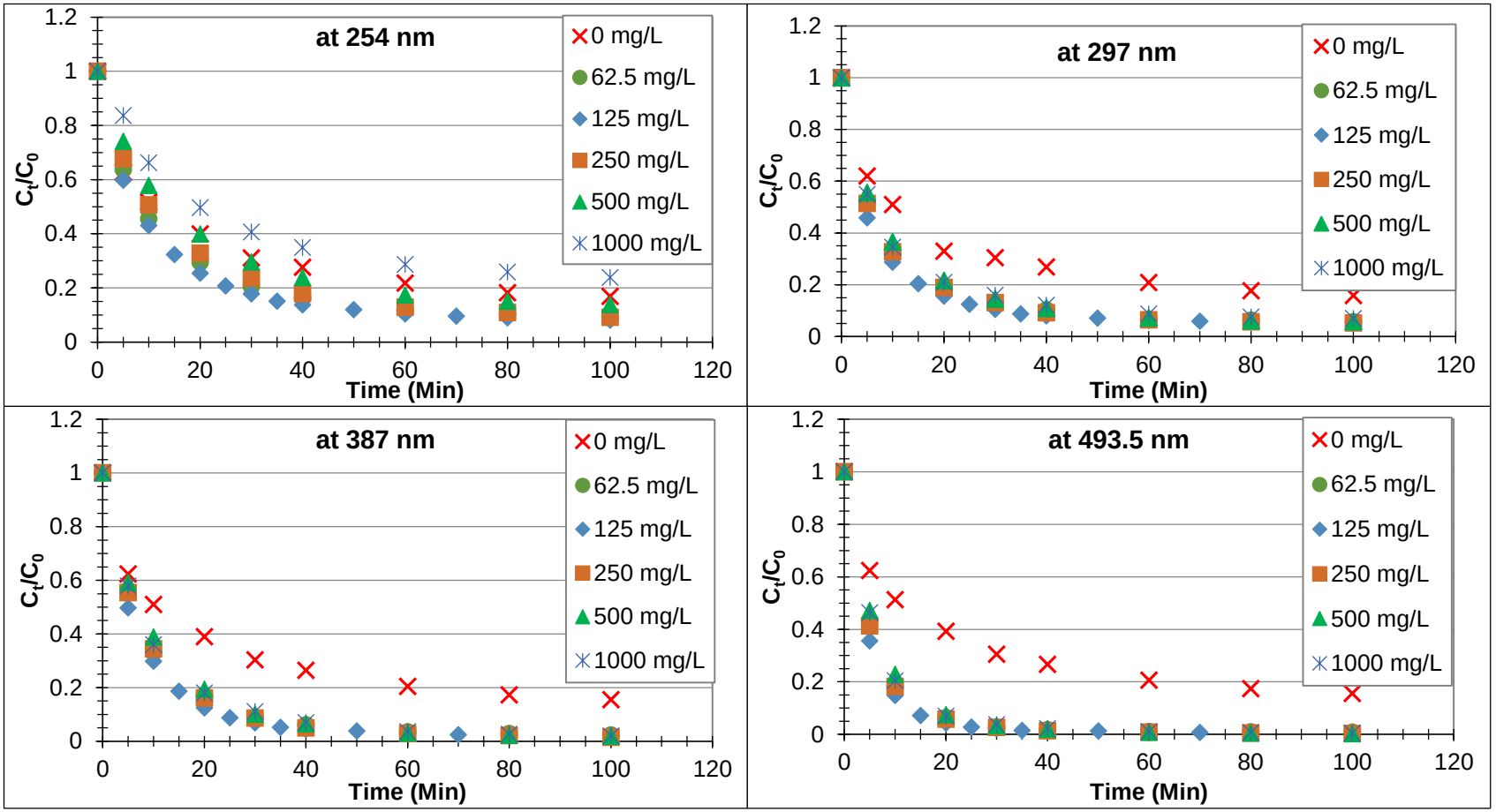

Figure 4-17: Influence of initial concentration of hydrogen peroxide on degradation of RO16.

[Experimental conditions: 6 g catalyst, pH 3 in 100 mL of RO16 solution (C_0 = 50 mg/L) at 30 °C.]

Previous study involving modified PAN catalyst and H_2O_2 also documented similar observation (Asuelimen, 2015). Asuelimenn, 2015 showed that, after one hour of catalysis, the consumption of H_2O_2 increased from 255 mg/L to 640 mg/L when the initial concentrations of H_2O_2 varied from 300 mg/L to 1,000 mg/L. At the same time the efficiency of humic acid removal (at 400 nm) improved by 6 % only (54 % to 60 %). Such an inefficient consumption of H_2O_2 increases the OPEX (Rivas *et al.*, 2003). Thus, in this study, an optimum initial concentration of H_2O_2 is considered as 125 mg/L.

It appears that, at 254 nm, removal of dye without H_2O_2 is higher than with 1,000 mg/L of H_2O_2. This does not agree with the removal trends at other bands. This is due to the additional absorbance contributed by the relatively high concentration of residual H_2O_2. Such contribution is significant, see Figure 4-18, at 254 nm when high concentration (1,000 mg/L) of H_2O_2 is used.

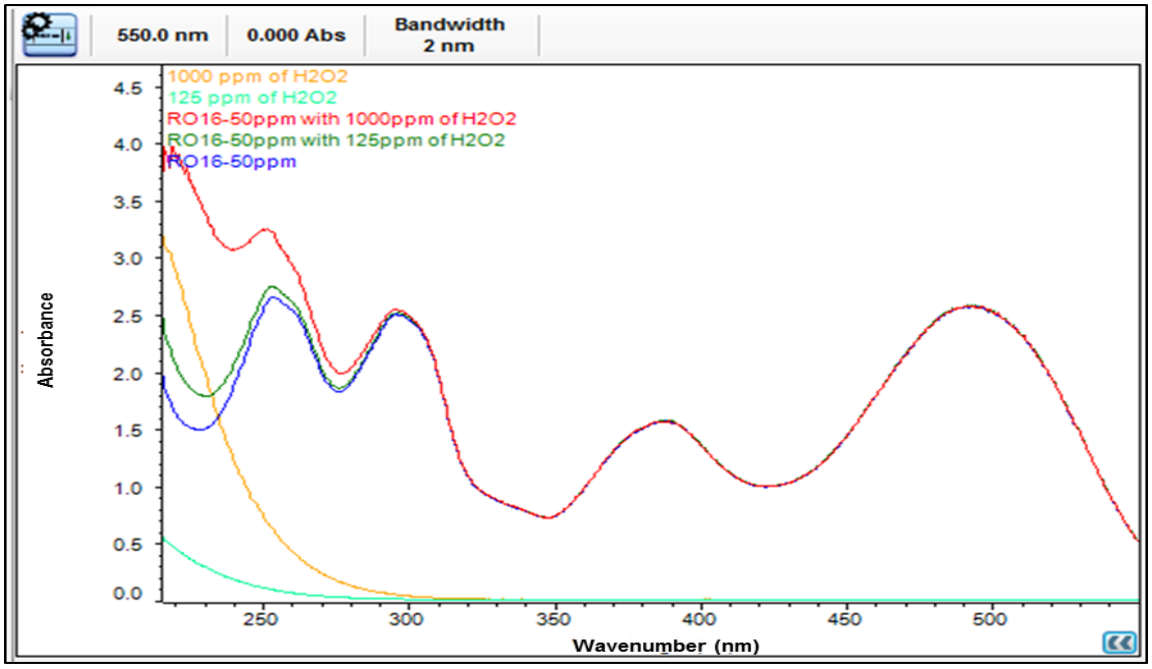

Figure 4-18: UV-Vis spectra comparing RO16 with and without H_2O_2.

The removal (~ 73 %) of RO16 in the absence of H_2O_2 (i.e. in the presence of catalyst only) may question the effectiveness of the catalyst. Although degradation of dye in the presence of dissolved oxygen (DO) is possible, results in section 4.5.3 confirm that the removal in the absence of H_2O_2 was mainly due to the adsorption of dye onto the modified PAN catalyst. According to Langmuir adsorption isotherm model, the maximum adsorption capacity of modified PAN catalyst is 0.68 mg/g. In this experimentation, 5 mg of RO16 (C_0 = 50 mg/L, reaction volume = 100 mL) was exposed to 6 g of catalyst. Thus, a maximum amount of 4.02 mg (80 %) of RO16 is expected to adsorbed onto the catalyst.

The adsorption and catalysis of the dye can be distinguished analytically and visually. The analytical comparison include the changes in dye spectra during the two processes, performing catalysis with much lower amounts of catalyst, removing oxidants such as DO from the dye solution by degassing with nitrogen or helium gas and changes in pH / conductivity over time. The visual comparison include the colour of the exposed catalyst, formation of bubbles (O_2 and / or CO_2) on the surface of catalyst etc.

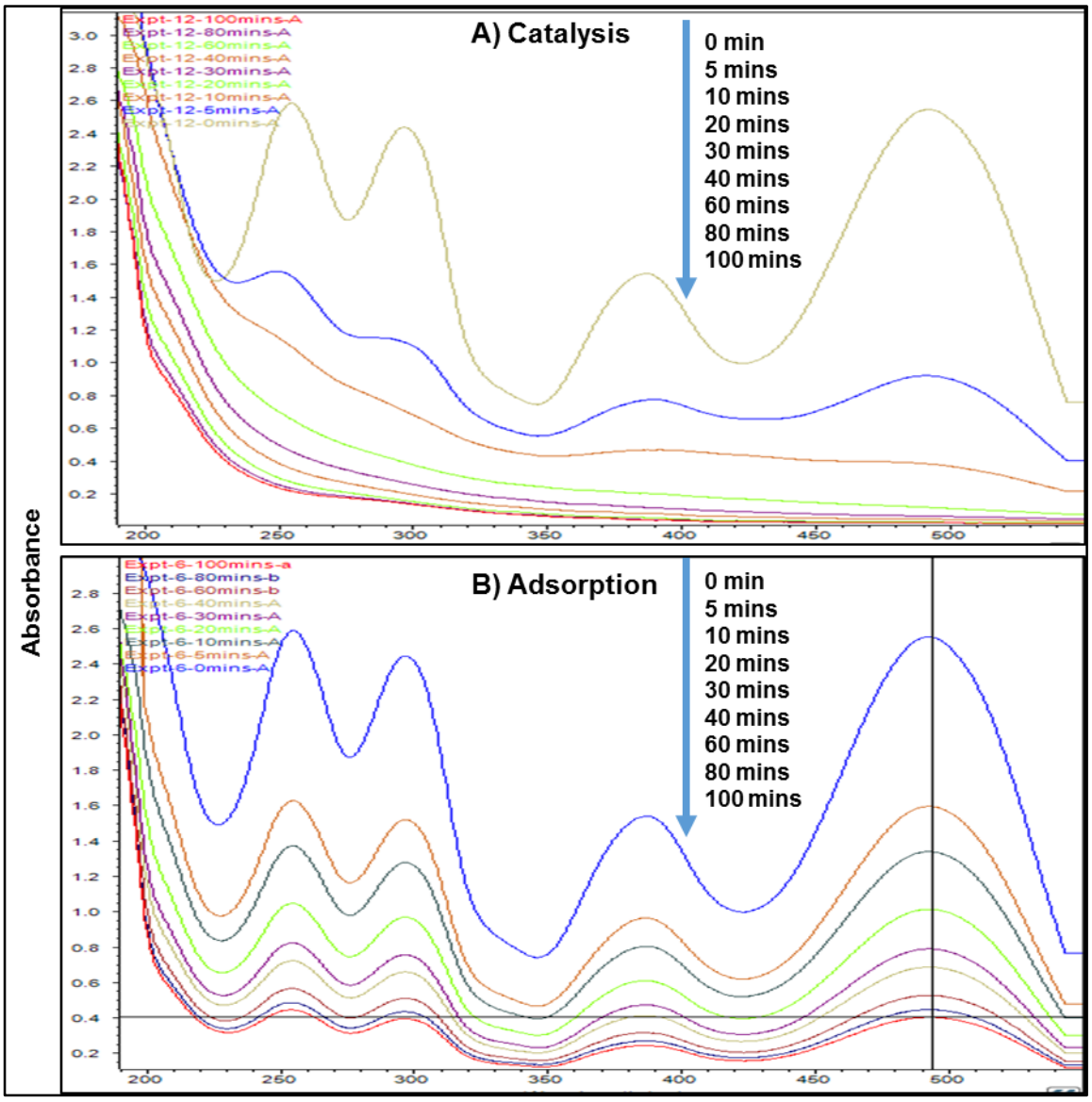

Figure 4-19: Spectral changes of RO16 during a) catalysis and b) adsorption.

[Experimental conditions: 6 g catalyst with (125 mg/L) and without H_2O_2 in 100 mL of RO16 solution (C_0 = 50 mg/L) at 30 °C.]

The removal efficiencies, by means of catalysis, corresponding to the four absorption bands during catalysis are discussed in previous section and found to be in the order of

493.5 nm > 387 nm > 297 nm > 254 nm. Accordingly, in catalysis, a non-proportional reduction of these bands is expected as the dye molecules are degrading over the time. However, in (physical) adsorption, a proportional reduction of absorbance is expected as the dye molecules are not degrading.

Figure 4-19 compares the spectra of RO16 during catalysis (with H_2O_2) and adsorption (without H_2O_2). The spectra of RO16 solution during adsorption show a proportional reduction in absorbance and the spectra remain alike over the time whereas no proportional reduction in absorbance and disappearance of peaks were observed during catalysis. In Figure 4-19-B, after 40 minutes, the removal efficiencies corresponding to absorption bands at 254 nm, 297 nm and 387 nm and 493.5 nm were 72.4 %, 73.2 %, 73.6 % and 73.4 % respectively. The similarity in removal efficiencies corresponding to these four bands supports a proportional reduction of absorbance due to adsorption of dye onto the catalyst.

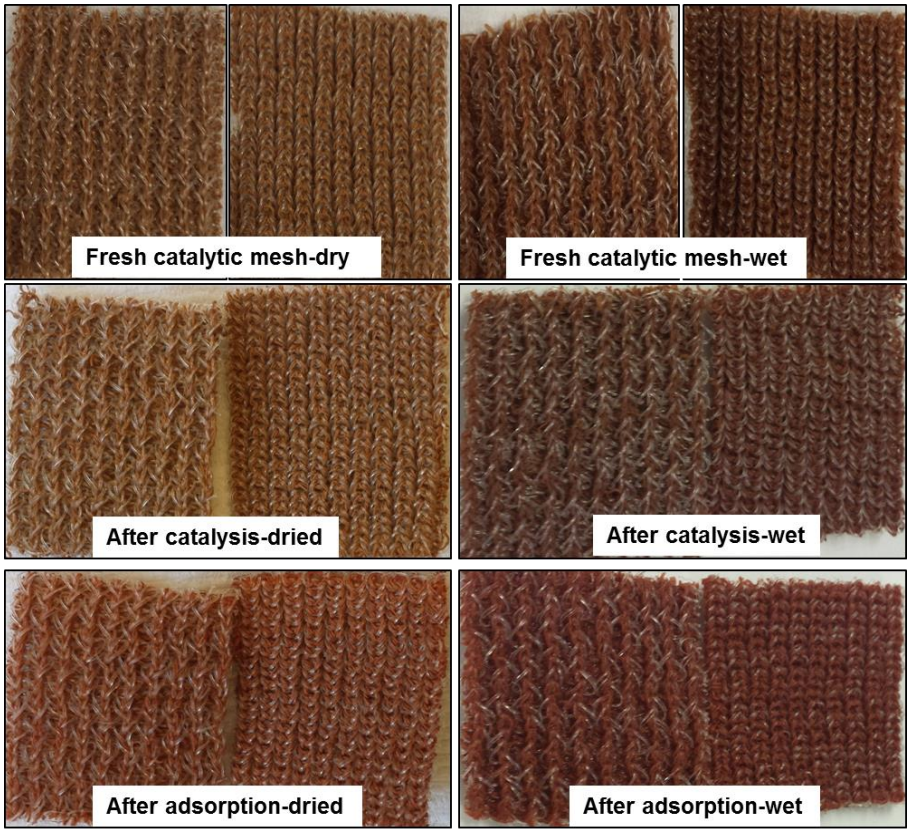

Figure 4-20: Photographic evidence to distinguish catalysis and adsorption of dye. Top row- fresh modified PAN catalyst. Middle row – modified PAN catalyst after 100 minutes of exposure in the presence of H_2O_2 – represents catalysis of dye. Bottom row – modified PAN catalyst after 100 minutes of exposure in the absence of H_2O_2 – represents adsorption of dye.

The photographic evidences taken at the end of experiments performed with and without H_2O_2 further help distinguish catalysis and adsorption processes. Figure 4-20 presents

the photographs of air-dried and wet catalyst exposed to the RO16 solution with and without H_2O_2. The catalyst exposed to the RO16 solution with H_2O_2 was not coloured by the dye whereas the catalyst exposed to the dye solution without H_2O_2 was coloured. In heterogeneous catalysis, the first step of the reaction is the adsorption of reactants (dye and H_2O_2) and favouring their activation (Jacques, 2017). Thus, in the presence of H_2O_2, the adsorbed dye was catalysed as the H_2O_2 was activated and the reaction occurred whereas the adsorbed dye remained unreacted as there was not oxidant to activate.

Moreover, Figure 4-21 compares the photographs taken at the end (after 100 minutes) of experiments performed with and without H_2O_2. The bubbles on the surface of the catalyst exposed to the dye solution with H_2O_2 are indicative to the formation of carbon dioxide and / or oxygen due to the mineralization of dye and concomitant decomposition of H_2O_2. Absence of bubbles on the surface of the catalyst exposed to the dye solution without H_2O_2 is indicative to adsorption of dye onto the catalyst.

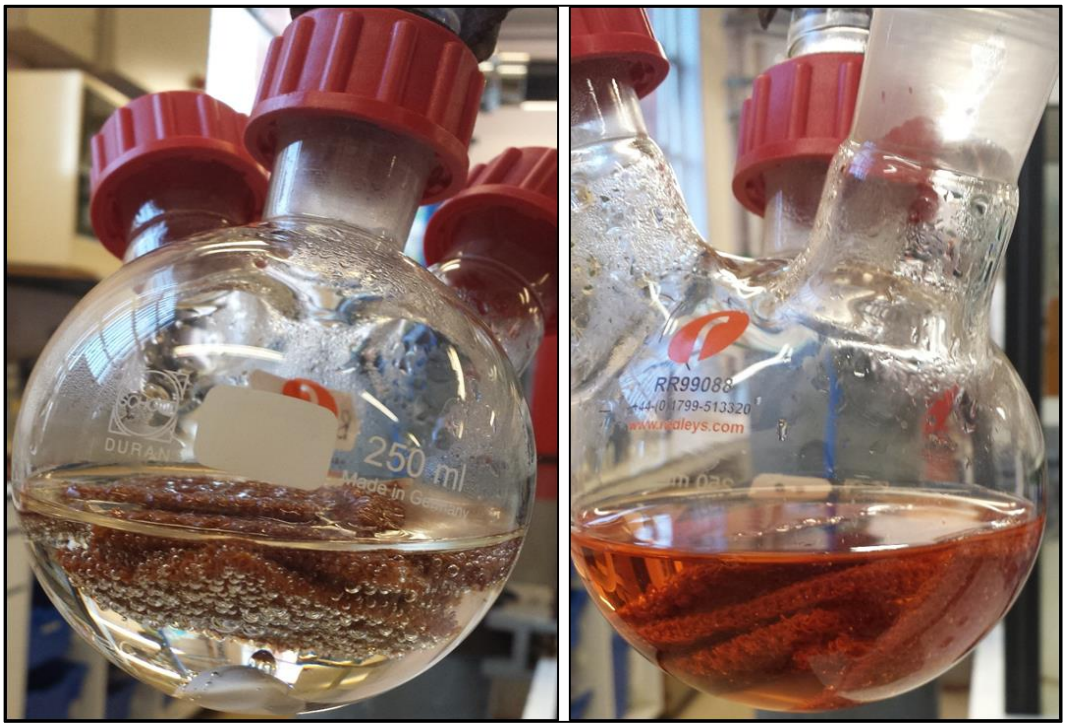

Figure 4-21: Photographs taken at the end of experiments performed with (left) and without (right) H_2O_2.

In addition to spectral and visual evidences discussed above, the difference between catalysis and adsorption was further investigated. It can be assumed that the difference between the extents of removals corresponding to the two processes would increase if the catalyst were exposed to a substrate load much higher than its maximum adsorption capacity. In other words, the removal of RO16 is expected to be much faster and higher

in the presence of H_2O_2 than in the absence of H_2O_2. Accordingly, an experiment was performed with a higher dye to catalyst ratio by using a lower amount of catalyst (2 g) keeping other parameters fixed. The results presented in Figure 4-22 clearly shows that the removal of RO16 in the presence of H_2O_2 occurred much faster than in the absence of H_2O_2. The difference between removals corresponding to catalysis and adsorption become larger. Figure 4-22 also shows that, after 40 minutes, the decolourization efficiencies (@ 493.5 nm) corresponding to catalysis and adsorption were 83.6 % and 41.2 % respectively. Similarly, the loss of aromaticity (@ 254 nm), after 40 minutes, were 66.2 % and 41.2 % respectively.

According to Figure 4-22, the differences in removal efficiencies for decolourization and loss of aromaticity during catalysis and adsorption processes, when performed with 2 g catalyst, become 42.4 % and 25 % respectively. Similarly, according to Figure 4-17, these differences, when performed with 6 g catalyst, become 25.7 % and 13.3 % respectively. This supports the assumption and confirms that the degradation of RO16 was due to the catalytic oxidation.

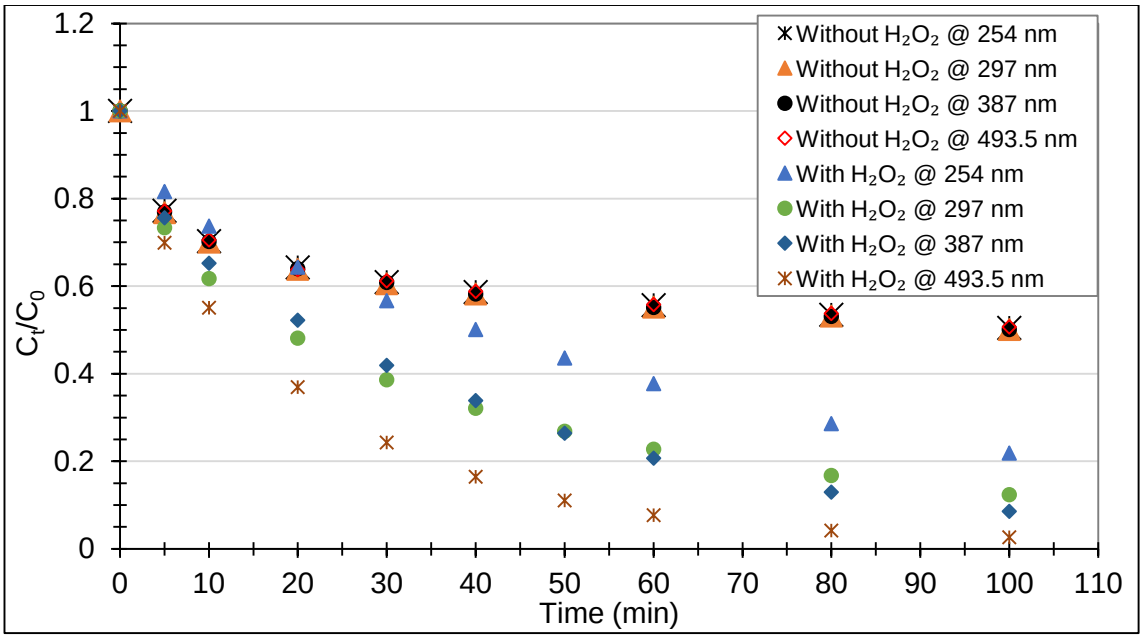

Figure 4-22: Investigation on catalysis and adsorption of RO16.

[Experimental Conditions: 2 g catalyst, with H_2O_2 (C_0 = 125 mg/L) and without H_2O_2 at pH 3 in 50 mL of RO16 solution (C_0 = 50 mg/L) at 30 °C].

Table 4-4 shows that the maximum adsorption capacity of modified PAN catalyst is 0.68 mg/g. Accordingly, the adsorption capacity of 2 g modified PAN catalyst becomes 1.36 mg. The mass of RO16 in 50 mL of dye solution (C_0 = 50 mg/L) become 2.5 mg. After

100 minutes, the removal efficiency (~ 50 %) in the absence of H_2O_2 corresponds to removal of 1.25 mg of RO16, which agrees with the Langmuir adsorption capacity and thus confirms adsorption of RO16.

The difference between initial and final (after 100 minutes of catalysis) pH values with respect to initial concentration of H_2O_2 is presented in Figure 4-23. The pH of the solution decreased while catalysis proceeded. The decrease in pH is indicative of the extent of mineralization and formation of acidic products (organic acids). The lowest final pH corresponding with 125 mg/L of initial amount of H_2O_2 also suggests that more acidic products have formed. In another word, 125 mg/L of H_2O_2 is an optimum initial concentration.

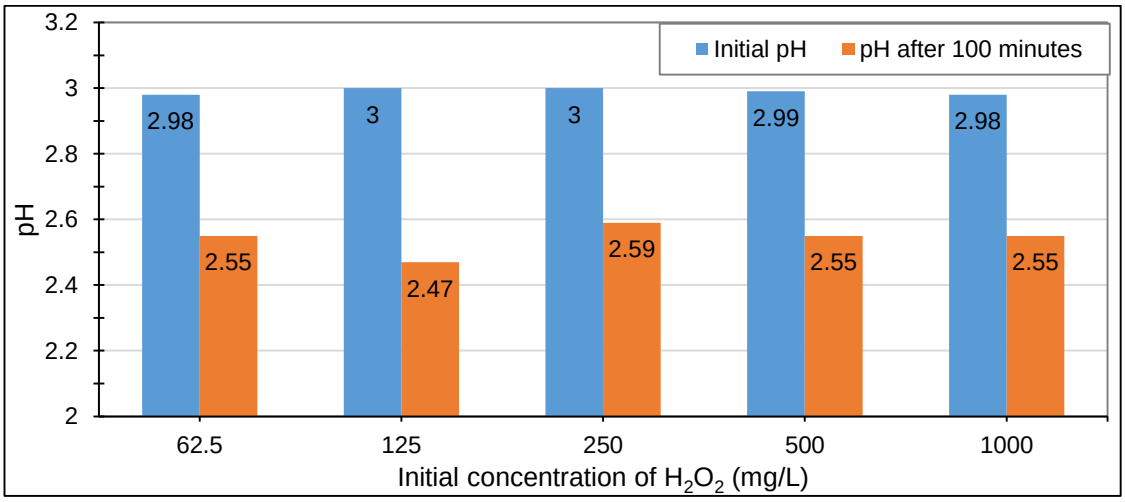

Figure 4-23: Average pH variation during the reaction process with respect to varying initial concentration of H_2O_2.

[Experimental conditions are similar to Figure 4-17]

4.5.4.2.1. EFFECT OF DISSOLVED OXYGEN ON THE DECOLOURIZATION OF RO16

The influence of dissolved oxygen (DO) and air on removal of RO16 was investigated. The dye solution was sparged with helium gas to remove the DO and air. Figure 4-24 shows that 53 % of RO16 was removed via sorption onto the catalyst (production roll 3 used in this case) when complete catalytic decolourization occurred. Decolourization of RO16 was expected to be faster in the presence of dissolved oxygen and in contact with air (not sparged). However, slightly faster decolourization was observed in deoxygenated condition (sparged), clearer picture could be seen before 60 minutes. It is believed that the faster decolourization observed before 60 minutes in the sparged condition was due to the higher adsorption of dye enforced by the pressure of helium gas, suggesting low probability of having catalytic decomposition of RO16 due to the presence of DO and air.

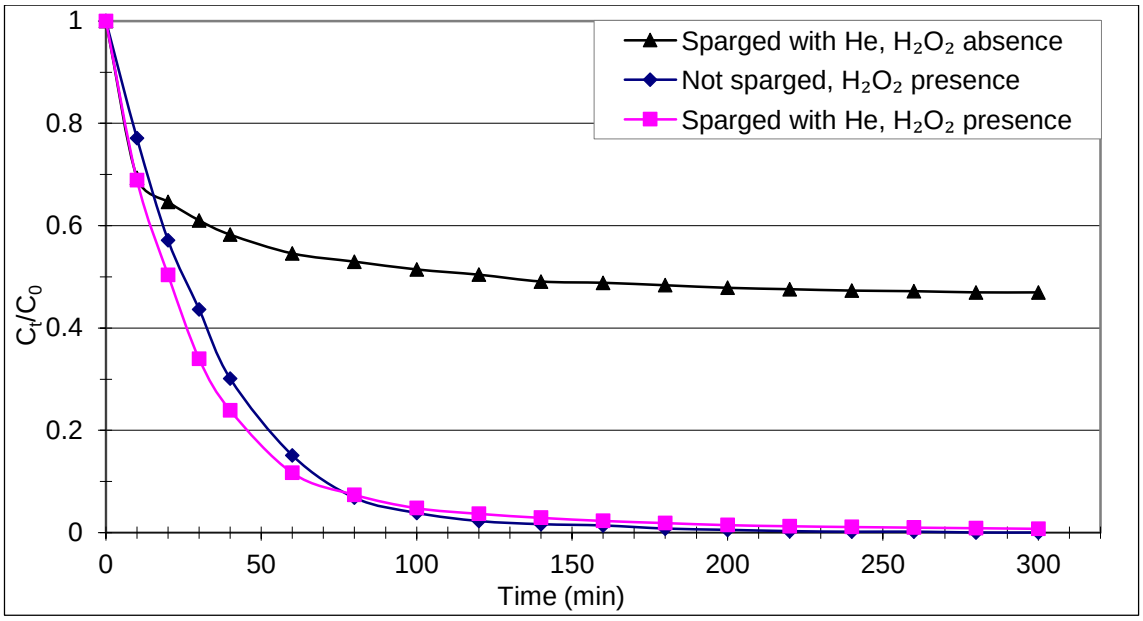

Figure 4-24: Influence of dissolved oxygen and air on decolourization (Vis - 493.5 nm) of RO16.

[Experimental conditions: 3 g catalyst (production roll 3), 1,000 mg/L H_2O_2, pH 3 in 50 mL of RO16 solution (C_0 = 50 mg/L) at room temperature (= 21°C)].

4.5.4.3. INFLUENCE OF PH ON DEGRADATION OF RO16

The pH of the reaction medium is one of the most influential parameters for the degradation of RO16. The influence of pH in Fenton-like system is discussed in the section 2.2.3.1.5, p. 42. The effect of pH on the degradation of RO16 was investigated by varying pH of the reaction medium in the range of pH 2 to pH 7, while keeping amount of catalyst and initial concentration of H_2O_2 fixed at 6 g and 125 mg/L respectively. The results are presented in Figure 4-25.

The rate of decolourization of RO16 (Vis-493.5 nm) and removal of aromaticity (UV-254 nm) decreased sharply by 73.4 % and 68.2 % respectively when the pH of the medium was increased from pH 3 to pH 5. The efficiencies of decolourization after 40 minutes corresponding to pH 3, pH 4 and pH 5 were 98.7 %, 57.5 % and 25.3 % respectively. Similarly, the efficiencies for loss of aromaticity after 40 minutes corresponding to pH 3, pH 4 and pH 5 were 86.2 %, 30.1 % and 18 % respectively. However, further increase in pH to 7 resulted in negative efficiencies for both decolourization (- 3 %) and loss of aromaticity (- 5 %). On the other hand, removal efficiency also decreased, more pronounced before 20 minutes, when the pH was further decreased below pH 3. The extent of decolourization and loss of aromaticity at pH 2 after 40 minutes were 98.3 % and 53 % respectively. The difference between removal at pH 2 and pH 3 for absorption band at 254 nm was more pronounced compared to other absorption bands. This is due

to higher absorbance as a result of the dissolution of iron from the catalyst at pH 2, seen (cloudy) during experimentation.

The decolourization efficiencies at pH 2 and pH 3 after 40 minutes seem similar but the difference between two pHs was significant at the beginning of the reaction, for example 26.7 % and 9.6 % after five and ten minutes respectively. Thus, pH 3 is adopted as an optimum pH for the removal of RO16. The decrease in removal of RO16 with respect to increasing pH can be attributed to a number of mechanisms which are discussed below.

The pH of the reaction medium exerts profound influence on the adsorption of adsorbate molecules by influencing the ionization / dissociation and the surface properties of the modified PAN catalyst (Pandiselvi and Thambidurai, 2013; Deng *et al.*, 2015). This is discussed in section 4.5.3.1.4.

The hydrolytic speciation of Fe (III) is strictly dependent on pH of the solution (see Figure 2-7). At pH 2.54, existence of equal concentrations of Fe^{3+} and $FeOH^{2+}$ and much smaller concentrations of $Fe(OH)_2^+$ and $Fe_2(OH)_2^{4+}$ have been reported by (Pignatello, Oliveros and Mackay, 2006). Badawy, Ghaly and Gad-allah, 2006 reported that more $Fe(OH)^+$ is formed at pH 2 to pH 4 and the activity of $Fe(OH)^+$ is higher than Fe^{2+}. Pignatello, Oliveros and Mackay, 2006 pointed two reasons for optimum pH of 3. First, above pH 3, the Fe^{3+} begins to precipitate in the form of hydrous oxyhydroxides. Second, $[Fe(HO_2)^{2+}]$ reaches a maximum around pH 3. The above explanations elucidate the highest removal of RO16 in the pH range of 2 to 3. At pH ≥ 4, complexation of Fe (III) via Fe^{3+} hydrolysis is also noted as a cause of reduced efficiency (Catrinescu *et al.*, 2003; Muruganandham and Swaminathan, 2004; Bokare and Choi, 2014; Queirós *et al.*, 2015).

Moreover, stability of H_2O_2 is also strictly dependent of pH. At low pH, higher stability of H_2O_2 favours the generation of $^{\bullet}OH$ radicals. However, stability of H_2O_2 decreases at higher pH as the concentration of the conjugate base of H_2O_2 increases according to Equation 4-18. The anions HO_2^- and OH^- further react with non-dissociated H_2O_2 molecules according to Equation 4-19 (Mitrović *et al.*, 2012) and Equation 2-22 (Boczkaj and Fernandes, 2017). Moreover, Mitrović et al., 2012 further argued that the $^{\bullet}OH$ reacts approximately 300 times faster with HO_2^- than with H_2O_2, resulting in quick decline in removal efficiency of RO16.

$$H_2O_2 \rightarrow HO_2^- + H^+, \qquad pK_a = 11.6$$ ***Equation 4-18***

$$HO_2^- + H_2O_2 \rightarrow H_2O + O_2 + OH^-$$ ***Equation 4-19***

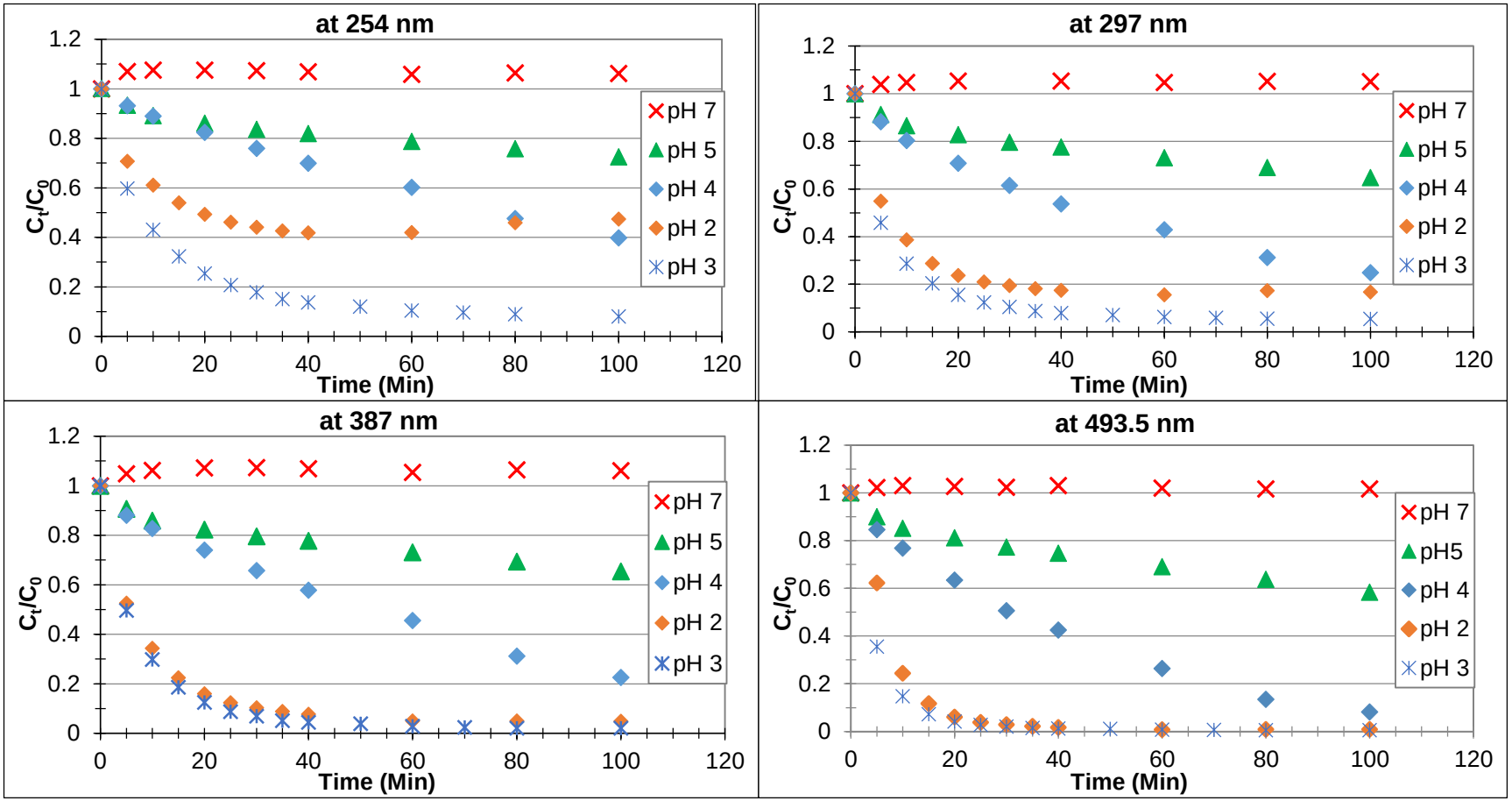

Figure 4-25: Influence of pH on degradation of RO16.

[Experimental conditions: 6 g catalyst, 125 mg/L H_2O_2, in 100 mL of RO16 solution (C_0 = 50 mg/L) at 30 °C.]

Additionally, at higher pH, auto-decomposition of H_2O_2 to molecular oxygen and water according to Equation 2-8 is reported (Catrinescu *et al.*, 2003; Badawy, Ghaly and Gad-allah, 2006; Queirós *et al.*, 2015). Further to this, the oxidation potential of $^{\bullet}OH$ radical also decreases rapidly with increasing pH (Neyens and Baeyens, 2003; Nidheesh, Gandhimathi and Ramesh, 2013), with values 2.65 V to 2.80 V at pH 3 and 1.90 V at pH 7 (Queirós *et al.*, 2015).

The slower removal rate corresponding to pH 2 is also attributed to a number of mechanisms that occur at very acidic pH. First, proton solvation of H_2O_2 leads to the formation of oxonium ion $(H_3O_2)^+$ as in Equation 2-20. Second, scavenging of $^{\bullet}OH$ radicals by excess protons (H^+) as in Equation 2-21. Third, speciation of iron in hexaquo ion $[Fe(H_2O)_6]^{2+}$ form which is relatively less reactive to H_2O_2 than other iron species (Nidheesh, Gandhimathi and Ramesh, 2013; Babuponnusami and Muthukumar, 2014; Queirós *et al.*, 2015; Fida *et al.*, 2017).

The relationship between adjusting acidic pH with inorganic acids (HCl, HNO_3, H_2SO_4 and H_2PO_4) and the rate of decolourization was studied by (Mitrović *et al.*, 2012). The authors reported that the anions (Cl^-, NO_3^-, SO_4^{2-} and PO_4^{3-}) evolve after dissociation of acids can scavenge $^{\bullet}OH$ radical and form inorganic radical ions such as $ClHO^{\bullet-}$. The study revealed the scavenging effect in the order of chloride > nitrate > sulfate > phosphate. Since, HCl was used to adjust the pH of the dye solution and to normalize the catalyst; this effect can have contributed to some extent as well.

Since production of more RO16 during catalysis was not possible, the negative removals at pH 7 is indicative to presence of products that absorb strongly at given absorption bands. This was investigated by performing control experiments at pH 7, only with H_2O_2 (i.e. without catalyst) and with catalyst (i.e. without H_2O_2). Results presented in Figure 4-26 show that increased absorbance in visible range (negative efficiency for decolourization) was due to catalyst and in UV range (negative efficiency for aromaticity loss) is linked to both catalyst and hydrogen peroxide.

At pH 7, additive effect (rather high absorbance at 254 nm) of catalyst and H_2O_2 is observed in the first 40 minutes. After 60 minutes, the absorbance at 254 nm become similar to that of catalyst only. This could be due to inefficient consumption of H_2O_2 as discussed in previous paragraphs. The increase in absorbance in the presence of catalyst only could be linked with the complexation of RO16 with the leached iron.

Moreover, catalyst alone could release hydroxylamine (NH_2OH), hydrazine (NH_2NH_2), ammonia (NH_3) and iron that might contribute to increase absorbance.

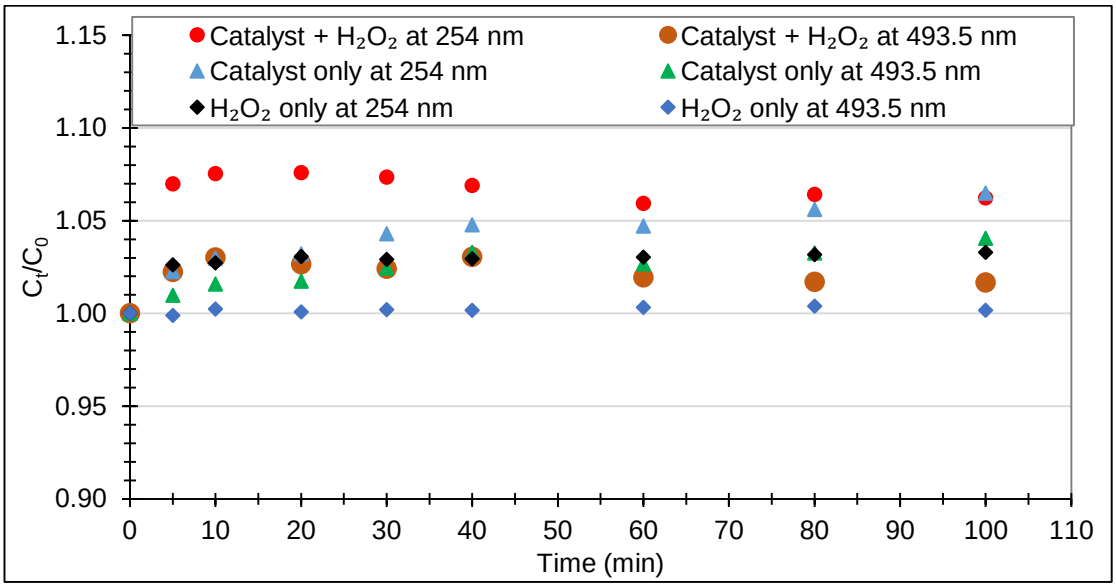

Figure 4-26: Investigation on negative removal of RO16 at pH 7.

[Experimental conditions: 100 mL of RO16 (C_0 = 50 mg/L) at 30 °C].

Some literature claimed that high-valent iron species, ferryl (IV), are produced in heterogeneous Fenton systems at neutral or basic pH (De-Laat and Gallard, 1999; Babuponnusami and Muthukumar, 2012; Bokare and Choi, 2014; He *et al.*, 2016). The negative removal at pH 7 rules out the oxidation via ferryl ion route. In other words, the degradation of RO16 occurred via $^{\bullet}OH$ radical route. In fact, a separate test involving radical trapping method confirmed the production of $^{\bullet}OH$ radicals at pH 3 but not at pH 7 (result not included here).

4.5.4.4. INFLUENCE OF INITIAL CONCENTRATION OF SUBSTRATE (RO16)

The initial concentration of substrate is known to influence Fenton-like oxidation processes. This is due to the change in ratio between substrate, catalyst and the oxidant. Increasing the concentration of substrate only adds the number of substrate molecules but not the number of active sites and the number of oxidant molecules. In other words, the higher the concentration of substrate the higher is the chemical oxygen demand which means more oxidant is required. Thus, it is generally believed that the removal efficiency decreases with respect to the increasing substrate concentration. This effect was investigated by varying the initial concentration of RO16 in the range of 12.5 mg/L to 100 mg/L, whilst keeping other parameters at optimum conditions.

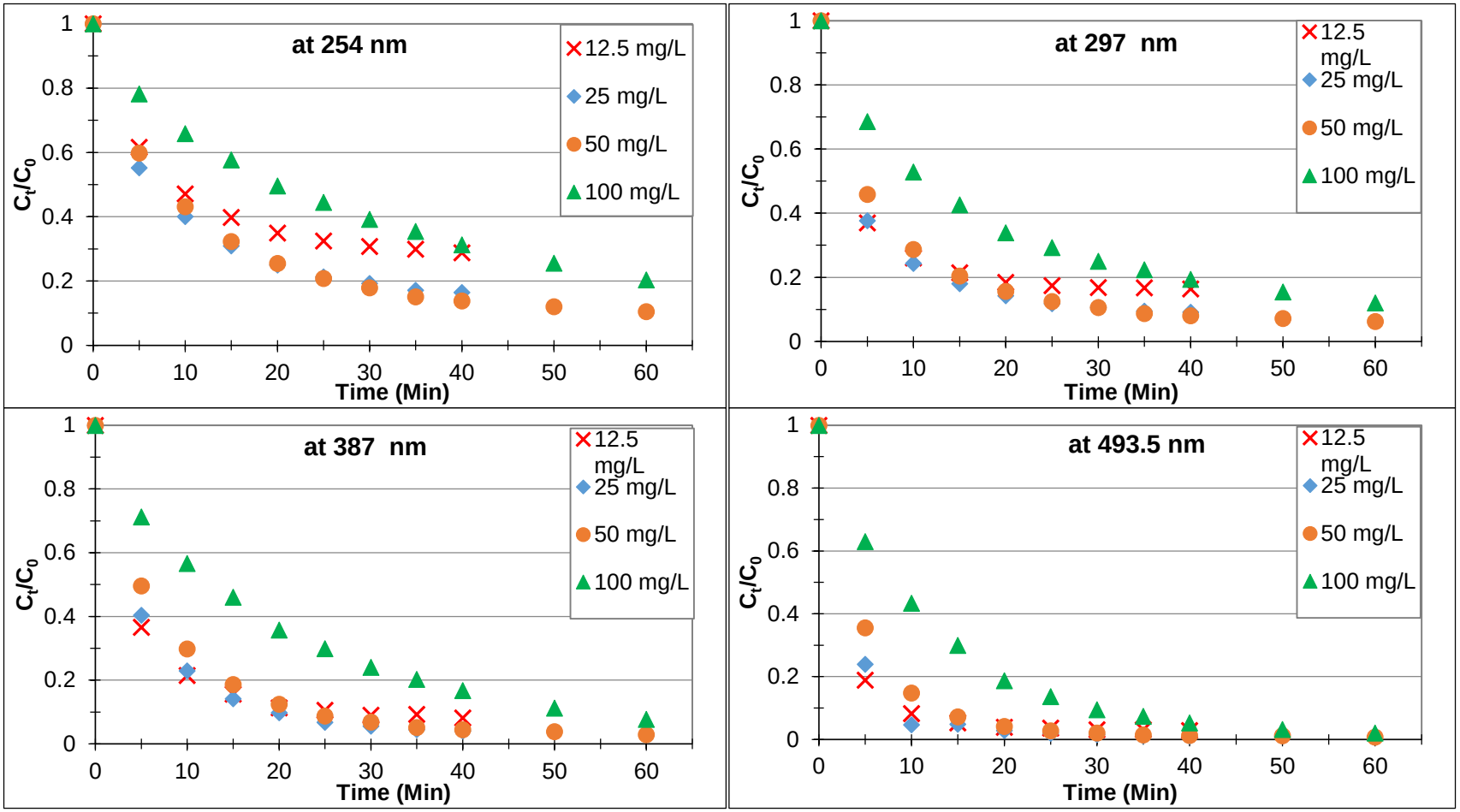

Figure 4-27: Influence of RO16 concentration on degradation process.

[Experimental conditions: 6 g catalyst, 125 mg/L H_2O_2, pH 3 in 100 mL of RO16 solution at 30 °C.]

Figure 4-27 presents the results for the influence of initial concentration of RO16 on degradation process. Since the reaction was quick, it is meaningful to compare the effect of RO16 concentration after ten minutes of catalysis. Accordingly, after 10 minutes of catalysis, the efficiency of decolourization, as measured at 493.5 nm, is 91.7 %, 95.3 %, 85.2 % and 56.6 % corresponding to 12.5 mg/L, 25 mg/L, 50 mg/L and 100 mg/L of RO16 respectively. Similarly, the loss of aromaticity, as measured at 254 nm, is 52.9 %, 60 %, 56.9 % and 34.2 % corresponding to 12.5 mg/L, 25 mg/L, 50 mg/L and 100 mg/L of RO16 respectively. Similar trends of removals at bands 297 nm and 387 nm were also observed. The results show that catalysis of RO16 was negatively influenced when initial concentration of RO16 increased or decreased beyond 25 mg/L. These results agree with the finding of previous studies by other authors (Kasiri, Aleboyeh and Aleboyeh, 2008; Hassan and Hameed, 2011; Idel-aouad *et al.*, 2011; Panda, Sahoo and Mohapatra, 2011).

The decrease in removal efficiency with respect to increase in concentration of RO16 (25 mg/L to 50 mg/L and 100 mg/L) can be explained in terms of production of $^{\bullet}OH$ radicals and competition with intermediate products. Idel-aouad et al., 2011varied the concentration of C.I. Acid Red 14 in the range of 50 mg/L to 200 mg/L and observed negative effect on decolourization rate. The authors argued that generation of $^{\bullet}OH$ radicals was hindered as the active sites on the surface of catalyst were occupied by dye ions. This is possible due to the increasing number of dye molecules. Panda, Sahoo and Mohapatra, 2011 also observed negative influence of decolourization of Methyl Orange while varying the concentration in the range of 300 mg/L to 800 mg/L. Supporting the afore mentioned statement, the author further mentioned that the intermediate products formed during dye-degradation compete with the dye molecules for the available active sites.

The improved in removal efficiency with respect to increase in concentration of RO16 (12.5 mg/L to 25 mg/L) can be explained in terms of collision theory. Since the lifetime of $^{\bullet}OH$ radicals is very short, for oxidation to occur, they must react (collide with dye molecules) only where they were formed. Thus, the frequency of effective collision increases by increasing the concentration of reactant(s). Kasiri, Aleboyeh and Aleboyeh, 2008 observed improvement in removal efficiency when concentration of Acid Blue 74 increased in the range of 0.0214 mM to 0.107 mM and drop in removal efficiency with further increased in dye concentration of Acid Blue 74 to 0.168 mM. The authors argued that increasing concentration increases the number of dye molecules per volume unit

enhances the probability of collision between dye molecules and the oxidant (•OH), resulting in the improvement in removal efficiency.

Hassan and Hameed, 2011 observed improvement in removal efficiency while varying the concentration of Acid Red 1 in the range of 25 mg/L to 100 mg/L. They also explained the effect in terms of collision theory.

4.5.4.5. INFLUENCE OF TEMPERATURE ON DEGRADATION OF RO16

The temperature of reacting medium is very crucial in wastewater treatment. Generally, higher the temperature the higher is the rate of reaction. However, Fenton-like systems can have negative influence of temperature. Therefore, the influence of temperature on the degradation of RO16 was investigated by varying the reaction temperature in the range of 20 °C to 35 °C and the results are presented in Figure 4-28.

As expected, the results show improved rate of decolourization and loss of aromaticity when the temperature of reaction medium increased from 20 °C to 35 °C. The efficiency of decolourization, after ten minutes of catalysis, corresponding to 20 °C, 25 °C, 30 °C and 35 °C were 28.7 %, 48.7 %, 85.2 % and 91.4% respectively. Similarly, the loss of aromaticity, after ten minutes of catalysis, corresponding to 20 °C, 25 °C, 30 °C and 35 °C were 15.1 %, 22.7 %, 56.9 % and 61.8 % respectively. Similar trends of removals for absorption bands at 297 nm and 387 nm were also observed. According to Figure 4-29, the decolourization and loss of aromaticity of RO16 seem linearly dependent within the temperature range studied. The results of this study are in line with previous studies (J. Herney Ramirez *et al.*, 2007; Chen, 2009; Mesquita *et al.*, 2012; Duarte *et al.*, 2013).

The increase in removal with respect to increasing temperature can be explained by Arrhenius law that relates exponential dependency of kinetic constant on temperature. Accordingly, the generation of •OH radicals increases with respect to increase in temperature, enhancing the degradation of dye. The influence of temperature in the removal of Chicago Sky Blue (Mesquita *et al.*, 2012) and Orange II (J. Herney Ramirez *et al.*, 2007) dyes revealed a linear relationship between dye removal and temperature in the range of 10 °C to 70 °C. However, the investigation on removal of Alcian Blue-tetrakis (methylpyridinium) chloride dye (Duarte *et al.*, 2013) revealed that the removal rate increased in the range of 10 °C to 50 °C only and decreased at 70 °C. These authors also argued the improvement in removal rate based on Arrhenius law and higher rates of •OH radicals formation.

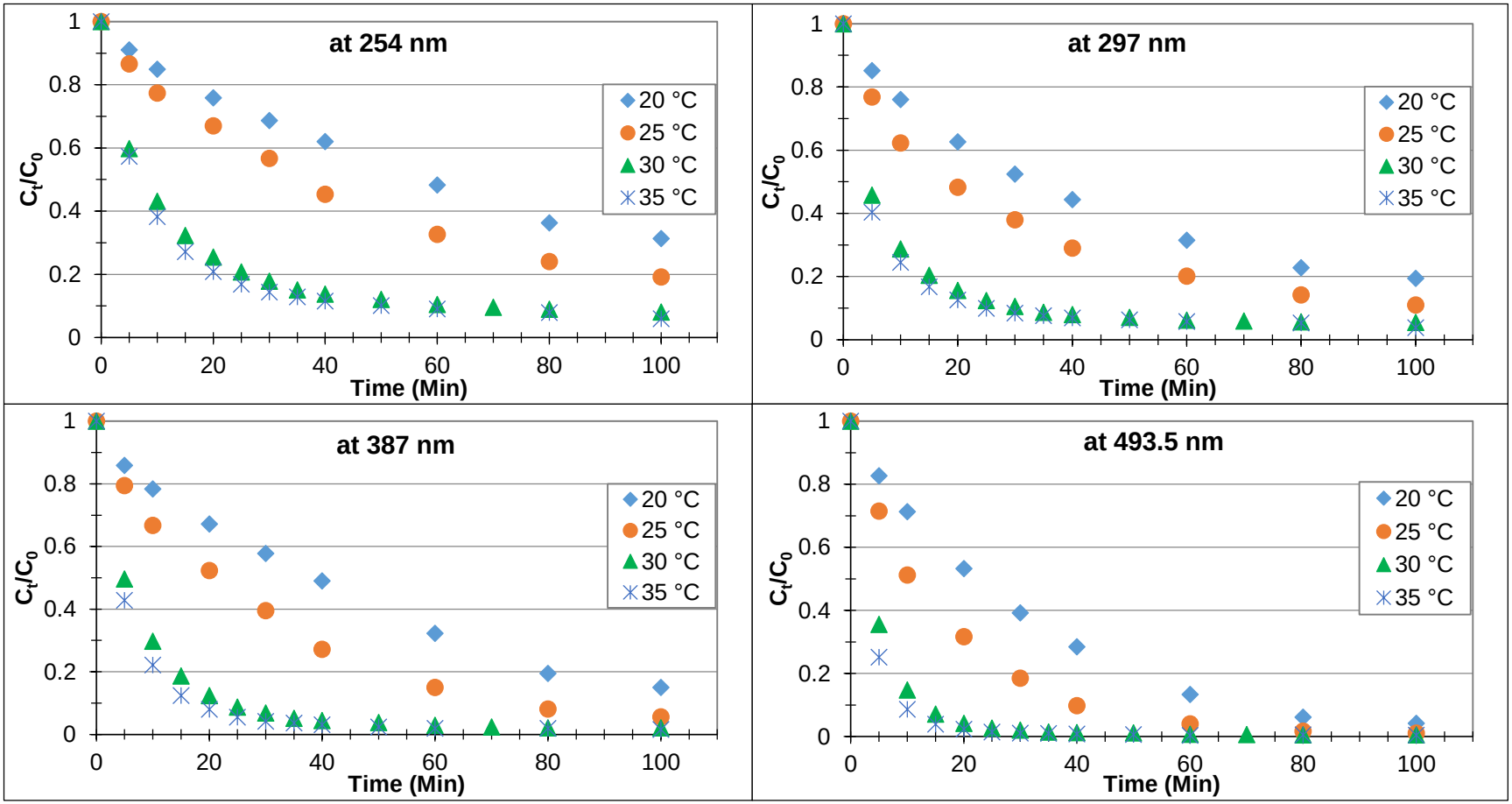

Figure 4-28: Influence of temperature on degradation of RO16.

[Experimental conditions: 6 g catalyst, 125 mg/L H_2O_2, pH 3 in 100 mL of RO16 (C_0 = 50 mg/L) solution.]

The Arrhenius equation is given as $k = Ae^{\frac{-Ea}{RT}}$ where k = rate constant, A = constant, Ea = activation energy, R = universal gas constant and T = temperature (Kelvin). The Arrhenius equation can be linearized as $\ln(k) = -\frac{Ea}{R} * \frac{1}{T} + \ln(A)$. A plot of ln(k) versus $\frac{1}{T}$ yields a straight line if Arrhenius equation is obeyed. The initial rate of the reaction can be calculated using the tangent at time zero in Figure 4-28. Then, activation energy (Ea) and constant (A) can be calculated from the slope (-$\frac{Ea}{R}$) and intercept {ln (A)} of the linear plot of ln(k) versus $\frac{1}{T}$.

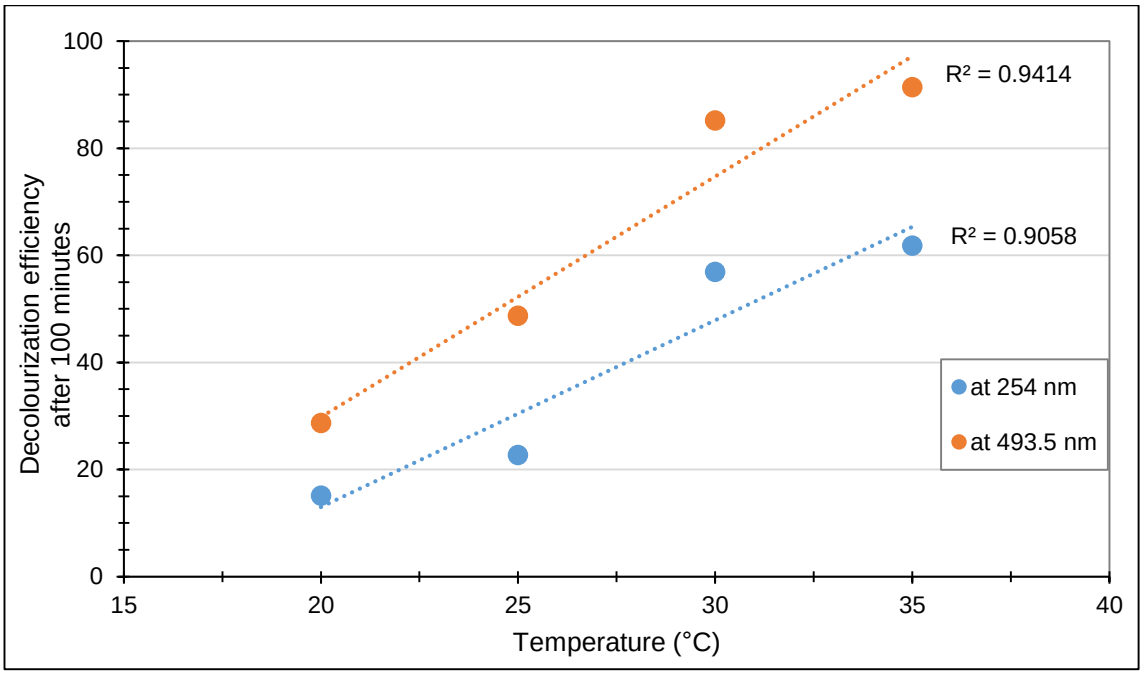

Figure 4-29: Decolourization and loss of aromaticity of RO16 dye as a function of temperature.

4.5.4.6. AMOUNT OF CATALYST LOSS WITH RESPECT TO PROCESS PARAMETERS

The amount of catalyst loss with respect to process parameters was evaluated in terms of leached iron. The concentration of leached iron was measured in the acidified samples collected at the end (100 minutes) of the experiments performed to investigate the influence of process parameters. Accordingly, Figure 4-30 presents the relationship between amounts of catalyst (iron) loss with respect to process parameters.

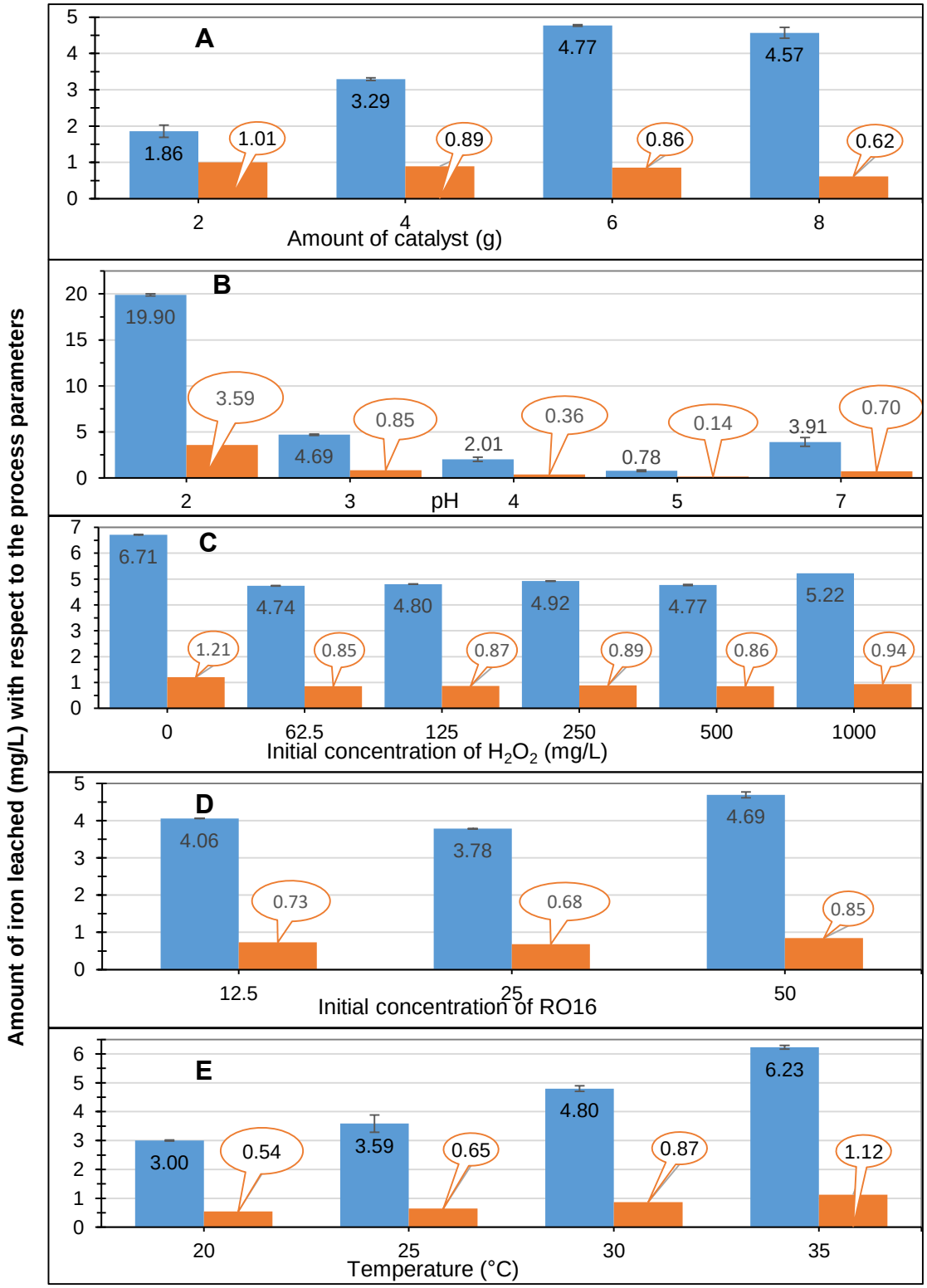

Figure 4-30: Amount of catalyst (Iron) loss with respect to process parameters.

[Experimental conditions: All experiments were performed with 6 g catalyst (varied in A), 125 mg/L of H_2O_2 (varied in C) at pH 3 (varied in B) in 100 mL of RO16 (C_0 = 50 mg/L, varied in D) at 30 °C (varied in E).

Figure 4-30-A shows increase in concentration of leached iron with respect to increase in amount of catalyst until the optimum amount (6 g) of catalyst. Beyond the optimum amount, the iron leaching remained insignificant. However, the relationship between the amounts of iron loss (% wt) with respect to mass of iron on the catalyst is found to be negative. This result is in agreement with the result of (J. Herney Ramirez *et al.*, 2007) who reported lower percentages of iron lost from the sample with higher iron content. The ration between iron and H_2O_2 decreased as the amount of catalyst increased, suggesting that leaching could be limited by H_2O_2. However, the result shown on Figure 4-30-B (that has same amount of iron and H_2O_2) does not support this argument as leaching at pH 2 was very high.

Figure 4-30-B shows that amount of leached iron was very high at pH 2 and decreased as initial pH of the medium increased to pH 5. This can be attributed to the increasing dissolution and accessibility of iron species with decreasing pH. These results are in agreement with other Fenton-like systems (Feng, Ã and Yue, 2006; J. Herney Ramirez *et al.*, 2007; Pastrana-Martínez *et al.*, 2015). The leaching of iron at pH 7 was higher than at pH 4 and pH 5. This can be explained in terms of stability of H_2O_2. Pastrana-Martínez et al., 2015 reported lower leaching of iron at higher H_2O_2 concentrations and explained in terms of stability of metal species promoted by H_2O_2. The authors further stated that H_2O_2 acts as an oxidizing agent and maintains the metal species in their oxide state. As discussed earlier, stability of H_2O_2 decreases with increase in pH, meaning that H_2O_2 concentration at the end of the reaction would be lower at higher pH than at lower pH. Thus, the lower the concentration of H_2O_2 the lower the metal oxide formation and hence the greater the leaching.

The amount of catalyst loss at pH 2 compared to loss at pH 3 together with the extent of removals, relatively better at pH 3, of the dye signify that the degradation of dye did not rely on the amount of leached iron. In other words, the system was relying on heterogeneous catalysis.

Although concentrations of leached iron at pH 3 is higher than the permitted discharge limit (2 mg/L) imposed by the European legislation, the loss of iron (%) from the catalytic mesh in terms of iron leaching is minimal. The loss of iron from the catalyst (0.85 %) at pH 3 ensures the longevity of catalyst.

Figure 4-30-C shows no direct relationship between amount of catalyst (iron) loss (%) and the initial concentration of H_2O_2. This result is in line with the finding of (Ramirez *et*

al., 2007; Ramirez *et al.*, 2007; Duarte *et al.*, 2013). Relatively higher amount of iron loss (%) was observed (Figure 4-30-C) when no H_2O_2 was used. This could be again explained in terms of stability of metal species promoted by H_2O_2 which is discussed above in this section. H_2O_2 is more stable in low pH meaning H_2O_2 is expected to present relatively longer than at basic pH. Thus, stability of metal species is promoted in the presence of H_2O_2 (Pastrana-Martínez *et al.*, 2015) whereas in the absence of H_2O_2 stability of metal species is not promoted. Thus, at pH 3, dissolution of catalyst was favoured in the absence of H_2O_2. Alternatively, in the absence of H_2O_2, it is possible that protons (H^+) can attack ligands, break Fe-ligand bonds, and release iron.

The result presented in Figure 4-30-D shows no relationship between iron loss and initial concentration of RO16. Figure 4-30-E presents the amount of iron loss with respect to the temperature of the reacting medium. A direct relationship between amount of iron loss and temperature was observed. The amount of iron loss increased with respect to the increase in temperature. The amount of iron loss (%) was doubled when the temperature increased by 1.5 folds, from 20 °C to 35 °C. This is expected as higher temperature increases the dissolution of catalyst. Alike increase in reaction rate, it is believed that breaking of Fe-ligand bonds is also favoured by high temperature.

4.5.4.7. EXTENT OF DECOLOURIZATION AND MINERALISATION OF RO16

Decolourization of dyes occurs mainly due to the cleavage of chromophoric groups (see section 4.5.1, p.94), for example, the azo bond (-N=N-) in the case of RO16. Cleavage of chromophoric group (decolourization) is an initial stage during the degradation process of a given dye. In case of RO16 degradation, this is evidenced by the higher removal corresponding to absorption band at 493.5 nm. Formation of more toxic intermediate products due to inefficient degradation of a dye is discussed in chapter two. Therefore, complete decolourization of a given dye may not result in complete mineralization. Thus, the extent of decolourization and mineralization of RO16 were evaluated. This work was done using previous batch of catalyst (production roll 3), which was less active than the current batch (production roll 7) used in optimization process discussed above.

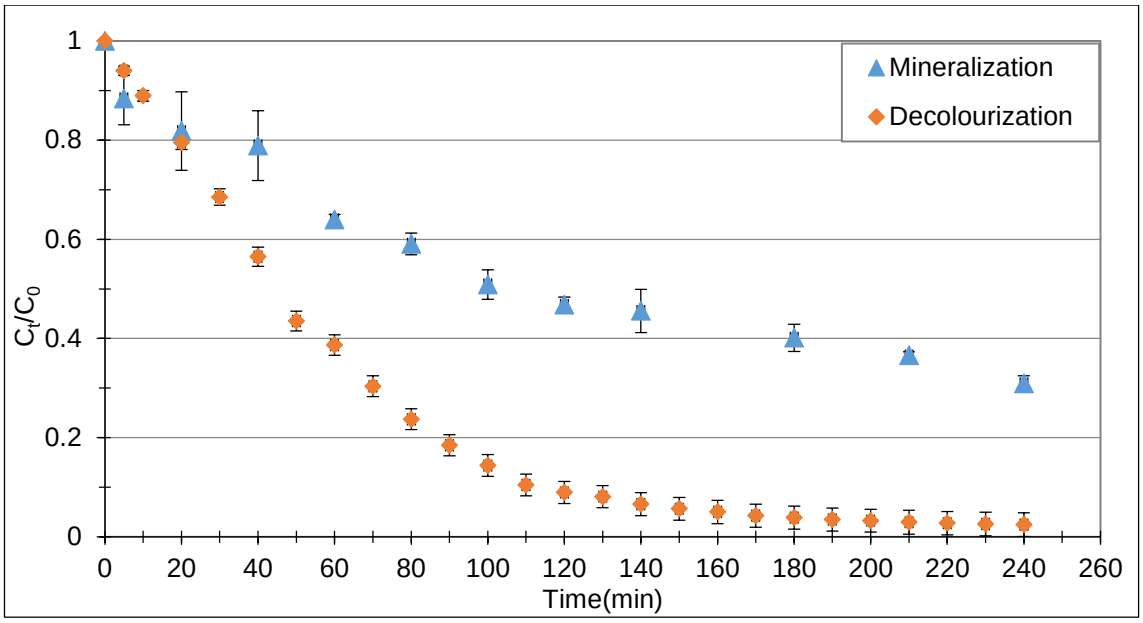

Figure 4-31: Extent of decolourization and mineralization of RO16.

[Experimental conditions: 6g catalyst (production roll 3), 1,000 mg/L H_2O_2, pH 3 in 100 mL RO16 solution (C_0 = 50 mg/L) at room temperature (= 23°C)].

Experiments were performed to measure the extent of decolourization and mineralization. The decrease in absorbance at 493.5 nm represents the extent of decolourization of RO16 due to the cleavage of chromophore group. The reduction in TOC value represents the extent of mineralization of RO16 into carbon dioxide and water (see section 4.3.3.3, p. 87). Figure 4-31 shows that decolourization of RO16 occurred much faster than the mineralization. After 4 hours, 70 % of RO16 was mineralized into CO_2 and H_2O whereas the decolourization efficiency become 97.5 %.

4.5.4.8. HOMOGENEOUS VERSUS HETEROGENEOUS CATALYSES

An ideal catalyst is expected to last forever. However, in reality, a catalyst eventually deactivates with respect to usage. One of the mechanisms that deactivates catalyst is leaching (Richardson, 1989; Argyle and Bartholomew, 2015). Thus, it is possible that a treatment system can undergo homogeneous catalysis with the leached catalyst. Therefore, it is important to investigate whether the treatment system relies on homogeneous or heterogeneous catalysis. Thus, investigation on homogeneous catalytic removal of RO16 was performed according to the procedure laid out in section 4.3.3.7.

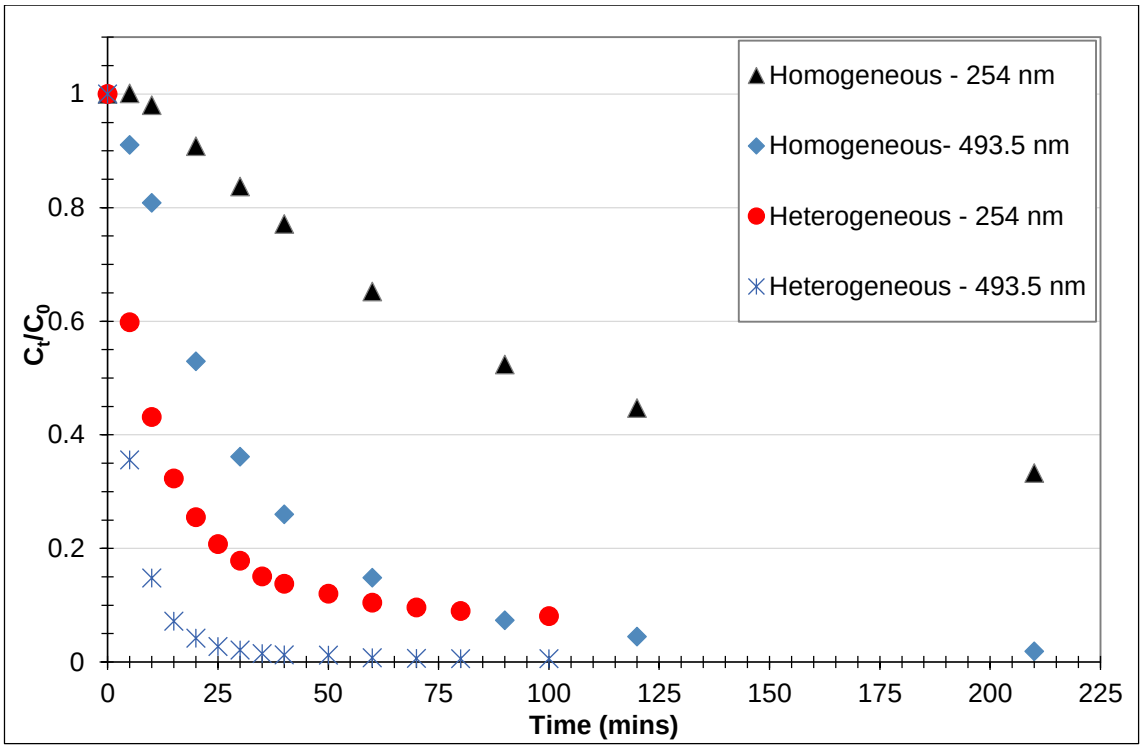

Figure 4-32: Comparison between homogeneous and heterogeneous catalytic decomposition of RO16.

[Experimental conditions: The iron in both processes was sourced from 6 g catalyst (see section 4.3.3.7), pH 3, 125 mg/L H_2O_2 in 100 mL RO16 (C_0 = 50 mg/L) at temperature = 30 °C].

Figure 4-32 compares the homogeneous and heterogeneous catalytic decomposition of RO16 at given conditions. It is clearly seen that decolourization of RO16 was more pronounced in heterogeneous catalysis compared to homogeneous catalysis. Approximately complete decolourization of RO16 occurred after 40 minutes in heterogeneous catalysis. Thus, it is meaningful to compare two processes within the first 40 minutes of the reaction. The difference in extent of decolourization of RO16 between two processes at five minutes was 55 % which further increased to 66 % at ten minutes and gradually declined with respect to time. Decolourization of RO16 in heterogeneous catalysis at ten minutes was approximately 4.5 folds faster than that of homogeneous catalysis.

Similarly, the difference in extent of aromaticity loss between two processes was 40.2 % at five minutes which gradually increased to maximum (65.8 %) at 30 minutes of and declined thereafter. Loss of aromaticity of RO16 at 30 minutes of heterogeneous catalysis was five folds faster than that of homogeneous catalysis. These observations are evident that the reaction was governed by means of heterogeneous catalysis.

It is noteworthy to mention that iron leaching is a gradual process and the iron concentration measured at the end of a batch experiment is the cumulative amount of iron leached from the beginning of the experiment. Thus, comparison of heterogeneous catalysis with the homogeneous catalysis using an amount of iron accumulated during a batch experiment is not a fair comparison. Comparison of two processes using an equivalent amount of iron from iron salts is also not truly correct as the speciation of iron could make a significant difference in reaction rate. It is expected that the leached iron from the modified PAN catalyst is complexed with ligands which could be water, dye and its intermediate products. The catalytic activity of complexed iron may not be similar to that of iron in iron salt. Therefore, in reality, the removal efficiency corresponding to homogeneous catalysis should be lower than the practically observed efficiency. Thus, the difference between two processes as discussed above would be even wider, revealing that the homogeneous system has null or negligible contribution, if any, in the catalytic decomposition of RO16.

4.5.4.9. TREATMENT OF EFFLUENT FROM THE DYE-BATH

4.5.4.9.1. THE SAMPLE AND THE CONSTITUENTS

The effectiveness of the treatment system was investigated with a semi-real effluent collected from a local Dyer in Leicester, UK. The sample was prepared by collecting the first wash of individual dye-baths as described in section 4.3.3.9. According to the technician of the company, the dyed fabric is washed up to six times. Thus, the representative sample was believed to be much more concentrated (up to six times) than the real effluent.

The Dyer was using a range of reactive and disperse dyes on sampling day. Amongst the reactive dyes were Yellow HE6G, Turq HA and Blue HEGN and those of disperse dyes were Red CC, Blue CC and Disperse Black. According to the technician of the company, the reactive dyes are more dominant in the wastewater than disperse dyes as the reactive dyes are very soluble in water and approx. only 60% of the dye goes to the fabric whereas disperse dyes are not very soluble in the water and very much less goes to wastewater. Besides dyes, the Dyer also used a wide range of auxiliaries during the dyeing process. These include sodium chloride (NaCl), acetic acid (CH_3COOH), sodium carbonate (Na_2CO_3), potassium hydroxide (KOH), sodium hydroxide (NaOH), sodium metabisulphite ($NaHSO_3$), hydrogen peroxide (H_2O_2) and enzymes. The use of enzymes is to decompose the excess hydrogen peroxide in the wastewater.

4.5.4.9.2. UV-VIS SCANNING OF DYES AND EFFLUENT SAMPLE

Generally, dyes are not 100 % pure. The Reactive Orange-16 used in this study supplied by Sigma Aldrich was 50 % pure. Therefore, the dyes samples collected from Jersey Dyer were also assumed as 50 % pure. The dyes (C_0 = 50 mg/L) used by the company while sampling were scanned individually using UV-Vis spectrophotometer.

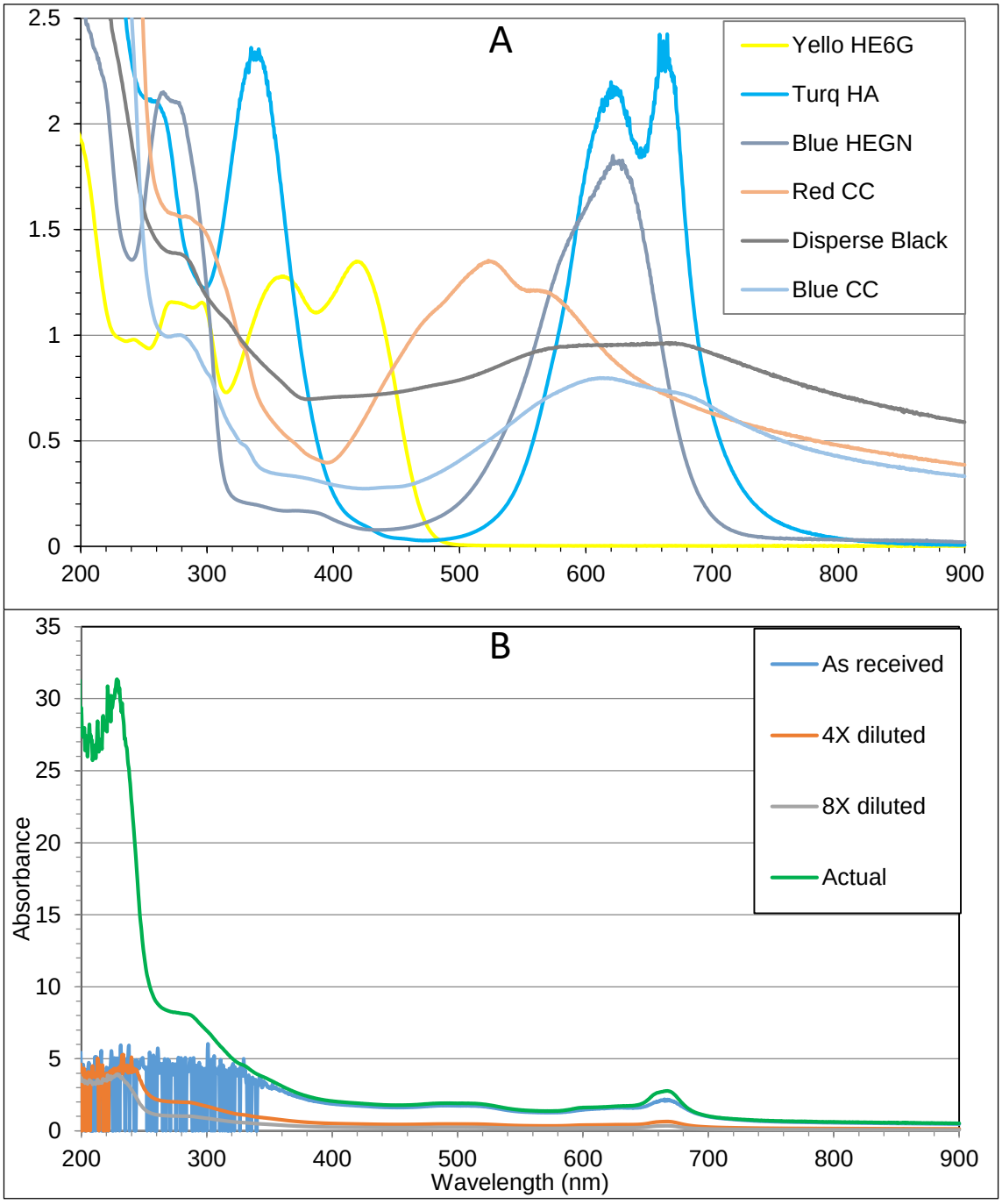

Figure 4-33: UV-Vis spectra of dyes used by the Dyer and the dye-bath effluent sample.

Figure 4-33-A and Figure 4-33-B present the spectra of the individual dyes used by the dyer on the sampling day and the dye-bath sample respectively. It can be seen that the maximum absorbance wavelength (λ_{max}) of each dye is different and many of the absorption bands overlap. This shows the complexity to quantify the rate of degradation of individual dye corresponding to its absorption band. For example, Blue CC and Disperse Black do not have distinctive peaks and they were masked by others. Therefore, to monitor the degradation of all dyes, the samples were taken as a function of time and scanned in the range of 200 nm to 900 nm, looking at changes in overall spectrum. Similarly, the change in spectra (Figure 4-33-B) in the visible region was not seen due to the very high absorbance in the UV region. Thus, the spectra of dye-bath effluent will be divided into UV and visible ranges with the reference wavelengths as 292 nm and 672 nm respectively.

4.5.4.9.3. CATALYSIS OF DYE-BATH EFFLUENT

4.5.4.9.3.1. INITIAL ASSESSMENT FOR THE CATALYSIS OF DYE-BATH EFFLUENT

The operating parameters (9 g catalyst, 1,000 mg/L H_2O_2, and pH 3 at 30 °C) of the treatment process during initial assessment were selected based on the knowledge gained from the optimization of RO16. In 24 hours, the removal efficiencies corresponding to 292 nm and 672 nm were 54 % and 78 % respectively. Further increase in residence time did not improve the removal efficiency. In 48 hours, the removal efficiencies corresponding to 292 nm and 672 nm become 58.5 % and 80 % respectively, indicating the need for further improvement in treatment process.

4.5.4.9.3.2. IMPROVEMENT OF THE TREATMENT PROCESS

In order to improve the performance of the system, at first, the initial concentration of H_2O_2 was increased to 2.5 g/L. Figure 4-34-A shows that, in 48 hours removal efficiencies corresponding to 292 nm and 667 nm increased to 85 % and 95 % respectively. After 48 hours, the system was out of H_2O_2, indicating further requirement of oxidant. Therefore, 2 g/L of H_2O_2 was redosed after 48 hours. After 24 hours of redosing, the corresponding removal efficiencies further improved to 95 % and 99.99 % respectively. Although, the dye-bath effluent was successfully decolourized, the significantly longer residence time (72 hours) suggests the need of further improvement in the treatment process. Accordingly, the amount of catalyst was increased to 12 g, initial H_2O_2 concentration 2.5 g/L, and pH 3 at 30 °C. H_2O_2 (1 g/L) was redosed after 24 hours and 30 hours

respectively. Figure 4-34-B shows that, in 48 hours, the new adjustment of parameters yielded 95 % and 98.5 % removals corresponding to 292 nm and 672 nm respectively.

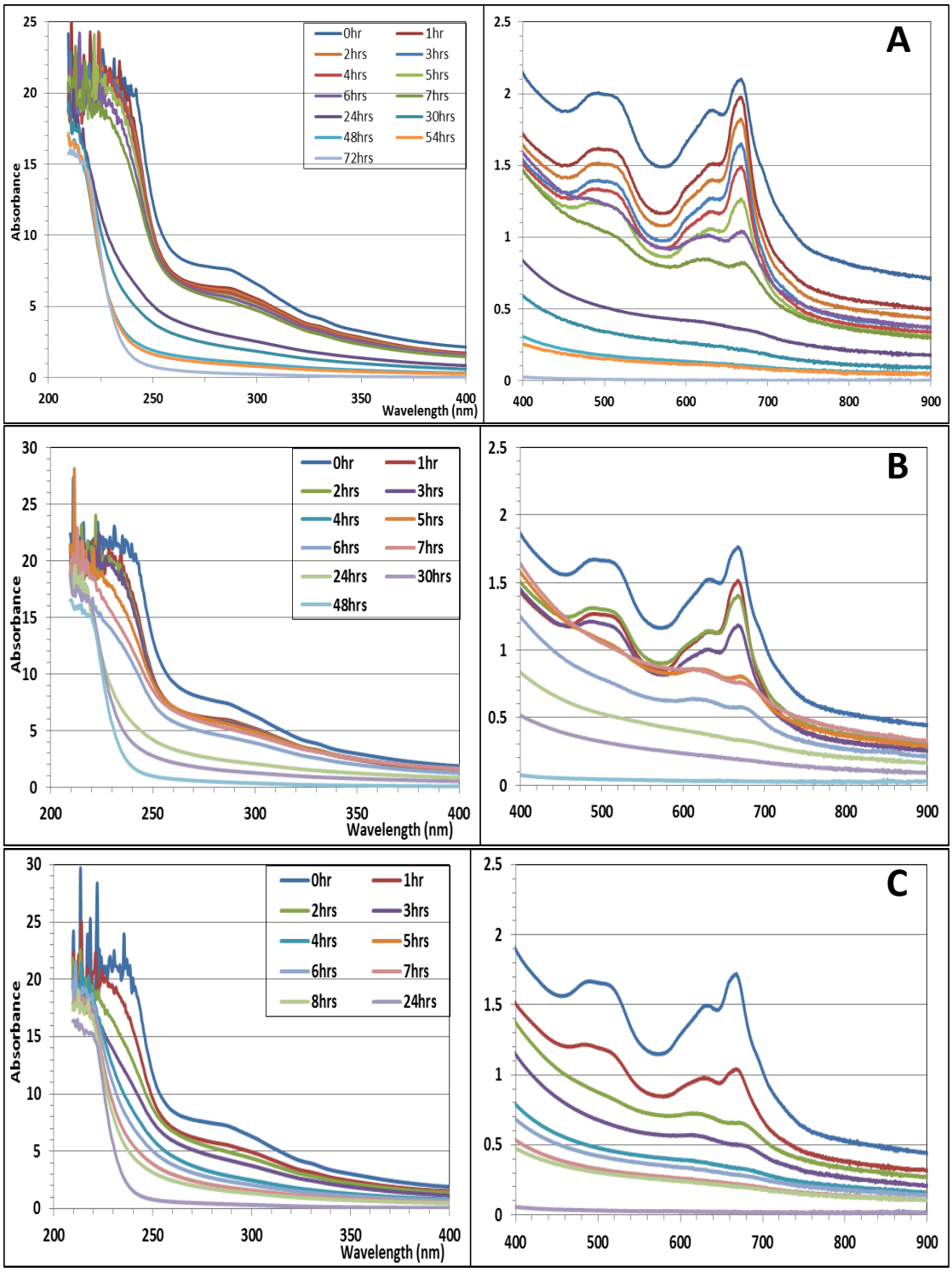

Figure 4-34: Improvement of catalytic degradation process of dye-bath effluent.

[Experimental conditions: A) 9 g catalyst (production roll 3), H_2O_2 = 4.5 g/L (initial 2.5 g/L, redosed 2 g/L after 48 hours), pH 3 in 100 mL of dye-bath effluent at 30°C. B) 12 g catalyst (production

roll 3), H_2O_2 = 4.5 g/L (initial 2.5 g/L, redosed 1 g/L each at 24 and 30 hours), pH 3 in 100 mL of dye-bath effluent at 30°C. C) 12 g catalyst (production roll 3), H_2O_2 = initial H_2O_2 2.5 g/L, pH 3 in 100 mL of dye-bath effluent at 40°C].

Further enhancement of the treatment process was made by increasing the reaction temperature to 40 °C, keeping the amount of catalyst to 12 g, initial H_2O_2 to 2.5 g/L at pH 3. According to Figure 4-34-C, the performance of the system doubled, compared to 30 °C, and removal efficiencies corresponding to 292 nm and 672 nm become 94.8 % and 98.8 % in 24 hours. The amount of H_2O_2 consumption was reduced to 2.5 g/L only reflects the effectiveness of treatment process in terms of decolourization of the dye-bath effluent. Figure 4-35 compares the effectiveness of catalytic treatment process in terms of decolourization of dye-bath effluent.

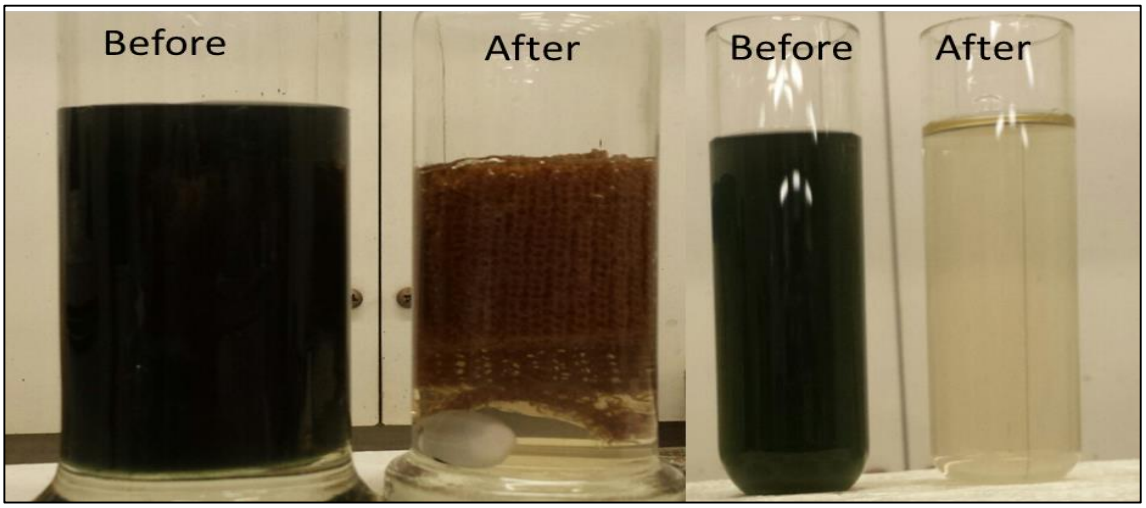

Figure 4-35: Dye-bath effluent before and after catalytic treatment process.

[The left two and the right two show with and without the modified PAN catalyst to make it easier to see the extent of decolourization].

4.6. SUMMARY

The effectiveness of heterogeneous modified PAN catalyst and H_2O_2 system on the treatment of textile effluent was investigated in a batch mode of operation. The treatment system was optimized by evaluating the influence of operating parameters on removal of model compound, the Reactive Orange 16 (RO16), an azo (reactive) dye. The removal of RO16 was measured in terms of decolourization (absorption band at 493.5 nm) and loss of aromaticity (absorption band at 254 nm). The system was found to be influenced by the pH, amount of modified PAN catalyst, initial concentration of oxidant (H_2O_2), initial concentration of substrate and temperature of the reacting medium.

The influence of process parameters; pH (2 to 7), amount of modified PAN catalyst (0 g to 8 g/100 mL), initial concentration of H_2O_2 (0 mg/L to 1000 mg/L), initial concentration of substrate (12.5 mg/L to 100 mg/L) and temperature (20 °C to 35 °C) on removal of dye were studied. The study revealed that the influences of pH and catalyst were more significant compared to the influence of H_2O_2, the pH being the most influential. The study established an optimum treatment condition for decolourization of RO16 as 6 g catalyst, pH 3, 125 mg/L H_2O_2 in 100 mL of RO16 solution (C_0 = 50 mg/L) at 30 °C. At optimum condition, 99.5 % decolourization (measured at 493.5 nm) and 91.9 % loss of aromaticity (measured at 254 nm) were achieved in 100 minutes. The study also revealed that ~ 70 % of the dye mineralized to carbon dioxide and water when decolourization was nearly completed. The pH of the reacting medium dropped by ~ 0.5 unit. The dissolved oxygen has no noticeable effect on removal of dye.

The sorption of dye onto the modified PAN catalyst was studied. The study of equilibrium adsorption isotherms revealed that adsorption of RO16 onto the modified PAN catalyst can be best described by Langmuir adsorption isotherm model. The best-fit of Langmuir isotherm model confirms the presence of monolayer adsorption surface with homogeneous sites. The maximum adsorption capacity was found to be 0.68 mg of RO16 per gram of modified PAN catalyst. The adsorption of RO16 onto the modified PAN catalyst was found to be heavily influenced by the pH of the dye solution.

The amount of catalyst loss was measured in terms of amount of iron leaching with respect to the changes in the process parameters. The study revealed a direct relationship of iron loss with respect to variations in pH and temperature of the treatment system. The more acidic the pH, the higher is the catalyst (iron) loss. The amount of iron leached at pH 2 was ~ 4.5 folds higher than at pH 3. Similarly, the higher the temperature, the higher is the catalyst loss. The iron leaching was found to be linearly dependent on temperature of the system. The amount of catalyst loss doubled when temperature increased from 20 °C to 35 °C. No direct relationship of catalyst loss with respect to initial concentration of H_2O_2 and substrate was found. However, the amount of iron loss increased with respect to the increase in amount of catalyst until an optimum point is reached. The amount of iron lost from the catalyst was below 1 % in all experiments listed in Table 4-3 except at pH 2 (3.6 %). The 0.87 % loss of iron from the catalyst at optimum condition ensures the long life of the system.

The possibility of having homogeneous catalysis of RO16 due to the leached iron was investigated. The heterogeneous catalysis was found to be 4.5 to five folds faster than

the homogeneous catalysis performed with the leached iron, indicating that homogeneous catalysis has negligible contribution in the catalytic decomposition of RO16.

The potential application of the treatment system in industrial scale was examined by evaluating its performance in the treatment of real dye-bath effluent, which was much more concentrated than usual textile effluent. The system also successfully treated the concentrated dye-bath effluent. The maximized extent of decolourization (measured at 672 nm) and loss of aromaticity (measured at 292 nm) were 99.99 % and 95 % respectively were achieved.

CHAPTER FIVE

5. CONTINUOUS FLOW TREATMENT OF REACTIVE ORANGE 16 (RO16) AND LIFETIME OF THE MODIFIED PAN CATALYST

5.1. INTRODUCTION

Adoption of a laboratory scale chemical process to the industrial scale is rarely successful. The great challenge is to reproduce results obtained at laboratory scale of treatment of a small quantity of wastewater, usually millilitres to litres, compared to cubic metres or millions of cubic metres at the industrial scale (Euzen, Trambouze and Wauquier, 1993). Therefore, it is necessary to gather accurate and meaningful information to establish a cost-effective industrial process that can achieve the same level of treatment as that of the laboratory scale and perhaps improve the industrial scale through additional experimental design, the steps of process development or scaling up (Euzen, Trambouze and Wauquier, 1993; Donati and Paludetto, 1997; Perego and Peratello, 1999). The stage of scaling up of a treatment process is decisive in the selection of the scale (bench, pilot, and demonstration unit) (Euzen, Trambouze and Wauquier, 1993) and the mode of operation (batch, semi-batch and continuous) (Donati and Paludetto, 1999; Perego and Peratello, 1999) of the treatment process.

At bench scale, certain aspects of the treatment process are studied handling relatively small quantities of wastewater, to minimize the consumption of resources (Euzen, Trambouze and Wauquier, 1993). Bench scale experiments are frequently performed as a predecessor to a full scale pilot experiment (Stephenson and Blackburn, 1998). The pilot scale experiment incorporates all the industrial constraints such as impurities, operation period, materials and equipment reliability etc. Pilot plant is a representative experimental rig of the industrial plant that facilitates the study of all the problems related to scaling up of the process. Demonstration unit is a first industrial unit on a modest scale and incorporates about $1/10^{th}$ of the size required for industrial process (Euzen, Trambouze and Wauquier, 1993; Stephenson and Blackburn, 1998).

Batch mode operates with the instantaneous introduction of reactants at the beginning and there is no in / out-flow of reactants as reaction proceeds for a set time. Semi-batch mode lies between batch and continuous flow modes of operation. In semi-batch mode, an initial amount of reactants is added into the reactor. Some components of reaction process can be added or withdrawn while the reaction proceeds. The continuous flow mode operates with the continuous flow of reactants into the reactor which emerges as a continuous stream of product (Lopez, Taghon and Levinton, 1989; Perego and Peratello, 1999; Jana, 2011; Speight, 2017).

There is no general rule to select the best operation mode for a treatment process. However, reaction time, economic balance, operation scale, flexibility of treatment,

process and product type may enforce the selection of an operation mode (Donati and Paludetto, 1999; Speight, 2017). Despite significant developments in agitator blade and baffle design, batch mode of operation is not an ideal solution as mixing in large batch reactors is limited by the amount of energy that can be supplied and a high agitator load can destabilise the shaft (Speight, 2017). Moreover, separation of catalyst (iron) from the treated effluent is time consuming and an inherent drawback of the batch treatment process and requires a secondary treatment (Nanda, 2008; Meshram *et al.*, 2011; Queirós *et al.*, 2015). Semi-batch processes are operated on non-steady state batch processes hence are not used as often as batch and continuous processes (Speight, 2017). Therefore, the continuous flow process, specifically with continuously mixed tank reactors (CMTR) are well known as continuously stirred tank reactors (CSTR), is an alternative to overcome the disadvantages of the batch and semi-batch process (Chaplin and Bucke, 1990; Donati and Paludetto, 1999; Nanda, 2008; Meshram *et al.*, 2011; Queirós *et al.*, 2015; Speight, 2017) .

Continuous flow reactors are used for a wide variety of processes within the industries. Mixing is an important aspect of the continuous flow process as efficient mixing of reactants improves the efficiency of heat and mass transfer. Depending on mixing mechanism, continuous flow reactors can be classified as mixing by diffusion, mixing by pumping and mixing by agitation. Mixing by diffusion relies on concentration and / or temperature gradients within the reactor. Mixing by diffusion is not practical in reactors with large flow channels and effluent with immiscible fluids. The turbulent flow generated by continuous pumping promote mixing if the fluid velocity is high. However, in long reactors, the drop in pressure hinders the mixing and this occurs with viscous effluents. Installation of baffles within the reactor minimizes this effect. Mixing by mechanical agitation ensures efficient mixing irrespective of reactant throughput and viscosity and thereby eliminates the need for long flow channels and subsequent pressure drop. The strong axial mixing created by mechanical agitators can be negated by subdividing the reactor into a series of mixed stages using baffles (Nanda, 2008; Speight, 2017).

The standard paradigm in scaling up of a treatment process is to begin with a bench scale batch followed by continuous flow experiment, then scaling up to pilot scale leading to the construction of the full scale industrial reactor according to the sequence shown in Figure 5-1. However, literature suggest that most studies available were performed in closed (batch) reactor (Donati and Paludetto, 1999; Hodaifa *et al.*, 2013; Queirós *et al.*, 2015) focussing on the main operating conditions and this is particularly true in case of

dyes (Duarte *et al.*, 2013; Zodi *et al.*, 2013). The second stage in the standard paradigm for scaling up of a treatment process, the bench scale continuous flow experiments, and specifically those of the Fenton / Fenton-like mechanism, are poorly dealt with in the literature (Melero *et al.*, 2009; Mesquita *et al.*, 2012; Duarte *et al.*, 2013). These experiments can provide better insights to understand reaction kinetics, mass transfer, energy consumption, start-up and shutdown operations and steady-state performance (Tokumura, Shibusawa and Kawase, 2013).

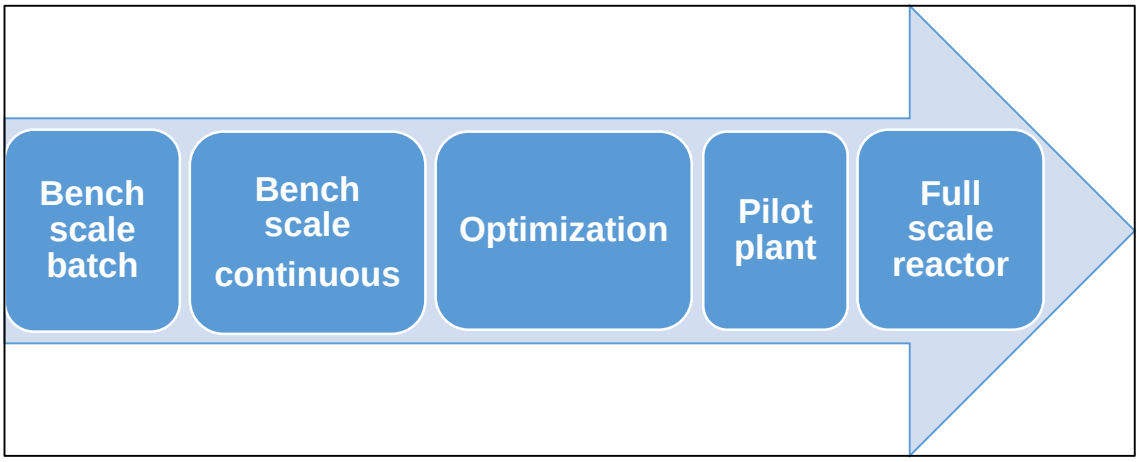

Figure 5-1: Standard paradigm in designing a chemical process.

Deactivation of a heterogeneous catalyst is inevitable and can occur physically and / or chemically. Physical deactivation occurs due to blocking of pores, loss of active sites due to agglomeration, closure of pores and adsorption of impurities. Chemical deactivation occurs due to chemisorption of impurities (poisoning, textural modification, coking) and fouling due to thermal degradation and leaching by the reaction mixture (Perego and Peratello, 1999; Nauman, 2001; Bisschops and Spanjers, 2003; Nanda, 2008; Argyle and Bartholomew, 2015). Since batch mode of operation is not reliable to study the deactivation mechanism of the catalyst, continuous flow mode of operation is the only choice (Perego and Peratello, 1999).

5.2. AIM AND OBJECTIVES

The aim of this study was to investigate the effectiveness of a heterogeneous modified polyacrylonitrile (PAN) catalyst in continuous flow treatment of Reactive Orange 16 (RO16) dye.

The aim of this study was achieved through the following objectives:

- To investigate the effect of H_2O_2 concentration on decolourization of RO16 dye

- To investigate the effect of residence time (≈ flow rate) on decolourization of dye
- To investigate the lifetime of PAN catalyst in relation to the treatment of dye
- To investigate the mechanism of catalyst deactivation
- To investigate the regeneration of catalyst
- To investigate the catalytic activity of regenerated catalyst in the treatment of RO16

5.3. MATERIALS AND METHODS

The reagents, materials and methodologies used in this study are discussed separately in the following sections.

5.3.1. REAGENTS

All the reagents used in this part of the project are listed in Table 4-1. They were used without further purification. The required solutions and dilutions were made using double distilled water.

5.3.2. MATERIALS

Apart from the conventional glassware (beaker, volumetric flask, Erlenmeyer flask, graduated and bulb pipettes) used in the laboratory; the other materials and instruments used in this part of the project are listed in Table 4-2.

5.3.3. ANALYTICAL PARAMETERS AND METHODOLOGIES

The methodology for the analytical parameters measured in this study are given in the following sections.

5.3.3.1. pH

The pH of the solution on the bench was measured using JENWAY 305 pH meter as described in section 4.3.3.1, p. 86. The influent and effluent pH values during continuous flow experiment were measured using online data loggers, model pHTemp2000, supplied by MadgeTech.

5.3.3.2. CONDUCTIVITY

The conductivity of samples was measured using Mettler Toledo conductivity meter. The electrode was rinsed with double distilled water and immersed into the sample and stable reading was taken.

5.3.3.3. DETERMINATION OF HYDROGEN PEROXIDE (H_2O_2)

Hydrogen peroxide was measured with the colourimetric method adopted from (Eisenberg, 1943). The method relies on an instantaneous reaction of residual H_2O_2 with titanium (IV) sulfate reagent and form yellow coloured complex, the pertitanic acid. The titanium (IV) sulfate reagent was prepared as described in (Ekpurke, 2018, p. 69). The absorbance of complex was recorded at maximum wavelength (λ = 408 nm). The absorbance (Y) obtained from the UV-Vis spectrophotometer was converted to concentration of H_2O_2 (X) using calibration Equation 5-1 obtained from the calibration curve presented in Figure 5-2. For some rapid tests, peroxide strips ranged 0 to 100 mg/L of H_2O_2 were used.

$$Y = 0.0125X - 0.0045$$ ***Equation 5-1***

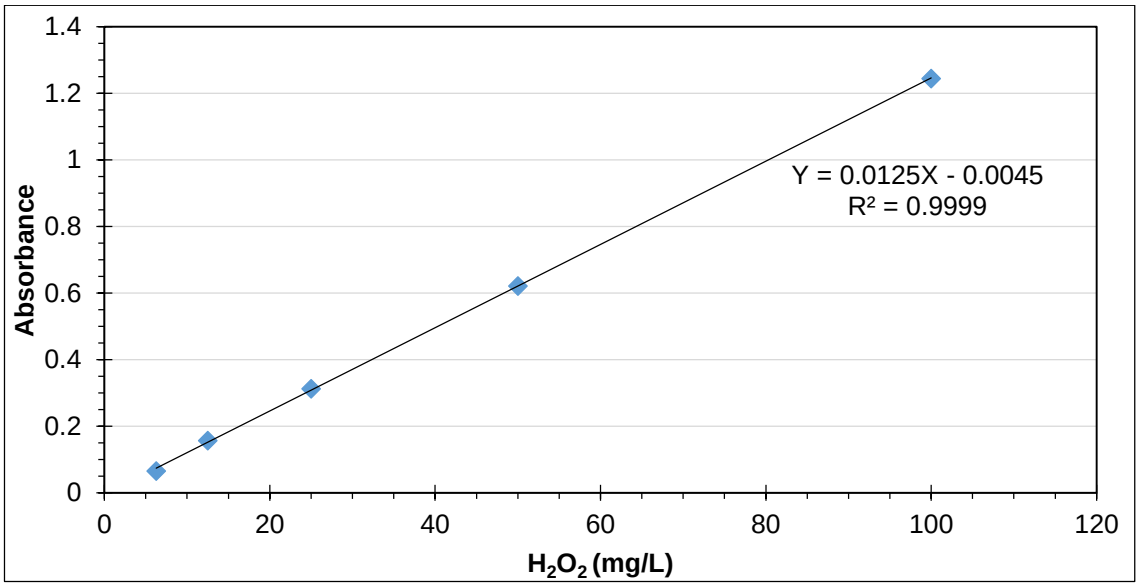

Figure 5-2: UV-Vis spectrophotometric calibration function for the analysis of hydrogen peroxide using titanium (IV) sulfate reagent.

5.3.3.4. DECOLOURIZATION OF REACTIVE ORANGE 16

Decolourization of Reactive Orange 16 was studies according to the procedures laid out in the section 4.3.3.2, p. 86.

5.3.3.5. MINERALIZATION

Mineralization of Reactive Orange 16 was determined according to the procedures laid out in the section 4.3.3.3, p. 87.

5.3.3.6. DETERMINATION OF IRON

5.3.3.6.1. IRON IN THE SOLUTION PHASE

The concentration of leached iron in the solution was determined according to the procedures laid out in the section 4.3.3.6, p. 90.

5.3.3.6.2. RESIDUAL IRON ON THE CATALYST

A vial containing a known amount of catalyst was filled with conc. HCl and placed in a heating block (pre-heated at 148 °C) for two hours. The vial was allowed to cool and the solution was transferred into a 100 mL flask. Above procedures repeated twice. Then, the catalyst was washed three times with dilute HCl (1 M) followed by distilled water making final volume to 100 mL. The solution was filtered through Whatman filter paper and analyzed using AAS accordingly as described in section 4.3.3.6.

5.3.3.7. CHEMICAL OXYGEN DEMAND (COD)

Chemical Oxygen Demand (COD) of the samples was determined according to the procedures laid out in the section 4.3.3.4, p.88 .

5.3.3.8. FUNCTIONAL STRUCTURE OF PAN CATALYST

The change in functional structure of catalyst before and after the treatment of RO16 was analyzed using Fourier transform infrared spectroscopy-attenuated total reflectance (FTIR-ATR) in the region 4,000 to 400 cm^{-1} and transmittance mode. The FTIR-ATR was run with OPUS software. The resolution was set to 4 cm^{-1} and number of scans for sample and background were set to 30 and 10 respectively. The instrument was wiped with acetone before measuring background (air). PAN threads were pulled out from the catalyst samples taken from the different catalytic discs in the reactor and a single strand at a time was scanned. Scan was performed at least for three replicates. The spectra thus obtained were manipulated using baseline correction and smoothness (value 13) functions. The data belonging to each spectra were transferred to Microsoft Excel and an average transmittance of replicates was taken to produce a spectrum for the corresponding sample.

5.3.3.9. REGENERATION OF DEACTIVATED PAN CATALYST

Regeneration of deactivated modified PAN catalyst was performed in two stages.

5.3.3.9.1. STEP 1: CLEANING WITH EXCESS AMOUNT OF H_2O_2

The deactivated catalyst was washed with excess amount of peroxide. The reactor was washed with H_2O_2 solution; 10 L of 500 mg/L followed by 5.5 L of 1,500 mg/L, at pH 3 in continuous flow mode. The H_2O_2 solution was fed in to the reaction at the same flow rate as used during the experiment.

5.3.3.9.2. STEP 2: REIMPREGNATION OF IRON (III) SALT

At first, the deactivated catalyst was decontaminated via homogeneous catalysis in batch mode. Homogeneous catalysis was performed in 1,000 mL solution with 25 mg/L (126.93 mg of $FeSO_4.7H_2O$ in 1,000 mL) of Fe (II) sulfate in conjunction with 1,000 mg/L of H_2O_2 at pH 3 and room temperature. Inlet and outlet channels were blocked and the solution was poured into the reactor. The rotation speed of the discs was increased to very high to ensure effective mixing and reaction. Homogeneous catalysis was performed for a set period; time varied at each reimpregnation stage, and the solution was drained. This procedure was repeated twice. After homogeneous catalysis, the reactor was washed twice (5 minutes per batch) with 1,000 mL of double distilled water to get rid of free Fe (II) and peroxide.

Reimpregnation of iron onto the deactivated catalyst was performed in batch mode, residence time 3 hours, using a regeneration solution containing 13.7 g/L of Fe (III) sulfate pentahydrate and 53.7 g/L of sodium sulfate decahydrate. The natural pH (~ 2.15) of the solution was not adjusted during the reimpregnation. The solution was poured into the reactor and the rotation speed of the catalytic discs increased to ensure effective mixing in the reactor. The reactor was drained and allowed to dry overnight. The reactor was rinsed twice with double distilled water in batch mode, each rinse lasting for 30 minutes.

5.3.3.9.3. HOMOGENEOUS CATALYSIS IN THE PRESENCE OF IRON EQUIVALENT TO LEACHED IRON

Homogeneous catalysis was performed in the presence of iron equivalent to the amounts of iron leached on the second day (by then process was stabilized) and in between day-11 to day-20 when maximum leaching of iron was observed. The equivalent amounts of iron was prepared using iron (III) sulfate pentahydrate ($Fe_2(SO_4)_3.5H_2O$). The pH of double distilled water was adjusted to pH 3 and used to prepared solutions. Stock solutions of RO16 (100 mg/L) and iron (20 mg/L) were prepared. Then 50 mL of each stock solutions were mixed together in a Radley's Carousel to obtain a solution

containing 50 mg/L of RO16 and 10 mg/L of iron. Then, 37.8 µL of conc. H_2O_2 (30 % wt/v) was added to the solution to obtain an initial concentration of H_2O_2 as 125 mg/L.

Similarly, to simulate as of Day-2, 50 mL each of RO16 (100 mg/L) and iron (6 mg/L) were mixed in Radley's Carousel to obtain a solution containing 50 mg/L of RO16 and 3 mg/L of iron. Then, 15.2 µL of conc. H_2O_2 (30 % wt/v) was added to the solution to obtain an initial concentration of H_2O_2 as 50 mg/L.

5.4. EXPERIMENTATION

The continuous flow experiment was performed using a Rotating Disc Reactor (RDR) loaded with the modified PAN catalyst. The description of the reactor and experimental set up are discussed in the following sections.

5.4.1. THE REACTOR

The reactor used in this study was a Rotating Disc Reactor (RDR), a modified version of a Rotating Biological Contactor (RBC). The horizontal cylindrical reactor drum made of 6 mm thick Perspex was attached to 10 mm thick supports at each end of the reactor. The inner length and radius of the reactor were 209 mm and 64 mm respectively. Ten rotating discs, radius 25 mm, loaded with modified PAN catalyst, were fitted onto a shaft connected to a motor (90 W) via timing belt. The motor was equipped with an inverter to vary rotation speed. The reactor also consists of two inlet channels, one each for substrate and oxidant (H_2O_2), on one side and an outlet channel on the opposite side-end. The outlet channel is positioned lower than the inlet channels to prevent back flow from the reactor. The drain tap was fitted at the bottom of outlet side of the reactor.

5.4.2. EXPERIMENTAL SET UP

Bench scale continuous flow treatment of RO16 dye was performed using PAN catalyst, production roll 7, normalized at pH 3. The catalyst was thoroughly washed according to the procedure laid out in the section 4.4.1 p. 92. Twenty circular pieces of modified PAN catalyst were cut and ten catalytic discs were prepared by stitching two circular PAN catalyst pieces together over a Perspex disc. The reactor set up is shown in Figure 5-3 and Figure 5-4 representing the schematic diagram and actual set up respectively.

The total amount of modified PAN catalyst in ten catalytic discs was derived by deducting the weight of ten plain Perspex discs from the weight of catalytic discs as shown in Equation 5-2. The total weight of modified PAN catalyst on ten catalytic discs was derived as 208 g.

$$W_{PANCAT} = W_{CD} - 10\,W_P$$ ***Equation 5-2***

Where, W_{PANCAT} = Total weight of PAN catalyst (g),

W_{CD} = Weight of ten catalytic discs (g),

W_P = Weight of a Perspex disc (g).

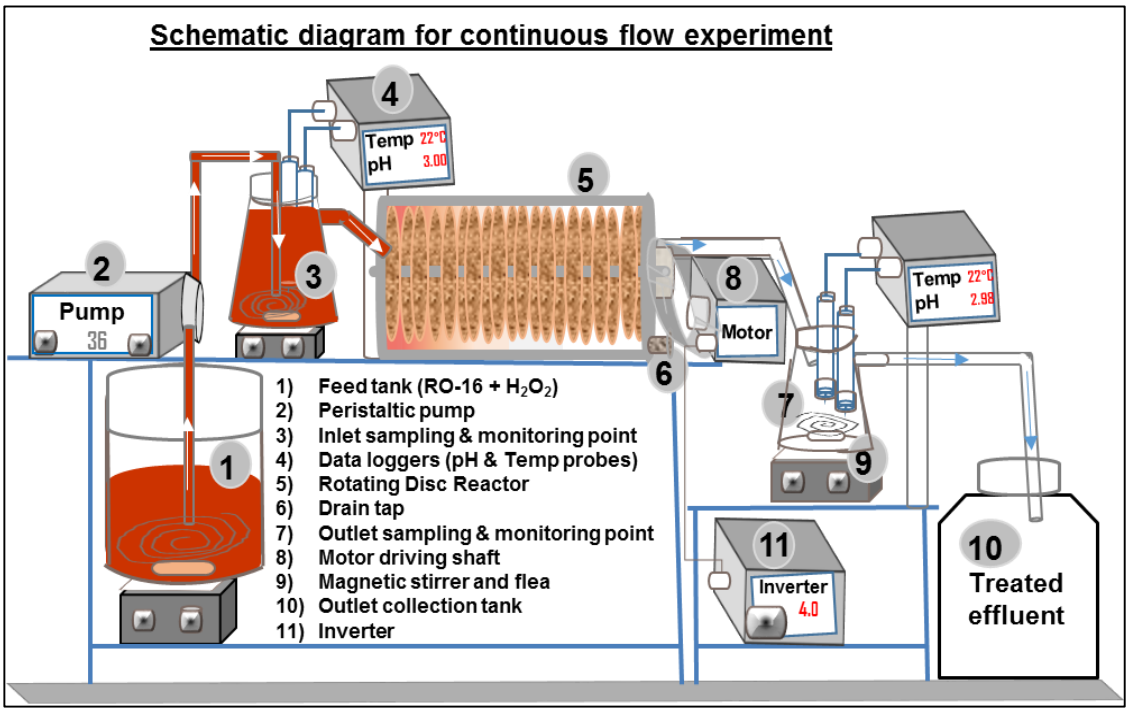

Figure 5-3: Schematic diagram showing experimental set-up for the treatment of RO16 in continuous flow mode.

Figure 5-4: Pictorial view of an experimental set-up in the laboratory for the treatment of RO16 in continuous flow mode. The insert is the close view of the rotating disc reactor. The description for the assigned numbers are same as of Figure 5-3.

In order to determine the reacting volume in the reactor, water was pumped into the reactor containing the dry catalytic discs whilst rotating. The reacting volume of the reactor was determined according to Equation 5-3. The volume retained in the drainpipe was not considered as contributing to the reacting volume. Thus, actual reacting volume was calculated as 860 mL.

$$V_R = V_{R+D} - V_D = 910 - 50 = 860\, mL \qquad \textbf{Equation 5-3}$$

Where, $V_R =$ Reacting volume (mL), $V_{R+D} =$ Volume retained in the reactor and drainpipe (mL), and $V_D =$ Volume retained in the drainpipe (mL).

The stability of RO16 in the presence of H_2O_2 (C_0 = 500 mg/L) was investigated. The result presented in Figure 4-8 shows 12.6 % and 2.7 % removals, after 24 hours, corresponding to absorption bands at 493.5 nm and 254 nm respectively. The minimum loss of substrate in the presence of H_2O_2 only envisaged to conduct the experiment with an isocratic (RO16 and H_2O_2) feed. However, to mitigate the loss of RO16 by photolysis, in the presence of H_2O_2, the initial concentration of H_2O_2 was decreased and the feed container was covered with aluminium foil and feed was stirred continuously. Fresh feed adjusted to pH 3 was fed into a feed container on a daily basis. Then, the feed was pumped into an Erlenmeyer flask (750 mL) and stirred continuously to ensure effective mixing. Eventually, gravity drives the feed to the reactor and, after set residence time, treated effluent flows out of the reactor to the effluent collection tank via outlet sampling point.

Data loggers were positioned at the Erlenmeyer flasks located up and down stream of the reactor where pH and temperature readings of influent and effluent samples were recorded in every two minutes. Influent samples at a given time were taken from the Erlenmeyer flask (number 3 in above figures) whereas effluent samples were collected in a beaker at effluent exit point (number 7 in above figures) at the given time. Experiment was performed with RO16 dye solution (C_0 = 50 mg/L) at room temperature, which, in theory, should be at the same temperature recorded at inlet and outlet sampling points. The corresponding COD and TOC values of RO16 (C_0 = 50 mg/L) were 76 mg/L of O_2 and 36 mg/L respectively. Effective mixing in the reactor was achieved by the spinning of catalytic discs mounted perpendicular to the flow of substrate. The concentration of H_2O_2 and residence time were varied in order to achieve the optimum operating condition.

5.5. RESULTS AND DISCUSSIONS

The performance of the system is evaluated based on the change in absorbance at the four absorption bands at 254 nm, 297 nm, 387 nm and 493.5 nm respectively. The presence of bands at these wavelengths is explained in section 4.5.1, p.94. The results of continuous flow experiment are discussed in the following sections.

5.5.1. EFFECT OF PROCESS PARAMETERS

The key features of Fenton based treatments are reagent conditions such as the initial concentration of H_2O_2, the amount of catalyst (Fe^{3+} in this study) and the reaction characteristics such as pH, temperature and the concentration of organic and inorganic constituents (Neyens and Baeyens, 2003; Soon and Hameed, 2011). As established from the batch treatment discussed in section 4.5.4.3, p.120, the best pH in Fenton's-like process is pH 3. Hence, the pH of the continuous flow treatment was kept to pH 3. The amount of catalyst plays a significant role but the reactor can only accommodate a certain amount of catalyst. According to Perego and Peratello, 1999, the amount of modified PAN catalyst inside a continuous flow treatment reactor remains constant with time. Thus, the amount of catalyst was chosen to be the maximum capacity the reactor can housed. The temperature was kept to the room temperature. The process parameters namely residence time (RT) and the initial concentration of H_2O_2 were varied in order to establish the optimum concentration of H_2O_2 for the maximum treatment capacity of the system.

Figure 5-5 presents the overall treatment performance of modified PAN catalyst (first exposure) before its deactivation. The breakthrough in the performance of the treatment system was considered when the treatment efficiency (decolourization) dropped to ≤ 80 % of the highest achieved. The breakthrough in the performance of the system occurred after 50 days and the removal efficiencies corresponding to the aromaticity (UV - 254 nm), decolourization (Vis - 493.5 nm), COD and TOC on day 50 were 30 %, 71 %, 16 % and -6 % respectively. The negative efficiency corresponding to TOC could be either due to a contribution from the catalyst or an instrumental error. Previous study (unpublished) also evidenced the contribution of catalyst to TOC.

The duration of continuous flow treatment is further divided into subsections A to G, each subsection representing a different set of experimental conditions, as shown in Figure 5-5 and the details of subdivisions are given in Table 5-1. To investigate the effect of parameters on removal of RO16, performing each experiment with fresh catalytic discs

would be ideal, however; considering the practical approach at the industrial scale treatment process, the effect of parameters in this study were investigated using the existing catalytic discs.

According to Perego and Peratello, 1999, continuous flow reactors are performed in steady state operation and an operation is said to be in steady state if the performance of the system at any chosen point is invariant with time. Thus, the performance of the system during each experimental condition (see Table 5-1) seemed to have stabilized within few hours of operation and attained a steady state operation mode as the removal efficiency (decolourization) remained invariant for the duration tested.

5.5.1.1. EFFECT OF RESIDENCE TIME

Residence time (τ) is the time required for processing one reactor volume of feed and is determined by dividing the reacting volume (*V*) by the volumetric flow rate (*Q*) of the feed as shown in Equation 5-4. In CSTR studies, some literature used the term space-time instead of residence time (Ramirez *et al.*, 2009; Karthikeyan *et al.*, 2011). According to Hodaifa et al., 2013, the space-time in CSTR is equal to the mean residence time. The flow rate determines the residence time and the mass transfer in the reactor. Lower flow rate decreases the pollutants load and increases the residence time and vice versa.

$$\tau = \frac{V\ (mL)}{Q\ (mL/min)} = min \qquad \textit{Equation 5-4}$$

The lower flow rate increases the contact time (RT) between the solution and the rotating discs. Thus, it is believed that lower flow rate ensures effective mass transfer and hence the removal efficiency. Flow rate was varied, in the first two weeks of the experiment, in order to investigate the effect of residence time on the treatment performance of the system. The flow rates used in this investigation were 5.5 mL/min, 4.5 mL/min and 3.6 mL/min respectively. With respect to the reacting volume of the reactor (860 mL), these flow rates correspond to 2 hours 35 minutes (2.6 hours), 3 hours 15 minutes (3.3 hours) and 4 hours respectively. These flow rates were used with different initial concentrations of H_2O_2 ranging from 50 mg/L to 250 mg/L. Figure 5-5 presents the removal of dye at different flow rates and Figure 5-6 presents the results with respect to variations in residence time.

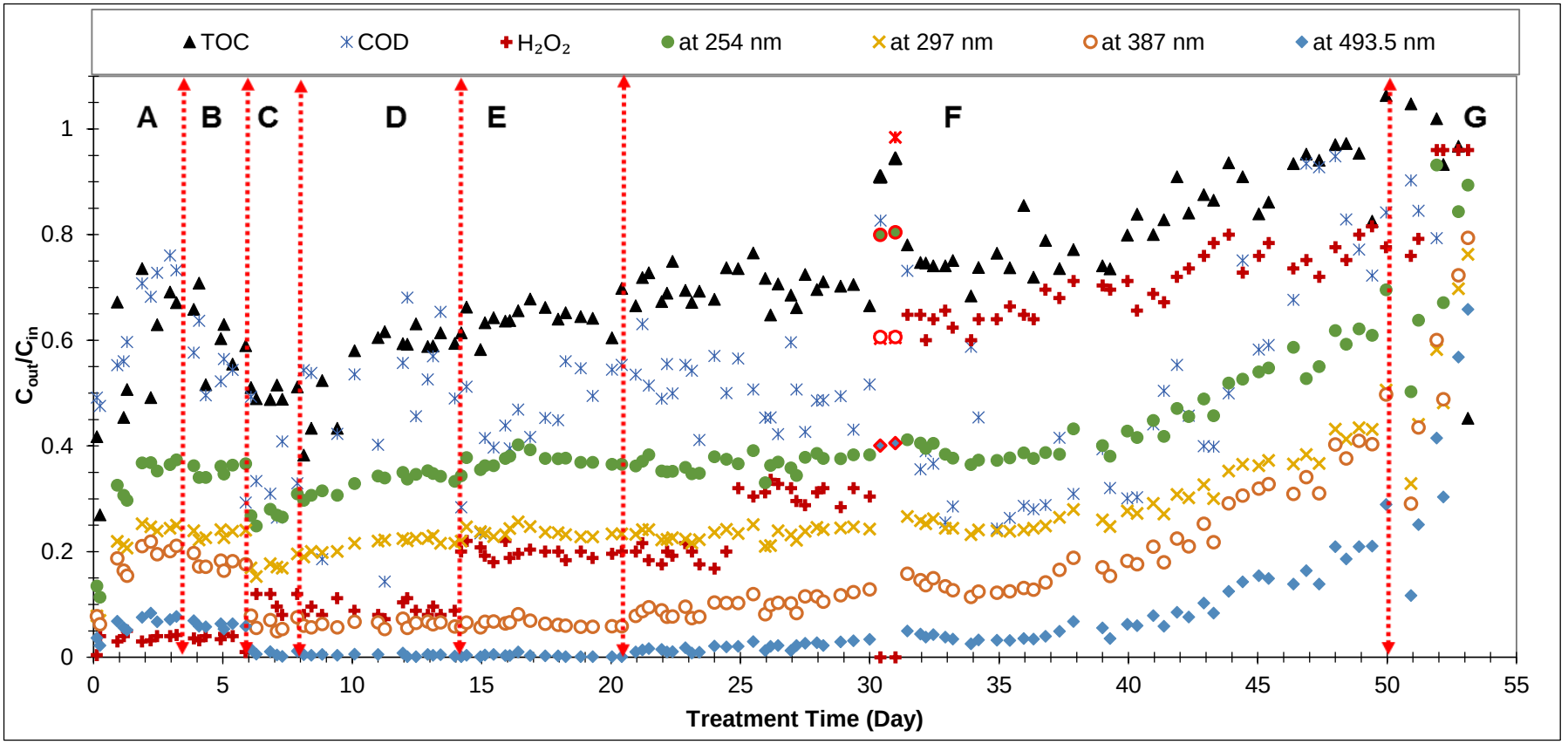

Figure 5-5: Comparison of efficiency of decolourization, degradation and mineralization of RO16 during bench scale continuous flow experiment.

Experimental conditions: 208 g catalyst on first exposure, 50 mg/L to 250 mg/L H_2O_2, 860 mL reaction volume of RO16 (C_0 = 50 mg/L) at pH 3 and room temperature (~ 20°C). The details of subdivisions are given in Table 5-1.

Table 5-1: Breakdown of continuous flow treatment for RO16 with respect to set initial concentration of H_2O_2 and residence time.

Experimental Sub-sections	H_2O_2 inlet / outlet (mg/L)	Average flow rate (mL) / RT (h)	Duration of treatment (h) / (day)	Average conc. of RO16 (mg/L)		Average degradation of RO16 (%)				Average TOC (mg/L)		Average mineralization	Average COD (mg/L)		Average COD removal
				Inlet	Outlet	254 nm	297 nm	387 nm	493.5 nm	Inlet	Outlet	(%)	Inlet	Outlet	(%)
A	50 / 1.7	5.5 / 2.6	0 to 79 = 79 / (3.2)	46.1	2.8	69.9	79.8	83.2	93.9	36.5	20.1	44.6	70.0	44.3	37.1
B	50 / 1.7	4.4 / 3.3	79 to 142 = 63 / (2.6)	48.6	2.9	64.5	76.6	82.2	93.9	35.4	21.5	39.1	74.0	38.4	48.1
C	125 / 12.8	4.5 / 3.25	142 to 192 = 50 / (2.1)	48.5	0.4	72.7	82.8	93.6	99.2	33.4	16.7	49.9	74.0	26.4	64.4
D	125 / 11.2	3.6 / 4.0	192 to 337 = 145 / (6.0)	48.2	0.2	66.8	78.5	93.8	99.6	34.5	18.8	44.4	73.6	35.3	52.1
E	250 / 49.6	3.5 / 4.1	337 to 490 = 153 / (6.4)	48.3	0.1	62.8	76.4	93.7	99.7	32.1	20.6	35.7	73.6	32.9	55.2
F	125 / 63.4	3.5 / 4.1	490 to 1,200 = 710 / (29.6)	49.1	3.5	56.7	71.5	81.6	92.9	35.0	27.5	22.1	74.9	38.4	48.8
G	125 / 110.1	3.4 / 4.2	1,200 to 1,275 = 75 / (3.2)	49.1	18.2	26.0	45.7	45.3	62.8	41.8	36.3	5.9	75.3	63.8	15.4

The experiment was begun with an initial H_2O_2 concentration of 50 mg/L and a residence time of 2.6 hours and run for 3.3 days (79 hours). Then, residence time was increased by 40 minutes (flow rate lowered to 4.5 mL/min), giving total residence time of 3.3 hours. The experiment was run for another 2.63 days (63 hours). According to Table 5-1, within 79 hours of treatment, the average loss of aromaticity (UV - 254 nm) and decolourization (Vis - 493.5 nm) were 69.9 % and 93.9 % for the subsection A and 64.7 % and 93.9 % for subsection B respectively. The reduction in extent of mineralization (TOC) and degradation (COD) in subsection A were 44.6 % and 37.1 % respectively. This cannot be true in principle as COD reduction is always less than or equal to that of reduction in TOC. This is also supported by the relatively higher extent of COD removal in other subsections. This bias could be due the influence in COD results by fibrils that were washed out from the system. Due to the fibrous nature of catalyst, it is very likely to lose more fibrils during initial stage of the treatment.

Table 5-1 shows same average removal rates corresponding to two residence times (2.6 hours and 3.3 hours). The average reduction in TOC has decreased to 38.4 % whereas the average reduction in COD increased to 48.1 %. The removal trends for subsection B (see Figure 5-5) can be used to argue that section B (longer RT) is better than section A (shorter RT) as reduction of TOC and COD is gradually improving towards the end of section B whereas it is gradually decreasing towards the end of section A. The gradual improve in section B could be due to the slow-cleansing of adsorbed dye and recalcitrant products formed and adsorbed on catalyst during the treatment in section A.

The effect of residence time on removal of dye was further investigated with higher dose of H_2O_2. After 5.92 days (142 hours), the H_2O_2 concentration was increased to 125 mg/L and residence time was maintained at 3.25 hours for 8 days (192 hours) in subsection C and 4 hours for another 6 days in subsection D. The corresponding results are shown in Figure 5-5, Figure 5-6 and Table 5-1.

When the initial concentration of H_2O_2 increased to 125 mg/L, keeping same residence time as of section B, the efficiency for decolourization (Vis - 493.5 nm) increased from 93.9 % in subsections A and B to 99.2 % in subsection C. The aromaticity removal in subsection C also increased to 72.7 %. Accordingly, the reduction of TOC and COD in subsection C also improved to 49.9 % and 64.4 % respectively.

Keeping the same initial concentration of H_2O_2, the residence time was further increased to 4 hours (flow rate 3.6 mL/min) after 8 days (192 hours - subsection D). With the

increasing residence time from 3.25 hours to four hours, the decolourization efficiency further improved from 99.2 % to 99.6 % whereas the efficiency for aromaticity removal dropped to 66.8 %. However, similar efficiencies for decolourization (95.8 %) and aromaticity (68.7 %) were achieved in batch treatment (see Figure 4.26 at 20 °C) with residence time of 100 minutes, suggesting that continuous flow require ~ 2.5 folds longer residence time than that of batch treatment.

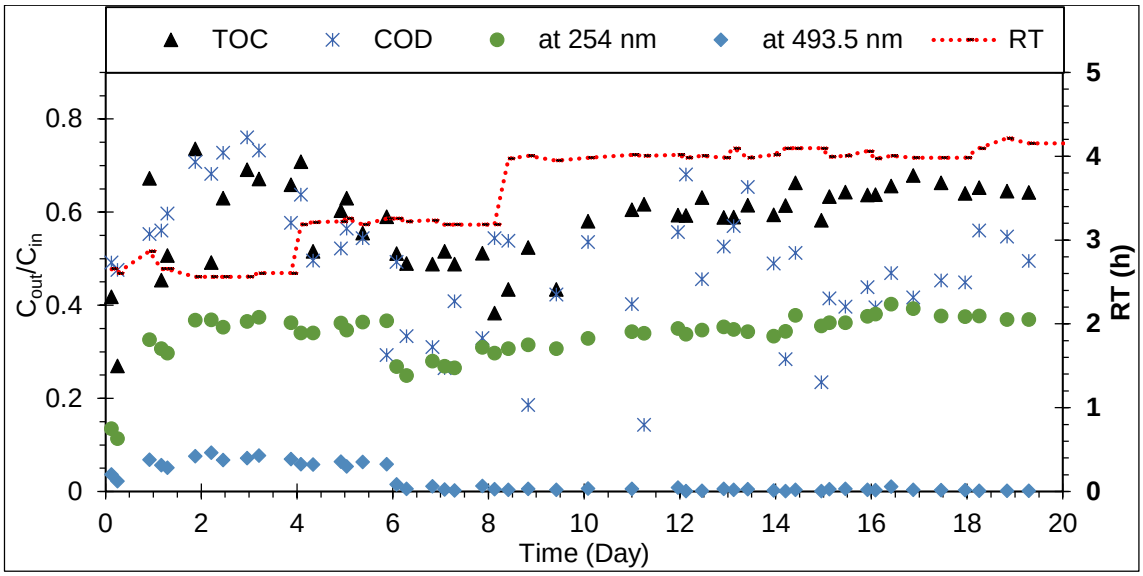

Figure 5-6: Effect of residence time on removal of RO16 in continuous flow treatment system.

[Experimental conditions are given in Table 5-1 and Figure 5-5].

5.5.1.2. EFFECT OF HYDROGEN PEROXIDE CONCENTRATION ON DECOLOURIZATION OF RO16.

Optimization of H_2O_2 concentration in a continuous flow treatment is crucial not only from the treatment performance basis but also from the operational cost basis as well. Therefore, effect of initial concentration of H_2O_2 on the decolourization of RO16 dye has been investigated. The stoichiometric requirement of H_2O_2 for the complete mineralization of RO16 (C_0 = 50 mg/L) is determined from the experimentally determined chemical oxygen demand (COD) of dye (76 mg/L) as shown in Equation 5-5 through Equation 5-7.

$$2H_2O_2 = 2H_2O + O_2 \qquad \textit{Equation 5-5}$$

Equation 5-5 shows that two moles of H_2O_2 requires to yield one mole of oxygen. Thus, the amount of oxygen (mmoles) required for given COD value is calculated using Equation 5-6.

$$mmoles\ of\ O_2\ required = \frac{COD\ (mg|L)}{molar\ mass\ of\ O_2(g|mol)} = \frac{76}{32} = 2.375 \quad \textit{Equation 5-6}$$

This suggests that complete mineralization of RO16 (C_0 = 50 mg/L, COD = 76 mg/L) requires 2.375 mmoles of oxygen. Using Equation 5-5, the mmoles of oxygen can be converted to required concentration (mg/L) of H_2O_2 as shown in Equation 5-7.

$$H_2O_2(mg|L) = 2 \times\ O_2\ (mmoles) \times molar\ mass\ of\ H_2O_2(g|mol) \quad \textit{Equation 5-7}$$
$$= 2 \times 2.375 \times 34.0147 = 161.57$$

The residual hydrogen peroxide inside the reactor is also consumed by non-selective nature of •OH radicals. Thus, the requirement of oxidant is generally higher than that of stoichiometric requirement (Queirós *et al.*, 2015). Thus, the initial concentration of H_2O_2 was varied from 50 mg/L to 250 mg/L in the first 20 days of the continuous flow experiment, while other process parameters, except residence time (RT), were kept constant. Table 5-2 and Figure 5-7 show the treatment performance of the system with respect to the initial concentration of H_2O_2.

Table 5-2: Treatment performance with respect to the effect of H_2O_2 concentration on removal of RO16.

Treatment time (Day)	Concentration of H_2O_2 (mg/L)			Average removal efficiency (%)			
	Inlet	Outlet	Used	254 nm	493.5 nm	TOC	COD
0 to 5.9	50	1.7	48.3	67.7	93.9	42.4	41.6
5.9 to 14	125	11.7	113.3	68.6	99.5	46.1	55.8
14 to 20.42	250	49.6	200.4	62.8	99.7	35.7	55.2
20.42 to 50	125	29.1	95.9	63.7	98.4	29.6	48.7

The experiment commenced with 50 mg/L of H_2O_2 and ran for 142 hours (6 days), subsections A and B in Figure 5-5. Even though residence time increased from subsection A to B, there was little improvement in removal efficiency. With 50 mg/L of initial concentration of H_2O_2, the average efficiency for aromaticity removal (UV - 254 nm) was 67.7 % and the decolourization (Vis - 493.5 nm) was 93.9 %. The average reduction in TOC and COD were 42.3 % and 41.6 % respectively. Table 5-2 shows that the concentration of residual H_2O_2 in the effluent was below 2 mg/L. The very high consumption (97 %) of H_2O_2 could be indication of insufficient dose of H_2O_2. The higher degree of TOC and COD removal in subsection A compared to subsection B also supports that H_2O_2 dose was not sufficient to push the reaction down the chain. As

heterogeneous catalysis begins with sorption, it is believed that the higher removal in subsection A was influenced by sorption.

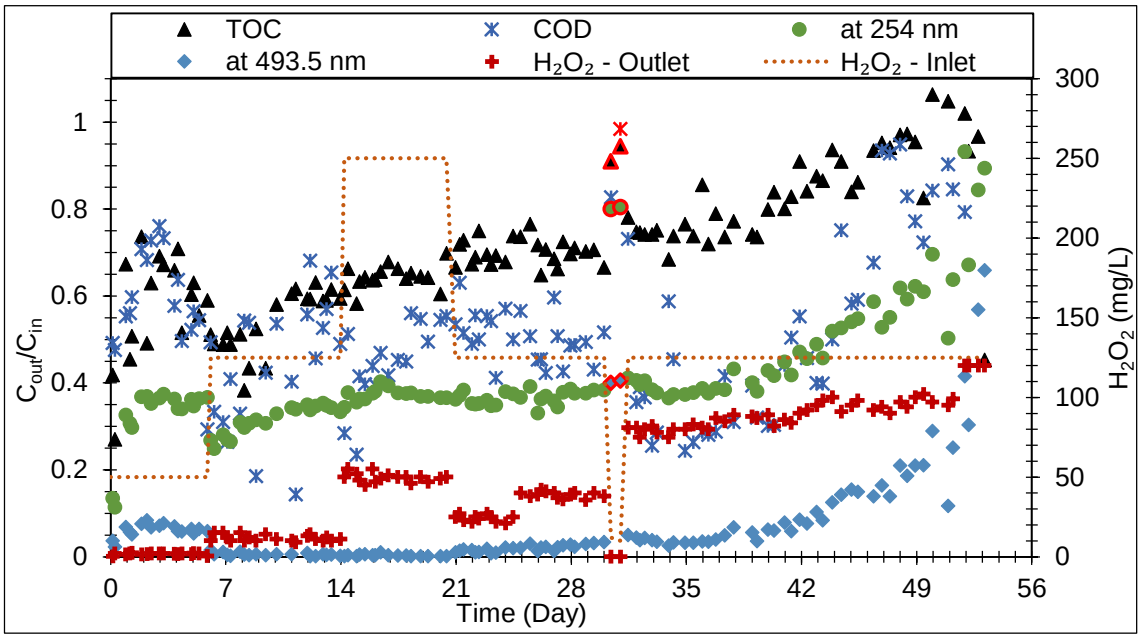

Figure 5-7: Effect of H_2O_2 concentration on removal of RO16 in continuous flow treatment.

Although decolourization (93.9 %) with respect to 50 mg/L H_2O_2 seems very high, the extent of treatment was not satisfactory in regards to aesthetic point. Presence of unreacted or escaped dye (due to plug flow in the reactor) and / or intermediate products formed during the early stage of decolourization / degradation of RO16 can contribute to the colour of the treated water. Formation of intermediates such as nitrosobenzene, nitrobenzene, hydroquinone and benzoquinone during ozonation of RO16 is documented by (Tizaoui and Grima, 2011). Similarly, formation of intermediates such as 6-acetylamino-3-amino-naphthalene-2-sulfonic acid and N-(3,4-bis-hydroxy-methyl-phenyl)-acetamide during photo oxidation of RO16 is also documented (Bilgi and Demir, 2005).

Nitrosobenzene – light-yellow (straw) (Sigma-Aldrich, 2017a), nitrobenzene – pale yellow (Madan, 2013) and quinones – dark yellow (Sigma-Aldrich, 2017b) coloured intermediates cannot degrade further due to the lack of hydroxyl radicals ($^{\bullet}OH$) formation because of insufficient amount of H_2O_2 in the system. This explains the dark yellowish (brown) colour observed (see Figure 5-8C) in the effluent during the period when the H_2O_2 concentration was kept at 50 mg/L. The incomplete decolourization of RO16 with 50 mg/L of H_2O_2 indicates the necessity of higher dose of H_2O_2. The pinkish-orange colour observed at the beginning (see Figure 5-8B) of the treatment is due to the system

not being stabilized. There was a high chance for the influent to pass through the bed (the gap between catalytic discs and the reactor bed) of the reactor without or with minimal contact with catalytic discs.

Moreover, the removal at the initial stage of the treatment may not be due to catalytic oxidation of RO16. It is widely believed that the first step in heterogeneous catalysis proceeds with the adsorption of substrate onto the heterogeneous catalyst (Soon and Hameed, 2011; Sun *et al.*, 2014; Wang *et al.*, 2014; Queirós *et al.*, 2015). The study in section 4.5.3, p.97 determined that the adsorption of RO16 onto the surface of modified PAN catalyst is favourable. Therefore, removal at the initial stage could have enhanced by adsorption as well.

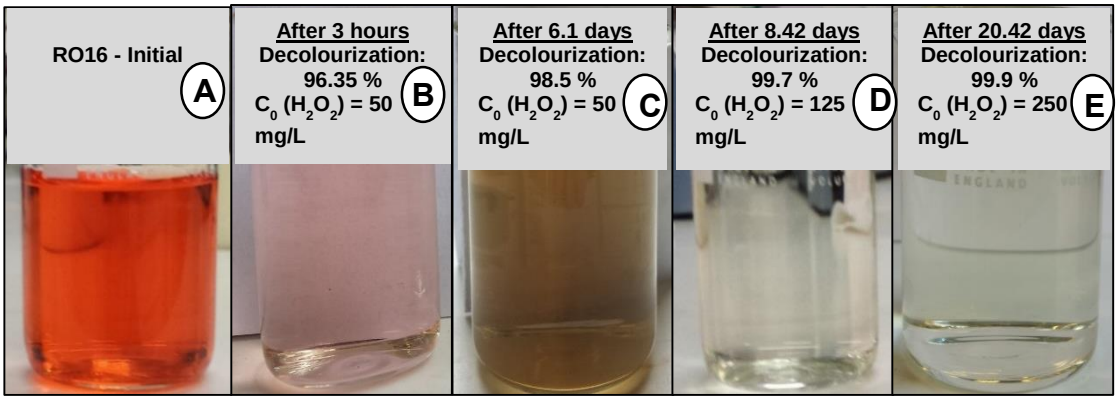

Figure 5-8: Comparison of colour of samples at different stages of treatment.

a) Influent, C_0-(RO16) = 50 mg/L, b) effluent at 3 hours, C_{RO16} = 1.73 mg/L, c) effluent on 6.1 day, C_{RO16} = 0.75 mg/L, d) effluent on 8.42 day, C_{RO16} = 0.18 mg/L and e) effluent at 20.42 day, C_{RO16} = 0.05 mg/L.

The initial concentration of H_2O_2 increased by 2.5 folds from 50 mg/L to 125 mg/L, the optimum concentration established in the batch treatment, and the system was run for another 195 hours (8 days). Figure 5-7 and Table 5-2 show that the system stabilized and the average degradation efficiency for decolourization (Vis - 493.5 nm) improved further and plateaued above 99 %. Similarly, efficiency for TOC and COD improved to 46.1 % and 55.8 % respectively. However, the removal efficiency for aromaticity remained similar (68.6 %).

Although decolourization of RO16 was visually complete (see Figure 5-8D) when initial concentration of H_2O_2 increased by 2.5 folds to 125 mg/L, the COD and TOC reduction limited to 55 % and 46 % respectively. The possible explanation could be that H_2O_2 was below the stoichiometric requirement (162 mg/L) as suggested by Equation 5-7.

According to Table 5-2, the residual H_2O_2 (11.7 mg/L) in the effluent suggests that 91 % (114 mg/L) of the initial H_2O_2 was consumed. Therefore, the initial concentration of H_2O_2 was doubled to 250 mg/L and treatment was run for a further 153 hours (6.4 days).

Figure 5-7 and Table 5-2 present the results with 250 mg/L of H_2O_2 and Figure 5-8-E shows the continued clarity of the treated sample. The performance of the system did not improve while doubling the H_2O_2 dose from 125 mg/L to 250 mg/L. The efficiency for decolourization and COD reduction remained similar whereas efficiency for aromaticity (UV - 254 nm) and TOC reduction dropped by 6 % and 10 % respectively. Therefore, the optimum concentration of H_2O_2 was considered as 125 mg/L and the rest of the treatment was performed with 125 mg/L.

The need for H_2O_2 in the treatment was observed around day 30 of the experiment as the feed was mistakenly prepared without H_2O_2.The concentration of H_2O_2 in influent become ~ 10 mg/L as a result of dilution with previous feed. Figure 5-7 shows that the removal efficiency for aromaticity and decolourization suddenly dropped to 20 % and 60 % respectively. Similar drop in TOC and COD was also observed. This emphasizes that H_2O_2 is necessary for the treatment process. In another word, the treatment is based on the liberation of $^{\bullet}OH$ radicals through the catalytic decomposition of H_2O_2.

The influence of H_2O_2 dose (50 mg/L to 200 mg/L) on decolourization of three reactive dyes (Reactive Black 5, RO16 and Reactive Blue 2) in fluidized-bed reactor was studied by Su et al., 2011. The study also observed the similar influence as of this study. The authors documented that decolourization rate increased when H_2O_2 dose doubled (from 50 mg/L to 100 mg/L) and changed insignificantly with H_2O_2 concentration up to 200 mg/L. Similar effect of H_2O_2 on removal of RO16 has been reported when H_2O_2 was used with copper oxide (Abdullah, Wong and Yaziz, 2010) and UV (Mitrović *et al.*, 2012).

Figure 5-9 compares the removal efficiency with respect to the consumption of H_2O_2 when the initial concentrations of H_2O_2 were 50 mg/L, 125 mg/L and 250 mg/L respectively. 48 mg/L, 113 mg/L, 200 mg/L of H_2O_2 were consumed respectively with respect to the initial concentrations mentioned above. Increase in consumption of H_2O_2 from 48 mg/L to 113 mg/L has improved the removal efficiencies for aromaticity, decolourization, TOC and COD. However, further increase in consumption from 113 mg/L to 200 mg/L did not improve the removal efficiencies instead deteriorated COD and TOC removals. This effect is widely discussed in the literature and explained as scavenging effect (Muruganandham and Swaminathan, 2004; Melero *et al.*, 2009;

Abdullah, Wong and Yaziz, 2010; Su *et al.*, 2011; Mitrović *et al.*, 2012; Babuponnusami and Muthukumar, 2014; Queirós *et al.*, 2015). This occurs due to the reaction of •OH radicals with residual H_2O_2 Equation 2-7, other radicals Equation 2-10 and recombination of •OH radicals Equation 2-9 in the system thereby reducing the number of free •OH radicals to oxidize dye. Consequently, decrease in efficiencies for COD and TOC were noted.

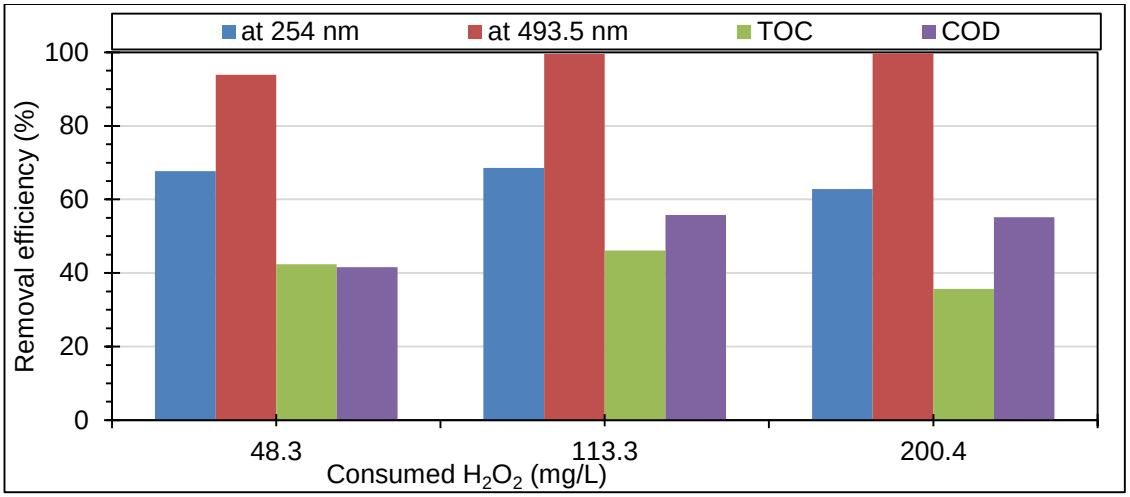

Figure 5-9: Removal efficiencies for aromaticity, decolourization, TOC and COD with respect to consumption of H_2O_2.

Hydroperoxyl radicals (HO_2•) formed according to Equation 2-7 could possibly react with dye molecules. However, their oxidation potential is lower than that of hydroxyl radicals resulting in the reduction in removal efficiencies (Queirós *et al.*, 2015). Karthikeyan et al., 2011 explained the retarded efficiency at higher ratio between H_2O_2 and catalyst is due to the conversion of •OH radicals into OH^- ions as in Equation 2-3 which leads to precipitation of ferric irons (Fe^{3+}).

5.5.2. INVESTIGATION ON MECHANISM OF CATALYST DEACTIVATION

Breakthrough of RO16 in the treatment system, using the modified PAN catalyst on its first exposure, occurred after 50 days. Deactivation of heterogeneous catalyst is an inevitable process and widely discussed. According to Bartholomew and Argyle, 2015; 15 % of 24,000 journal articles, presentations, reports, reviews, and books and more than 33,000 patents published / registered in last 35 years (1980 to 2015) were made in the last three years (Bartholomew and Argyle, 2015). There are various mechanisms for catalyst deactivation and they are either physical or chemical alterations on the catalyst (Nauman, 2001; Trimm, 2001; Argyle and Bartholomew, 2015; Bartholomew and Argyle, 2015). In a review of deactivation and regeneration of a heterogeneous catalyst, Argyle

and Bartholomew, 2015, grouped various paths that can lead to catalyst deactivation into six fundamental mechanisms as: fouling, poisoning, thermal degradation, vapour compound formation and / or leaching accompanied by transport from the catalyst surface or particle, vapour-solid and/or solid-solid reactions, and attrition / crushing. Amongst these, the possible mechanisms that can lead to deactivation of modified PAN catalyst used in this study are fouling, poisoning, leaching of catalyst and attrition. Mechanisms of catalyst deactivation involving leaching of catalyst (Iron), modification of catalyst by means of changes in functional groups and physical changes on the catalyst have been studied. A brief description of possible mechanisms linked to this study are summarized in Table 5-3.

Table 5-3: Mechanisms of catalyst deactivation (Argyle and Bartholomew, 2015).

Mechanisms	Brief definition / description
Fouling	Physical deposition of species onto the catalytic surface and in catalyst pores thereby block active sites. Carbonaceous deposits, commonly known as coke deposition, is a common example.
Poisoning	Strong chemisorption of species of the feed on catalytic sites which block sites for catalytic reactions. For example, poisoning by products of catalysis.
Leaching of catalyst	leaching accompanied by transport from the catalyst surface or particle
Attrition / crushing	Loss of catalytic material due to abrasion; loss of internal surface area due to mechanical-induced crushing of the catalyst particle

5.5.2.1. LEACHING OF IRON FROM THE CATALYST

In order to establish a mechanism that attributed to the breakthrough of the treatment system by means of catalyst deactivation, leaching of iron from the catalyst was investigated. Leached iron content in the samples taken during the 50 day-long continuous flow experiment was analyzed according to the procedure laid out in section 5.3.3.6 and the results are presented in Figure 5-10, Figure 5-12 and Table 5-4 respectively.

Figure 5-10 shows a gradual increase in iron leaching from the catalyst until 246 hours (11.25 days) then plateauing at the maximum leaching rate for 10 days (246 hours to 492 hours) followed by a gradual decline. Within the 50-days period, the lowest (1.81 mg/L) and the highest (10.7 mg/L) values for iron leaching observed at 1,200 hours (50

days) and 346 hours (14.5 days) respectively. Figure 5-10 shows the leaching of iron in three phases: the 'log' phase, the 'stationary' phase and the 'death' phase. The leaching in log and death phases are linear with coefficients of determination (R^2) as 0.965 and 0.94 respectively. However, the slope of the curve in log phase (0.8103) is ~ 3.5 folds higher than that of death phase (-0.2328). The sign (+/-) of slope indicative to incline and decline of iron leaching.

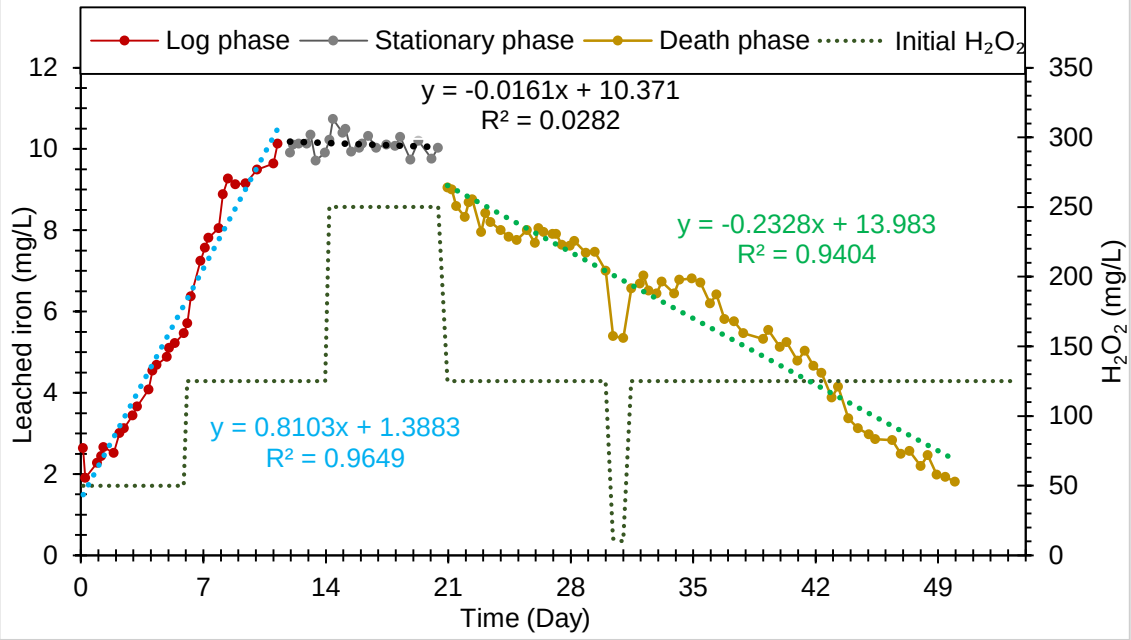

Figure 5-10: Iron leaching and initial concentration of H_2O_2 with respect to treatment time.

It is stated that deactivation of iron catalyst takes place with higher doses of H_2O_2 (Karthikeyan *et al.*, 2011). Increase in daily amount of leached iron with respect to increase in initial concentration of H_2O_2 has been reported in a continuous flow treatment of humic acid in column reactor using modified PAN catalyst (Production Roll 3) (Asuelimen, 2015). Figure 5-10 shows no evidences favouring them. Regardless of initial concentration of H_2O_2, leaching of iron was increasing linearly until it reached its maximum, after which further increase in H_2O_2 did not affect the iron leaching. Thus, no direct relationship between H_2O_2 concentration and iron leaching was observed in this study. Similar results were observed during heterogeneous Fenton oxidation of Alcian Blue-tetrakis (methylpyridinium) chloride (Duarte *et al.*, 2013), Orange II (Queirós *et al.*, 2015) in continuous flow and Orange II (J. Herney Ramirez *et al.*, 2007) in batch treatment. It is argued that iron leaching with higher dose of H_2O_2 could be low due to the higher stability of metal species favoured by H_2O_2, as an oxidizing agent, thus maintaining the metal species in their oxide state (Pastrana-Martínez *et al.*, 2015). Other

authors have also documented the stability of catalysts, in terms of leaching of metal, with respect to the higher dose of H_2O_2. A decreasing trend of iron leaching with respect to increasing concentration of oxidant was observed and explained in terms of shielding effect of surrounding metal-H_2O_2 complex species which prevents leaching (Pastrana-Martínez *et al.*, 2015). On the other hand, it is also documented that the stability of catalyst towards leaching solely relies on the ratio of oxidant dose and catalyst loading (Martínez *et al.*, 2005; Molina *et al.*, 2006; Babuponnusami and Muthukumar, 2014). Thus, stability of catalyst in terms of metal leaching is a complex behaviour and strictly depends on the experimental conditions.

Figure 5-12 shows no correlation in removal efficiencies for aromaticity (UV - 254 nm), decolourization (Vis - 493.5 nm), COD and TOC with respect to the amount of iron leached off the catalyst. In other words, either the system relies on heterogeneous catalysis or homogeneous catalysis has a minimal contribution.

5.5.2.1.1. MASS BALANCE OF IRON ON THE MODIFIED PAN CATALYST

The mass balance of iron in the system was evaluated by calculating the residual iron content on the catalytic discs and total amount of iron leached off the system. The residual iron content on deactivated catalyst was determined via digestion of catalyst samples according to procedures laid out in section 5.3.3.6.2. The total amount of iron leached off the catalyst was determined by calculating the area under the curve (see Figure 5-11) for leached iron using trapezium rule computation in Microsoft Excel. The area of a trapezium was calculated using Equation 5-8.

$$\sum_{i=1}^{n} A_i = \frac{1}{2}(C_{t_1} + C_{t_2})(v_2 - v_1) \qquad \textit{Equation 5-8}$$

Where, $A =$ Area of trapezium (mg), $n =$ total number of trapeziums = total number of samples, $C_{t_1}\ and\ C_{t_2}$ are the sides of the trapezium = concentrations of iron at time t_1 and t_2, (mg/L), and $(v_2 - v_1) =$ height of trapezium = volume treated at time (t_2- t_1), (L).

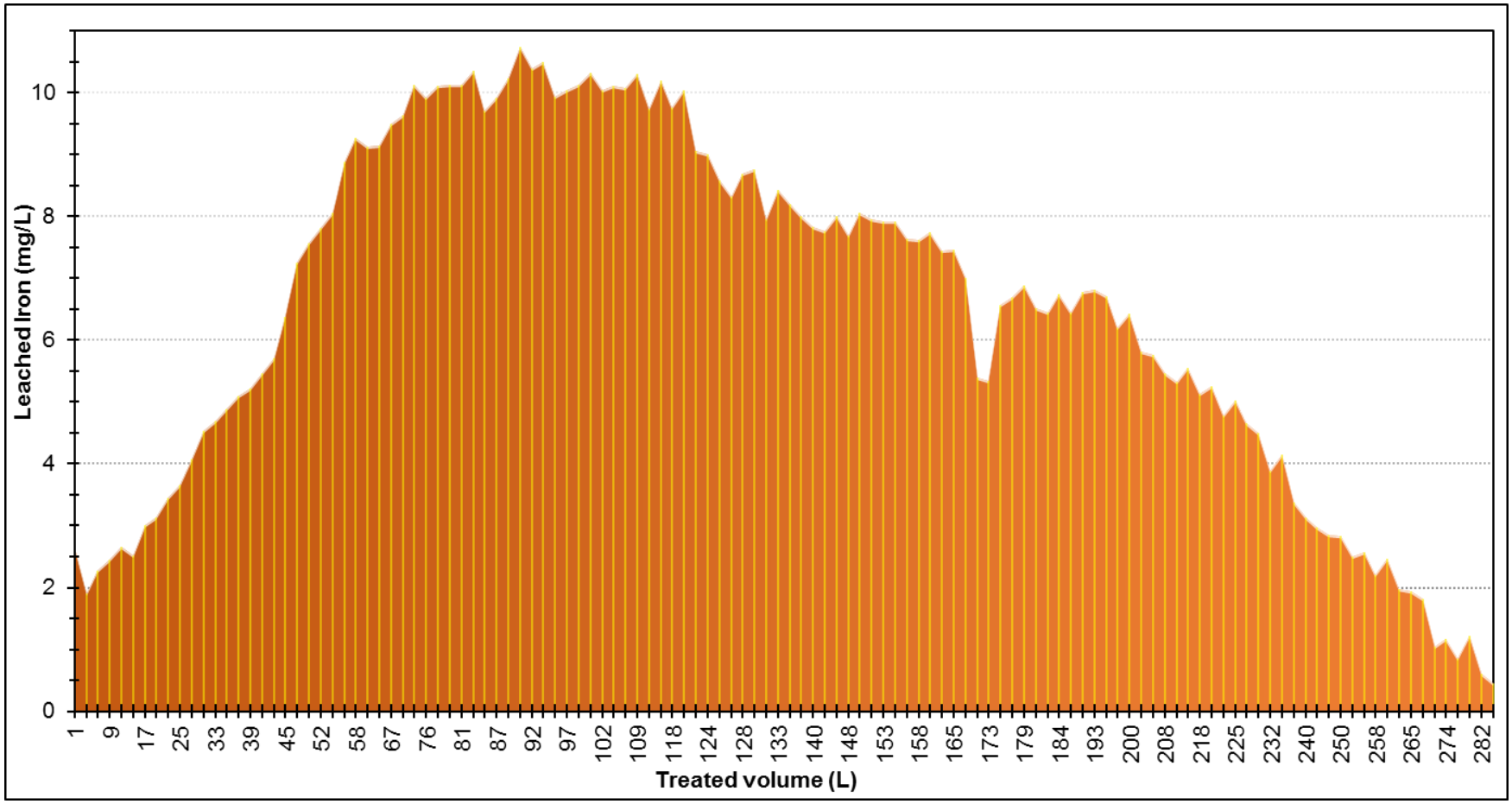

Figure 5-11: Amount of iron leached off the catalyst with respect to the volume treated.

Table 5-4: Mass balance of iron during continuous flow treatment with fresh catalyst.

Initial iron content of the catalyst (mg/g mesh)				Amount of catalyst used (g)	Initial iron content of the system (mg) $= A * B$	Iron remained on the first disc after 50 days (mg/g mesh)			Iron remained on the ninth disc after 50 days (mg/g mesh)			Average iron content of the system after 50 days (mg/g mesh) $= \frac{D+E}{2}$	Total iron content of the system after 50 days (mg) $= B * F$
Rep 1	Rep 2	Rep 3	Average **(A)**	**(B)**	**(C)**	Rep 1	Rep 2	Average **(D)**	Rep 1	Rep 2	Average **(E)**	**(F)**	**(G)**
9.10	9.11	9.51	9.24	208.00	1921.92	1.44	1.25	1.34	1.44	1.58	1.51	1.425	296.4

Total iron content of the system after 53 days (mg) **(H)**	Area under the curve (leached iron) after 50 days (mg) **(I)**	Area under the curve (leached iron) after 53 days (mg) **(J)**	Iron in the regenerated solution (26 L) (mg) **(K)**	Total loss of iron after 53 days (mg) $= J + K$ **(L)**	Mass balance after 50 days (mg) $= G + I$ **(M)**	Mass balance after 53 days (mg) $= H + L$ **(N)**	Loss of iron based on area under the curve (leached iron) (%)		Loss of iron based on residual iron on the deactivated catalyst (%)	
							After 50 days	After 53 days	After 50 days	After 53 days
238.33	1740.22	1750.34	22.32	1772.66	2036.62	2010.99	90.54	92.23	84.57	87.6

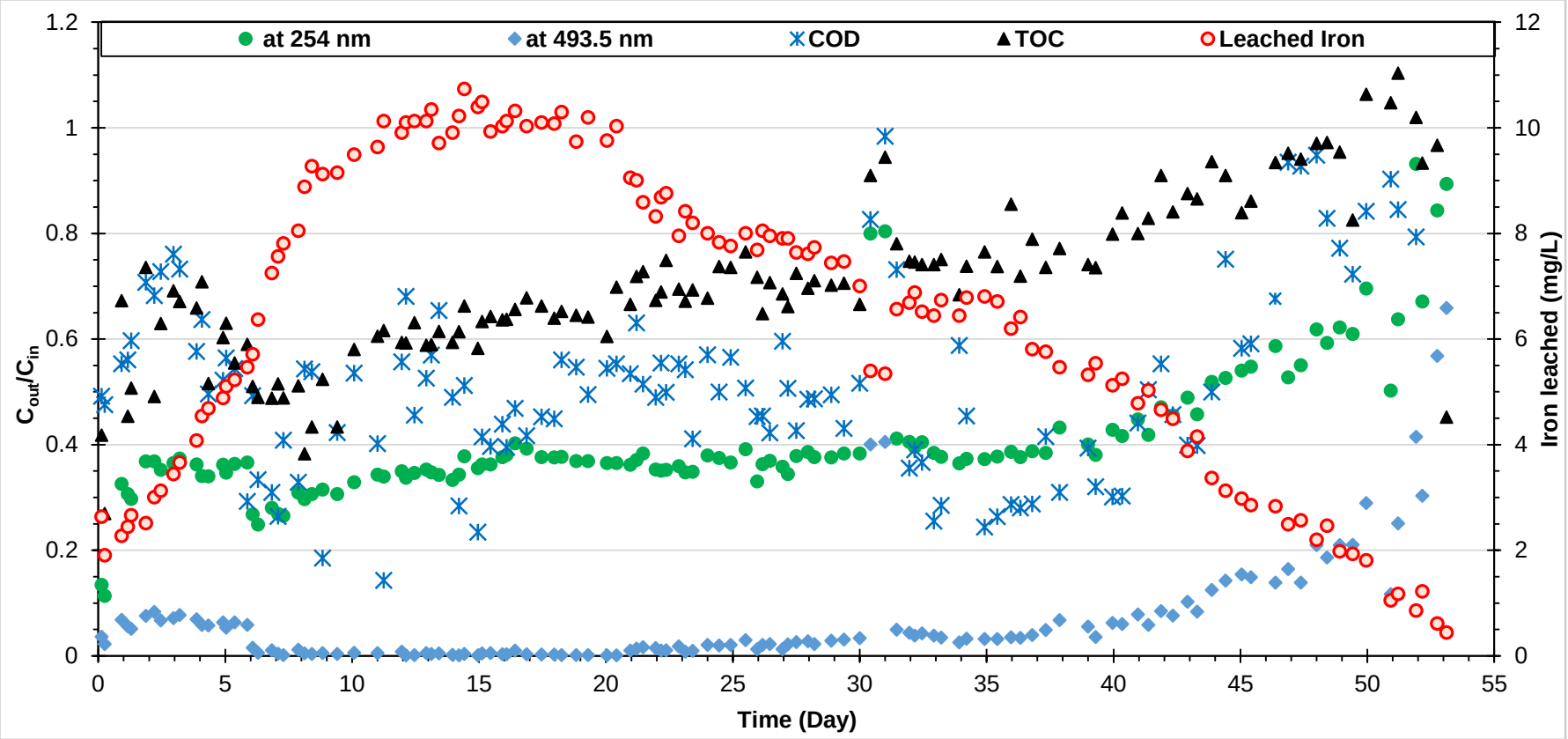

Figure 5-12: Leached iron and removal efficiencies for aromaticity, decolourization, COD and TOC with respect to treatment time.

Experimental conditions: 208 g catalyst (first exposure), 50 mg/L to 250 mg/L H_2O_2, 860 mL reaction volume of RO16 (C_0 = 50 mg/L) at pH 3 and room temperature (~20°C).

Table 5-4 presents the mass balance of iron during the continuous flow experiment. The initial iron content of the modified PAN catalyst on the disc was determined using the catalyst after pH normalization to three. The iron content was found to be 9.24 mg/g mesh (0.165 mmol/g mesh). Therefore, the total amount of iron in the reactor loaded with 208 g of catalyst was 1922.10 mg. According to the area under the curve, total iron leached off the system when breakthrough occurred (50 days) was 1740.22 mg, which is 90.54 % of the initial iron content of the system.

In order to evaluate the mass balance of the system, residual iron content on catalytic discs after 50 days was determined using average iron content (1.43 mg/g mesh) calculated from the iron content of the first disc (1.34 mg/g mesh) and the ninth disc (1.54 mg/g mesh). Thus, total residual iron in the system was 296.65 mg, which is 15.4 % of the initial iron content. The total iron, sum of leached iron and residual iron on the catalyst, of the system after breakthrough found to be 2036.87 mg, which is 5.97 % higher than that of initial iron on the system. After breakthrough on day 50, the system was cleaned with H_2O_2 solution (see section 5.3.3.9.1) and run for another 3 days. The total iron leached in 53 days was 1750.34 mg, which is 92.23 % of the initial iron content of the system. The mass balance of iron after 53 days, sum of leached iron, residual iron on the catalyst and iron leached during regeneration process, of the system found to be 2010.99 mg, which is 4.6 % higher than that of initial iron content of the system. Thus, the very high (> 90 %) leaching of iron from the catalyst is an evidence and a major cause for the deactivation of the catalyst.

A significantly low (12.73 %) amount of iron loss has been reported in a continuous flow treatment of humic acid in column reactor using modified PAN catalyst (Production Roll 3) (Asuelimen, 2015). Continuous flow treatment of RO16 in a column reactor was performed using the same batch of catalyst (production roll 3) (Fe content 0.2723 mmol/g mesh) [Experimental conditions: 55 g catalyst, 300 mg/L H_2O_2, pH-3 in 210 mL of reactor volume, flow rate = 1.56 mL/min at room temperature (~ 20 °C)]. The iron leaching was found in agreement to that of production roll 7 (see Figure 5-11 and Table 5-4) as 76 % of iron was leached off the catalyst when breakthrough on the treatment system occurred. This is indicative that leaching of iron may vary with respect to the nature of the substrate.

Elemental analysis of PAN threads taken from the active mesh, deactivated-unwashed, and deactivated-washed (with 500 mg/L of H_2O_2 at pH 3) were performed using Scanning Electron Microscope (SEM). The results shown in Figure 5-13 also agree with the AAS

results discussed above. Both, iron in terms of weight and atomic mass, show that loss of iron from the surface of the catalyst was ~ 90 %. Figure 5-14 shows the SEM images and mapping of iron on PAN threads taken from the active and deactivated catalysts. There is a huge difference in term of iron (the white pixels) mapping between active and deactivated catalysts. Similarly, presence of iron (white granules) on the active catalyst is more pronounced than that of deactivated catalyst.

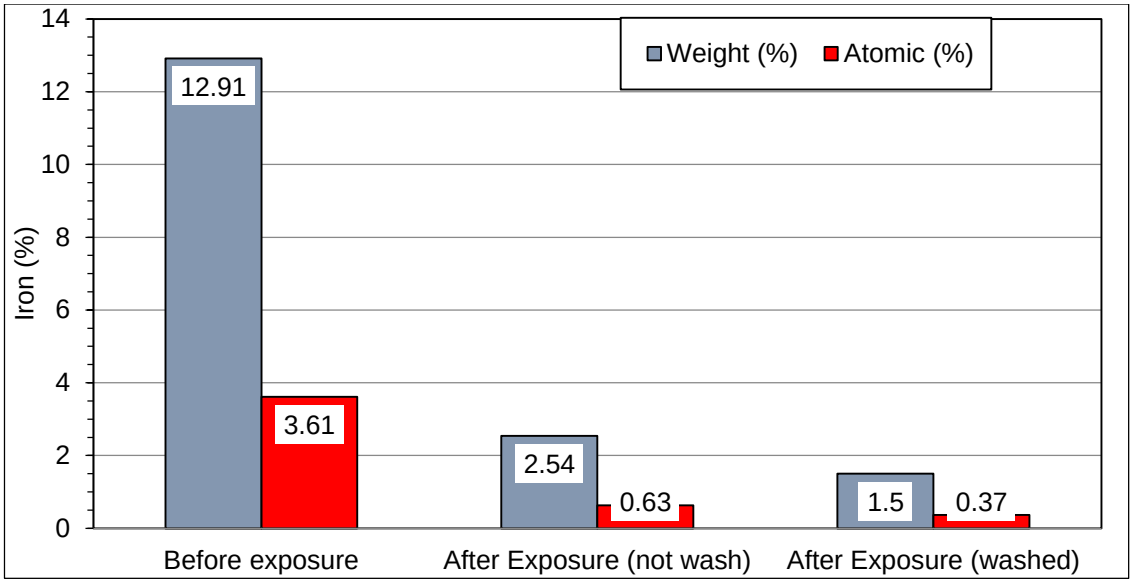

Figure 5-13: SEM analysis for iron content of the active and deactivated catalysts.

The above results suggest that deactivation of catalyst was mainly due to the loss of iron from the catalyst. The physicochemical changes within the treatment system may also favours the leaching iron. Hence, the potential parameters responsible for the physicochemical changes of the treatment system are thus investigated.

5.5.2.2. PHYSICOCHEMICAL CHANGES IN THE TREATMENT SYSTEM

The physicochemical changes in the treatment system such as changes in pH and functional groups of modified PAN catalyst can occur and lead towards deactivation of catalyst thereby failure of the treatment system. These are discussed in following sections.

5.5.2.2.1. TEMPORAL CHANGES IN PH, CONDUCTIVITY AND TEMPERATURE

The pH and temperature of the system were recorded in two minutes intervals using online data loggers positioned before inlet and after outlet of reactor (see Figure 5-3 and Figure 5-4). The conductivity of influent and effluent were also monitored. The temporal changes in pH, conductivity and temperature are shown in Figure 5-15.

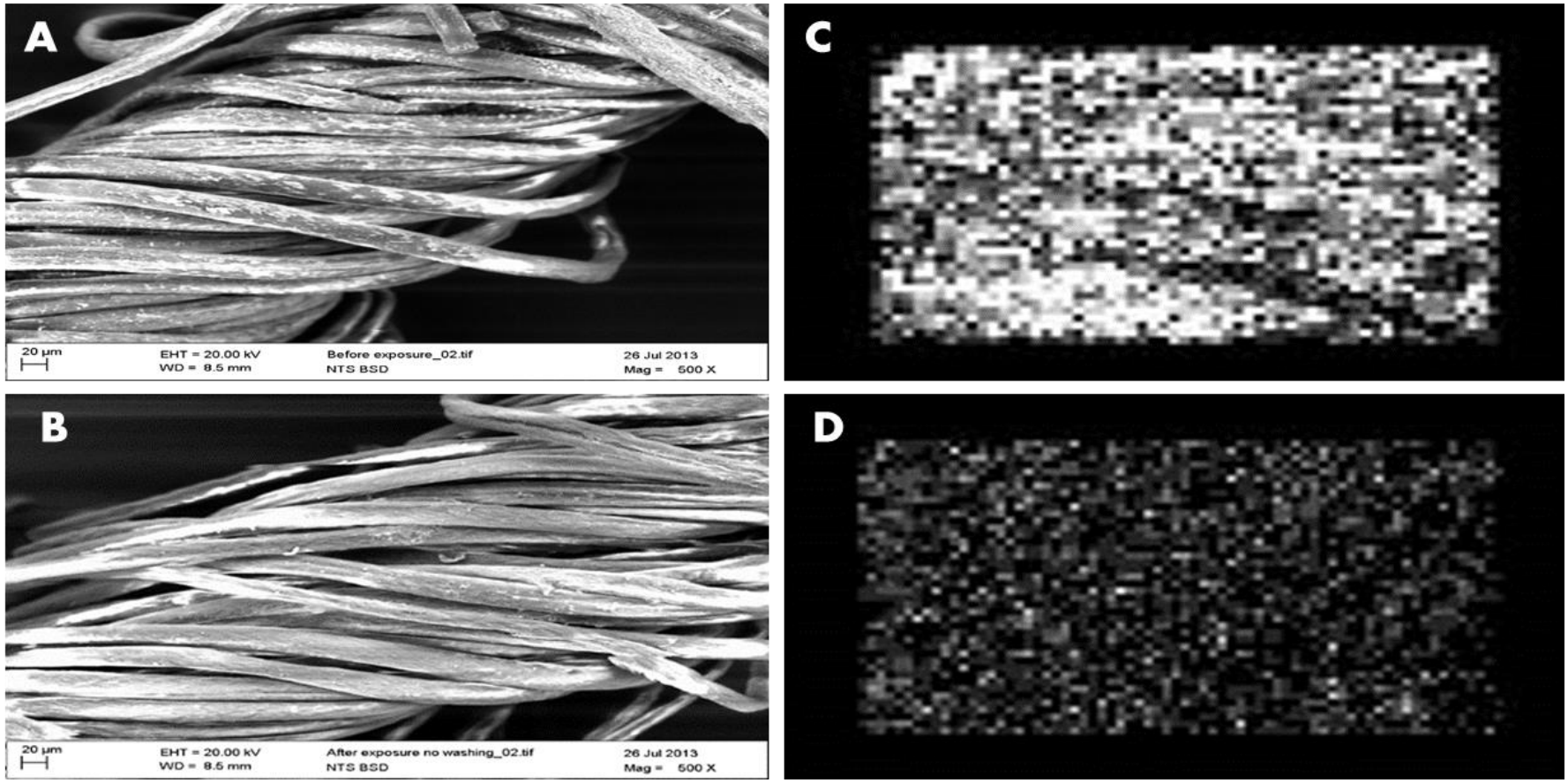

Figure 5-14: SEM images and mapping of iron on PAN threads taken from the active and deactivated catalysts. A) SEM image of PAN thread taken from the active modified PAN catalyst B) SEM image of PAN thread taken from the deactivated modified PAN catalyst C) Mapping of iron on PAN thread taken from the active modified PAN catalyst and D) Mapping of iron on PAN thread taken from the deactivated catalytic mesh.

[Conditions: EHT = 20.00 kV, WD = 8.5 mm, Magnification = 500X].

The daily fluctuations in temperature during the experiment are expected. The temperature during the experiment was around 21 °C. The slight difference between influent and effluent temperatures could be related to the heat generated by continuous stirring with a relatively bigger stirrer at influent compared to smaller stirrer used at effluent sampling point.

The pH of the effluent was slightly lower than the pH of influent. The difference between influent and effluent pH was 0.05 unit to 0.2 unit. The decrease in pH of effluent was due to the formation of acidic intermediate products, such as organic acids, during oxidation of RO16. This result agrees with the results of Fenton oxidation of Amido Black 10B (Sun *et al.*, 2007), photocatalytic degradation of Acid Orange 7 (Stylidi, Kondarides and Verykios, 2004), UV/H_2O_2 decolourization of RO16 (Mitrović *et al.*, 2012), Electro-Fenton treatment of photographic processing wastewater (Bensalah *et al.*, 2013), ozonation and photo degradation of Disperse Red 354 (Neamtu *et al.*, 2004). The changes in pH was found more prominent in near neutral (pH 6.86), weak acidic (pH 5.36) and weakly basic (pH 8.86) media than in strong acidic (pH 2.8 and 3.2) and basic (pH 10.12) media (Mitrović *et al.*, 2012). The small changes of effluent pH in this study could be due to the formation of low molecular weight organic acids. Formation of oxalic, acetic, formic, phthalic, succinic, malonic, fumaric, and maleic acid during degradation of dyes have been reported (Stylidi, Kondarides and Verykios, 2004; Tizaoui and Grima, 2011; Mitrović *et al.*, 2012). The significant drop in pH during oxidation of azo dyes has been attributed to carboxylic acids and primarily to sulphuric acid formed by the rupture of the sulfonate group (—HSO_3) (Hu and Pei, 2002; Sun *et al.*, 2007; Tizaoui and Grima, 2011).

The drop in pH of the effluent due to formation of acidic intermediates is further backed up by the rise in conductivity of the effluent. The increase in conductivity of effluent is due to the formation of ionic species. Apart from the above mentioned acids, formation of inorganic ions such as sulphate (SO_4^{2-}), nitrate (NO_3^-), nitrite (NO_2^-) and ammonium (NH_4^+) during degradation of azo dyes have been reported (Neamtu *et al.*, 2004; Stylidi, Kondarides and Verykios, 2004; Tizaoui and Grima, 2011; Mitrović *et al.*, 2012; Bensalah *et al.*, 2013). The bigger difference between conductivity of influent and effluent compared to pH could be due the presence of inorganic ions released into the system on dye degradation.

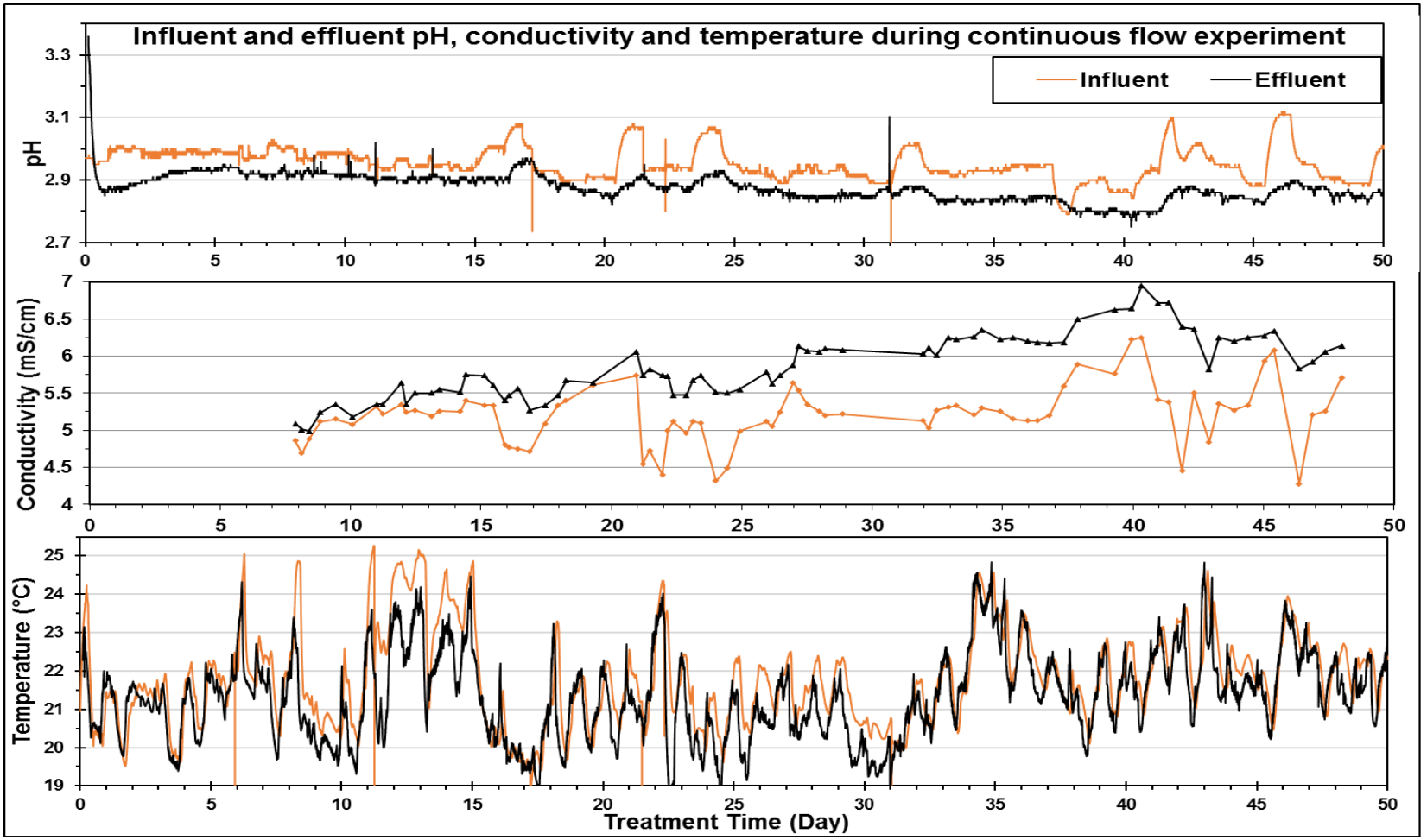

Figure 5-15: Influent and effluent pH, conductivity and temperature recorded during continuous flow experiment.

Deactivation of heterogeneous catalysts due to leaching of metals has been widely discussed and the leaching is attributed to the acidic pH of the reacting solutions (Martínez *et al.*, 2005; J. Herney Ramirez *et al.*, 2007; Chen and Zhu, 2009; Soon and Hameed, 2011; González-Bahamón *et al.*, 2011; Duarte *et al.*, 2013; Babuponnusami and Muthukumar, 2014; Sun *et al.*, 2014; Pastrana-Martínez *et al.*, 2015; Queirós *et al.*, 2015; Ribeiro *et al.*, 2015; Wang *et al.*, 2016; He *et al.*, 2016). The drop of pH due to the formation of acidic intermediates favoured the loss of iron from the catalyst. The iron leaching can arise from the complexation of these intermediates such as carboxylic acids generated during the degradation of dye (Chen and Zhu, 2009; González-Bahamón *et al.*, 2011). Figure 5-16 shows a sharp drop of pH at the beginning of continuous flow experiments performed using column reactor (CR) and rotating disc reactor (RDR) loaded with modified PAN catalyst from production roll 3 and roll 7 respectively. As discussed above, the drop of pH was due to formation of acidic intermediates.

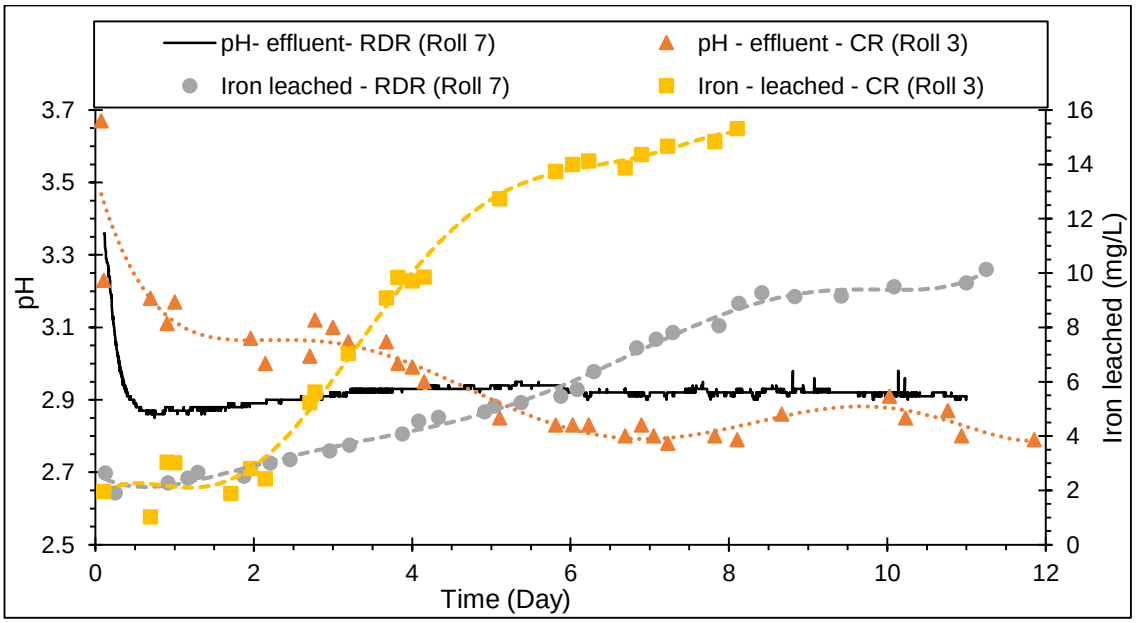

Figure 5-16: pH and iron leaching during the continuous flow treatment of RO16 (C_0 = 50 mg/L) in column reactor (CR) and rotating disc reactor (RDR) with catalyst from production roll 3 and roll 7 respectively.

It is difficult to establish a relationship between pH and iron leaching in rotating disc reactor loaded with catalyst from roll 7 due to lack of readings for leached iron within the first 8 hours of treatment, after which the pH was stabilized around 2.9. However, as seen in Figure 5-17, a linear correlation (R^2 = 0.8814) between pH and the iron leaching was found during the continuous flow experiment performed in column reactor using catalyst from production roll 3. The correlation established in this study is similar to the linear correlation between iron leaching and the formation of oxalic acid reported during

phenol degradation (Zazo *et al.*, 2006). Thus, it is evident that iron leaching favoured by decrease in pH is a cause for the deactivation of catalyst.

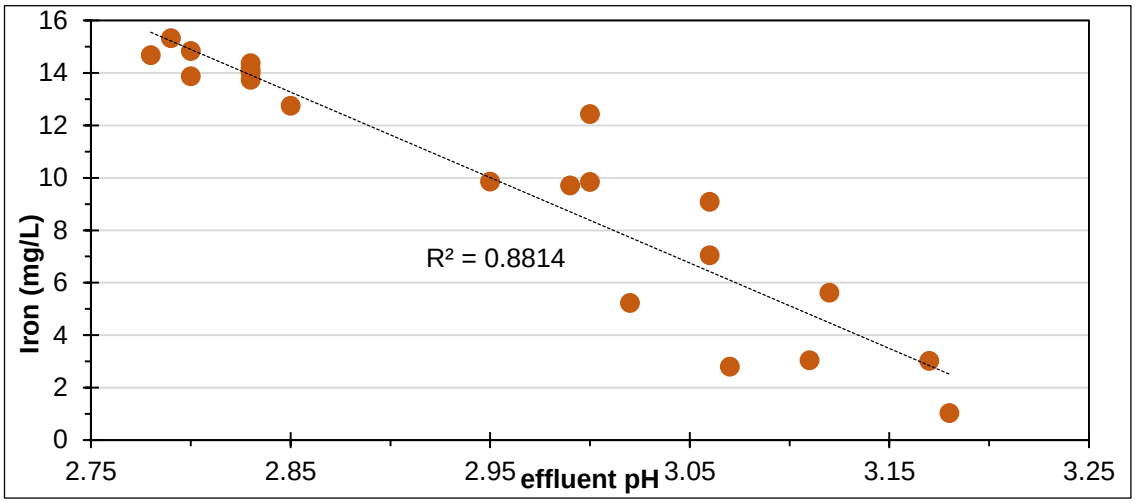

Figure 5-17: Leaching of iron as a function of pH during continuous flow experiment in column reactor loaded with catalyst from production roll 3.

5.5.2.2.2. CHANGES IN FUNCTIONAL GROUPS OF MODIFIED PAN CATALYST

Changes in functional groups within the modified PAN catalyst can occur during reaction. The infrared spectrum arise from vibration of specific sets of chemical bonds from within a molecule. This is considered to be a unique characteristic which can be used as a fingerprint for identification and comparison of changes in molecular backbone or associated functional groups (Coates, 2000). FTIR-ATR analysis of active and deactivated catalysts was performed according to procedures outlined in section 5.3.3.8. The principal infrared bands associated in raw and modified PAN are given in Table 5-5.

Table 5-5: Principal IR bands associated in PAN and modified PAN fibre.

Wavenumber (cm^{-1})	**Functional groups**
3,400	O-H hydroxyl group H-bonded stretch
3,324	N-H stretch in primary amine ($-NH_2$)
3,210 – 3,190	N-H stretch of imino compounds (=N-H)
2,950 – 2,970	Asymmetric vibration of aliphatic $-CH_3$ groups
2,924	C-H asymmetrical stretch of methylene (CH_2)
2,850	C-H symmetrical stretch
2,242	C≡N saturated
1,733	C=O as in esters

Wavenumber (cm^{-1})	**Functional groups**
1,640	C=O as in amide $–CONH_2$
1,613	N-H, primary amine bend
1,650 - 1,580	C=N (includes C=N in oximes and imidines), N-H bend mixed
1,540	Acid salts
1,445	C-H bend of methylene
1,384	CH_3 bending mode
1,236	C-N, C-C, mixed
1,106	N-N stretch of hydrazide group
1,080	stretch in C-O-Fe
1,070 – 1,100	C-O stretch of primary alcohol, secondary alcohol
1,130 - 1,080	Inorganic sulfate usually accompanied by a peak at 680 - 610 cm^{-1}
1,036	C-O stretch in C-O-C
938	Vinyl out of plane bend
920	N-O bend of Oxime, usually accompanied by N-O stretch at 1240-1,215 cm^{-1}, and bonded OH stretch at 3,300-3,150 cm^{-1}
828	Nitrate usually accompanied by a peak at 1,410-1,340 cm^{-1}
695	Bending motion of O=C-N group in amides

Source: reproduced from (Chi, 2008, p. 64).

Figure 5-18 presents the FTIR-ATR spectra of PAN threads taken from the active and deactivated catalysts. The following changes in the spectra were observed.

- The broad peak at 3,200 cm^{-1} assigned to amine ($-NH_2$) and hydroxyl (O-H) groups showed decreased intensity in the deactivated catalyst. This could be due to the loss of amino or amide groups during continuous flow treatment of RO16 (Orlova, 2010).
- The peak at 2,919 cm^{-1} attributed to C-H stretch appeared with decrease in intensity. This could be due to the coverage of the C-H bond, the backbone of the modified catalyst (Coates, 2000; Chi, 2008; Chi and Huddersman, 2011).
- Broadening of peak at 1,630 cm^{-1} with increase in intensity indicates the formation of carboxyl groups (C=O) upon hydrolysis of amine groups, and intermediate acid adsorbing to the catalyst (Chi, 2008; Asuelimen, 2015).
- The peaks at 1,355 cm^{-1} and 1,245 cm^{-1} broadened with increase in intensity.

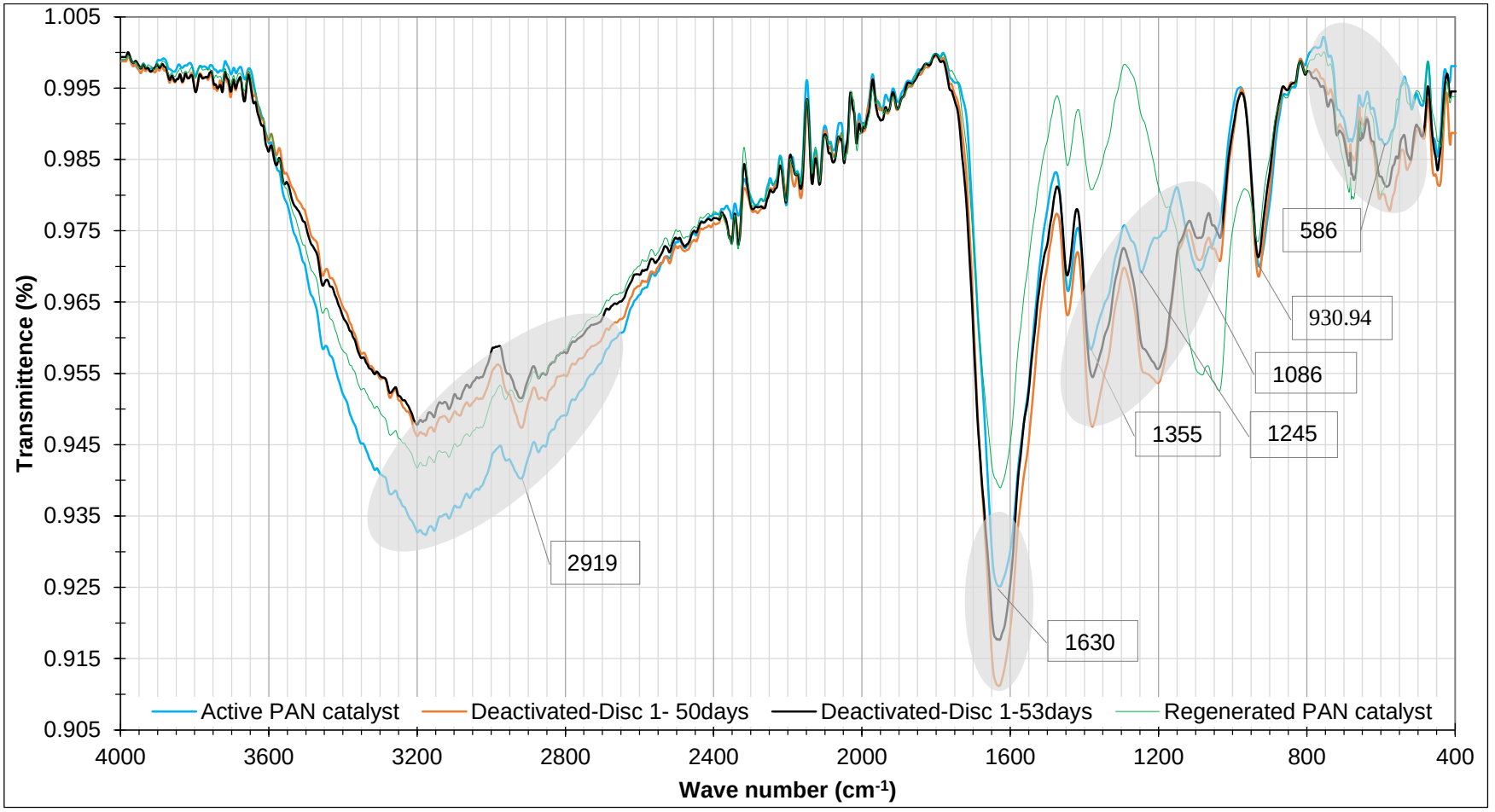

Figure 5-18: Overlaid baseline corrected and normalized FTIR-ATR spectra for active and deactivated catalyst samples.

- The peak at 1,086 cm^{-1} assigned to a C-O-Fe stretch narrowed with decrease in intensity, indicating loss of iron.
- A new peak emerged at 1,035 cm^{-1}. According to Table 5-5, the peak at 1,035 cm^{-1} is assigned to C-O stretch in C-O-C.
- The peak at 930.94 cm^{-1} assigned to oxime groups remained unaffected.
- The peaks at lower wave number 700 cm^{-1} to 450 cm^{-1} gained intensity.
- The peak at 1,080 cm^{-1} in regenerated modified PAN catalyst broadened either side. This is due to the presence of iron sulfate. The peak is so broad that it adjoined with the peak at 1,036 cm^{-1} that, according to Table 5-5, is due to C-O stretch in C-O-C. Besides this change, the overall spectrum corresponding to regenerated mesh appeared as less intense. However, the peak to base ratio of active (unexposed) and regenerated modified PAN catalyst are similar.

The above observations evident that the failure of the treatment system and the deactivation of catalyst is also linked to the changes in functional groups in the catalyst that occurred due to the loss or gain of organic and inorganic compounds on the modified PAN catalyst.

5.5.3. REGENERATION OF DEACTIVATED CATALYST

The possible mechanisms for the catalyst deactivation have been already discussed in section 5.5.2. The deactivated catalyst can be regenerated, recycled or disposed. The regeneration of deactivated catalyst is preferred mainly on environmental and economic grounds as it facilitates prolonged use of the catalyst, minimizing the use of new raw materials. The main purpose of regeneration is to eliminate the temporary poisons and foulants from the surface of catalyst as well as restoration of the active sites.

The regeneration of catalyst can be performed off-site / ex-situ and on-site / in-situ (Trimm, 2001; Bartholomew and Argyle, 2015; Gumerov *et al.*, 2016). Regeneration of deactivated heterogeneous catalyst can be performed by washing off foulants and poisons with surfactants, acid or base etc., rinsing with deionized water, pressurized wet and dry treatments of coke (carbonaceous deposits), reimpregnation of active catalytic materials and drying at low heating rates (Trimm, 2001; Argyle and Bartholomew, 2015; Gumerov *et al.*, 2016). Thus, attempts were made for the in-situ regeneration of deactivated modified PAN catalyst by washing with higher dose of oxidant followed by reimpregnation of active catalytic sites onto the deactivated modified PAN catalyst. An important point to be noted is that complete restoration of catalytic activity is not possible

and even with continual regeneration, the catalytic activity would gradually decline and have a certain life (Nauman, 2001).

5.5.3.1. REGENERATION OF DEACTIVATED CATALYST VIA WASHING WITH HIGHER DOSE OF OXIDANT

It is very likely that the catalyst was fouled and or poisoned by recalcitrant degradation products such as carboxylic acids. According to Trimm, 2001, total removal of foulants and poisons by means of washing is rare however; it can be effective to regenerate significant proportion of the original catalytic activity. Washing with oxidant not only physically removes the foulants but also catalyses the poisons (Trimm, 2001). In-situ regeneration of deactivated modified PAN catalyst was successfully performed by washing with 10 g/L H_2O_2 at pH 3 (Asuelimen, 2015). Thus, in order to restore the catalytic activity, deactivated modified PAN catalyst after 50 days of operation was washed with higher doses of H_2O_2 at pH 3.

The reactor was drained to remove RO16 solution. Then, the system was washed with 11 L (12.8 times the reacting volume) of H_2O_2 (500 mg/L, four times higher than optimum dose) at pH 3 followed by washing with double distilled water at pH 3. The washing was done in batch mode, each cycle lasting about 30 minutes. The rotating speed of the discs was increased to get vigorous mixing. The treatment operation of RO16 was resumed to evaluate the performance of the system. The results (from day 50 to 52) are shown in subsection G of Figure 5-5.

The removal efficiency for decolourization and aromaticity, compared to that at the time of breakthrough (71 % and 30 % respectively), have improved immediately after washing and reached to 88 % and 50 % respectively. However, the improvement did not last long and dropped to 58 % for decolourization and 36 % for aromaticity within 46 hours. It is believed that sudden enhancement in removal efficiency was partly due to sorption and partly due to the cleansing of foulants and or poisons.

Second attempt was made to regenerate the deactivated modified PAN catalyst by washing with a three-folds higher dose of H_2O_2 than previously used. Accordingly, 15 L (17.5 times the reacting volume) of H_2O_2 (1,500 mg/L) at pH 3 was fed through the system and washed with double distilled water at pH 3. The results on day 52 to 53 are in line with the results from the first attempt. The sudden improvement did not last for 24 hours and the removal efficiency for decolourization and aromaticity dropped to 34 %

and 10 % respectively. The results of regeneration by means of washing with H_2O_2 do not agree with the results of (Asuelimen, 2015).

In summary, the regeneration of deactivated catalyst by means of washing with higher dose of H_2O_2 was not successful. Continual decline in the performance of the system after washing with H_2O_2 indicates that deactivation of catalyst was not occurred due to the blockage of active sites by foulants and poisons. This suggests that the deactivation of catalyst was occurred due to the loss of active catalytic sites which agrees with the high degree of iron leaching from the catalyst discussed in section 5.5.2.1. Therefore, regeneration of active catalytic sites via reimpregnation of catalytic material onto the deactivated catalyst was thus investigated in the following sections.

5.5.3.2. REGENERATION OF DEACTIVATED CATALYST VIA REIMPREGNATION OF ACTIVE CATALYTIC SITES

Since the regeneration of deactivated catalyst via washing with oxidant was not successful, an alternative method of regeneration was considered. The degree of iron leaching was very high and almost 90 % of the iron was leached off the catalyst. With this very fact, regeneration via reimpregnation of iron as catalytic sites was chosen. The iron from iron (III) sulfate pentahydrate $\{Fe_2(SO_4)_3.5H_2O\}$ was impregnated onto the deactivated catalyst. It was desired to reimpregnate the same amount of iron (15 mg/g mesh) as of fresh catalyst during production. Therefore, regenerations of deactivated catalyst after each exposure was performed using a solution containing 13.7 g/L of ferric sulfate pentahydrate and 53.3 g/L of sodium sulfate decahydrate (calculation shown in Appendix 9-4). The pH of the solution (pH 2.2) was not adjusted. The results are discussed separately in the following sections.

5.5.3.2.1. ACTIVITY OF FIRST-TIME REGENERATED CATALYST

Reimpregnation of iron onto the deactivated catalyst was performed according to the procedures laid out in section 5.3.3.9.2. The regenerated catalyst was subsequently applied for the treatment of the RO16. Figure 5-19 shows that the catalytic activity of deactivated catalyst was successively restored via reimpregnation of active catalytic sites. The treatment performance of the regenerated catalyst found to be similar to the performance of fresh catalyst. The removal efficiencies corresponding at 254 nm, 297 nm, 387 nm and 493.5 nm follow the same order as in the first exposure of catalyst. The highest removal efficiencies for decolourization (Vis - 493.5 nm) and loss of aromaticity (UV - 254 nm) were 100 % and 66 % respectively. The highest TOC removal was 51 %.

The poor removals related to 254 nm, 297 nm and 387 nm observed at the beginning are due to the absorbance contributed by leached of iron as shown in Figure 5-20.

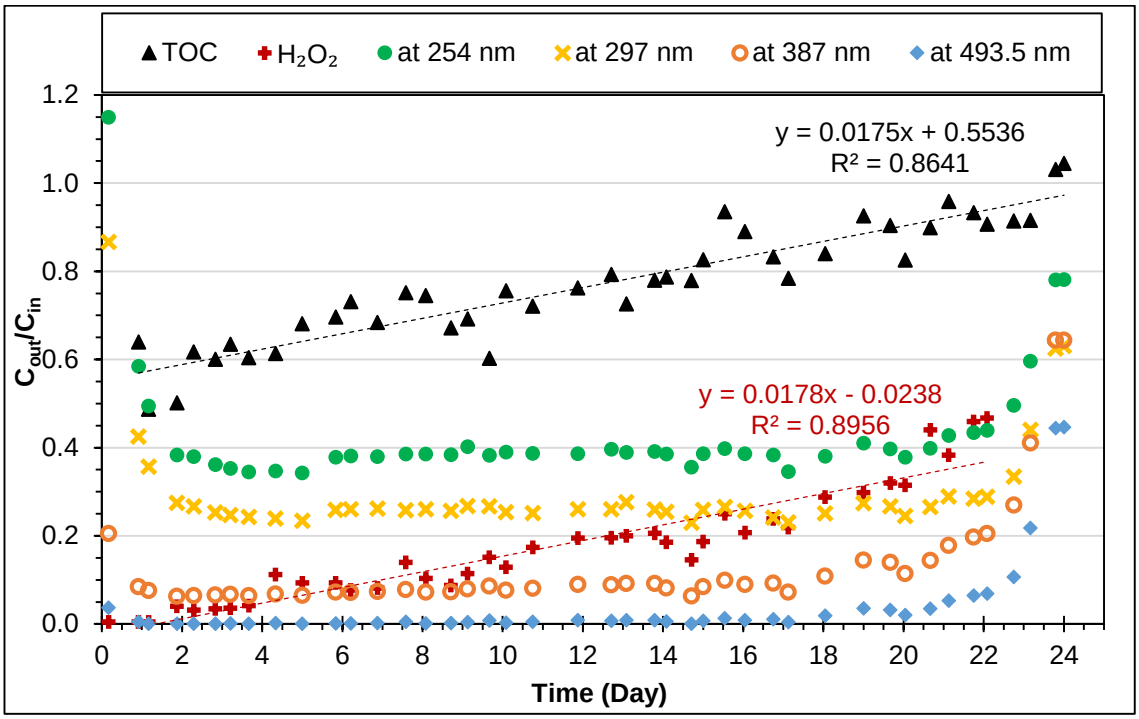

Figure 5-19: Treatment of RO16 in continuous flow mode of operation using first-time regenerated PAN catalyst.

[Experimental conditions: 208 g of regenerated catalyst, 125 mg/L H_2O_2, pH 3 in 860 mL reacting volume, RT = 4 hours at room temperature ~ 21 °C].

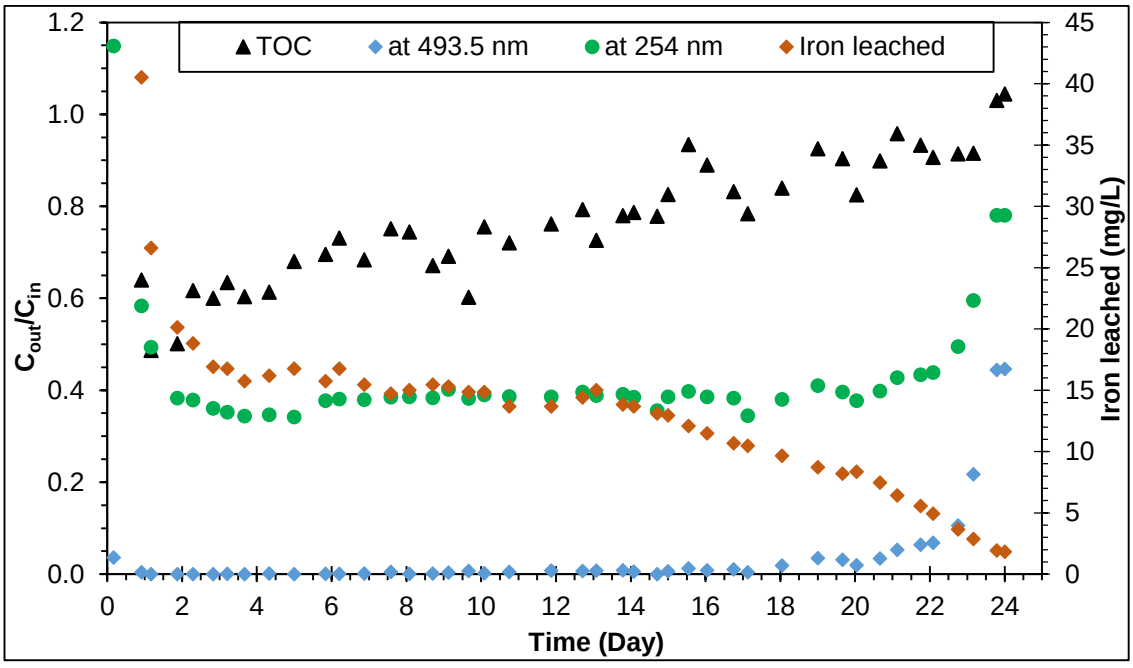

Figure 5-20: Removal efficiencies for decolourization, aromaticity and TOC with respect to iron leaching.

The trend for H_2O_2 consumption in the presence of reactivated catalyst was also similar to that with catalyst before deactivation. The consumption of H_2O_2 decreases with decreasing extent of mineralization (TOC). It is noteworthy to mention that H_2O_2 consumption and TOC removal were decreasing linearly with respect to time and were parallel (similar slopes) to each other (see Figure 5-19).

The regenerated catalyst was equally effective, in the treatment of RO16, as fresh active catalyst. However, compared to the fresh catalyst, the lifetime of the regenerated catalyst was halved and the breakthrough in the treatment system occurred on 24th day of the treatment. The removal efficiencies for aromaticity (UV - 254 nm) and decolourization (Vis - 493.5 nm) at the time of breakthrough were 22 % and 56 % respectively. The lifetime of regenerated catalyst, by iron reimpregnation, was much longer than the one observed by Asuelimen, 2015 who regenerated the deactivated catalyst in similar manner as in this study and applied in the removal of humic acid and observed complete failure (20.5 % for decolourization (Vis - 400 nm) and 0.1 % for aromaticity (UV - 254 nm) after 9 days.

The reduced lifetime of regenerated catalyst could either be due to a higher degree of iron leaching from the catalyst due to loose bonding of iron salt onto the catalyst or not having the same amount of iron on the regenerated catalyst as of fresh catalyst. Therefore, mass balance of iron during the exposure of first-time regenerated catalyst was investigated and the results are discussed in section 5.5.3.3.1.

5.5.3.2.2. TEMPORAL CHANGES IN PH AND TEMPERATURE OF THE FIRST-TIME REGENERATED SYSTEM.

Figure 5-21 shows the pH and temperature of influent and effluent during the treatment period after the first regeneration. The influent and effluent temperature trends show similar daily fluctuation and the average temperature during the treatment was ~ 21 °C. However, there was difference in pH of influent and effluent. Similar to previous exposure, drop of effluent pH was observed and the difference between influent and effluent is more pronounced (0.4 unit drop in pH) compared to the differences shown during treatment with fresh catalyst. Thus, relatively lower pH of the solution also contributed to higher leaching of iron from the regenerated catalyst.

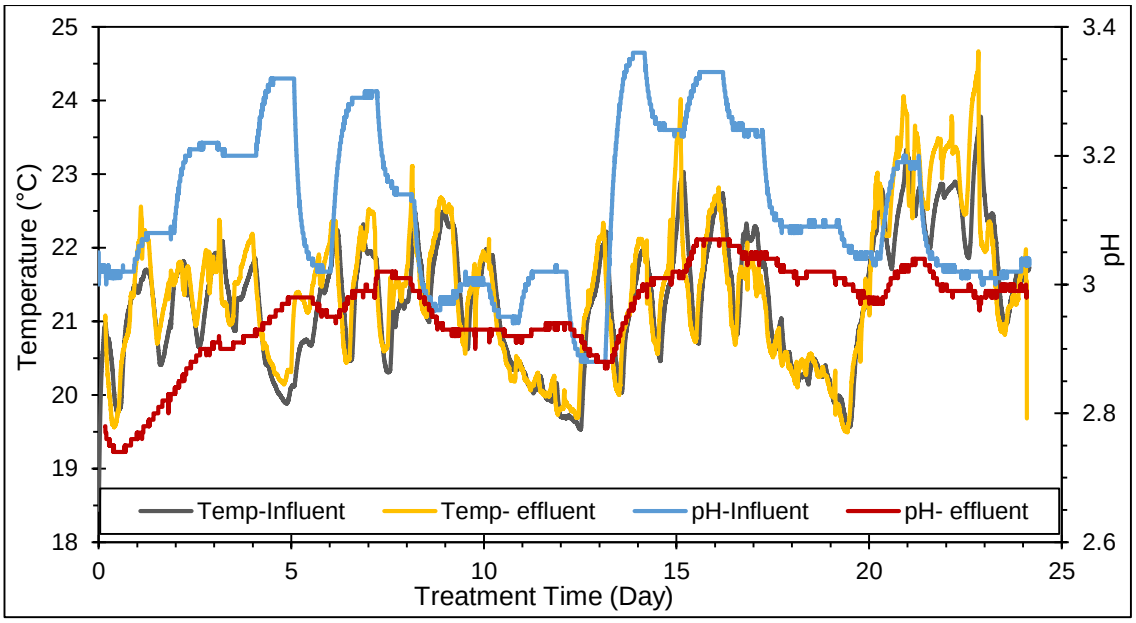

Figure 5-21: pH and temperature of influent and effluent during continuous flow treatment of RO16 using first-time regenerated catalyst.

5.5.3.2.3. ACTIVITY OF SECOND-TIME REGENERATED CATALYST

Second regeneration of deactivated catalyst was performed using the amount of iron and sodium salts as calculated in Appendix 9-4 and procedures given in section 5.3.3.9.2. The catalyst thus prepared was then applied in the treatment of RO16 using the experimental conditions as of previous exposures and the results are presented in Figure 5-22 and Figure 5-23. The removal efficiencies corresponding to 254 nm, 297 nm, 387 nm and 493.5 nm are in the same order as of first-time regenerated and fresh catalysts. The trends for TOC, COD and consumption of H_2O_2 are similar to those observed with fresh and first-time regenerated catalysts. The highest removals corresponding to decolourization (Vis - 493 nm), aromaticity (UV - 254 nm), TOC and COD were 99.86 %, 68 %, 36 % and 83 % respectively.

The second-time regenerated catalyst was equally effective in terms of removal of RO16. However, the lifetime of catalyst decreased by 66 % and 30 % compared to fresh catalyst (50 days) and the first-time regenerated catalyst (24 days). The breakthrough occurred on the 17th day of the treatment and the removal efficiencies for aromaticity (UV-254 nm) and decolourization (Vis- 493.5 nm) dropped to 39% and 79 % respectively. The cause of deactivation, as established during previous experiments, is expected as loss of iron and functional changes of modified PAN catalyst. Therefore, mass balance of iron during the exposure of second-time regenerated catalyst was investigated and the results are discussed in section 5.5.3.3.2.

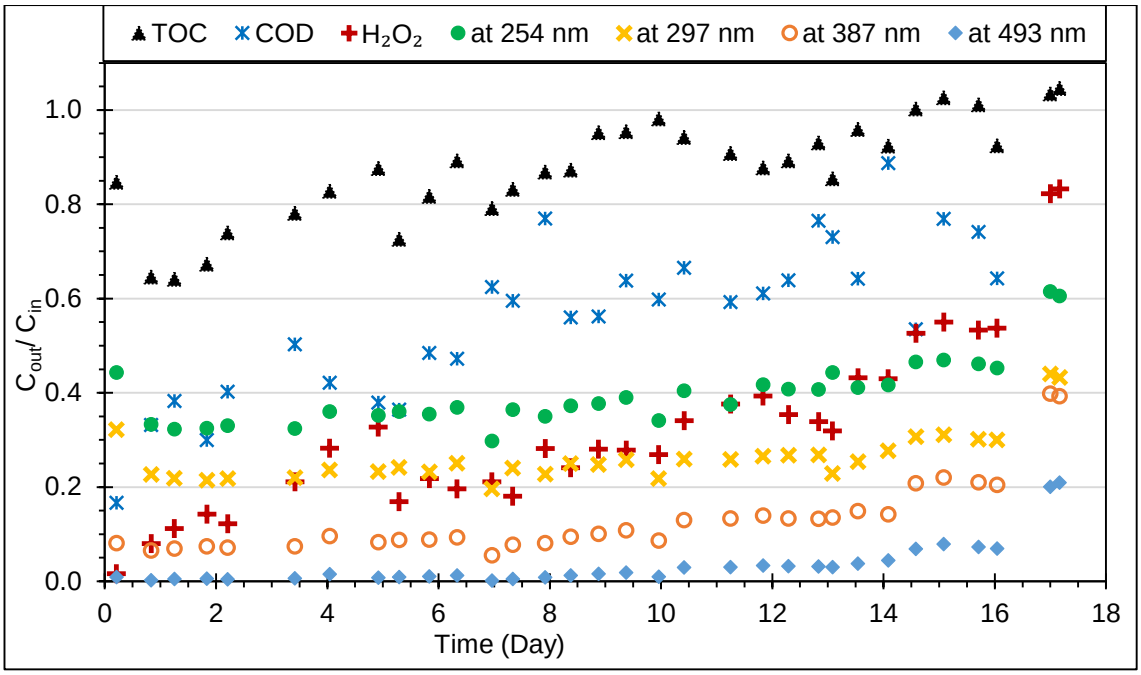

Figure 5-22: Treatment of RO16 in continuous flow mode of operation using second-time regenerated PAN catalyst.

[Experimental conditions: 208 g of regenerated catalyst, 125 mg/L H_2O_2, pH 3 in 860 mL reacting volume, RT = 4 hours at room temperature ~ 21 °C].

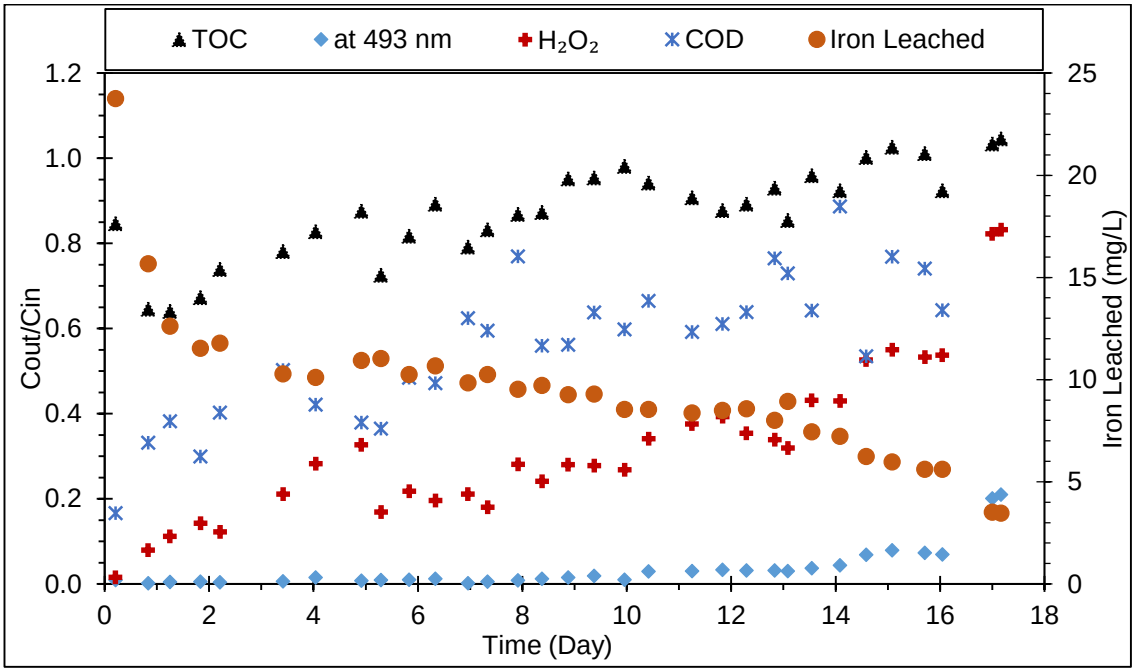

Figure 5-23: Removal efficiencies and iron leaching during continuous flow experiment with second-time regenerated catalyst.

[Experimental conditions are similar as in Figure 5-22].

5.5.3.2.4. TEMPORAL CHANGES IN pH AND TEMPERATURE OF THE SECOND-TIME REGENERATED SYSTEM

Figure 5-24 presents the temporal changes in pH and temperature of influent and effluent. It is clear that influent and effluent temperature remained similar where as decrease in pH from influent to effluent was observed. The average temperature during the treatment was ~21 °C. The drop in effluent pH resulted by the formation of acidic intermediates and related discussion can be found in the previous sections.

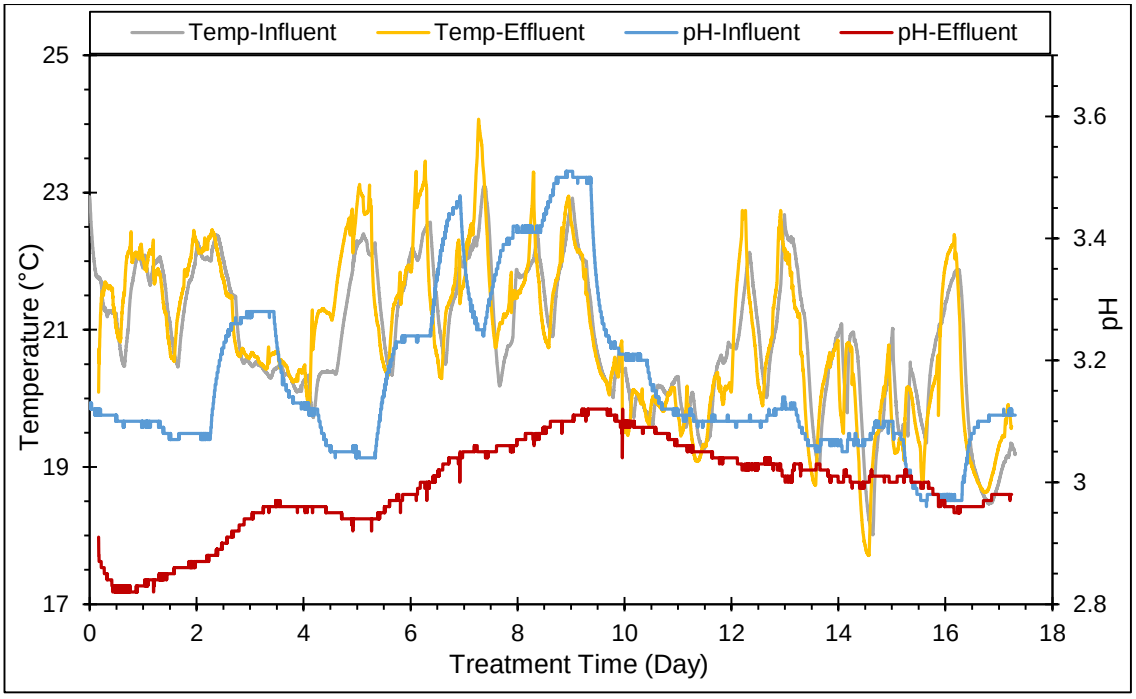

Figure 5-24: pH and temperature of influent and effluent during continuous flow treatment of RO16 using second-time regenerated catalyst.

5.5.3.2.5. ACTIVITY OF THIRD-TIME REGENERATED CATALYST

The deactivated catalyst was regenerated as in previous regenerations. The regenerated catalyst was subsequently applied in the treatment of RO16 and the results obtained are presented in Figure 5-25. It can be seen that the regenerated catalyst was equally effective as in previous cycle. However, the effectiveness did not last as long as in previous cycles. The performance of catalyst started to decline from the fourth day of the treatment. The removal efficiencies corresponding to 254 nm, 297 nm, 387 nm and 493.5 nm dropped to 47 %, 62 %, 68 % and 84 % respectively on 9th day of the treatment. The highest removals observed corresponding to these wavelengths were 73 %, 82 %, 93 % and 99.13 % respectively.

Although the removal of COD does not follow a smooth trend, decline in COD removal can be traced. The fluctuation in COD removals related to the fluctuation in room temperature. It was observed that the samples taken in the evening show higher COD removal compared to the samples taken in the morning. This is expected as the room temperature in the evening used to be relatively higher than in the morning. The lifetime of third-time regenerated catalyst was reduced by 82 %, 62.5 % and 48 % compared to fresh, first-time and second-time regenerated catalysts respectively. The possible causes for the deactivation of catalyst described in previous exposures and established as loss of iron that is discussed in section 5.5.3.3.3.

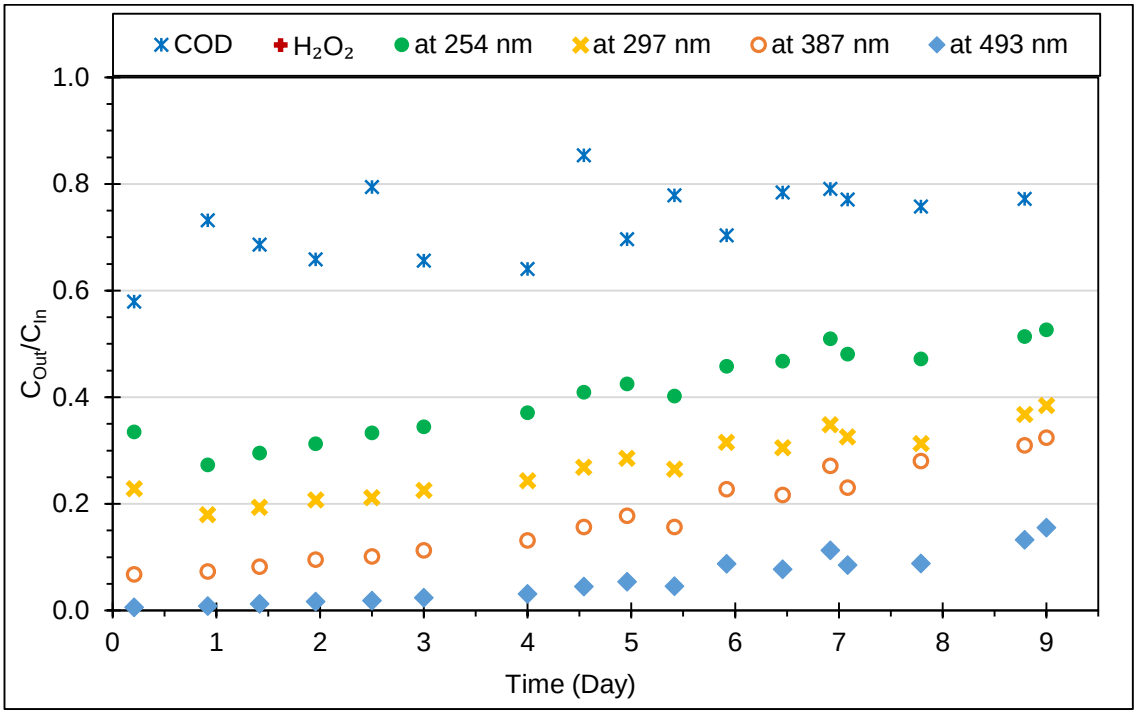

Figure 5-25: Treatment of RO16 in continuous flow mode of operation using third-time regenerated PAN catalyst.

[Experimental conditions are similar as in Figure 5-22].

5.5.3.2.6. TEMPORAL CHANGES IN PH AND TEMPERATURE OF THE THIRD-TIME REGENERATED SYSTEM

The temporal fluctuations in pH and temperature during the exposure of third-time regenerated catalyst are presented in Figure 5-26. The daily fluctuation in temperature was within the range of 18.5 °C to 24 °C. The variation between influent and effluent pH is similar to those observed during the previous exposures. The difference in influent and effluent pH decreases when catalyst starts to deactivate.

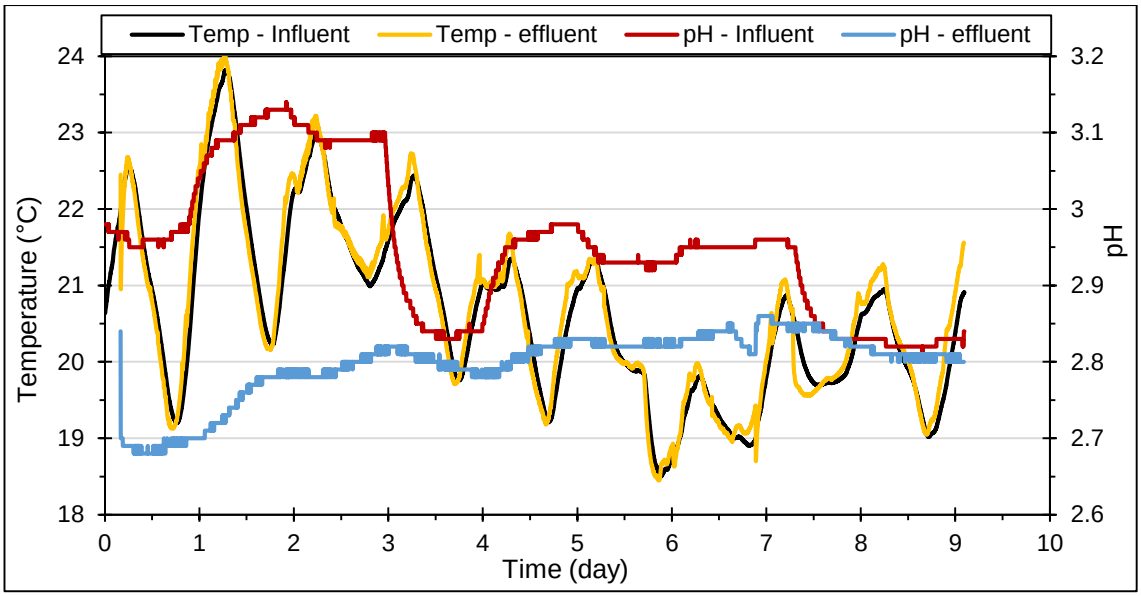

Figure 5-26: Changes in pH and temperature during the fourth exposure of PAN catalyst.

5.5.3.3. MASS BALANCE OF IRON DURING THE EXPOSURES OF REGENERATED CATALYST

Mass balance of iron during the application of first-time regenerated catalyst has been evaluated by determining the amount of iron impregnated onto the catalytic discs, leached into the effluent, and residual iron left on the catalytic discs after breakthrough in the system. The total amount of leached iron was calculated by calculating the area under the curve using trapezium method as explained in section 5.5.2.1.1. The mass balance of iron during continuous flow treatment of RO16 using regenerated catalyst is given in Table 5-6.

5.5.3.3.1. FIRST-TIME REGENERATED CATALYST

Although, it was desired to impregnate 15 mg of iron per gram of catalyst, only 7.12 mg Fe/g (1480.69 mg in 208 g) of catalyst was achieved. This, along with the residual iron (238.33 mg in 208 g) on the deactivated catalyst, gives 8.26 mg Fe/g of regenerated catalyst. Thus, the regenerated catalyst held a total of 1719.02 mg of iron, which is 203.08 mg less than the total iron held on the fresh catalyst. The reduction in iron loading on regenerated catalyst could be due the loss of polymeric support (functional groups) on the modified PAN resulted from continuous washing or it could be due to limited access of iron salt to the inner fibrils of PAN threads. The extent of iron loss from the first-time regenerated catalyst was calculated as 92.27 % (based on area under the curve of leached iron) and 84.57 % (based on residual iron on the catalyst) when breakthrough of the system occurred. The extent of iron loss from regenerated catalyst is similar to

that of the fresh catalyst, 90.54 % based on area under the curve and 84.57 % based on residual concentration on the catalyst.

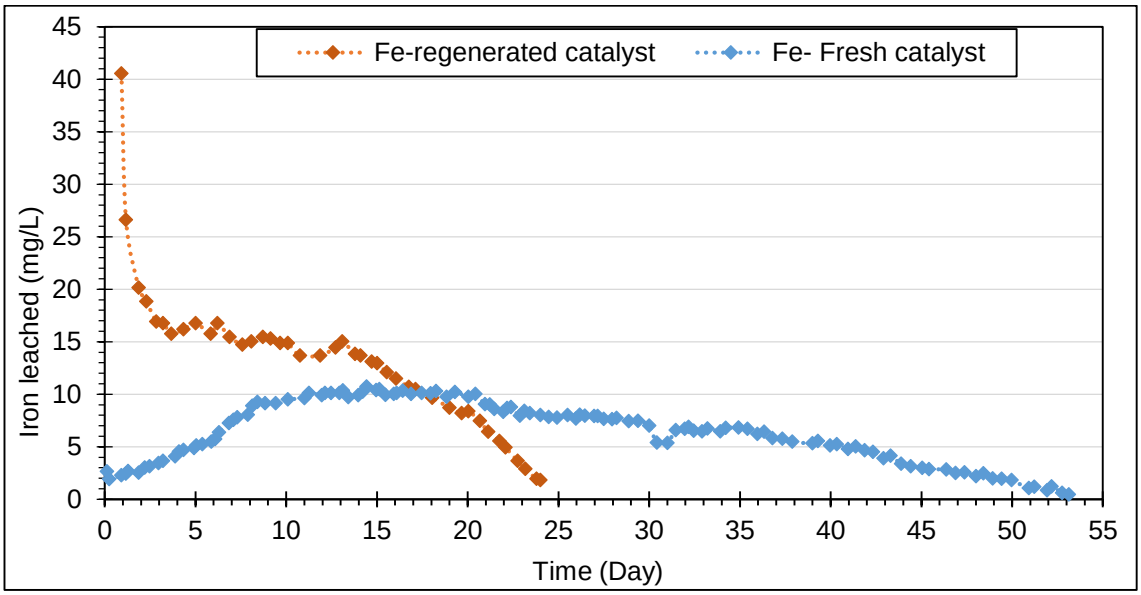

Figure 5-27: Comparison of iron leaching from fresh and regenerated PAN catalyst during continuous flow treatment of RO16.

Figure 5-27 compares the iron leaching during continuous flow treatment of RO16 using fresh and regenerated catalysts. Although the total leaching (%) of iron from fresh and regenerated catalysts seem to be similar, the rate at which iron leached from regenerated catalyst was higher than fresh catalyst. Figure 5-27 shows that iron leaching from the fresh catalyst was slower and increases gradually over time and is stable for some time then gradually decreases whereas iron leaching from the regenerated catalyst was the highest at the beginning and gradually decreases over time. The very high leaching at the beginning signifies inadequate washing after regeneration. The regenerated catalyst did not show the three phases of leaching of iron as did the fresh catalyst.

Based on the total iron loading on fresh and regenerated catalysts, the lifetime of regenerated catalyst was not proportional to the lifetime of fresh catalyst. Fresh catalyst with iron loading of 1,922.10 mg lasted for 50 days. Thus, by proportion, regenerated catalyst was supposed to last ~ 45 days. However, it lasted 24 days only. The shorter lifetime of regenerated catalyst resulted from the higher leaching of iron. The causes of higher leaching of iron could be related to the strength of iron legation to the regenerated catalyst and pH of the reacting solution.

Table 5-6: Mass balance of catalyst (iron) during second, third and fourth exposures of regenerated PAN catalyst.

Total amount of residual iron on the deactivated catalyst carried over from previous exposure (mg) **(A)**		Total amount of iron in the solution before impregnation (mg) **(B)**	Total amount of iron in the solution after impregnation (mg) **(C)**	Total amount of iron in the washed solution, after impregnation (mg) **(D)**	Total amount of iron impregnated onto the catalyst (mg) **(E)** $= \mathbf{B} - (\mathbf{C} + \mathbf{D})$
First-time regenerated catalyst	238.33	3,241.50	1,307.00	453.81	1,480.69
Second-time regenerated catalyst	257.92	3,185.00	1,049.00	1,087.20	1,048.80
Third-time regenerated catalyst	314.86	3,158	2,136	504.9	517.1

Total amount of iron leached into the effluent (mg) **(F)**		Total amount of residual iron on the catalyst deactivated after exposure (mg) **(G)**	Mass Balance for iron		Iron loss (%)	
			Mass of iron before exposure (mg) $\boldsymbol{M_B = A + E}$	Mass of iron after exposure (mg) $\boldsymbol{M_A = F + G}$	Based on area under the curve $= \frac{\boldsymbol{F}}{\boldsymbol{M_B}} * \mathbf{100}$	Based on residual iron on the catalyst $= \frac{\boldsymbol{G}}{\boldsymbol{M_B}} * \mathbf{100}$
First-time regenerated catalyst	1,586.10	257.92	1,719.02	1,844.02	92.27	84.57
Second-time regenerated catalyst	827.21	314.86	1,306.72	1,078.20	63.31	75.90
Third-time regenerated catalyst	273.07	342.88	831.96	615.95	32.82	58.78

5.5.3.3.2. SECOND-TIME REGENERATED CATALYST

The mass balance of iron during the exposure of second-time regenerated catalyst is shown in Table 5-6. Although, it was aimed to impregnate 15 mg of iron per gram of deactivated catalyst, only 5.04 mg (1,048.8 mg in 208 g) of iron per gram of deactivated catalyst was impregnated. This is less than iron impregnated during the first regeneration (7.12 mg/g). Therefore, with residual iron (257.92 mg in 208 g), the total iron loading on second-time regenerated catalyst become 6.28 mg/g (1,306.72 mg in 208 g) of catalyst. The total amount of iron after third exposure was calculated as 1,078.20 mg, which is 82.51 % of initial loading (1306.72 mg).

The loss of iron computed based on area under the curve (effluent concentration) and residual concentration on deactivated catalyst were 63.31 % and 75.9 % respectively. This is ~ 10 % (based on residual iron) to ~ 30 % (based on leached iron) less compared to extent of iron loss during previous exposures. The disparity in the data might have resulted from the computation performed using the same initial amount of catalyst (208 g). It should be noted that there was a continual washing-off of catalytic fibres during each experimental run. The exact loss of catalyst after each set of experiment was not known. However, an approximation can be made based on the loss of catalyst (~ 4 g) observed during 33-day long continuous flow treatment of RO16 in a vertical column reactor loaded with 55 g catalyst. It is also noteworthy to mention that, after each deactivation, catalyst samples were taken for FTIR-ATR analysis and digestion. Thus, it is obvious to obtain more iron loss calculated based on the residual iron on the catalyst.

The first-time regenerated catalyst was washed with four times the reacting volume and a very high amount (~ 40 mg/L) of iron leaching was observed at the beginning of exposure (see Figure 5-20). This indicates the inadequate washing of regenerated catalyst. Thus, to ensure proper washing of regenerated catalyst, second-time regenerated catalyst was washed with seven times the reacting volume. However, Figure 5-23 shows that iron leaching was still high (23.75 mg/L) which also indicates inadequate washing of regenerated catalyst or the iron was loosely held on catalyst and not ligated. The trend for iron leaching from the second-time regenerated catalyst was found to be similar to that from the first-time regenerated catalyst.

5.5.3.3.3. THIRD-TIME REGENERATED CATALYST

The mass balance of iron during the exposure of third-time regenerated catalyst was performed in the same manner to those for previous exposures and the results are

presented in Table 5-6. As in previous regenerations, the targeted loading of iron on the catalyst was not achieved. Instead, compared to the first (7.12 mg/g) and the second (5.04 mg/g) impregnations, the iron loading during the third (2.48 mg/g) impregnation was significantly decreased. This indicates a sequential loss of functional groups as ligands during each exposure.

The total loading of iron after third impregnation become 831.96 mg. The total amount of iron after the exposure of third-time regenerated catalyst was calculated as 615.95 mg (residual – 342.88 mg, leached – 273.07 mg) which is 74 % of the initial loading. The difference in mass balance of iron increases after every successive exposure. This difference could have arisen from the change in total amount of catalyst as the amount of catalyst in every exposure was considered same as of beginning (208 g). However, in reality, amount of catalyst changes with respect to time due to loss of catalytic fibrils.

The impregnated amount of iron decreased in each successive regenerations and loading of iron onto the deactivated catalyst as on fresh catalyst was not achieved. Looking at the amount of reimpregnated iron during the first, second and third regenerations, iron salt adequate for two-third, half and one-third of the iron loading on the fresh catalyst could be enough. However, due to the concentration effect, the iron loading may further decrease. Therefore, further investigation on reimpregnation is needed.

5.5.4. HOMOGENEOUS VERSUS HETEROGENEOUS CATALYSES

The possibility of having homogeneous catalysis due to leached iron is discussed in section 4.5.4.8, p.133. Homogeneous catalysis of RO16 was performed in batch as described in section 5.3.3.9.3. The amount of iron used in homogeneous study were equivalent to the amounts of iron leached on the second day (~ 3 mg/L) and in between Day-11 and Day-20 (~ 10 mg/L – the maximum leaching observed) during continuous flow treatment of RO16. Figure 5-28 presents the results of homogeneous catalysis of RO16 in the presence of iron equivalent to the amount of leached iron. The residence times on Day-2 and Day-11 to Day-20 were about 2.5 hours and 4 hours respectively. Accordingly, the removal efficiencies observed at these residence times with respect to homogeneous catalysis of RO16 are compared in Figure 5-29.

After 2.5 hours of homogeneous catalysis of RO16 in the presence of iron equivalent to the leached iron (3 mg/L) on Day-2 of continuous flow treatment, the removal efficiencies corresponding to decolourization, loss of aromaticity and mineralization (reduction in

TOC) were 89.4 %, 45.4 % and 16.9 % respectively. The efficiency for decolourization shows no significant difference to decolourization efficiencies observed on Day-2 of continuous flow treatment. This suggests that continuous flow treatment relied on homogeneous catalysis due to the leached iron. However, significant differences between two processes in terms of efficiencies corresponding to loss of aromaticity and mineralization strongly disagree with above statement. The continuous flow treatment resulted in much higher efficiencies than homogeneous catalysis. According to Figure 5-5, the removal efficiencies corresponding to loss of aromaticity and mineralization in continuous flow treatment on Day-2 were 63.2 % and 50.8 % respectively. According to Figure 5-28, the corresponding efficiencies in homogeneous catalysis limited to 45.4 % and 16.9 % respectively. The results show that continuous flow treatment was 1.4 to three folds faster than homogeneous catalysis. The photographic evidence presented in Figure 5-4 (insert) also supports above statement as the RO16 solution was decolourized halfway through the reactor. This suggests that continuous flow treatment relied on heterogeneous catalysis.

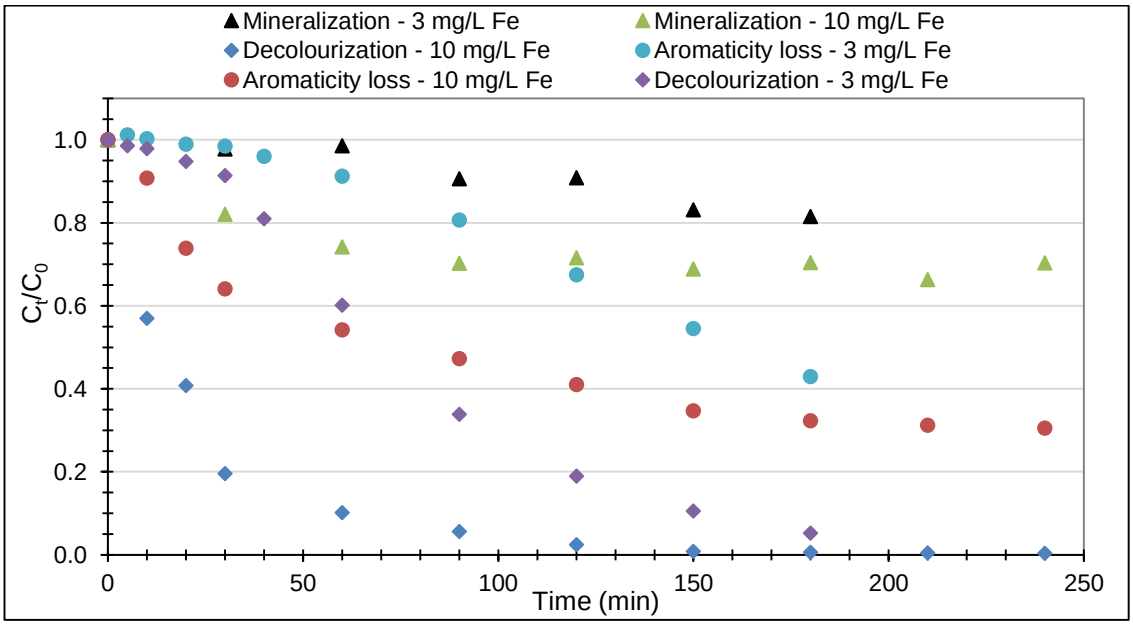

Figure 5-28: Homogeneous catalysis of RO16 using an equivalent amount of leached iron during continuous flow treatment of RO16. The source of iron was iron (III) sulfate pentahydrate.

After four hours of homogeneous catalysis of RO16 in the presence of iron equivalent to the leached iron (~ 10 mg/L) on Day-11 of the continuous flow treatment, the removal efficiencies corresponding to decolourization, loss of aromaticity and mineralization were 99.6 %, 69.5 % and 29.7 % respectively. The efficiencies corresponding to decolourization and loss of aromaticity show no significant difference between two

processes. This suggests that continuous flow treatment relied on homogeneous catalysis due to the leached iron. However, the extent of mineralization in continuous flow treatment resulted higher (39.5 %) compared to homogeneous catalysis (29.7 %), suggesting continuous flow treatment did not rely only on leached iron.

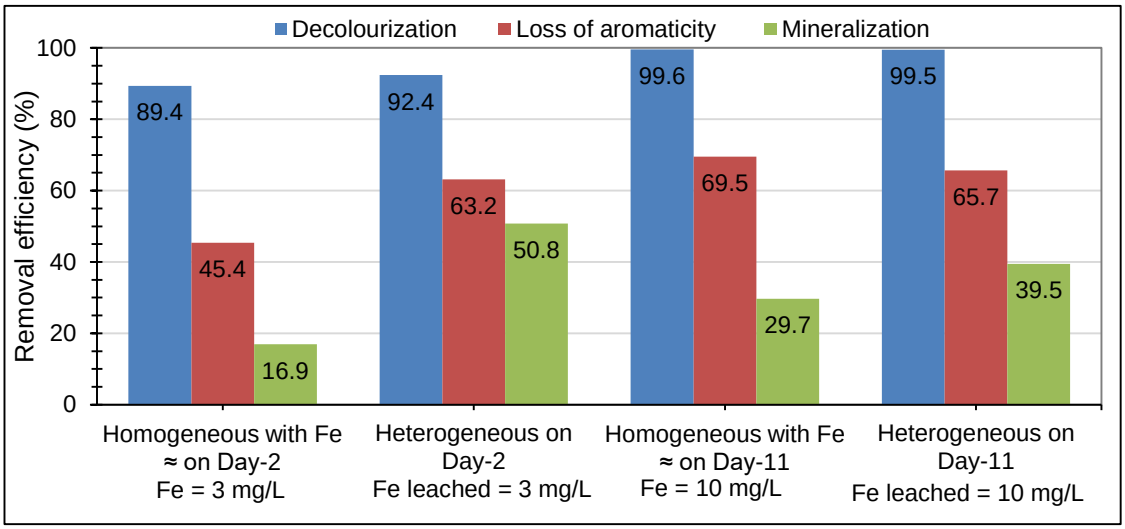

Figure 5-29: Comparison of performance of continuous flow treatment with homogenous catalysis performed in the presence of iron equivalent to the leached iron.

In order to conclude whether continuous flow treatment relied on homogeneous catalysis, the following points must be considered.

- It is not fair to compare the results of a batch and a continuous flow treatment. Generally, due to mixing effect, a batch process results in better performance than a continuous flow process.
- It is not fair to use the amount of iron equivalent to the amount of leached iron in continuous flow treatment. The amount of leached iron in continuous flow treatment is the quantity accumulated over a certain residence time, for example 2.5 to four hours in this study. Thus, exposing an equivalent amount of iron that leached after certain residence time from the beginning in homogeneous catalysis (batch) is in favour of homogenous catalysis.
- The iron concentration in the reactor builds up towards the outlet of the reactor. The photographic evidence in Figure 5-4 (insert) shows decolourization of RO16 midway through the reactor where concentration of leached iron would be expected to much lower than that at effluent.
- The comparison using an equivalent amount of iron from iron salt would not be fair as the speciation of iron may be different. It is believed that the leached iron is complexed with ligands such as water, substrate and intermediate products.

In conclusion, based on the results on Day-2 of continuous flow treatment and homogeneous catalysis with an equivalent amount of iron as of Day-2 and considering the above mentioned points, it can be concluded that the continuous flow treatment mainly relied on heterogeneous catalysis. However, looking at the results of Day-11 of continuous flow treatment and homogeneous catalysis with an equivalent amount of iron as of Day-11, the process can be said to be assisted by homogenous catalysis.

5.5.5. THE LIFETIME OF THE MODIFIED PAN CATALYST

An ideal catalyst is expected to last forever. In practicality, this would not happen and the catalyst eventually deactivate with respect to the use (Richardson, 1989). Thus, it is important to know the lifetime of a catalyst. The lifetime of a catalyst can be measured in terms of various properties. An effective catalyst supposed to possess properties such as; high catalytic activity, high selectivity, long life-time, easy regeneration, highly resistance to deactivation, and higher mechanical strength (Derouane *et al.*, 2002). Although, there are no universal methods for testing and controlling catalytic activity and selectivity, the common properties used to determine the suitability of a catalyst for an industrial process are activity, selectivity and stability (deactivation behaviour) (Derouane *et al.*, 2002; Hagen, Chorkendorff and Niemantsverdriet, 2006).

5.5.5.1. ACTIVITY

The activity of a catalyst is the ability to accelerate chemical reaction. The rate of reaction is the absolute measure for catalyst activity (Derouane *et al.*, 2002). However, catalyst activity can be measured in terms of other parameters such as space-time yield (STY), space velocity, turnover frequency (TOF), turnover number (TON) and temperature of reactions (Hagen, Chorkendorff and Niemantsverdriet, 2006).

The continuously mixed tank reactor models assumed to operate at steady state. Hence, the computation of rate of reaction accordingly considers the parameters at steady state. Thus, determination of rate of reaction with respect to fresh catalyst applied in this study is irrelevant as the process parameters such as flow rate and H_2O_2 were varied during the experimentation. Therefore, activity of modified PAN catalyst is discussed in terms of TOF and TON for which determination of the oxidized mass of substrate is a prerequisite.

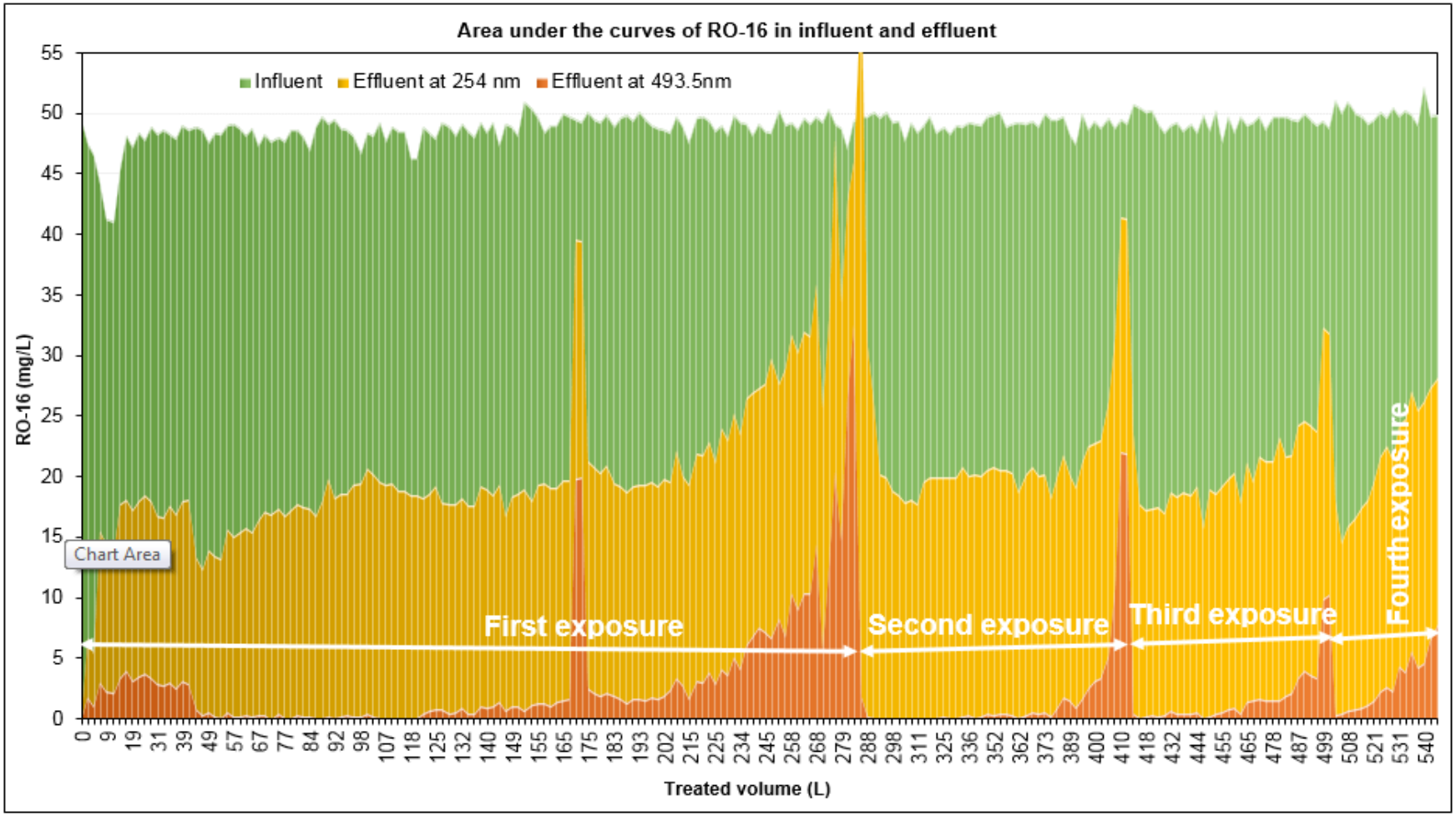

Figure 5-30: Concentrations of RO-16 in the influent and effluent with respect to treated volume.

5.5.5.1.1. MASS BALANCE OF REACTIVE ORANGE 16

The mass balance during the continuous flow treatment of RO16 is calculated in terms of total mass of RO16 fed in, oxidized and exited the reactor. The mass fed into the reactor (M_i) is equal to the total area of the plot in Figure 5-30. The total decomposed mass (M_d) of RO16 is equal to the area above the dynamic curve. The total exited mass (M_o) of RO16 is equal to the area under the dynamic curve. The area above the curve was determined by subtracting the area under the dynamic curve from the total area of the plot (see Equation 5-9). The area under the curve was computed by summing up the area of the trapezoids under the dynamic curve produced by plotting the concentrations of RO16 in the effluent with respect to treated volume at time (t). The area of the plot was also computed by summing up the area of trapezoids under the curve produced by plotting the concentrations of RO16 in the influent. The area of trapezium was calculated using Equation 5-8.

$$M_d = M_i - M_o \qquad \textit{Equation 5-9}$$

Where, M_d = mass of RO16 decomposed (mg) = area above the curve. M_i = mass of RO16 entered into the reactor (mg) = total area of the plot (graph) and M_o = mass of RO16 exited from the reactor (mg) = area under the curve (mg).

Table 5-7: Mass balance of RO16 quantified interms of decolourization and loss of aromaticity during four exposures of catalyst.

Experimental cycle	Total mass entered into the reactor **(M_i)** (mg)	Total mass of RO16 exited from the reactor **(M_o)** (mg)		Total mass of RO16 decomposed **(M_d)** (mg)	
		Based on decolourization	Based on aromaticity loss	Based on decolourization	Based on aromaticity loss
Fresh catalyst	13,777.06	1,017.61	6,013.04	12,759.45	7,764.02
First regeneration	6,292.93	204.28	2,791.63	6,088.64	3,501.30
Second regeneration	4,392.01	151.11	1,831.83	4,240.90	2,560.17
Third regeneration	2,322.43	135.30	9,98.87	2,187.13	1,323.56
Over all	**26,784.42**	**1,508.3**	**11635.38**	**25,276.12**	**15,149.05**

Table 5-7 presents the calculation and Figure 5-30 shows graphical representation for mass balance during the continuous flow treatment of RO16 with fresh and regenerated catalyst. The mass balance of RO16 during continuous flow treatment was estimated based on decolourization and loss of aromaticity. The yellow and orange area in Figure 5-30 represent the untreated mass of RO16 based on decolourization and loss of aromaticity respectively. Therefore, green, yellow and orange; green; and green and yellow areas in Figure 5-30 represent the total mass of RO16 entered to the reactor and mass of RO16 decomposed based on loss of aromaticity (at 254 nm) and decolourization (at 493.5 nm) respectively.

5.5.5.1.2. TURNOVER FREQUENCY (TOF)

TOF is simply defined as the number of revolutions of the catalytic cycle per unit time (Boudart, 1995). Thus, TOF measures the total number of molecules decomposed by one mole of active catalytic site per time at specified experimental conditions (Hagen, Chorkendorff and Niemantsverdriet, 2006; Ilsen and Avci, 2016) and is given by the Equation 5-10.

$$TOF = \frac{moles\ of\ RO16\ converted}{moles\ of\ iron\ per\ gram\ catalyst * mass\ of\ catalyst * time} = \frac{mmol}{\left(\frac{mmol}{g}\right) * g * t} = \frac{1}{t} = t^{-1} \qquad \textit{Equation 5-10}$$

Table 5-8 shows the TOF values for the fresh catalyst and catalyst after every successive regenerations. TOF can be used to compare the catalytic activities of different catalysts. The larger the TOF, the more active is the catalyst. It can be seen that TOF improved slightly in every successive regeneration. The overall TOF of modified PAN catalyst for the treatment of RO16 based on aromaticity removal and decolourization were found as $1.6*10^{-4}$ h^{-1} and $9.56*10^{-5}$ h^{-1} respectively. This means that $1.6*10^{-4}$ mmol of RO16 can be decolourized per hour by one mmol of iron before being inactive. These TOF values are much lower compared to relevant industrial applications in which TOF ranges; 0.01 to 100 s^{-1} (Hagen, Chorkendorff and Niemantsverdriet, 2006) and 0.01 to 1,000 s^{-1} (Ilsen and Avci, 2016). It is noteworthy to mention here that the dye content of model compound was 50 % and the other 50 % was not known. Thus, the TOF values calculated should take into account of 50 % impurities as well.

Although TOF has been widely used to define the catalyst activity, it is equally accepted that measurements of active sites in heterogeneous catalysts based on TOF values may not truly represent the activity of catalyst (Boudart, 1995; Hagen, Chorkendorff and Niemantsverdriet, 2006). Moreover, active sites in heterogeneous Fenton processes can exist in multiple forms which may not be active equally (Soon and Hameed, 2011). The approximation of active sites may lead to the big errors, thus some literature recommend not to use TOF and / or TON for characterization of industrial catalysts (Petrov, 2002).

In the case of modified PAN catalyst, amount of active sites (iron) decrease as iron leaches continuously with respect to the treatment time. Thus, TOF may not be a true reflection of catalytic activity of modified PAN catalyst towards the degradation of RO16 over the time period chosen.

Table 5-8: Turnover frequency (TOF) for fresh and regenerated PAN catalysts.

Experimental cycle	Moles of RO16 decomposed (mmol)		Iron (mmol/g catalyst)	Amount of catalyst (g)	Time (hours)	TOF (hr^{-1})	
	Decolourized	Aromaticity loss				Decolourization	Aromaticity
Fresh catalyst	20.662	12.573	0.1654	208	1275	$4.71*10^{-4}$	$2.87*10^{-4}$
First regeneration	9.8595	5.6697	0.1479	208	576	$5.56*10^{-4}$	$3.2*10^{-4}$
Second regeneration	6.8674	4.1458	0.1124	208	412	$7.13*10^{-4}$	$4.3*10^{-4}$
Third regeneration	3.5417	2.1433	0.0716	208	216	$1.1*10^{-3}$	$6.66*10^{-4}$
Overall	**40.931**	**24.531**	**0.4974**	**208**	**2479**	**$1.6*10^{-4}$**	**$9.56*10^{-5}$**

Since the parameters, such as TOF, measuring catalytic activity are not precise, the priority of target properties of a catalyst during industrial application is given the following order: selectivity > stability > activity (Hagen, Chorkendorff and Niemantsverdriet, 2006; Ilsen and Avci, 2016). Thus, despite low activity reflected by TOF, Figure 5-31 proves that modified PAN catalyst was selective and stable for the treatment of dye with the average removals measured in terms of aromaticity loss and decolourization as 56.56 % and 94.37 % respectively and total lifetime of 104 days (3.5 months) in continuous flow treatment.

According to Figure 5-31, the performance (decolourization, loss of aromaticity and lifetime) of the system dropped approximately by half on each successive exposures.

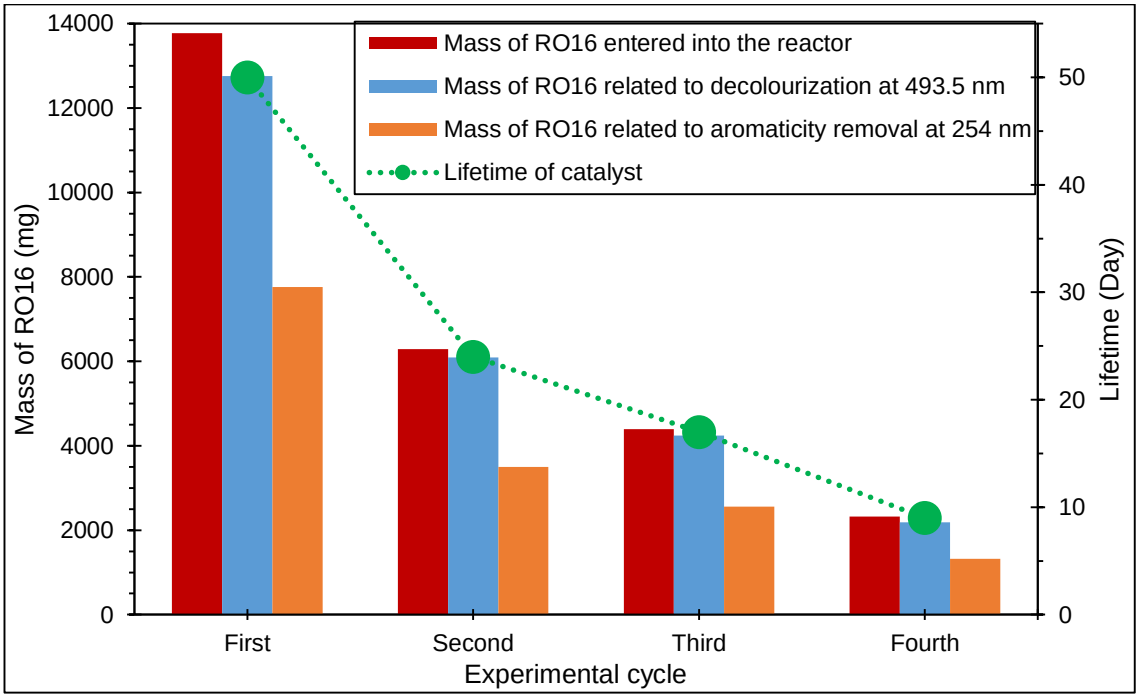

Figure 5-31: Comparison of experimental cycles with respect to treatment performance and lifetime of catalyst.

5.5.6. POST TREATMENT ACTIVITY

The colour of the effluent becomes brownish-yellow when catalytic activity declines nearer the time of breakthrough of the system. The colour of the effluent disappeared afterwards in a collection tank and become colourless. This suggests continual oxidation of the effluent. It is clear that the effluent contained leached iron and unreacted H_2O_2 that can favour homogeneous Fenton process. Thus, post treatment activity was examined with effluent samples taken nearer to and after the breakthrough in the system. The effluent sample at 1,081 hours (45 days) of treatment was taken in a beaker and stirred

using magnetic stirrer. The concentrations of iron, RO16 and H_2O_2 in the sample were 2.91 mg/L, 7.6 mg/L and 95 mg/L respectively.

Figure 5-32 shows the results of post treatment activity in the effluent. It can be seen that decolourization, loss of aromaticity, extent of mineralization (TOC) continuously increase whereas pH and H_2O_2 decrease over the time. Figure 5-33 shows photographic evidence of post treatment activity in the effluent sample taken at 325 hours of the third exposure. This suggests that having a post treatment reservoir would be beneficial. This would help to not only reduce COD but also eliminate H_2O_2 and leached iron by favouring precipitation.

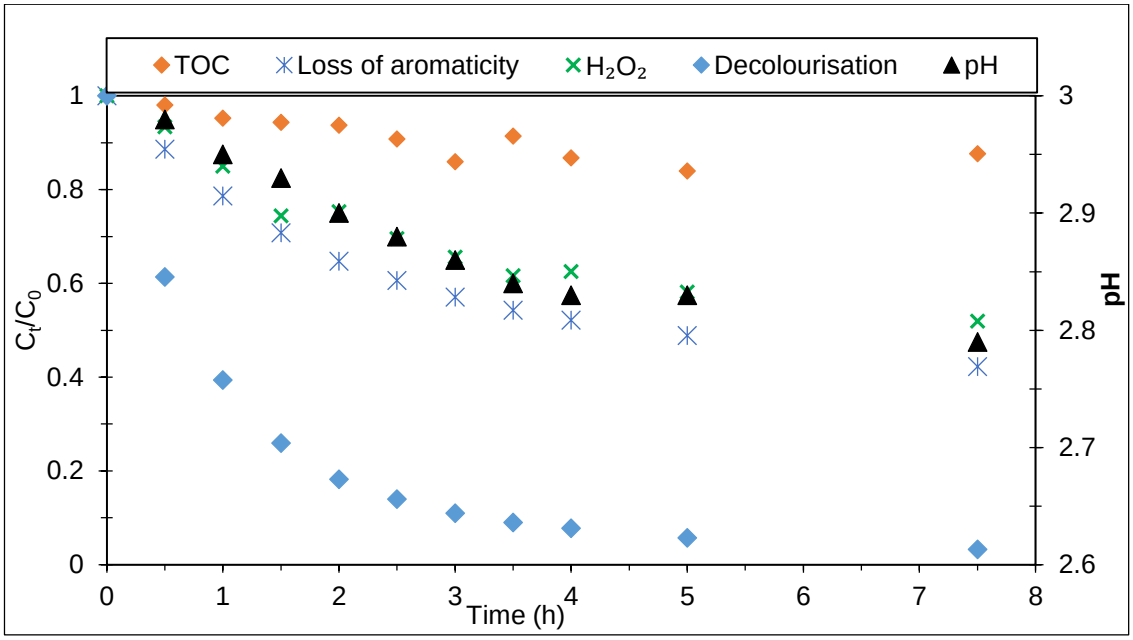

Figure 5-32: Post treatment activity in the effluent sample collected on the Day-45 of the the treatment.

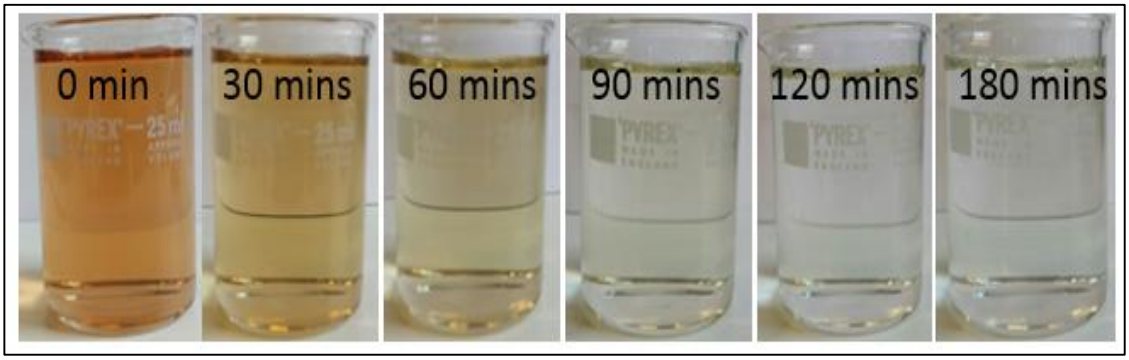

Figure 5-33: Photographic evidence of post treatment activity in the effluent sample taken at 325 hours of third exposure of PAN catalyst.

The effluent colour shown in Figure 5-8 (C) and Figure 5-33 (0 min) does not match with the colour imparted by RO16. In order to investigate whether the colour imparted by

RO16 or intermediate products, RO16 solution equivalent to that of effluent concentration (1.8 mg/L) was made and scanned. Figure 5-34 presents the UV/Vis spectra of RO16 in influent, effluent sampled at 325 hours of the third exposure and RO16 solution with concentration equivalent to effluent. It can be seen that the spectrum for RO16 solution with concentration equivalent to effluent is identical to the spectrum of RO16 in influent. All the four characteristic peaks are present. However, the spectrum corresponding to effluent sampled at 325 hours during third exposure shows no characteristic peaks, confirming loss of peaks. This confirms that the presence of colour in the effluent is associated with the degradation products that can be degraded due to post-treatment reaction.

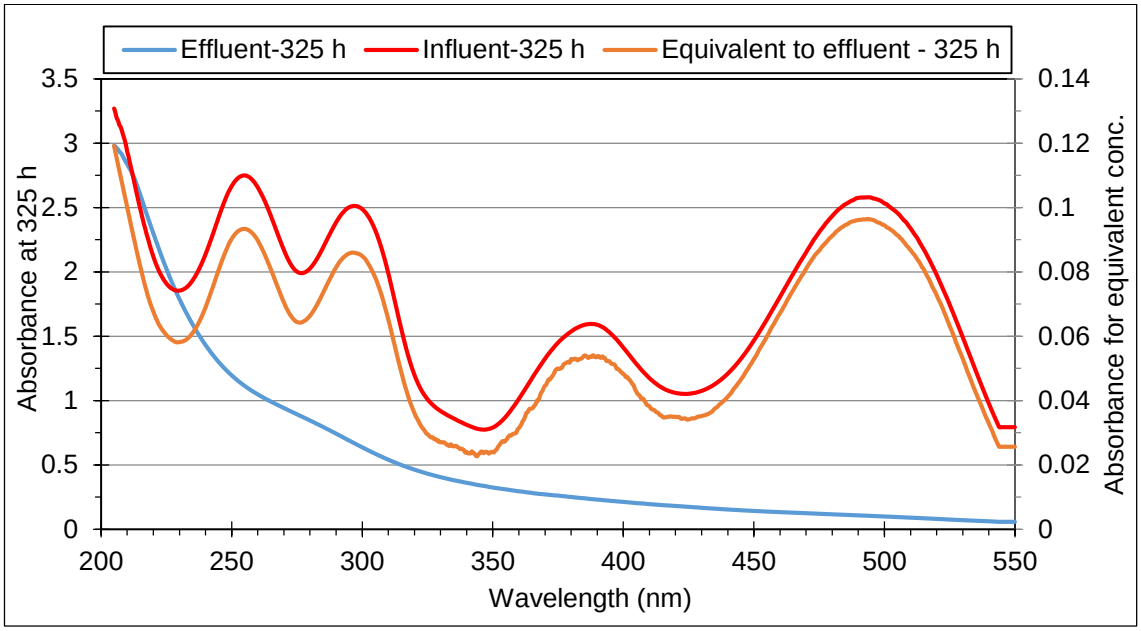

Figure 5-34: Comparison of RO16 spectra for influent, effluent and effluent-equivalent concentrations.

5.6. CONCLUSION

Continuous flow treatment of Reactive Orange 16 dye has been successfully performed at bench scale using a prototype of rotating disc contactor loaded with 208 g of modified PAN catalyst. The effect of residence time and H_2O_2 dose on removal of RO16 has been investigated using 50 mg/L RO16 solution at pH 3. The residence time and H_2O_2 doses were varied in the range of 2.6 hours to four hours and 50 mg/L to 250 mg/L respectively. The efficiencies of 99.2 % and 73 % corresponding to decolourization and loss of aromaticity respectively were achieved when 125 mg/L of H_2O_2 (optimum concentration established in batch) was used with an extended residence time, ~ 2.5 folds longer than that of batch. The removal of COD and TOC were up to 64.4 % and 50 % respectively

when 125 mg/L of H_2O_2 was used. However, no further improvement in COD and TOC was observed above125 mg/L of H_2O_2.

The breakthrough in the performance of the system during the exposure of fresh, first-time, second-time and third-time regenerated catalyst occurred after 50, 24, 17 and 9 days respectively. The deactivation of catalyst occurred mainly due to the loss of active sites (iron) with a minor contribution due to chemical alternation of catalyst legating groups. The iron leaching was enhanced by a drop in pH due to the formation of acidic intermediate products and hydrolysis of iron complexes (see Equation 7-1). A three-phase (log-phase, steady-phase and lag-phase) iron loss was observed when fresh catalyst was used whereas a gradual decline of iron loss with respect to time was observed with regenerated catalyst. The mass balance study shows that, at the time of breakthrough, 92.2 %, 84.6 %, 75.9 % and 58.8 % of iron was leached from the surface of fresh and successively regenerated catalyst.

In-situ regeneration of the deactivated modified PAN catalyst was successfully performed for three times. The impregnated amount of iron and the lifetime of regenerated catalyst decreased after each successive regeneration. The amount of iron reimpregnated onto the deactivated catalyst during the first, second and third regeneration were 46 %, 32.3 % and 16.4 % respectively of the total amount of iron in the regenerating solution. The rate of iron loss was found to be higher with regenerated catalyst. However, the total loss of iron decreased after each exposure suggesting higher influence of poisoning and / or chemical modification of polymeric supports.

Although regenerated catalyst appeared to have higher TOF, the lifetime, total mass of RO16 decomposed by the fresh catalyst were two to six folds better than that of regenerated catalysts. The total mass of RO16 decolourized during the first, second, third and the fourth experimental cycles were 12.76 g, 6.09 g, 4.24 g, and 2.19 g respectively. The lifetimes corresponding to the fresh catalyst, first-time, second-time and third-time regenerated catalyst were 50 days, 24 days, 17 days and 9 days respectively. The total mass of RO16 for loss of aromaticity corresponding to the first, second, third and fourth experimental cycle were 7.76 g, 3.5 g, 2.56 g, and 1.32 g respectively. Similarly, the treated volume of effluent corresponding to these experimental cycles were 283.59 L, 128.75 L, 88 L and 46.33 L respectively. In summary, in 103 days, 546.7 L of dye solution that carried 26.78 g of RO16 was treated and 25.3 g of RO16 was decolourized.

Post-treatment oxidation of intermediate products continues with residual H_2O_2 and leached iron. Therefore, having a post-treatment reservoir with two to four hours residence time would be beneficial to minimize the COD and possibly the iron as well. The COD will be reduced due to oxidation of H_2O_2 and intermediate products whereas iron concentration may reduce due to precipitation.

The possibility of having homogeneous catalysis due to leached iron was investigated using an equivalent amount of iron leached on Day-2 (when the process stabilized) and Day-11 (when iron leaching was maximum) of the continuous flow treatment. Based on the performance observed on Day-2 of continuous flow treatment and homogeneous catalysis with iron equivalent to amount of leached iron as of Day-2, it can be concluded that the continuous flow treatment relied on heterogeneous catalysis. However, looking at the results observed on Day-11 of continuous flow treatment and homogeneous catalysis with iron equivalent to amount of leached iron as of Day-11, the process can be said to be assisted by homogenous catalysis.

CHAPTER SIX

6. REMEDIATION OF MINING INFLUENCED WATERS

6.1. INTRODUCTION

Mine water discharges from coal and metal mines and the problems associated with such waters (discussed in chapter three) emphasized the need of remediation before discharging into the natural water system. A brief discussion on the existing remediation technologies available for the removal of metals such as zinc, cadmium and lead from the mine waters is also given in chapter three. A range of active and passive treatment technologies have been employed in the treatment of mine waters (Younger, Banwart and Hedin, 2002; Pearce, 2014; USEPA, 2014). Sorption (adsorption and ion exchange) based processes are considered as potential alternatives for the removal of metals (Gode and Pehlivan, 2006; Inglezakis and Poulopoulos, 2006; Fu and Wang, 2011). A range of modified polyacrylonitrile (PAN) fibres have been developed to remove metals; zinc (Zhang *et al.*, 1994) cadmium and lead (Zhang *et al.*, 2009; Deng *et al.*, 2016). Ishtchenko, Huddersman and Vitkovskaya, 2003, modified a PAN fibre to produce a heterogeneous catalyst. The modified PAN mesh after modification stage two in section 2.2.3.2, p. 46 and pictured in Figure 3-12 contains both cation and anion exchange groups and hence is a potential sorbent (adsorbent and ion exchanger). Therefore, this chapter focusses on determining the ion exchange capacity of the modified PAN mesh and evaluate its effectiveness in the remediation of mine waters.

The batch and continuous flow experiments were performed to determine the metal uptake capacity of modified mesh. The batch experiments were performed to investigate the influence of pH, initial concentration of metal and contact time on uptake of metal. Zinc sulfate heptahydrate solution was used as a source of metal.

The continuous flow experiment was performed at pilot scale with real mine effluent. The pilot project was commissioned to investigate the effectiveness of ion exchange mesh technology in the treatment of mine waters contaminated with metals. The mine water used in this project was drainage water infiltrating through the White Tip site, part of former Snailbeach lead mine at Minsterley, a village in Shropshire, England. The non-coal mine water was circum-neutral pH and heavily contaminated with “heavy metals” mainly zinc (Zn), cadmium (Cd) and lead (Pb). The concentrations of these metals exceed the Environmental Quality Standards (EQS) levels, for example 75 µg/L for zinc in fresh water with hardness range 100 to 250 mg/L of $CaCO_3$ (Maycock *et al.*, 2010), thereby emphasising the need for treatment. The metals investigated in this pilot trial project were zinc (Zn), cadmium (Cd) and lead (Pb). The pilot trial was conducted at the premises of The Coal Authority’s coalmine water treatment scheme at A Winning,

Fordbridge Lane, Blackwell, Alfreton, Derbyshire, DE55 5JY. This trial was commissioned on 5th November 2014 with the initial operation permit for twelve weeks and extended for a further twelve weeks ending on 17th August 2015. The treatment process was stopped for two weeks (19th December 2014 to 4th January 2015) during Christmas and New Year holidays and 14 weeks (27th March 2015 to 2nd July 2015) due to a change in contractor from Integrated Water Services (IWS) to Severn Trent Water Services (STS). Therefore, the trial was run for a total of 24 weeks and 2 days (170 days).

Figure 6-1: Map locating Snailbeach lead mine at Minsterley, UK. (Source: Google Map)

6.2. AIM AND OBJECTIVES

This study aimed to investigate the effectiveness of ion exchange mesh for the remediation of mine waters contaminated with metals. Afore mentioned aim was achieved through the objectives listed below:

- To determine the ion exchange capacity of ion exchange mesh
- To determine the uptake capacity of ion exchange mesh with respect to the
  - Influence of pH
  - Influence of contact time (residence time)
  - Equilibrium adsorption isotherms
- To determine the influence of regeneration of ion exchange mesh in continuous flow experiment
- To determine the influence of residence time (≈ flow rate) in continuous flow experiment
- To determine the influence of rotation speed of the discs

6.3. MATERIALS AND METHODS

The reagents, materials and methodologies used in this study are given separately in the following sections.

6.3.1. REAGENTS

The reagents used in this part of the thesis are listed in Table 4-1. They were used without further purification. The required solutions and dilutions were made using double distilled water.

6.3.2. MATERIALS

Apart from the conventional glassware (beaker, volumetric flasks, Erlenmeyer flask, graduated and bulb pipette) used in the laboratory; the other materials and instruments used in this part of thesis are listed in Table 4-2.

6.3.3. EXPERIMENTAL SET UP

6.3.3.1. BATCH EXPERIMENTS

The batch experiments were performed with 50 mL solutions with known concentrations of metal (zinc) ions ranging from 50 mg/L to 2,000 mg/L. The initial pH of the solution, when required, adjusted using HCl and NaOH. 50 mL of solutions were transferred into the reaction bottles (plastic) and a known amount of ion exchange mesh was immersed into the solution. The bottles were clamped onto the rotating drum and the effective contact between solution and ion exchange mesh was ensured by thorough mixing using rotator. Samples were withdrawn with respect to time and processed for AAS analysis. The influence of pH, contact time and the initial concentration of metal ions on the uptake of metal ions onto the modified PAN mesh was also studied. The influence of pH was studied in the range of 2.08 to 6.6. The influence of concentration was studied in the the range of 0 to 2,000 mg/L. The influence of time was studied within five hours.

6.3.3.2. PILOT SCALE FIELD TRIAL

The rotating discs reactor (RDR) consists of a 60 L tank comprising thirty discs housing 11 kg of ion–exchange mesh and a lid with see-through polypropylene windows on two sides and on top. The reactor had four distinct sections separated by baffles containing a small hole at the bottom of each baffle for ease of draining. The flow windows were designed on top of opposite sides of each baffle to prevent a direct inlet-outlet laminar

flow. The first and second sections from the inlet side of the reactor contained seven discs each whereas the third and fourth sections contained eight discs each. These discs were fixed onto a shaft which was connected to a motor via a timing belt. The motor drives the shaft and rotates the disc covered with ion exchange mesh. The motor was equipped with an inverter which enables the rotation speed to be varied. The power input of the motor was 90 W. The reactor also consist of a tap at the bottom on the inlet side for ease of draining. The outlet of the reactor was positioned 1 cm lower than the inlet to prevent back flow from the reactor to the feed tank. Mistakenly, for the first five weeks, the treatment process was run with the feed connected to the outlet side of the reactor. The connection was reversed to the true inlet and outlet on Day-36 and the discs were reoriented during New Year holiday when the process was halted. This reorientation did not have any impact on performance and results.

The reactor was bolted onto a table sitting inside a drip tray of 250 L holding capacity. A dosing pump was stationed nearby in a separate bund. The dosing pump was connected to a 5 m^3 influent storage tank and to the inlet side of the reactor. The outlet of the reactor was connected to a collection pump station comprising a tank (300 L capacity) and a submersible pump with a float switch. There were two taps each for inlet and outlet sample collection. The inlet sampling tap was located between reactor inlet and the dosing pump whereas the outlet sampling tap was located between reactor outlet and the collection pump station. Data loggers comprising pH and temperature probes were positioned inside the reactor at both inlet and outlet ends and reading were taken every two minutes. pH of influent and effluent samples were also monitored on daily basis in the laboratory.

Mine water with a circum-neutral pH containing a mixture of metal cations (mainly Zn ~ 50 mg/L, Cd ~ 0.14 mg/L and Pb ~ 0.06 mg/L) was pumped by the dosing pump from the 5 m^3 influent storage tank into the reactor where the rotating discs ensured effective mixing and contact with the novel ion exchange mesh. The desired typical residence time was approximately two hours. The residence time was determined using reactor dimensions and the flow rates. The flow rate was determined by measuring the volume exiting the reactor in unit time. The average flow rate into the reactor during this trial is calculated as 32.22 L/hr (0.54 L/min). However, the flow rate was varied to study the effect of residence time on removal of metals. The treated effluent was fed by gravity from the reactor outlet into the outlet pump station which was pumped into the 5 m^3 effluent storage tank for disposal.

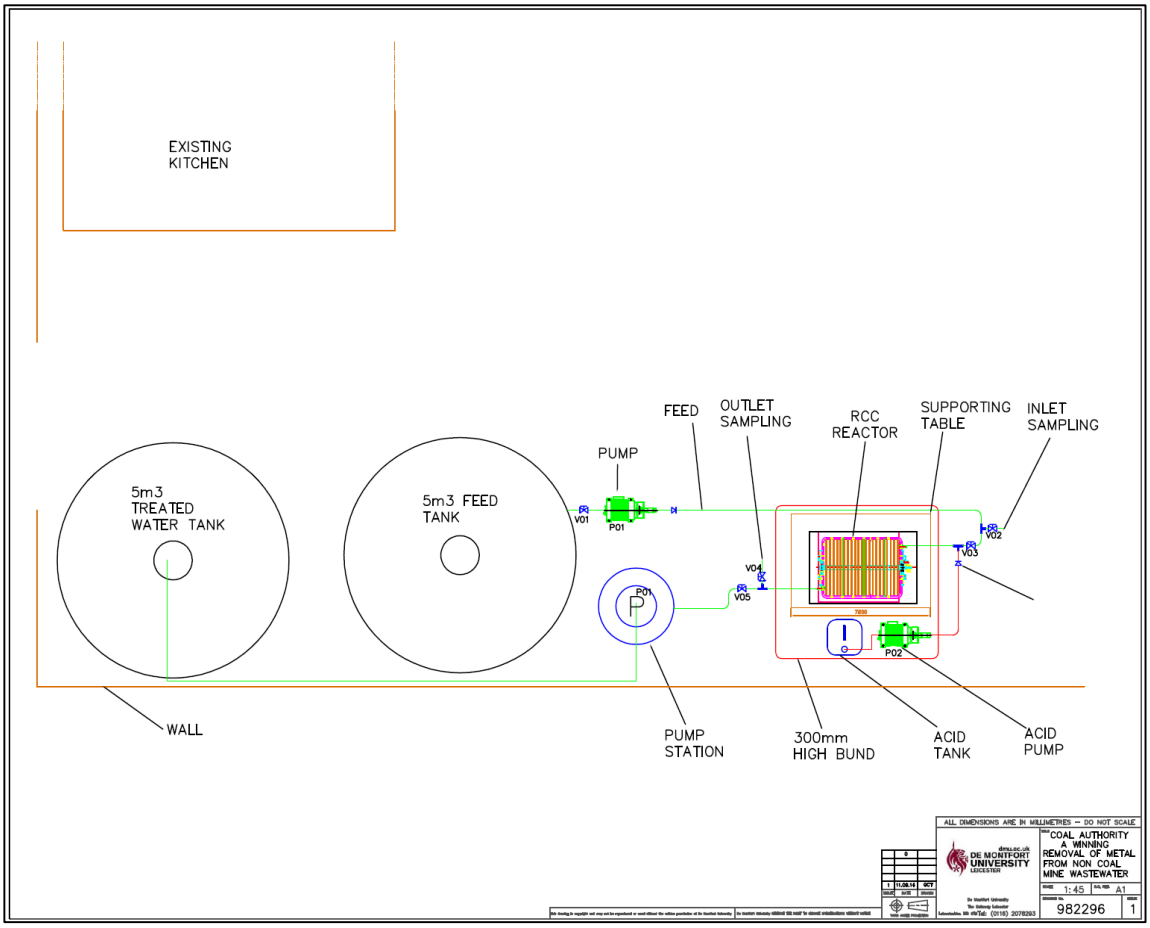

Figure 6-2: Engineering layout of the treatment plant at A Winning, Derbyshire, UK.

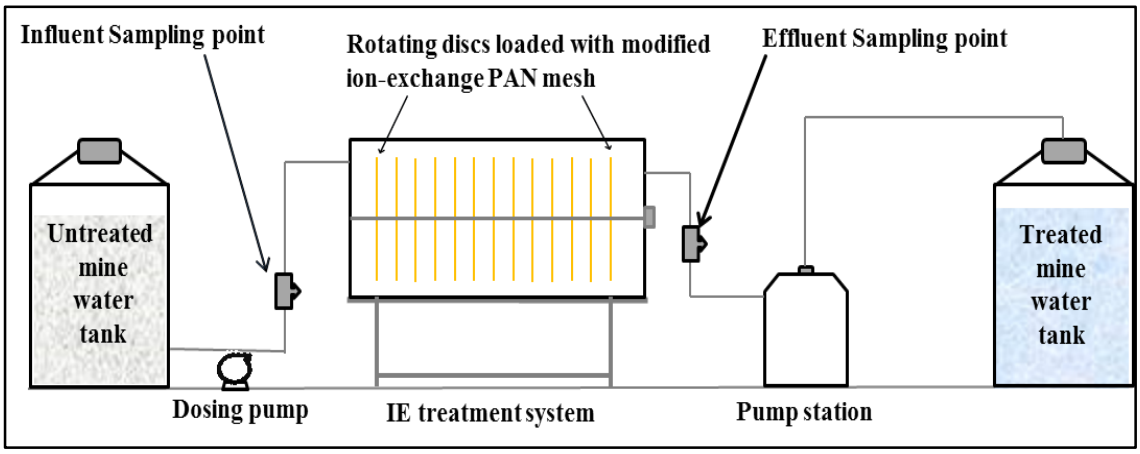

Figure 6-3: Schematic diagram of treatment plant on site at A Winning, Derbyshire, UK.

Integrated Water Services (IWS) tankered non-coal mine water from Minsterley to the trial site until Day-125 after which they were replaced by Severn Trent Water Services (STS). The treated mine water in the outlet storage tank was discharged into the settlement lagoons of the operational mine water treatment scheme for additional treatment by dilution, precipitation and polishing in constructed wetlands prior to final

discharge into nearby watercourse. The general engineering layout and schematic diagram of the treatment plant on site at A Winning, Derbyshire, UK are given in Figure 6-2 and Figure 6-3 respectively.

6.3.4. SAMPLING, SAMPLE HANDLING AND ANALYSES

6.3.4.1. BATCH EXPERIMENT

Samples were withdrawn with respect to time and diluted with double distilled water. The required dilution factor was determined by dividing the initial concentration with the highest value on the calibration. The diluted samples were analyzed using AAnalystTM 200 Flame Atomic Absorption Spectrophotometer (F-AAS), Perkin Elmer Instruments, LLC. The concentrations obtained were multiplied by dilution factor to obtain the actual residual concentrations.

6.3.4.2. PILOT TRIAL

Inlet and outlet samples were collected directly from sampling points into sample bottles (plastic, 1 L) five days per week for analysis at DMU. Samples were stored in the fridge on site and transported to DMU in a cool box. The procedures for sample preparation, measurement of pH and analyses of zinc, cadmium and lead are given in sections 6.3.4.4 to 6.3.4.6. Jenway pH meter 305 and F-AAS, were used to analyze the water samples. Samples were allowed to settle and the supernatants of the samples were taken for the analyses. Double distilled water was used in all analyses when dilution was required. To determine the metal content on ion exchange mesh, samples of ion exchange mesh were taken from the reactor discs (first and last) for acid digestion as described in section 5.3.3.6.2, p.148. An analytical balance was used to weigh the mesh samples used in acid digestion.

Weekly inlet and outlet samples were collected for analysis by the United Kingdom Accreditation Service (UKAS) accredited external commercial laboratory, Environmental Scientific Group (ESG).

6.3.4.3. PH

The pH of the collected samples was measured as described in section 4.3.3.1, p. 86. The influent and effluent pH during field trial were also measured using MadgeTech online data loggers.

6.3.4.4. ZINC (ZN)

Before each analysis, the AAS was calibrated using calibration standards prepared from an AAS standard solution of concentration 1,000 mg/L of Zn in nitric acid supplied by Fisher Scientific. It is noteworthy to mention that in every calibration the coefficient of determination (R^2) was greater than 0.99.

Since the concentration of zinc in the mine water samples was well above the linear range of calibration (1 mg/L-10 mg/L until Day-125 and 0.031 mg/L – 2 mg/L afterward), all the inlet and outlet samples were diluted accordingly. The samples were aspirated in to the AAS to determine the zinc concentration. The absorbance for zinc was recorded at the wavelength of 213.86 nm. The obtained instrumental value was then multiplied by the dilution factor to obtain the actual zinc concentration in the samples. This analysis at DMU is equivalent to the dissolved zinc (Zn-D) concentration reported by ESG.

6.3.4.5. CADMIUM (CD)

Before each analysis, AAS was calibrated using calibration standards which were prepared by serial dilution of an AAS standard solution of concentration of 1,000 mg/L of Cd in nitric acid supplied by Fisher Scientific.

As the concentration of cadmium in the water samples was within the linear range of calibration (0.0781 mg/L - 5 mg/L until day125 and 0.019 mg/L – 1.25 mg/L afterward), all the samples were analyzed without further treatment. The samples were allowed to settle and the supernatant of each water sample was taken and aspirated in to the AAS. The absorbance for cadmium was recorded at the wavelength of 228.8 nm. This analysis is equivalent to the dissolved cadmium (Cd-D) concentration reported by ESG.

6.3.4.6. LEAD (PB)

Before the start of each analysis, AAS was calibrated using calibration standards which were prepared through a serial dilution of an AAS standard solution of concentration of 1,000 mg/L of Pb in nitric acid which was supplied by Fisher Scientific.

In the first 125 days of the trial, the concentration of lead in the water samples was below the calibration range (0.078 mg/L- 5 mg/L until Day-125 and 0.062 mg/L – 2 mg/L afterward).Thus, all the samples were concentrated by 10 folds. This was done from the start of the trial until Day-125 (27th March 2015). Concentration was effected by evaporating 250 mL of supernatant of each sample to 25 mL. Initially, about 5 mL of 2.5

% hydrochloric acid (HCl) was added to each 250 mL water sample, to prevent deposition of metal salts onto the walls of the beaker. The samples were then evaporated to 10 - 15 mL. The beaker was rinsed with 2.5 % HCl to make a final volume of 25 mL. The concentrated water samples were aspirated in to the AAS and the corresponding absorbance recorded at a wavelength of 283.31 nm. The occurrence of lead in mine water was mostly in lead-total form (see section 6.4.4.2.1.4), as much of the lead was in an insoluble form. Therefore, the analysis (dissolution of supernatant of settled samples with acid) used in this study gives a lead concentration in between that of lead-dissolved and lead-total reported by ESG.

6.3.5. DETERMINATION OF ION EXCHANGE CAPACITY OF ION EXCHANGE MESH

The ion exchange capacity of modified PAN ion exchange mesh was carried out by means of titrimetric technique that involves acid-base titration. Acid-base titration was used by various authors to determine the ion exchange capacity of ion exchangers such as modified PAN fibre (Orlova, 2010, pp. 65–68), a range of DOWEX resins (Soldatov, Sosinovich and Mironova, 2004), PAN fibre Nitron D (Shunkevich *et al.*, 2005), KB-4 (carboxylic acid resin containing methylmethacrylate with 5 % divinylbenzene) (Soldatov *et al.*, 2004) and Kanecaron modacryl fibre (Nesteronok and Soldatov, 2011). The acid-base titration used in this study was adopted from (Orlova, 2010, pp. 65–68).

6.3.5.1. TOTAL ION EXCHANGE CAPACITY (TIEC)

The ion exchange fibres were pulled out of ion exchange mesh. Approximately 0.5 g of ion exchange fibre was submerged in 50 mL of NaOH (0.1 M) for 24 hours, converting the fibre in Na/OH form. The excess NaOH was washed-off with 3.5 mmol/L (mM) NaOH until the pH of the washed solution attained the initial pH of the 3.5 mM NaOH solution (i.e. pH 11.44). The washed fibre was air-dried, weighed and submerged in 50 mL of HCl (0.1 M = 0.1 N) for 30 minutes. The fibres were filtered from the solution and 10 mL aliquot of filtrate was taken and titrated against NaOH (0.1 M = 0.1 N). Methyl orange was used as an indicator to determine endpoint. Above procedure was repeated for three samples and an average value of NaOH consumed was used to determine the TIEC as shown in Equation 6-1.

$$TIEC\ (mmol/g) = \frac{(V_I/V_A) \times C \times (V_A \times f_{HCl} - V_T \times f_{NaOH})}{m} \qquad \textit{Equation 6-1}$$

Where, C = normality (0.1 M) of the acid; V_I = Initial volume of acid (50 mL) used to treat air-dried fibre; V_A = volume of aliquot (10 mL) taken in titration; V_T = volume of titre,

0.1M NaOH (mL); f_{HCl} = factor of the acid; f_{NaOH} = factor for alkali; $m =$ mass (g) of fibre used.

The f_{HCl} and f_{NaOH} are coefficients that account for the normality of the titrant (HCl or NaOH), if differ from 0.1 N. The reaction of titration is given in Equation 6-2.

$$NaOH + HCl = NaCl + H_2O$$ ***Equation 6-2***

Where NaOH and HCl react in equimolar (1:1) ratio. Thus, the actual normality of the titrant can be determined by the relationship between their normality and volume as given in Equation 6-3. The HCl used in the titration was a standardized 0.1 N. Therefore, its factor is considered as unity. The actual normality of NaOH can be determined as in Equation 6-4, where the volume of HCl consumed (V_{HCl}) can be determined by the blank titration of 10 mL of NaOH against standardized 0.1 N HCl.

$$N_{HCl} \times V_{HCl} = N_{NaOH} \times V_{NaOH}$$ ***Equation 6-3***

$$N_{NaOH} = \frac{V_{HCl}}{V_{NaOH}} \times N_{HCl}$$ ***Equation 6-4***

In this case, the f_{NaOH} could be presented and determined according to Equation 6-5.

$$f_{NaOH} \times N_{NaOH} = 0.1$$ ***Equation 6-5***

6.3.5.2. CATION EXCHANGE CAPACITY (CEC)

The ion exchange fibre (0.5 g) was submerged in 50 mL of HCl (0.1 M) for 24 hours. The treatment of fibre by HCl converts the fibre in H/Cl form. The excess acid was washed-off with hot double distilled water. The required extent of washing was examined by adding few (2 – 3) drops of $AgNO_3$ in 10 mL of washed solution. The washing was continued until no precipitate of AgCl was observed. The washing converts the $–NH_3Cl$ to $-NH_3OH$.

The air-dried sample was immersed into 50 mL of NaOH (0.1 M) for one hour, converting –COOH groups to –COONa. The residual fibre was filtered and 10 mL aliquot of filtrate was titrated against HCl (0.1 M). Methyl orange was used as an indicator to determine the endpoint of the titration. Above procedure was repeated for three samples and an average value of HCl consumed during titration was used to determine the CEC as given in Equation 6-6.

$$CEC\ (mmol/g) = \frac{V_I/V_A \times C \times (V_A \times f_{NaOH} - V_T \times f_{HCl})}{m}$$ ***Equation 6-6***

Where, $V_I =$ Initial volume of alkali (50 mL) used to treat air-dried fibre, $C =$ normality of alkali (0.097N) (see Appendix 9.5, p.); and other symbols carry same definition as in Equation 6-1. The normality and factor of NaOH are calculated as in Equation 6-4 and Equation 6-5.

6.3.5.3. ANION EXCHANGE CAPACITY (AEC)

The fibre (0.5 g) was prepared as in CEC by treating with HCl (0.1 M) followed by hot double distilled water washing. The air-dried sample was immersed into 50 mL of HCl (0.1 M) for one hour, converting $–NH_3OH$ groups to $–NH_3Cl$. The residual fibre was filtered and 10 mL aliquot of filtrate was titrated against NaOH (0.1 M). The endpoint of the titration was determined with methyl orange as an indicator. Above procedure was repeated for three samples and an average value of NaOH consumed during titration was used to determine the AEC as given in Equation 6-7.

$$AEC\ (mmol/g) = \frac{V_I/V_A \times C \times (V_A \times f_{HCl} - V_T \times f_{NaOH})}{m} \qquad \textit{Equation 6-7}$$

Where the symbols carry same definition as in Equation 6-1. The normality and factor of NaOH (f_{NaOH}) are calculated as in Equation 6-4 and Equation 6-5.

6.3.6. SORPTION OF METALS

The batch experiments were set up as described in section 6.3.3.1. Metal concentrations were determined using AAS. The sorption capacity per unit mass of ion exchange mesh was calculated through Equation 6-8. The percentage sorption capacity of ion exchange mesh was calculated according to Equation 6-9.

$$q_t(mg/g) = \frac{(C_0 - C_t)V}{m} \qquad \textit{Equation 6-8}$$

$$q_t(\%) = \frac{(C_0 - C_t)}{C_0} * 100 \qquad \textit{Equation 6-9}$$

Where, q_t is the mass (mg/g) of metal adsorbed at time t; C_0 and C_t are the concentrations (mg/L) at time zero (initial concentration) and time (t) respectively; V is the volume (L) of metal contaminated solution ; and m is the mass (g) of the ion exchange mesh used. The adsorption capacity q_e (mg/g) at the time of equilibrium can be calculated using concentration of metal at the time of equilibrium (C_e).

6.3.7. REGENERATION OF THE SYSTEM (PILOT UNIT)

The regeneration process was successfully carried out as described below. The main access to the building (roller shutter door) was kept open during the regeneration process to ensure effective ventilation. All health and safety procedures were observed and related personal protective equipment (PPE), especially acid resistant gloves, apron, face shield and safety specs were used. Acid and alkali for dilution was dispensed using the siphon pump. The operational parameters of the reactor were not altered. Summarily, the regeneration process was carried out as below.

The unit was switched off, data loggers removed and immersed in water, and acid pump and pipe work connected to the unit.

A 50 L solution of 5 % HCl (~ 1.55 M HCl) was prepared from the 37 % stock solution and pumped into the reactor unit. It was left to react for approximately 30 minutes with the discs rotating.

1) A brown slightly muddy solution was formed and some foaming observed – attributed to the wash-off of suspended solids trapped on the mesh and digestion of humic substances and decomposition of carbonates respectively.

2) A sample of the liquor was collected and the reactor drained directly by gravity into the collection pump station. Step 2 above was repeated twice. The second acid solution after regeneration was cleaner and the third was clean. Samples of the regenerated solutions were collected for each step for further analysis. A picture showing each batch of solution can be seen in Appendix 9-8.

3) The reactor was rinsed with 60 L of tap water for 15 minutes. Liquid samples were collected and the reactor was drained. The pH sensors and data loggers were reinstalled.

4) 60 L of NaOH (0.16 M) solution was prepared from the 40 % w/v stock and pumped into the reactor. It took approximately two hours for the pH of the system to stabilise at a pH of about 3. The concentration of the NaOH solution was topped up at intervals, making sure that the solution pH never exceeded 12.5. Water samples were collected and the reactor drained.

5) Step 6 was repeated and the final pH of the system was 8.5.

6) Samples of the ion exchange mesh at both inlet and outlet ends of reactor were collected for characterisation.

7) The acid / alkali pumping line was disconnected; the mine water pumping line reconnected and the treatment process was restarted.

About 235 moles of hydrochloric acid and only about 19 moles of alkali (NaOH) were used in the regeneration. To neutralise the regenerated solution in the holding tank ~ 18.6 L of 40 % (w/v) NaOH was added. The neutralised regenerated solution containing the dissolved metal cations e.g. Zn, Cd, Pb was then passed to the outlet storage tank where it was diluted with treated mine water to give a total volume of ~ 3,000 L.

6.4. RESULTS AND DISCUSSIONS

6.4.1. ION EXCHANGE CAPACITY OF ION EXCHANGE MESH

The ion exchange groups available in ion exchange mesh are discussed in section 3.3.2.8.3.1, p.78. The ion exchange capacity of mesh was determined according to the procedures laid out under section 6.3.5. The results are presented in Table 6-1.

The total ion exchange capacity (TIEC) of modified PAN fibre is calculated as 3.49 mmol/g with cation and anion exchange capacities as 1.99 mmol/g and 1.46 mmol/g respectively. The values presented are related to PAN threads which account ~ 50 % of the mesh. Thus, the ion exchange capacity of the ion exchange mesh would be half of the values determined. The results suggest that the ion exchange mesh contains ~ 60 % cation exchangers and ~ 40 % anion exchangers. On the modification of modacrylic PAN-vinylchloride fibre, Nesteronok and Soldatov, 2011 reported that the fibre preserves its integrity, by mechanical properties, up to the exchange capacity of 3.5 meq/g. Thus, the exchange capacity of 3.49 mmol/g of PAN fibre which is equivalent to 1.745 mmol/g of PAN mesh supports the excellent mechanical properties as reported by Ishtchenko, Vitkovskaya and Huddersman, 2003.The value of TIEC determined in this study is equivalent to that of Orlova, 2010, however, the values for CEC and AEC differ. The author reported ~ 80 % cation exchangers and ~ 20 % anion exchangers.

Since the reacting species hydrogen, sodium, hydroxyl ion and chlorine have same valency (1) and the reaction between them is an equimolar, the ion exchange capacity expressed as mmol/g is also equal to milliequivalent per unit mass (meq/g) of ion exchange mesh.

Table 6-2 shows a comparison of ion exchange capacity of the PAN mesh used in this study with the ion exchange capacities of commercial and non-commercial ion exchangers reported in the literature. The ion exchange mesh used in this study can be considered amongst the good ion exchangers.

Table 6-1: Ion exchange capacities of modified PAN fibre.

S. N.	Mass of fibre (g)		Initial volume (V_I) (mL)	Volume of aliquot (V_A) (mL)	Volume of titre, (V_T) (mL)				Normality of HCl (N)	Normality of NaOH (N)	f_{HCl}	f_{NaOH}	Ion exchange capacity (mmol/g) (≈ meq/g)	Average Ion exchange capacity (mmol/g) (≈ meq/g)
	Initial	Air dried			Rep 1	Rep 2	Rep 3	Average						
1	0.5343	0.5037	50	10	6.2	6.2	6.3	6.23	0.1	0.097	1	1.031	3.55	TIEC = 3.49
2	0.5283	0.5026	50	10	6.4	6.2	6.4	6.33	0.1	0.097	1	1.031	3.45	
3	0.524	0.501	50	10	6.3	6.3	6.4	6.33	0.1	0.097	1	1.031	3.46	
4	0.5308	0.494	50	10	8.25	8.35	8.35	8.32	0.1	0.097	1	1.031	1.96	CEC = 1.99
5	0.5218	0.4878	50	10	8.3	8.35	8.3	8.32	0.1	0.097	1	1.031	1.98	
6	0.5238	0.4888	50	10	8.25	8.25	8.3	8.27	0.1	0.097	1	1.031	2.03	
7	0.5122	0.4977	50	10	8.2	8.2	8.3	8.23	0.1	0.097	1	1.031	1.52	AEC =1.46
8	0.5111	0.4906	50	10	8.3	8.3	8.3	8.30	0.1	0.097	1	1.031	1.47	
9	0.5116	0.4931	50	10	8.3	8.5	8.3	8.37	0.1	0.097	1	1.031	1.39	

Table 6-2: Comparison of ion exchange capacity of ion exchange PAN mesh with other ion exchangers.

Name of Ion exchanger	Functional groups	Ion exchange capacity	References
Ion exchange PAN fibre	-COOH, NH_2, Oxime	TIEC = 3.49 mmol/g CEC = 1.99 mmol/g AEC = 1.46 mmol/g	Current study
PAN electrospun fibre	-COOH	CEC = 2.3 meq/g	(Jassal *et al.*, 2014)
PAN fibre Nitron-D	-COOH	3.5 meq/g	(Shunkevich *et al.*, 2005)
FIBAN K-3	-COOH	5 meq/g	(Kosandrovich and Soldatov, 2012, pp. 333–334)
FIBAN K-5	-COOH	5 meq/g	
VION KN-1	-COOH	5 – 7 meq/g	
Species of zeolites		2.29 – 3.87 meq/g	(Inglezakis and Poulopoulos, 2006, p. 253)
Chelex-100	Iminodiacetic acid	0.4 mmol/mL ≈ 0.4 mmol/g	(Gode and Pehlivan, 2006, p. 331)
Lewatit S 100	Sulfonic acid	2.0 eq/L ≈ 2 meq/g	
TWTT SBWA-8 (amphoteric ion exchange resin)	Trimethylamine ($-N(CH_3)_3$), -COOH	TIEC = 3.3 meq/mL CEC = 1.2 meq/mL AEC = 1.1 meq/mL	(TWTT, 2018)

6.4.2. SORPTION OF METAL IONS ONTO MODIFIED PAN ION EXCHANGE MESH

Sorption of metal ions onto ion exchange material is influenced by process parameters such as pH, initial concentration of metal ions, contact time (≈ residence time) and temperature (Fu and Wang, 2011). This study investigated the influence of above variables except temperature. Sorption of metal by ion exchange mesh was studied with solution spiked with zinc from zinc sulfate heptahydrate. The adsorption capacity was calculated according to the Equation 6-8 and Equation 6-9. The influence of each variables on sorption of zinc ions onto the ion exchange PAN mesh is discussed below.

6.4.2.1. INFLUENCE OF PH ON SORPTION OF ZINC

The influence of solution pH on the sorption of zinc ions was investigated by varying the initial pH of the solutions. Selection of pH range depends on the initial concentration of zinc as pH, concentration of zinc and precipitation are interrelated. The pH of the solution decreases with increase in concentration of zinc, for example pH 7.1 (50 mg/L) and 6.1 (1,500 mg/L). The precipitation of zinc is favoured at higher pH. Zinc solution (1,000 mg/L) remained clear at pH 6.5 and became cloudy at pH 6.7 and above. Thus, the highest pH was chosen to be 6.6. Known amounts (0.8 ± 0.05 g) of non-normalized ion exchange PAN mesh was exposed in 50 mL of zinc solution (C_0 = 1,00 mg/L) for five hours and the results are presented in Figure 6-4-A.

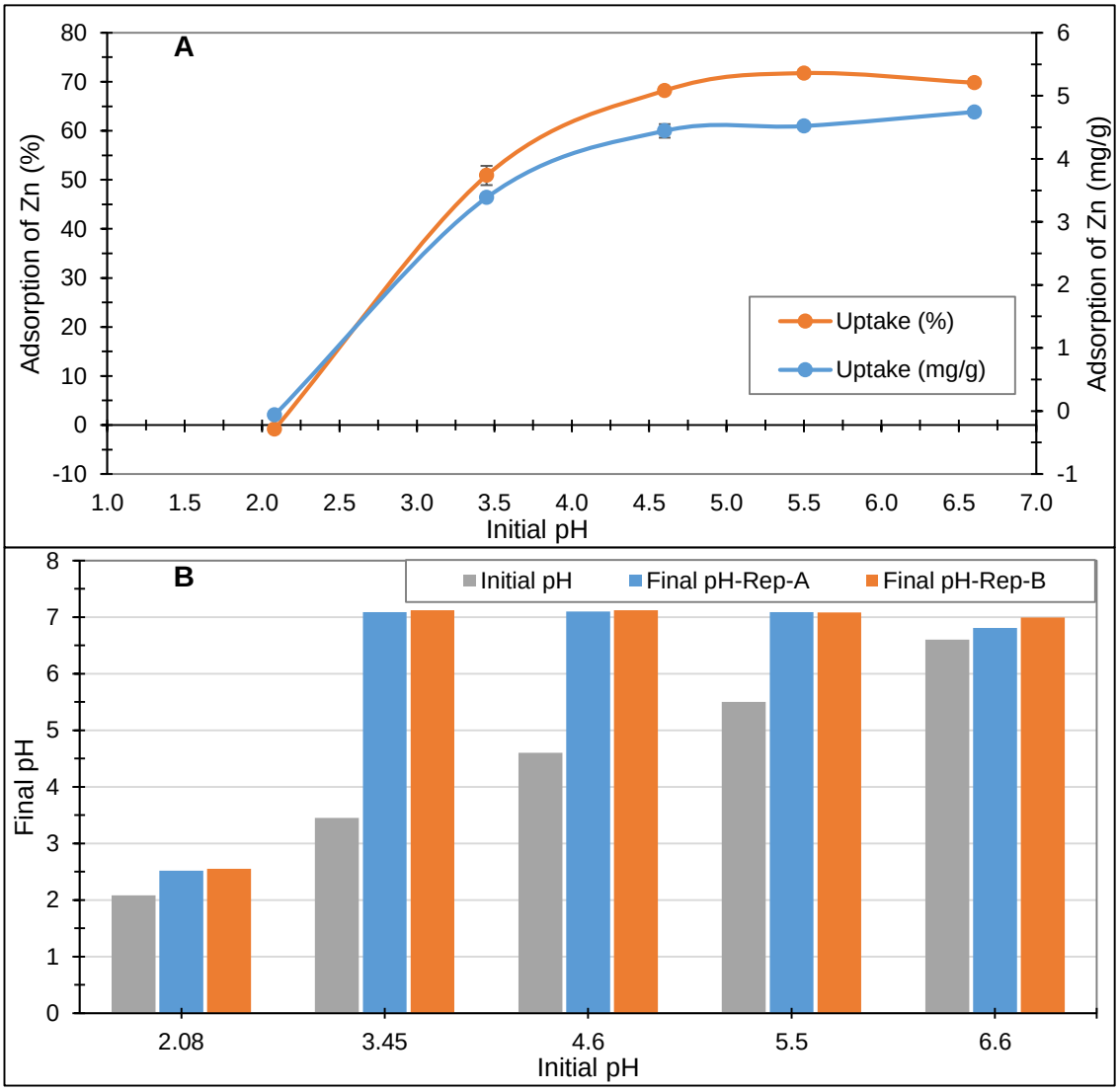

Figure 6-4: A) Influence of pH on adsorption of zinc B) pH variation during adsorption process.

[Experimental conditions: 0.8 ± 0.05 g of ion exchange PAN mesh in 50 mL of zinc solution (C_0 = 100 mg/L), contact time of five hours at room temperature (25 °C)].

It can be seen that the adsorption capacity of ion exchange PAN mesh increased with increase in initial pH of the solution. Accordingly, 0 %, 50 %, 68.8 %, 71 % and 70 % of removal of zinc was observed at initial pH of 2.08, 3.45, 4.6, 5.5 and 6.6 respectively. These efficiencies correspond to adsorption capacity of ion exchange mesh as 0 mg/g, 3.38 mg/g, 4.44 mg/g, 4.52 mg/g, and 4.74 mg/g respectively. The results are also supported by the similar trend of coefficient of distribution (K_d) with respect to the pH, shown in Figure 6-5. Coefficient of distribution is a measure of the effectiveness of an ion exchanger to remove metal ions from a given aqueous solution. It is defined as a ratio between concentrations of metal ions in solid and liquid phases. K_d is generally determined from batch experiments and higher values are always desirable (Alyüz and Veli, 2009; Kiani, Sheikhloie and Arsalani, 2011; Inamuddin. and Luqman, 2012, p. 17). At a given pH, K_d reflects the affinity of an ion exchange sorbent for metal ions (Liu, Zhang and Tang, 1999). The above results confirm that the best adsorption of zinc occurs at pH ≥ 5.5. The results of this study agree with other study (Jain and Ram, 1997; Mishra and Patel, 2009).

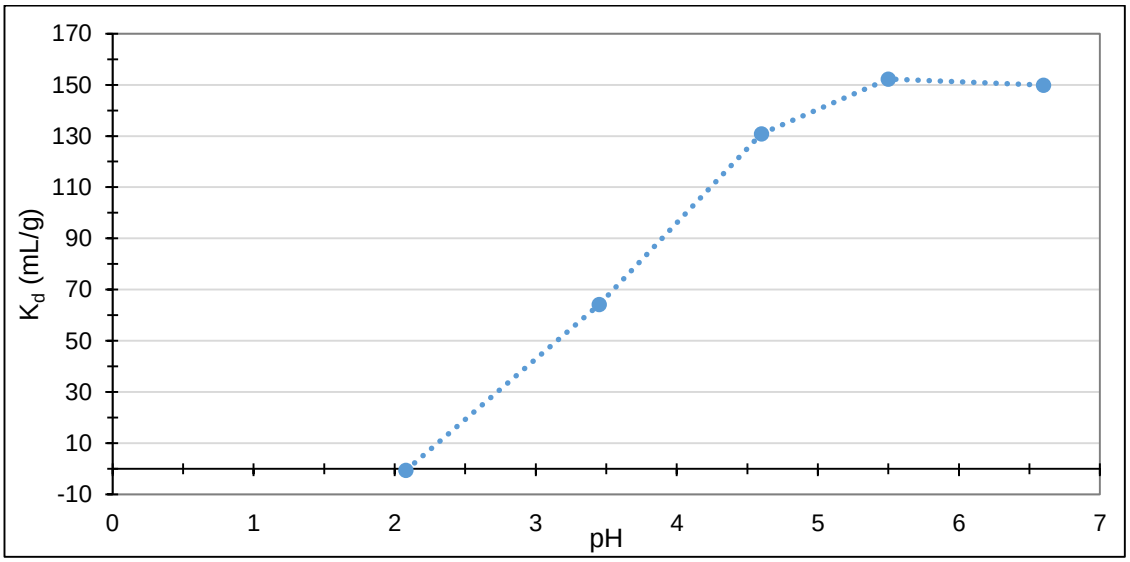

Figure 6-5: Distribution coefficients with respect to initial pH of solution.

Figure 6-4-B shows the pH variation during adsorption process. After five hours, the solution with initial pH of 2.08 stabilized to pH 2.5 whereas the solutions with initial pH of 3.45, 4.6, 5.5 and 6.6 attained to neutral pH. A rise in pH was expected as the ion exchange mesh was produced through an alkaline (NaOH) treatment and hence leaching of OH^- ions was expected. The large rise in pH corresponding to initial pH 3.45 compared to initial pH of 2.08 can be explained with the help of pH curve. In the

experimental pH range (above pH 3), a rapid rise in pH is expected even with the addition of small quantity of alkali such as NaOH.

After the experiment, the solution phase and the ion exchange PAN mesh were inspected carefully. The solution was clear and no precipitate was observed on the surface of exposed mesh. The exposed mesh was found to be shrunk and more brittle compared to unexposed mesh, suggesting some degree of crosslinking between fibre (ligands) and metal. The graph relating theoretical solubility of zinc hydroxide and pH presented by Ayres, Davis and Gietka, 1994, p.13,(Ayres, Davis and Gietka, 1994, p. 13) (see Appendix 9-7**)** suggests that an aqueous solution of a zinc salt at 100 mg/L at pH 7 would have almost all zinc in dissolved form. Thus, it is evident that the removal of zinc was by means of adsorption and not by precipitation.

The lower adsorption capacity at acidic pH conditions is influenced by mechanisms related to surface charge (ionization) of mesh and competition between ions (Kubilay *et al.*, 2007). The surface charge of mesh as a function of pH is discussed in section 4.5.3.1.4, p.106. In summary, the charge of mesh in acidic (below pzc) and alkaline (above pzc) pH values result in a net positive and net negative charge respectively. Accordingly, the surface of mesh become more repulsive and attractive to metal cations at acidic and alkaline conditions respectively. Also, at low pH, the metal ions also compete with H^+ ions for the available sites, reducing the coefficient of distribution (K_d) (Aksu, 2001; Gode and Pehlivan, 2006; Kubilay *et al.*, 2007; Kampalanonwat and Supaphol, 2014). The functional groups such as oxime groups on the mesh may take part in adsorption of metal through the complexation process which is also a pH dependent process (Mustafa and Ünlü, 2006).

6.4.2.2. INFLUENCE OF CONTACT TIME ON SORPTION

The influence of contact time on the sorption of zinc ion was investigated and the results are presented in Figure 6-6**.** It is clearly seen that the adsorption of zinc (C_0 =100 mg/L) increased with respect to the increase in contact time and attained equilibrium state after four hours. Further increase in contact time had insignificant influence on sorption. The sorption process was faster at the beginning due to high abundance of sites. The adsorption capacity (q_t) of ion exchange PAN mesh at equilibrium found to be 4.08 mg/g, which corresponds to 60.1 % of the initial zinc loading.

The pH of the solution was monitored with respect to the contact time and the results are presented in Figure 6-6-B. The initial pH (6.76) increased by 0.5 unit pH in first 30

minutes and plateaued afterwards. The rise in pH is due to the release of OH^- ions from the mesh. The adsorption was high in the first half hours due to the availability of a large number of unoccupied sites on the surface of mesh and the high solute concentration gradient was high. The number of sites reduces with the increase in contact time and adsorption become difficult due to repulsive forces between metal ions in solid and liquid phases (Alyüz and Veli, 2009; Mishra and Patel, 2009; Kampalanonwat and Supaphol, 2014).

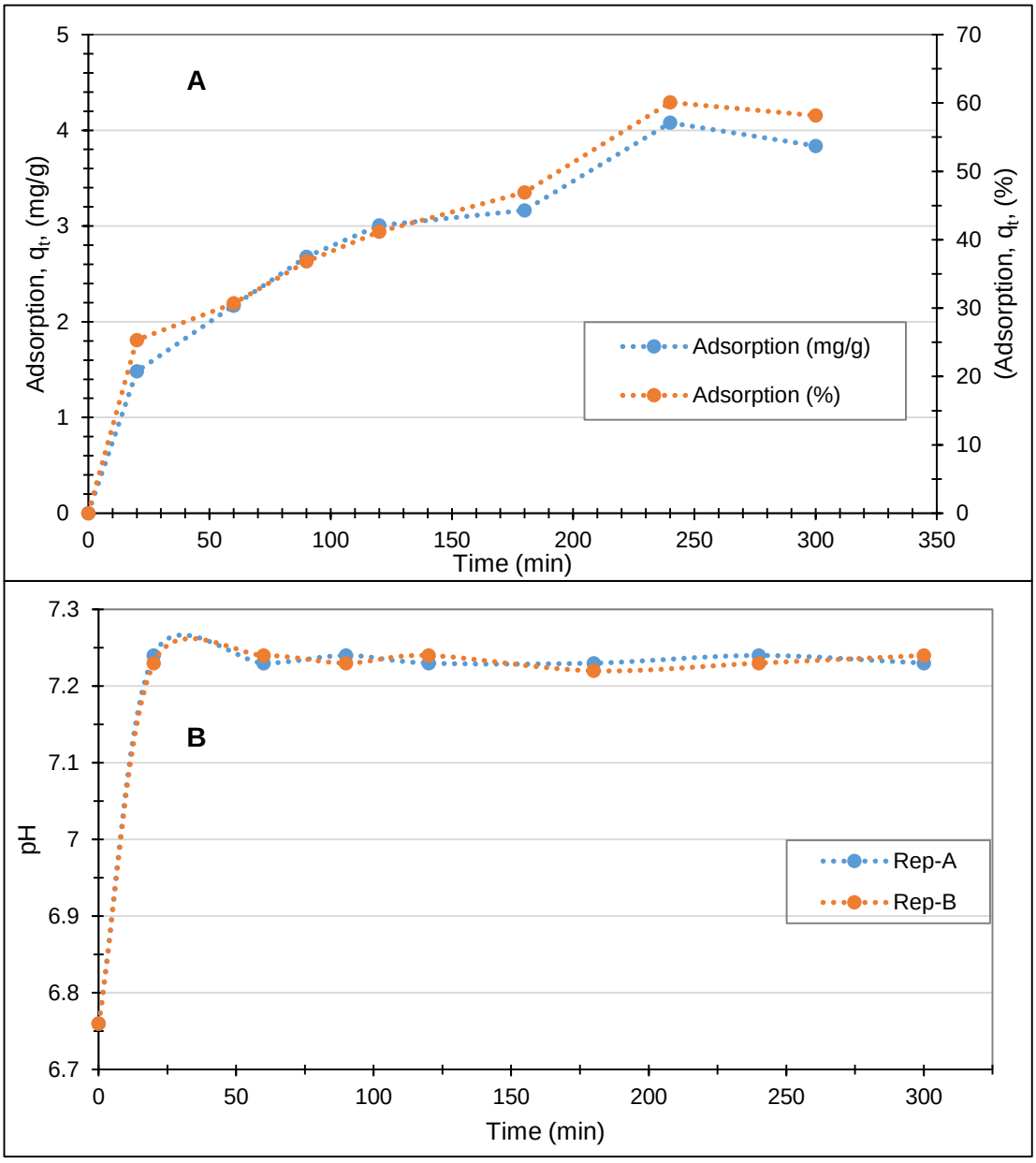

Figure 6-6: A) Adsorption of zinc as a function of time B) pH variation with respect to time during adsorption process.

[Experimental conditions: 0.75 ± 0.05 g of ion exchange mesh in 50 mL of zinc solution (C_0 = 100 mg/L), initial pH 6.76 and at room temperature (25 °C)].

6.4.2.3. INFLUENCE OF INITIAL CONCENTRATION OF METAL IONS

The influence of initial concentration of metal ions on adsorption was investigated by varying the concentration of zinc in the range of 50 mg/L to 2,000 mg/L. Figure 6-7 shows that the adsorption capacity per unit mass of ion exchange mesh increased gradually until an initial concentration of 1,500 mg/L. Further increase in concentration to 2,000 mg/L resulted in slight decline in adsorption capacity per unit mass of mesh. The maximum adsorption capacity of mesh was determined to be 12.3 mg/g mesh. However, the percentage adsorption capacity of mesh decreased with respect to increase in initial concentrations. Accordingly, the maximum (97.5 %) and minimum (10.7 %) adsorption capacities correspond to the initial concentrations of 50 mg/L and 2,000 mg/L zinc respectively. The adsorption capacity per unit mass of mesh corresponding to these concentrations were 2.94 mg/g and 11.5 mg/g respectively.

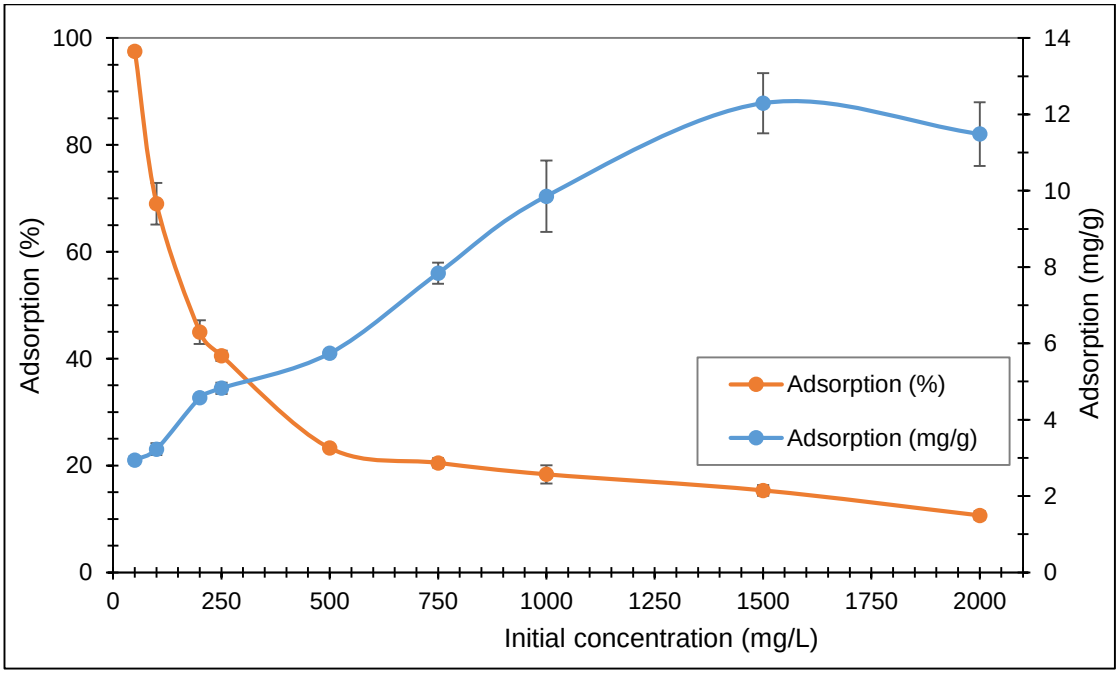

Figure 6-7: Influence of initial concentrations of zinc on adsorption.

[Experimental conditions: 1.0 ± 0.05 g of ion exchange mesh in 50 mL of zinc solution, initial pH 6.45 to 6.85 at room temperature (25 °C) and contact time of 8 hours].

In the case of lower initial concentrations, the ratio between available sites to the metal ions is larger. Thus, adsorption process becomes independent of initial concentration. Increasing the initial concentration of metal decreases the rate of adsorption, but the adsorption density per unit mass of mesh increases. Similarly, the adsorption density per unit mass of mesh decreases with respect to the lower initial concentrations (Gode and Pehlivan, 2006).

Figure 6-8 presents the distribution coefficients (K_d) with respect to the equilibrium concentration (C_e) of zinc. A very high K_d value at lowest concentration indicates the involvement of more favourable sites (Kubilay et al., 2007). The increase in adsorption capacity per unit mass of mesh with respect to increasing initial concentration is due to the increased driving force for mass transfer between mesh and solution (Mishra and Patel, 2009; Anis, Haydar and Bari, 2013).

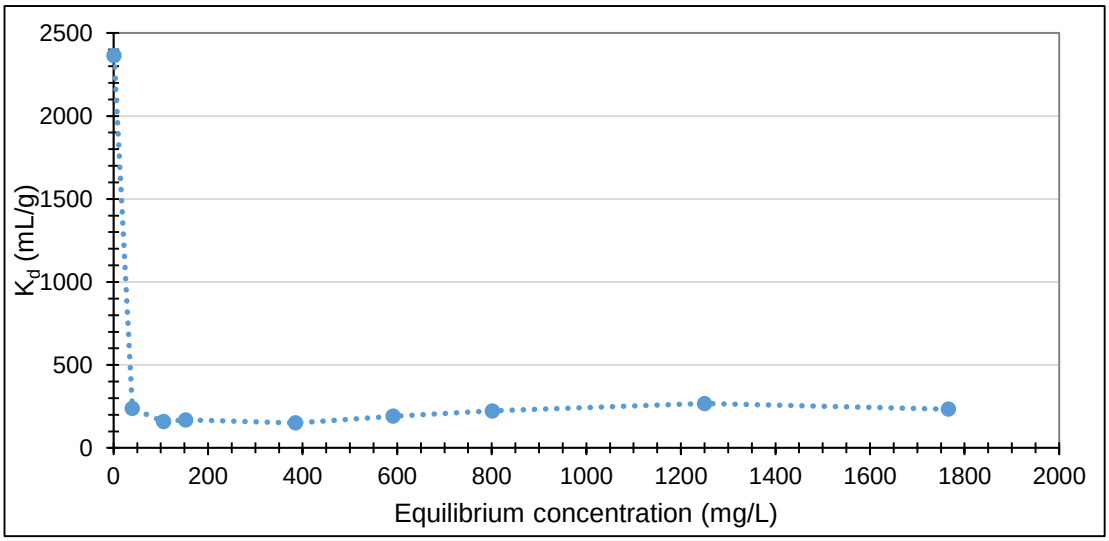

Figure 6-8: Distribution coefficients (Kd) with respect to the equilibrium concentration (Ce) of zinc.

6.4.2.4. EQUILIBRIUM ADSORPTION ISOTHERMS

An equilibrium isotherm is a useful tool that helps understand the nature of a surface. Selection of the best adsorption model depicts a true scenario of the surface (Kubilay et al., 2007) and informs how metal ions interact with the ion exchange mesh thereby reveals an idea of the adsorption capacity per unit mas of mesh, surface property and affinity to the ion exchange mesh (Liu et al., 2012; Wawrzkiewicz, 2013; Wawrzkiewicz and Hubicki, 2015). The experimental data at equilibrium concentrations determined from the influence of initial concentration of metal ions on adsorption can be used to describe the type of adsorption model (Mustafa and Ünlü, 2006). The regression correlation coefficient (R^2) dictate the best-fit adsorption model (Suteu, Zaharia and Malutan, 2011; Anis, Haydar and Bari, 2013; Yagub et al., 2014). Amongst the several adsorption models mentioned in section 4.5.3.1, p.100, Langmuir and Freundlich models are the most commonly found in the literature (Aksu, 2001; Anis, Haydar and Bari, 2013; Deng et al., 2015).

6.4.2.4.1. LANGMUIR ADSORPTION ISOTHERM MODEL

The Langmuir isotherm model assumes adsorption free energy independent of surface coverage and the formation of monolayer where the solid surface reaches saturation (Mohan and Singh, 2002). Further information and expressions, Equation 4-11 to Equation 4-14, related to Langmuir model are discussed in section 4.5.3.1.1, p.100. Figure 6-9 and Figure 6-10 present the adsorption capacities of ion exchange mesh with respect to equilibrium concentrations and Langmuir adsorption isotherm model-1.

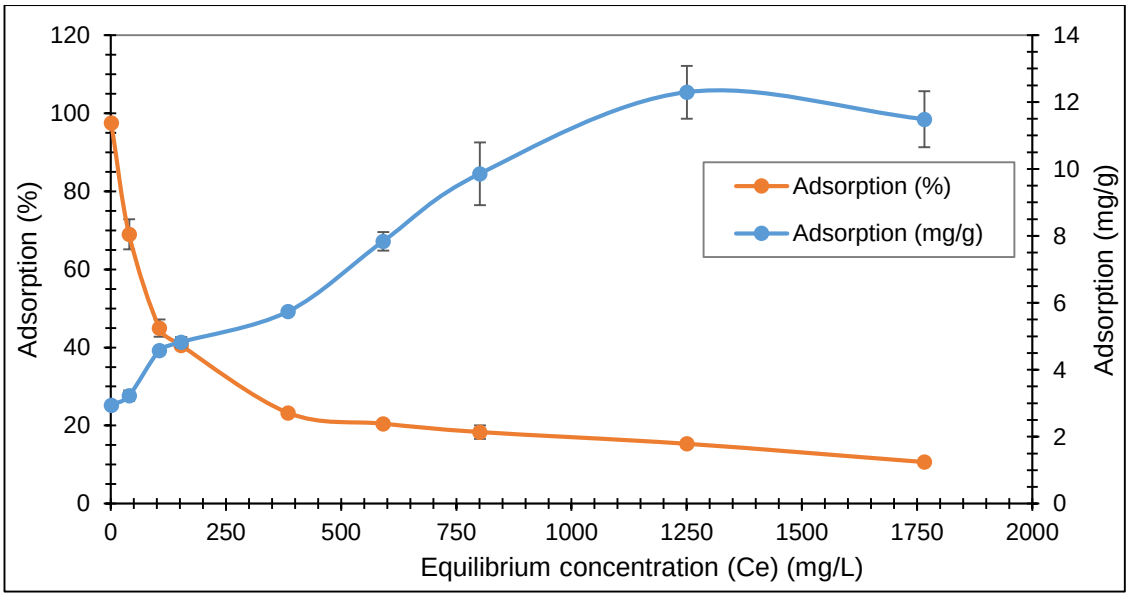

Figure 6-9: Adsorption capacity of ion exchange mesh with respect to the equilibrium concentrations.

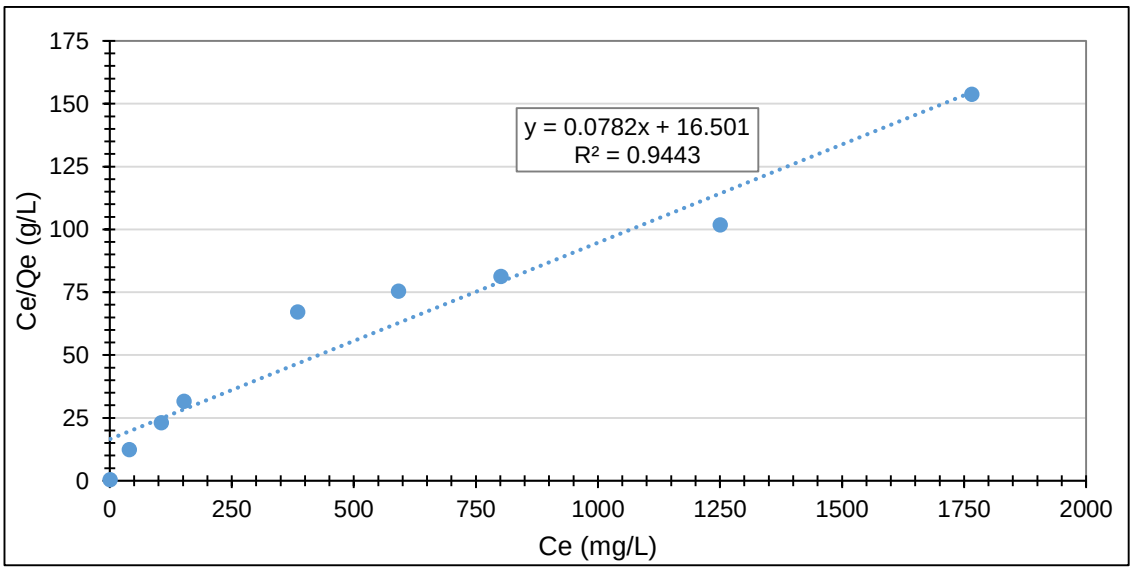

Figure 6-10: Langmuir isotherm model for the adsorption of zinc onto the ion exchange PAN mesh.

Table 6-3 presents the related parameters of Langmuir adsorption isotherm model. With the correlation coefficient (R^2) equal to 0.9443, Langmuir adsorption model estimated the maximum adsorption capacity (Q_m = 1/slope) per unit mass of ion exchange mesh as 12.8 mg/g which becomes 25.6 mg/g per unit mass of modified PAN fibre.

Table 6-3: Langmuir adsorption isotherm parameters for the adsorption of zinc onto ion exchange PAN mesh.

Langmuir isotherm	Slope	Intercept	R^2	Q_m (mg/g)	K_L (L/mg)
Model-1	0.0782	16.501	0.9443	12.79	0.0047

The separation factor (R_L) is considered as more reliable indicator of adsorption capacity and classify whether adsorption of zinc onto the ion exchange mesh is favourable or unfavourable (Pandiselvi and Thambidurai, 2013; Yagub *et al.*, 2014; Xiong *et al.*, 2015).

Figure 6-11 presents the separation factors (R_L), calculated from the Equation 4-15, corresponding to the initial concentrations of zinc. The separation factor corresponding to an initial concentration (1,500 mg/L) that yielded maximum adsorption capacity per unit mass of mesh in Figure 6-9 is calculated as 0.123. The calculated R_L values corresponding to all initial concentrations of zinc fall between zero and unity ($0 < R_L < 1$), thus adsorption of zinc onto ion exchange mesh is favourable. The R_L decreases towards zero with respect to increase in metal concentration, suggests that adsorption with high concentration could be irreversible. Similarly, R_L increases towards unity with respect to decrease in concentration, suggests that adsorption at low concentration could be linear.

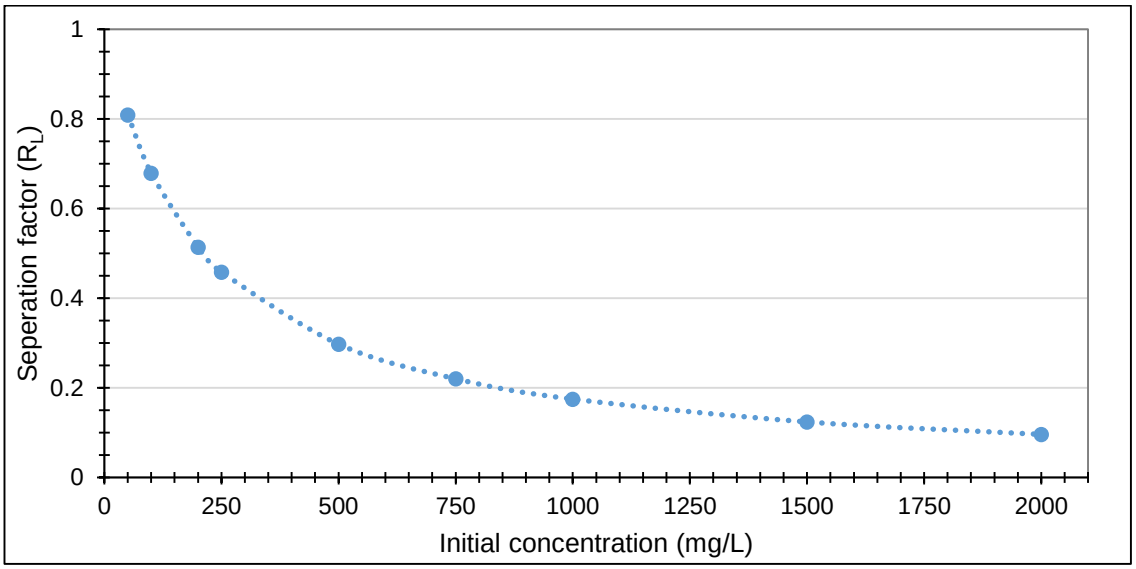

Figure 6-11: Separation factors with respect to the initial concentrations of zinc.

6.4.2.4.2. FREUNDLICH ADSORPTION ISOTHERM MODEL

Freundlich isotherm model assumes a heterogeneous adsorption surface that has exponentially distributed sites with different energies of adsorption (Suteu, Zaharia and Malutan, 2011; Yagub et al., 2014). This model does not predict saturation of the solid surface by the adsorbate. Thus, surface covering being mathematically unlimited (Mohan and Singh, 2002). Freundlich isotherm expression are given in Equation 4-16 and Equation 4-17. Freundlich adsorption isotherm model and related parameters are presented in Figure 6-12 and Table 6-4 *respectively*. Since 1/n < 1 (n >1), the adsorption can be explained as a normal Langmuir isotherm. Dafa et al., 2012 mentioned that adsorption is favourable if n lies between one and ten.

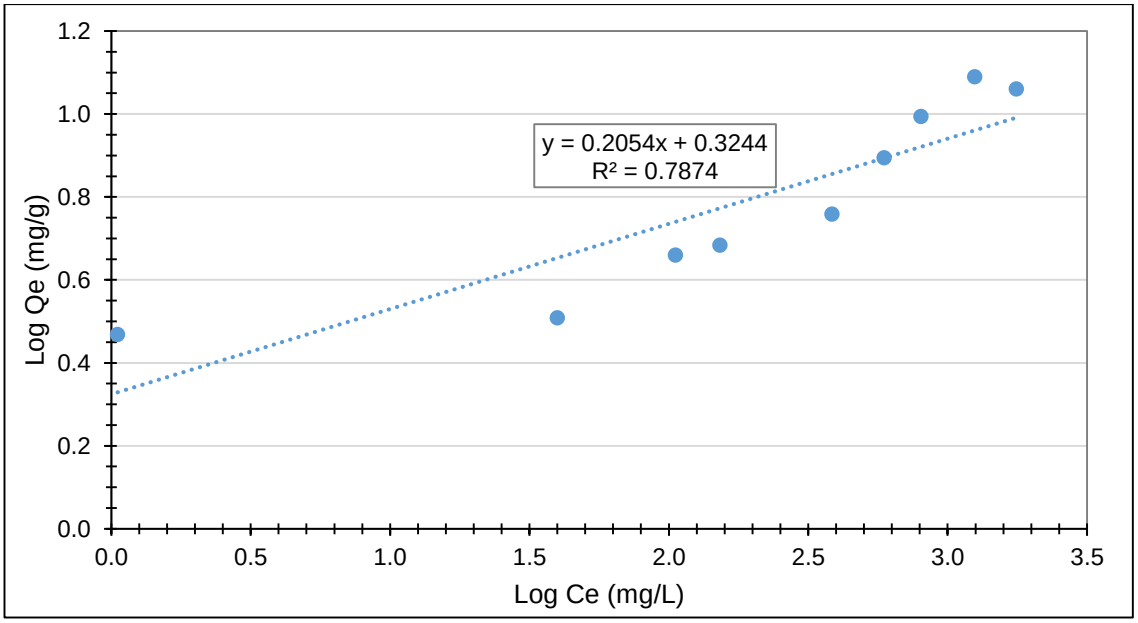

Figure 6-12: Freundlich adsorption isotherm model for the adsorption of zinc onto the ion exchange PAN mesh.

Table 6-4: Parameters related to Freundlich adsorption isotherm model.

Freundlich isotherm model	**Slope**	**Intercept**	**R^2**	***n* = *1/slope***	**K_F = antilog (intercept) (mg/g)**
	0.2054	0.3244	0.7874	4.78	2.11

6.4.2.4.3. SELECTION OF THE BEST-FIT MODEL

The values of correlation coefficient (R^2) is commonly accepted in the literature to determine the goodness of fit criterion. The R^2 values obtained for Langmuir and Freundlich isotherm models are 0.9443 and 0.7874 respectively. The R^2 value for Langmuir isotherm model is higher compared to Freundlich isotherm model. The trend

line in Langmuir plot represents four data points whereas in Freundlich plot only one data point is represented. Therefore, Langmuir model is considered to the best-fit model, confirming the presence of monolayer adsorption of zinc onto the ion exchange mesh. Accordingly, the maximum adsorption capacity (Q_m) per unit mass of ion exchange mesh at pH 6.5 and 25 °C is estimated as 12.8 mg/g, corresponding to 25.6 mg/g fibre. The maximum adsorption capacity per unit mass of mesh derived experimentally is 11.8 mg/g, corresponding to 23.6 mg/g fibre.

Table 6-5 compares the adsorption capacity per unit mass of ion exchange mesh used in this study with values reported by other literature. The ion exchange mesh used in this study can be considered as an average adsorbent in terms of the removal of metal.

Table 6-5: Comparison of maximum adsorption capacities of various adsorbents predicted by Langmuir model.

Q_m (mg/g)	Adsorbents	Reference
25.6 (fibre)	Ion exchange PAN mesh	This study
31.11	Activated carbon derived from bagasse	(Mohan and Singh, 2002)
101.01	Rice husk modified with phosphoric acid	(Dada et al., 2012)
15.06	Bentonite	(Kubilay et al., 2007)
11.24	Active carbon	(Mishra and Patel, 2009)
65.40	Polyamidoxime / organobentonite composite	(Anirudhan and Ramachandran, 2008)
59.88	Activated carbon made from palm oil mill effluent	(Adebisi, Chowdhury and Alaba, 2017)

6.4.3. REMOVAL OF METALS FROM THE REAL MINE EFFLUENT

In order to assess the potential application of ion exchange mesh in the remediation of mine waters contaminated with metals, experiments were conducted with real effluent from an abandoned mine from White Tip site at Snailbeach at Minsterley. The mine water was drainage water infiltrating through the site and heavily contaminated with metals such as zinc, lead etc. The experiments were performed in batch mode and the results

for the removal of zinc and lead are presented in Figure 6-13 and Figure 6-14 respectively.

Figure 6-13 shows that removal efficiencies of zinc corresponding to the controlled experiments, residence time six hours, with no mesh (mine water only) and with unmodified PAN mesh were almost zero and below 15 % respectively. However, removal efficiency of zinc corresponding to modified PAN mesh gradually increased with respect to increase in residence time and plateaued around 70 % at six hours. When exposed to real mine effluent, the uptake capacity of ion exchange PAN mesh further improved. Compared to the removal of zinc from zinc sulfate heptahydrate solution, the uptake capacities of ion exchange PAN mesh, even with a significant change in ratio between ion exchange PAN mesh to liquor, according to Figure 6-7 (1 g : 50 mL) and Figure 6-13 (1 g : 167 mL) are ~ 2.8 mg/g and 5.83 mg/g respectively.

Minimal removal (15 %) of zinc in the presence of unmodified PAN mesh is due to the absence of functionalized groups that control the surface ionization of the mesh. The almost zero removal of zinc in the absence of PAN mesh signifies the lack of precipitation of zinc in the solution phase. In fact the, independent analysis by UKAS accredited laboratory confirmed the presence of zinc was in a dissolved form, see section 6.4.4.2.1.4. The results evidenced the enormous potential of ion exchange mesh in the remediation of circum-neutral mine water.

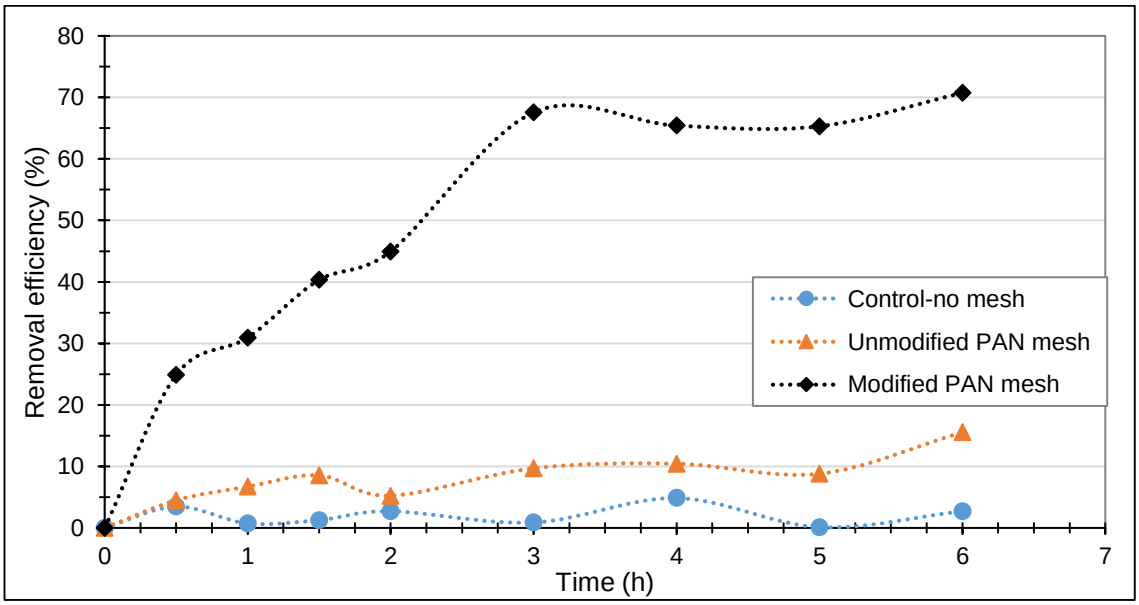

Figure 6-13: Removal of zinc from real mine effluent from White site Tip, Minsterley, UK.

[Experimental conditions: 30 g of mesh in 5 L of real mine effluent (C_0-Zn = 50 mg/L), as natural pH (7.24), contact time of six hours and at room temperature (23 °C)].

According to Figure 6-14, the removal efficiencies of lead corresponding to the controlled experiments, residence time six hours, with no mesh (mine water only) and with unmodified and modified PAN mesh as 29 %, 43.6 % and 60 % respectively. A significant amount of removal (29 %) in the absence of PAN mesh is indicative the removal through other mechanisms. Removal through electrostatic interaction between lead and the glass container can be ruled out as surface conductivity on borosilicate glass container by free electron is reported as null (Muray, 1962). After the experiments, the whitish residue was seen on the surface of air-dried glass container, indicating deposition of lead onto the surface of glass container. This suggests the occurrence of lead in solid phase, favouring precipitation. In fact, an independent analysis by UKAS accredited laboratory confirmed the presence of lead as in lead-total form; see section 6.4.4.2.1.4, with little in the dissolved form.

In the presence of unmodified PAN mesh, the removal efficiency further increased to 43.6 %. This is probably due to additional surface area of mesh for the deposition of lead-total. The removal efficiency further improved to 60 % in the presence of modified PAN mesh. This is expected as the functionalized surface of modified PAN mesh favoured the sorption (ion exchange and adsorption) of lead in the solution phase, lead-dissolved.

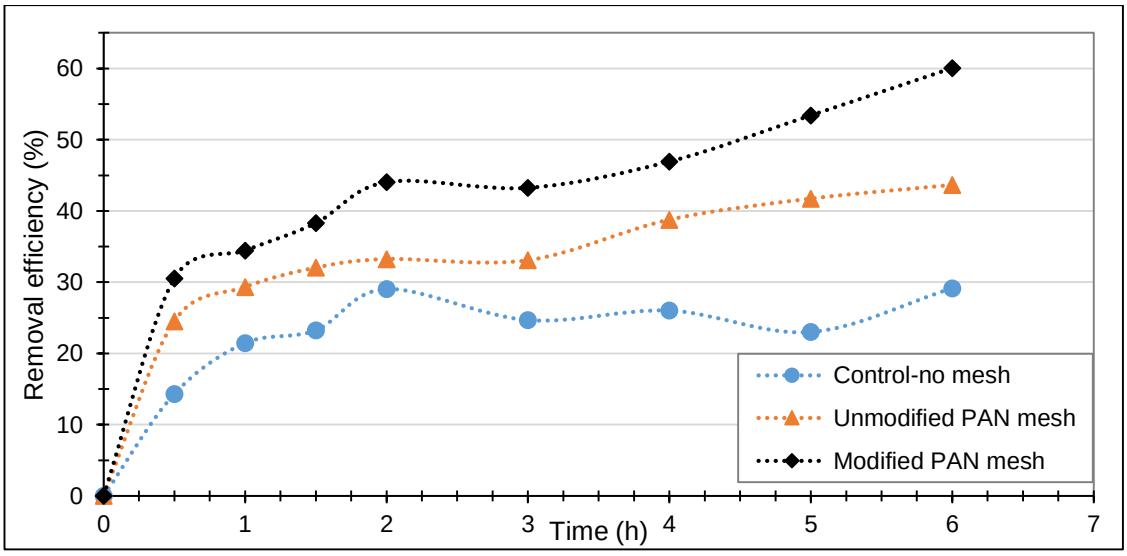

Figure 6-14: Removal of lead from real mine effluent from White site Tip, Minsterley, UK.

[Experimental conditions: 30 g of mesh in 5 L of real mine effluent (C_0-Pb = 125 µg/L), at natural pH (7.24), contact time of six hours and at room temperature (23 °C)].

6.4.3.1. INFLUENCE OF PH ON REMOVAL OF METALS FROM REAL MINE EFFLUENT

It is clear from section 6.4.2.1 that pH of the mine water effluent determines the success of remediation process. Therefore, the influence of pH on remediation of real effluent

from White site Tip was investigated. The initial pH of the effluent was adjusted to pH 3 and pH 5 and the results are presented in Figure 6-15. At pH of 3 and 5, after six hours, the effieciency for zinc removal dropped significantly below 5 %. Similarly, the removal efficiency for lead, after six hours, dropped to 13.5 % and 31.6 % at pH 3 and pH 5 respectively. This is due to changes in surface ionization of the mesh which is discussed in section 6.4.2.1. (Florence, 1982) reported that pH 5.7 was adequate to prevent adsorption of free metal ions. The significant drop in removals of zinc and lead at pH 3 and 5 is possibly indicative that the technology could be limited to the remediation of waters at circum-neutral pH.

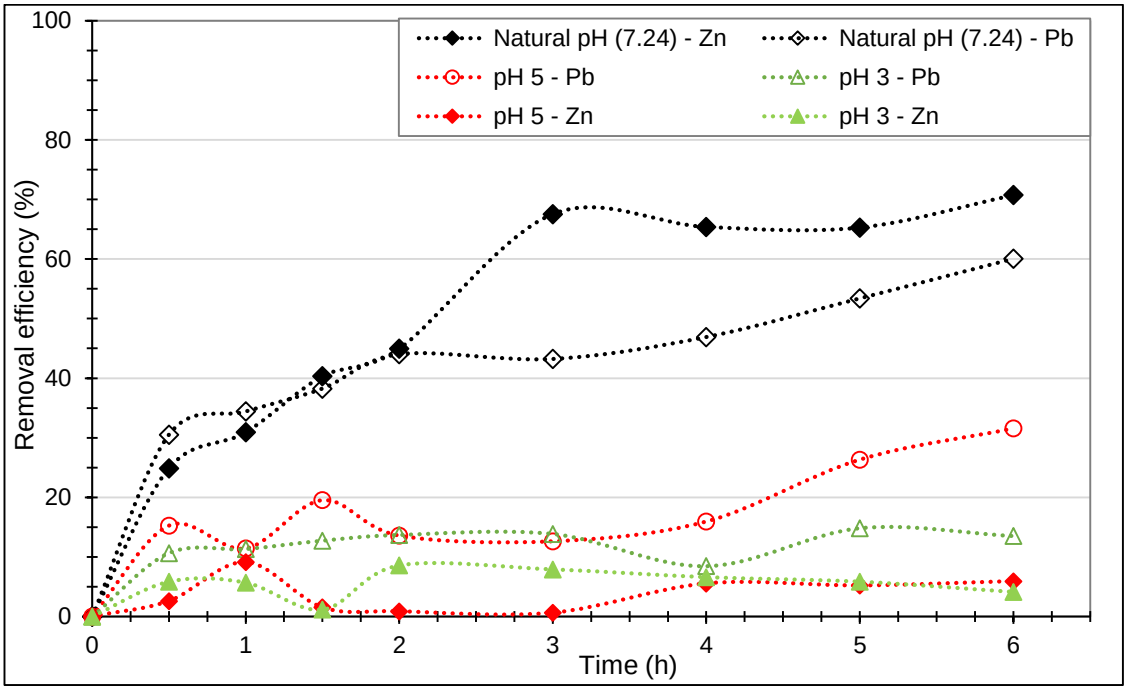

Figure 6-15: Influence of pH on removal of metals from real mine effluent from White site Tip, Minsterley, UK.

[Experimental conditions: 30 g of mesh in 5 L of real mine effluent (C_0-Zn = 50 mg/L, C_0-Pb = 125 µg/L), contact time of six hours at room temperature (23 °C)].

In order to investigate the suitability of the treatment system for acid mine drainage (AMD), the pH of the the real effluent was first lowered to pH 2.5 to obtain a simulated AMD and readjusted to pH (7.67), upper range of natural pH of the effluent received in the field trial. Then, the pH adjusted effluent was exposed to the mesh for six hours. The results are presented in Figure 6-16.

It is clearly seen in Figure 6-16 that the higher extent of zinc removal achieved with simulated effluent than in as-received effluent. The removal efficiencies after six hours

corresponding to simulated and as received effluents become 84 % and 70.7 %. The additional removal of 14 % in simulated effluent is due to the differences in pH of the medium which determines the solubility of zinc (see Figure 3-5 and Appendix 9-7). The higher removal of zinc corresponding to simulated effluent helps draw conclusion that AMDs can be treated with this technology which yields the best results at circum-neutral pH.

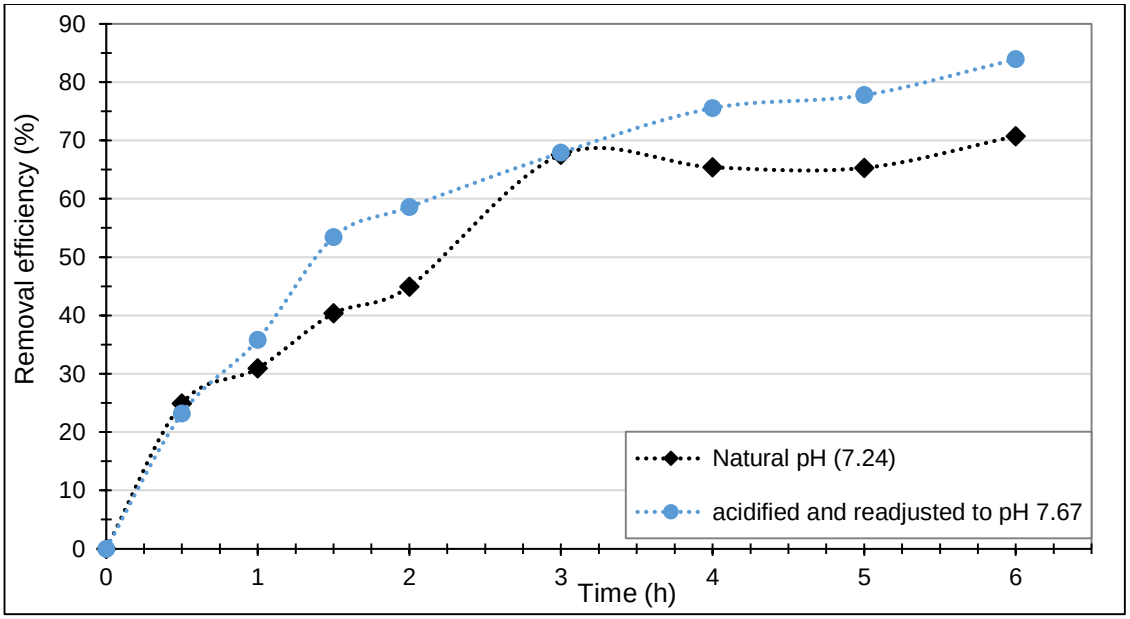

Figure 6-16: Removal of zinc from real mine effluents: as received and pH acidified and readjusted to pH = 7.67.

[Experimental conditions: 30 g of mesh in 5 L of real mine effluent (C_0-Zn = 50 mg/L) at natural pH (7.24) and readjusted to pH (7.67), contact time of six hours and room temperature (23 °C)].

6.4.4. PILOT SCALE FIELD TRIAL

The results of this pilot scale field trial discussed in the following sections were provided to the Coal Authority, UK as a formal report. These results were presented in an international conference organized by International Mine Water Association (IMWA) and held in Leipzig, Germany in July (11-15), 2016. Accordingly, a part of these results were published in conference proceedings (Upreti *et al.*, 2016).

6.4.4.1. REMOVAL OF METALS

The treatment process was run for a total of 24 weeks and 2 days (170 days). During this period, the estimated weighted average (see Appendix 9.9) flow rates for overall treatment, before and after the regeneration process were calculated as 32.22 L/hr, 28.18 L/hr and 35.60 L/hr respectively. This corresponds to the estimated total volume

of 131.46 m^3 of treated mine water. The estimated total volumes of mine water treated before and after the regeneration process were 53.43 m^3 and 77.75 m^3 respectively. Table 6-6 summarizes the estimated average flow rate, amount of mine water treated during this trial and break down into before and after the regeneration process. The average flow rates were calculated using weighted mean as shown in Appendix 9-9.

Table 6-6: The summary of time, flow rate and amount of treated mine water during this project

	Overall (Day-1 to Day-170)	**Before regeneration** (Day-1 to Day-79)	**After regeneration** (Day-80 to Day-170)
Time (day)	170.00	79.00	91.00
Average flow rate (L/hr)	32.22	28.18	35.60
Volume treated (m^3)	131.46	53.43	77.75

The process was halted on two occasions which are annotated in the results presented in following sections with a blue vertical line marking the date of regeneration process. The removal of individual metal ions and comparison of internal (analyzed at DMU) and external (analyzed by ESG) results are discussed separately in the following sections.

6.4.4.1.1. COMPARISON OF INTERNAL (DMU) AND EXTERNAL (ESG) ANALYSES FOR METAL IONS

Figure 6-17, Figure 6-18 and Figure 6-19 show that there was no significant difference between DMU and ESG results in terms of removal efficiencies for zinc, cadmium and lead. However, a significant variation in the concentrations of zinc, especially, in the inlet water samples was observed. Figure 6-20 compares the pH, concentrations of zinc, cadmium and lead analyzed at DMU and ESG. Comparing the ESG and DMU results for the corresponding dates, an average variation of 11.3 mg/L with the highest 38.8 mg/L (only observed in one sample) and the lowest 1.94 mg/L was observed in the concentration of zinc in the inlet water samples. Comparing the average concentration of zinc in the inlet water derived from the overall analyses performed at DMU with the average concentration derived from the ESG analyses, this variation reduce to 9.14 mg/L of zinc.

The values were close to each other for the zinc (outlet), cadmium (inlet and outlet) and lead (inlet and outlet). Mostly, ESG analyses resulted in higher concentrations than DMU analyses. This variation can arise from the analytical technique used, sensitivity of

instrument and sampling time. Samples for external analyses at ESG were usually collected in the afternoon on the tankering day, after refilling the inlet tank whereas for internal analyses, samples were usually collected in the morning. The new feed had mixed the sediments settled in the inlet tank which could have contributed to the high concentration of metal ions in the inlet water. Analyses at DMU were performed using AAS whereas ESG analyses were performed using inductively coupled plasma- mass spectroscopy (ICP-MS) which, compared to AAS, is a more sensitive and better technique. For dissolved metal analyses at ESG, an aliquot (100 mL) of the water sample was filtered through a 0.45 µm filter and then acidified with 0.15 mL of nitric acid. DMU analyses were performed with settled samples without further treatment. It is well known that the analyses vary to some extent between laboratories, instruments and analytical techniques.

Table 6-7, Figure 6-17, Figure 6-18 and Figure 6-19 compare the removal efficiencies of zinc, cadmium and lead analyzed at DMU and ESG. Removal efficiencies for zinc, lead and cadmium obtained from ESG analyses appear higher compared to corresponding removal efficiencies obtained from DMU analyses. However; Figure 6-17, Figure 6-18, and Figure 6-19 show similar removal trends for both DMU and ESG analyses.

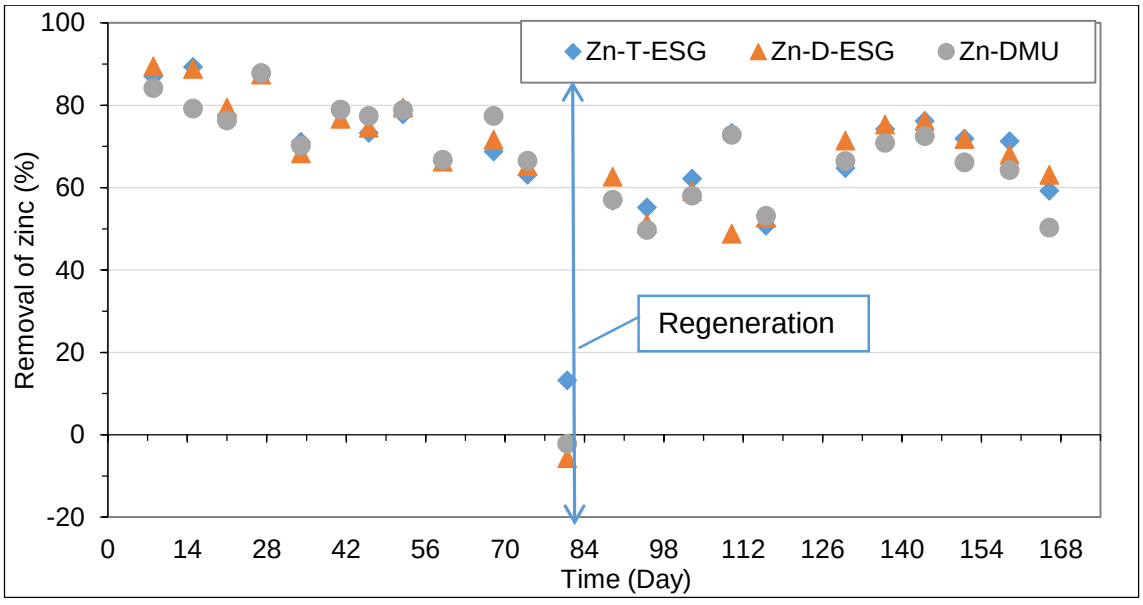

Figure 6-17: Comparison of removal efficiencies of zinc analyzed at DMU and ESG.

Table 6-8 presents the average removal efficiencies, maximum and minimum concentrations of all the water quality parameters analyzed by ESG. Table 6-9 presents removal of metals, with removal efficiency higher than 20 %, expressed as milliequivalents per gram of mesh (meq/g mesh). In this calculation, the concentrations

expressed less than limit of detection (LOD) were considered to be at LOD. This is why the removal efficiencies for lithium and arsenic-D show no removal. In addition, for some other parameters, the average concentrations would be lower than tabulated values. Therefore, these results represent the minimum removal efficiencies for the corresponding parameters.

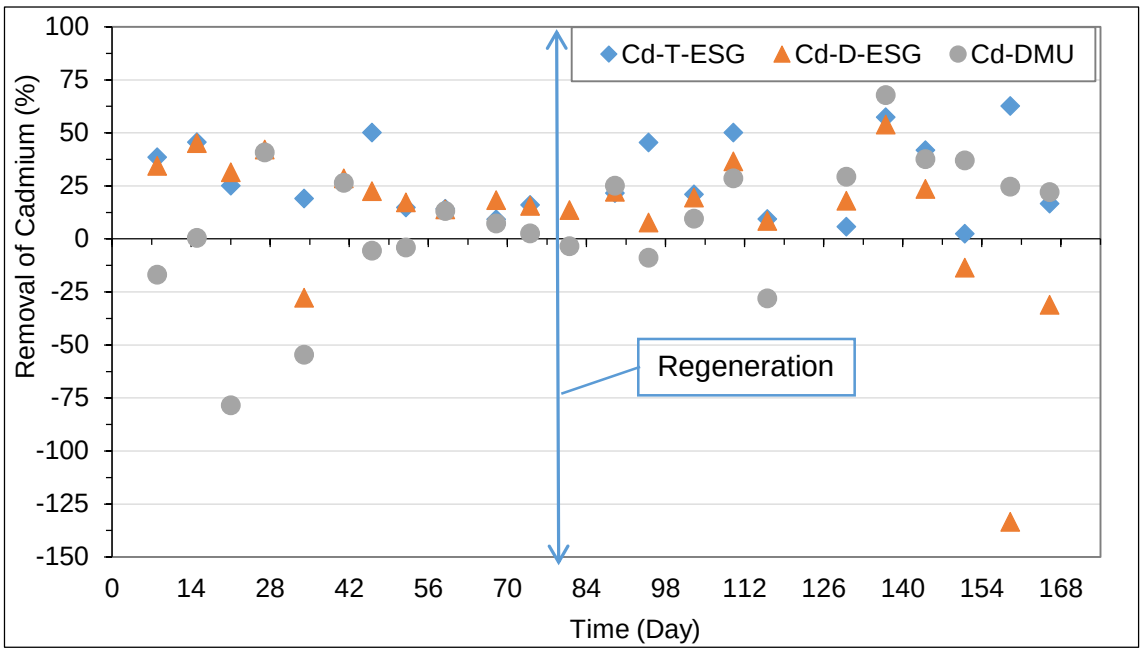

Figure 6-18: Comparison of removal efficiencies of cadmium analyzed at DMU and ESG.

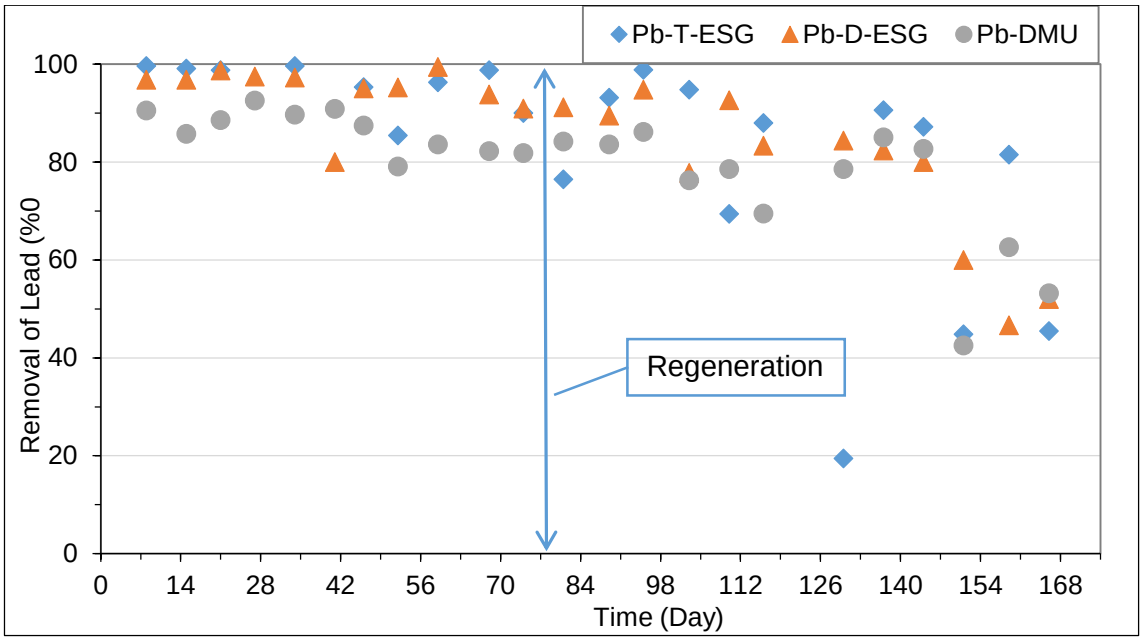

Figure 6-19: Comparison of removal efficiencies of lead analyzed at DMU and ESG.

Table 6-7: DMU and ESG analyses comparing the average concentrations, removal efficiencies and total amounts of zinc, cadmium, lead and suspended solids removed from the mine water.

Parameters	Average concentration (mg/L)			Total amount passed to the system (g)			Removal efficiency (%)			Total amount of removal (g)		
	Overall	Before regeneration	After regeneration	Overall	Before regeneration	After regeneration	Overall	Before regeneration	After regeneration	Overall	Before regeneration	After regeneration
Zn-T-ESG	62.86	72.62	55.55	8264.21	3879.85	8264.21	67.65	75.66	59.8	5590.74	2935.50	2582.77
Zn-D-ESG	58.28	68.10	49.29	7661.95	3638.49	7661.95	68.77	77.51	57.7	5269.12	2820.19	2211.09
Zn-DMU	49.14	53.43	45.36	6460.31	2854.76	6460.31	64.18	70.41	58.79	4146.23	2010.04	2073.37
Cd-T-ESG	0.26	0.37	0.18	34.02	19.80	34.02	25.06	28.23	20.02	8.53	5.59	2.72
Cd-D-ESG	0.24	0.32	0.16	31.27	17.31	31.27	23.63	25.18	20.74	7.39	4.36	2.57
Cd-DMU	0.19	0.25	0.14	24.82	13.28	24.82	22.37	21.54	23.09	5.55	2.86	2.46
Pb-T-ESG	0.16	0.21	0.11	20.39	11.31	20.39	89.16	97.53	77.36	18.18	11.03	6.78
Pb-D-ESG	0.03	0.05	0.02	4.30	2.54	4.30	91.08	95.97	79.91	3.92	2.44	1.19
Pb -DMU	0.05	0.04	0.06	6.95	2.26	6.95	75.04	77.73	72.75	5.22	1.76	3.51
SS-ESG	47.91	67.18	30.25	6298.25	3589.43	2351.94	77.31	86.87	58.85	4869.18	3118.14	1384.12

Figure 6-21 presents the percentage removals of water quality parameters analyzed by ESG (excluded parameters analyzed twice or less: ionic balance, total anions and cations, TOC and phosphate). From Table 6-8 and Figure 6-21, it is clear that in addition to the metals of interest (Zn, Cd and Pb); the system also removed most of the metals and metalloids analyzed by ESG. These include in particular iron (Fe), aluminium (Al), copper (Cu), manganese (Mn), barium (Ba), nickel (Ni) and arsenic (As). The system also removed non-metallic parameters; such as acidity, suspended solids (SS), alkalinity, nitrate (NO_3-N), conductivity and total anions but contributed to the ammoniacal nitrogen (NH_3-N), sulphate (SO_4-S), hardness and total cations. Although, the contribution to ammoniacal nitrogen in terms of percentage appears very high, in terms of concentrations the contribution is minimal. This result was skewed by the leaching of ammoniacal nitrogen from the mesh within the first four weeks after which the ammoniacal nitrogen dropped in the range of 0.12 mg/L to 0.5 mg/L, with most of the outlet concentrations within the range of 0.2 mg/L to 0.3 mg/L (see Appendix 9-10). There were only two readings at 0.5 mg/L of ammoniacal nitrogen. These readings occurred following the regeneration process. The concentration of leached ammoniacal nitrogen will be less in the upscaled treatment system as the liquor to mesh ratio will be changed. In this trial the reactor was loaded heavily by placing PAN mesh discs very close together which cannot be maintained in the large reactor. This loss of mesh means that the mesh to liquor ratio will be reduced and hence the NH_3-N. To maintain the same performance, the loss can be compensated by increasing the residence time. The initial release of ammonia can be lowered by prewashing of mesh at the manufacturing stage.

The pH of the mine water increased on treatment as a result of degassing of carbon dioxide. The precipitation of carbonate is favourable at higher pH which results in the reduction of alkalinity, see Equation 6-10 and Equation 6-11.

The ESG results expressed for ionic balance, TOC, total anions and total cations in Table 6-8, are based on one-day (Day-42) sample. Similarly, the results for nitrate and phosphate are based on two days, Day-21 and Day-42. Therefore, these results may not represent the overall treatment period. On Day-21, the concentrations of phosphate in inlet and outlet samples were reported as less than 0.01 mg/L. However, on Day-42, the inlet concentration remained the same (< 0.01 mg/L) and outlet concentration was reported as 0.31 mg/L. There was no source of phosphate in the mesh, if any then the leaching would be expected to be higher at the beginning of the treatment. Thus, this

result could be an outlier or error. In fact, in some analyses, ESG reported higher concentrations for dissolved metal than total metal.

The pH of the inlet and outlet end of the reactor were monitored using data loggers and the results are discussed in section 6.4.4.4.

Table 6-8: Concentrations of water quality parameters and the corresponding average removals analyzed by ESG.

Parameters	Inlet			Outlet			Removal (%)		
	Max	Min	Avg	Max	Min	Avg	Max	Min	Avg
pH	7.2	6.6	6.9	7.8	6.9	7.4	2.82	-11.94	-6.54
Conductivity (µS/cm)	1800	807	1479.43	1760	1210	1457.8	9.29	-49.94	1.46
SS (mg/L)	193	5	47.9	35	5	10.9	97.01	-266.67	77.31
Alkalinity-T (mg/L)	211	114	165.2	162	69	115.7	60.12	-39.47	29.93
Acidity-T (mg/L)	36	0	4.8	0	0	0	100	100	100
Hardness-T (mg/L)	1110	8.3	859.3	1140	778	907	4.31	-12.85	-5.55
Cl (mg/L)	41	18	29.3	41	19	29.4	51.22	-33.33	-0.30
S-SO_4 (mg/L)	920	590	720.4	920	610	740.9	4.05	-29.23	-2.84
Ca-T (mg/L)	420	295	341	419	290	337.6	10.00	-8.47	0.99
Ca-D (mg/L)	423	285	334.7	432	290	338.9	4.55	-13.89	-1.26
Mg-T (mg/L)	15	12	13.6	15	13	13.6	7.14	-8.33	0.00
Mg-D (mg/L)	14	12	13.4	14	13	13.5	0.00	-8.33	-0.98
Ba-T (mg/L)	0.13	0.03	0.065	0.06	0.03	0.04	69.23	-25.00	30.53
Ba-D (mg/L)	0.31	0.03	0.06	0.05	0.03	0.04	90.32	-33.33	28.03
Sr-T (mg/L)	0.31	0.25	0.28	0.31	0.027	0.264	90.36	-4.00	4.04

Parameters	Inlet			Outlet			Removal (%)		
	Max	Min	Avg	Max	Min	Avg	Max	Min	Avg
Sr-D (mg/L)	0.31	0.026	0.26	0.31	0.028	0.25	90.00	-8.00	3.99
Na-T (mg/L)	30	16	21.6	28	16	20.95	40.00	-13.04	2.87
Na-D (mg/L)	29	16	21.3	28	16	20.96	37.93	-22.73	1.43
K-T (mg/L)	7	6	6.5	7	6	6.5	14.29	-16.67	0.00
K-D (mg/L)	8	6	6.5	8	6	6.5	14.29	-16.67	-0.67
Ni-T (mg/L)	0.1	0.064	0.078	0.66	0.037	0.084	53.16	13.04	-7.47
Ni-D (mg/L)	0.091	0.066	0.077	0.071	0.034	0.054	58.02	9.09	29.49
Cr-T (mg/L)	0.002	0.001	0.001	0.001	0.001	0.001	50.00	0.00	12.50
Cr-D (mg/L)	0.005	0.001	0.001	0.005	0.001	0.001	0.00	0.00	0.00
Cd-T (mg/L)	0.5539	0.0278	0.2588	0.4143	0.0317	0.194	62.75	-5.78	25.06
Cd-D (mg/L)	0.5488	0.0042	0.2379	0.3764	0.0076	0.1817	63.13	-133.33	23.64
Cu-T (mg/L)	0.019	0.001	0.006	0.004	0.001	0.002	92.31	-50.00	66.92
Cu-D (mg/L)	0.01	0.001	0.003	0.01	0.001	0.002	66.67	-50.00	25.81
Pb-T (mg/L)	0.611	0.01	0.155	0.1	0.001	0.017	99.61	19.44	89.16
Pb-D (mg/L)	0.17	0.009	0.033	0.012	0.001	0.003	99.41	46.67	91.08
Zn-T (mg/L)	93.62	38.61	62.86	53.38	7.804	20.33	89.28	13.19	67.66
Zn-D (mg/L)	91.21	34.38	58.28	51.22	7.64	18.20	89.44	-5.63	68.77
Mn-T (mg/L)	0.64	0.33	0.40	0.3	0.1	0.2	84.38	9.09	51.73
Mn-D (mg/L)	0.42	0.3	0.36	0.3	0.1	0.2	70.59	9.09	47.02
Fe-T (mg/L)	12.2	0.24	1.89	2.54	0.17	0.48	98.20	-39.22	74.58
Fe-D (mg/L)	0.85	0.17	0.33	0.32	0.16	0.21	78.82	-13.64	36.58

Parameters	Inlet			Outlet			Removal (%)		
	Max	Min	Avg	Max	Min	Avg	Max	Min	Avg
As-T (mg/L)	0.003	0.001	0.002	0.001	0.001	0.001	66.67	0.00	27.59
As-D (mg/L)	0.001	0.001	0.001	0.001	0.001	0.001	0.00	0.00	0.00
B-T (mg/L)	0.09	0.02	0.05	0.06	0.03	0.05	40.00	-50.00	5.77
B-D (mg/L)	0.06	0.02	0.05	0.06	0.03	0.048	50.00	-150.00	5.22
BOD (mg/L)	4.5	2	2.7	6.4	2	2.6	37.50	-42.22	0.00
Al-T (mg/L)	1.17	0.04	0.29	0.48	0.02	0.08	97.53	0.00	73.87
Al-D (mg/L)	0.09	0.01	0.03	0.07	0.01	0.03	77.78	-133.33	5.08
Si-D (mg/L)	4.4	3.1	3.8	4.2	2.6	3.6	35.00	-3.23	4.78
Anions-T (meq c)	17.9	17.9	17.9	17.5	17.5	17.50	2.23	2.23	2.23
Cations-T (meq c)	17.8	17.8	17.8	19	19	19.00	-6.74	-6.74	-6.74
NO_3-N (mg/L)	2.7	2.2	2.45	2.2	2.2	2.20	18.52	0.00	10.20
PO_4-P (mg/L)	0.01	0.01	0.01	0.31	0.01	0.16	0.00	-3000.0	-1500.0
Li-T (mg/L)	0.01	0.01	0.01	0.01	0.01	0.01	0.00	0.00	0.00
Li-D (mg/L)	0.01	0.01	0.01	0.01	0.01	0.01	0.00	0.00	0.00
NH_3-N (mg/L)	2.7	0.04	0.29	4.7	0.12	0.65	40.00	-900.00	-123.72
Ionic Balance (% c)	-0.3	-0.3	-0.30	4	4	4.00	1433.33	1433.33	1433.33
TOC (mg/L)	3.2	3.2	3.20	3.4	3.4	3.40	-6.25	-6.25	-6.25

Table 6-9: Removal of metals, with removal efficiency higher than 20 %, expressed as milliequivalents per gram of mesh (meq/g).

Parameters	Total amount passed to the system (g)			Total amount of removal (g) (W)			Atomic Weight (X)	Valency (Y)	Equivalents of total amounts removed (eq) $(Z = W \times Y/X)$			meq/g mesh $(Z \times 1000/11 \times 1000)$		
	Overall	Before regeneration	After regeneration	Overall	Before regeneration	After regeneration			Overall	Before regeneration	After regeneration	Overall	Before regeneration	After regeneration
Zn-T	8264.21	3879.85	4319.01	5590.74	2935.50	2582.77	65.38	2	171.02	89.80	79.01	15.55	8.16	7.18
Zn-D	7661.95	3638.49	3832.04	5269.12	2820.19	2211.09	65.38	2	161.18	86.27	67.64	14.65	7.84	6.15
Zn-DMU	6460.31	2854.76	3526.74	4146.23	2010.04	2073.37	65.38	2	126.83	61.49	63.43	11.53	5.59	5.77
Cd-T	34.02	19.80	13.61	8.53	5.59	2.72	112.41	2	0.15	0.10	0.05	0.01	0.01	0.00
Cd-D	31.27	17.31	12.36	7.39	4.36	2.57	112.41	2	0.13	0.08	0.05	0.01	0.01	0.00
Cd-DMU	24.82	13.28	10.66	5.55	2.86	2.46	112.41	2	0.10	0.05	0.04	0.01	0.00	0.00
Pb-T	20.39	11.31	8.76	18.18	11.03	6.78	207.20	2	0.18	0.11	0.07	0.02	0.01	0.01
Pb-D	4.30	2.54	1.49	3.92	2.44	1.19	207.20	2	0.04	0.02	0.01	0.00	0.00	0.00
Pb-DMU	6.95	2.26	4.82	5.22	1.76	3.51	207.20	2	0.05	0.02	0.03	0.00	0.00	0.00
Ba-T	8.20	3.21	4.99	2.50	0.83	1.68	127.33	2	0.04	0.01	0.03	0.00	0.00	0.00

Parameters	Total amount passed to the system (g)			Total amount of removal (g) (W)			Atomic Weight (X)	Valency (Y)	Equivalents of total amounts removed (eq) $(Z = W \times Y/X)$			meq/g mesh $(Z \times 1000/11 \times 1000)$		
	Overall	Before regeneration	After regeneration	Overall	Before regeneration	After regeneration			Overall	Before regeneration	After regeneration	Overall	Before regeneration	After regeneration
Ba-D	7.54	2.53	5.18	2.11	0.24	2.07	127.33	2	0.03	0.00	0.03	0.00	0.00	0.00
Ni-D	10.06	3.99	6.08	2.97	1.32	1.60	58.70	2	0.10	0.05	0.05	0.01	0.00	0.00
Cu-T	0.83	0.39	0.43	0.56	0.28	0.27	63.55	2	0.02	0.01	0.01	0.00	0.00	0.00
Cu-D	0.35	0.20	0.13	0.09	0.06	0.03	63.55	2	0.00	0.00	0.00	0.00	0.00	0.00
Mn-T	52.93	23.41	28.77	27.38	14.18	12.12	54.94	4	1.99	1.03	0.88	0.18	0.09	0.08
Mn-D	47.26	20.36	26.69	22.22	11.04	10.95	54.94	4	1.62	0.80	0.80	0.15	0.07	0.07
Fe-T	248.92	143.87	90.25	185.64	119.93	50.47	55.85	3	9.97	6.44	2.71	0.91	0.59	0.25
Fe-D	43.44	17.49	25.92	15.89	6.46	9.39	55.85	3	0.85	0.35	0.50	0.08	0.03	0.05
As-T	0.18	0.08	0.10	0.05	0.02	0.03	74.91	5	0.00	0.00	0.00	0.00	0.00	0.00
Al-T	37.84	16.66	20.67	27.95	12.14	15.49	26.98	3	3.11	1.35	1.72	0.28	0.12	0.16

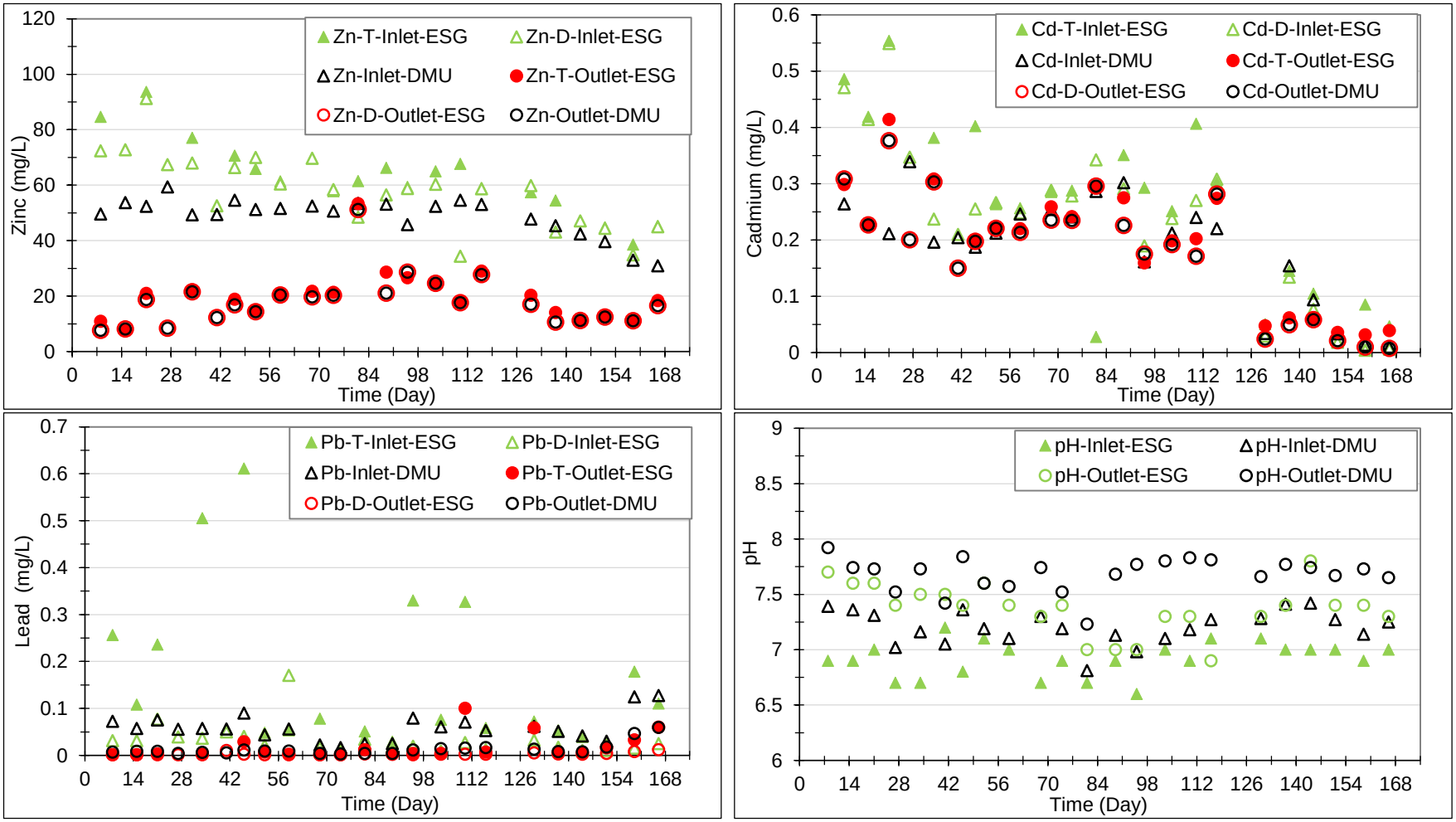

Figure 6-20: Comparison of concentrations of metals (zinc, cadmium and lead) and pH analyzed at DMU and ESG.

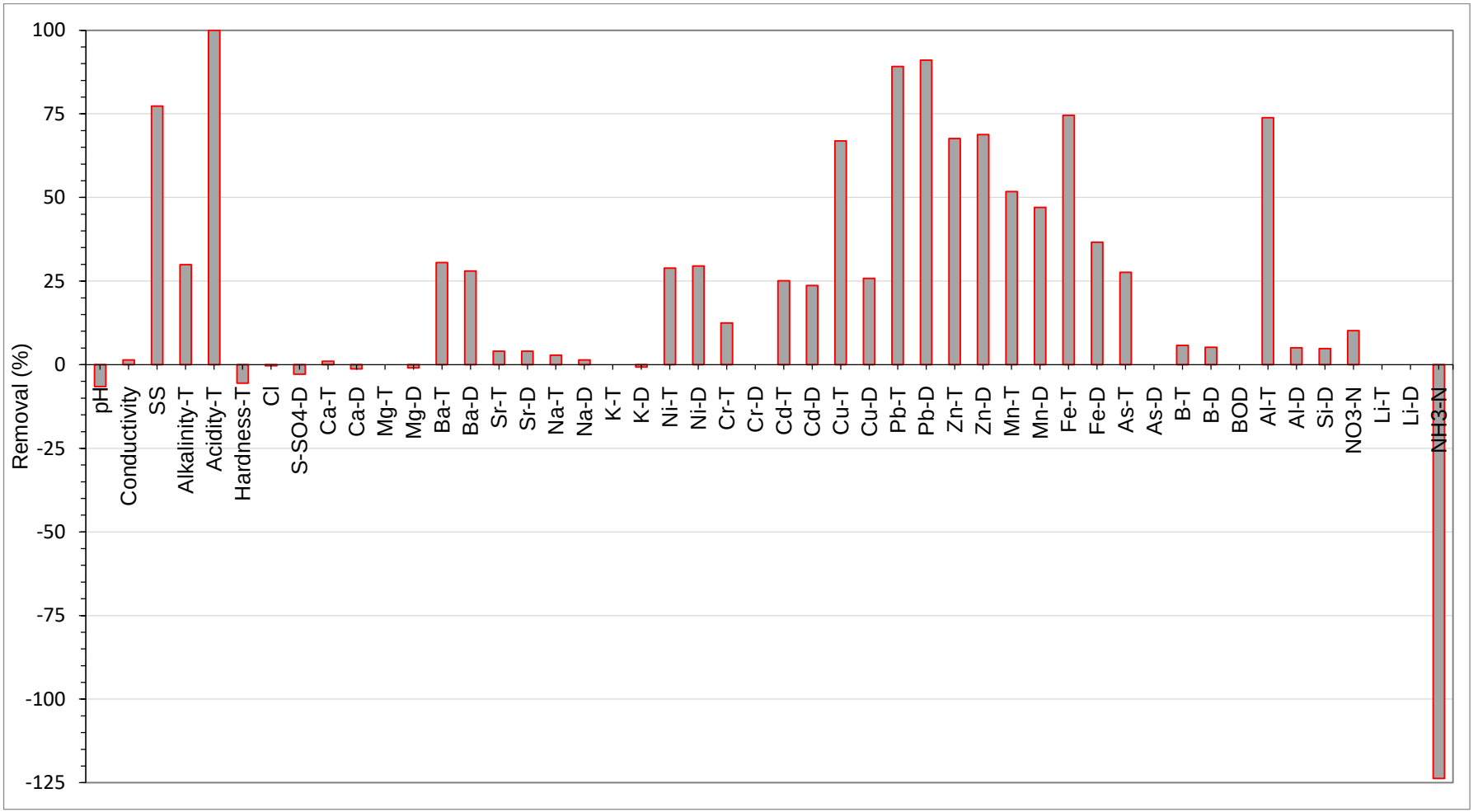

Figure 6-21: Average removal efficiencies of water quality parameters obtained from ESG.

6.4.4.1.2. REMOVAL OF ZINC

The mine water contains a high concentration of zinc. Figure 6-22 presents the DMU results for concentrations of zinc before and after treatment and the corresponding percentage removals. The average concentration of zinc in the Minsterley non-coal mine water was 49.14 mg/L with the lowest and the highest values as 26.0 mg/L and 63.55 mg/L respectively. The average removal of zinc in this trial was 64.18 % with the highest removal at 90.58 %. The least removal (-15.32 %) was observed on the very next day, Day-79, after the regeneration process. Usually, at that time, water samples used to be very clear but on that particular day the outlet sample was found very dirty. It is suspected that the outlet sample was collected without draining the sampling tube thus including part of the regenerated solution.

Considering the average concentration of zinc and the total amount of mine water passed through the system, a total of 6.46 kg of zinc passed through the system. Considering an average removal rate of 64.18 %, a total of 4.15 kg of zinc was removed by the system. This total removal of zinc can be further quantified in terms of removals before and after the regeneration process. The average removal rates for zinc before and after the regeneration process were calculated as 70.4 % and 58.78 % respectively. The estimated average flow rate and concentration of zinc in mine water before regeneration process were 28.18 L/hr and 53.43 mg/L respectively. Thus, before the regeneration process, a total of 2.85 kg of zinc passed through the system of which 2.01 kg was removed. Similarly, after regeneration process, the total amount of zinc passed through and removed by the system are calculated as 3.53 kg and 2.07 kg respectively. The reduction in average removal rate after regeneration process can be related to a number of factors such as, washout of zinc (negative removal) immediately after regeneration process, decrease in inlet concentration and fluctuation of process parameters, mainly the flow rate. The removal of zinc as a function of flow rate is discussed separately in section 6.4.4.2.2.

Similarly, in Table 6-7, ESG analyses show the average concentrations of zinc-total (Zn-T) and zinc-dissolved (Zn-D) in inlet mine water during this trial were as 62.86 mg/L and 58.28 mg/L respectively. The average removal rates of Zn-T and Zn-D were 67.65 % and 68.77 % respectively. Based on these values, the estimated amount of 8.26 kg (Zn-T) and 7.66 kg (Zn-D) of zinc was passed through the system of which 5.59 kg (Zn-T) and 5.27 kg (Zn-D) was removed.

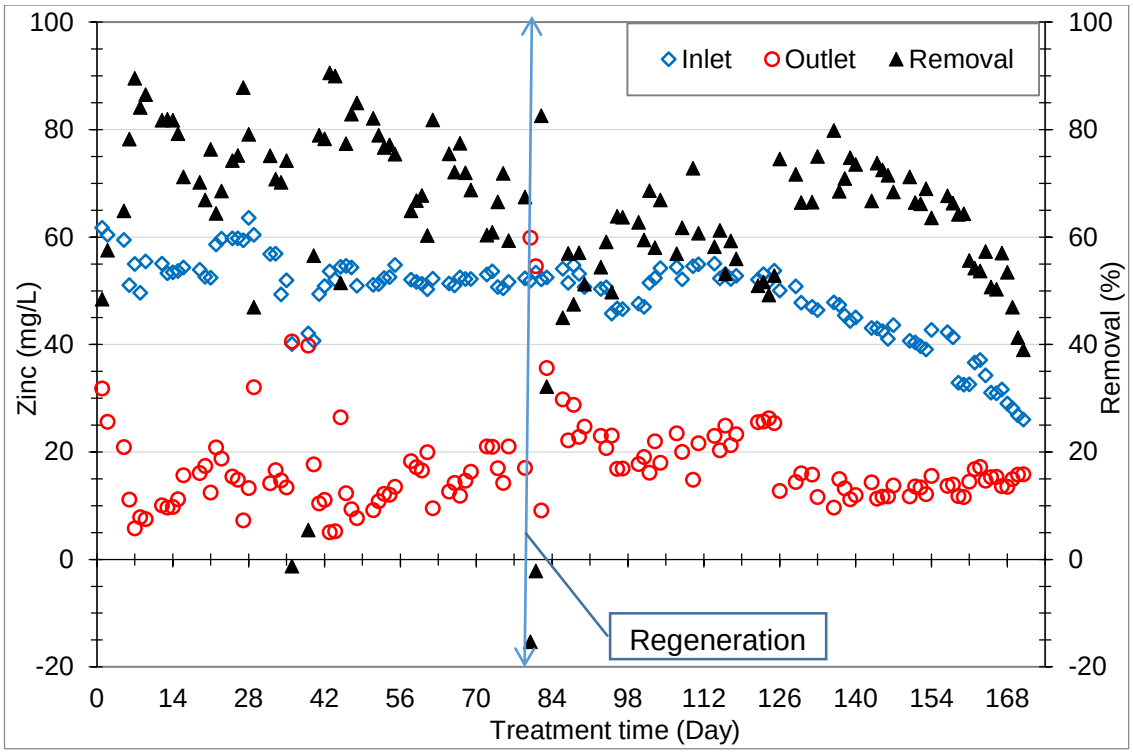

Figure 6-22: Inlet and outlet concentrations of zinc and the corresponding percentage removals measured at DMU.

6.4.4.1.3. REMOVAL OF CADMIUM

Figure 6-23 shows the DMU results for inlet and outlet concentrations of cadmium and corresponding removal rates. During this trial, the average concentration of cadmium in the mine water was 188.80 µg/L with the lowest and the highest concentrations measured as 39.00 µg/L and 373.00 µg/L. The average removal rate for cadmium was 22.37 %.

Considering the average concentration of cadmium (188.80 µg/L) and a total volume of treated mine water (131.46 m^3), a total estimated amount of 24.82 g of cadmium passed through the system. Considering an average removal rate of 22.37 %, 5.55 g of cadmium was removed by the system. The removal of cadmium can be quantified in terms of removal before and after the regeneration process. The average inlet concentration and removal rate of cadmium before the regeneration process were 248.5 µg/L and 21.54 % respectively. This results in to an estimated total amount of 13.28 g of cadmium exposed to the system of which 2.86 g was removed. Similarly, with an average inlet concentration of 137.1 µg/L and removal rate of 23.08 %, after the regeneration process, a total of 10.66 g of cadmium was exposed to the system of which 2.46 g was removed. The average removal efficiencies for cadmium before and after the regeneration process

seem consistent; however, the fluctuation in daily removal efficiencies was high. The relationship between fluctuation in removal efficiencies and pH and temperature does not establish a defined particular trend.

In Table 6-7, ESG analyses show the average concentrations of cadmium-total (Cd-T) and cadmium-dissolved (Cd-D) as 258.80 µg/L and 237.90 µg/L respectively. The average removal rates of Cd-T and Cd-D were 25.05 % and 23.63 % respectively. Based on these values, an estimated amount of 34.02 g (Cd-T) and 31.27 g (Cd-D) of cadmium was passed through the system of which 8.53 g (Cd-T) and 7.39 g (Cd-D) was removed.

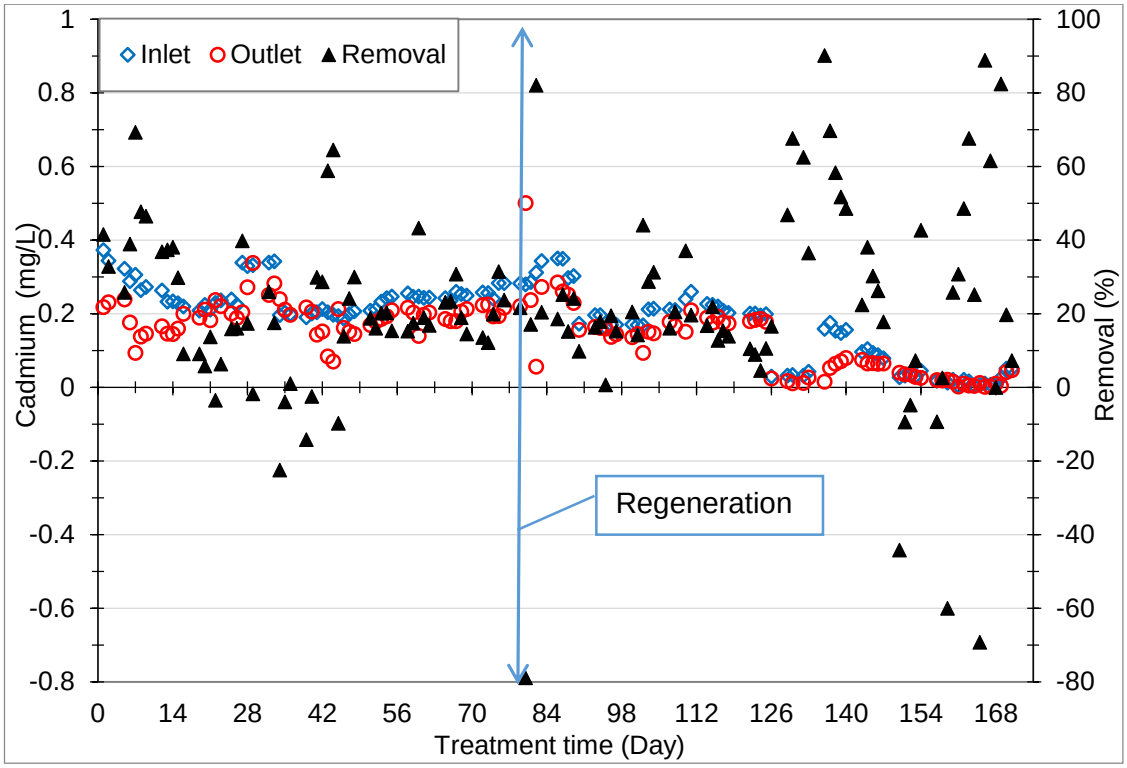

Figure 6-23: Inlet and outlet concentrations of cadmium and corresponding percentage removals measured at DMU.

6.4.4.1.4. REMOVAL OF LEAD

Amongst the three metals monitored by DMU, lead has the lowest concentration in the mine water. Figure 6-24 presents the DMU results for inlet and outlet concentrations of lead and corresponding percentage removals. During this trial, the average concentration of lead in the mine water was measured as 53.00 µg/L. The average removal rate of lead was 75.04 % with the highest and the lowest as 97.28 % and 40.42 % respectively. Using similar calculations as in above sections, an estimated total amount of 6.95 g of lead was exposed to the system of which 5.22 g was removed.

Before the regeneration process, the average concentration and removal rate of lead were 42.30 µg/L and 77.73 % respectively. This results into an estimated total amount of 2.26 g of lead exposed to the system of which 1.76 g was removed. Similarly, after the regeneration process, the average concentration and removal rate of lead were 62.00 µg/L and 72.75 % respectively. This results into a total amount of 4.82 g of lead exposed to the system of which 3.51 g was removed. Despite of variations of lead in the inlet mine water, the average removal efficiencies of lead before and after the regeneration process seem consistent. The correlation between concentrations of lead in the inlet water and the corresponding removals was examined (see Appendix 9-11).The values of correlation coefficient (r = - 0.237) and coefficient of determination (R^2 = 0.0562) suggest that the correlation between inlet concentration of lead and the corresponding removal efficiency is very weak.

In Table 6-7, ESG analyses show the average concentrations of lead-total (Pb-T) and lead-dissolved (Pb-D) as 155.10 µg/L and 32.60 µg/L respectively. The average removal rates of Pb-T and Pb-D were 89.16 % and 91.08 % respectively. Based on these values, an estimated amount of 20.39 g (Pb-T) and 4.30 g (Pb-D) of lead was passed through the system of which 18.18 g (Pb-T) and 3.92 g (Pb-D) was removed.

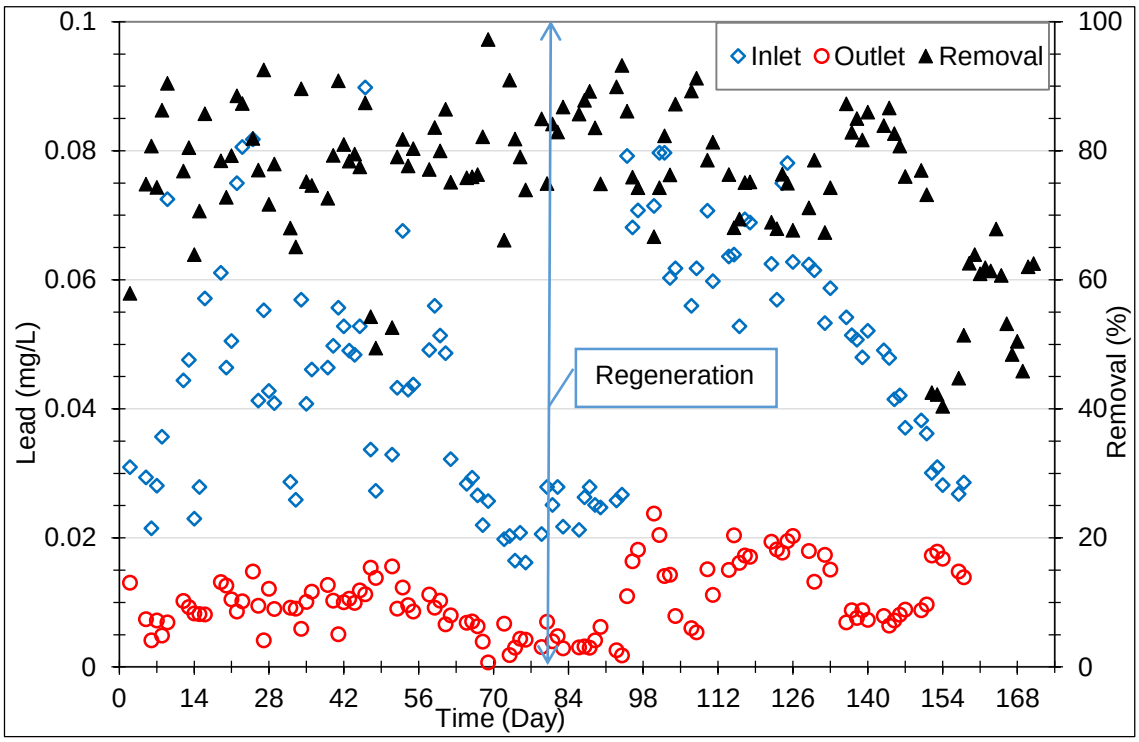

Figure 6-24: Inlet and outlet concentrations of lead and the corresponding percentage removals measured at DMU.

6.4.4.2. EFFECTIVENESS OF PROCESS PARAMETERS ON REMOVAL OF METAL IONS

The effectiveness of process parameters were studied by investigating the effect of individual parameters on the treatment process. Three process parameters were investigated for their effect on metal ions removal in the treatment process. These were regeneration of the ion exchange mesh, the residence time/flow rate and the rotation speed of the discs. The individual effects of each parameter are discussed in the following sections.

6.4.4.2.1. EFFECT OF REGENERATION OF ION EXCHANGE PAN MESH ON REMOVAL OF METALS

The regeneration of the ion exchange mesh was performed on Day-79 according to the procedures laid out in section 6.3.7, p. 216. The most time consuming phase during the regeneration process was the pH adjustment. This took about four to five hours for the pH to stabilize. This could be improved by using moderately concentrated NaOH (0.25 M or 0.5 M).

Figure 6-22 reveals that, after the regeneration process, the removal efficiencies of zinc gradually increased and reached over 80 %. However, on average, removal efficiency dropped by 10 % and stabilized around 65 %. However, as seen in Figure 6-23 and Figure 6-24, the removal efficiencies for cadmium and lead were not affected by the regeneration process. The detail calculation regarding the estimated total amounts of zinc, cadmium and lead desorbed during the regeneration process are given separately in the following sections.

6.4.4.2.1.1. AMOUNT OF ZINC DESORBED DURING THE REGENERATION PROCESS

As discussed in section 6.4.4.1.2, before the regeneration process, a total amount of 2.01 kg of zinc was removed by the system. Table 6-10 shows a total amount of 1.71 kg of zinc was desorbed off the mesh during the regeneration process. The amount desorbed off the mesh accounts 85.08 % of the total removal by the system. It is noteworthy to mention that more than 60 % (1.04 kg) of the total desorbed zinc (1.71 kg) was desorbed in the first batch of acid wash. The amount of metals desorbed off the mesh is expected to decrease in each subsequent acid wash. The higher amount present in the third acid wash could be as a result of slight variation in the duration of each acid wash which were performed for approximately 30 minutes. In addition, solutions for

regeneration were prepared crudely using bucket chemistry. Therefore, it is possible that the acid strength varied slightly in each acid wash.

Table 6-10: Concentration of zinc in the regenerated solutions.

Samples	Concentration of zinc after dilution (mg/L)	Dilution factor	Concentration of zinc before dilution (mg/L)	Volume used (L)	Total amount of desorbed zinc (g)
First acid wash	4.166	5,000.0	20,830.00	50	1041.50
Second acid wash	2.687	1,250.0	3,358.75	60	201.52
Third acid wash	6.535	625.0	4,084.37	60	245.06
Water wash	6.435	416.66	2,681.20	60	160.87
First NaOH wash	3.157	312.50	986.56	60	59.19
				Total (g)	1,708.15

After the regeneration process, mesh samples from inlet and outlet sides of the reactor were collected. These samples were digested in conc. HCl (~ 37 %) for two hours at 148 °C to determine the metal concentration per unit mass of regenerated mesh. Table 6-11 shows the metal ions content per gram of regenerated mesh. According to Table 6-11, the average zinc content was 3.6 mg/g of regenerated mesh. This sums to a total amount of 39.63 g of zinc which remained on the 11 kg of ion exchange mesh in the reactor. This suggests that the regeneration of the system desorbed 98.03 % of the total zinc (2.01 kg) off the mesh. The total amount of zinc in the regenerated solutions (1708.15 g) and the total amount of zinc on the regenerated mesh (39.63 g) equals to 86.95 % of the total zinc (2.01 kg) removed by the system. The remaining 13.05 % of zinc can be defined in terms of negative removals (washing off) in Figure 6-22 on days 80 and 81 when the treatment was restarted. It is also noteworthy to mention that the 2nd NaOH wash was not included in the calculation. The metal content is higher in outlet-side disc than inlet-side disc. In the regeneration process, the acid entered the reactor from the inlet side of the reactor. It is possible that there was some slight exhaustion of the acid on reaching

the outlet side. This would account for the slightly higher amount of metal ions remaining on the outlet side discs.

Table 6-11: Residual concentrations of zinc, cadmium and lead on per unit mass of regenerated PAN mesh

Samples	Zn (mg/g mesh)	Cd (mg/g mesh)	Pb (mg/g mesh)
Inlet side- Rep-1	2.696	0.0351	0.077
Inlet side- Rep-2	2.549	0.0314	0.081
Outlet side- Rep-1	4.332	0.0674	0.113
Outlet side- Rep-2	4.835	0.0628	0.108
Average (mg/g mesh)	3.603	0.0492	0.094
Total in the reactor (g)	39.633	0.541	1.034

6.4.4.2.1.2. AMOUNT OF CADMIUM DESORBED DURING THE REGENERATION

As discussed in section 6.4.4.1.3, before the regeneration process, a total amount of 2.86 g of cadmium was removed by the system. Table 6-12 shows that a total amount of 2.02 g of cadmium was desorbed off the mesh during the regeneration process. The desorbed amount of cadmium accounts 70.63 % of the total removal (2.86 g) by the system. Table 6-11 shows that the average residual concentration of cadmium on regenerated mesh was 0.0492 mg/g of mesh. This sums to a total amount of 0.54 g of cadmium which was remained on 11 kg of ion exchange mesh in the reactor. The residual amount of cadmium on regenerated mesh suggests that the regeneration of the system desorbed 81.12 % of the total cadmium (2.86 g) from the mesh.

Table 6-12: Concentration of cadmium in the regenerated solutions.

Samples	Concentration of cadmium after dilution (mg/L)	Dilution factor	Concentration of cadmium before dilution (mg/L)	Volume used (L)	Total amount of desorbed cadmium (g)
First acid wash	0.565	25	14.12	50	0.70
Second acid wash	0.389	25	9.72	60	0.58
Third acid wash	0.276	25	6.90	60	0.41

Samples	Concentration of cadmium after dilution (mg/L)	Dilution factor	Concentration of cadmium before dilution (mg/L)	Volume used (L)	Total amount of desorbed cadmium (g)
Water wash	0.352	10	3.52	60	0.21
First NaOH wash	0.175	10	1.75	60	0.10
			Total (g)		2.02

The total amount of cadmium (2.02 g) desorbed in the regenerated solutions and the total amount of cadmium remained on the regenerated mesh (0.54 g) equals to 89.51 % of the total cadmium (2.86 g) removed by the system. The remaining 10.49 % of cadmium can be defined in terms of negative removals (washing off) in Figure 6-23 on Day-80.

6.4.4.2.1.3. AMOUNT OF LEAD DESORBED DURING THE REGENERATION PROCESS

As discussed in section 6.4.4.1.4, before the regeneration process, a total amount of 1.76 g of lead was removed by the system. Table 6-13 shows that a total amount of 1.73 g of lead was desorbed off the mesh during the regeneration process. The desorbed amount of lead accounts 98.30 % of the total removal by the system.

Table 6-13: Concentration of lead in the regenerated solutions.

Samples	Concentration of lead after dilution (mg/L)	Dilution Factor	Concentration of lead before dilution (mg/L)	Volume used (L)	Total amount of desorbed lead (g)
First acid wash	6.802	2	13.604	50	0.6802
Second acid wash	3.732	2	7.464	60	0.44784
Third acid wash	5.23	1	5.23	60	0.3138
Water wash	3.958	1	3.958	60	0.23748
First NaOH wash	0.758	1	0.758	60	0.04548
			Total (g)		1.7248

Table 6-11 shows that the average lead content on the regenerated mesh was 0.094 mg/g. This sums to a total amount of 1.03 g of lead which remained on the 11 kg of mesh

in the reactor. This, contrary to Table 6-13, suggests that only 41.48 % of the total lead (1.76 g) was desorbed off the mesh.

The total amount of lead in the regenerated solutions (1.73 g) and the total amount of lead remained on the regenerated mesh (1.03 g) equals to 156.82 % of the total lead (1.76 g) removed by the system. Figure 6-24 shows no washing-off of lead after the regeneration process. Therefore, the excess 56.82 % of lead can be defined in terms of contribution from the lead total (Pb-T) and the solid residue filtered by the mesh. This is elaborated in the following section.

6.4.4.2.1.4. OCCURRENCE OF METALS IN THE MINE WATER

Figure 6-25 compares the average values of total and dissolved concentrations of zinc, cadmium and lead in the inlet water before the regeneration process and throughout this trial. As seen in Figure 6-25, most of zinc and cadmium were present in the dissolved form whereas most of lead was present as total (solid) lead.

Figure 6-26 presents the ratio of zinc-total to zinc-dissolved (Zn-T/Zn-D), cadmium-total to cadmium-dissolved (Cd-T/Cd-D) and lead-total to lead-dissolved (Pb-T/Pb-D). The ratios of Zn-T/Zn-D and Cd-T/Cd-D before regeneration process were 1.04 and 1.22 respectively whereas the ratio of Pb-T/Pb-D was 5.76. This shows that all the zinc was present in the dissolved form and over 80 % of cadmium were also present in the dissolved form. However, contrary to zinc and cadmium, only 17 % of lead was present in the dissolved form, suggesting 83 % of the lead was present as solids.

As shown in Table 6-7 and Figure 6-21, on average, 77.31 % of suspended solids (SS) were removed during this trial. The average concentration of suspended solids in the inlet water samples was 47.9 mg/L. In 24 weeks 2 days, this results in a total amount of 6.30 kg of suspended solids which passed through the system. This suggests that 4.87 kg of suspended solids was removed by the system. This removal can also be quantified as removal before the regeneration process. Before the regeneration process, the average concentration and removal rates for suspended solids were 67.2 mg/L and 86.87 % respectively. Therefore, before the regeneration process, a total of 3.59 kg of suspended solids was passed through the system of which 3.12 kg was retained by the system.

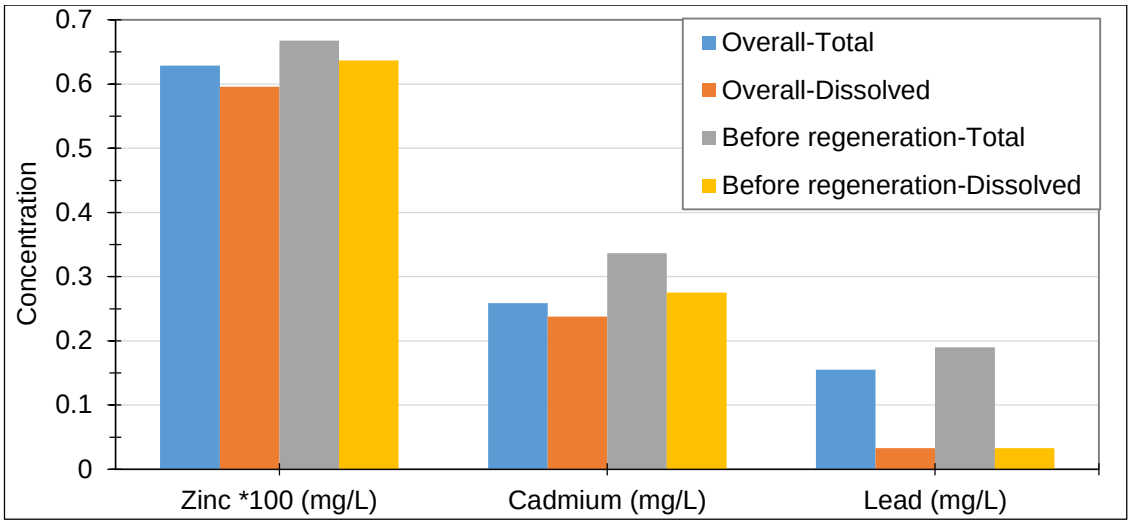

Figure 6-25: Average inlet concentrations of zinc, cadmium and lead before the regeneration process and throughout the trial analyzed by ESG.

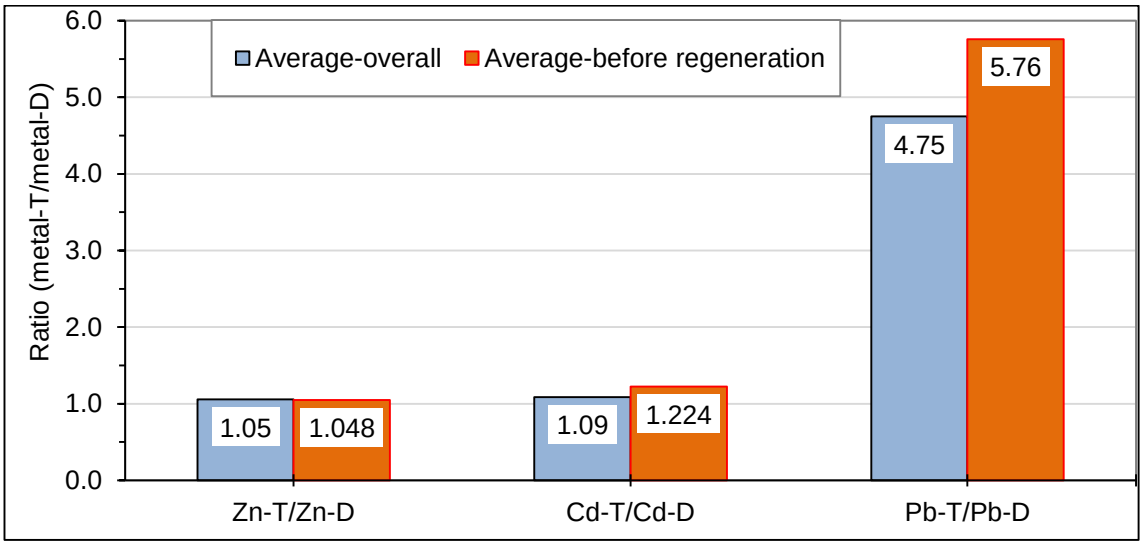

Figure 6-26: Ratio of average concentrations of total to dissolved metals in the inlet mine water.

The first acid wash regenerant in Appendix 9-8 shows that the regeneration process was successful in removing significant amount of total solids retained on the modified PAN mesh. Significant amount of soil was present in the inlet water, especially, during heavy rainfall in the Minsterley catchment. The soil was exposed to the system mostly on tankering day as a result of fresh feed mixing with sludge settled in the feed tank. Therefore, if the water samples for external analyses were not taken on the tankering day then the total amount of suspended solids passed to the system could be much higher than above calculation. Therefore, the higher amount of suspended solids would result in higher lead content. Possibly, this could be the best explanation for the excess amount (56.82 %) of lead desorption during regeneration process.

6.4.4.2.2. EFFECT OF FLOW RATES ON REMOVAL OF METAL IONS

The flow rate determines the residence time (RT) and the mass transfer in the reactor. Lower flow rate decreases the pollutants load and increases the residence time and vice versa. It is believed that the lower flow rate increases removal efficiency by ensuring effective mass transfer between the solution and the rotating discs. This effect was investigated by increasing the flow rate from 30 L/hr to 45 L/hr and 60 L/hr respectively. The reactor volume was 60 L. Therefore, flow rates of 30 L/hr, 45 L/hr and 60 L/hr correspond to residence time of two hours, 1.33 hours and one hour respectively. The effect of flow rate on removal of metal ions was also observed when the dosing pump behaved erratically by reducing / increasing the desired set flow rate. It is noteworthy to mention here that after increasing the flow rate, STS had to tanker more frequently and there were some significant variations in inlet water quality. For example, there was a significant decrease in zinc concentration from ~ 50 mg/L to ~ 25 mg/L and presence of algae. The gradual variation in zinc concentration in inlet mine water is not due to the seasonal change on site at White Tip. It is found that STS did not use same tankering methodology as IWS and collected water from run-off entering a pond. The routine monitoring at White Tip did not show same variation in concentrations suggesting it was sampling bias rather than the seasonal variation in water quality.

Figure 6-27 presents the results from day 125 to the end of this project. The flow rate of 30 L/hr increased to 45 L/hr on Day-143 and further increased to 60 L/hr on Day-159. The average flow rates from Day-125 to Day-143, Day-144 to Day-159 and Day-160 to Day-170 were 31.36 L/hr, 43.7 L/hr and 59.45 L/hr respectively. The corresponding removal efficiencies for zinc during these periods were 71.84 %, 67.61 % and 50.86 % respectively. Similarly, the corresponding removal efficiencies for lead were 79.36 %, 61.45 % and 57.76 % respectively. However, the removal of cadmium did not follow a particular trend.

In the case of zinc, there was no significant drop in removal efficiency when the flow rate was increased by 1.5 folds (30 L/hr to 45 L/hr). Meanwhile, a 21% reduction in the removal efficiency of zinc was observed when the flow rate was doubled (30 L/hr to 60 L/hr). The removal efficiency for lead dropped by 18 % when the flow rate increased by 1.5 folds from 30 L/hr to 45 L/hr. However, a further increase in flow rate did not result in a significant reduction in removal efficiency bringing the reduction in removal of lead to 21 % when the flow rate doubled.

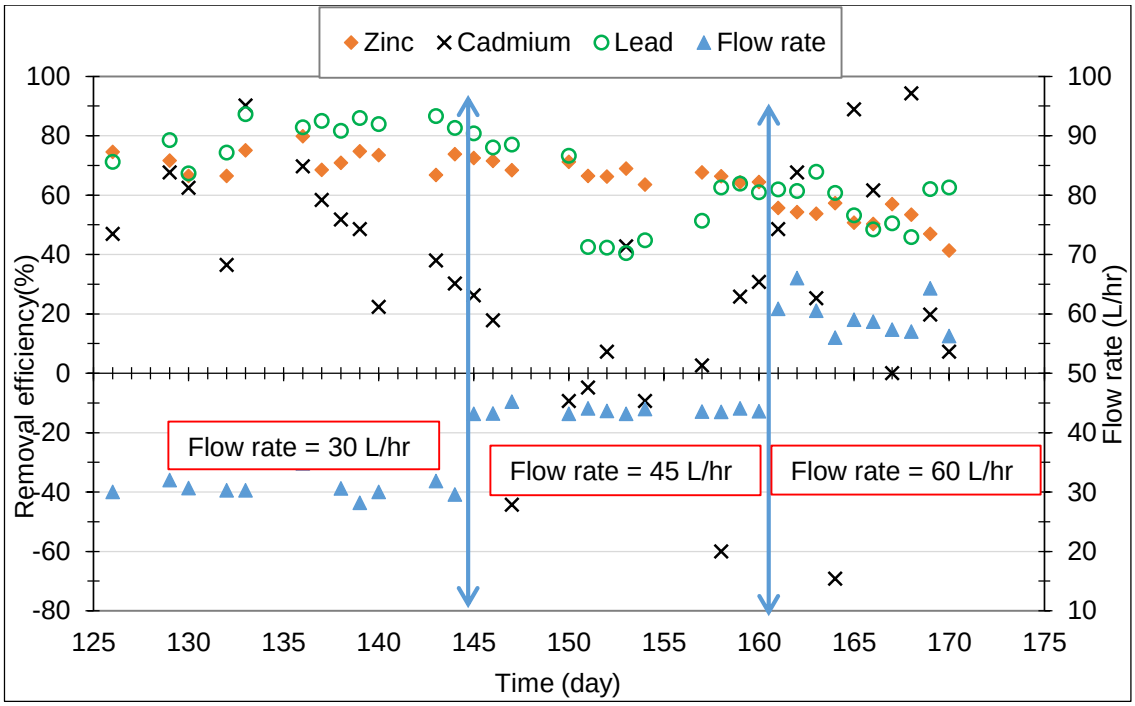

Figure 6-27: Effect of flow rate on removal of zinc, cadmium and lead (DMU analyses from Day-125 to Day-170).

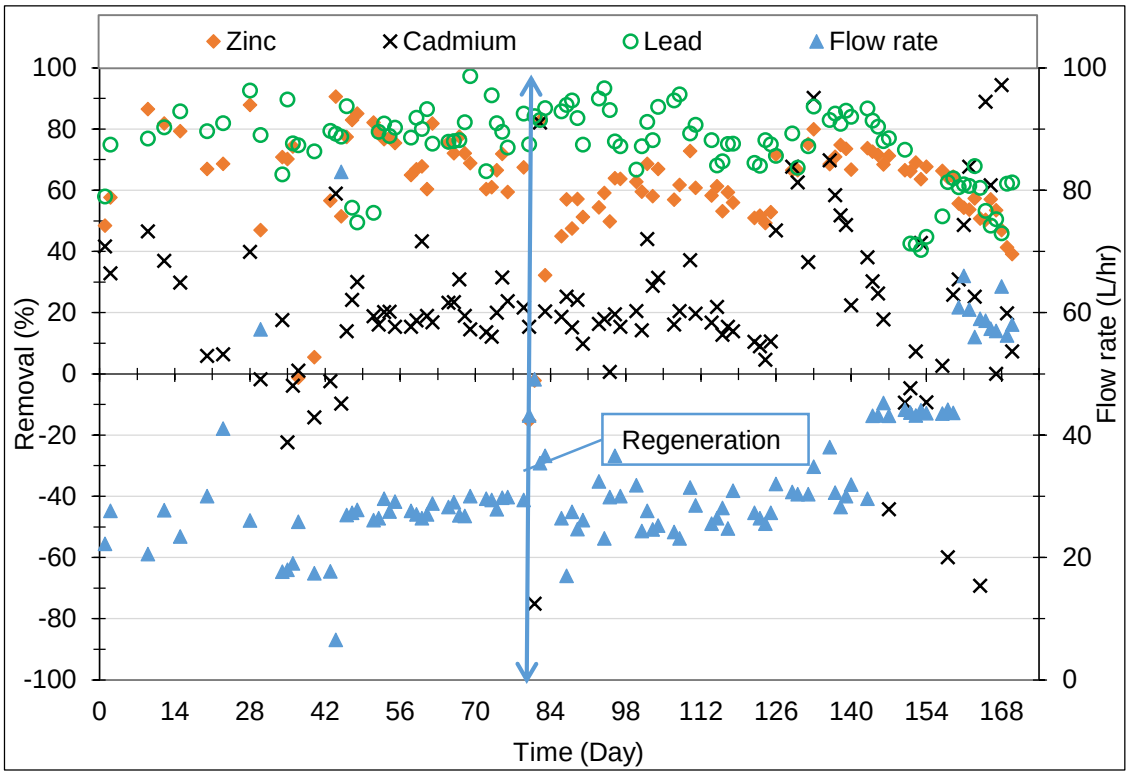

Figure 6-28: Comparison of removal rates of zinc, cadmium and lead as a function of flow rate (DMU analyses from day 1 to day 170).

Figure 6-28 compares the removal rates of zinc, cadmium and lead as a function of flow rate from the beginning to the end of the trial. The removal of zinc reduced to 47 % on

Day-32 when a flow rate of 57.24 L/hr was measured implying a reduction in the residence time by half from two hours to one hour. This is in contrast to the average 70 % removal of zinc observed before and after Day-32 when the residence time was ~ 2.25 hours. Similarly, a high removal (90 %) of zinc was achieved on Day-44 when a flow rate of 6.5 L/hr was measured. This flow rate increased the residence time by ~ 5 folds from two hours to 9.25 hours.

Figure 6-29 compares the removal rates of zinc, cadmium and lead as a function of flow rates in ascending order. Figure 6-29 suggests that for the removal of zinc, cadmium and lead, the ideal flow rate should be kept at or below 45 L/hr (RT ≥ 1.33 hours). This will obviously vary depending on the flow rate, reactor size, water quality and amount of mesh loaded on the discs.

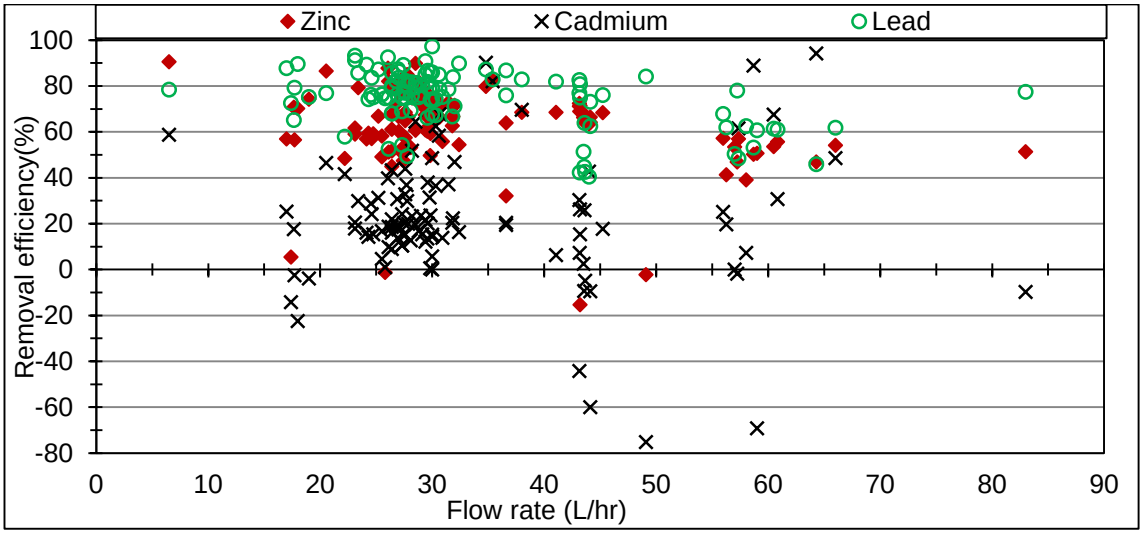

Figure 6-29: Removal rates of zinc, cadmium and lead as a function of flow rate.

6.4.4.2.3. EFFECT OF ROTATION SPEED OF THE DISCS ON METAL IONS REMOVAL

The rotation speed of the discs influences the removal efficiency of metals by influencing mixing and contact time. It is believed that faster rotation enhances mixing of the mine water but reduces mesh-water contact time. This effect was investigated by varying the rotation speed of the discs. This trial commenced with an initial rotation speed of the discs at ten revolutions per minute (rpm). The rotation speed was lowered to 2.5 rpm on Day-118 and the system was run for three weeks, until Day-125 where upon it reverted to 10 rpm. Figure 6-30 presents the DMU results for removal rates of zinc, cadmium and lead with respect to rotation speed of the discs from Day-83 to Day-143. Lowering the rotation speed by a factor of four did not affect the removal of metal ions with the removal

trends for zinc, cadmium and lead remained almost the same. The removal trends for zinc, cadmium and lead can also be seen in Figure 6-17, Figure 6-18 and Figure 6-19 respectively.

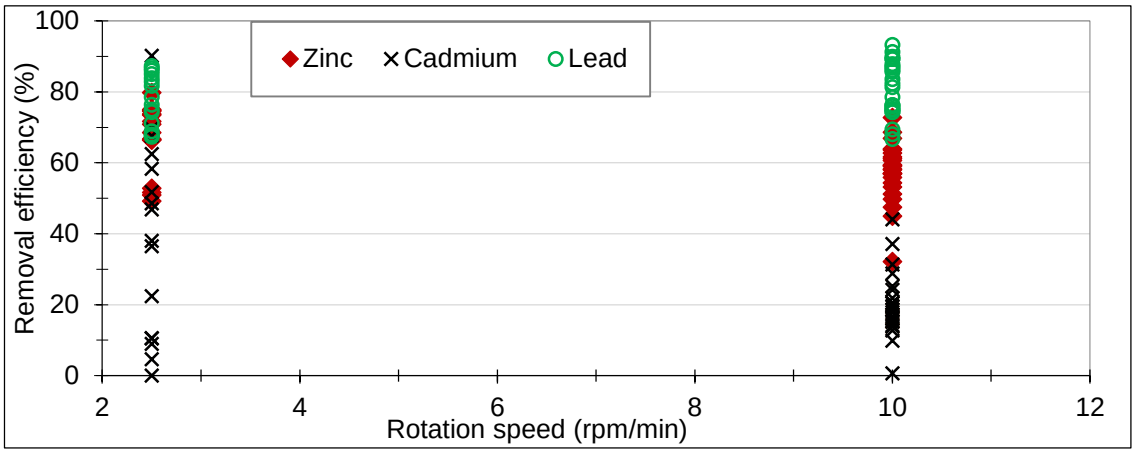

Figure 6-30: Removal (%) of zinc, cadmium and lead as a function of rotation speed of the discs.

6.4.4.3. MECHANISM OF REMOVAL: ION EXCHANGE / SORPTION / PRECIPITATION

In order to assess the amounts of metals sorbed onto the ion exchange mesh, samples of mesh were taken, at the end of the experiment, from the first and last discs in each sections of the reactor. The first and the second sections contained seven discs each and the third and the fourth sections contained eight discs each. The samples from the first disc of each section were taken from the inlet side of the disc whereas from the last disc samples were taken from the outlet side of the disc. Before analyses, all the mesh samples were air-dried to get rid of moisture (see Appendix 9-12). The mesh discs became darker due to soiling, suspended solids removed (1.36 kg) by the system. The discs towards inlet end of the reactor were darker than those on the outlet end.

To enable an estimation of metal content per gram of mesh arising from precipitation in comparison to ion exchange / sorption, the solid residues were removed from the mesh samples at the end of the trial by gently squeezing and tapping the mesh onto a paper sheet (see Appendix 9-13). Mesh samples were weighed before and after removing solid residues. The difference between the two was considered as the weight of solid residues that comprised both soil and metal salts precipitate. The residues and the voided mesh were each digested separately in replicates as described in section 6.4.4.2.1. The amount of metal digested off each mesh sample and the amount of metal contained in each corresponding residue were used to calculate the total metal content per gram of mesh for each sample. Metal content was calculated based on the weight of dried mesh after digestion.

Possible sources of error are that some residue might have remained on the mesh resisting digestion, resulting in a metal content per gram of mesh that is lower than the true value. Similarly, it is possible to lose some fibrils during digestion and filtration. The contribution from these is believed to be insignificant. The metal contents from the two replicates were found to be close and the average values were used in the calculation. Table 6-14,

Table 6-15 and

Table 6-16 present the results (average of two replicates) of digestions of mesh samples and their residues. Table 6-14 shows that the total amount of zinc content in reactor was 2.64 kg. This is close to the estimated total amount of zinc (2.07 kg) that was removed after the regeneration process, Day-79 to Day-170. Table 6-14 reveals an important finding that, on average, at least 76.5 % of the total zinc removed by the system was precipitated onto the mesh.

Table 6-15 shows that the total amount of cadmium content in reactor was 2.54 g. This is also equivalent to the estimated total amount of cadmium (2.46 g) that was removed after the regeneration process. Table 6-15 again reveals that, on average, at least 47 % of the total cadmium removed by the system was precipitated onto the mesh.

Similarly,

Table 6-16 shows that the total amount of lead content in reactor was 7.77 g. This is 2.2 folds higher than the estimated total amount of lead (3.51 g) that was removed after the regeneration process. The higher amount of lead desorbed off the mesh is related to the higher value of lead total (Pb-T) which is not accounted in the DMU estimation and is discussed in section 6.4.4.2.1.4. ESG results in Table 6-7 show that, after the regeneration process, an estimated total amount of 8.76 g of Pb-T passed through the system. Considering an average removal efficiency of lead (77.36 %) after the regeneration process, 6.78 g of Pb-T was removed by the system. This amount is equivalent to the total amount of lead desorbed during digestion of mesh samples.

Table 6-16 again reveals that, on average, at least 63.2 % of the total lead removed by the system was precipitated onto the mesh.

The estimated total amounts of zinc (2.64 kg), cadmium (2.54 g) and lead (7.77 g) desorbed off the mesh samples (taken at the end of the trial) are equivalent to the estimated total amounts of zinc (2.58 kg), cadmium (2.72 g) and lead (6.78 g) removed by the system after the regeneration process. This suggests that the metal ions were removed by means of ion exchange and precipitation facilitated by the mesh. This also provides the evidence that the precipitation occurred onto the surface of mesh and not at the base of reactor.

The average metal content in each sections of the reactor, according to Table 6-14,

Table 6-15 and
Table 6-16, is the highest in the first section followed by the second, the third and the fourth sections respectively. Figure 6-31 shows a linear reduction of zinc, cadmium and lead concentration with respect to subsequent reactor sections. This is expected as the discs towards the inlet side of the reactor are the first to be contacted with the fresh feed. Therefore, the metal ions loading reduces as the feed flows through each section.

The amounts of zinc removed before (2.01 kg) and after (2.07 kg) the regeneration process suggest the uptake capacities of ion exchange mesh as 182.73 mg/g and 188.2 mg/g respectively. These capacities are much larger than the maximum sorption capacity (12.79 mg/g mesh) predicted by Langmuir adsorption isotherm model given in Table 6-3, indicating the existence of two or more removal mechanisms. The uptake capacity of mesh in the presence of multiple removal mechanisms is not known at this stage as treatment was halted before having breakthrough in the performance. Assuming the earliest possible saturation scenario by considering the metal content in the first section of the reactor as the concentration close to the saturation, as shown in

Table 6-17, the treatment system can remove at least an additional 1.2 kg of zinc, 0.97 g of cadmium and 3.21 g of lead. This suggests that the system could have been in operation for at least a further six weeks (Table 6-14,

Table 6-15 and

Table 6-16 show 2.64 kg of Zn, 2.54 g of Cd and 7.77 g of Pb removed in 13 weeks) without interruption.

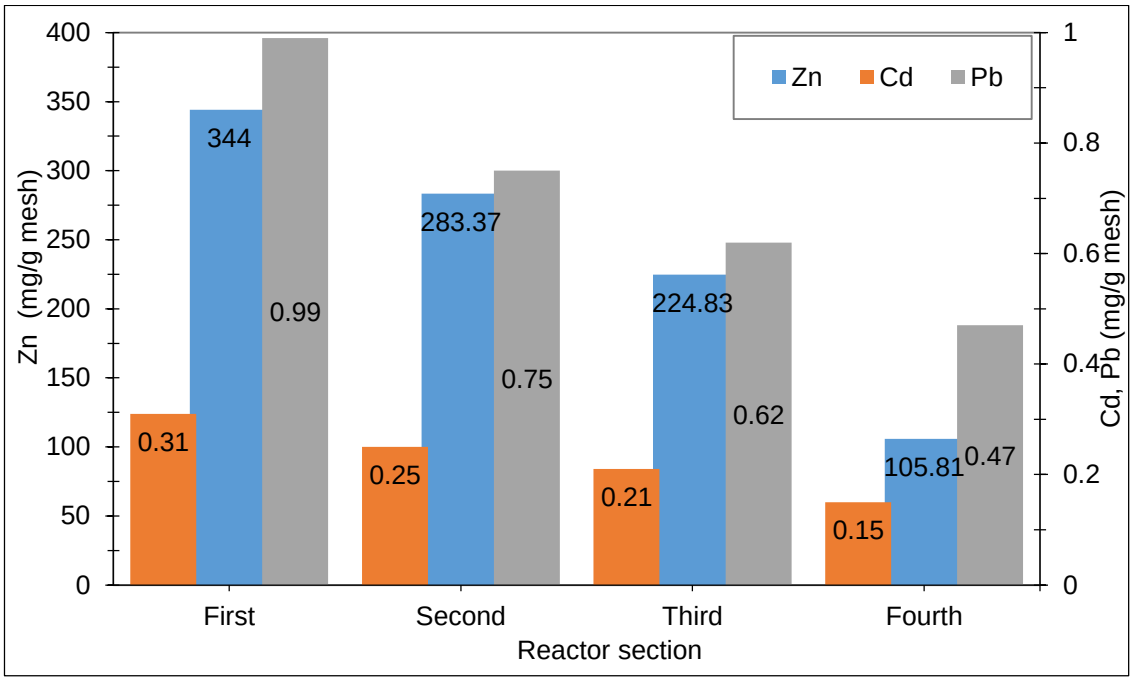

Figure 6-31: Removal of zinc, cadmium and lead with respect to the reactor sections.

Table 6-14 : Concentrations of zinc (recovered after the regeneration process) on mesh samples taken from the discs at the end of the trial.

Samples taken from	Average weight of mesh (g)			Weight of residue (g) (D= A-B)	Amount of zinc desorbed (mg)				Amount of zinc (mg/g mesh) (H=G/C)	Average amount of zinc (mg/g mesh) (H=G/C)
	Before removing residue (A)	After removing residue (B)	After digestion (C)		Mesh (E)	Residue (F)	Total (G=E+F)	Zinc in residue (%) ((F/G)*100)		
Section 1 First disc	0.8950	0.5795	0.4934	0.3155	38.06	133.2	171.26	77.77	347.13	**344.00**
Section 1 Last disc	1.2435	0.776	0.6512	0.4676	51.84	170.16	222.00	76.64	340.91	
Section 2 First disc	1.0199	0.6963	0.5912	0.3237	39.97	138.44	178.41	77.59	301.77	**283.37**
Section 2 Last disc	1.0627	0.7636	0.6452	0.2992	45.72	125.24	170.96	73.25	264.97	
Section 3 First disc	0.9442	0.7274	0.6321	0.2168	30.42	91.88	122.29	75.13	193.49	**224.83**
Section 3 Last disc	0.8578	0.6138	0.5409	0.2441	24.59	113.96	138.55	82.25	256.18	
Section 4 First disc	0.7064	0.5987	0.5409	0.1077	12.25	41.66	53.91	77.27	99.68	**105.81**
Section 4 Last disc	0.8818	0.74	0.6621	0.1418	23.28	50.84	74.124	68.58	111.95	
		Average zinc (mg)			33.26	108.17	141.44	76.48	239.51	
		Total amount of zinc in the reactor (kg) (H*11 kg (amount of mesh in the reactor))							**2.64**	

Table 6-15: Concentrations of cadmium (recovered after the regeneration process) on mesh samples taken from the discs at the end of the trial.

Samples	Average weight of mesh (g)			Weight of residue (g) (D=A-B)	Amount of cadmium desorbed (mg)				Amount of Cd (mg/g mesh) (H=G/C)	Average amount of Cd in each section of the reactor (mg/g mesh)
	Before removing residue (A)	After removing residue (B)	After digestion (C)		Mesh (E)	Residue (F)	Total (G=E+F)	Cd in residue (%) ((F/G)*100)		
First disc section 1	0.8950	0.5795	0.4934	0.3155	0.06	0.07	0.13	54.16	0.27	**0.31**
Last disc section 1	1.2435	0.776	0.6512	0.4676	0.09	0.14	0.23	62.32	0.30	
First disc section 2	1.0199	0.6963	0.5912	0.3237	0.08	0.06	0.13	45.89	0.24	**0.25**
Last disc section 2	1.0627	0.7636	0.6452	0.2992	0.08	0.08	0.17	50.09	0.26	
First disc section 3	0.9442	0.7274	0.6321	0.2168	0.07	0.04	0.12	37.49	0.19	**0.21**
Last disc section 3	0.8578	0.6138	0.5409	0.2441	0.07	0.05	0.12	44.15	0.2	
First disc section 4	0.7064	0.5987	0.5409	0.1077	0.06	0.02	0.08	25.52	0.15	**0.15**
Last disc section 4	0.8818	0.74	0.6621	0.1418	0.07	0.03	0.11	28.97	0.16	
		Average cadmium (mg)			0.07	0.06	0.14	46.77	0.23	
		Total amount of cadmium in the reactor (g) (H*11 kg (amount of mesh in the reactor))							**2.54**	

Table 6-16: Concentrations of lead (recovered after the regeneration process) on mesh samples taken from the discs at the end of the trial.

Samples	Average weight of mesh (g)			Weight of residue (g) (D=A-B)	Amount of lead desorbed (mg)				Amount of lead (mg/g mesh) (H=G/C)	Average amount of lead in each section of the reactor (mg/g mesh)
	Before removing residue (A)	After removing residue (B)	After digestion (C)		Mesh (E)	Residue (F)	Total (G=E+F)	Lead in residue (%) ((F/G)*100)		
First disc section 1	0.8950	0.5795	0.4934	0.3155	0.15	0.32	0.47	67.43	0.95	**0.99**
Last disc section 1	1.2435	0.776	0.6512	0.4676	0.20	0.47	0.67	69.92	1.03	
First disc section 2	1.0199	0.6963	0.5912	0.3237	0.14	0.32	0.46	69.72	0.78	**0.75**
Last disc section 2	1.0627	0.7636	0.6452	0.2992	0.16	0.30	0.46	64.77	0.72	
First disc section 3	0.9442	0.7274	0.6321	0.2168	0.14	0.22	0.36	60.85	0.56	**0.62**
Last disc section 3	0.8578	0.6138	0.5409	0.2441	0.12	0.24	0.36	67.75	0.67	
First disc section 4	0.7064	0.5987	0.5409	0.1077	0.14	0.11	0.26	42.57	0.47	**0.47**
Last disc section 4	0.8818	0.74	0.6621	0.1418	0.18	0.14	0.32	44.61	0.48	
		Average lead (mg)			0.15	0.26	0.42	63.17	0.71	
		Total amount of lead in the reactor (g) (H*11 kg (amount of mesh in the reactor))							**7.77**	

Table 6-17: Estimated additional amount of metal ions that can be removed by the second, third and fourth section of the reactor.

Total mesh in the reactor (kg) (A)	Total no. of discs in the reactor (B)	Reactor section	Number of discs in the reactor section (C)	Amount of mesh in the section (kg) [D=(A/B)*C]	Average metal content in the reactor sections after the regeneration process (mg/g mesh)			Estimated amount of additional metal ions that can be removed by 2nd, 3rd and 4th sections of the reactor (g)		
					Zinc	Cadmium	Lead	Zinc	Cadmium	Lead
11	30	First section	7	2.57	344.02	0.31	0.99			
11	30	Second section	7	2.57	283.37	0.25	0.75	155.66	0.16	0.61
11	30	Third section	8	2.93	229.23	0.21	0.61	336.72	0.29	1.09
11	30	Fourth section	8	2.93	105.81	0.15	0.47	698.74	0.45	1.51
			Additional total amounts of metal that can be removed (g)					**1191.13**	**0.97**	**3.21**

6.4.4.4. pH AND TEMPERATURE

pH and temperature were monitored by two sets of MadgeTech data loggers which were positioned nearer to the inlet and outlet ends of the reactor. Data loggers were set to record temperature and pH at every two minutes intervals.

Figure 6-32 shows the inlet and outlet water temperatures recorded during this trial. There was sudden rise in temperature on day 79 when the regeneration process was performed. During the regeneration process, temperature probes were taken off the reactor and immersed into warm tap water. Figure 6-32 shows that the treatment process was operated within the temperature range of 0.7 °C to 20 °C. Figure 6-17, Figure 6-18 and Figure 6-19 show no effect of temperature fluctuation on the removal of zinc, cadmium and lead.

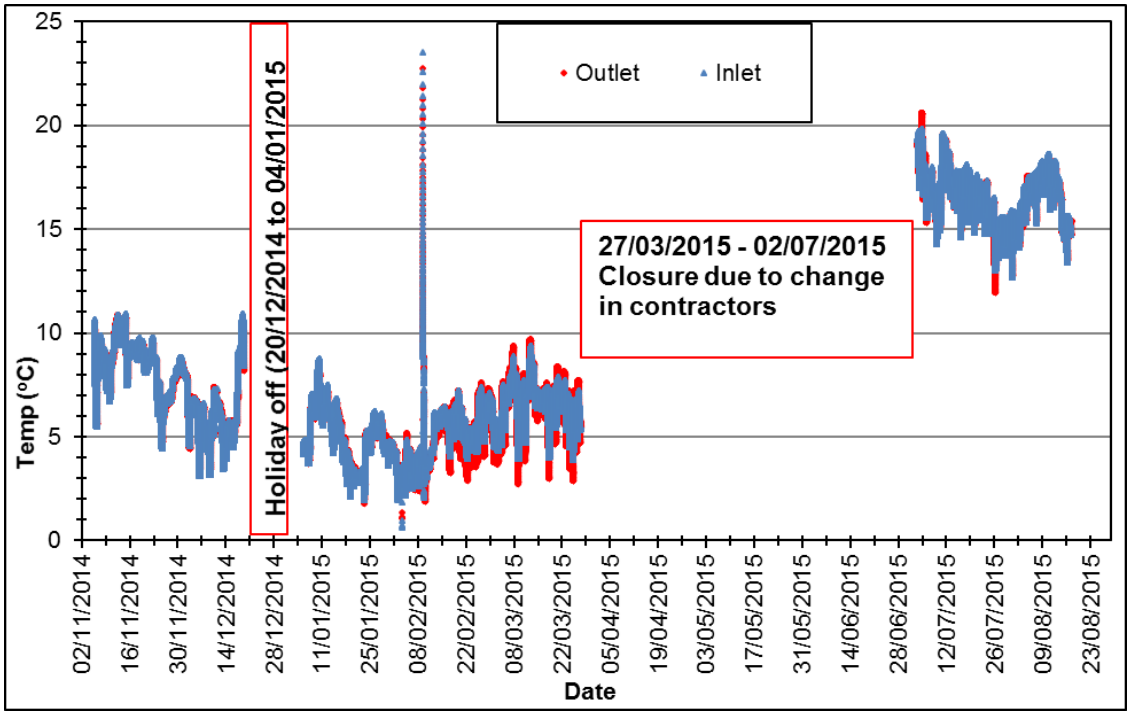

Figure 6-32: Reactor inlet-end and outlet-end water temperatures recorded by online data loggers.

Figure 6-33 shows the inlet and outlet water pH recorded during this trial. The system started with a high pH (10.2) arising from residual alkali used in mesh production process and quickly stabilized at just below pH 8 within 24 hours. The sharp fluctuation in pH on Day-79 marks the regeneration process. The minimal differences in inlet and outlet pH values indicate the effective mixing of water in the reactor. The true pH readings of inlet and outlet samples were measured with a manual pH meter at DMU and the results are shown in Figure 6-34. The average pH of inlet water was 7.21 with standard deviation

0.15. An average rise of ~ 0.5 unit pH was observed in treated water samples. In order to investigate the rise of pH in treated water, a control experiment was performed with five litres of mine water stirred with an overhead mechanical stirrer.

Figure 6-35 shows the result of the control experiment performed to investigate pH rise. Mine water with a starting natural pH of 7.99 eventually stabilized to a pH of 8.30. It is believed that the rise in pH was due to degassing of dissolved carbon dioxide from the mine water. Degassing of dissolved carbon dioxide shifts the equilibrium from bicarbonate towards carbonic acid resulting in the consumption of hydrogen ions thus increasing the pH. The relatively lower and slower rise of 0.31 unit pH in control experiment compared to ~ 0.5 unit pH rise during this trial could be attributed to the natural degassing of carbon dioxide during the six months storage of mine water in the control experiment.

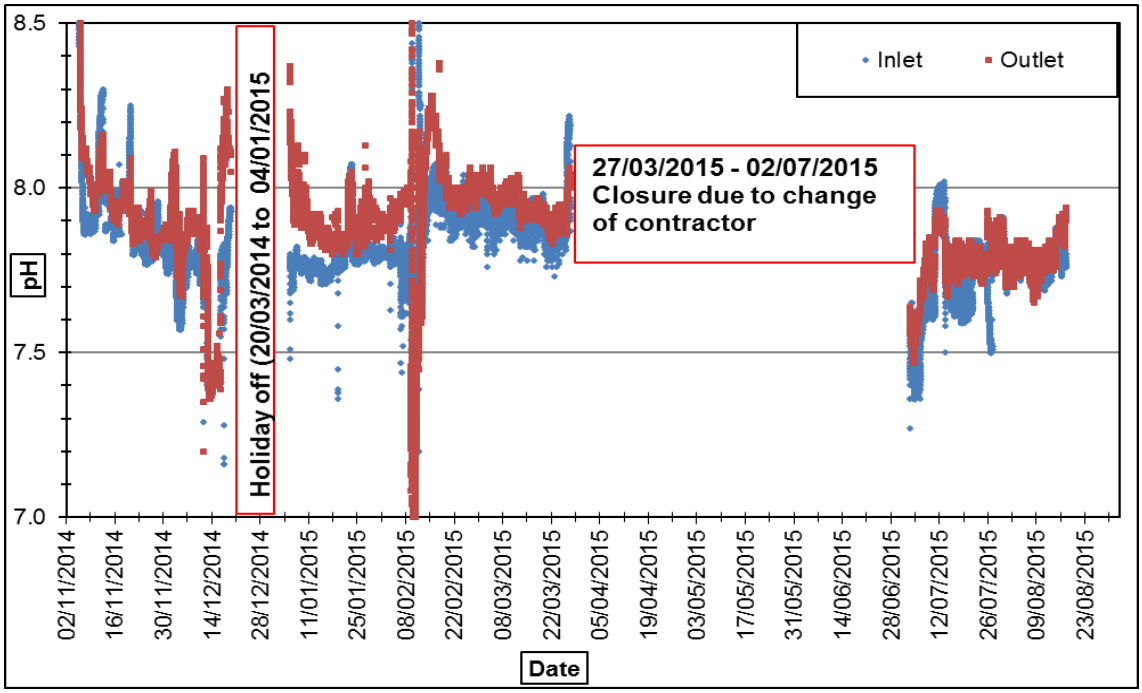

Figure 6-33: Reactor inlet-end and outlet-end water pHs recorded by online data loggers.

The degassing of carbon dioxide also occurs naturally. The initial pH (pH = 7.99) of the mine water was relatively higher in the control experiment performed at DMU laboratory compared to the pH of inlet water samples (pH ~ 7.3) collected in the third week of March, 2015. This rise in pH of mine water during storage (for six months) supports the notion of the natural degassing of carbon dioxide from the mine water. Natural degassing is also expected to occur to some extent in the storage tank. Accordingly, a gradual rise in pH over the week followed by a drop in pH after tankering days would be expected.

However, this was not observed during this trial as presented in Figure 6-34. This could be because of very slow degassing process and mixing of fresh feed with residual (~ 0.5 - 1.0 m^{-3}) feed.

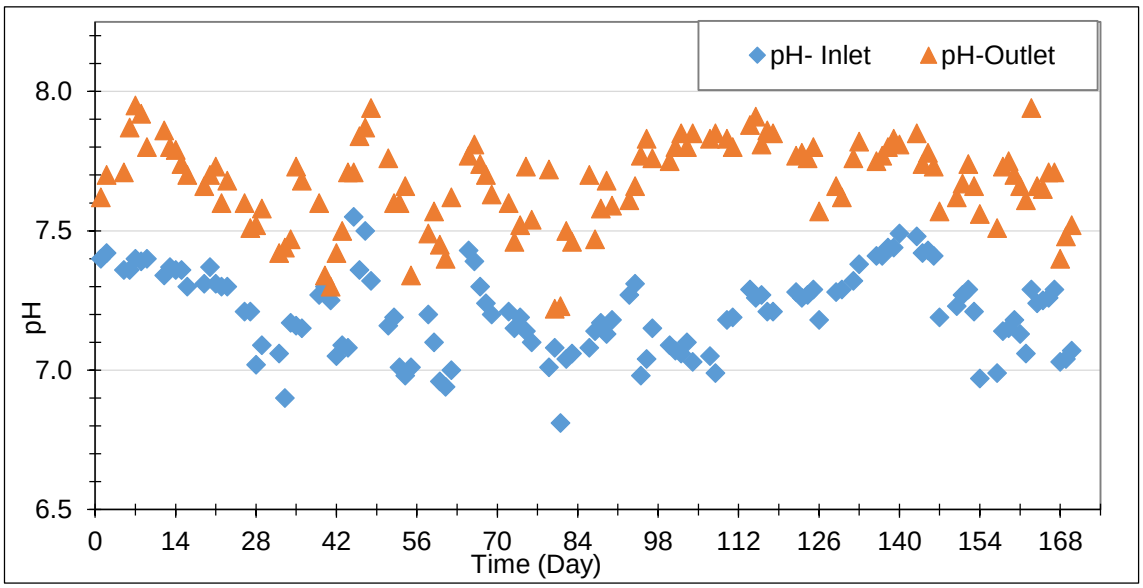

Figure 6-34: pH of inlet and outlet water samples measured at DMU laboratory.

At circum-neutral pH, very small changes in hydroxyl ion (OH^-) concentration could result in a variation in pH, for example, the concentration of OH^- ions at pH 7 equals to $1*10^{-7}$ $molL^{-1}$ whereas at pH 7.5 the $[OH^-]$ equals to $3.162 * 10^{-7}$ $molL^{-1}$ (see

Appendix 9-14). Whilst the slight rise in pH could be as a result of leached residual alkali arising from the manufacturing process of the mesh. It would be expected to reduce with respect to time. Therefore, the consistent rise of pH by ~ 0.5 throughout the treatment is attributed to the degassing of carbon dioxide.

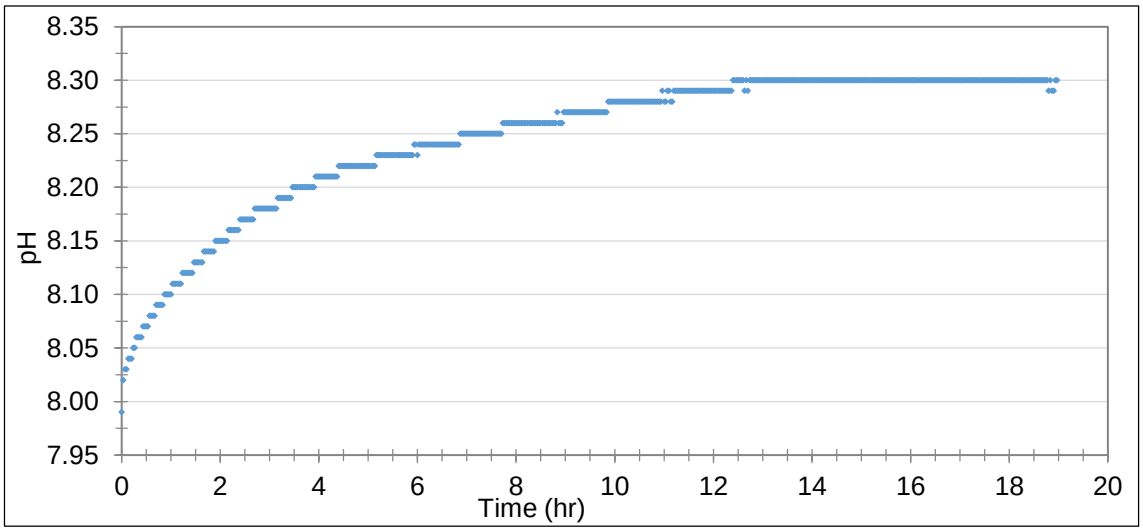

Figure 6-35: Control experiment to investigate rise in pH of mine water.

6.4.4.5. MECHANISM OF ZINC REMOVAL

Based on laboratory equilibrium studies using a model solution of zinc sulphate heptahydrate in double distilled water, saturation of the mesh in the reactor was anticipated in 4.16 days at the average flow rate of the mine water and the zinc concentration used in the trial (Appendix 9-15). The first sample taken for analysis by ESG was after nine days, when the inlet and outlet concentrations for sodium were found to be the same as 16 mg/L. This supports the conclusion that monitoring the release of sodium in the ion exchange reaction had been missed. The mesh had reached saturation via ion exchange by the first measurement and that no further ion exchange of sodium for zinc was occurring.

Continual removal of zinc even after saturation by ion exchange suggests that there was another removal mechanism, which is likely to be sorption / co-precipitation. This reaction was aided by the persistent rise in pH of ~ 0.5 units from an average inlet pH value of 7.21 to an average outlet pH value of 7.67 after treatment as described in section 6.4.4.4. The rise in pH was likely to be due to degassing of dissolved carbon dioxide in the mine water aided by the rotation of the mine water laden mesh into and out of the reactor tank containing the mine drainage water, see Equation 6-10 and Equation 6-11.

Equation 6-10

$$CO_{2(g)} + H_2O_{(l)} \rightleftharpoons H_2CO_{3(l)}$$

Equation 6-11

$$H_2CO_{3(l)} \rightleftharpoons H^+_{(l)} + HCO^-_{3(l)} \rightleftharpoons 2H^+_{(l)} + CO^{2-}_{3(l)}$$

The degassing of carbon dioxide also resulted in a loss of alkalinity although this was only one of the two mechanisms resulting in loss of alkalinity. This is evidenced by the overall reduction of 29.3 % in alkalinity over the trial period as shown in Table 6-8.

The activity (concentration) of free metal ion may be dictated by the solubility equilibrium with mineral phases such as related metal oxides or hydroxide in the solid phase. The predominant species in the mine water changes with rise in pH. Zinc ion concentrations are determined by pH and the conditional solubility constant (K_{so}) (Younger, Banwart and Hedin, 2002). Nuttall and Younger, 2000 performed computational calculations using the well-known WATEQ4F code (Ball and Nordstrom, 1991). On raising the pH from 6 to 8.5, the zinc carbonate and zinc hydroxide species increase at the expense of free zinc ions and zinc sulphate. According to Hem, 1972, a stable zinc carbonate (smithsonite) can be formed over a narrow pH range of 7.5 - 8.0 in natural waters. The solubility of zinc

carbonate has been documented in a review by Clever, Derrick and Johnson, 1992 and it was found that the solubility of zinc carbonate depends on temperature, ionic strength, pH and partial pressure of carbon dioxide. Solubility increases with temperature and partial pressure of carbon dioxide and decreases rapidly as pH rises around circum-neutral.

Paulson et al., 1989 studied the solubility of hydrozincite, a basic zinc carbonate, in solution with a total dissolved CO_2 of 2 mM and reported the formation of crystalline hydrozincite at pH below 8.2, poorly crystalline hydrozincite at pH between 8.2 to 10.5 and eventually zinc oxide (ZnO) at pH above 10.5. This is further backed up by Alwan and Williams, 1979 who explained the anomalous stability of hydrozincite in nature based on the calculated solubility product constant of hydrozincite in natural waters as log K_{sp} = -14.9.

Stumm and Morgan, 1979 suggested that below pH 7.5 zinc carbonate is the most insoluble species and as the pH increases (as it did in this trial to pH 7.7 to 7.8 on average) a basic zinc carbonate, hydrozincite, becomes controlling. The above supports the powder X-Ray Diffraction (XRD) analysis of the white precipitate on the mesh which was confirmed as some variant of hydrozincite (a basic zinc carbonate) with general formula $Zn_4(CO_3)(OH_6).H_2O$. The diffraction peaks were extremely broad, indicating a very small particle size in the powdered specimen (Appendix 9-16).

The removal of cations by sorption onto an amphoteric surface is dependent on pH and is best at the pH which correlates with the point of zero charge (pzc) (Miller, Figueroa and Wildeman, 2011). The surface of functionalised mesh used in this trial is a complex material comprising both anion exchanging ($-NH_2^-$), cation exchanging (-COOH) and complexometric (-NOH) sites. At pH of around circum-neutral the amine ($-NH_3^+$) sites are likely to be partially protonated, carboxylic (-COOH) sites completely deprotonated and oxime (-NOH) sites unchanged. Thus, the mesh provides excellent sites to support both ion exchange and sorption of zinc cations and carbonate / hydroxide etc. ions. Miller et al. 2011 further documented that extent of zinc removal depends on a complex interplay between the nature of the aqueous medium and the speciation of the surface. As pH increases, CO_3^{2-} sorbs onto the surface of the substrate to form zinc carbonate and as pH increases further zinc sorption increases forming zinc hydroxides.

There is competition between aqueous and substrate phases for zinc complexation. As pH and alkalinity increase, the increased concentration of CO_3^{2-} in the aqueous phase

outcompetes the substrate bound CO_3^{2-} stripping zinc from the surface of the substrate resulting in increased concentration of zinc carbonate in the solution.

When surface sites are in abundance, the pH dependent removal dominates and alkalinity effects are minimal. When surface sites are restricted then a more complex behaviour is exhibited dependent on pH, alkalinity and number of sites. For example, a drainage water of zinc at 1.3 mg/L, at low pH 2.67 - 6.63 and low alkalinity of 0 - 89.2 mg/L, very little zinc was precipitated or sorbed onto limestone ($CaCO_3$). However, for pH of 6.66 - 6.77 and alkalinity of 106 - 122 mg/L, the amount of zinc in solution dropped by 40 % due to sorption and precipitation. However, this trend is reversed when the pH rises to 6.83 - 7.02 and alkalinity rises to 150 - 183 mg/L (Miller, Figueroa and Wildeman, 2006, p. 1308, 2011, pp. 126–127).

The presence of alkalinity and dissolved iron in the drainage water helped to remove the solution phase zinc by precipitation or sorption onto precipitated iron oxy, hydroxyl species (Miller, Figueroa and Wildeman, 2011). This is further backed up by Mayes, Potter and Jarvis, 2009 using high surfaced area hydrous ferric oxide in the presence of similar alkalinity but higher pH than Miller, Figueroa and Wildeman, 2011 to remove zinc from solution containing zinc in the range of 1.5 - 2.2 mg/L to 0.9 - 1.5 mg/L. On moving to continuous flow field trial, Miller, Figueroa and Wildeman, 2011 reduced the residence time on limestone drain to one to two hours, compared to 4 days in batch mode, the removal efficiencies were significantly reduced almost to zero.

A range of materials was used to investigate the circum-neutral removal of zinc (23.5 mg/L, 15 minutes retention time and flow rate 1 L/min) in beds containing 1.5 - 12 kg of materials. The best material was found to be fly ash which significantly reduced zinc to below 0.02 mg/L before saturation at 16.7 hours of treatment. However, poor permeability through the fly ash reduced the flow rate which was exacerbated by the presence of iron in the wastewater which formed Fe-oxy-hydroxide precipitates reducing flow rates to almost zero (Warrender *et al.*, 2010). A significant advantage of the ion exchange mesh used in this study is the openness of the mesh and which together with its high surface area combined with agitation from the rotating discs allows excellent flows whilst providing a variety of charged sites for sorption (ion exchange and adsorption) / precipitation of zinc.

6.4.4.6. APPLICABILITY OF THE TECHNOLOGY

The results shown in section 6.4.4 show the tremendous potential of this technology in the treatment of non-coal mine water. The system not only removes metals from non-coal mine water but also non-metallic water quality parameters such as suspended solids, anions, and nitrate. The system is very effective in the removal of lead, iron, aluminium, zinc, manganese and copper. Compared to these metals, removal of cadmium was less successful. The treatment process was not affected by temperature variations suggesting that the treatment system can be used for the continuous flow treatment of mine water under ambient conditions throughout the year. The system is very scalable from a portable treatment system to systems of municipal size and a number of reactors can be situated in series and / or in parallel to achieve desired results.

As discussed above, the trial showed that saturation of the mesh had not occurred in three months and as there was no drop in performance (no significant breakthrough), it can be estimated that regeneration would not be needed for at least six to twelve months. In this particular situation, regeneration would be needed only when the mesh becomes heavily loaded affecting rotation of the discs, the mesh becomes clogged or the residue starts to slough off the mesh. Alternatively, regeneration can be initiated when the removal of zinc drops to a predetermined value e.g. to 80 % of its initial value as an example.

It is believed that this technology would be suitable for all mine water contaminated with metals. However, if the pH of the mine water is acidic (pH < 2) and alkalinity is low then uptake for some metal ions e.g. Zn is likely to reduce. Pre-treatment such as pH dosing by passing through Oxic Limestone Drains (OLDs) would be appropriate in this situation. These have been shown to increase pH and alkalinity in only a two to three hour residence time (Younger, Banwart and Hedin, 2002). If flow velocities of the mine water are kept high then this keeps any precipitated hydroxides in suspension preventing blocking of the drain material. In contrast to Anoxic Limestone Drains (ALDs), OLDs are able to treat wastewaters with iron content greater than 1 mg/L.

If the amount of suspended solids is very high then settlement pre-treatment might be advised. If the mine water contains low concentration of metal ions then it may be necessary to increase the residence time, as longer residence time improves ion exchange and precipitation processes by enhancing contact between metal ions and the active sites on the mesh. If the mine water contains an excessively high concentration of

iron then pre-treatment to precipitate it might be necessary to prevent clogging of mesh with ochre. Pre-treatment may avoid competition of iron with the uptake of the desired metal ions. However, as discussed above the presence of iron is likely to enhance the precipitation / sorption of the zinc. If the mine water contains low concentrations of iron then this will be removed together with other metal ions by an ion exchange process and will eventually assist in the co-precipitation / sorption of the other metal ions onto the mesh.

The spent mesh can be disposed in many ways. The spent mesh can be used as a support for metal oxide catalyst by Sol Gel method. It can be used as a ground cover or underlying layer to prevent soil erosion. It can be incinerated to recover energy. The precipitated residue rich in zinc can be used in agricultural fertilizer (Whysner *et al.*, 2012). The highly concentrated regenerant is suitable for electrochemical recovery of metals (Figueroa and Wolkersdorfer, 2014).

Thus, in summary, the DMU patented ion exchange PAN mesh treatment system is good at treating mine waters with high alkalinity and circum-neutral pH, which the literature suggests is difficult to treat. The presence of iron and other metals principally iron, aluminium and manganese should on balance enhance the removal of zinc by (co)precipitation / sorption mechanisms. For mine waters where the pH is low and alkalinity is low then it would be advisable to flow the waters through a limestone drain to increase alkalinity and pH to circum-neutral. For mine waters of low pH and alkalinity where the zinc concentration is very low and there are no competing cations then a pure ion exchange mechanism could potentially be used. Laboratory studies at DMU on a simulated North Pennine Nent mine water showed that the mesh was successful in taking up nearly all the zinc from solutions with zinc concentrations of 2 mg/L and 10 mg/L. This was when iron (0.33 mg/L) was competing and pH circum-neutral. This was described in detail in previous correspondence to the Coal Authority.

6.4.4.7. UPSCALING OF THE SYSTEM

Based on the operating parameters used in this field trial (reactor volume – 60 L, residence time – two hours, flow rate – 30 L/hr and amount of ion exchange mesh – 11 kg), upscaling of the treatment process can be estimated. The standard sized reactor has approximate dimensions of 7.1 m length, 3 m depth and 3.15 m width. This gives a foot print area of 22.4 m^2 per reactor. These types of reactors are very scalable and can be used for many different flows including the treatment of municipal wastewater where

there are high flows per day. Table 6-18 summarizes the estimated process parameters, and average treatment cost (calculation not disclosed) per cubic metre of mine water for a period of 25 years. The power requirements for these reactors are low (1.65 kWh/reactor) as required only to rotate (usually 2 to 5 rpm) the shaft. If pumps are needed for inflow and outflow, these do not use much energy. For example, for a flow of 5 L/s (18 m^3/h) to raise water by 10 m requires a hydraulic pump with 0.49 KW/h power (Pump Power Calculator, 2017). The power requirement for pumping of acid during the regeneration process is minimal. The energy requirement can be obtained by coupling with renewable energy sources for example wind, solar and hydropower provided the energy can be stored. The energy consumption can be further reduced by maintaining gravity driven process.

Table 6-18: Upscaling of treatment system and estimated costs.

Flow rate (L/s)	Residence time (hour)	Number of reactors	Amount of mesh (kg)	Average treatment cost per m^3 for 25 years (£)*
5	2.79	4	6,761.20	0.86
10	2.79	7	11,832.10	0.71
15	2.79	9	15,212.70	0.60
25	2.79	14	41,412.35	0.55

* The costs based on the manufacturer in the UK.

6.5. CONCLUSION

The ion exchange capacities of modified PAN mesh have been determined through titrimetric technique. The total ion, cation and anion exchange capacities of the modified PAN fibre were calculated as 3.49 mmol/g, 1.99 mmol/g and 1.46 mmol/g respectively. Based on the ion exchange capacities of commercial and non-commercial ion exchangers reported in the literature, the ion exchange mesh used in this study can be considered amongst the good ion exchangers.

Sorption of metal ions onto the ion exchange mesh was investigated using zinc solution. The influence of initial pH, contact time and initial concentration of metal ions was studied. The pH of the solution was found as the most influential parameter. The best pH for the maximum sorption of metal ions was found to be pH ≥ 5.5. The sorption capacity per unit mass of mesh increased with respect to increase in contact time and attained

equilibrium after four hours. The sorption capacity per unit mass of mesh also increased with respect to increase in initial concentration of metal ions up to 1,500 mg/L. The maximum amount of zinc adsorbed onto the mesh was determined to be 12.3 mg/g mesh or 24.6 mg/g fibre. However, the percentage adsorption capacity of mesh increased with decrease in initial concentration of metal ions. The percentage adsorption capacities of mesh become 97.5 % and 10.5 % with respect to initial concentrations of 50 mg/L and 2,000 mg/L zinc solutions respectively.

The equilibrium study of ion exchange mesh in relation to the zinc was performed. The higher value of coefficient of determination (R^2) for Langmuir adsorption isotherm model (0.9443) compared to Freundlich adsorption isotherm model (0.7874) confirmed the presence of monolayer sorption over the heterogeneous sites. The maximum adsorption capacity per unit mass of ion exchange mesh predicted by Langmuir isotherm model become 12.8 mg/g mesh that corresponds to 25.6 mg/g fibre. The separation factors corresponding to the initial concentrations fall between zero and unity ($0 < R_L < 1$), suggesting adsorption of metal ions onto the ion exchange mesh was favourable.

The ion exchange mesh developed at De Montfort University and incorporated in the innovative rotating discs contactor has been successfully applied to a pilot scale field trial in order to remove metal ions from non-coal mine drainage heavily contaminated with zinc, cadmium and lead. The removal efficiencies vary depending on metal. Lead had the highest removal efficiency followed by zinc and cadmium.

DMU results show the average influent concentrations of zinc, cadmium and lead were 49.14 mg/L, 0.19 mg/L and 0.05 mg/L respectively and the average removal efficiencies for zinc, cadmium and lead were 64.18 %, 22.37 %, and 75.04 % respectively. Accordingly, 4.15 kg of zinc, 5.55 g of cadmium and 5.22 g of lead were removed from 131.46 m^3 of non-coal mine water during a period of 24 weeks and 2 days.

Analyses by an UKAS accredited independent laboratory, ESG, show that the average influent concentrations of Zn-D, Cd-D and Pb-D were 58.8 mg/L, 0.24 mg/L and 0.03 mg/L respectively and removal efficiencies for Zn-D, Cd-D and Pb-D were 68.77 %, 23.63 % and 91.08 % respectively. Accordingly, 5.27 kg of zinc, 7.39 g of cadmium, and 3.92 g of lead were removed. Similarly, the average influent concentrations of Zn-T, Cd-T and Pb-T were 62.86 mg/L, 0.26 mg/L and 0.16 mg/L respectively. The removal efficiencies for Zn-T, Cd-T and Pb-T were 67.65 %, 25.06 % and 89.16 % respectively correspond to 5.59 kg, 8.53 g and 18.18 g zinc, cadmium and lead respectively. ESG results also show that the system had removed other metals / metalloids such as iron,

aluminium, manganese, copper, barium, arsenic, nickel, boron, chromium and small amounts of sodium, potassium and strontium.

The system also removed other water quality parameters such as acidity, suspended solids, alkalinity and small amounts of nitrate (NO_3-N) and total anions, however; contributed to small amount of ammoniacal nitrogen (NH_3-N), sulphate (SO_4-S) and hardness. An average rise of pH by ~ 0.5 unit in treated water was also observed. Conductivity was also reduced by the system.

The effects of process parameters such as regeneration ability of the system, variation of flow rate and rotation speed of the discs were investigated. The performance of the treatment system was not significantly affected by the regeneration process and rotation speed of the discs. The treatment system was successfully regenerated in-situ, indicating minimal downtimes for full-scale units. The treatment process was not affected by temperature variations within the range of 0.7 °C to 20 °C. This suggests that the treatment system can be used for the continuous flow treatment of mine water under ambient conditions throughout the year. The maximized removals of metals were observed when flow rates were at or below 45 L/hr which corresponds to a residence time at or above 1.33 hours. However, this will obviously vary depending on the liquor to mesh ratio and water quality.

The system had removed the metals mainly by ion exchange initiated (co)precipitation / sorption onto the surface of the mesh. The openness of the mesh does not result in blocking of the sites when the zinc is (co)precipitated / sorbed onto the mesh with no reduction in flow rates unlike particulate systems. It is suitable for systems with high alkalinity and circum-neutral pH and will not be hindered by mine waters with iron, rather the removal process is likely to be enhanced. For mine waters of low pH and alkalinity, it is suggested that an Oxic Limestone Drain pre-treatment be used to increase these parameters to the desired values. However, if the zinc content is very low then the mesh could be used in a purely ion exchange removal process with possibly more frequent regeneration. The spent mesh can be reused or recycled.

6.6. LESSONS LEARNT FROM THE FIELD TRIAL

The following lessons have been learnt from this trial.

- Based on lab results, saturation of mesh was expected in about one weeks. However, in the field, saturation was not reached even after elven weeks. Therefore, it is important to perform laboratory investigation, before field trial, with real mine water.

This will help to understand the removal mechanism. Undertaking geochemical calculation of saturation indices in the planning phase, especially for carbonates, will help predict if precipitation is a likely removal mechanism.

- Positioning the data loggers within reactor bias the true readings for inlet and outlet samples. In addition, in one occasion, the rotation of discs was paused as the probes in the inlet side of the reactor hooked onto the mesh. Therefore, the positioning of data loggers should be outside the reactor. This will ensure true readings of treated and untreated water and eliminate hooking onto the mesh.
- The outlet feeding tube was broken, the inlet feeding tube was cracked, and there was a slow leakage. Therefore, those tubes should be made of strong and flexible materials. This will prevent any leakage and hassles during operation. The feeding of water through outlet side was amended to inlet side and the discs were reoriented. Therefore, that change did not impact on the results.
- At the beginning of this project, the mine water was very clean. Therefore, analyses were performed with supernatant of samples without further treatment. But, later on, especially once the tankering frequency increased, the samples became dirty. That made difficulties in analyses. Therefore, it is advised to follow the same sample preparation techniques as of external analyses. This will not only make consistency in analyses but also minimize the difference between external and internal results. None the less, it is not unusual to have sets of total, dissolved and settled wastewater analyses.
- There were occasions in which the dosing pump was running dry and the outlet tank was over filled and flooded. Therefore, early communication and planning are needed.

CHAPTER SEVEN

7. CONCLUSIONS AND RECOMMENDATIONS

7.1. CONCLUSION

This project has successfully investigated the effectiveness of a modified heterogeneous PAN-(Fe^{3+}) catalyst and hydrogen peroxide system and a modified ion exchange PAN mesh in the treatment of textile and mining influenced effluents respectively. The findings of these treatments are discussed separately in the following sections.

7.1.1. TREATMENT OF TEXTILE EFFLUENT- THE BATCH MODE

A modified PAN-(Fe^{3+}) catalyst and H_2O_2 system was employed in the treatment of textile effluent. Reactive Orange (RO16), an azo dye, was used as a model dye. The treatment system was investigated in both batch (chapter four) and continuous flow (chapter five) mode of operations.

The influence of process parameters such as pH, amount of catalyst, initial concentration of hydrogen peroxide, initial concentration of substrate and temperature of the reacting medium were investigated in batch experiments to optimize the treatment process. The performance of the system was measured in terms of decolourization (measure of absorption band at 493.5 nm) and loss of aromaticity (measure of absorption band at 254 nm). The system was found to be influenced by the process parameters studied. The parameters were studied in the range as pH (2 to 7), amount of modified PAN catalyst (0 g to 8 g/100 mL), initial concentration of H_2O_2 (0 mg/L to 1,000 mg/L), initial concentration of substrate (12.5 mg/L to 100 mg/L) and temperature (20 °C to 35 °C).

The investigation revealed that the influence of pH and catalyst was more significant compared to the influence of H_2O_2, the pH being the most influential. The investigation on oxidation of dye established an optimum treatment condition as 6 g catalyst, pH 3, 125 mg/L H_2O_2 in 100 mL of RO16 solution (C_0 = 50 mg/L) at 30 °C. At optimum condition, 99.5 % decolourization and 91.9 % loss of aromaticity were achieved in 100 minutes. The study also revealed that ~ 70 % of the dye mineralized to carbon dioxide and water. The pH of the reacting medium dropped by ~ 0.5 unit. The dissolved oxygen has no noticeable effect on removal of dye.

The sorption of dye onto the surface of modified PAN catalyst was studied through Langmuir and Freundlich equilibrium adsorption isotherm models. The study revealed that adsorption of RO16 onto the modified PAN catalyst was favourable and can be best described by Langmuir adsorption isotherm model. The best-fit of Langmuir isotherm model confirms the presence of monolayer surface on homogeneously distributed sites. The maximum adsorption capacity of modified PAN catalyst was found to be 0.68 mg of

RO16 per gram of PAN catalyst. The influence of pH on sorption of RO16 onto the surface of modified PAN catalyst was also studied. The adsorption of RO16 was found to be heavily influenced by the pH of the dye solution with maximum adsorption (87.15 %) occurring at pH 2.

The amount of catalyst loss was measured in terms of iron leaching from the surface of the modified PAN catalyst. The iron leaching was measured with respect to the changes in the process parameters studied in batch experiments. A direct relationship between amount of leached iron, pH and temperature was established. The lower the pH of the medium, the more iron leached from the modified PAN catalyst. About 4.5 folds higher amount of iron was leached at pH 2 compared to pH 3. Iron leaching was found to be linearly dependent on temperature of the system. The amount of leached iron at 35 °C was doubled compared to that at 20 °C. No direct relationship between catalyst loss and initial concentration of H_2O_2 and substrate was observed. However, amount of leached iron increased with respect to increase in amount of catalyst until an optimum amount of catalyst only. The amount of leached iron was below one percent, except at pH 2 (1.12 %), with 0.87 % loss at optimum condition. The minimum loss of iron ensures longer lifetime of the modified PAN catalyst and hence the treatment system.

The contribution of leached iron on the removal of dye by means of homogeneous catalysis was investigated. The heterogeneous catalysis (in the presence of modified PAN catalyst) was found to be 4.5 folds faster than that of homogenous catalysis (in the presence of leached iron), revealing no significant contribution of leached iron in the removal of RO16.

The potential use of treatment system in the industrial scale was examined using a real dye-bath effluent, which was much more concentrated than usual textile effluent. The successful treatment of the concentrated dye-bath effluent ensures the suitability of the system in the treatment of industrial effluents. The maximized extent of decolourization (measured at 672 nm) and loss of aromaticity (measured at 292 nm) were 99.99 % and 95 % respectively.

7.1.2. TREATMENT OF TEXTILE EFFLUENT- THE CONTINUOUS FLOW MODE

A modified PAN-(Fe^{3+}) catalyst and H_2O_2 system was successfully employed in the continuous flow treatment of RO16 dye using a bench scale prototype of a rotating discs contactor loaded with 208 g of modified PAN catalyst. The influence of residence / contact time (≈ flow rate) and H_2O_2 dose on removal of RO16 was studied. The residence

time was varied in the range of 2.4 to 4 hours and the H_2O_2 dose in the range of 50 mg/L to 250 mg/L respectively. The optimum dose of H_2O_2 was found to be the same as established in batch mode (125 mg/L) whereas the residence time was extended by ~ 2.5 fold. At optimum condition, the removal efficiencies corresponding to decolourization, loss of aromaticity, COD and TOC were 99.2 %, 73 %, 64.4 % and 50 % respectively.

The breakthrough of the system occurred on 50^{th}, 24^{th}, 17^{th} and 9the days respectively when performed with fresh and successively regenerated catalyst. The breakthrough of the treatment system was observed mainly due to deactivation of the modified PAN catalyst occurred due to loss of iron. The iron leaching was favoured at low pH generated by the formation of acidic intermediate products and hydrolysis of iron complexes. A three-phase (log-phase, steady-phase and lag-phase) iron leaching was observed with fresh catalyst whereas a gradual decline of iron with respect to time was observed with regenerated catalysts.

Three in-situ regenerations of the deactivated modified PAN catalyst were successively performed. The amount of reimpregnated iron and lifetime of regenerated catalyst reduced after each regeneration. The rate of iron leaching was relatively higher with regenerated catalyst. However, the total percentage of leached iron decreased after each exposure, suggesting increasing poisoning and / or chemical modification of polymeric supports. The mass balance of iron shows that 92.2 %, 84.6 %, 75.9 % and 58.8 % of iron was leached from the fresh and successively regenerated catalyst.

The continuous flow experiment ran for 103 days (3.4 months) in total. During this period, a total volume of 546.7 L of dye solution carrying 26.78 g of RO16 was treated and a total mass of 25.3 g (12.76 g, 6.09 g, 4.24 g, and 2.19 g in each successive exposure) of RO16 was successfully decolourized by the system.

The possibility of having homogeneous catalysis due to leached iron was investigated using an equivalent amount of iron leached on Day-2 (when the process was stabilized) and Day-11 (when iron leaching was maximum) of the continuous flow treatment. Based on the performance observed on Day-2 of continuous flow treatment and homogeneous catalysis with iron equivalent to amount of leached iron as of Day-2, it can be concluded that the continuous flow treatment was solely relied on heterogeneous catalysis. However, looking at the results observed on Day-11 of continuous flow treatment and homogeneous catalysis with iron equivalent to amount of leached iron as of Day-11, the process can be said to be assisted by homogenous catalysis.

7.1.3. REMEDIATION OF MINING INFLUENCED EFFLUENT

The ion exchange capacity of modified PAN mesh was determined using an acid-base titrimetric technique. The total ion, cation and anion exchange capacities of the modified PAN fibre were calculated as 3.49 mmol/g, 1.99 mmol/g and 1.46 mmol/g respectively. The sorption of metal (zinc) ions onto the ion exchange mesh was studied as a function of initial pH, contact time and initial concentration of metal ions. These parameters were varied in the range as; pH (2 to 6.6), contact time (30 minutes to five hours) and initial concentrations of zinc (50 mg/L to 2,000 mg/L). The pH of solution was found to be the most influential parameter and maximum sorption was observed at initial solution pH ≥ 5.5. The sorption capacity of modified ion exchange PAN mesh increased with respect to increase in contact time and attained an equilibrium after four hours. The sorption capacity of mesh also increased with increase in initial concentration of metal and the maximum sorption of metal ions observed with 1,500 mg/L of zinc solution. However, the sorption capacity (%) of ion exchange mesh decreased with increase in initial concentration of metal ions. The sorption capacity (%) of ion exchange mesh with respect to 50 mg/L and 2,000 mg/L zinc solutions was 97.5 % and 10.5 % respectively.

The sorption of metal ions onto the surface of modified ion exchange PAN mesh was studied through Langmuir and Freundlich equilibrium adsorption isotherm models. The sorption of metal ions onto the modified ion exchange PAN mesh was favourable and can be best described by Langmuir adsorption isotherm model. The maximum adsorption capacity per unit mass of ion exchange PAN mesh was predicted by Langmuir isotherm model was 12.8 mg of zinc per gram of PAN mesh that corresponds to 25.6 mg of zinc per gram of modified PAN fibre.

The modified ion exchange PAN mesh incorporated in the rotating discs contactor was successfully applied to pilot scale field trial in the remediation of mining influenced effluent heavily contaminated with zinc, cadmium and lead. The trial was run for a total of 170 days (24 weeks and 2 days), treating 131.46 m^3 of non-coal mine water. The average inlet concentrations of zinc, cadmium and lead, according to DMU analyses, were 49.14 mg/L, 0.19 mg/L and 0.05 mg/L respectively. DMU results show the average removal efficiencies of 64.18 %, 22.37 % and 75.04 % for zinc, cadmium and lead respectively. These removals are equivalent to 4.15 kg of zinc, 5.55 g of cadmium and 5.22 g of lead respectively.

The performance of the system was also evaluated through an independent body, an UKAS accredited independent laboratory, ESG. The analyses by ESG showed the

average concentrations of zinc-dissolved (Zn-D), zinc-total (Zn-T), cadmium-dissolved (Cd-D), cadmium-total (Cd-T), lead-dissolved (Pb-D) and lead-total (Pb-T) were 62.86 mg/L, 58.28 mg/L, 0.26 mg/L, 0.24 mg/L, 0.16 mg/L and 0.03 mg/L respectively. The removal efficiencies for Zn-D, Cd-D and Pb-D were 68.77 %, 23.63 % and 91.08 % respectively. Accordingly, 5.27 kg of zinc, 7.39 g of cadmium, and 3.92 g of lead were removed. Similarly, the removal efficiencies for Zn-T, Cd-T and Pb-T were 67.65 %, 25.06 % and 89.16 % respectively. The corresponding removals for zinc, cadmium and lead were 5.59 kg, 8.53 g and 18.18 g respectively. ESG results also show that the system had removed other metals / metalloids such as iron, aluminium, manganese, copper, barium, arsenic, nickel, boron, chromium and small amounts of sodium, potassium and strontium.

The treatment system also consumed acidity and removed other water quality parameters such as suspended solids, alkalinity, small amounts of nitrate (NO_3-N) and total anions. However, the system contributed to small amount of ammoniacal nitrogen (NH_3-N), sulphate (SO_4-S) and hardness. An average rise of pH by ~ 0.5 unit in treated water was also observed. Conductivity was also reduced by the system.

Influence of in-situ regeneration ability, variation in contact time (≈ flow rate) and rotation speed of the discs were investigated. The in-situ regeneration of the system was successfully performed on Day-79 of the treatment and the performance of the system was not influenced by the regeneration, indicating minimum downtimes for the full scale units. The performance of the system was not affected by the seasonal and daily variation in temperature with the range of 0.7 °C to 20 °C. The best performance of the system was observed when the contact / residence time was maintained at or above 1.33 hours.

The uptake capacity per unit mass of ion exchange mesh observed, before system attaining the saturation state, during the field trial clearly exceeded the maximum sorption capacity predicted by Langmuir adsorption isotherm model, suggesting the existence of additional removal mechanisms. The removal mechanism was ion exchange initiated (co)precipitation / sorption onto the surface of PAN mesh. The openness of the mesh did not result in blocking of the sites when the zinc is (co)precipitated / sorbed onto the mesh with no reduction in flow rates unlike particulate systems. It is suitable for systems with high alkalinity and circum-neutral pH and will not be hindered by mine waters with iron; rather the removal process is likely to be enhanced. The application of this technology

on simulated acid mine drainage (AMD) suggests the need of pre-treatment to raise the pH and alkalinity. The spent mesh can be reused or recycled.

7.2. RECOMMENDATIONS

Based on the knowledge and experience gained from this project, it is felt that further investigations would fulfil the gaps highlighted in this project and make this research complete and meaningful. Accordingly, some future studies relevant to each experimental chapter are proposed below.

7.2.1. RECOMMENDATIONS FOR CHAPTER 4 - OPTIMIZATION OF REACTION PROCESS IN BATCH MODE OF OPERATION

- It is recommended to study the degradation pathway and identify the intermediate products of RO16. The possibility of forming more toxic intermediate products has been discussed in literature. Thus, this study will help understand the potential post-treatment toxicity to aquatic environment that can be evaluated by a test against *Daphnia Magna,* a freshwater insect. Literature establishing degradation pathway of RO16 using Fenton's catalysis could not be found. However, literature based on photocatalytic (Chen, 2009), photo-oxidative (Bilgi and Demir, 2005), ozone (Tizaoui and Grima, 2011) and fungal (Svobodová *et al.*, 2007) degradations have documented a range of intermediate products. An attempt to identify intermediates was made based on the method described in (Tizaoui and Grima, 2011). However, the intermediates could not be traced as products fragmented into numerous products (see Appendix 9-3). Thus, it is advised to either develop a new method or use more powerful technique such as GC-MS-MS.
- It is recommended to study the effect of anions on the decomposition of RO16. The anions such as Cl^-, NO_3^-, SO_4^{2-} and PO_4^{3-} are known to scavenge $^{\bullet}OH$ radical. Thus, this study will help understand the influence of such ions and corroborate the treatment process accordingly.
- It is recommended to study the effectiveness of modified PAN catalyst and H_2O_2 system in the decomposition of dyes with different chromophores and functional groups. This study will help improve the treatment process by covering a wider range of dyes discharged in textile effluent.
- It is recommended to optimize the design of space through design of experiment (DOE). DOE is considered as a better approach over traditional one-factor-at-a-time (OFAT) approach. DOE reveals a better space for setting of process parameters,

which could be more cost-effective. DOE was performed using six control variables (pH, H_2O_2, catalyst, substrate concentration, temperature and time) and two response factors (decolourization and loss of aromaticity). A suitable model could not be developed. The factor setting for pH (3 to 5), H_2O_2 (0 to 1,000 mg/L) and catalyst (1 to 7 g) was too wide. In addition, using too many variables makes the study unnecessarily complex. Thus, it is advised to avoid time, substrate and temperature as variables and narrow down factor settings towards the centre point. The optimized setting in batch can be used as a guidance for centre point.

7.2.2. RECOMMENDATIONS FOR CHAPTER 5 – CONTINUOUS FLOW TREATMENT OF DYE

- It is recommended to reintroduce the functional groups onto the deactivated catalyst (used in this study) followed by the reimpregnation of iron and testing in continuous flow experiment. This will help understand the possibility of further extending the lifetime of the modified PAN catalyst.
- It is recommended to perform a continuous flow treatment, if possible using a real textile effluent, if not using a mock effluent. This will help determine a more realistic performance of the treatment system and the lifetime of the catalysis.
- It is recommended to perform continuous flow treatment of textile effluent in combination with UV and microwave. This will help understand the additive and / or synergistic effects of combined technology.
- It is recommended to perform tracer study. This will help understand the mixing and true residence time. This might help understand how leached iron distributes or accumulates in the reactor.
- It is recommended to use a baffled reactor and measure the amount of leached iron in each section. This will help understand the iron leaching with respect to the reactor length thus provides better picture of leaching mechanism and distribution of leaching.
- It is recommended to investigate the reimpregnation of iron with respect to initial iron content of the PAN catalyst. Despite of using iron and sodium salts sufficient to reimpregnate an equivalent amount of iron as of fresh catalyst, the amount of reimpregnated iron reduced significantly in each successive regeneration. It is felt that similar extents of iron loading could have achieved even if two-third, half and one-third of the iron and sodium salts were used in corresponding regenerations. If so, this will help allocate resources accordingly and mitigate the economic and environmental burdens.

- It is recommended to investigate the pH fluctuation with respect to iron concentration. The difference between influent and effluent pH did not show any relationship with concentration of leached iron when fresh catalyst was used (Figure 5-15). However, when performed with the regenerated catalyst (Figure 5-21, Figure 5-24 and Figure 5-26), the difference between influent and effluent pH was greater when iron leaching is the greatest. This suggests that the pH of treated effluent decreased not only due to formation of acidic products but also due to hydrolysis of iron (Fe^{3+}) complexes as given in Equation 7-1.

$$[Fe^{III}(H_2O)_6]^{3+} \rightleftharpoons [Fe^{III}(H_2O)_5OH]^{2+} + H^+ \qquad \textit{Equation 7-1}$$

7.2.3. RECOMMENDATIONS FOR CHAPTER 6 – REMEDIATION OF MINING INFLUENCED WATER

- It is recommended to run the treatment process until saturation point is reached. This will give a true uptake capacity and better understanding of the system and help save time, cost and resources.
- It is recommended to perform the selectivity study for ion exchange mesh. Selectivity study would reveal the affinity of metals towards ion exchange mesh which would be useful to assess the suitability of this technology in the remediation of other mine waters.
- It is recommended to test this technology with real acid mine drainage (AMD). This will also give a better understanding of the system and suitability of this technology in the treatment of mine waters with wide pH range.
- It is recommended to investigate the effect of a treatment process in series. This will help to answer whether environmental quality standards (EQS) levels can be achieved or not.
- It is recommended to maintain, if possible, a gravity driven feed for full scale plants. This will ensure a consistent flow rate and save cost.
- It is recommended to avoid the sludge feeding into the reactor. Physical solids will block the ion exchange sites on the mesh.
- It is recommended to determine the ion activity product (IAP) and solubility product (K_{sp}) for related metal species. These will help to determine saturation index (SI), [= log (IAP/K_{sp})]. Saturation index will help understand the degree of saturation. If SI equal approximately zero, the water is at equilibrium. If SI > 0, the water is supersaturated with mineral hence precipitation would be favoured. If SI < 0, the water is undersaturated with mineral hence mineral would be dissolved in water (Ball and

Nordstrom, 1991, p. 4; Stumm and Morgan, 1996, p. 357; Younger, Banwart and Hedin, 2002, p. 115). WATWQ4F simulation provides this information.

- It is recommended to perform an initial laboratory testing with real mine water on the laboratory scale rotating disc reactor if the new site has mine water with very different pH or very different parameters from the Minsterley mine water.

8. REFERENCES

REFERENCES

Abdullah, A. H., Wong, W. Y. and Yaziz, M. I. (2010) 'Decolorization of reactive orange 16 dye by copper oxide system', *Sains Malaysiana*, 39(4), pp. 587–591.

Adebisi, G. A., Chowdhury, Z. Z. and Alaba, P. A. (2017) 'Equilibrium, kinetic, and thermodynamic studies of lead ion and zinc ion adsorption from aqueous solution onto activated carbon prepared from palm oil mill effluent', *Journal of Cleaner Production*. Elsevier Ltd, 148, pp. 958–968.

Adinew, B. (2012) 'Textile effluent treatment and decolorization techniques - A review.', *Chemistry: Bulgarian Journal of Science Education*, 21(3), pp. 434–456.

Aksu, Z. (2001) 'Equilibrium and kinetic modelling of cadmium (II) biosorption by C . vulgaris in a batch system : effect of temperature', *Separation and Purification Technology*, 21, pp. 285–294.

Al-Kdasi, A., Idris, A., Saed, K. and Guan, C. T. (2005) 'Treatment of textile wastewater by advanced oxidation processes - a rieview', *Global Nest: the International Journal*, 6(3), pp. 222–230.

Alchin, D. and Wansbrough, H. (2002) 'Ion exchange resins'. Aukland: New Zealand Institute of Chemistry, pp. 1–7.

Allen, R. L. M. (1971) *Studies in Modern Chemistry : Colour Chemistry*. First. New York: Appleton Century Crofts.

Allen, S. J., Mckay, G. and Porter, J. F. (2004) 'Adsorption isotherm models for basic dye adsorption by peat in single and binary component systems', *Journal of Colloid And Interface Science*, 280, pp. 322–333.

Alsamkari, L. (2011) *The Application of a Novel Polymer Supported Catalyst in the Fenton's Decomposition of Hydrogen Peroxide , Chlorphenols and Dyes*. De Montfort University.

Alyüz, B. and Veli, S. (2009) 'Kinetics and equilibrium studies for the removal of nickel and zinc from aqueous solutions by ion exchange resins', *Journal of Hazardous Materials*, 167, pp. 482–488.

American Chemical Society (2017) *A closer look at what caused the Flint water crisis*. Available at: https://phys.org/news/2017-02-closer-flint-crisis.html (Accessed: 2

March 2018).

Andreozzi, R., Caprio, V., Insola, A. and Marotta, R. (1999) 'Advanced oxidation processes (AOP) for water purification and recovery', *Catalysis Today*, 53(1), pp. 51–59.

Anirudhan, T. S. and Ramachandran, M. (2008) 'Synthesis and characterization of amidoximated polyacrylonitrile / organobentonite composite for Cu(II), Zn(II), and Cd(II) Adsorption from Aqueous solutions and industry wastewaters', *Industrial and Engineering Chemistry Research*, 47(16), pp. 6175–6184.

Anis, M., Haydar, S. and Bari, A. J. (2013) 'Adsorption of lead and copper from aqueous solution using unmodified wheat straw', *Environmental Engineerig and Management Journal*, 12, pp. 2117-21–24.

Anjaneyulu, Y., Chary, N. S. and Raj, D. S. S. (2005) 'Decolourization of Industrial Effluents – Available Methods and Emerging Technologies – A Review', *Environmental Science and Bio/Technology*, 4(4), pp. 245–273.

Annie, L. (2009) *O Ecotextiles*, *O Ecotextiles*. Available at: https://oecotextiles.wordpress.com/category/chemicals/dyes/ (Accessed: 13 October 2017).

Annie, L. (2018) *Why does the Cape Town water crisis impact the textile industry?*, *O Ecotextiles*. Available at: https://oecotextiles.wordpress.com/author/oecotextiles/ (Accessed: 7 March 2018).

Arends, I. W. C. E. and Sheldon, R. A. (2001) 'Activities and stabilities of heterogeneous catalysts in selective liquid phase oxidations : recent developments', *Applied Catalysis A: General*, 212, pp. 175–187.

Argyle, M. and Bartholomew, C. (2015) 'Heterogeneous Catalyst Deactivation and Regeneration: A Review', *Catalysts*, 5(1), pp. 145–269.

Arslan-Alaton, I. (2007) 'Degradation of a commercial textile biocide with advanced oxidation processes and ozone', *Journal of Environmental Management*, 82, pp. 145–154.

Arslan, I. and Balcioğlu, I. A. (1999) 'Degradation of commercial reactive dyestu € s by heterogenous and homogenous advanced oxidation processes : a comparative study', *Dyes and Pigments*, 43, pp. 95–108.

Arslan, S., Eyvaz, M., Gürbulak, E. and Yüksel, E. (2016) 'A Review of State-of-the-Art Technologies in Dye- Containing Wastewater Treatment – The Textile Industry Case', in *Textile Wastewater Treatment*. InTech, pp. 1–28.

Asghar, A., Raman, A. A. A. and Daud, W. M. A. W. (2015) 'Advanced oxidation processes for in-situ production of hydrogen peroxide/hydroxyl radical for textile wastewater treatment: A review', *Journal of Cleaner Production*. Elsevier Ltd, 87(1), pp. 826–838.

Asuelimen, L. I. (2015) *Remediation of polycyclic aromatic hydrocarbon (PAH) and humic acid contaminated water using heterogeneous modified PAN catalyst*. De Montfort.

Augugliaro, V., Loddo, V., Palmisano, G., Palmisano, L. and Pagliaro, M. (2010) *Clean by Light Irradiation: Practical Applications of Supported TiO2*. Cambridge: The Royal Society of Chemistry.

Ayres, D. M., Davis, A. P. and Gietka, P. M. (1994) *Removing Heavy Metals from Wastewater*. Maryland.

Babuponnusami, A. and Muthukumar, K. (2012) 'Removal of phenol by heterogenous photo electro Fenton-like process using nano-zero valent iron', *Seperation and Purification Technology*. Elsevier B.V., 98, pp. 130–135.

Babuponnusami, A. and Muthukumar, K. (2014) 'A review on Fenton and improvements to the Fenton process for wastewater treatment', *Journal of Environmental Chemical Engineering*. Elsevier Ltd, 2(1), pp. 557–572.

Badawy, M. I., Ghaly, M. Y. and Gad-allah, T. A. (2006) 'Advanced oxidation processes for the removal of organo- phosphorus pesticides from wastewater', *Desalination*, 194, pp. 166–175.

Bailey, S. E., Olin, T. J., Bricka, R. M. and Adrian, D. D. (1999) 'A review of potentially low-cost sorbents for heavy metals', *Water Research*, 33(11), pp. 2469–2479.

Balan, D. S. L. and Monteiro, R. T. R. (2001) 'Decolorization of textile indigo dye by ligninolytic fungi', *Journal of Biotechnology*, 89, pp. 141–145.

Ball, J. W. and Nordstrom, D. K. (1991) *User's manual for WATEQ4F, with revised thermodynamic data base and text cases for calculating speciation of major, trace, and redox elements in natural waters*.

Banat, I. M., Nigam, P., Singh, D. and Marchant, R. (1996) 'Microbial decolourization of textile-dye-contaning effluents: a review', *Bioresource Technology*, 58(3), pp. 217–227.

Barakat, M. A. (2011) 'New trends in removing heavy metals from industrial wastewater', *Arabian Journal of Chemistry*. King Saud University, 4(4), pp. 361–377.

Bartholomew, C. H. and Argyle, M. D. (2015) 'Advances in catalyst deactivation and regeneration', *Catalysts*, 5(1), pp. 949–954.

Baumann, W. and Lacasse, K. (2004) *Textile Chemicals : Environmental Data and Facts*. First. Berlin: Springer-Verlag.

Bautista, P., Mohedano, A. F., Gilarranz, M. A., Casas, J. A. and Rodriguez, J. J. (2007) 'Application of Fenton oxidation to cosmetic wastewaters treatment', *Journal of Hazardous Materials*, 143, pp. 128–134.

Benatti, C. T., Tavares, C. R. G. and Guedes, T. A. (2006) 'Optimization of Fenton ' s oxidation of chemical laboratory wastewaters using the response surface methodology', *Journal of Environmental Management*, 80, pp. 66–74.

Bensalah, N., Bedoui, A., Chellam, S. and Abdel-Wahab, A. (2013) 'Electro-Fenton Treatment of Photographic Processing Wastewater', *Clean - Soil, Air, Water*, 41(7), pp. 635–644.

Bianco, B., Michelis, I. De and Vegliò, F. (2011) 'Fenton treatment of complex industrial wastewater : Optimization of process conditions by surface response method', *Journal of Hazardous Materials*. Elsevier B.V., 186, pp. 1733–1738.

Bilgi, S. and Demir, C. (2005) 'Identification of photooxidation degradation products of C.I. Reactive Orange 16 dye by gas chromatography-mass spectrometry', *Dyes and Pigments*, 66(1), pp. 69–76.

Bisschops, I. and Spanjers, H. (2003) 'Literature review on textile wastewater characterisation', *Environmental Technology*, 24(11), pp. 1399–1411.

Boateng, M. K., Price, S. L., Huddersman, K. D. and Walsh, S. E. (2011) 'Antimicrobial activities of hydrogen peroxide and its activation by a novel heterogeneous Fenton's-like modified PAN catalyst', *Journal of Applied Microbiology*, 111, pp. 1533–1543.

Boczkaj, G. and Fernandes, A. (2017) 'Wastewater treatment by means of advanced

oxidation processes at basic pH conditions : A review', *Chemical Engineering Journal*. Elsevier B.V., 320, pp. 608–633.

Bokare, A. D. and Choi, W. (2014) 'Review of iron-free Fenton-like systems for activating H_2O_2 in advanced oxidation processes', *Journal of Hazardous Materials*. Elsevier B.V., 275, pp. 121–135.

Börnic, H. and Schmidt, T. C. (2006) 'Amines', in Reemtsma, T. and Jekel, M. (eds) *Organic Pollutants in the water cycle: properties, occurrence, analysis and environmental relevance of polar compounds*. Berlin: Wiley-VCH Verlag GmbH & Co. KGaA, p. 363.

Boudart, M. (1995) 'Turnover Rates in Heterogeneous Catalysis', *Chemical Reviews*, 95(3), pp. 661–666.

Brillas, E. and Martínez-Huitle, C. A. (2015) 'Decontamination of wastewaters containing synthetic organic dyes by electrochemical methods. An updated review', *Applied Catalysis B: Environmental*, 166–167.

Brookins, D. G. (1998) *Eh-pH Diagrams for Geochemistry*. New York: Springer-Verlag.

Brown, D. and Anliker, R. (1988) 'Dyestuffs and the environment-A risk assessment.', *Risk Assessment of Chemicals in the Environment*, pp. 398–413.

Brown, M., Barley, B. and Wood, H. (2002) *Minewater Treatment Technology, Application and Policy*. London: IWA Publishing.

Butler, E., Hung, Y.-T., Ahmad, M. Al and Fu, Y.-P. (2016) 'Treatment and Management of Industrial Dye Wastewater for Water Resources Protection', in *Handbook of Environmental Engineering 17 Natural Resources and Control Processes*. Geneva: Springer International Publishing AG Switzerland, pp. 187–224.

Carmen, Z. and Daniela, S. (2012) 'Textile organic dyes – characteristics , polluting effects and separation / elimination procedures from industrial effluents – a critical overview', in Puzyn, T. and Mostrag-Szlichtyng, A. (eds) *Organic pollutants ten years after the Stockholm Convention - environmental and analytical update*. Rijeka: InTech, p. 482.

Carta, R. and Desogus, F. (2013) 'The enhancing effect of low power microwaves on phenol oxidation by the Fenton process', *Biochemical Pharmacology*. Elsevier B.V., 1(4), pp. 1292–1300.

Catalkaya, E. C. and Kargi, F. (2007) 'Color , TOC and AOX removals from pulp mill effluent by advanced oxidation processes : A comparative study', *Journal of h*, 139, pp. 244–253.

Catanho, M., Malpass, G. R. P. and Motheo, A. J. (2006) 'Photoelectrochemical treatment of the dye reactive red 198 using DSA® electrodes', *Applied Catalysis B: Environmental*, 62, pp. 193–200.

Catrinescu, C., Teodosiu, C., Macoveanu, M., Miehe-brendl, J. and Dred, R. Le (2003) 'Catalytic wet peroxide oxidation of phenol over Fe-exchanged pillared beidellite', *Water Research*, 37, pp. 1154–1160.

Chamarro, E., Marco, A. and Esplugas, S. M. (2001) 'Use of fenton reagent to improve organic chemical biodegradability', *Water Research*, 35(4), pp. 1047–1051.

Chaplin, M. F. and Bucke, C. (1990) *Enzyme Technology*, *Enzyme Technology*. Cambridge: Cambridge University Press. Available at: http://www1.lsbu.ac.uk/water/enztech/ (Accessed: 20 April 2017).

Chaudhary, B. K. and Farrell, J. (2014) 'Preparation and Characterization of Homopolymer Polyacrylonitrile-Based Fibrous Sorbents for Arsenic Removal', *Environmental Engineering Science*, 31(11), pp. 593–601.

Chemical Book (2017) *2-Acetamido-8-naphthol-6-sufonic acid (N-acetyl gamma acid)*. Available at: http://www.chemicalbook.com/ChemicalProductProperty_EN_CB8875534.htm (Accessed: 19 March 2018).

Chen, C.-Y. (2009) 'Photocatalytic Degradation of Azo Dye Reactive Orange 16', *Water Air and Soil Pollution*, 202, pp. 335–342.

Chen, H. W., Kuo, Y. L., Chiou, C. S., You, S. W., Ma, C. M. and Chang, C. T. (2010) 'Mineralization of reactive Black 5 in aqueous solution by ozone/H_2O_2 in the presence of a magnetic catalyst', *Journal of Hazardous Materials*, 174(1–3), pp. 795–800.

Chen, J. P., Yang, L., Ng, W.-J., Wang, L. K. and Thong, S.-L. (2006) 'Ion Exchange', in Wang, L. K., Hung, Y.-T., and Shammas, N. K. (eds) *Handbook of Environmental Engineering: Advanced Physicochemical Treatment Processes*. Volume 4. New Jersey: Human Press, p. 697.

Chen, J. and Zhu, L. (2009) 'Comparative study of catalytic activity of different Fe-pillared

bentonites in the presence of UV light and H_2O_2', *Separation and Purification Technology*, 67(3), pp. 282–288.

Chequer, F. M. D., De Oliveira, G. A. R., Ferraz, E. R. A., Zanoni, M. V. B. and De Oliveira, D. P. (2013) 'Textile Dyes : Dyeing Process and Environmental Impact', in Guenay, M. (ed.) *Eco-Friendly Textile Dyeing and Finishing*. INTECH, pp. 151–176.

Chi, G. T. (2008) *Synthesis, chemical charaterisation and scale up of a heterogeneous catalyst for the oxidation of organic pollutants in wastewater*. De Montfort University.

Chi, G. T., Churchley, J., Huddersman, K. D., Trent, S., Road, S. M. and Cv, C. (2013) 'Pilot-Scale Removal of Trace Steroid Hormones and Pharmaceuticals and Personal Care Products from Municipal Wastewater Using a Heterogeneous Fenton ' s Catalytic Process', *International Journal of Chemical Engineering*, 2013, pp. 1–10.

Chi, G. T. and Huddersman, K. D. (2011) 'Maleic Acid Oxidation Using A Heterogeneous Modified Polyacrylonitrile (PAN) Fibrous Catalyst', *Journal of Advanced Oxidation Technology*, 14(2), pp. 235–243.

Chi, G. T., Nagy, Z. K. and Huddersman, K. D. (2011) 'Kinetic modelling of the Fenton-like oxidation of maleic acid using a heterogeneous modified polyacrylonitrile (PAN) catalyst', *Progress in Reaction Kinetics and Mechanism*, 36, pp. 189–214.

Chiron, S., Fernandez-alba, A., Rodriguez, A. and Garcia-Calvo, E. (2000) 'Pesticide chemical oxidation: state-of-the-art', *Water Research*, 34(2), pp. 366–377.

Choudhury, A. K. R. (2006) *Textile Preparation and Dyeing*. Enfield: Science Publishers.

Christie, R. M. (2007) *Environmental aspects of textile dyeing*. Edited by R. M. Christie. Cambridge: Woodhead Publishing Limited.

Chronicle, D. (2016) *3,400 ducks die after consuming contaminated effluent water*, *Deccan Chronicle*. Vellore. Available at: http://www.deccanchronicle.com/nation/current-affairs/150716/3400-ducks-die-after-consuming-contaminated-effluent-water.html (Accessed: 13 October 2017).

Chung, K., Fulk, G. E. and Egan, M. (1978) 'Reduction of Azo Dyes by Intestinal Anaerobes', *Applied and Environmental Microbiology*, 35(3), pp. 558–562.

Cihanoğlu, A., Gündüz, G. and Dükkanci, M. (2015) 'Degradation of acetic acid by heterogeneous Fenton-like oxidation over iron-containing ZSM-5 zeolites', *Applied*

Catalysis B: Environmental, 165.

Clarke, E. A. and Anliker, R. (1980) 'Organic Dyes and Pigments', in *The Handbook of Environmental Chemistry: Anthropogenic compounds*. 3rd edn. Heidelberg: Springer, pp. 181–215.

CNN (2017) *Flint Water Crisis Fast Facts*, *CNN Library*. Available at: https://edition.cnn.com/2016/03/04/us/flint-water-crisis-fast-facts/index.html (Accessed: 27 February 2018).

Coal Authority (2016) *Metal mine water treatment*. Available at: https://www.gov.uk/government/collections/metal-mine-water-treatment (Accessed: 3 November 2017).

Coates, J. (2000) 'Interpretation of Infrared Spectra , A Practical Approach', *Encyclopedia of Analytical Chemistry*. John Wiley & Sons, I.

Coelho, A., Castro, A. V. and Sant' Anna Jr., G. L. (2006) 'Treatment of petroleum refinery sourwater by advanced oxidation processes', *Journal of Hazardous Materials*, 137, pp. 178–184.

Comninellis, C., Kapalka, A., Malato, S., Parson, S. A., Poulios, I. and Mantzavinos, D. (2008) 'Advanced oxidation processes for water treatment-advances and trends for R &D.', *Journal of Chemical Technology and Biotechnology*, 83(6), pp. 769–776.

Cook, S. M. F. and Linden, D. R. (1997) 'Use of Rhodamine WT to Facilitate Dilution and Analysis of Atrazine Samples in Short-Term Transport Studies', *Journal of Environmental Quality*, 26(5), pp. 1438–1440.

Cooper, P. (1995) *Colour in Dyehouse Effluent*. Bradford: Society of Dyers and Colourists.

Dada, A. O., Olalekan, A. P., Loatunya, A. M. and Dada, O. (2012) 'Langmuir , Freundlich , Temkin and Dubinin – Radushkevich Isotherms Studies of Equilibrium Sorption of Zn^{2+} Unto Phosphoric Acid Modified Rice Husk', *Journal of Applied Chemistry*, 3(1), pp. 38–45.

Dantas, T. L. P., Mendonça, V. P., José, H. J., Rodrigues, A. E. and Moreira, R. F. P. M. (2006) 'Treatment of textile wastewater by heterogeneous Fenton process using a new composite Fe2O3/carbon', *Chemical Engineering Journal*, 118(1–2), pp. 77–82.

De-Laat, J. and Gallard, H. (1999) 'Catalytic Decomposition of Hydrogen Peroxide by Fe(III) in Homogeneous Aqueous Solution : Mechanism and Kinetic Modeling', *Environmental Science and Technology*, 33(16), pp. 2726–2732.

Deng, S., Wang, P., Zhang, G. and Dou, Y. (2016) 'Polyacrylonitrile-based fiber modified with thiosemicarbazide by microwave irradiation and its adsorption behavior for Cd (II) and Pb (II)', *Journal of Hazardous Materials*. Elsevier B.V., 307, pp. 64–72.

Deng, S., Zhang, G., Wang, X., Zheng, T. and Wang, P. (2015) 'Preparation and performance of polyacrylonitrile fiber functionalized with iminodiacetic acid under microwave irradiation for adsorption of Cu (II) and Hg (II)', *Chemical Engineering Journal*. Elsevier B.V., 276, pp. 349–357.

Derouane, E. G., Parmon, V., Lemos, F. and Ribeiro, F. R. (2002) *Principles and Methods for Accelerated Catalyst Design and Testing*.

Dewil, R., Mantzavinos, D., Poulios, I. and Rodrigo, M. A. (2017) 'New perspectives for Advanced Oxidation Processes', *Journal of Environmental Management*. Elsevier Ltd, 195, pp. 93–99.

Dharani, M. and Balasubramanian, S. (2015) 'Synthesis and characterization of chitosan-g-N-methyl piperazinium chloride - A hybrid flocculant', *International Journal of Biological Macromolecules*, 81, pp. 778–784.

Donati, G. and Paludetto, R. (1997) 'Scale up of chemical reactors', *Catalysis Today*, 34, pp. 483–533.

Donati, G. and Paludetto, R. (1999) 'Batch and semibatch catalytic reactors (from theory to practice)', *Catalysis Today*, 52(2–3), pp. 183–195.

Duarte, F., Morais, V., Maldonado-Hódar, F. J. and Madeira, L. M. (2013) 'Treatment of textile effluents by the heterogeneous Fenton process in a continuous packed-bed reactor using Fe/activated carbon as catalyst', *Chemical Engineering Journal*, 232.

Eisenberg, G. (1943) 'Colorimetric Determination of Hydrogen Peroxide', *Industrial and Engineering Chemistry, Analytical Edition*, 15(5), pp. 327–328.

Ekpurke, A. O. (2018) *Application of a Novel Heterogeneous-Fenton Catalyst in the Treatment of BTEX Contaminated Waters*. De Montfort University.

Elshafei, G. M. S., Yehia, F. Z., Dimitry, O. I. H., Badawi, A. M. and Eshaq, G. (2014)

'Ultrasonics Sonochemistry Ultrasonic assisted-Fenton-like degradation of nitrobenzene at neutral pH using nanosized oxides of Fe and Cu', *Ultrasonics - Sonochemistry*. Elsevier B.V., 21(4), pp. 1358–1365.

Emami, F., Tehrani-bagha, A. R., Gharanjig, K. and Menger, F. M. (2010) 'Kinetic study of the factors controlling Fenton-promoted destruction of a non-biodegradable dye', *Desalination*. Elsevier B.V., 257(1–3), pp. 124–128.

Engelke, P. (2016) *Will the world's next wars be fought over water?*, *Los Angeles Times*. Available at: http://www.latimes.com/world/global-development/op-ed/la-fg-global-water-oped-story.html (Accessed: 8 March 2018).

Environment Agency (2009) *How to comply with your environmental permit-additional guidance for: The Textile Sector (EPR 6.05)*. Bristol.

Environment Canada and Health Canada (2012) *The Chemical Management Plan Substance Groupings Initiative: Aromatic Azo- and Benzidine-Based Substances.*

Esteves, F. and Sousa, E. (2015) 'Electrochemical degradationof C.I. reactive orange 16 in the presence of H_2O_2/Cu+ ions', *International Journal of Industrial Chemistry*, (6), pp. 285–295.

European Comission (2014) *Environmental Improvement Potential of textiles (IMPRO Textiles)*.

European Commission (2003a) *Passive In-situ Remediation of Acidic Mine / Industrial Drainage*.

European Commission (2003b) *Technical Guidance Document on Risk Assessment*. Ispra.

European Commission (2013) *The Seventh Report on the Implementation of the Urban Waste Water Treatment Directive, 91/271/EEC*.

Euzen, J.-P., Trambouze, P. and Wauquier, J.-P. (1993) *Scale-up methodology for chemical processes*. Paris: Editions Technip.

Feng, J., Ã, X. H. and Yue, P. L. (2006) 'Effect of initial solution pH on the degradation of Orange II using clay-based Fe nanocomposites as heterogeneous photo-Fenton catalyst', *Water Research*, 40, pp. 641–646.

Fenton, H. J. H. (1894) 'Oxidation of tartaric acid in presence of iron', *Journal of the*

Chemical Society, 65, pp. 899–910.

Fida, H., Zhang, G., Guo, S. and Naeem, A. (2017) 'Journal of Colloid and Interface Science Heterogeneous Fenton degradation of organic dyes in batch and fixed bed using La-Fe montmorillonite as catalyst', *Journal of Colloid And Interface Science*. Elsevier Inc., 490, pp. 859–868.

Field, M. S., Wilhelm, R. G., Quinlan, J. F. and Aley, T. J. (1995) 'An assessment of the potential adverse properties of fluorescent tracer dyes used for groundwater tracing', *Environmental Monitoring and Assessment*, 38(1), pp. 75–96.

Figueroa, L. and Wolkersdorfer, C. (2014) 'Electrochemical Recovery of Metals in Mining Influenced Water : State of the Art', in Sun, Y. and Wang, C. (eds) *An Interdisciplinary Response to Mine Water Challenges*. Xuzhou,: China University of Mining and Technology, pp. 627–631.

Florence, T. M. (1982) 'Development of physico-chemical speciation procedures to investigate the toxicity of copper, lead, cadmium and zinc towards aquatic biota', *Analytica Chimica Acta*, 141, pp. 73–94.

Forgacs, E., Cserháti, T. and Oros, G. (2004) 'Removal of synthetic dyes from wastewaters: A review', *Environment International*, 30(7), pp. 953–971.

Freedonia (2015) *World Dyes & Organic Pigments*. Freedonia. Available at: https://www.freedoniagroup.com/industry-study/world-dyes-organic-pigments-3264.htm.

Frey, D. D., Frey, D. D., Engelhardt, F. and Greitzer, E. M. (2003) 'A role for " one-factor-at-a-time "experimentation in parameter design A role for one-factor-at-a-time experimentation in parameter design', *Research in Engineering Design*, 14(May 2015), pp. 65–74.

Frey, D. D. and Jugulum, R. (2003) 'How one-factor-at-a-time experimentation can lead to greater improvements than orthogonal arrays', in *International Design Engineering Technical Conferences and Computers and Information in Engineering Conference*. Chicago: American Society of Mechanical Engineers, pp. 1–9.

Fu, F. and Wang, Q. (2011) 'Removal of heavy metal ions from wastewaters : A review', *Journal of Environmental Management*. Elsevier Ltd, 92(3), pp. 407–418.

Fytianos, K., Voudrias, E. and Kokkalis, E. (2000) 'Sorption - desorption behaviour of 2

, 4-dichlorophenol by marine sediments', *Chemosphere*, 40, pp. 3–6.

Gallard, H., De Laat, J. and Legube, B. (1999) 'Spectrophotometric study of the formation of iron(III)-hydroperoxy complexes in homogeneous aqueous solutions', *Water Research*, 33(13), pp. 2929–2936.

Garrel, R. M. and Thompson, M. E. (1960) 'Oxidation of pyrite by iron sulfate solutions', *American Journal of Science*, 258–A, pp. 57–67.

Geological Survey of Japan (2005) *Atlas of Eh-pH diagrams: Intercomparison of thermodynamic databases*. Takeno.

Ghaly, A. E., Ananthashankar, R., Alhattab, M. and Ramakrishnan, V. V (2014) 'Chemical Engineering & Process Technology Production , Characterization and Treatment of Textile Effluents : A Critical Review', *Chemical Engineering & Process Technology*, 5(1), pp. 1–18.

Ghiselli, G., Jardim, W. F., Litter, M. I. and Mansilla, H. D. (2004) 'Destruction of EDTA using Fenton and photo-Fenton-like reactions under UV-A irradiation', *Journal of Photochemistry and Photobiology A: Chemistry*, 167(1), pp. 59–67.

Glaze, W. H. and Kang, J. W. (1989) 'Advanced oxidation processes. Test of a kinetic model for the oxidation of organic compounds with ozone and hydrogen peroxide in semibatch reactor.', *Industrial and Engineering Chemistry Research*, 28(11), pp. 1573–1580.

Gleick, P. H., Cooley, H., Katz, D., Lee, E., Morrison, J., Palaniappan, M., Samulon, A. and Wolf, G. H. (2006) *The World's Water 2006-2007: The Biennial Report on Freshwater Resources*. London: ISLANDPRESS.

Gode, F. and Pehlivan, E. (2006) 'Removal of chromium (III) from aqueous solutions using Lewatit S 100 : The effect of pH , time , metal concentration and temperature', *Journal of Hazardous Materials*, 136, pp. 330–337.

Goldenberg, S. (2014) *Why global water shortages pose threat of terror and war*, *The Gurdian*. Available at: https://www.theguardian.com/environment/2014/feb/09/global-water-shortages-threat-terror-war (Accessed: 8 March 2014).

Gomes, L., Freitas, R. G., Malpass, G. R. P., Pereira, E. C. and Motheo, A. J. (2009) 'Pt film electrodes prepared by the Pechini method for electrochemical decolourisation of Reactive Orange 16', *Journal of Applied Electrochemistry*, 39(1), pp. 117–121.

Gomes, L., Miwa, D. W., Malpass, G. R. P. and Motheo, A. J. (2011) 'Electrochemical degradation of the dye reactive orange 16 using electrochemical flow-cell', *Journal of the Brazilian Chemical Society*, 22(7), pp. 1299–1306.

González-Bahamón, L. F., Mazille, F., Benítez, L. N. and Pulgarín, C. (2011) 'Photo-Fenton degradation of resorcinol mediated by catalysts based on iron species supported on polymers', *Journal of Photochemistry and Photobiology A: Chemistry*, 217(1), pp. 201–206.

Graf, E., Mahoneys, J. R., Bryant, R. G. and Eaton, J. W. (1984) 'Iron-catalyzed Hydroxyl Radical Formation. Stringent requirement for free iron coordination site.', *The Journal of Biological Chemistry*, 259(6), pp. 3620–3624.

Greluk, M. and Hubicki, Z. (2013) 'Effect of basicity of anion exchangers and number and positions of sulfonic groups of acid dyes on dyes adsorption on macroporous anion exchangers with styrenic polymer matrix', *Chemical Engineering Journal*. Elsevier B.V., 215–216, pp. 731–739.

Guimarães, I. R., Oliveira, L. C. A., Queiroz, P. F., Ramalho, T. C., Fabris, J. D. and Ardisson, J. D. (2008) 'Modified goethites as catalyst for oxidation of quinoline : Evidence of heterogeneous Fenton process', *Applied Catalysis A: General*, 347, pp. 89–93.

Gumerov, F. M., Neindre, B. Le, Bilalov, T. R. and Sagdeev, A. A. (2016) 'Regeneration of Spent Catalyst and Impregnation of Catalyst by Supercritical Fluid', pp. 51–65.

Gupta, V. K., Khamparia, S., Tyagi, I., Jaspal, D. and Malviya, A. (2015) 'Decolorization of mixture of dyes : A critical review', *Global J. Environmental Science and Management*, 1(1), pp. 71–94.

Gürses, A. (2016) 'Classification of Dye and Pigments', in *Dyes and Pigments*, pp. 31–45.

Gürses, A., Acikyildiz, M., Güenes, K. and Gürses, M. S. (2016) *Springer briefs in Molecular Science, Green Chemistry for Sustainability: Dyes and Pigments*. Edited by S. K. Sharma. Switzerland: Springer Nature.

Hagen, J., Chorkendorff, I. and Niemantsverdriet, J. W. (2006) *Industrial Catalysis: A practical Approach*, *Simulation*.

Hao, O. J., Kim, H. and Chiang, P. (2000) 'Decolorization of wastewater: Critical review',

Critical Reviews in Environmental Science and Technology, 30(4), pp. 449–505.

Harland, C. E. (1994) *Ion Exchange: Theory and Practive*. Second. Cambridge: Royal Society of Chemistry.

Hartley, S. (2009) *Remediation of abandoned metal mine drainage using dealginated seaweed*, *Aberystwyth University*. Aberystwyth University.

Hasan, D. B., Aziz, A. R. A. and Daud, W. M. A. W. (2012) 'Oxidative mineralisation of petroleum refinery effluent using Fenton-like process', *Chemical Engineering Research and Design*. Institution of Chemical Engineers, 90(2), pp. 298–307.

Hassaan, M. A. and Nemr, A. El (2017) 'Advanced Oxidation Processes for Textile Wastewater Treatment', *International Journal of Photochemistry and Photobiology*, 2(3), pp. 85–93.

Hassan, H. and Hameed, B. H. (2011) 'Fenton-like Oxidation of Acid Red 1 Solutions Using Heterogeneous Catalyst Based on Ball Clay', *International Journal of Environmental Science and Development*, 2(3), pp. 218–222.

He, J., Yang, X., Men, B. and Wang, D. (2016) 'Interfacial mechanisms of heterogeneous Fenton reactions catalyzed by iron-based materials: A review', *Journal of Environmental Sciences (China)*. Elsevier B.V., 39, pp. 97–109.

Hegazi, H. A. (2013) 'Removal of heavy metals from wastewater using agricultural and industrial wastes as adsorbents', *HBRC Journal*. Housing and Building National Research Center, 9(3), pp. 276–282.

Hem, J. D. (1972) 'Chemistry and Occurrence of Cadmium and Zinc in Surface Water and Groundwater', *Water Resources Research*, 8(3), pp. 661–679.

Herber, R. F. M., Verschoor, M. A. and Wibowo, A. A. E. (1988) 'A Review of the Kinetics and Kidney Effects of Cadmium - Recent Epidemiological Studies', in Stoeppler, M. and Piscator, M. (eds) *Cadmium-Environmental Toxin Series*. Berling: Springer, pp. 115–131.

Hodaifa, G., Ochando-Pulido, J. M., Rodriguez-Vives, S. and Martinez-Ferez, A. (2013) 'Optimization of continuous reactor at pilot scale for olive-oil mill wastewater treatment by Fenton-like process', *Chemical Engineering Journal*, 220, pp. 117–124.

Hoigné, J. (1997) 'Inter-calibration of OH radical sources and water quality parameters',

Water Science and Technology, 35(4), pp. 1–8.

Holkar, C. R., Jadhav, A. J., Pinjari, D. V, Mahamuni, N. M. and Pandit, A. B. (2016) 'A critical review on textile wastewater treatments : Possible approaches', *Journal of Environmental Management*. Elsevier Ltd, 182, pp. 351–366.

Horning, R. H. (1978) *Textile Dyeing Wastewaters: Characterization and Treatment*. Washington, DC.

Hu, W. and Pei, H. (2002) 'Decomposed characteristic of azo dyes by ozonization with ultrasonic enhancement', *Chinese Science Bulletin*, 47(12), pp. 986–989.

Huang, H.-H. (2016) 'The Eh-pH Diagram and Its Advances', *Metals*, 6(1), p. 23.

Hudson-Edwards, K. A., Macklin, M. G., Brewer, P. A. and Dennis, I. A. (2008) *Assessment of Metal Mining-Contaminated River Sediments in England and Wales protecting and improving the environment in England and Wales*. Bristol.

Hunger, K. (1991) 'On the Toxicology and Ecology of Organic Colorants', *Chimia*, 45(1010), pp. 297–300.

Hunger, K. (2003) *Industrial Dyes: Chemistry, Properties, Applications*.

Idel-aouad, R., Valiente, M., Yaacoubi, A., Tanouti, B. and López-Mesas, M. (2011) 'Rapid decolourization and mineralization of the azo dye C . I . Acid Red 14 by heterogeneous Fenton reaction', *Journal of Hazardous Materials*. Elsevier B.V., 186(1), pp. 745–750.

Igwe, J. C. (2007) 'A Review of Potentially Low Cost Sorbents for Heavy Metal Removal and Recovery', *Terrestrial and Aquatic Environmental Toxicology*.

Ilsen, Z. and Avci, A. K. (2016) *Multiphase Catalytic Reactors: Theory, Design, Manufacturing, and Applications*. Edited by Z. . Önsan and A. K. Avci. New Jersery: John Wiley & Sons, Inc.

Inamuddin. and Luqman, M. (2012) *Ion Exchange Technology I -Theory and Materials*. Edited by Inamuddin and M. Luqman. London: Springer.

Inglezakis, V. J. and Poulopoulos, S. G. (2006) *Adsorption, Ion Exchange and Catalysis: Design of Operations and Environmental Applications*. First, *Adsorption, Ion Exchange and Catalysis*. First. Athens: Elsevier.

Interstate Technology Regulatory Council (2010) *Mining Waste Treatment Technology*

Selection, *Technology Overviews*. Available at: http://www.itrcweb.org/miningwaste-guidance/technology_overviews.htm (Accessed: 6 November 2017).

Ishtchenko, V. V, Huddersman, K. D. and Vitkovskaya, R. F. (2003) 'Part 1. Production of a modified PAN fibrous catalyst and its optimisation towards the decomposition of hydrogen peroxide', *Applied Catalysis A: General*, 242, pp. 123–137.

Jacques, C. V. (2017) 'Heterogeneous Catalysis on Metal Oxides', *Catalysts*, 7(11), p. 341.

Jadhav, J. P., Kalyani, D. C., Telke, A. A., Phugare, S. S. and Govindwar, S. P. (2010) 'Evaluation of the efficacy of a bacterial consortium for the removal of color, reduction of heavy metals, and toxicity from textile dye effluent', *Bioresource Technology*. Elsevier Ltd, 101(1), pp. 165–173.

Jain, C. K. and Ram, D. (1997) 'Adsorption of lead and zinc on bed sediments on the river Kali', *Water Research*, 31(1), pp. 154–162.

Jana, A. K. (2011) *Chemical Process Modelling and Computer Simulation*. Second. New Delhi: PHI Learning Private Limited.

Jassal, M., Bhowmick, S., Sengupta, S., Patra, P. K. and Walker, D. I. (2014) 'Hydrolyzed Poly(acrylonitrile) Electrospun Ion-Exchange Fibers', *Environmental Engineering Science*, 31(6), pp. 288–299.

Jiang, C., Pang, S., Ouyang, F., Ma, J. and Jiang, J. (2010) 'A new insight into Fenton and Fenton-like processes for water treatment', *Journal of Hazardous Materials*, 174, pp. 813–817.

Johnston, D., Parker, K. and Pritchard, J. (2007) 'Management of abandoned minewater pollution in the United Kingdom', in Cidu, R. and Frau, F. (eds) *Water in Mining Environments*. Cagliari: International Mine Water Association.

Johnston, D. and Rolley, S. (2008) 'Abandoned Mines and the Water Framework Directive in the United Kingdom', in *Mine Water and the Environment*. Czech Republic: VSB-Technical University of Ostrava, pp. 529–532.

Johnston, D., Watson, I., Potter, H., Jones, C., Rolley, S. and Pritchard, J. (2008) *Abandoned mines and the water environment*. Bristol.

Kampalanonwat, P. and Supaphol, P. (2014) 'The Study of Competitive Adsorption of

Heavy Metal Ions from Aqueous Solution by Aminated Polyacrylonitrile Nanofiber Mats', *Energy Procedia*. Elsevier B.V., 56, pp. 142–151.

Karthik, T. and Rathinamoorthy, R. (2015) 'Recycling and Reuse of Textile Effluent Sludge', in Senthikannan Muthu, S. (ed.) *Environmental Implications of Recycling and Recycled*. Hong Kong: Springer, pp. 213–258.

Karthikeyan, S., Titus, A., Gnanamani, A., Mandal, A. B. and Sekaran, G. (2011) 'Treatment of textile wastewater by homogeneous and heterogeneous Fenton oxidation processes', *Desalination*. Elsevier B.V., 281(1), pp. 438–445.

Kasiri, M. B., Aleboyeh, H. and Aleboyeh, A. (2008) 'Degradation of Acid Blue 74 using Fe-ZSM5 zeolite as a heterogeneous photo-Fenton catalyst', *Applied Catalysis B : Environmental*, 84, pp. 9–15.

Kelly, M. (1988) *Mining and the freshwater environment*. London: Elsvier in association with The British Petroleum Company.

Khalid, A., Arshad, M. and Crowley, D. (2010) 'Bioaugumentation of Azo Dyes', in Erkurt, H. A. (ed.) *The handbook of environmental chemistry*. Ninth. Heidelberg: Springer, pp. 1–121.

Khataee, A., Salahpour, F., Fathinia, M., Seyyedi, B. and Vahid, B. (2015) 'Iron rich laterite soil with mesoporous structure for heterogeneous Fenton-like degradation of an azo dye under visible light', *Journal of Industrial and Engineering Chemistry*, 26.

Kiani, G. R., Sheikhloie, H. and Arsalani, N. (2011) 'Heavy metal ion removal from aqueous solutions by functionalized polyacrylonitrile', *Desalination*. Elsevier B.V., 269, pp. 266–270.

Knackmuss, H.-J. (1996) 'Basic knowledge and perspectives of bioelimination xenobiotic compounds', *Journal of Biotechnology*, 51, pp. 287–295.

Kosandrovich, E. G. and Soldatov, V. S. (2012) 'Fibrous Ion Exchangers', in Inamuddin. and Luqman, M. (eds) *Ion Exchange Technology I Theory and Materials*. London: Springer, p. 561.

Kubilay, Ş., Gürkan, R., Savran, A. and Şahan, T. (2007) 'Removal of Cu(II), Zn(II) and Co(II) ions from aqueous solutions by adsorption onto natural bentonite', *Adsorption*, 13, pp. 41–51.

Kumar, R., Pant, N. and Srivastava, S. (2000) 'Chlorinated pesticides and heavy metals', *International Journal of Andrology*.

Kuo, W. G. (1992) 'Decolorizing dye wastewater with Fenton's reagent', *Water Research*, 26(7), pp. 881–886.

Kušić, H., Božić, A. L. and Koprivanac, N. (2007) 'Fenton type processes for minimization of organic content in coloured wastewaters : Part I : Processes optimization', *Dyes and Pigments*, 74, pp. 380–387.

Langmuir, D. (1997) *Aqueous Environmental Geochemistry*. Edited by R. McConnin. New Jersey: Prentice Hall Inc.

Lewis, T. J., Richards, D. H. and Salter, D. A. (1963) 'Peroxy-complexes of inorganic ions in hy- drogen peroxide–water mixtures. Part I. Decomposition by ferric ions', *Journal of Chemical Society*, pp. 2434–2446.

Li, R., Gao, B., Sun, J., Yue, Q., Wang, Y. and Xu, X. (2016) 'Synthesis , characterization of a novel lignin-based polymer and its behavior as a coagulant aid in coagulation / ultra fi ltration hybrid process', *International Biodeterioration & Biodegradation*. Elsevier Ltd, 113, pp. 334–341.

Liu, R. X., Zhang, B. W. and Tang, H. X. (1999) 'Synthesis and characterization of poly (acrylaminophosphonic- carboxyl-hydrazide) chelating fibre', *Reactive and Functional Polymers*, 39, pp. 71–81.

Liu, W., Yao, C., Wang, M., Ji, J., Ying, L. and Fu, C. (2012) 'Kinetics and Thermodynamics Characteristics of Cationic Yellow X-GL Adsorption on Attapulgite / Rice Hull-Based Activated Carbon Nanocomposites', *Environmental Progress & Sustainable Energy*, 32(3), pp. 655–662.

Lopez, A., Mascolo, G., Detomaso, A., Lovecchio, G. and Villani, G. (2005) 'Temperature activated degradation (mineralization) of 4-chloro-3-methyl phenol by Fenton's reagent', *Chemosphere*, 59, pp. 397–403.

Lopez, G., Taghon, G. and Levinton, J. (1989) *Ecology of Marine Deposits Feeders*. Edited by G. Lopez, G. Taghon, and J. Levinton. New York: Springer-Verlag.

Luna, L. A. V. De, Thiago, H. G., Pupo, R. F., Kummrow, F. and Umbuzeiro, G. A. (2014) 'Aquatic toxicity of dyes before and after photo-Fenton treatment', *Journal of Hazardous Materials*. Elsevier B.V., 276, pp. 332–338.

Lv, H., Zhao, H., Cao, T., Qian, L., Wang, Y. and Zhao, G. (2015) 'Efficient degradation of high concentration azo-dye wastewater by heterogeneous Fenton process with iron-based metal-organic framework', *Journal of Molecular Catalysis. A: Chemical*. Elsevier B.V., 400, pp. 81–89.

Ma, J., Song, W., Chen, C., Ma, W., Zhao, J. and Tang, Y. (2005) 'Fenton degradation of organic compounds promoted by dyes under visible irradiation', *Environmental Science and Technology*, 39(15), pp. 5810–5815.

Ma, L., Zhuo, R., Liu, H., Yu, D., Jiang, M., Zhang, X. and Yang, Y. (2014) 'Efficient decolorization and detoxification of the sulfonated azo dye Reactive Orange 16 and simulated textile wastewater containing Reactive Orange 16 by the white-rot fungus Ganoderma sp. En3 isolated from the forest of Tzu-chin Mountain in China', *Biochemical Engineering Journal*, 82, pp. 1–9.

MacKay, K. M., MacKay, R. A. and Henderson, W. (2002) *Introduction to Modern Inorganic Chemistry*. Sixth. Cheltenham: Nelson Thornes.

Madan, R. L. (2013) *Organic Chemistry*. New Delhi: Tata McGraw-Hill Education Private Limited.

Manhan, S. E. (2011) *Water Chemsitry: Green Science and Technology of Nature's Most Renewalbe Resource*. London: CRC Press - Taylor & Francis Group.

Marin-morales, M. A., Ventura-camargo, B. D. C. and Marin-morales, M. A. (2013) 'Azo Dyes : Characterization and Toxicity – A Review', *Textiles and Light Industrial Science and Technology*, 2(2).

Martínez, F., Calleja, G., Melero, J. A. and Molina, R. (2005) 'Heterogeneous photo-Fenton degradation of phenolic aqueous solutions over iron-containing SBA-15 catalyst', *Applied Catalysis B: Environmental*, 60(3–4), pp. 181–190.

Martins, R. C., Rossi, A. F. and Quinta-Ferreira, R. M. (2010) 'Fenton ' s oxidation process for phenolic wastewater remediation and biodegradability enhancement', *Journal of Hazardous Materials*, 180, pp. 716–721.

Maycock, D., Peters, A., Merrington, G. and Crane, M. (2010) *Proposed EQS for Water Framework Directive Annex VIII substances : zinc (For consultation)*. Edinburgh.

Mayes, W. M., Gozzard, E., Potter, H. and Jarvis, A. P. (2006) 'Identifying diffuse sources of inorganic pollutants in post-industrial catchments', in *4th Annual CIWEM*

conference. Newcastle upon Tyne, pp. 1–9.

Mayes, W. M., Potter, H. A. B. and Jarvis, A. P. (2009) 'Novel approach to zinc removal from circum-neutral mine waters using pelletised recovered hydrous ferric oxide', *Journal of Hazardous Materials*, 162, pp. 512–520.

Melero, J. A., Martínez, F., Botas, J. A., Molina, R. and Pariente, M. I. (2009) 'Heterogeneous catalytic wet peroxide oxidation systems for the treatment of an industrial pharmaceutical wastewater', *Water Research*, 43(16), pp. 4010–4018.

Menini, L., Silva, M. J., Lelis, M. F. F., Fabris, J. D., Lago, R. M. and Gusevskaya, E. V (2004) 'Novel solvent free liquid-phase oxidation of β-pinene over heterogeneous catalysts based on $Fe_{3-x}M_xO_4$ (M = Co and Mn)', *Applied Catalysis A: General*, 269, pp. 117–121.

Meshram, S., Limaye, R., Ghodke, S., Nigam, S., Sonawane, S. and Chikate, R. (2011) 'Continuous flow photocatalytic reactor using ZnO-bentonite nanocomposite for degradation of phenol', *Chemical Engineering Journal*. Elsevier B.V., 172(2–3), pp. 1008–1015.

Mesquita, I., Matos, L. C., Duarte, F., Maldonado-Hódar, F. J., Mendes, A. and Madeira, L. M. (2012) 'Treatment of azo dye-containing wastewater by a Fenton-like process in a continuous packed-bed reactor filled with activated carbon', *Journal of Hazardous Materials*. Elsevier B.V., 237–238, pp. 30–37.

Mestre, M. A. (2009) *Environmental impact of mine drainage and its treatment on aquatic communities*. Univeristy of Birmingham.

Migliorini, F. L., Braga, N. A., Alves, S. A., Lanza, M. R. V, Baldan, M. R. and Ferreira, N. G. (2011) 'Anodic oxidation of wastewater containing the Reactive Orange 16 Dye using heavily boron-doped diamond electrodes', *Journal of Hazardous Materials*. Elsevier B.V., 192(3), pp. 1683–1689.

Mijin, D. Ž., Dabić, D. M., Mirković, J. M., Božić, B. Đ. and Grgur, B. N. (2016) 'Influence of microwave irradiation on hypochlorite decolorisation of synthetic dyes', *Zaštita materijala*, 57(1), pp. 63–70.

Miller, A., Figueroa, L. and Wildeman, T. (2006) 'Mechanism of nickel and zinc removal in oxic limestone systems and the application to metal mine drainages', in Barnhisel, R. I. (ed.) *International Conference on Acid Rock Drainage (ICARD)*. St. Louise:

American Society of Mining and Reclamation (ASMR), pp. 1302–1313.

Miller, A., Figueroa, L. and Wildeman, T. (2011) 'Zinc and nickel removal in simulated limestone treatment of mining influenced water', *Applied Geochemistry*. Elsevier Ltd, 26(1), pp. 125–132.

Miller, A., Wildeman, T. and Figueroa, L. (2013) 'Zinc and nickel removal in limestone based treatment of acid mine drainage : The relative role of adsorption and co-precipitation', *Applied Geochemistry*. Elsevier Ltd, 37, pp. 57–63.

Ming, T. K. (2011) *Removal of Reactive Orange 16 using chemicall modified pineapple peels*. Tunku Abdul Rahman.

Mishra, P. C. and Patel, R. K. (2009) 'Removal of lead and zinc ions from water by low cost adsorbents', *Journal of Hazardous Materials*, 168, pp. 319–325.

Mitrović, J., Radović, M., Bojić, D., Anbelković, T., Purenović, M. and Bojić, A. (2012) 'Decolorization of the textile azo dye Reactive Orange 16 by the UV/H_2O_2 process', *Journal of the Serbian Chemical Society*, 77(4), pp. 465–481.

Mohan, D. and Singh, K. P. (2002) 'Single- and multi-component adsorption of cadmium and zinc using activated carbon derived from bagasse - an agricultural waste.', *Water Research*, 36, pp. 2304–2318.

Molina, R., Martínez, F., Melero, J. A., Bremner, D. H. and Chakinala, A. G. (2006) 'Mineralization of phenol by a heterogeneous ultrasound/Fe-SBA-15/H_2O_2 process: Multivariate study by factorial design of experiments', *Applied Catalysis B: Environmental*, 66(3–4), pp. 198–207.

Muhammad, A., Shafeeq, A., Butt, M. A., Rizvi, Z. H., Chughtai, M. A. and Rehman, S. (2008) 'Decolorization and removal of COD and BOD from raw and biotreated textile dye bath effluent through advanced oxidation processes (AOPS)', *Brazilian Journal of Chemical Engineering*, 25(3), pp. 453–459.

Mullinger, N. (2004) 'Assessing the Impacts of Metal Mines in Wales', in Jarvis, A. P., Dudgeon, B. A., and Younger, P. L. (eds). Newcastle upon Tyne: International Mine Water Association, pp. 209–217.

Muñoz, I., Rieradevall, J., Torrades, F., Peral, J. and Domènech, X. (2006) 'Environmental assessment of different advanced oxidation processes applied to a bleaching Kraft mill effluent', *Chemosphere*, 62(1), pp. 9–16.

Muray, J. J. (1962) 'Surface Conductivity of Borosilicate Glass', *Journal of Applied Physics*, 33(4).

Muruganandham, M. and Swaminathan, M. (2004) 'Decolourisation of Reactive Orange 4 by Fenton and photo-Fenton oxidation technology', *Dyes and Pigments*, 63(3), pp. 315–321.

Mustafa, E. and Ünlü, N. (2006) 'Adsorption characteristics of heavy metal ions onto a low cost biopolymeric sorbent from aqueous solutions', *Journal of Hazardous Materials B*, 136, pp. 272–280.

Muthu, S. S. (2017) *Textiles and Clothing Sustainability: Sustainable Technologies*. Singapore: Springer Nature.

Nanda, S. (2008) 'Reactors and Fundamentals of Reactors Design for Chemical Reaction', *Pharmaceutical Engineering*.

Narayanan, Y. (2015) *Religion, Heritage and the Sustainable City: Hinduism and Urbanisation in Jaipur*. New York: Routledge.

National Centre for Biotechnology Information (2018) *Reactive Orange 16*, *PubChem Compound Database; CID=6509773*.

National Rivers Authority (1994) *Abandoned mines and the water environment*. Bristol.

Nauman, E. B. (2001) *Chemical Reactor Design, Optimization and Scaleup*.

Neamtu, M., Yediler, A., Siminiceanu, I. and Kettrup, A. (2003) 'Oxidation of commercial reactive azo dye aqueous solutions by the photo-Fenton and Fenton-like processes', *Journal of Photochemistry and Photobiology A: Chemistry*, 161, pp. 87–93.

Neamtu, M., Yediler, A., Siminiceanu, I., Macoveanu, M. and Kettrup, A. (2004) 'Decolorization of disperse red 354 azo dye in water by several oxidation processes - a comparative study', *Dyes and Pigments*, 60(1), pp. 61–68.

NepaliSansar (2018) *Nepal Welcomes Holi 2018, A Festival of Colours*, *NepaliSansar*. Available at: http://www.nepalisansar.com/culture/nepal-welcomes-holi-festival-colors/ (Accessed: 3 March 2018).

Nesteronok, P. V and Soldatov, V. S. (2011) 'Acid – base properties of ion exchangers : V . Synthesis and properties of ion exchangers on the base of modacrylic polyacrylonitrile – vinylchloride fibers', *Reactive and Functional Polymers*. Elsevier

Ltd, 71(10), pp. 1033–1039.

Neyens, E. and Baeyens, J. (2003) 'A review of classic Fenton's peroxidation as an advanced oxidation technique', *Journal of Hazardous Materials*, 98(1–3), pp. 33–50.

Ngah, W. S. W. and Hanafiah, M. A. K. M. (2008) 'Removal of heavy metal ions from wastewater by chemically modified plant wastes as adsorbents : A review', *Bioresource Technology*, 99, pp. 3935–3948.

Nidheesh, P. . V. (2015) 'Heterogeneous Fenton catalysts for the abatement of organic pollutants from aqueous solution: a review', *Rsc Advances*, 5(51), pp. 40552–40577.

Nidheesh, P. V., Gandhimathi, R. and Ramesh, S. T. (2013) 'Degradation of dyes from aqueous solution by Fenton processes: A review', *Environmental Science and Pollution Research*, 20(4), pp. 2099–2132.

Nigam, P., Banat, I. M., Singh, D. and Marchanv, R. (1996) 'Microbial Process for the Decolorization of Textile Effluent Containing Azo , Diazo and Reactive Dyes', *Process Biochemistry*, 31(5), pp. 435–442.

Nordstrom, D. K. (1982) 'Aqueous pyrite oxidation and the consequent formation of secondary minerals', in Kittrick, J., Fanning, D., and Hosner, L. (eds) *Acid Sulfate Weathering*. Madison: Soil Sciences Society of America, pp. 37–56.

NPCS Board of Consultants and Engineers (2009) *Handbook on Textile Auxiliaries, Dyes and Dye Intermediates Technology*. New Delhi: Asia Pacific Business Press Inc.

Nuttall, C. A. and Younger, P. L. (2000) 'Zinc removal from hard, circum-neutral mine waters using a novel closed-bed limestone reactor', *Water Research*, 34(4), pp. 1262–1268.

Oliveira, G. A. R., Ferraz, E. R. A., Chequer, F. M. D., Grando, M. D., Angeli, J. P. F., Tsuboy, M. S., Marcarini, J. C., Mantovani, M. S., Osugi, M. E., Lizier, T. M., Zanoni, M. V. B. and Oliveira, D. P. (2010) 'Chlorination treatment of aqueous samples reduces , but does not eliminate , the mutagenic effect of the azo dyes Disperse Red 1 , Disperse Red 13 and Disperse Orange 1', *Mutation Research - Genetic Toxicology and Environmental Mutagenesis*. Elsevier B.V., 703(2), pp. 200–208.

Oller, I., Malato, S. and Sánchez-pérez, J. A. (2011) 'Science of the Total Environment Combination of Advanced Oxidation Processes and biological treatments for wastewater decontamination — A review', *Science of the Total Environment*. Elsevier

B.V., 409(20), pp. 4141–4166.

Øllgaard, H., Frost, L., Galster, J. and Hansen, O. C. (1998) *Survey of azo-colorants in Denmark : Consumption , use , health and envi- ronmental aspects*.

Orlova, M. V. (2010) *Development of Catalyst on Polymer Support for Organic Compounds Destruction*. De Montfort University.

Pagga, U. and Brown, D. (1986) 'The degradation of dyestuffs: Part II Behaviour of dyestuffs in aerobic biodegradation tests', *Chemosphere*, 15(4), pp. 479–491.

Pahari, A. K. and Chauhan, B. S. (2006) *Engineering Chemistry*. New Delhi: Laxmi Publications (P) LTD.

Panda, N., Sahoo, H. and Mohapatra, S. (2011) 'Decolourization of Methyl Orange using Fenton-like mesoporous Fe2O3-SiO2 composite', *Journal of Hazardous Materials*, 185(1), pp. 359–365.

Pandiselvi, K. and Thambidurai, S. (2013) 'Synthesis of porous chitosan – polyaniline / ZnO hybrid composite and application for removal of reactive orange 16 dye', *Colloids and Surfaces B: Biointerfaces*. Elsevier B.V., 108, pp. 229–238.

Panel on New Directions in Catalytic Science and Technology, N. R. C. (1992) *Catalysis Looks to the Future*. Washington, D.C.: National Academy Press.

Parson, S. (2004) *Advanced Oxidation Processes for Water and Wastewater Treatment*. London: IWA Publishing.

Pastrana-Martínez, L. M., Pereira, N., Lima, R., Faria, J. L., Gomes, H. T. and Silva, A. M. T. (2015) 'Degradation of diphenhydramine by photo-Fenton using magnetically recoverable iron oxide nanoparticles as catalyst', *Chemical Engineering Journal*, 261.

Pearce, C. I., Lloyd, J. R. and Guthrie, J. T. (2003) 'The removal of colour from textile wastewater using whole bacterial cells : a review', *Dyes and Pigments*, 58, pp. 179–196.

Pearce, S. (2014) *Metal Mine Water Treatment Review: A report prepared for The Coal Authority*. Manchester.

Pera-titus, M., Garc, V., Baños, M. A., Giménez, J. and Esplugas, S. (2004) 'Degradation of chlorophenols by means of advanced oxidation processes : a general review', *Applied Catalysis B: Environmental*, 47, pp. 219–256.

Perego, C. and Peratello, S. (1999) 'Experimental methods in catalytic kinetics', *Catalysis Today*, 52(2–3), pp. 133–145.

Pereira, L. and Alves, M. (2016) 'Dyes-Environmental Impact and Remediation', in Susskind, L. and Jain, R. (eds) *Strategies for Sustainability*. Springer, pp. 111–162.

Petrov, L. (2002) 'Problems and challenges about accelerated testing of the catalytic activity of catalysts', in Derouane, E. G., Lemos, F., and Ribeiro, F. R. (eds) *Principles and Methods for Accelerated Catalyst Design and Testing*. 69th edn. Vilamoura: Springer, Dordrecht, p. 503.

Pignatello, J. J., Oliveros, E. and Mackay, A. (2006) 'Advanced Oxidation Processes for Organic Contaminant Destruction Based on the Fenton Reaction and Related Chemistry', *Critical Reviews in Environmental Science and Technology*, 36(1), pp. 1–84.

Pizzolato, T. M., Carissimi, E., Machado, E. L. and Schneider, I. A. H. (2002) 'Colour removal with NaClO of dye wastewater from an agate-processing plant in Rio Grande do Sul , Brazil', *International Journal of Mineral Processing*, 65, pp. 203–211.

Powell, R. M., Blowes, D. W., Gillham, R. W., Schultz, D., Sivavec, T., Puls, R. W., Vogan, J. L., Powell, P. D. and Landis, R. (1998) *Permeable Reactive Barrier Technologies for Contaminant Remediation*. Washington, DC.

Price, S., Huddersman, K., Shen, J. and Walsh, S. (2012) 'Mycobactericidal activity of Hydrogen Peroxide Activated by a Novel Heterogeneous Fentons-like Catalyst System', *Letters in Applied Microbiology*, 56(2), pp. 83–87.

Purnama, H. (2005) 'Photocatalytic decolourization of reactive orange 16 (R3R) dye', *Jurnal Teknik Gelagar*, 16(2), pp. 85–90.

Queirós, S., Morais, V., Rodrigues, C. S. D., Maldonado-Hódar, F. J. and Madeira, L. M. (2015) 'Heterogeneous Fenton's oxidation using Fe/ZSM-5 as catalyst in a continuous stirred tank reactor', *Separation and Purification Technology*, 141.

Rahim Pouran, S., Abdul Aziz, A. R., Wan Daud, W. M. A. and Embong, Z. (2015) 'Niobium substituted magnetite as a strong heterogeneous Fenton catalyst for wastewater treatment', *Applied Surface Science*, 351.

Ramirez, J. H., Costa, C. A., Madeira, L. M., Mata, G., Vicente, M. A., Rojas-Cervantes, M. L., López-Peinado, A. J. and Martín-Aranda, R. M. (2007) 'Fenton-like oxidation of

Orange II solutions using heterogeneous catalysts based on saponite clay', *Applied Catalysis B: Environmental*, 71(1–2), pp. 44–56.

Ramirez, J. H., Duarte, F. M., Martins, F. G., Costa, C. A. and Madeira, L. M. (2009) 'Modelling of the synthetic dye Orange II degradation using Fenton's reagent: From batch to continuous reactor operation', *Chemical Engineering Journal*, 148(2–3), pp. 394–404.

Ramirez, J. H., Maldonado-Hódar, F. J., Pérez-Cadenas, A. F., Moreno-castilla, C., Costa, C. A. and Madeira, L. M. (2007) 'Azo-dye Orange II degradation by heterogeneous Fenton-like reaction using carbon-Fe catalysts', *Applied Catalysis B : Environmental*, 75(3–4), pp. 312–323.

Ranade, V. V. and Bhandari, V. M. (2014) *Industrial wastewater treatment, recycling and reuse*. Oxford: Elsevier.

Rauf, M. A. and Ashraf, S. S. (2009) 'Fundamental principles and application of heterogeneous photocatalytic degradation of dyes in solution', *Chemical Engineering Journal*, 151(1), pp. 10–18.

Razo-Flores, E., Luijten, M., Donlon, B., Lettinga, G. and Jim, F. (1997) 'Biodegradation of selected azo dyes under methanogenic conditions.', *Water Science and Technology*, 36(6–7), pp. 65–72.

Ribeiro, A. R., Nunes, O. C., Pereira, M. F. R. and Silva, A. M. T. (2015) 'An overview on the advanced oxidation processes applied for the treatment of water pollutants defined in the recently launched Directive 2013/39/EU', *Environment International*.

Richardson, J. T. (1989) *Principles of Catalyst Development*. First. New York: Springer-Science+Business Media, B.V.

Rifai, R. (2016) *State of emmergency in US city after water poisoned*, *Aljazeera*. Available at: https://www.aljazeera.com/news/2015/12/state-emergency-city-water-poisoned-151229165652041.html (Accessed: 2 March 2018).

Risk and Policy Analysis Ltd. (1997) *Analysis of the advantage and drawback of banning azo dyes and products treated with azo dyes. Final Report for Director General III of the European Commission, Great Britain*.

Rivas, F. J., Beltrán, F. J., Gimeno, O. and Alvarez, P. (2003) 'Optimisation of Fenton's reagent usage as a pre-treatment for fermentation brines', *Journal of Hazardous*

Materials, 96, pp. 277–290.

Robertson, A. J. B. (1975) 'The Early History of Catalysis', *Platinum Metal Review*. Johnson Matthey Technology, 19(2), pp. 64–69.

Robinson, T., Mcmullan, G., Marchant, R. and Nigam, P. (2001) 'Remediation of dyes in textile effluent : a critical review on current treatment technologies with a proposed alternative', *Bioresource Technology*, 77(3), pp. 247–255.

Rodríguez, M. (2003) *Fenton and UV-vis based advanced oxidation processes in wastewater treatment: Degradation, mineralization and biodegradability enhancement*. University of Barcelona.

Rozas, A. C. (2017) *Textile Toxicity: What lurks in your clothes*, *Fashion United*. Available at: https://fashionunited.uk/news/fashion/textile-toxicity-what-lurks-in-your-clothes/2017061424828 (Accessed: 13 October 2017).

Ruppert, G., Bauer, R., Heisler, G. and Novalic, S. (1993) 'Mineralization of cyclic organic water contaminants by the photo-Fenton reaction: influence of structure and substituents', *Chemosphere*, 27(8), pp. 1339–1347.

Salleh, M. A. M., Mahmoud, D. K., Karim, W. A. W. A. and Idris, A. (2011) 'Cationic and anionic dye adsorption by agricultural solid wastes: a comprehensive review', *Desalination*, 280(1–3), pp. 1–13.

Saratale, R. G., Saratale, G. D., Chang, J. S. and Govindwar, S. P. (2011) 'Bacterial decolorization and degradation of azo dyes : A review', *Journal of the Taiwan Institute of Chemical Engineers*. Taiwan Institute of Chemical Engineers, 42(1), pp. 138–157.

Satishkumar, G., Landau, M. V., Buzaglo, T., Frimet, L., Ferentz, M., Vidruk, R., Wagner, F., Gal, Y. and Herskowitz, M. (2013) 'Fe/SiO_2 heterogeneous Fenton catalyst for continuous catalytic wet peroxide oxidation prepared in situ by grafting of iron released from $LaFeO_3$', *Applied Catalysis B: Environmental*, 138–139.

Scottish Environment Protection Agency (2014) *Supporting Guidance (WAT-SG-05) Point Source Discharge Constituents*.

Sebesta, F., John, J., Moti, A. and Stamberg, K. (1995) *Evaluation of Polyacrylonitrile (PAN) as a Binding Polymer for Absorbers Used to Treat Liquid Radioactive Wastes*. Prague.

Şengil, I. A. and Özacar, M. (2009) 'The decolorization of C.I. Reactive Black 5 in aqueous solution by electrocoagulation using sacrificial iron electrodes', *Journal of Hazardous Materials*, 161(2–3), pp. 1369–1376.

SenGupta, A. K. (2017) *Ion Exchange in Environmental Processess: Fundamentals, Applications and Sustainable Technology*. First. Edited by A. K. SenGupta. Belthlehem: Wiley.

Shahidi, D., Roy, R. and Azzouz, A. (2015) 'Advances in catalytic oxidation of organic pollutants – Prospects for thorough mineralization by natural clay catalysts', *Applied Catalysis B, Environmental*. Elsevier B.V., 174–175, pp. 277–292.

Sharma, S., Ruparelia, J. P. and Patel, M. L. (2011) 'A general review on Advanced Oxidation Processes for waste water treatment', in *Nirma University International Conference*. Ahmedabad, Gujarat, pp. 1–7.

Sharma, S., Saxena, R. and Gaur, G. (2014) 'Study of Removal Techniques for Azo Dyes by Biosorption : A Review', *IOSR Journal of Applied Chemistry*, 7(10), pp. 6–21.

Sharma, V. K., Triantis, T. M., Antoniou, M. G., He, X., Pelaez, M., Han, C., Song, W., Shea, K. E. O., De, A. A., Kaloudis, T., Hiskia, A. and Dionysiou, D. D. (2012) 'Destruction of microcystins by conventional and advanced oxidation processes : A review q', *Separation and Purification Technology*. Elsevier B.V., 91, pp. 3–17.

Shaul, G. M., Holdsworth, T. J., Dempsey, C. R. and Dostal, K. A. (1991) 'Fate of water soluble azo dyes in the activated sludge process', *Chemosphere*, 22(1–2), pp. 107–119.

Sheldon, R. A. and Downing, R. S. (1999) 'Heterogeneous catalytic transformations for environmentally friendly production', *Applied Catalysis A: General*, 189, pp. 163–183.

Shore, J. (2002) *Colorants and auxiliaries: Volume 2 - Auxiliaries*. Second. Edited by J. Shore. Bradford: Society of Dyers and Colourists.

Shunkevich, A. A., Akulich, Z. I., Mediak, G. V and Soldatov, V. S. (2005) 'Acid – base properties of ion exchangers . III . Anion exchangers on the basis of polyacrylonitrile fiber', *Reactive and Functional Polymers*, 63, pp. 27–34.

Sigma-Aldrich (2017a) *Safety Data Sheet-Nitrosobenzene*, *Sigma Aldrich*. Available at: www.sigma-aldrich.com.

Sigma-Aldrich (2017b) *Safety Data Sheet-p-Benzoquinone*, *Sigma-Aldrich*. Available at: www.sigma-aldrich.com.

Singh, H. (2006) *Mycoremediation : Fungal Bioremediation*. New Jersey: John Wiley & Sons, INC., Publication.

Slokar, Y. M. and Marechal, M. Le (1998) 'Methods of Decoloration of Textile Wastewaters', *Dyes and Pigments*, 37(4), pp. 335–356.

Smith, D. R. and Nordberg, M. (2014) 'General Chemistry, Sampling, Analytical Methods, and Speciation', in Nordberg, G. F., Fowler, B. A., and Nordberg, M. (eds) *Handbook on the Toxicology of Metals*. Fourth. London: Elsevier, p. 1422.

Smith, K. S. (1999) 'Metal Sorption on Mineral Surfaces: An Overview with Examples Relating to Mineral Deposits', *Economic Geology: The Environmental Geochemistry of Mineral Deposits*, 6A and 6B, pp. 161–182.

Society of Dyers and Colourists & American Association of Textile Chemists and Colourists (2017) *Definition of a dye and a pigment*. Available at: https://colour-index.com/definitions-of-a-dye-and-a-pigment (Accessed: 25 June 2017).

Sokolowska-gajda, J., Freeman, H. S. and Reife, A. (1996) 'Synthetic Dyes Based on Environmental Considerations. Part 2: Iron Complexed Formazan Dyes', *Dyes and Pigments*, 30(1), pp. 1–20.

Soldatov, V. . S., Sosinovich, Z. I., Korshunova, T. A. and Mironova, T. V. (2004) 'Acid – base properties of ion exchangers . I . Optimising of potentiometric titration of ion exchangers exemplified by carboxylic acid resins', *Reactive and Functional Polymers*, 58, pp. 3–12.

Soldatov, V. . S., Sosinovich, Z. I. and Mironova, T. V. (2004) 'Acid – base properties of ion exchangers . II . Determination of the acidity parameters of ion exchangers with arbitrary functionality', *Reactive and Functional Polymers*, 58, pp. 13–26.

Soon, A. N. and Hameed, B. H. (2011) 'Heterogeneous catalytic treatment of synthetic dyes in aqueous media using Fenton and photo-assisted Fenton process', *Desalination*. Elsevier B.V., 269(1–3), pp. 1–16.

Speight, J. . (2017) *Handbook of Petroleum Refining*. Florida: CRC Press.

Sponza, D. T. and Işik, M. (2007) 'Fate and toxicity of azo dye metabolites under batch

long-term anaerobic incubations', *Enzyme and Microbial Technology*, 40(4), pp. 934–939.

Srinivasan, A. and Viraraghavan, T. (2010) 'Decolorization of dye wastewaters by biosorbents: A review', *Journal of Environmental Management*, pp. 1915–1929.

Stephenson, R. L. and Blackburn, J. B. J. (1998) *The Industrial Wastewater Systems Handbook*. Florida: Lewis Publishers.

Stumm, W. and Morgan, J. J. (1996) *Aquatic Chemistry: Chemical Equilibria and Rates in Natural Waters*. Third. New York: Wiley-Interscience.

Stylidi, M., Kondarides, D. I. and Verykios, X. E. (2004) 'Visible light-induced photocatalytic degradation of Acid Orange 7 in aqueous TiO2 suspensions', *Applied Catalysis B: Environmental*, 47(3), pp. 189–201.

Su, C. C., Pukdee-Asa, M., Ratanatamskul, C. and Lu, M. C. (2011) 'Effect of operating parameters on decolorization and COD removal of three reactive dyes by Fenton's reagent using fluidized-bed reactor', *Desalination*. Elsevier B.V., 278(1–3), pp. 211–218.

Suib, S. L. (2013) *New and future developments in catalysis: Catalysis for remediation and environmental concerns*. Oxford: Elsevier.

Sukhdev, A., Manjunatha, A. S. S. and Puttaswamy (2017) 'Decolorization of reactive orange 16 azo dye in wastewater using CAT/IrCl3/ HClO4 redox system : Delineation of kinetic modeling and mechanistic approaches', *Journal of Taiwan Institute of Chemical Engineering*. Elsevier B.V., 70, pp. 150–160.

Sun, J. H., Sun, S. P., Wang, G. L. and Qiao, L. P. (2007) 'Degradation of azo dye Amido black 10B in aqueous solution by Fenton oxidation process', *Dyes and Pigments*, 74(3), pp. 647–652.

Sun, L., Yao, Y., Wang, L., Mao, Y., Huang, Z., Yao, D., Lu, W. and Chen, W. (2014) 'Efficient removal of dyes using activated carbon fibers coupled with 8-hydroxyquinoline ferric as a reusable Fenton-like catalyst', *Chemical Engineering Journal*. Elsevier B.V., 240, pp. 413–419.

Supaka, N., Juntongjin, K., Damronglerd, S., Delia, M. L. and Strehaiano, P. (2004) 'Microbial decolorization of reactive azo dyes in a sequential anaerobic-aerobic system', *Chemical Engineering Journal*, 99(2), pp. 169–176.

Suteu, D., Zaharia, C. and Malutan, T. (2011) 'Removal of Orange 16 reactive dye from aqueous solutions by waste sunflower seed shells', *Journal of the Serbian Chemical Society*, 76(4), pp. 607–624.

Svobodová, K., Senholdt, M., Novotný, Č. and Rehorek, A. (2007) 'Mechanism of Reactive Orange 16 degradation with the white rot fungus Irpex lacteus', *Process Biochemistry*, 42(9), pp. 1279–1284.

Swedish Chemicals Agency (2014) *Chemicals in textiles – Risks to human health and the environment, Report from a government assignment. Report 6/14*. Stockholm.

Taylor, P., Brown, M. A. and Vito, S. C. De (1993) 'Predicting Azo Dye Toxicity', *Critical Reviews in Environmental Science and Technology*, 23(3), pp. 249–324.

Tekin, H., Bilkay, O., Ataberk, S. S., Balta, T. H., Ceribasi, I. H., Sanin, F. D., Dilek, F. B. and Yetis, U. (2006) 'Use of Fenton oxidation to improve the biodegradability of a pharmaceutical wastewater', *Journal of h*, 136, pp. 258–265.

The Editors of Encyclopaedia Britannica (2015) *Eh-pH diagram*, *Encyclopædia Britannica*. Encyclopædia Britannica, inc.

The Engineering ToolBox (2017) *Pump Power Calculator*. Available at: https://www.engineeringtoolbox.com/pumps-power-d_505.html (Accessed: 23 February 2018).

The Guardian (2017) *Flint officials may face jail for water crisis*, *The Guardian*. Available at: https://www.theguardian.com/commentisfree/2017/jun/15/flint-officials-may-face-jail-water-crisis-bittersweet-news (Accessed: 27 February 2018).

The International Network for Acid Prevention (2014) *The International Network for Acid Prevention Global Acid Rock Drainage Guide*.

Tijani, J. O., Fatoba, O. O., Madzivire, G. and Petrik, L. F. (2014) 'A Review of Combined Advanced Oxidation Technologies for the Removal of Organic Pollutants from Water', *Water Air and Soil Pollution*, 9(225), p. 2102.

Timmy, K. and Satake, M. (1989) *Environmental Pollution*. New Delhi: Anmol Publications.

Tizaoui, C. and Grima, N. (2011) 'Kinetics of the ozone oxidation of Reactive Orange 16 azo-dye in aqueous solution', *Chemical Engineering Journal*. Elsevier B.V., 173(2),

pp. 463–473.

Tokumura, M., Shibusawa, M. and Kawase, Y. (2013) 'Dynamic simulation of degradation of toluene in waste gas by the photo-Fenton reaction in a bubble column', *Chemical Engineering Science*. Elsevier, 100, pp. 212–224.

Toronto Water Treatment Company (2018) *Ionexchange.ca*. Available at: http://www.ionexchange.ca/products (Accessed: 28 March 2018).

Trimm, D. L. (2001) 'The regeneration or disposal of deactivated heterogeneous catalysts', *Applied Catalysis A: General*, 212(1–2), pp. 153–160.

Trumm, D. (2010) 'Selection of active and passive treatment systems for AMD', *New Zealand Journal of Geology and Geophysics*, 53(2–3), pp. 195–210.

Tüfekci, N., Sivri, N. and Toroz, İ. (2007) 'Pollutants of Textile Industry Wastewater and Assessment of its Discharge Limits by Water Quality Standards', *Turkish Journal of Fisheries and Aquatic Sciences*, 103(7), pp. 97–103.

Tunay, O., Kaddasli, I., Orhon, D. and Cansever, G. (1999) 'Use and minimization of water in leather tanning processes', *Water Science and Technology*, 40, pp. 237–244.

United States Environmental Protection Agency (2014) *Reference Guide to Treatment Technologies for Mining-Influenced Water*.

United States Geological Survey (2016) *Water Hardness*. Available at: https://water.usgs.gov/edu/hardness.html (Accessed: 18 January 2018).

Upreti, P. D., Tangyie, G. C., Huddersman, K. and Smail, I. (2016) 'Field trial of an ion exchange based metal removal technology in the treatment of mine waters', in Drebenstedt, C. and Paul, M. (eds) *Mining Meets Water- Conflicts and Solutions*. Leipzig: International Mine Water Association, pp. 828–835.

USEPA (1985) *Textile Dyes and Dyeing Equipment Classification, Properties*, *National Service Centre for Environmental Publications (NSCEP)*.

Valh, J. V. and Marechal, A. M. Le (2009) 'Decolouration of Textile Wastewaters', in Lang, A. R. (ed.) *Dyes and Pigments : New Research*. New York: Nova Science Publishers, Inc., pp. 175–199.

Vandevivere, P. C., Bianchi, R. and Verstraete, W. (1998) 'Review Treatment and Reuse of Wastewater from the Textile Wet-Processing Industr y : Review of Emerging

Technologies', *Journal of Chemical Technology and Biotechnology*, 72, pp. 289–302.

Vatutsina, O. M., Soldatov, V. S., Sokolova, V. I., Johann, J., Bissen, M. and Weissenbacher, A. (2007) 'A new hybrid (polymer / inorganic) fibrous sorbent for arsenic removal from drinking water', *Reactive and Functional Polymers*, 67, pp. 184–201.

Vietnamnet (2016) *Amid Serious situation, China eyes soil pollution law in 2017*, *Talkvietnam*. Available at: https://www.talkvietnam.com/2016/03/amid-serious-situation-china-eyes-soil-pollution-law-in-2017/ (Accessed: 13 October 2017).

Voudrias, E., Fytianos, K. and Bozani, E. (2002) 'Sorption Description isotherms of Dyes from aqueous solutions and Waste Waters with Different Sorbent materials', *Global Nest International Journal*, 4(1), pp. 75–83.

Wagner, R. W. and Lindsey, J. S. (2009) 'Boron-dipyrromethene dyes for incorporation in synthetic-pigment light-harvesting arrays', *Pure and Applied Chemistry*, 68(7), pp. 1373–1380.

Wahid, Z. and Nadir, N. (2013) 'Improvement of One Factor at a Time Through Design of Experiments', *World Applied Sciences Journal*, 21, pp. 56–61.

Wang, L. K., Hung, Y.-T. and Shammas, N. K. (2007) *Handbook of Environmental Engineering: Advanced Physicochemical Treatment Technologies*. Volume 5. New Jersey: Human Press.

Wang, L., Yao, Y., Zhang, Z., Sun, L., Lu, W., Chen, W. and Chen, H. (2014) 'Activated carbon fibers as an excellent partner of Fenton catalyst for dyes decolorization by combination of adsorption and oxidation', *Chemical Engineering Journal*. Elsevier B.V., 251, pp. 348–354.

Wang, N., Zheng, T., Zhang, G. and Wang, P. (2016) 'A review on Fenton-like processes for organic wastewater treatment', *Journal of Environmental Chemical Engineering*. Elsevier B.V., 4(1), pp. 762–787.

Waring, D. R. and Geoffrey, H. (1990) *The Chemistry and Application of Dyes*. First. Edited by D. R. Waring and H. Geoffrey. New York and London: Plenum Press.

Warrender, R. (2009) *Remediation of circum-neutral metal mine drainage using laboratory-scale permeable reactive barriers.* Aberystwyth University.

Warrender, R., Pearce, N. J. G., Perkins, W. T., Brown, A., Sapsford, D., Bowell, R. and Dey, M. (2010) 'Field Trials of Low-Cost Permeable Reactive Media for the Passive Treatment of Circum-Neutral Metal Mine Drainage in mid-Wales , UK " Mine Water and Innovative Thinking "', in *Mine Water and Innovative Thinking*. Sydney: International Mine Water Association, pp. 291–294.

Wawrzkiewicz, M. (2013) 'Removal of C . I . Basic Blue 3 dye by sorption onto cation exchange resin, functionalized and non-functionalized polymeric sorbents from aqueous solutions and wastewaters', *Chemical Engineering Journal*, 217, pp. 414–425.

Wawrzkiewicz, M. and Hubicki, Z. (2015) 'Anion Exchange Resins as Effective Sorbents for Removal of Acid , Reactive , and Direct Dyes from Textile Wastewaters', in Kilislioglu, A. (ed.) *Ion Exchange - Studies and Applications*. InTech, p. 204.

Weber, E. J. (1991) 'Studies of benzidine-based dyes in sediment-water systems', *Environmental Toxicology and Chemistry*, 10(5), pp. 608–618.

Weber, E. J. and Wolfe, N. L. E. E. (1987) 'Kinetics studies of reduction of aromatic azo compounds in anaerobic sediment/water systems', *Environmental Toxicology and Chemistry*, 6, pp. 911–919.

Wei, J. F., Wang, Z. P., Zhang, J., Wu, Y. Y., Zhang, Z. P. and Xiong, C. H. (2005) 'The preparation and the application of grafted polytetrafluoroethylene fiber as a cation exchanger for adsorption of heavy metals', *Reactive and Functional Polymers*, 65, pp. 127–134.

Wei, X., Tao, J., Li, M., Zhu, B., Li, X., Ma, Z., Ye, L. and Qi, X. (2017) 'Polyacrylamide-based inorganic hybrid fl occulants with self- degradable property', *Material Chemistry and Physics*, 192, pp. 72–77.

Weschenfelder, S. E., José, H. J., Gebhardt, W. and Schröder, H. F. (2007) 'Monitoring the Physicochemical and Chemical Treatment of Textile Wastewater using GC/MS, LC/MS and -MS/MS Techniques', *Separation and Purification Technology*, 42, pp. 1535–1551.

WFD-UKTAG (2015) *Updated Recommendations on Environmental Standards River Basin Management (2015-21)*.

WFD-UKTAG (2017) *An updated list of hazardous substances*. Available at:

http://wfduk.org/resources/groundwater-hazardous-substances-standards.

WHO (1996) *Zinc in Drinking-water Background document for development of WHO Guidelines for Drinking-Water Quality*. Geneva.

WHO (2011) *Cadmium in Drinking-water Background document for development of WHO Guidelines for Dirnking-water Quality*. Geneva.

WHO-IARC (2010) 'IARC monographs on the evaluation of carcinogenic risks to humans', *IARC Monographs on the Evaluation of Carcinogenic Risks to Humans*, 93, pp. 9–38.

Whysner, K., Figueroa, L., Petri, E. and Holmes, M. (2012) 'Economic recovery of zinc from Mining Influenced Water (MIW)', in *Advancing Solutions for a New Legacy*. Denver: USEPA.

Wingenfelder, U., Hansen, C., Furrer, G. and Schulin, R. (2005) 'Removal of Heavy Metals from Mine Waters by Natural Zeolites', *Environmental Science and Technology*, 39(12), pp. 4606–4613.

Wolf, S. and Stanley, N. (2003) *Wolf and Stanley on Environmental Law*. Fourth. London: Cavendish Publishing Limitied.

Won, S. W., Choi, S. B. and Yun, Y. (2006) 'Performance and mechanism in binding of Reactive Orange 16 to various types of sludge', *Biochemical Engineering Journal*, 28, pp. 208–214.

Wu, J., Zhao, J., Du, F. and Han, Z. (2009) 'Development of Environmentally Friendly Modified Fe-PAN Fibrous Catalyst and Its Application in Degradation of Dye', *Journal of Sustainable Development*, 2(3), pp. 214–220.

Xing, X., Yang, H., Tao, M. and Zhang, W. (2015) 'An overwhelmingly selective colorimetric sensor for Ag+ using a simple modified polyacrylonitrile fiber', *Journal of Hazardous Materials*. Elsevier B.V., 297, pp. 207–216.

Xiong, C., Li, Y., Wang, G., Fang, L., Zhou, S., Yao, C., Chen, Q., Zheng, X., Qi, D., Fu, Y. and Zhu, Y. (2015) 'Selective removal of Hg (II) with polyacrylonitrile-2-amino-1 , 3 , 4-thiadiazole chelating resin : Batch and column study', *Chemical Engineering Journal*. Elsevier B.V., 259, pp. 257–265.

Xu, G., Zhao, Y., Hou, L., Cao, J., Tao, M. and Zhang, W. (2017) 'A recyclable phosphinic

acid functionalized polyacrylonitrile fiber for selective and efficient removal of Hg^{2+}', *Chemical Engineering Journal*. Elsevier B.V., 325, pp. 533–543.

Xu, H., Liu, W., Qi, S., Li, Y. A. N., Zhao, Y. and Li, J. (2014) 'Kinetics and optimization of the decoloration of dyeing wastewater by a schorl-catalyzed Fenton-like reaction', *Journal of the Serbian Chemical Society*, 79(3), pp. 361–377.

Xu, X.-R., Li, H.-B., Wang, W.-H. and Gu, J.-D. (2005) 'Decolorization of dyes and textile wastewater by potassium permanganate', *Chemosphere*, 59, pp. 893–898.

Yagub, M. T., Sen, T. K., Afroze, S. and Ang, H. M. (2014) 'Dye and its removal from aqueous solution by adsorption : A review', *Advances in Colloid and Interface Science*. Elsevier B.V., 209, pp. 172–184.

Yang, Z., Ishtchenko, V. V and Huddersman, K. D. (2006) 'Novel Fibrous Catalyst in Advanced Oxidation of Photographic Processing Effluents', *Journal of Enviornmental Science and Health Part A*, 4529, pp. 129–141.

Yao, Y., Wang, L., Sun, L., Zhu, S., Huang, Z., WangyangLu, Y. M. and Chen, W. (2013) 'Efficient removal of dyes using heterogeneous Fenton catalysts based on activated carbon fibers with enhanced activity', *Chemical Engineering Science*. Elsevier, 101, pp. 424–431.

Yap, C. L., Gan, S. and Ng, H. K. (2011) 'Fenton based remediation of polycyclic aromatic hydrocarbons-contaminated soils', *Chemosphere*. Elsevier Ltd, 83(11), pp. 1414–1430.

Yeap, K. L., Teng, T. T., Poh, B. T., Morad, N. and Lee, K. E. (2014) 'Preparation and characterization of coagulation / flocculation behavior of a novel inorganic – organic hybrid polymer for reactive and disperse dyes removal', *Chemical Engineering Journal*. Elsevier B.V., 243, pp. 305–314.

Younger, P. L. and Adams, R. (1999) *Predicting Mine Water Rebound*. Bristol.

Younger, P. L., Banwart, S. A. and Hedin, R. S. (2002) *Environmental Pollution Mine Water: Hydrology, Pollution, Remediation*. Edited by B. J. Alloway and J. T. Trevors. Springer-Science+Business Media, B.V.

Zagorodni, A. A. (2007) *Ion Exchange Materials Properties and Applications*. First. Stockholm: Elsevier.

Zazo, J. A., Casas, J. A., Mohedano, A. F. and Rodríguez, J. J. (2006) 'Catalytic wet peroxide oxidation of phenol with a Fe/active carbon catalyst', *Applied Catalysis B: Environmental*, 65(3–4), pp. 261–268.

Zero Discharge of Hazardous Chemicals (2015) *Textile industry wastewater discharge quality standards*.

Zhang, B. W., Fisher, K., Bieniek, D. and Kettrup, A. (1994) 'Synthesis of carboxyl group containing hydrazine-modified polyacrylonitrile fibres and application for the removal of heavy metals', *Reactive Polymers*, 24(1), pp. 49–58.

Zhang, L., Zhang, X., Li, P. and Zhang, W. (2009) 'Reactive & Functional Polymers Effective Cd^{2+} chelating fiber based on polyacrylonitrile', *Reactive and Functional Polymers*. Elsevier Ltd, 69(1), pp. 48–54.

Ziemkiewicz, P. F., Skousen, J. G. and Simmons, J. (2003) 'Long-term Performance of Passive Acid Mine Drainage Treatment Systems', *Mine Water and the Environment*, 22, pp. 118–119.

Zissi, U. and Lyberatos, G. (1996) 'Azo-dye biodegradation under anoxic conditions', *Water Science and Technology*, 34(5–6), pp. 495–500.

Zodi, S., Merzouk, B., Potier, O., Lapicque, F. and Leclerc, J. P. (2013) 'Direct red 81 dye removal by a continuous flow electrocoagulation/flotation reactor', *Separation and Purification Technology*. Elsevier B.V., 108, pp. 215–222.

Zollinger, H. (2003) *Colour Chemistry: Syntheses, Properties, and Applications of Organic Dyes and Pigment*. Third. Zurich: Wiley-VCH.

9. APPENDICES

APPENDIX 9-1: CHARACTERIZATION OF TEXTILE EFFLUENT.

Table 9-1: Characterization of textile effluent with respect to water quality parameters.

Characteristics parameters	**Pollution load**	**References**
pH	6 – 10	
	12.1	(Muhammad et al., 2008)
Temperature (°C)	35 - 45	
BOD (mg/L)	80 – 6,000	
COD (mg/L)	150 – 12,000	
Total Organic Carbon (TOC) (mg/L)	144	(Karthikeyan et al., 2011)
Total Dissolved Solids (TDS) (mg/L)	2,900 – 3,100	
	8,000 - 12,000	(Al-Kdasi et al., 2005)
Total Suspended Solids (TSS) (mg/L)	15 – 8,000	
Chlorine (mg/L)	1,000 – 6,000	
Free Chlorine (mg/L)	<10	
Sodium (mg/L)	70	
Iron (Fe) (mg/L)	<10	
Zinc (Zn) (mg/L)	<10	
Calcium (Ca^{2+}) (mg/L)	60	(Karthikeyan et al., 2011)
Copper (Cu) (mg/L)	<10	
Arsenic (As) (mg/L)	<10	
Nickel (Ni) (mg/L)	<10	
Boron (B) (mg/L)	<10	

Characteristics parameters	**Pollution load**	**References**
Florin (F) (mg/L)	<10	
Manganese (Mn) (mg/L)	<10	
Vanadium (V) (mg/L)	<10	
Mercury (Hg) (mg/L)	<10	
Phosphate (PO_4) (mg/L)	<10	
Cyanide (Cn) (mg/L)	<10	
Oil and grease (mg/L)	10 - 30	
Nitrate (NO_3-N) (mg/L)	< 5	
Free ammonia (mg/L)	<10	
Sulphate (SO_4) (mg/L)	600 – 1,000	
Silica (mg/L)	<15	
Total Kjeldahl Nitrogen (mg/L)	70 - 80	
Colour (Pt-Co) (Platinum-Cobalt)	50 – 2,500	
Total Hardness ($CaCO_3$) (mg/L)	375 - 400	(Jadhav et al., 2010) - (Karthikeyan et al., 2011)
Conductivity (µS/m)	3.84	(Jadhav et al., 2010)
Oxidation reduction potential (ORP) (mV)	+ 525	(Karthikeyan et al., 2011)
Surfactant (mg/L)	9.71	(Karthikeyan et al., 2011)
Volatile Dissolved Solids (mg/L)	1.064	(Karthikeyan et al., 2011)

Reproduced from (Ghaly et al., 2014) and additional sources are referenced separately.

APPENDIX 9-2: COUNTRY WISE DISCHARGE LIMITS FOR WATER QUALITY PARAMETERS.

Table 9-2: Discharge limits for water quality parameters in various countries (Concentrations are expressed in mg/L unless otherwise stated).

Parameters	Canada (CCME)	China	India (BIS)	Hong Kong	USA (FEPA)	Mexico	Thailand	Philippines	Indonesia	Bangladesh	Sri Lanka	EU	UK
pH	6.5 - 8.5	6 - 9	5.5 - 9	6 - 10	6 - 9	6 - 8.5	5 - 9	6 - 9	6 - 9	6.5 - 9	6 - 8.5		6.5 - 8.5***
Temperature (°C)	30	-	50	43	40	-	40*	40	-	40-45	40	-	
Colour (Pt-Co)	100	80	400	1 (Lovibond)	7 (Lovibond)	-	-	100-200	-	-	30	-	Absorbance (400 nm to 800nm) < 0.1**
TDS (g/L)	2.0	-	2.1	-	2.0	-	2.0 - 5.0	1.2	-	2.1	2.1	-	
TSS	40	50 - 70*	100	800	30	-	30 -150	90	50*-60	100	50*	35*	10-30**
Sulphide	0.2	0.5*-1.0	2.0	1.0	0.2	-	1.0*	-	0.3*	1.0	2.0	-	
Free Chlorine	1.0	-	1.0	-	1.0	-	-	1.0	-	-	-	-	
COD	80	80-100*	250	2000	80	<125	120 - 400	200 - 300	250	200	600	125*	25**
BOD_5	50	20*-60	30	800	50	<30	20 - 60	30 - 200	85	150	200	25*	5-25**
Oil and Grease	-	-	10	20	10	-	300	5-15	5	10	30	-	
Dissolved Oxygen	6.0	-	-	≥ 4.0	-	-	-	1.0 - 2.0	-	4.5 - 8.0	-	-	8 - 15***

Parameters	Canada (CCME)	China	India (BIS)	Hong Kong	USA (FEPA)	Mexico	Thailand	Philippines	Indonesia	Bangladesh	Sri Lanka	EU	UK
Nitrate (mg/L)	13.0	-	10.0	-	20.0	10.0	-	-	-	10.0	45.0	-	
Ammonia	0.1	10 - 15*	50*	0.5	0.2	-	-	-	8*	5 – 50*	50-60*	-	
Phosphate	<4.0	1.0	5.0	5.0	5.0	-	-	-	2.0	-	2.0	-	
Calcium	-	-	-	-	200	-	-	200	-	-	240	-	
Magnesium	200	-	-	-	200	-	-	-	-	-	150	-	
Chromium	0.001	0.5 – 1.5 *	0.1	0.1	<0.1	0.05	0.5	0.05-0.5	0.5	2	0.05	-	
Aluminium	5	-	-	-	<1.0	5.0	-	-	-	-	-	-	
Copper	<1.0	1.0	3.0	1.0	<1.0	1.0	1.0 -2.0*	1.0	2.0	0.5	3.0	-	
Manganese	0.005	2.0	2.0	0.5	0.005	0.2	5.0	1.0-5.0	-	5.0	0.5	-	
Iron	0.3	-	3.0	1.5	20	1.0	-	1.0-20	5.0	2.0	1.0	-	
Zinc	0.03	2*- 5.0	5.0	0.6	<10	10	5.0*	5.0-10.0	5.0	5.0	2*-10	-	
Mercury	0.026	0.05*	0.01*	1.0	0.05	-	0.005*	0.005	-	10	0.0005*	-	0.005**
Arsenic	-	0.5*	0.2*	-	-	-	0.25*	-	-	0.2*	0.2*	-	

CCME- Canadian Council of Ministers of the Environment, BIS – Bureau of Indian Standards, FEPA – Federal Environmental Protection Agency (United States) Source : Reproduced from (Ghaly et al., 2014), * (ZDHC, 2015), ** (Environment Agency, 2009), ***(Scottish Environment Protection Agency, 2014).

APPENDIX 9-3: GC-MS SPECTRA OF RO16 SAMPLES TAKEN DURING CATALYTIC OXIDATION.

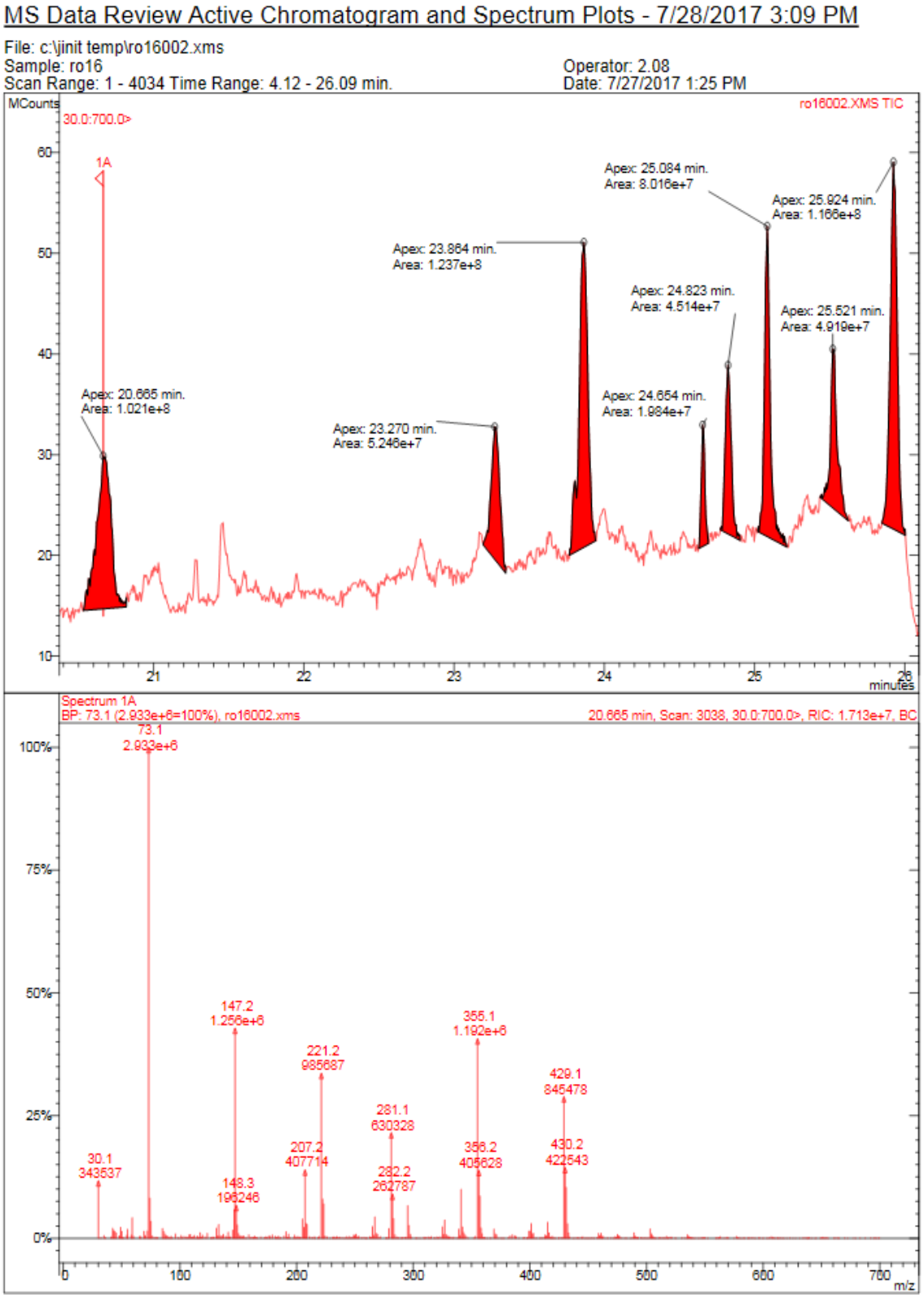

Figure 9-1: GC-MS spectrum of RO16 before (zero minute) catalysis.

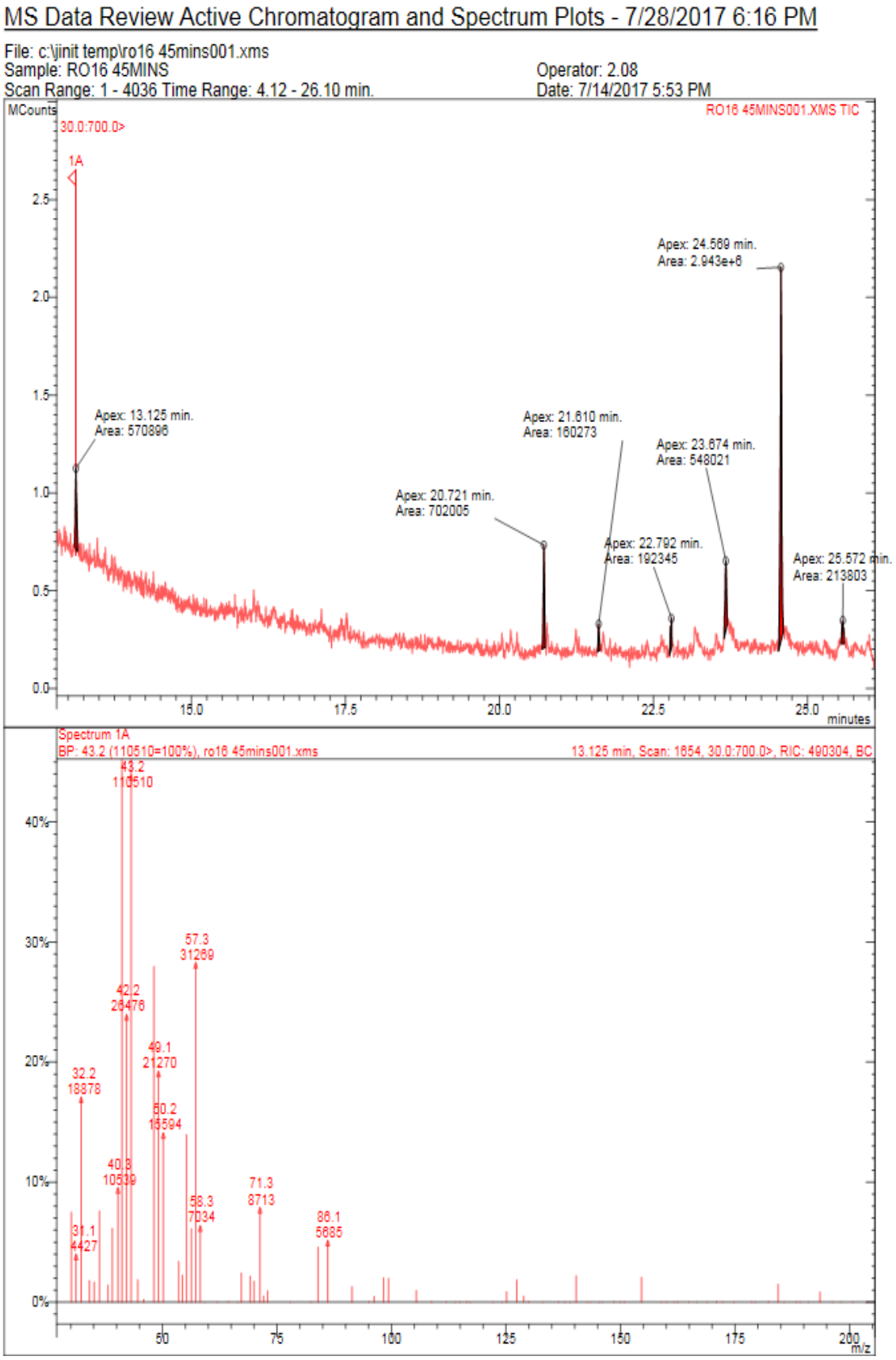

Figure 9-2: GC-MS spectrum of RO16 after 45 minutes of catalysis.

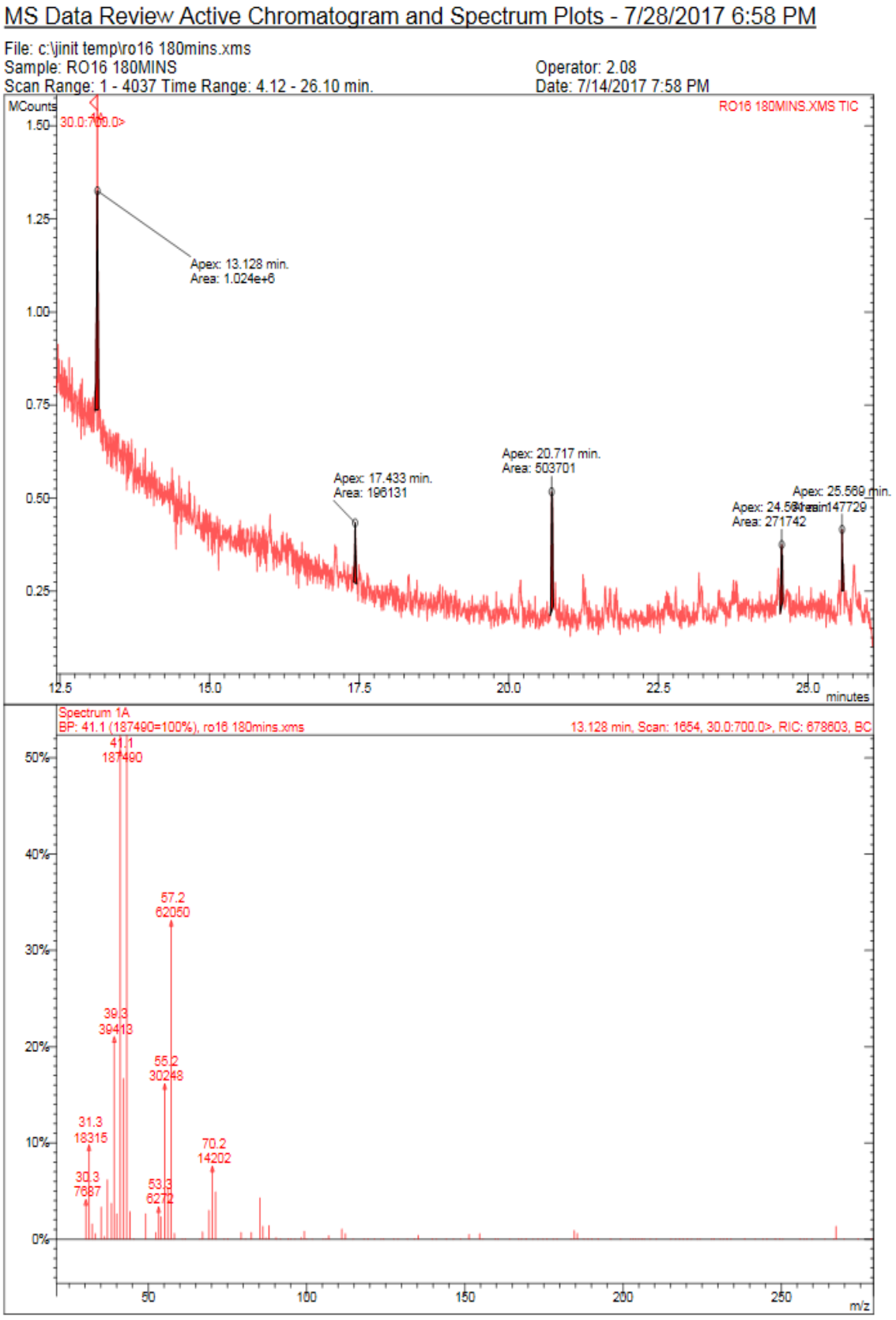

Figure 9-3: GC-MS spectrum of RO16 after 180 minutes of catalysis.

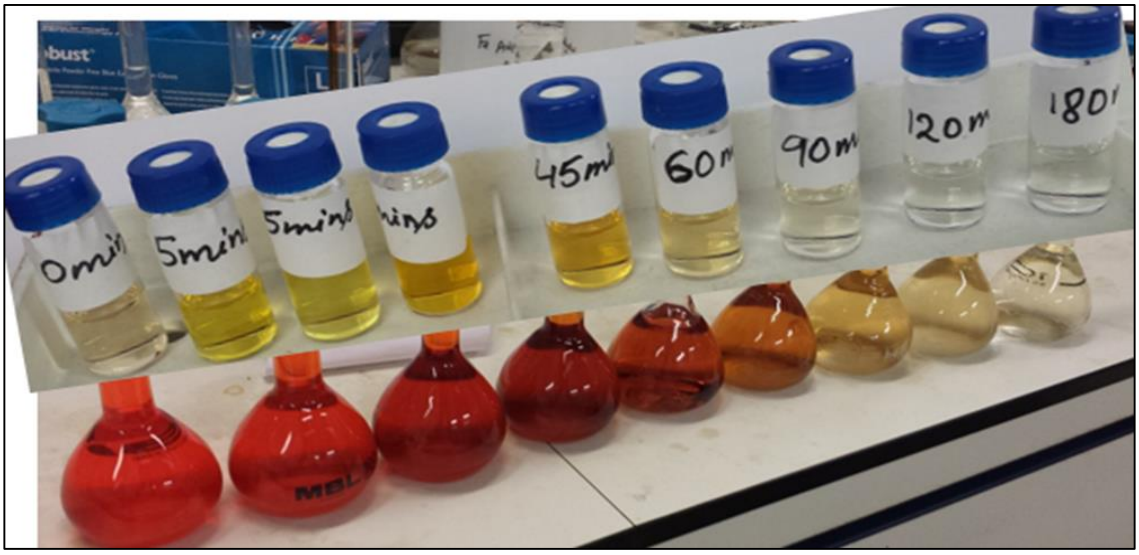

Figure 9-4: RO16 samples taken at different stages of catalysis. The samples from left to right belongs to 0, 15, 30, 45, 60, 90, 120 and 180 minutes of catalysis. The small vials represent the corresponding samples after extraction.

APPENDIX 9-4: CALCULATION OF AMOUNT OF SALTS USED DURING REGENERATION OF DEACTIVATED CATALYST.

Desired amount of iron to reimpregnate per gram of deactivated catalyst = 15 mg.

Weight of deactivated catalyst = 208 g

Total amount of iron needed for 208 g of deactivated catalyst$= 208 \times 15 = 3120$ mg.

Iron content in $Fe_2(SO_4)_3.5H_2O$ = 22.8 %.

∴ Total amount of $Fe_2(SO_4)_3.5H_2O$ needed to obtain 3,120 mg of iron $= 3{,}120 \div (\frac{22.8}{100}) = 13684.21\ mg = 13.7\ g$. Therefore, 13.7 g of $Fe_2(SO_4)_3.5H_2O$ dissolved in double distilled water and made up to 1 L.

Similarly, amount of sodium salt, Sodium sulfate decahydrate ($Na_2SO_4.10H_2O$), needed for reimpregnation was calculated by maintaining the iron salt to sodium salt ratio as of manufacturing stage. The amounts of $Fe_2(SO_4)_3.5H_2O$ and $Na_2SO_4.10H_2O$ used during manufacturing were 8.2 g/L and 31.9 g/L respectively. This gives a ratio of 1:3.89.

∴ Amount of $Na_2SO_4.10H_2O$ required with 13.7 g of $Fe_2(SO_4)_3.5H_2O = 13.7 * 3.89 = 53.3\ g$.

APPENDIX 9-5: STANDARDIZATION OF SODIUM HYDROXIDE.

The NaOH was standardized by titrimetric technique. The actual normality of NaOH used during acid-base titration was determined by blank titration with standardized HCl (0.1 N). 10 mL of NaOH was titrated against HCl (0.1 N). This was done in triplicate and the average value was taken for the calculation. The results are shown below.

Table 9-3: Standardization of NaOH used to determine the ion exchange capacity.

S.N.	Volume of NaOH (mL)	Volume of titre (HCl) (mL)	Normality of HCl (N)	Normality of NaOH (N)
1	10	9.7	0.1	0.097
2	10	9.6	0.1	0.096
3	10	9.7	0.1	0.097
			Average	**0.097**

APPENDIX 9-6: DETERMINATION OF FACTORS FOR ACID (F_{HCL}) AND ALKALI (F_{NAOH}).

The acid used in above titration was a standardized 0.1 N HCl. Thus, its factor f_{HCl} is considered as unity. The factor of alkali (NaOH), f_{NaOH}, is calculated from Equation 6-5 as $f_{NaOH} \times N_{NaOH} = 0.1 \Rightarrow \boldsymbol{f_{NaOH}} = \frac{0.1}{N_{NaOH}} = \frac{0.1}{0.097} = \mathbf{1.031}$.

APPENDIX 9-7: THEORETICAL SOLUBILITY OF ZINC HYDROXIDE WITH RESPECT TO PH.

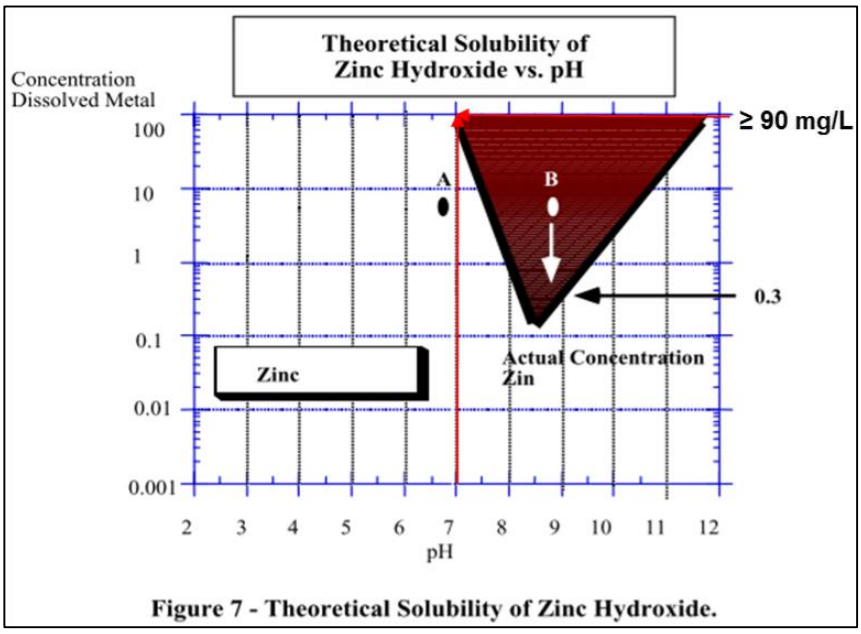

Figure 9-5: theoretical solubility of zinc hydroxide with respect to pH.

*"Figure 7 can be used to determine how the concentration of zinc in water is affected by pH. Suppose a wastewater contains dissolved zinc at 4 mg/L and is at pH = 6.8. This is shown at point **A** in the diagram. Since this point is below the bold lines in the solubility graph, this indicates that zinc is only present as a dissolved metal. It is not in a solid form and under these conditions it will not precipitate"*(Ayres, Davis and Gietka, 1994).

*"Since this is contrary to what we hope to achieve in zinc removal, we need to adjust the pH of the water by adding caustic. Point **B** reveals this pH adjustment from pH 6.8 to 8.6 (i.e., a horizontal line). Above the dark solubility lines, zinc forms zinc hydroxide solids, as is shown by the shaded area. At this new pH value, for example, most of the zinc forms zinc hydroxide and precipitates out of solution. The dissolved zinc concentration is obtained from the solubility line at this pH (i.e., 0.3 mg/L). This is the theoretical amount of zinc that would be in the discharged wastewater after this treatment. The difference of 3.7 mg/L has formed a solid - the metal hydroxide, which is the sludge".*

"The metal solubilities presented in the previous figures are based on an ideal wastewater. Some variations in the exact values of the metal concentrations will occur due to the presence of other substances in the wastewater. Compounds such as cyanide or ammonia can inhibit precipitation of metals, and limit their removal to the point where discharge limits can be exceeded. Also, note that not all metals have the same minimum solubility. Therefore, in a wastewater where multiple metals are present, as a general rule, pH should be adjusted to an average value, approximately 9" (Ayres, Davis and Gietka, 1994, p. 13).

APPENDIX 9-8: SAMPLES OF REGENERATED SOLUTIONS TAKEN DURING REGENERATION OF ION EXCHANGE PAN MESH

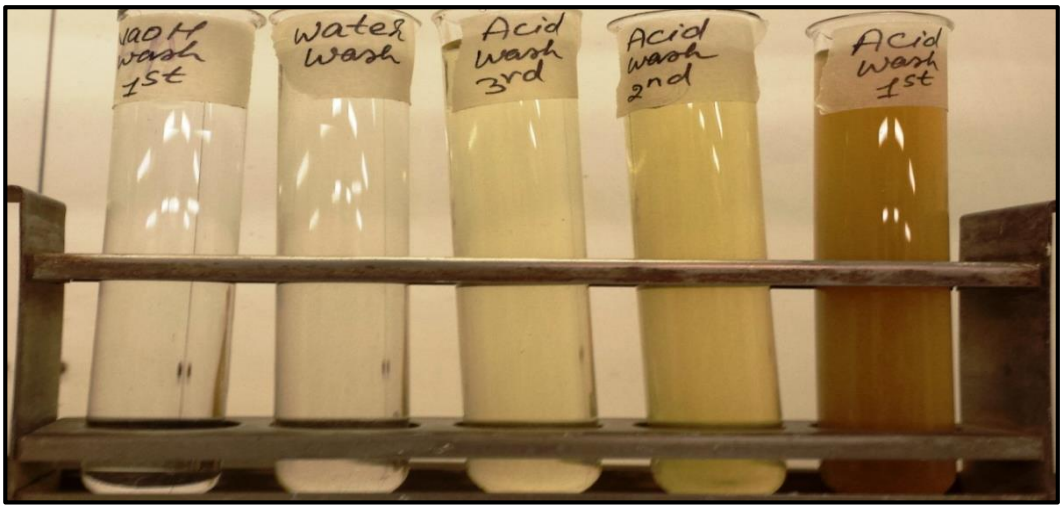

Figure 9-6: Samples of regenerated solutions taken during the regeneration process of ion exchange mesh.

APPENDIX 9-9: CALCULATION OF AVERAGE FLOW RATES AND CORRESPONDING VOLUMES

The flow rates were varied as part of the investigation. The desired flow rates investigated were 30 L/hr, 45 L/hr and 60 L/hr. The period of investigation for these flow rates were not equal. The flow rate was maintained at ~ 30 L/hr, ~ 45 L/hr and ~ 60 L/hr for 143, 16 and 11 days respectively. Hence, the weighting corresponding to each flow rate differs and needs to be taken into account. Therefore, the data obtained were skewed (tested and found as significantly skewed to the right) hence, the general average (arithmetic mean) was skewed. To obtain the better representation of average flow rate, average values were calculated based on corresponding weighting.

Average flow rate for desired flow at 30 L/hr run for 143 days = 28.84 L/hr

Average flow rate for desired flow rate at 45 L/hr run for 16 days = 43. 7 L/hr

Average flow rate for desired flow rate at 60 L/hr run for 11 days = 59.45 L/hr

Average flow for 170 days = $\frac{(143 \times 28.84)+(16\times 43.7)+(11\times 59.45)}{(143+16+11)} = \mathbf{32.22\ L/h}$

Total volume treated in 170 days $= 32.22 \times 24 \times 170 = \mathbf{131,477.6\ L}$

Average flow rate before the regeneration process (79 days) = **28.18 L/hr**

Total Volume treated before the regeneration process $= 28.18 \times 24 \times 79 = \mathbf{53,429.28\ L}$

After the regeneration process, flow rate was maintained at ~ 30 L/hr for 64 days, ~ 45 L/hr for 16 days and ~ 60 L/hr for 11 days. Therefore,

Average flow rate after the regeneration process (91 days) = $\frac{(64 \times 29.47)+(16\times 43.7)+(11\times 59.45)}{(64+16+11)} = \mathbf{35.60\ L/h}$

Total volume treated after the regeneration process $= 35.6 \times 24 \times 91 = \mathbf{77,750.4\ L.}$

APPENDIX 9-10: AMMONIACAL NITROGEN IN THE INLET AND OUTLET WATER SAMPLES ANALYZED BY ESG

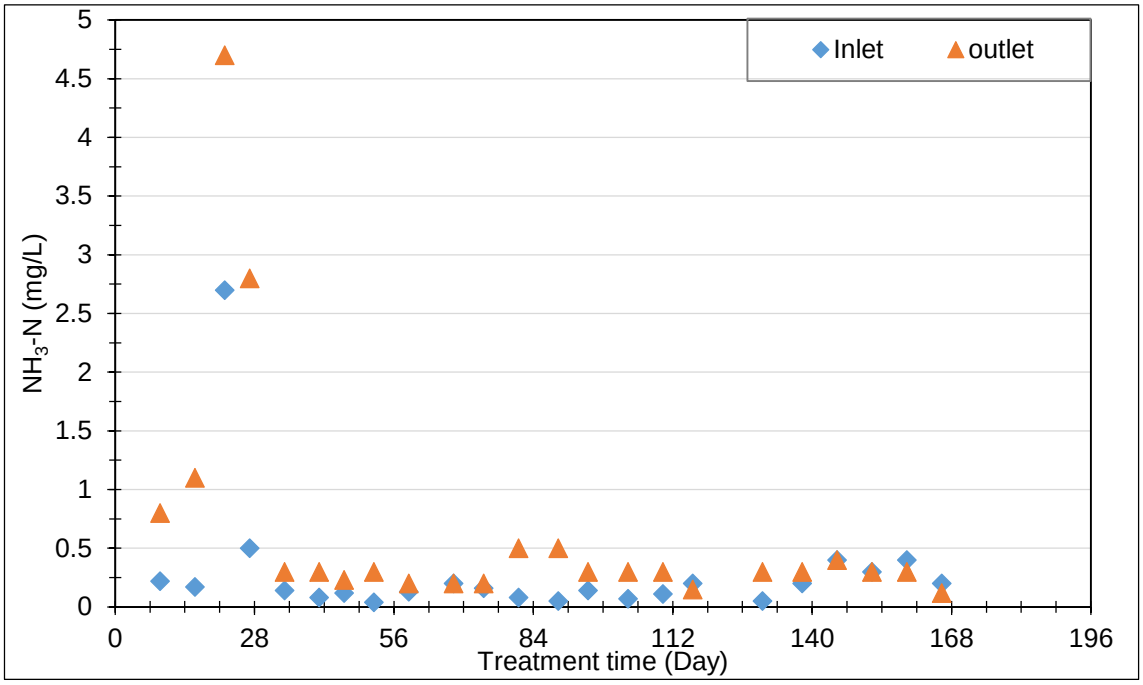

Figure 9-7: Ammoniacal nitrogen in the inlet and outlet water samples, analyzed by ESG, before regeneration process.

APPENDIX 9-11: CORRELATION PLOT FOR LEAD CONCENTRATIONS AND THE CORRESPONDING REMOVAL RATES

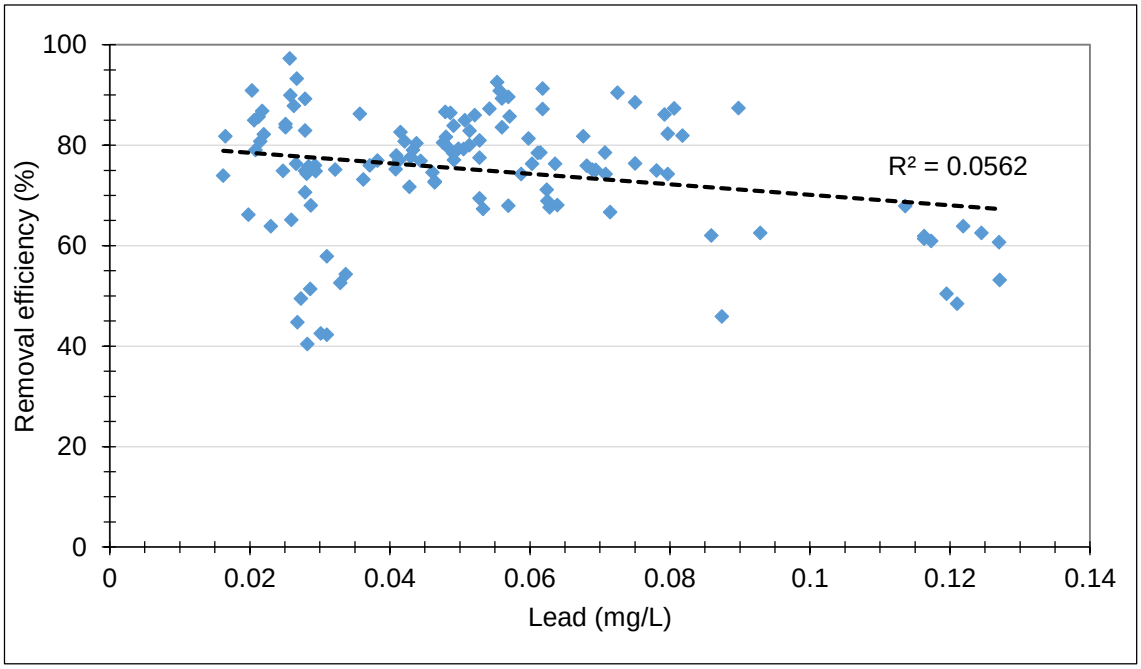

Figure 9-8: Correlation between lead concentrations in the influent samples and the corresponding removal efficiencies.

APPENDIX 9-12: AIR-DRIED ION EXCHANGE PAN MESH SAMPLES COLLECTED FROM THE DISCS.

Figure: 9-9: Air-dried samples of ion exchange mesh taken on day-79 (before regeneration) of the treatment.

APPENDIX 9-13: EXPOSED ION EXCHANGE PAN MESH SAMPLES BEFORE AND AFTER REMOVING RESIDUES

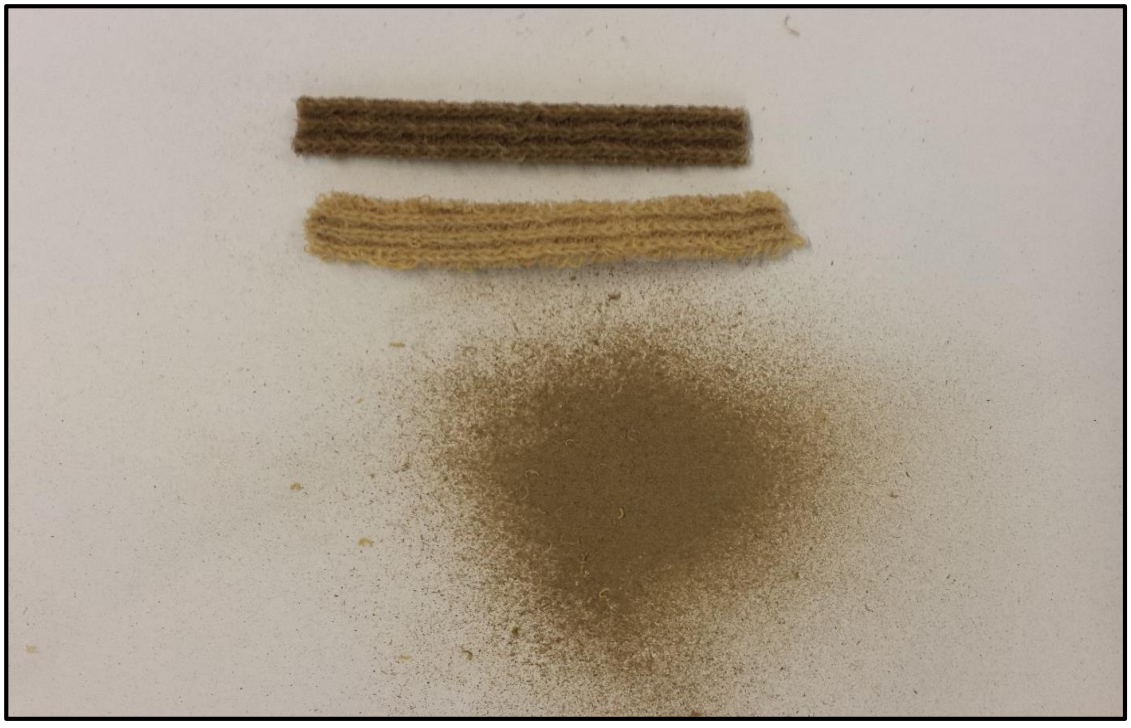

Figure 9-10: Mesh samples from Figure 8-9 before and after removing residues.

APPENDIX 9-14: CALCULATION OF HYDROXYL IONS CONCENTRATIONS AND CORRESPONDING PH VALUES.

$\mathrm{pH} + \mathrm{pOH} = 14$

pH is defined as negative logarithmic of hydrogen ion concentration.

i.e. $\mathrm{pH} = -\log[\mathrm{H}^+]$

Therefore, $[\mathrm{H}^+] = \mathrm{antilog}\,[-\mathrm{pH}]$

Therefore, at $\mathrm{pH} = 7$,

$[\mathrm{H}^+] = [\mathrm{OH}^-] = \mathrm{antilog}\,(-7) = \mathbf{1 * 10^{-7} molL^{-1}}$

And at $\mathrm{pH} = 7.5$, $\mathrm{pOH} = 14 - \mathrm{pH} = 14 - 7.5 = 6.5$

$\therefore [\mathrm{OH}^-] = \mathrm{antilog}\,(-6.5) = \mathbf{3.162 * 10^{-7} molL^{-1}}$

APPENDIX 9-15: CALCULATION OF ANTICIPATED SATURATION TIME FOR ION EXCHANGE PROCESS IN PILOT STUDY.

According to the Langmuir adsorption isotherm model, the maximum uptake capacity of ion exchange mesh is predicted as 12.79 mg/g. Considering this uptake as a reference, the 11 kg mesh in the reactor can remove $12.79 * 11{,}000\ \mathrm{mg} = 140.7\ \mathrm{g}$ of zinc.

Considering an average zinc concentration of 50 mg/L as analyzed by DMU, the amount of mine water feeding 140.7 g of zinc is equals to $\frac{140.7 \times 1000}{50} = 2{,}814\ \mathrm{L}$.

Considering an average flow rate of 28.18 L/hr (Table 6-6) time required to feed 2,814 L of mine water = $\frac{2814}{28.18} = 99.86\ \mathrm{hours} = 4.16\ \mathrm{days}$.

APPENDIX 9-16 : X-RAY DIFFRACTION (XRD) ANALYSIS OF RESIDUE TAKEN FROM THE PAN MESH PERFORMED AT SHEFFIELD UNIVERSITY.

ANalytical X'Pert3 powder X-ray diffractometer, and also collected data on the powder specimen using our new X-ray Fluorescence spectrometer, which gives a good quantitative analysis of the element present in the sample. As it was a powder specimen, we have to run under helium gas, so we lose information from elements lighter than Neon, but it has still proven vital in analysing the data.

Table 9-4: The XRF elemental analysis to determine the composition of residue taken from the mesh samples (Figure 9-10):

S.N.	Elements	Composition (%)
1	Zinc (Zn)	92.804
2	Silica (Si)	1.714
3	Calcium (Ca)	1.480
4	Sodium (Na)	1.221
5	Aluminium (Al)	0.658
6	Iron (Fe)	0.658
7	Phosphorus (P)	0.323
8	Potassium (K)	0.171

The XRF is a new instrument for us, and this is a service we are not providing commercially as yet. Zn and Na are hard to distinguish via XRF analysis, but it is a fairly safe bet that the main 'heavy' element in the specimen is zinc.

Feeding this into the XRD analysis, the best matches were all some variant of hydrozincite, some hydrated and others less so: $Zn_4(CO_3)(OH_6).H_2O$ - all of those numbers should be subscripted. The diffraction peaks were extremely broad, indicating a very small particle size in the powdered specimen. The data from the second sample were of much poorer quality due to the nature of the sample and the very small quantity, but matched those from the powder also.

One additional, sharper, reflection can be seen in the data at around 27°2θ; this is likely from some small amount of a more crystalline secondary phase. The best match I could find was ZnF_2 - zinc fluorite, but it is not possible to give a definite identification from a single peak - we would need at least three peaks for a definite id.

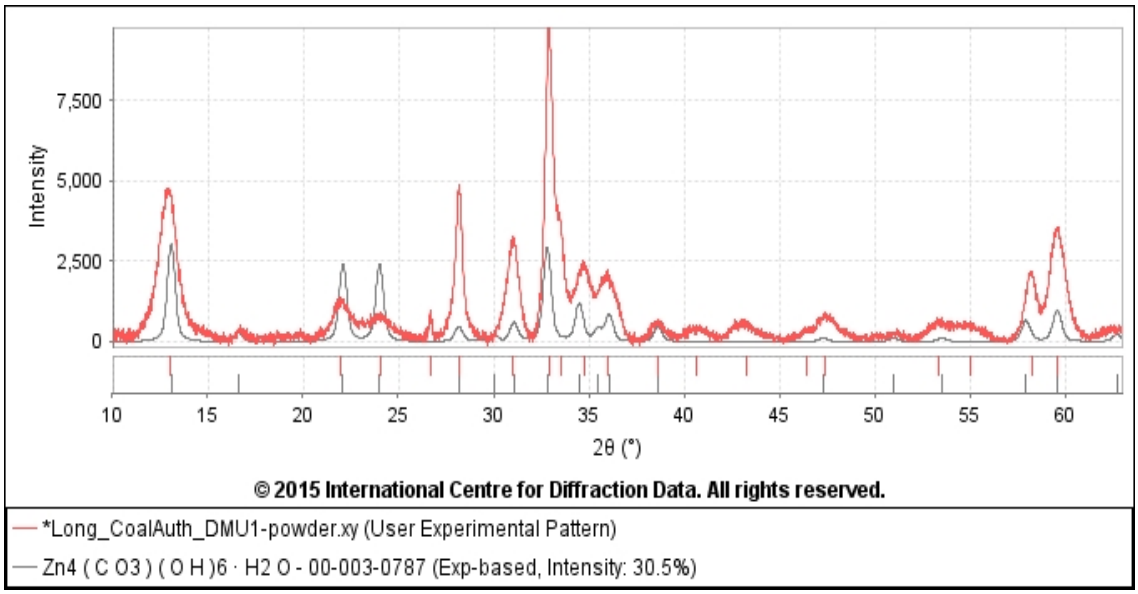

Figure 9-11: XRD spectrum of residue collected from the mesh samples (Figure 9-10).

Dr Nik Reeves-McLaren
Research and Teaching Fellow
Department of Materials Science & Engineering
Sir Robert Hadfield Building
University of Sheffield
Portobello Street
SheffieldS1 3JD